KERNFORSCHUNGSANLAGE JÜLICH GmbH
Institut für Kernphysik

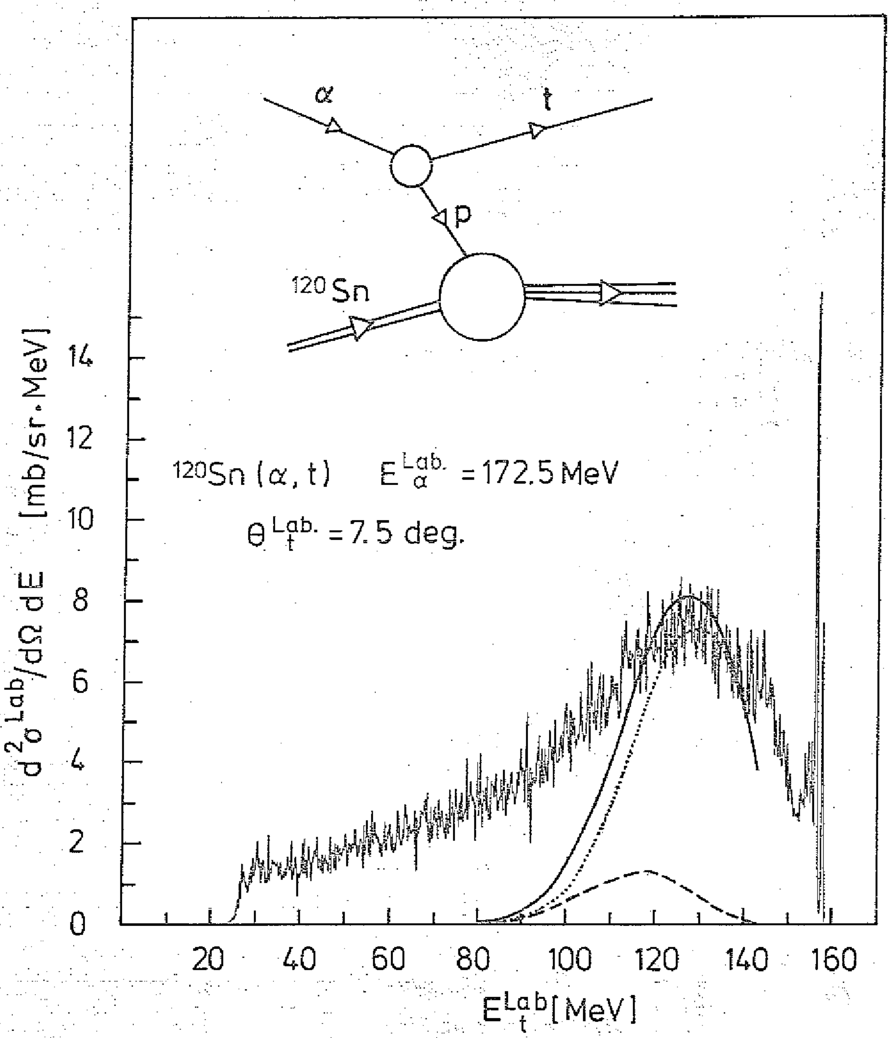

Jül - Spez 255
April 1984
ISSN 0170-8937

Annual Report 1983

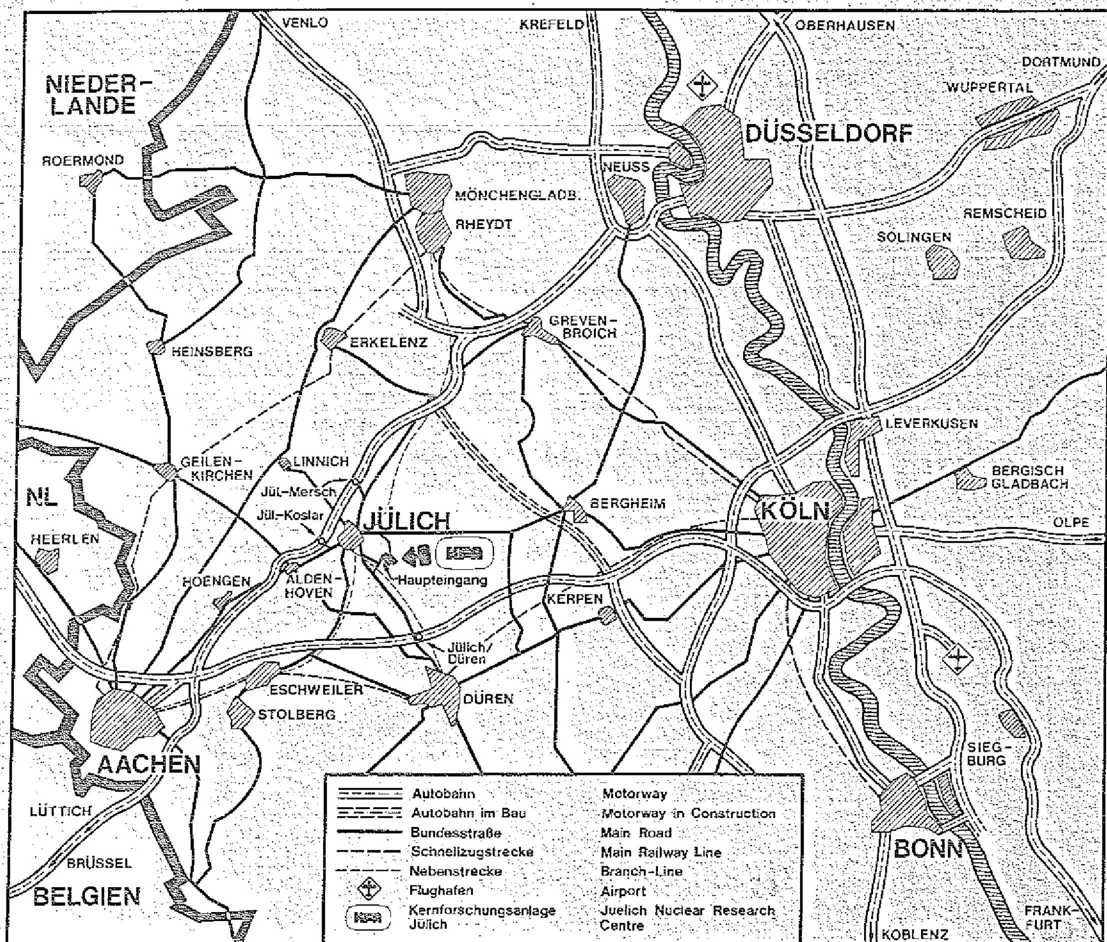

Als Manuskript gedruckt

Spezielle Berichte der Kernforschungsanlage Jülich - Nr. 255
Institut für Kernphysik Jül - Spez - 255

Zu beziehen durch: ZENTRALBIBLIOTHEK der Kernforschungsanlage Jülich GmbH
Postfach 1913 · D-5170 Jülich (Bundesrepublik Deutschland)
Telefon: (0 24 61) 610 · Telex: 8 33 556 kfa d

Annual Report 1983

Front cover: Inclusive triton spectra in 172.5 MeV α-particle induced reactions on ^{120}Sn at very forward angles as measured at JULIC. The theoretical calculations show the contribution of the inclusive break-up mechanism (continuous line) where the elastic and all inelastic interactions of the unobserved proton with the target nucleus are included (dashed and dotted line, respectively). The breakup reactions reveal information about ground state momentum distributions and single particle motion in the continuum.

P R E F A C E

This annual report of the Institut für Kernphysik (IKP) at the Kernforschungsanlage (KFA) Jülich covers the period from January to December 1983. Here we report on research activities and on technical developments performed by members of our institute and by guest groups using our cyclotron JULIC.

The Institut für Kernphysik consists of two experimental institutes, a theoretical institute, a newly created unit "Betrieb und Entwicklung kernphysikalischer Großgeräte", and several common support groups. The solar energy group is included in one of the experimental institutes.

The majority of the experimental research has been performed at the Jülich Isochronous Cyclotron (JULIC), and for about 50 % of the experiments the magnet spectrograph BIG KARL has been used as detector system. The cyclotron accelerates protons, deuterons, ^{3}He and α-particles from 22-45 MeV/nucleon, which have been used in basic research as well as for the radio-isotope production for bio medical application. About 20 % of the available beam time of the cyclotron has been used by guest scientists and users from other institutes of the KFA. In addition some of the experiments have been carried out at the KFA reactors: Neutron rich nuclei were studied with the on-line separator for fission fragments (JOSEF), and the Aachen-IKP collaboration searched for γ-events in connection with the question about the existence of axions.

Also in the past year there was an intense scientific and technical exchange due to guest groups at the cyclotron and many visiting scientists in the various units. There existsan especially strong collaboration with Prof. Hagedoorn and his groups of the Technische Hogeschool Eindhoven. Prof. Hagedoorn is temporarily here in a position as consultant.

The investigationsof giant resonances were concentrated on the charge exchange reaction (^{3}He,t) around zero degree to study isovector giant resonances in heavy nuclei.

Investigations in nuclear spectroscopy showed the low lying rotational bands in the Os-isotopes combined with low frequencies in the region of band-crossing. Other nuclear spectroscopy studies have revealed excited nuclear states which result from the coupling of two nucleons with one- and two phonon octupole vibrations. In the A=100 region rotational bands have now been observed systematically and Nilsson assignments have been made.

The theoretical work has concentrated on the role of the $\Delta(3/2\ 3/2)$-isobar resonance in nuclear structure and in charge exchange reactions, investigations of heavy-ion reactions with microscopic models, and the Coulomb-dissociation processes at relativistic energies.

The work on the external heavy ion source ISIS has been carried according to the time schedule. The test source (5 GHz) has been improved considerably to yield currents of 200 μA He^{2+} and 1 μA N^{6+}-ions.

In connection with the proposed neutron spallation source (SNQ) at the KFA, the IKP and interested scientists started to study various possibilities of isotope separation facilities in order to investigate exotic nuclei. For this reason a workshop was organized by our institute.

The proposal for the γ-ray detector system 'OSIRIS' was finished and presented to an international audience during a workshop on 'high-spin states' at the IKP.

After intense discussions, the study group 'COSY' under the leadership of Prof. T. Mayer-Kuckuk (University of Bonn) was created, which involves scientists from the universities of Bochum, Bonn, Köln, and Münster and the IKP of the KFA. The aim of the study group is to prepare a proposal for a cooler synchrotron, which can use the linac of the SNQ as well as our cyclotron as injector. In this connection the Institute also organized a workshop in the 'Physik Zentrum' at Bad Honnef.

The senior of the directors at the IKP, Prof. Dr. CLAUS MAYER-BÖRICKE, fell seriously ill in the beginning of the year 1982. He retired on October 1, 1983 after having led the Institute of Experimental Nuclear Physics I (IEKP I) as its director for a period of 16 years.

It was Claus Mayer-Böricke, who laid the plans for the large isoschronous cyclotron JULIC to be the main research instrument of the Nuclear Physics Institute (IKP) at the Kernforschungsanlage (KFA) Jülich. He planned and brought to realization the acceleration and extraction of protons, deuterons, ^{3}He and α-beams for nuclear physics experiments, the double monochromator for studies at higher resolution, and he initiated work on the large magnetic spectrometer Big Karl. In order to increase the potential of JULIC, he planned and started the installation of an ECR-source (project ISIS) for external injection of light ions.

Claus Mayer-Böricke was the director responsible for JULIC until the year of his retirement. Due to his constant and intense care, this facility could be used with high efficiency by the research groups of the IKP, by other groups of the KFA and by numerous guest groups.

As planned by Claus Mayer-Böricke, the IKP includes three institutes (IEKP I, IEKP II and Theory), and it is operated now as a department.

In spite of the large burden of his duties as director of the IEKP I and responsible director for JULIC and ISIS, Claus Mayer-Böricke remained an active scientist, and he ensured a high level research program at his institute. Only two of its most successful accomplishments will be mentioned here: (1) the backbending effect itself and its explanation by crossing of two rotational bands in deformed nuclei; (2) the discovery of the isoscalar giant quadrupole resonance in light nuclei. Both of these results received international recognition, indicating the high standard of the scientific program of his Institute.

April 1984 J. Speth

INSTITUTE FOR NUCLEAR PHYSICS

Managing director:	Prof. Dr. J. Speth
Experimental Nuclear Physics I, director:	Prof. Dr. C. Mayer-Böricke
Experimental Nuclear Physics II, director:	Prof. Dr. O. Schult
Theoretical Physics, director:	Prof. Dr. J. Speth

Kernforschungsanlage Jülich GmbH
Postfach 1913, 5170 Jülich, W.-Germany

CONTENTS

I. EXPERIMENTAL NUCLEAR PHYSICS

1. NUCLEAR REACTIONS AND SCATTERING PROCESSES

I EXPERIMENTAL NUCLEAR PHYSICS

1. NUCLEAR REACTIONS AND SCATTERING PROCESSES

1.1. Investigation of high lying M1 states in ^{40}Ca(p,p') at E_p = 45 MeV

B. Brinkmöller+*, G.P.A. Berg, G. Hlawatsch, A. Magiera, J. Meißburger, D. Paul*+*, J. Römer, G. Sondermann*+*, J.L. Tain*

In high resolution proton scattering experiments[1,2] at relatively low incident energies (E_p = 45, 65 MeV) several 1^+ states have been identified. A particular strong M1 excitation has been found[1] at E_x = 10.21 MeV in ^{48}Ca with a spin unsaturated closed $f_{7/2}$ neutron shell. In the simple independent particle shell model no 0 ħω M1 excitation is expected in ^{40}Ca. The observed 1^+ states[3,4,5] in ^{40}Ca indicate ground state correlations in the neutron and proton shells. A strong 1^+ state has been observed in ^{40}Ca at E_x = 10.31 MeV. Another 1^+ state was seen at E_x = 9.87 MeV[5]. The angular distribution of a peak at this energy is reported to be consistent with an unresolved doublet of 2^+ and 1^+ states in a backward angle electron scattering experiment[3] and a 200 MeV proton scattering experiment[4]. In addition a state with an l = 0 angular distribution was observed[4] at E_x=12.03 MeV with unknown parity.

To get more information about these states we measured ^{40}Ca(p,p') at 44.8 MeV proton energy using the high resolution magnetic spectrograph BIG KARL. States from 8.5 to 12.3 MeV excitation energy have been measured with a resolution of 14 keV at forward and 23 keV at backward angles due to incomplete kinematic matching. A sample spectrum of Θ_{lab} = 13.2° of the complete range of measured excitation energies is shown in fig. 1. The excitation energies are taken from ref. 6. This was one of the first experiments with the new multi-wire drift time chamber[7], which allowed to measure 75 cm of the focal plane of the spectrometer. Special care was taken in the off-line analysis to find and correct for effects of differential efficiency variations in the new detector. In order to show details of the states around E_x = 10 MeV, fig. 2 displays the enlarged range from E_x = 9.8 MeV to E_x = 10.5 MeV at three different scattering angles. At E_x = 10.33 MeV where two possible states have been reported[6] we resolve only one state in our measurements.

The angular distributions will be compared with DWBA calculations in order to determine the transfered angular momentum of the measured states and to identify possible 1^+ states.

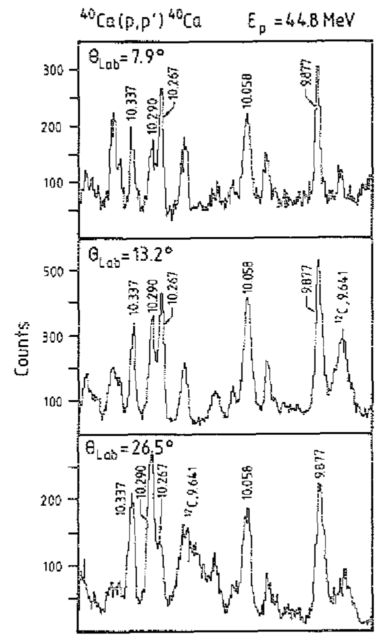

Fig. 2: Enlarged part of ^{40}Ca(p,p') spectra at 44.8 MeV incident energy for the scattering angles Θ_{lab} = 7.9°, 13.2°, 26.5° showing the states around E_x ∿ 10 MeV.

References

1) G.P.A. Berg et al., Phys. Rev. C25
2) M. Fujiwara et al., Nucl. Phys. A410 (1983) 137
3) W. Steffen et al., Phys. Lett. 95B (1980) 23
4) N. Anantaraman et al., Phys. Rev. Lett. 46 (1981) 1318
5) D.M. Pringle et al., Phys. Lett. 115B (1982) 291
6) H. Ejiri et al., Phys. Rev. C24 (1981) 2001
7) G.P.A. Berg et al., Annual Report 1982, IKP-KFA, Jül-Spez 202 (1983) 116

+ Institut für Kernphysik, Universität Münster

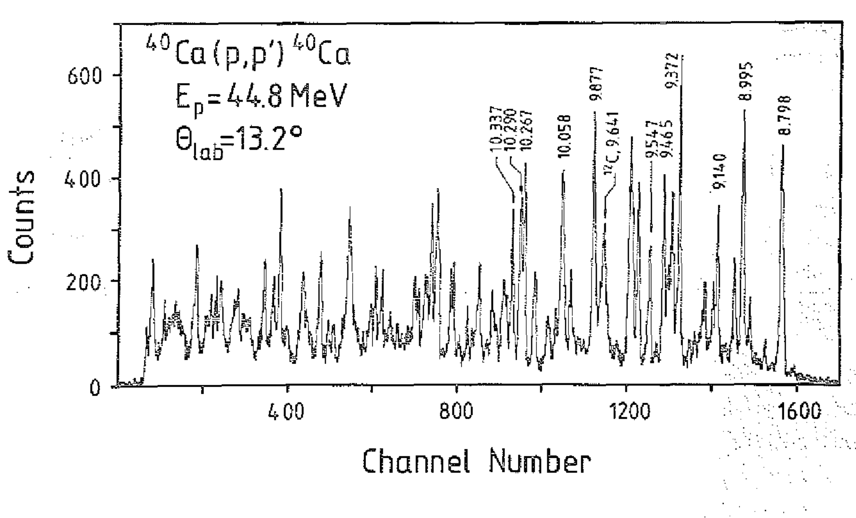

Figure 1:
Sample spectrum of ^{40}Ca(p,p') at 44.8 MeV incident energy from 8.7 to 10.3 MeV excitation energies at Θ_{lab} = 13.2°.

1.2. Excitation of 1^+ States in ^{58}Ni by Inelastic Proton Scattering at 45 MeV

G.P.A. Berg, G. Gaul[+]*, J. Meißburger, D. Paul, J.G.M. Römer, G. Sondermann*[+] *and J.L. Tain*

In our previously reported[1] $^{58}Ni(p,p')$ measurements at 45 MeV incident proton energy using the high resolution magnet spectrometer BIG KARL the 1^+ state at 2.903 MeV and the 1^+ state at 10.66 MeV are strongly excited. Spectra of these measurements have already been shown in ref. 1). The excitation of the 10.66 MeV state was also reported at 201 MeV[2] and 65 MeV[3] incident energy. Fig. 1 shows the comparison of the angular distributions of this state at the different incident energies plotted as function of the transfered momentum q. For $q \gtrsim 100$ MeV/c the cross sections are very similar for the three different energies. For $q < 100$ MeV/c, however the observed shapes of the angular distributions are very different. The higher the incident energies the larger is the cross section at very forward angles.

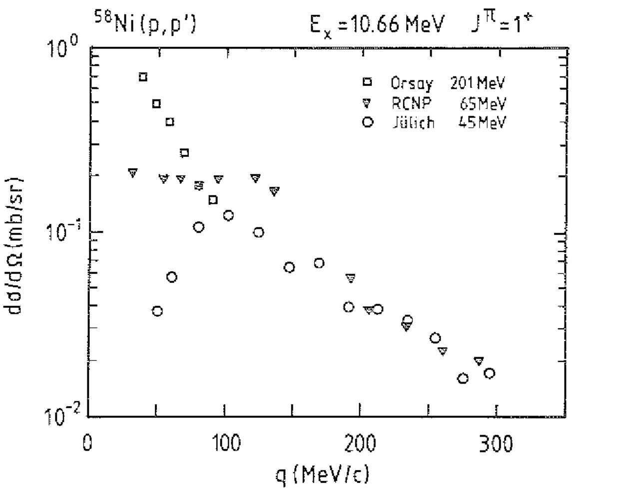

Fig. 1: Experimental angular distributions for the 1^+ state at 10.66 MeV in ^{58}Ni measured at various bombarding energies in (p,p') scattering.

This behaviour has been reproduced in preliminary microscopic DWBA calculations[4] and reflects the enhancement of the $\ell = 0$ relative to the $\ell = 2$ contribution with increasing energy.

We conclude that for energies 45 MeV $\lesssim E_p \lesssim$ 65 MeV the cross section maxima for M1 transitions occurs at $q \sim 100$ MeV/c while for higher energies the cross section increases with decreasing q, suggesting experiments for M1 investigations at $E_p > 65$ MeV in the energy window 150 - 400 MeV of spin flip excitations and extremely forward angles.

Low energy investigations of M1 transitions are limited to states with concentrated M1 strength like the 1^+ state[5] at E_x = 10.21 MeV in ^{48}Ca and the reported 1^+ state at E_x = 10.66 MeV in ^{58}Ni. Consequently we do not observe individual levels of the broad M1 (T = 1) resonance reported around $E_x \sim 8.8$ MeV in ^{58}Ni at E_p = 201 MeV. Among the expected 1^+ states there exists some confusion about the excitation of the state at 3.594 MeV for which one assumes a pure $(p_{3/2}\, p_{1/2})1^+$ configuration[6]. While the excitation of this state was not observed with an upper limit of 5 µb/sr in inelastic proton scattering at 65 MeV[3] it was excited with a cross section of 15 - 20 µb/sr in our (p,p') measurement at E_p = 45 MeV. Fig. 2 shows spectra including this 3.594 MeV state at Θ_{lab} = 15°, 20° and 25°. The spin-parity assignments of the 3.531 and 3.594 MeV states were taken from Ref. 6 while excitation energies, spins and parities of the other levels were taken from Ref. 7.

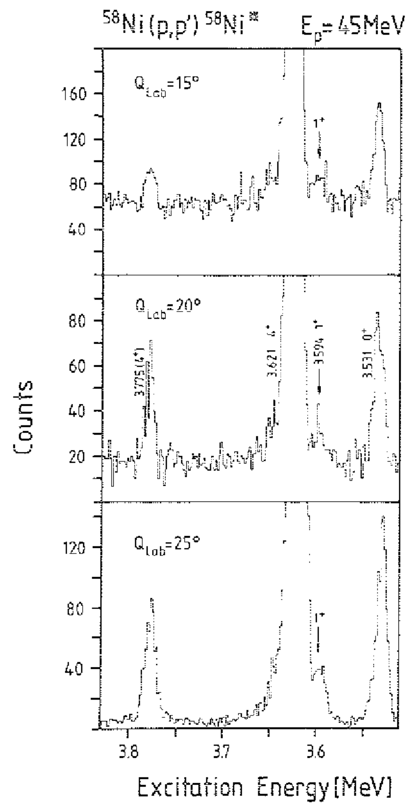

Fig. 2: Spectra including the 3.594 MeV state measured in ^{58}Ni (p,p') at Θ_{lab} = 15°, 20° and 25°.

References

1) G.P.A. Berg, G. Gaul, D. Grzonka, W. Hürlimann, J. Meißburger, D. Paul, J.G.M. Römer, G. Sondermann and J.L. Tain, KFA Institut für Kernphysik, Annual Report 1981, Jül-Spez 202 (1983) 1

2) C. Djalali, N. Marty, M. Morlet, A. Willis, J.C. Jourdain, N. Anantaraman, G.M. Crawley, A. Galonsky and P. Kitching, Nucl. Phys. A388 (1982) 1

3) M. Fujiwara, Y. Fujita, I. Katayama, S. Morinobu, T. Yamazaki, H. Ikegami, S.I. Hayakawa and K. Katori, Nucl. Phys. A410 (1983) 137

4) F. Osterfeld, private communication

5) G.P.A. Berg, W. Hürlimann, I. Katayama, S.A. Martin, J. Meissburger, J. Römer, B. Styczen, F. Osterfeld, G. Gaul, R. Santo and G. Sondermann, Phys. Rev. C25 (1982) 2100

6) H.P. Blok, J.J. Kraushaar, P.A. Batay-Csorba and F.E. Cecil, Nucl. Phys. A386 (1982) 61

7) Table of Isotopes ed. by C.M. Lederer and V.S. Shirley, John Wiley & Sons, Inc. 1978

[+] Institut für Kernphysik, Universität Münster

1.3. Identification of the second $13/2^+$ state of the octupole multiplet in ^{143}Nd

L. Trache[+], *J. Wrzesinsky*[++], *C. Wesselborg*[+++], *A. Clauberg*[+++], *R. Reinhardt*[+++], *P. von Brentano*[+++], *K.O. Zell*[+++], *Ch. Morris*[*], *G.P.A. Berg, B. Brinkmöller, G. Hlawatsch, J. Meißburger, D. Paul, J.G.M. Römer, J.L. Tain*

It has been reported recently[1)] that the complete particle-octupole multiplet in the N=83 nucleus ^{143}Nd has been identified by high-resolution inelastic proton scattering at E_p = 25 MeV using the BIG KARL spectrometer.
Earlier (d,p) experiments[2)] presented evidence for a splitting of the $13/2^+$ state into two levels at 1230 and 2807 keV due to configuration mixing with the $i_{13/2}$ single particle state in the major neutron shell with N=83-126[1,3)].

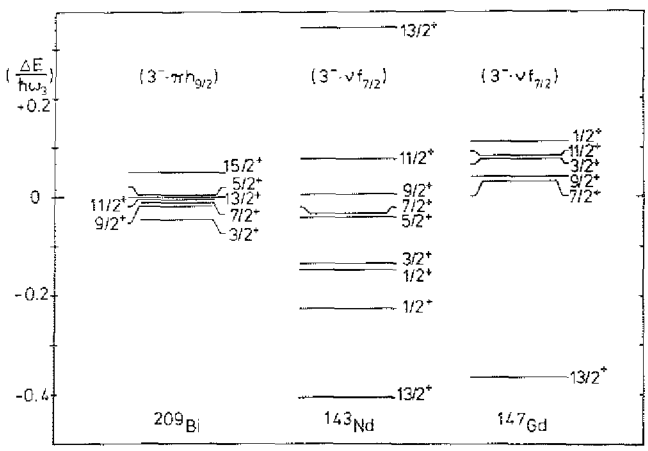

Fig. 1: Comparison of splitting of the octupole-multiplets arising from particle-core coupling in ^{209}Bi, ^{143}Nd and ^{147}Gd. The energies have been normalized to the energies of the corresponding core states.

In Fig. 1 the measured splitting in ^{143}Nd is compared with the splitting of the octupole multiplet in ^{209}Bi[4)] with a doubly magic core, and in ^{147}Gd[5)] with a core of magic neutron and semi-magic proton numbers. Both levels have been seen in our previous experiment[1)]. In the present experiment we measured the 2804 keV state with better statistics covering the energy range up to $E_x \approx$ 3.4 MeV. Fig. 2 shows a part of a sample spectrum taken with the new 90 cm long position sensitive detector[6)] in the focal plane of the magnet spectrometer BIG KARL. In this part of the spectrum the resolution was about 6 keV. For higher and lower excitation energies the resolution was worse by a factor of 3 - 4 because we did not yet work out an optimized set of H_t parameters for the correction of higher order aberrations. The measured angular distributions of both 13/2 states and the 3^- state in the ^{142}Nd core nucleus are shown in Fig. 3.

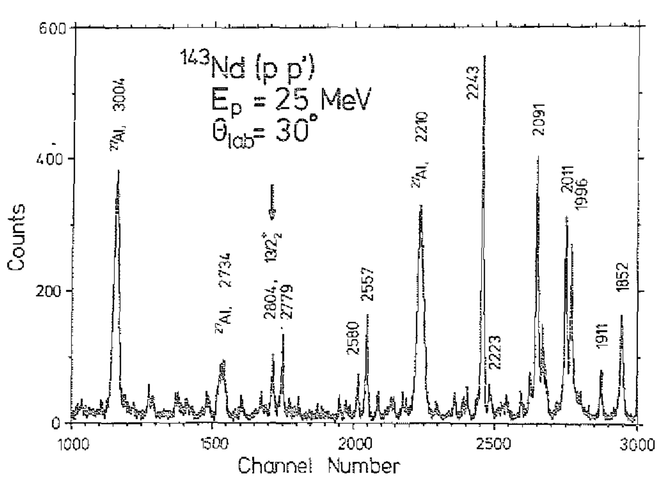

Fig. 2: $^{143}Nd(p,p')$ spectrum in the energy range from about 2 to 3 MeV.

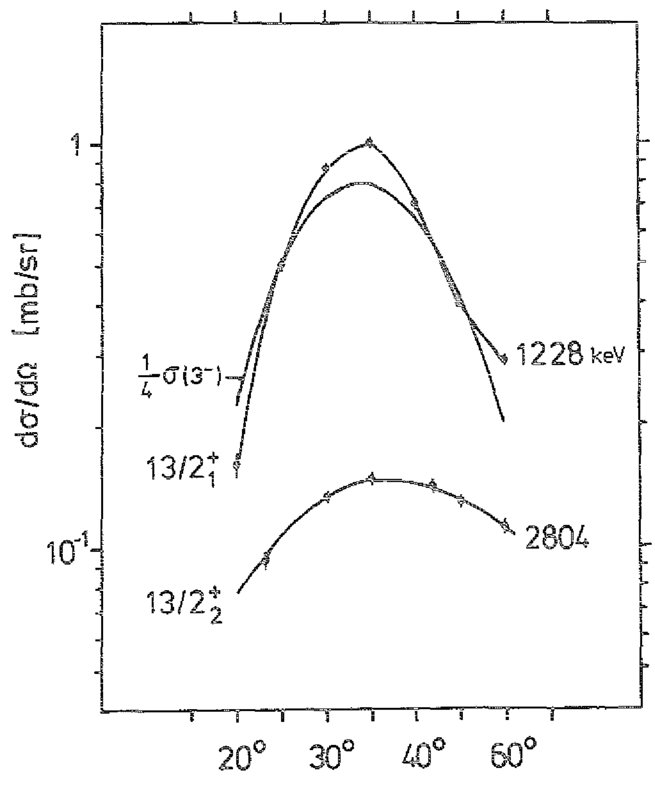

Fig.3 : Angular distribution of the two $13/2^+$ states compared to the octupole core state.

References

1) L. Trache et al., Ann. Rep. KFA-Jülich (1982) 2
L. Trache et al., Phys. Lett. B131 (1983) 285
2) W. Booth et al., Nucl. Phys. A238 (1975) 301
3) A.A.C. Klaasse, V. Paar, Nucl. Phys. A297 (1978) 45
4) J. Ugrin et al., Mat. Fys. Medd. Dan. Ved. Selsk. 38 (1971) no. 8
5) M. Piiparinen et al., Z. f. Physik A309 (1982) 87
6) G.P.A. Berg et al., Ann. Rep. KFA-Jülich (1982)

+ Institute for Physics and Nuclear Engineering, Bucharest, Romania
++ Institute of Nuclear Physics, Cracow, Poland
+++ Institut für Kernphysik, Universität zu Köln
* Los Alamos Scientific Laboratory, New Mexico, USA

1.4. States at E_x = 16 - 22 MeV in ^{8}Be excited in the $^{12}C(d,^{6}Li)^{8}Be$ and $^{11}B(^{3}He,^{6}Li)^{8}Be$ reactions

L. Jarczyk+, *A. Strzalkowski*+, *B. Styczen*+, *G.P.A. Berg*, *B. Brinkmöller*, *G. Hlawatsch*, *A. Magiera*++, *J. Meißburger*, *W. Oelert*, *D. Prasuhn*, *P. von Rossen*, *J.G.M. Römer and J.L. Tain*

The problem of the structure and especially of the isotopic spin assignment of the ^{8}Be states with excitation in the region 16 to 19 MeV is a long standing and still broadly discussed problem[1]. The investigation of excitation of this states in different cluster transfer reactions starting from the various entrance channels can shed light on this problem.

Two such reactions were measured using 78 MeV deuteron and 71.8 MeV ^{3}He beams from cyclotron JULIC namely $^{12}C(d,^{6}Li)^{8}Be$ and $^{11}B(^{3}He,^{6}Li)^{8}Be$. In both cases different clusters (α-particle or triton) with different isospin are transfered.

The ^{6}Li ions from $^{12}C(d,^{6}Li)$ were measured at few scattering angles Θ_{lab} = 10^{0} - 30^{0} using two ΔE-E semiconductor counter telescopes for particle identification. A typical example of the measured spectrum is shown in fig. 1. In the high excitation region the 16.63/16.92 MeV doublet is observed. The 18.15 MeV state is weakly populated. A broad group of states around 19 MeV is excited with a considerable cross section. No sign of excitation of the state at 17.64 MeV is visible in the spectra.

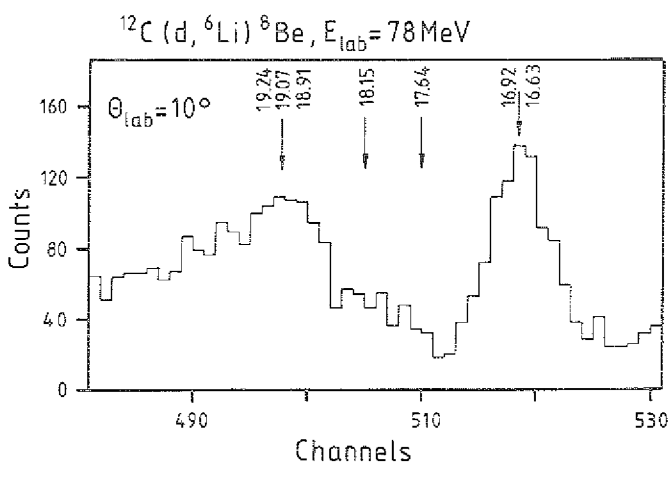

Fig. 1: Sample spectrum of the $^{12}C(d,^{6}Li)^{8}Be$ reaction

The spectra of ^{6}Li of the $^{11}B(^{3}He,^{6}Li)$ reaction were measured by means of the magnet spectrometer BIG KARL for scattering angles Θ_{lab} = 8^{0} - 42^{0}. The ΔE gas - E plastic counter telescope placed behind the position sensitive MWPC detector in the focal plane allowed the particle identification. In fig. 2 the spectrum between 16 and 20 MeV excitation energies measured in two runs is shown for an angle Θ_{lab} = 10 ^{0}. The different relative transition strengths to various ^{8}Be levels in both reactions under investigation is evident. In order to get more information on the excitation mode calculations of the angular distributions in the DWBA framework are in progress.

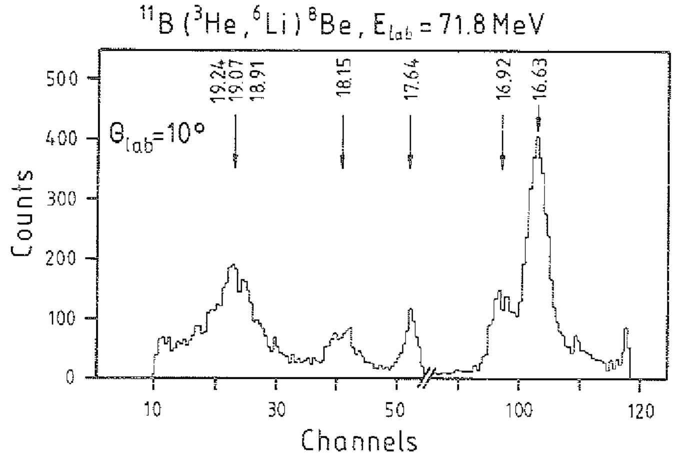

Fig. 2: Sample spectrum of the $^{11}B(^{3}He,^{6}Li)^{8}Be$ reaction

Reference

1) E.C. Barker, Nucl. Phys. 83 (1966) 48
V. Yamaya et al., Phys. Lett. 90B (1980) 219

+ Institute of Physics, Jagellonian University, Cracow, Poland

++ on leave from the Institute of Physics, Jagellonian University, Cracow, Poland

1.5. Reaction Mechanism of the $^{22}Ne(d,^{6}Li)^{18}O$ Reaction

W. Oelert and G. Pálla

As part of a systematic study of the alpha transfer among nuclei of the sd shell the $(d,^{6}Li)$ reaction has been measured at a bombarding energy of 80 MeV on ^{22}Ne. Angular distributions were obtained in an angular range of 8^{0} to 35^{0} lab. In the framework of finite-range Distorted-wave Born Approximation (FR-DWBA) calculations alpha-spectroscopic factors were extracted. Experimental data and FR-DWBA analysis leading to spectroscopic information were presented in an earlier report[1] and will be published[2]. Due to structure reasons and experimental limits qualitative comparison to sd-shell model calculations[3] can be made only for the low lying states with excitation energies less than 4 MeV. Fig. 1 displays these results for the low lying states and shows that these re-

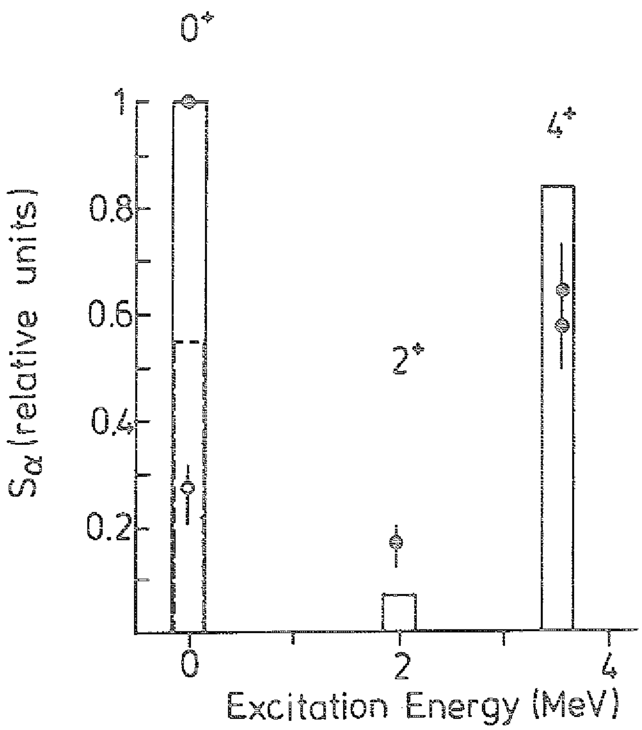

Figure 1: Relative spectroscopic factors for the members of the ground state band in ^{18}O. The full points (solid lines) denote experimental (theoretical) spectroscopic factors relative to the ground state transition, the open point (dashed line) relative to the $^{20}Ne \rightarrow ^{16}O_{g.s.}$ transition.

lative spectroscopic factors for the 2_1^+ and 4_1^+ final states agree to shell model calculations within a factor of two relative to the ground state transition (full data points, solid lines for theory) and that the ground state transition relative to the $^{20}Ne(d,^{6}Li)^{16}O_{g.s.}$ transition is a factor of two smaller than predicted by the shell model calculations. Since the absolute cross sections are believed to be accurate within 20 % the factor of two discrepancy seems to be significant at least for the comparison of relative experimental and theoretical results for the investigated system.

The strong collectivity of the low lying states suggests the neccessity of employing the coupled reaction channels formalism (CRC). Indeed an analysis in the framework of CC-DWBA resulted in rather good agreement between theore-

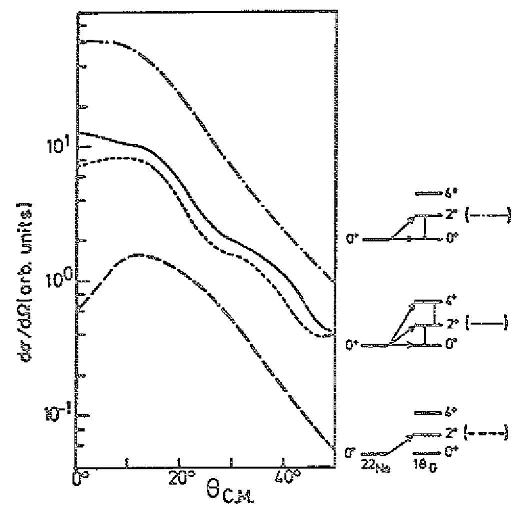

Figure 2: Influence of inclusion of different reaction pathes to the one-step transition for the final 2^+ state in ^{18}O.

tical and experimental angular distributions in view of both the shape and the magnitude. Fig. 2 demonstrates the influence of two step pathes on the final 2^+ state in ^{18}O. Whereas the direct one step process (dashed line) leads to very low cross sections an increase of a factor of 20 is observed due to the contribution of the reaction path via the ground state transition followed by the inelastic excitation (dashed-dotted line). Inclusion of the two step path via the transfer to the 4^+ state in ^{18}O (solid line) leads to a destructive interference and gets the cross section down, close to the experimental values which are indicated by the dashed line underneath the solid line. Results of the CC-DWBA calculations are given in Ref. 4. In extension of the CC-DWBA calculation we tried to describe all three members of the ground state band in the CRC framework i.e. to describe the 0^+, 2^+ and 4^+ states in ^{18}O by the solution of the Schrödinger-equation system of the coupled channel problem (including only two step contributions explicitly). Since the parameters entering into this type of calculations are mutually interdependent, effects of possible uncertainties are eventually qualitatively and quantitatively more sensitive and of stronger significance than in usual DWBA calculations. Here we only can list such uncertainties, a more detailed discussion will be given elsewhere[2]:

a) phases entering into the calculations have to be consistent among the different transfer spectroscopic amplitudes themselves as well as with the phases of the inelastic transition ones and, furthermore, with conventions used in the computer code for calculating the angular distributions,
b) absolute values of spectroscopic factors were calculated by a shell model code[3], however, the degree of reliability of these values is unknown,
c) optical model and bound state parameters are subject to considerable uncertainties for the simple DWBA as well as (because of mutual interdependence even stronger) for the case of CRC calculations.

For the present CRC calculations spectroscopic amplitudes and phases were obtained using the shell model code of Chung et al.[3]; the deformation parameters were selected from experimental results from the literature[5-8]; the coupled channel code CHUCK[9] was used; employing the coupling scheme as shown in Fig. 3; and optical model and bound state parameters were employed as in the FR-DWBA calculations[1,2], changing the radius parameter of the bound state from 1.56 $A^{1/3}$ fm to 1.65 $A^{1/3}$fm. The radius parameter of the deuteron optical potential was lowered to 1.15 fm according to the results of the analysis of scattering experiments[10].

Figure 4 shows the results of the calculations and demonstrates that the experimental angular distributions for the 0^+, 2^+ and 4^+ state in ^{18}O are well described in amplitude as well as in shape using the CRC formalism. However, two changes of parameters entering into the calculations were made: i) the phases of the spectroscopic amplitudes leading from the 2^+ state in ^{22}Ne to final states in ^{18}O were multiplied by -1 and ii) the potential depth of the real volume part of the ^{6}Li optical potential for ^{6}Li - $^{18}O_{g.s.}$ was lowered by 12 % (not for the other states of ^{18}O). Both changes might have some physical justifiaction, which has to be investigated by further studies on the same and on different systems. In spite of these questions we may conclude: Employing the rather complex CRC analysis good agreement between experimental results and theoretical predictions is observed. The spectroscopic factors predicted by shell model calculations prove to be very reliable in the sense that any significant change of one of the individual transition strength did worsen and not improve the simultaneous description of the data for the three members of the ground state band in the final nucleus ^{18}O.

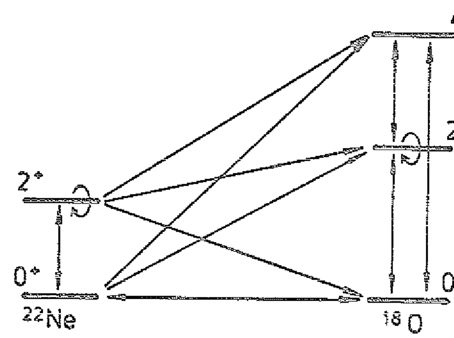

Figure 3: Coupling scheme used for the CRC calculations.

References

1) M.G. Betigeri et al., Annual Report 1980, KFA-IKP, Jül-Spez-99, p. 26
2) W. Oelert et al., to be published
3) W. Chung, Ph.D. thesis, Michigan State University, 1976, spectroscopic factor shell model calculations, using the computer code of W. Chung
4) W. Oelert and G. Pâlla, International Symposium, Osaka 1983, pp 420
5) H. Rebel et al., Nucl. Phys. A182 (1982) 145
6) J.L. Escudié et al., Phys. Rev. C10 (1974) 1645 and C11 (1975) 639
7) B.G. Harvey et al., Phys. Rev. 146 (1966) 712
8) R. Vandenbosch et al., Nucl. Phys. A230 (1974) 59
9) P.D. Kunz, Univ. of Colorado, code CHUCK, modified by J.R. Comfort
10) J.D. Childs et al., Phys. Rev. C10 (1974) 217, W.W. Daehnick et al., Phys. Rev. C21 (1980) 2253

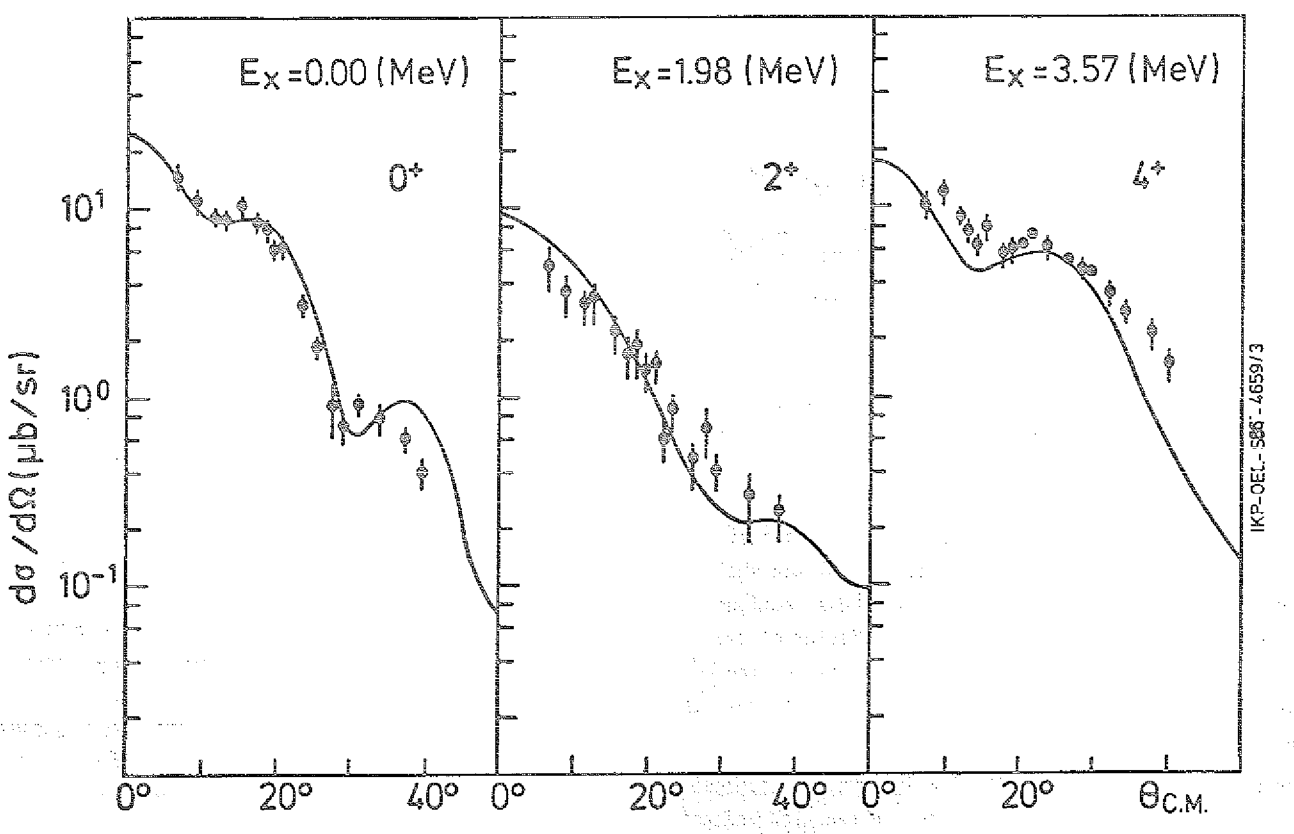

Figure 4: Experimental angular distributions of the (d,^{6}Li) reaction leading to final states in ^{18}O compared to CRC calculations.

1.6. Excitation of $K^{\pi} = 2^-$ Band States in ^{20,22}Ne via the (d,^{6}Li) Reaction

G. Pálla and W. Oelert

Recent analyses (preceding contribution and ref. [1]) have shown, that the strong collectivity of the low lying states makes necessary to employ coupled channels (CC) formalism in the interpretation of α-transfer reactions on sd-shell nuclei. In general both, one- and two-step processes feed a state contributing coherently to the reaction cross section and their interference effects, the magnitude and the shape of the angular distributions. The ^{24,26}Mg(d,^{6}Li)^{20,22}Ne reactions leading to the low lying members of the K=2$^-$ rotational band were analyzed by using a coupled channel (CC) DWBA method (code CHUCK[2]). Experimentally the $J^{\pi} = 3^-$ states (5.61 MeV in ^{20}Ne and 5.91 MeV in ^{22}Ne) were strongly populated, the transitions to the unnatural parity $J^{\pi} = 2^-$ (4.968 MeV) and $J^{\pi} = 4^-$ (7.004 MeV) states have been found to have medium yields in ^{20}Ne (in ^{22}Ne they were not resolved)[3], even though the excitation of these latter transitions are forbidden via direct α-transfer in a zero-range approximation. Since the B(E2) transition strengths between the 3^--2^- and 3^--4^- states are large the excitation of these states were assumed to proceed primarily through multi step pathes.

The coupling schemes used in CC calculation are shown in the Fig's. Existing no strong inelastic coupling between the members of the ground state and K=2$^-$ bands, in this calculation the K=-2 band is included explicitly only, the α-transfer transitions to the g.s. band members have been taken into account through the imaginary potential and have been investigated separatly in a CC-analysis[1]. For the α-cluster 2N+L=7 was used for the transitions to π = - states with $(sd)^3(0p)^{-1}$ configurations. The transfer form factors were calculated in a zero-range approximation applying finite range correction and proper zero range normalization. Potential parameters used are the same as in ref. [4]. The deformation parameters for the g.s. band were taken from inelastic scattering analysis and scaled according to βR. For the $K^{\pi} = 2^-$ band 25 % larger β_2 values were used[5]. The angular distribution results are presented in fig. 1 and fig. 2, the spectroscopic factors in table 1 including a corresponding SU(3) prediction[6]. The experimental spectroscopic factors

Transition	ℓ_{tr}	$S/S_{g.s.}$		
		SU(3)[6]	CCBA	DWBA[2]
^{24}Mg→^{20}Ne				
0^+→3^-	3	2.65	3.06	3.81
2^+→2^-	3		0.35	
2^+→4^-	3		-1.1	
2^+→4^-	5		0.26	
^{26}Mg→^{22}Ne				
0^+→3^-	3	0.50	0.5	2.44
0^+→5^-	5	0.99	-0.99	<0.2
2^+→3^-	3		-0.17	

Table 1: α-spectroscopic factors.

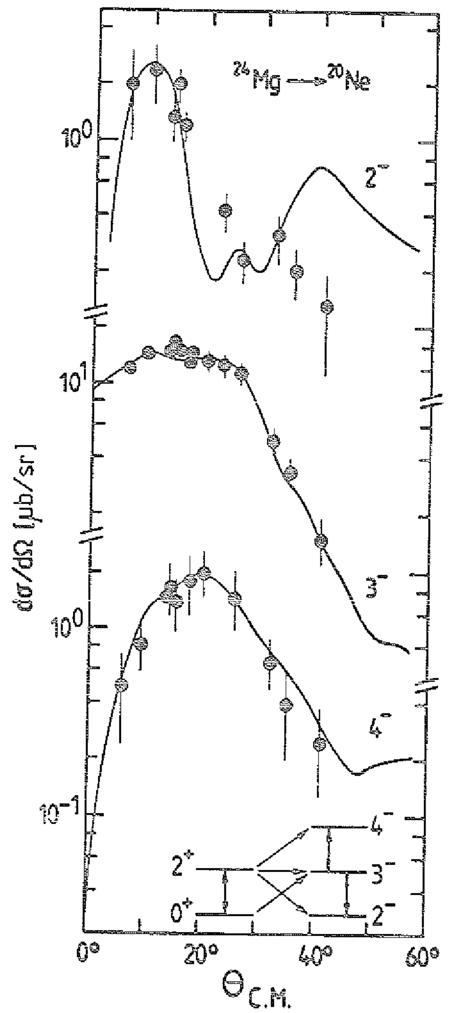

Figure 1: CC calculated and experimental angular distributions for negative parity states in ^{20}Ne.

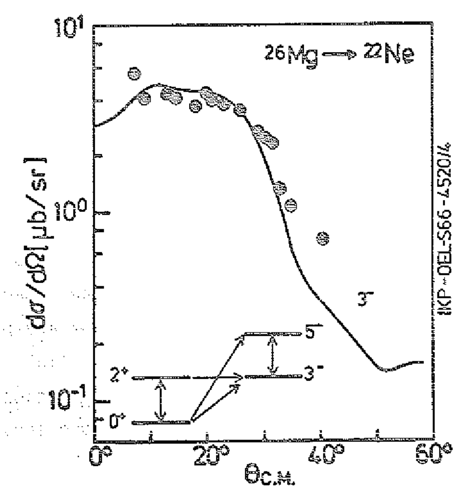

Figure 2: Predictions of a coupled channel calculation compared to the experimental angular distribution for the 3^- states in ^{22}Ne.

deduced by CC calculation are related to that of the ground state arising from CC analysis regarding the g.s. band[1]. The results prove the justification of the assumption of a multi step reaction mechanism.

References

1) G. Pálla, W. Oelert, Proc. of the Int. Conf. on Nuclear Physics, Florence, 1983, Vol. 1, pp 243
2) P.D. Kunz, Univ. of Colorado
3) W. Oelert et al., Phys. Rev. C22 (1980) 408
4) W. Oelert et al., Phys. Rev. C28 (1983) 73
5) D.K. Olsen et al., Phys. Rev. Lett. 29 (1972) 1178
6) J.C. Vermeulen et al., Nucl. Phys. A361 (1981) 189

1.7. Proton-Hole States in Co-Isotopes Observed via the (d,^{3}He) Reaction

A. Marinov[*]*, G.P.A. Berg, J. Bojowald, S. Gopal*[**]*, G. Hlawatsch, S.A. Martin, C. Mayer-Böricke, J. Meißburger, W. Oelert, D. Paul, J.G.M. Römer, M. Rogge, J.L. Tain, P. Turek, L. Zemło, R.B.M. Mooy*[+]*, P.W.M. Glaudemans*[+]*, S. Brant*[++]*, V. Paar*[++]*, M. Vouk*[++]*, V. Lopac*[++]

The structure of the cobalt nuclei is interesting from a theoretical point of view, since, on the basis of the simple shell model, they are characterized by one proton hole structure in the $1f_{7/2}$ shell. Therefore, we investigated the (d,^{3}He) reaction on Ni-isotopes leading to final states in Co. Experimental results of the ^{62}Ni(d,^{3}He)^{61}Co reaction were presented earlier[1,2]. Here we compare these data to theoretical predictions. The analysis of the ^{58}Ni(d,^{3}He)^{57}Co reaction is in progress . Preliminary results are available in the sense that the high resolution data taken with the magnetic spectrometer BIG KARL in the angular range of 3^0 to 25^0 are analyzed. The measurements of the same reaction in the scattering chamber are planned for the near future. The ΔE-E counter telescope technique is complementary necessary to obtain energy spectra over a wide excitation energy range and to ensure the absolute normalisation for the cross section measurement.

In the present analysis of the ^{62}Ni(d,^{3}He)^{61}Co reaction at E_d = 78 MeV we in particular consider the importance of the finite range effects on the validity of the DWBA calculations at high energies. At first, zero range calculations with the finite range effects taken into account by means of a local energy approximation have been performed using the code DWUCK4[3] with a value of 0.77 fm for the finite range correction factor and deuteron optical potentials as extracted from the global set of Daehnick et al.[4]. ^{3}He potentials (H1, H2 and H3) were derived from Hyakutuke et al.[5] (which are all shallow potentials with $V_R \sim$ - 108 MeV) and (H4) from Shepard et al.[6] (a deep potential with V_R = - 160.13 MeV). Two bound state parameter sets (P1 and P2) were tested with these ^{3}He potentials. Details on the individual parameters are given in Ref. 2. Figure 1 shows some examples of DWBA calculations employing the various potential combinations. It seems that the zero range approximation, with finite range effects taken into account by the local energy approximation, cannot reproduce all the tested angular distributions. Exact finite range calculations have therefore been performed using the code DWUCK5[3]. Results of these calculations for four states are shown in Fig. 2, using a shallow potential (H1) as well as a deep potential (H4) for the ^{3}He particles. It is demonstrated that, by using the deep potential for the ^{3}He particles, it is now possible to reproduce all of the four selected experimental angular distributions for the final levels in ^{61}Co quite nicely. Full finite range DWBA calculations have therefore been performed for the excited states analyzed in our work, using the DWUCK5 program and the deep potential for the ^{3}He particles.

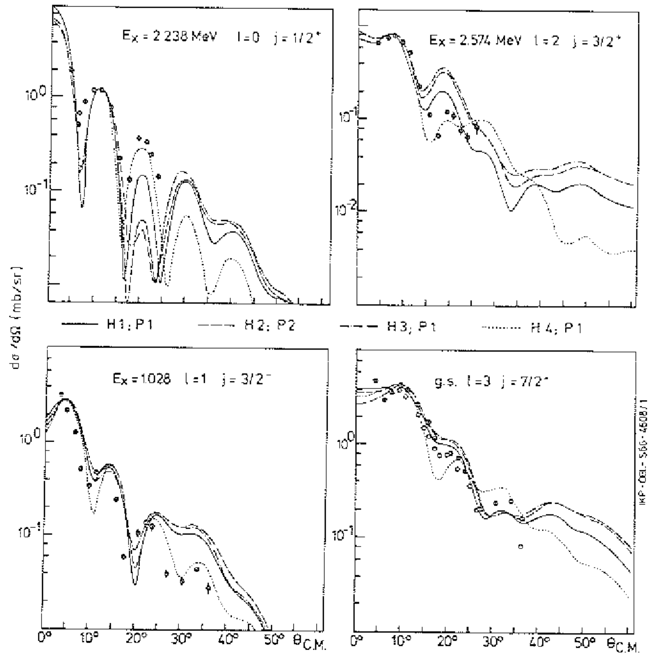

Figure 1: Results of zero range DWBA calculations together with a selection of experimental angular distributions.

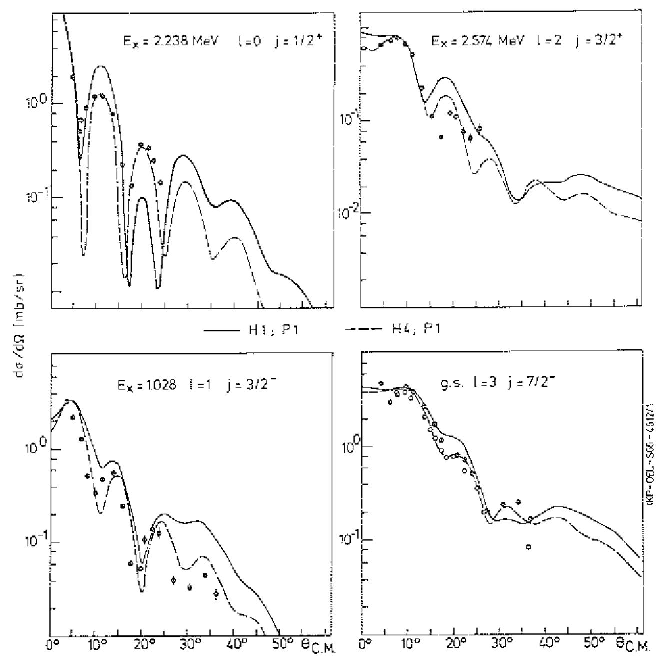

Figure 2: Results of full finite range DWBA calculations together with a selection of experimental angular distributions. H1 and H4 are Shallow and deep ^{3}He optical potentials, respectively.

Shell-model calculations for the system ^{62}Ni-^{61}Co were performed in the model space:

^{62}Ni: $f_7^{16}r^6 + f_7^{15}r^7$ $\qquad$ ^{61}Co: $f_7^{15}r^6 + f_7^{14}r^7$

where f_7 denotes the $1f_{7/2}$ orbit and r stands for any of the orbits $2p_{3/2}$, $1f_{5/2}$ and $2p_{1/2}$. Both terms of the wave function of ^{61}Co contribute to $f_{7/2}$ pick-up, whereas the first term only contributes to pick-up of an r particle. The interaction has been obtained empirically from a fit to experimental excitation energies of A=52-60 nuclei[7]. Excitation of one $f_{7/2}$ particle into the upper fp-shell orbits is assumed in the model space. Figure 3 compares the experimentally observed level scheme to the shell mo-

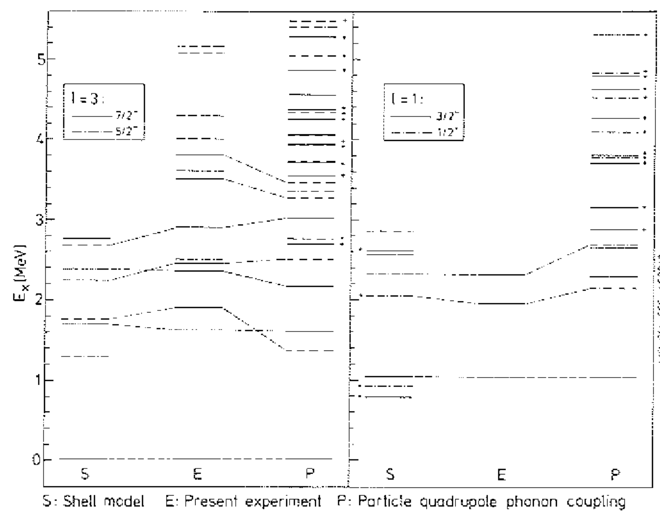

Figure 3: Calculated (shell model), experimental, and calculated (PTQM) energy spectrum of ^{61}Co for $7/2^-$, $5/2^-$ and $3/2^-$, $1/2^-$ final states. Levels denoted by + have a very small spectroscopic strength. The experimental states are tentatively assigned to the theoretical levels.

del predictions together with further theoretical predictions of the particle-quadrupole phonon coupling. The association of the theoretical predicted levels to the experimentally observed ones is not unique and has been made on the basis of: excitation energy, known and/or determined spin and parity assignment and predicted versus observed spectroscopic strengths.

The calculations for the energy spectrum of ^{61}Co were performed by coupling a proton quasiparticle to the anharmonic quadrupole vibrational core, employing a Hamiltonian characterized by the SU(6) symmetry: the core nucleus ^{62}Ni is described in the SU(6) quadrupole phonon model TQM, which is equivalent to the well known IBM, and ^{61}Co is described in the SU(6) particle-quadrupole phonon coupling model PTQM, which is equivalent to IBFM. An explicite description of the evaluation of the energy spectrum of ^{61}Co is given in Ref. 2) and in references cited therein. The negative and positive parity spectra of ^{61}Co obtained by diagonalization of the PTQM Hamiltonian are presented in Fig. 3 and in Fig. 4, respectively.

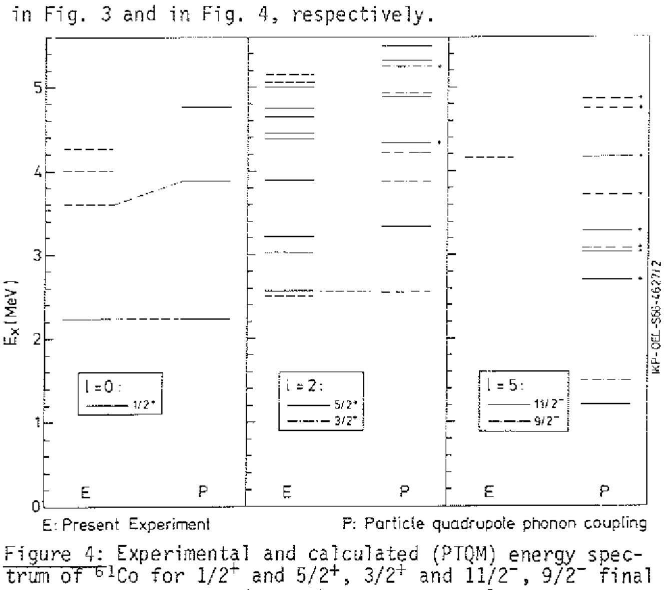

Figure 4: Experimental and calculated (PTQM) energy spectrum of ^{61}Co for $1/2^+$ and $5/2^+$, $3/2^+$ and $11/2^-$, $9/2^-$ final states. Levels denoted by + have a very small spectroscopic strength. The experimental states are tentatively assigned to the theoretical levels.

Using PTQM wave functions of the low-lying states in ^{61}Co and the TQM wave function of the ground state of ^{62}Ni we calculated the spectroscopic factors for the reaction ^{62}Ni(d,^{3}He)^{61}Co. The sums of the spectroscopic factors as functions of excitation energies are presented in Fig. 5. The spectroscopic information has been collected

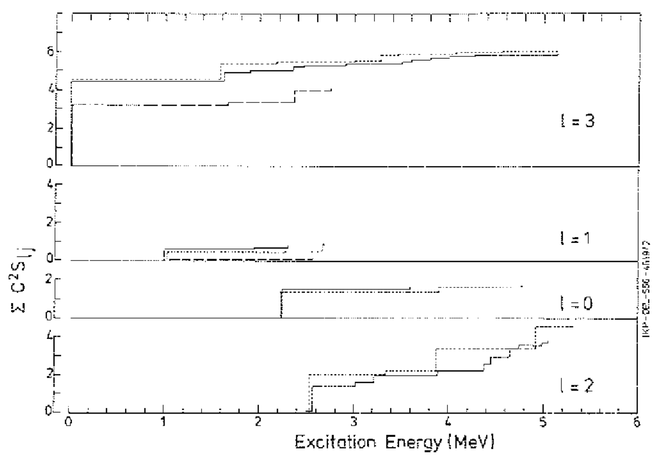

Figure 5: Experimental (solid lines) sum of spectroscopic strength versus excitation energy plotted for ℓ = 3, 1, 0 and 2 transfers, compared to the predictions of shell-model calculations (dashed lines) and of the PTQM calculation (dotted lines).

for the individual ℓ-transfers only, since experimentally a j-dependence is not detectable. For ℓ = 3 the shell model predictions are too small relative to the experimental values whereas the PTQM calculations show a very good agreement. Quantitatively the same is true for the ℓ = 1 results, where the shell model calculation fails to predict the observed occupation of the $p_{3/2}$ orbit.

For ℓ = 0 and ℓ = 2 transfers the shell model calculations are not suitable to predict strength because of the truncated model space. The agreement between experimental data and PTQM calculations is also very reasonable, but obviously some additional states outside the configuration space of the present calculation appear for the ℓ = 2 transfer strength in the energy range considered.

For ℓ = 5 the PTQM calculations predict very small spectroscopic factors for the first excited theoretical states $11/2^-$ and $9/2^-$ which lie at about 1.5 MeV. The corresponding experimental states have not been detected most likely because of very low cross sections; however, preliminary results of the ^{58}Ni(d,^{3}He)^{57}Co reaction reveal in this energy region two relatively weakly populated states excited by ℓ = 5 transfer. Especially interesting theoretical challenge is posed by the fact that the experimental spectroscopic factor of the first $3/2^-$ state at 1.028 MeV excitation energy is sizeably (spectroscopic factor s = 0.17) larger than those of higher-lying $3/2^-$ states ($3/2^-$ state at 1.953 MeV: s = 0.014; $3/2^-$ state at 2.313 MeV: s = 0.017). The admixture of the high lying $p_{3/2}$ quasiparticle state into the first $3/2^-$ wave function is naturally small; in our PTQM wave function the $|j, nI; J\rangle = |p_{3/2}, 00; 3/2\rangle$ component (the quasiparticle j and the n-phonon state of angular momentum I are coupled to the total angular momentum J) amounts to less than 2 %. Taking into account low occupation probability of the $p_{3/2}$ state ($\gtrsim 0.1$) the spectroscopic factor due to this component would result in a spectroscopic factor $S_{p_{3/2}} \approx 0.002$; which is two orders of magnitude below the experimental value. However, due to further terms in the PTQM transfer operator, we get a sizable contribution to $S_{p_{3/2}}$ from the dominant component $|f_{7/2}, 1\ 2; 3/2>$, this one phonon multiplet component amounts to 90 % of the norm of the wave function.

On the other hand, due to more scattered components in the wave functions of higher-lying $3/2^-$ states (as in the neighbouring nuclei) the total contribution to $S_{p_{3/2}}$ is smaller.

Thus, PTQM in a physically transparent way accounts for interesting pattern of the spectroscopic factors of $3/2^-$ states, which at the first sight contradicts to the particle-core concept.

References

1) A. Marinov et al., Annual Report 1982, KFA-IKP, Jül-Spez 202, p. 8
2) A. Marinov et al., to be published in Nucl. Phys. A
3) P.D. Kunz, computer codes DWUCK, Univ. of Colorado, Boulder, unpublished
4) W.W. Daehnick et al., Phys. Rev. C21 (1980) 2253
5) M. Hyakutake et al., Nucl. Phys. A333 (1980) 1
6) J.R. Shepard et al., Phys. Lett. 56B (1975) 135
7) R.B.M. Mooy and P.W.M. Glaudemans, Z. Phys. A312 (1983) 59

* The Hebrew University of Jerusalem, Israel

** University of Mysore, India

\+ Rijksuniversiteit, Utrecht, The Netherlands

++ University of Zagreb, Yugoslavia

1.8. Inelastic two-step processes in single-nucleon transfer reactions

G. Pálla, W. Oelert, A. Djaloeis, P. Turek, and L. Zemlo

The role of two-step processes in single-nucleon transfer of different type, namely, neutron and proton transfer in both of pick-up and stripping reactions on ^{28}Si target is revealed. A complete measurement is in progress undertaken concerning the reactions ^{28}Si(d,x), x = d,d',τ,t; ^{28}Si(τ,y), y = τ,τ',d,α and ^{28}Si(α,z), z = α,α',τ,t, which should offer an excellent possibility to show the importance of the higher-order transfer processes involving inelastic transitions of quadrupole nature preceded or followed by a transfer step. The data are analysed in the framework of the coupled channels reaction theory, the spectroscopic amplitudes needed in analysis are calculated, using the code CHUCK[1] and the SM-code from Chung et al.[2], respectively.

References

1) P.D. Kunz, University of Colorado
2) W. Chung et al., Phys. Lett. 79B (1978) 381

1.9. Observation of the 1.6 MeV level in ^{9}B

A. Djaloeis, J. Bojowald, G. Paić, and B. Antolković**

In spite of numerous experimental endeavours[1-5] to measure the parameters of the ^{9}B state analog to the first excited $1/2^{+}$ E_x = 1.68 MeV level in ^{9}Be, its existence has so far not been clearly demonstrated[6]. Although anomalous structures have been observed in the right region of ^{9}B excitation, it was always possible to explain the features in an alternative manner, and not as a state[3,4]. This is mainly due to the fact that the searches are generally based on the analysis of inclusive spectra where the continuum yields due to three- and four-body breakups may add to the discrete spectrum and could in principle obscure the state in question.

Details of the experiment and some preliminary results have been presented previously[7]. Figure 1 shows a "clean"

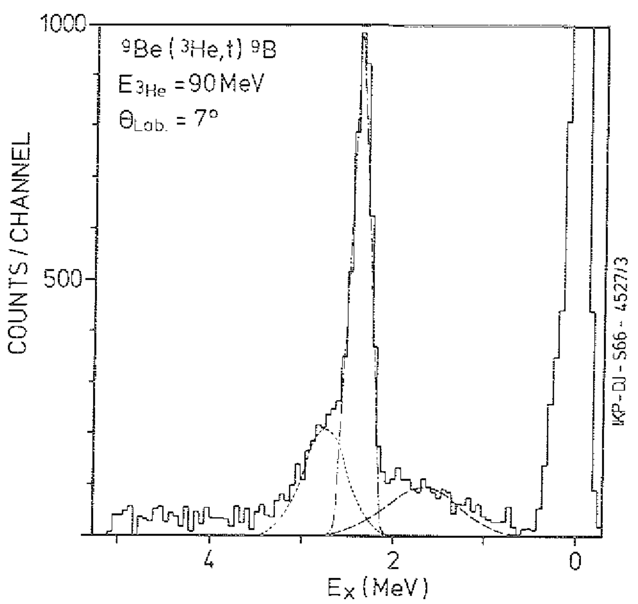

Figure 1: "Clean" triton spectrum (i.e. after subtraction of a linear background from the $^{9}Be(^{3}He,t)^{9}B$ reaction at 90 MeV. The dashed, dotted-dashed and dotted curves represent, respectively, the 1.6, 2.36 and 2.79 MeV peaks as obtained by the fitting routine.

spectrum (after subtraction of a linear background) at $\theta_{Lab} = 7^{0}$. The existence of two peaks, one on each flank of the 2.36 MeV level is clearly demonstrated. The clean spectrum was subjected to an automatic fitting program. In this procedure, the respective centroid positions E_c of the states at E_x = 2.36 and 2.79 MeV were fixed from the known energy calibration. The observed width Γ_0 of the 2.36 MeV state was assumed to be given by the experimental resolution Γ_{exp}, taken to be equal to the observed width of the ground-state peak. The other three quantities (i.e. E_c and Γ_0 of the 1.6 MeV and Γ_0 of the 2.79 MeV state) were treated as free parameters and determined from the optimum fit by the fitting routine.

From the analysis of spectra taken at 7^{0}, 8.5^{0} and 10^{0} the extracted centroid position and natural width Γ (where $\Gamma^2 = \Gamma_0^2 - \Gamma_{exp}^2$) of the 1.6 MeV state are 1.65 ± 0.03 MeV and 1.0 ± 0.2 MeV, respectively, while the width of the 2.79 MeV level is found to be 0.66 ± 0.06 MeV. It should be noted that the quoted errors are considerably larger than the estimated uncertainties introduced by assuming different background shapes in the analysis of the $\theta_{Lab} = 7^{0}$ spectrum.

The centroid positions of the peaks are corrected for the shift introduced by the fact that the Breit-Wigner shape of the resonance is affected (according to the Fermi's Golden Rule) by the phase space of the particular multiparticle final state to which the structure of the state belongs. The analytical expression for the shift (for a resonant state measured via a reaction channel involving a threebody final state) has been given by Delbar[8]. Assuming a $p+^{8}Be$ ($\alpha+\alpha$) structure of the ^{9}B 1.6 MeV level, the shift (calculated in accordance with the theory for the analog ^{9}Be state[9]) is found to be -36 keV, bringing the resonance energy of the first excited level of ^{9}B to E_x = 1.61 ± 0.03 MeV. The width of the level remains Γ = 1.0 ± 0.2 MeV since this is not significantly affected by the correction. The position of the state, as extracted from the present experiment, is very close to those determined in earlier attempts[1-5] judged inconclusive so far. The width for the 2.79 MeV level is in excellent agreement with that quoted in Ref. 6.

References

1) G.D. Symons and P.B. Treacy, Phys. Lett. 2 (1962) 175
2) E. Terranishi and B. Furubayaki, Phys. Lett. 9 (1964) 157
3) E.F. Farrow and H.J. Hay, Phys. Lett. 11 (1964) 50
4) J.J. Kroepfl and C.P. Browne, Nucl. Phys. A108 (1968) 289
5) G.C. Ball and J. Cerny, Phys. Rev. 177 (1969) 1466
6) F. Ajzenberg-Selove, Nucl. Phys. A320 (1979) 1
7) A. Djaloeis, J. Bojowald, G. Paić and B. Antolković, Annual Report 1982, IKP-KFA Jülich, Jül-Spez-202 (1983) 22
8) Th. Delbar, Thesis, Université de Louvain, Louvain-la-Neuve, Belgium, 1981 (unpublished) and Th. Delbar, Gh. Grégoire, B. Antolković and G. Paić, to be published
9) W. Zahn, Nucl. Phys. A269 (1976) 138

* Institute Rudjer Bosković, Zagreb, Yugoslavia

1.10. Relative contribution of α-particle and ^{4}H-like fragment transfers in ^{11}B + ^{3}He systems

L. Jarczyk+, A. Strzalkowski+, B. Styczen+, G.P.A. Berg, B. Brinkmöller, G. Hlawatsch, A. Magiera++, J. Meissburger, W. Oelert, D. Prasuhn, P. v. Rossen, J.G.M. Römer and J.L. Tain

Observation of ^{7}Be and ^{7}Li reaction products from the transfer reaction in the ^{11}B + ^{3}He system allows to study the relative contribution of different clustering models: the α- or ^{4}H-cluster transfer as shown in fig. 1.

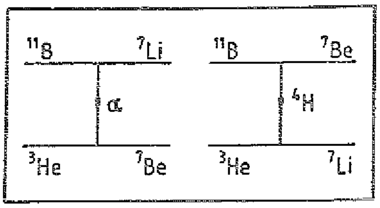

Fig. 1: Possible reaction channels in ^{11}B + ^{3}He: α- or ^{4}H-cluster transfer, left side, respectively right side

The experiment was performed at the cyclotron JULIC using the ^{3}He beam at E_{lab} = 71.8 MeV. Detection of the emitted ^{7}Li and ^{7}Be nuclei by means of the BIG KARL magnet spectrometer allowed the separation of the ground state transition from that leading to the first excited states of ^{7}Li or ^{7}Be. Identification of ^{7}Li and ^{7}Be particles in the focal plane of the spectrometer was performed using a ΔE(gas) - E(plastic) telescope placed behind the MWPC position sensitive detector. For some angles the transition with the simultaneous excitation of both nuclei was also observed although with much lower cross section. An example of the measured spectra is shown in fig.2.

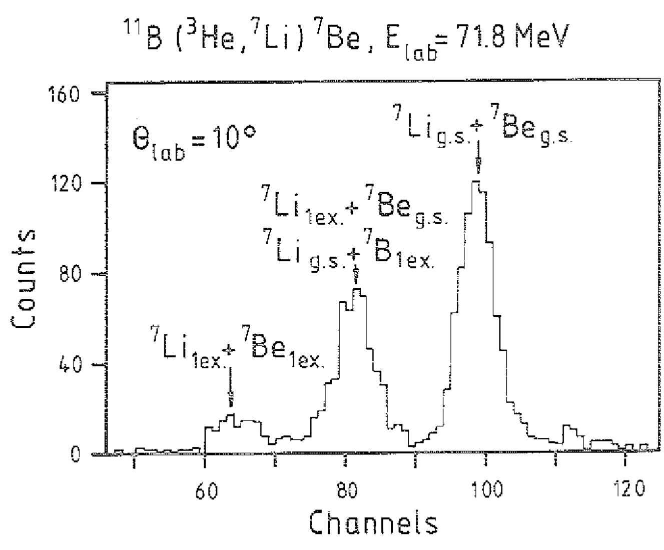

Fig. 2: ^{7}Li spectrum of the ^{11}B(^{3}He,^{7}Li)^{7}Be

The preliminary results for the measured angular distributions in a wide angular region (up to ∼ 80° for ^{7}Li and 60° for ^{7}Be) are presented in fig. 3 for the ground and the first excited state. The absolute cross sections were determined using the ^{11}B + ^{3}He elastic scattering data for the normalisation.

+ Institute of Physics, Jagellonian University, Cracow, Poland

++ on leave from the Inst. of Phys. Jagellonian University, Cracow, Poland

As expected it was found that the cross sections for the α transfer are by about an order of magnitude larger than for the transfer of the ^{4}H fragment. The results will be analyzed in the coupled reaction channels (CRC) formalism as single step transfer or sequential and simultaneous two subcluster transfer.

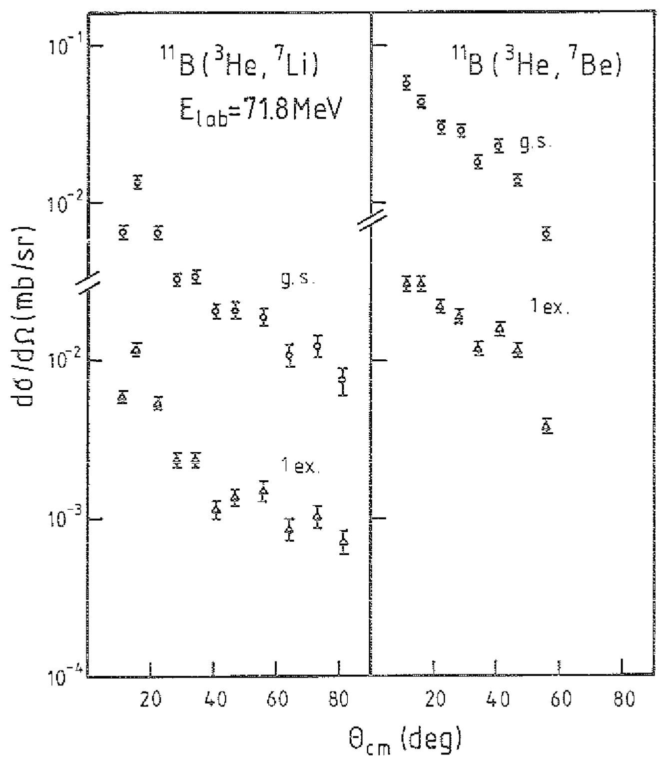

Fig. 3: Measured angular distribution in the ^{11}B(^{3}He,^{7}Li)^{7}Be and ^{11}B(^{3}He,^{7}Be)^{7}Li reactions

Besides being interesting on its own the investigated reaction is one step of the possible two step transfer processes into which the ^{12}C(d,^{7}Be)^{7}Li reaction[1] could be split as seen from fig. 4.

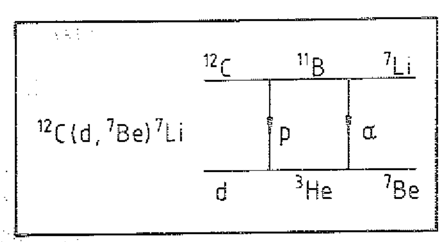

Fig. 4: Possible two step transfer in ^{12}C(d,^{7}Be)^{7}Li

The spectroscopic information on this analysis will be used in the CRC calculation to normalize this contribution to the two step processes of the 5 nucleon transfer in ^{12}C(d,^{7}Be)^{7}Li. The ^{3}He energy of E_{lab} = 71.84 MeV was chosen to match the deuteron energy E_{lab} = 78 MeV in the ^{12}C(d,^{7}Be)^{7}Li experiment in order to obtain the same center of mass energy in the exit channel of the ^{11}B + ^{3}He system.

Reference

1) L. Jarczyk, B. Kamys, A. Strzalkowski, B. Styczen, G.P. A. Berg, G. Hlawatsch, W. Hürlimann, I. Katayama, J.L. Tain, J. Meißburger, W. Oelert, J.G.M. Römer, A. Magiera and J. Krug, Annual Report 1982, IKP KFA Jülich, Jül-Spez 202 (1983) 14

1.11. High Lying T=3/2 Analog States in ^{13}C via the $^{14}C(^3He,\alpha)^{13}C$ Reaction

J.G.M. Römer, G.P.A. Berg, B. Brinkmöller, F. Hinterberger[+]*, G. Hlawatsch, A. Magiera, J. Meissburger, W. Oelert, D. Paul, D. Prasuhn, P. von Rossen, J.L. Tain*

In order to explore the rather unknown region[1] of excitation energies above the first T=3/2 analog state at E_x= 15.10 MeV in ^{13}C, we started an investigation of the spectrum of T=1/2 states in the region of this lowest T=3/2 state in ^{13}C and other T=3/2 states. Due to the relatively long lifetime, the widths of the T=3/2 states are very narrow compared to the T=1/2 states.

The experiment was performed using the high resolution magnet spectrometer BIG KARL[2] with the variable dispersion set to 14.8 cm/%. The dispersion of the beam line operated in dispersive mode was matched to the spectrograph's dispersion. This allowed to open the beam line slits and to obtain the relatively high beam current of 40-50 nA, which corresponds to about 5% transmission through the monochromator without loosing resolution. The solid angle was dΩ = 1.6 msr limited by a strong R_{346}-term of the spectrograph. The possible correction of this term, which would have allowed an opening angle of 2.5 msr, was not carried out since this would have taken one day of beam-time. For position detection, angle measurements and particle identification, independent detectors were used:

1. In the focal plane a 0.8 cm thick multi-wire drift chamber (MWDC)[3] with an active area of 90 cm x 8 cm was used for position measurements horizontally and vertically.
2. A 3.5 cm thick ΔE_{gas}-counter for energy-loss signals.
3. At a distance of 18 cm behind the first counter, a second MWDC for horizontal position measurements allowed to define the angle of the particle track in the focal plane.
4. A 0.5 cm thick ΔE-plastic scintillation counter[4] provided light output signals.
5. An E-plastic scintillation counter was used as an anticoincidence counter to suppress the high background from ^3He break-reactions.

Single charged $^3He^{1+}$ particles were suppressed by a stripper foil inserted between both dipoles of the spectrograph.

With this arrangement we measured an angular distribution from Θ_{lab} = 13° to 46° in the excitation energy range E_x=14.5 - 20 MeV at an incident energy of 68 MeV. A typical spectrum is shown in fig. 1. Special care was taken to correct for nonlinearities of the MWDC and its drift-time calibration. Energy calibration was done using ^{12}C and ^{28}Si targets. The data analysis is in progress. We acknoledge the fabrication of the ^{14}C target by H.J. Maier from the University of Munich.

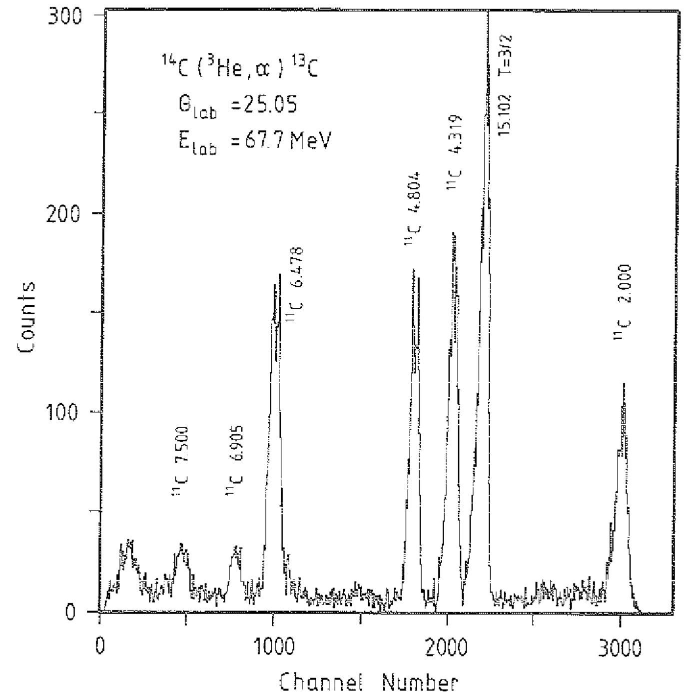

Figure 1: Sample spectrum of the $^{14}C(^3He,\alpha)^{13}C$ reaction.

References

1) Ajzenberg-Selove, Nucl. Phys. A360 (1981) 1
2) S.A. Martin, A. Hardt, J. Meissburger, G.P.A. Berg, U. Hacker, W. Hürlimann, J.G.M. Römer, T. Sagefka, A. Retz, O.W.B. Schult, K.L. Brown, K. Halbach, Nucl. Instr. & Meth. 214 (1983) 281
3) G.P.A. Berg, P. von Brentano, B. Brinkmöller, G. Hlawatsch, J. Meissburger, G.F. Moore, D. Paul, J.G.M. Römer, M. Rogge, S.J. Seestrom-Morris, J.L. Tain, L. Zemlo, IKP Annual Report 1982, Jül-Spez 202, p. 116 and D. Paul, Diplomarbeit (1983), University Münster
4) G. Müller, G.P.A. Berg, A. Hardt, H.J. Kelleter, S.A. Martin, J. Meissburger, A. Retz, Jül-Spez 84 (1980)

+Institut für Strahlen- und Kernphysik, University Bonn, F.R. Germany

1.12. Measurements of electron capture and stripping cross sections for Al, Ni, Ag and Au targets at 68, 99 and 130 MeV ^3He beams

I. Katayama[+], *G.P.A. Berg, G. Gaul*[++], *H. Hasai*[+++], *W. Hürlimann*[*], *S.A. Martin, J. Meißburger, W. Oelert, M. Rogge, A. Retz, J.G.M. Römer, J.L. Tain and L. Zemlo*[**]

In our previous work[1,2] we have shown:
1) electron stripping cross sections σ_s for $^3He^{1+}$ of 68, 99 and 130 MeV in C, N and Ne are well exlained by Gillespie's Born approximation calculation,
2) the projectile velocity dependence of σ_s for Ar, however, shows the systematic deviation[2] from the calculation and
3) electron capture cross sections σ_c for $^3He^{2+}$ of the same energies in C, N, Ne and Ar are close to the calculations by the present electron capture theories, but the velocity dependence in the region of $v_1 = 30 - 40\ v_0$ (v_1: ^3He projectile velocity and v_0: velocity in atomic units) cannot be explained by any theorie . We measured $\sigma_s(^3He^{1+} \rightarrow {}^3He^{2+})$ and $\sigma_c(^3He^{1+} \rightarrow {}^3He^{2+})$ on Al, Ni, Ag and Au targets of different thicknesses at 68, 99 and 130 MeV ^3He energies using the beam of the cyclotron JULIC focussed on a target in the scattering chamber of the magnetic spectrograph BIG KARL[3]. Details of the beam transport and geometry of the experiment have been described in ref. 1). The 40 targets were mounted on a multiple target drive[4] and remotely controlled to change the position one by one. A ^{242}Th α source and a Si surface barrier detector were mounted just above the beam position so that we could measure the energy loss of 6 MeV α particles in the target foils without breaking the vacuum. The thickness of the carbon backings on which most of the targets were evaporated was determined by measuring the elastic scattering yield of the 68 MeV ^3He particles at $\theta_{lab} = 8^0$ where the carbon elastic line is clearly separated from Al, Ni, Ag and Au lines. Using energy loss calculations the thickness of the 40 targets was determined. The results show a good agreement within 10 % with those from target weighting method. The $^3He^{1+}$ yield from the targets was analyzed by the magnetic spectrograph BIG KARL at $\theta_{lab} = 0^0$. The beam current was monitored using another Si surface barrier counter.

As a typical result of present experiment the thickness dependence of the $^3He^{1+}$ yield from Ag is shown in fig. 1. The curves are fitted by a least square fit to $y = y_0(t_0) \times e^{-\sigma_s t} + N(\sigma_c/\sigma_s)(1 - e^{-\sigma_s t})$, with $y_0(t_0)$ the $^3He^{1+}$ yield from the carbon backing and estimated from previous results[1], t_0 the thickness of the carbon backing, N the beam intensity and t target thickness. The results for σ_s at $E_{^3He} = 130$ MeV as function of the target atomic number Z_t are shown in fig. 2. The present results are quite well explained by the Gillespie's calculation for C, N, Ne, Al and Ar. We observe deviations for Ni, Ag and Au which are according to Gillespie[5] due to inaccuracies of the wave functions.

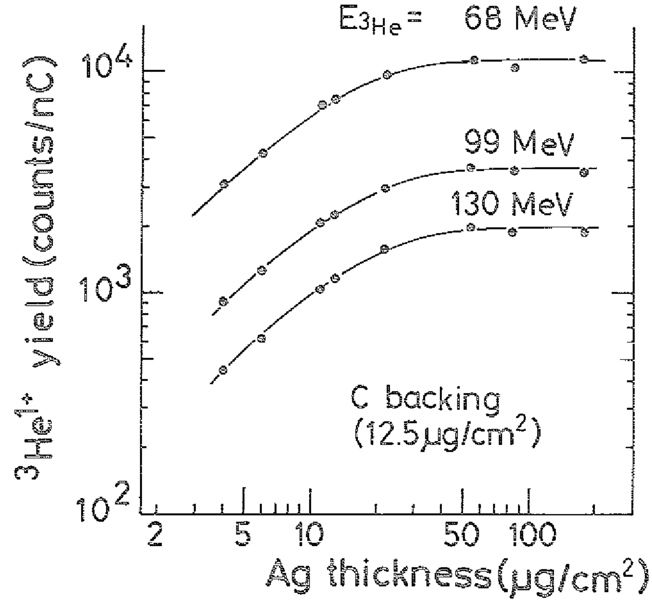

Fig. 1: $^3He^{1+}$ yield in units of nanoseconds (nC) as function of the thickness of the Ag target

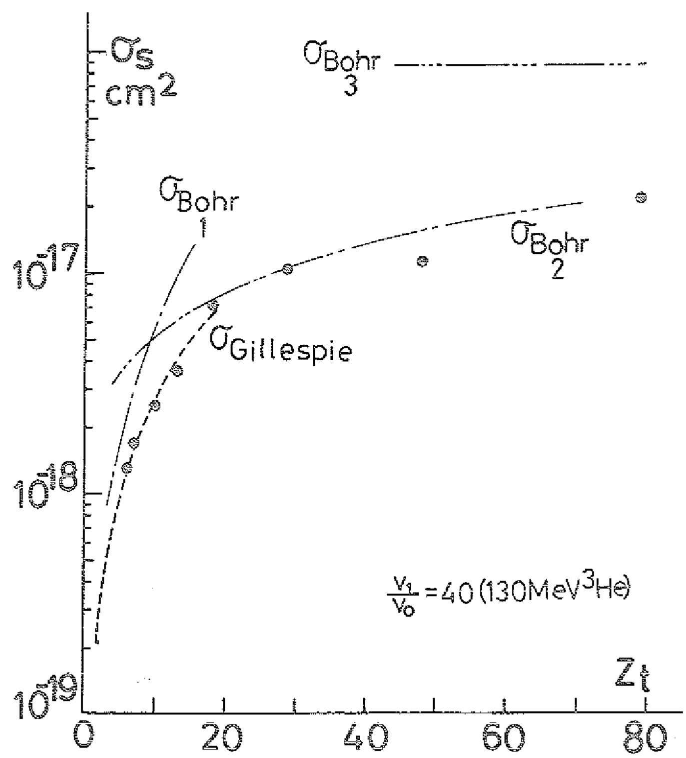

Fig. 2: Stripping cross section σ_s as function of the target atomic number Z_t at 130 MeV ^3He

Preliminary experimental results for the electron capture σ_c are shown in fig. 3. The projectile velocities of 30 - 40 v_0 are not sufficiently high to expect K shell capture in ^3He atoms from Ni, Ag and Au atoms. These data will be compared to current theoretical models.

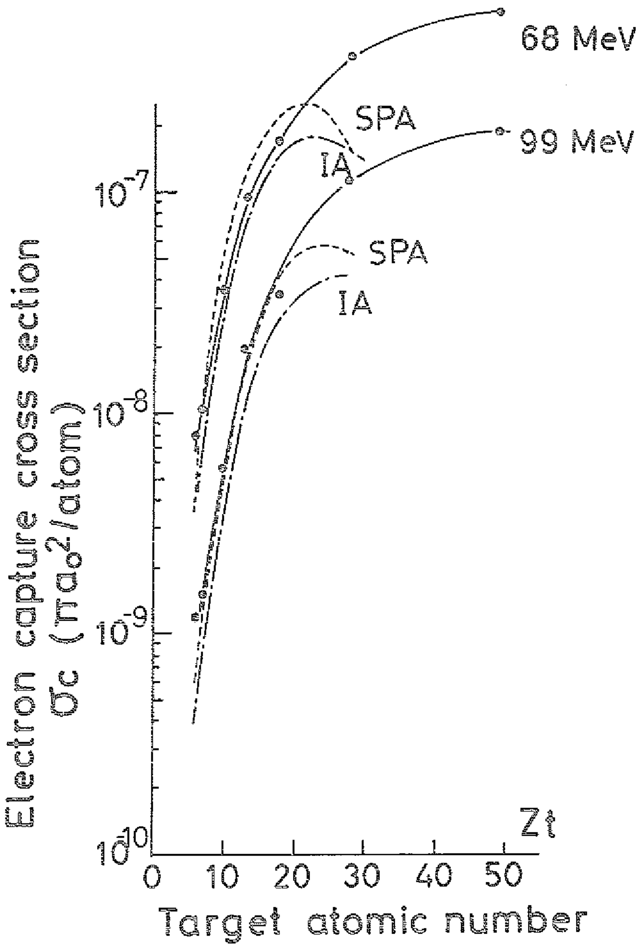

Fig. 3: Preliminary results of the measured and calculated electron capture cross sections σ_C for various targets with atomic number Zt. For the calculations see ref. 2.

References

1) I. Katayama, G.P.A. Berg, W. Hürlimann, S.A. Martin, J. Meissburger, W. Oelert, M. Rogge, J.G.M. Römer, J. Tain, B. Styczen and G. Gaul, Phys. Lett. 92A (1982) 385

2) I. Katayama, G.P A. Berg, W. Hürlimann, S.A. Martin, J. Meissburger, W. Oelert, M. Rogge, J.G.M. Römer, J.L. Tain, L. Zemlo and G. Gaul, J. Phys. B: At. Mol. Phys. 17 (1983) L23

3) S.A. Martin, A. Hardt, J. Meissburger, G.P.A. Berg, U. Hacker, W. Hürlimann, J.G.M. Römer, T. Sagefka, A. Retz, O.W.B. Schult, K.L. Brown and K. Halbach, Nucl. Instr. Meth. 214 (1983) 281

4) W. Briell, D. Groß, A. Retz, U. Rindfleisch, H. Schwan, Annual Report 1982, IKP-KFA, Jül-Spez 202 (1983) 131

5) Gillespie (1983), private communication

+ RCNP, University of Osaka, Japan

++ Institut für Kernphysik, Universität Münster

+++ Faculty of Engineering, University of Hiroshima, Japan

* Present address: Motor Columbus, Baden, Switzerland

** INR, Warsaw, Poland

1.13. The $^{90}Zr(^{3}He,t)^{90}Nb$ reaction and the Gamow-Teller strength

J.L. Tain, G.P.A. Berg, B. Brinkmöller, G. Hlawatsch, A. Magiera, J. Meißburger, W. Oelert, J.G.M. Römer and G. Sondermann[+]

There exists a considerable amount of experimental information on the localization of the Gamow-Teller (GT) strength in medium and heavy nuclei mainly from the (p,n) charge exchange reaction. In ^{90}Zr a discrepancy exists between the (p,n) reaction[1] and the (^{3}He,t) reaction[2] where the structure of the bump above the isobaric analog state (IAS) is seen to be composed of two parts. The lower part is identified as GT from the shape of the angular distribution and has an excitation energy considerably smaller than reported in ref. 1.

To clarify this discrepancy we measured the $^{90}Zr(^{3}He,t)^{90}Nb$ reaction using the highest incident beam energy $E_{^3He}$ = 135 MeV from the cyclotron JULIC. In order to measure at small scattering angles with good energy resolution we used the magnetic spectrograph BIG KARL. The position spectra of the momentum analyzed particles were measured with the 30 cm multi-wire proportional chamber (MWPC). A dispersion of D = -4 cm/% was used to obtain the large energy range of ΔE_x = 12 MeV. The resolution of 180 keV was mainly limited by the target thickness of 4.2 mg/cm^2. A sample spectrum is shown in fig. 1.

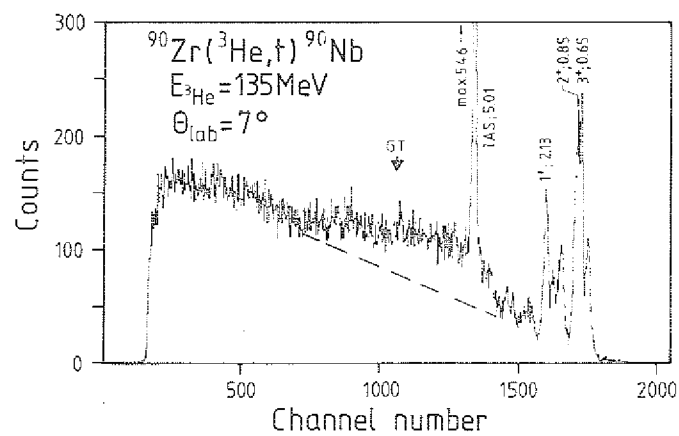

Fig. 1: Triton spectrum of the $^{90}Zr(^{3}He,t)$ reaction at 7°. Spin-parity and excitation energies of some identified peaks are indicated. The dashed line represents the extracted linear background under the GT bump.

The broad bump above the strong IAS and some of the low lying ($\pi g_{9/2}\ \nu g_{9/2}^{-1}$) states are clearly seen. Although there is some structure in the bump it is not clear, that there are two parts with different angular distributions in the measured range from Θ_{lab} = 3° to Θ_{lab} = 9°. The centroid of the broad structure is ∿ 8.3 MeV and the width is ∿ 4.5 MeV in agreement with the result of ref. 1.

The measured angular distribution is shown in fig. 2 together with the angular distribution of the low lying 1^+, 2^+, 3^+ states and the IAS. The similarity between the angular distribution of the broad structure and the low lying 1^+ state confirms that it contains mainly GT strength.

The reaction mechanism of the (^{3}He,t) reaction is not fully understood. Knock-on exchange[3] and two-step contributions[4] are assumed to be important. A better understanding is essential if one wants to use the (^{3}He,t) reaction as an effective spectroscopic tool. Therefore we were also interested in studying the reaction mechanism at the present incident energy of 135 MeV.

The ^{90}Zr target is well suited for such studies since the structure of the strongly populated states is simple. Here we assumed the configuration $(\pi 1g_{9/2}\ \nu 1g_{9/2}^{-1})$ while the GT resonance is $(\pi 1g_{7/2}\ \nu 1g_{9/2}^{-1})$. We used a microscopic DWBA description with a ^{3}He-nucleon folded type interaction. Calculations were carried out with the code DWBA83[5]. Optical model potentials were taken from Djaloeis et al.[6]. The shapes of the calculated angular distributions were sensitive to the choice of the optical potential. The best fits were obtained with the shallow potential family with volume absorption of ref. 6. The effective ^{3}He-nucleon interaction was taken from ref. 4. The results are shown as solid curves in fig. 2 and are normalized to the data. The normalization factors N ($N = \sigma_{exp}/\sigma_{calc.}$) needed are: $N_{IAS} = 4$, $N_{2^+} = 2.5$, $N_{1^+} = N_{3^+} = 0.6$, $N_{GT} = 1.4$.

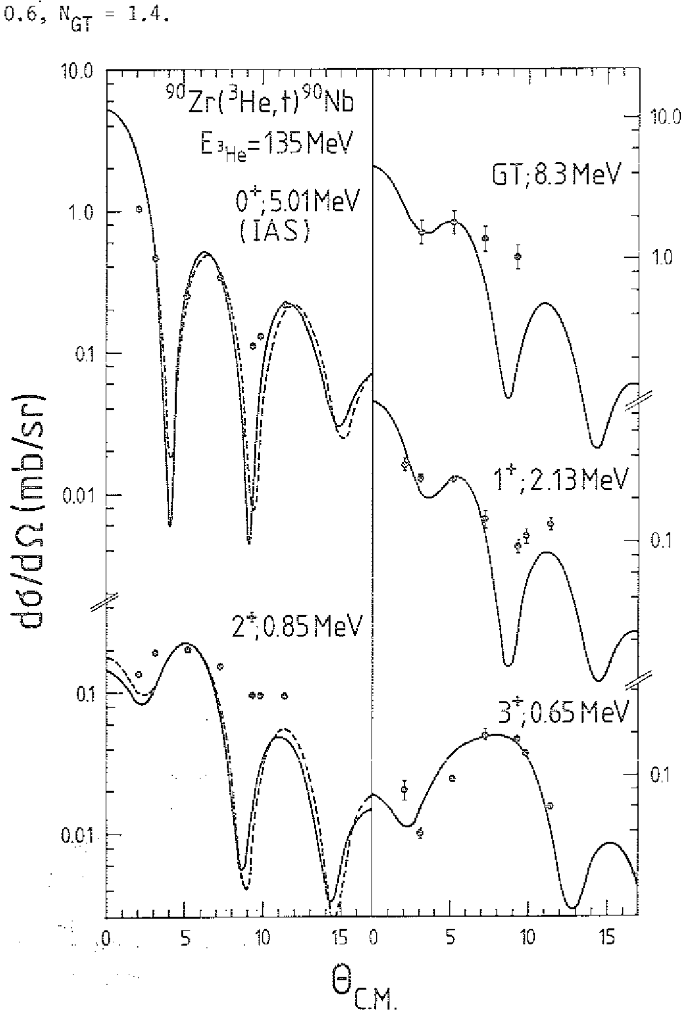

Fig. 2: Experimental and calculated angular distributions for the GT bump and some of the measured states. Theoretical curves are normalized to the experimental points. For the meaning of the different curves see the text.

For the natural parity states another more realistic effective central interaction was also used. It was obtained by folding the Paris effective nucleon-nucleon interaction[7] with a Gaussian 3-nucleon wave function. The folding was done analytically by converting the Yukawa type Paris interaction into an equivalent Gaussian interaction. The calculations are shown as dashed curves in fig. 2. The renormalization factors are $N_{IAS} = 3.7$, $N_{2^+} = 2$, similar to those with the simpler interaction.

The effects of the approximate inclusion of knock-on exchange are under investigation.

References

1) D.E. Bainum et al., Phys. Rev. Lett. 44, 1751 (1980)
2) D. Ovazza et al., Phys. Rev. 18C, 2438 (1978)
3) R. Schaeffer, Nucl. Phys. A158, 321 (1970)
4) C. Gaarde et al., Nucl. Phys. A334, 248 (1980)
5) J. Raynal, DWBA Computer Code (unpublished), modified version by H.V. von Geramb and L. Rikus
6) A. Djaloeis et al., Nucl. Phys. A306, 221 (1978)
7) N. Anantaraman et al., Nucl. Phys. A398, 269 (1983)

+ Institut für Kernphysik, Universität Münster

1.14. Study of giant resonances in small angle α scattering experiments

H.P. Morsch, P. Decowski, M. Rogge, P. Turek, L. Zemło, G.P.A. Berg, J. Meißburger and J.G.M. Römer

We have completed our study[1] of giant resonances in ^{208}Pb in small angle α scattering in the angular range 1.5 - 8° using the magnetic spectrometer BIG KARL. The spectra reveal a rather complicated structure of giant resonances with excitations of quite different multipolarities. The resulting multipole strength distributions for even multipolarities are given in fig. 1, details are discussed in ref. 2.

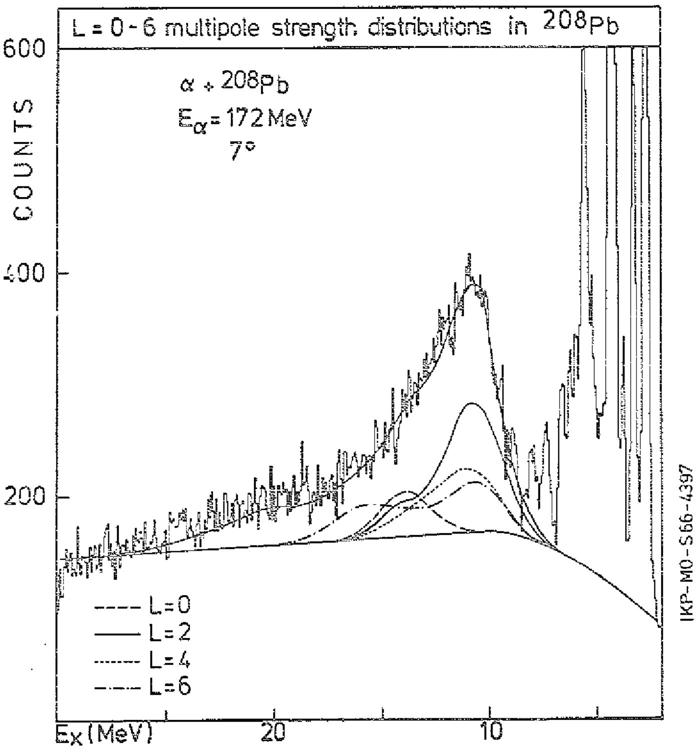

Figure 1: Multipole strength distributions for even multipolarities in ^{208}Pb obtained from our analysis in comparison with a 7° (α,α') spectrum. The odd multipole strength is located mainly between E_x = 15 and 25 MeV.

Further, we have investigated the experimental conditions for 0° measurements in BIG KARL. Since for giant resonance experiments[2] a small dispersion is used (2-3 cm p/100 % Δp) it is not possible to let the primary beam completely through the spectrometer system because the last quadrupole is strongly defocussing in Y direction. We have tested whether it is possible to catch the beam on a carbon block between the two dipole magnets. We found experimental conditions under which the last cross over is rather close to the place where we stop the beam. Measurements on ^{12}C and ^{208}Pb targets have shown that we can cut the inelastic spectrum at excitation energies ≤ 4 MeV without much disturbing the higher energy spectrum. We expect that the remaining background can be cut by retracing the particle trajectories.

References

1) H.P. Morsch, P. Decowski, M. Rogge, P. Turek, L. Zemło, G.P.A. Berg, J. Meißburger, J.G.M. Römer and J.L. Tain, Annual Report 1982, IKP, KFA Jülich, Jül-Spez-202 (1983) 15

2) H.P. Morsch, P. Decowski, R. Rogge, P. Turek, L. Zemło, S.A. Martin, G.P.A. Berg, W. Hürlimann, J. Meißburger and J.G.M. Römer, Phys. Rev. C28 (1983) 1947

1.15. Study of the (^{3}He,t) charge exchange reaction at $E_{^3He}$ = 135 MeV

H.P. Morsch, P. Decowski, G.P.A. Berg, J.L. Tain, M. Rogge, P. Turek, L. Zemło, J. Meißburger and J.G.M. Römer

We continued our efforts[1] to study the (^{3}He,t) reaction on heavy nuclei. The main aspects of this investigation are a) excitation of the isobaric analog state (IAS), b) study of the Gamow-Teller (GT) resonances and c) isovector giant resonances at higher excitation energies. Experiments were performed at triton angles 0°-5° using the magnetic spectrometer BIG KARL. At 0° the primary beam was stopped on an aluminum plate inside the first dipole magnet of the spectrometer. (^{3}He,t) spectra for ^{120}Sn and ^{208}Pb taken at 0° are shown in fig. 1. The excitation of the IAS and the underlying GT-resonance is clearly seen on top of a continuous background.

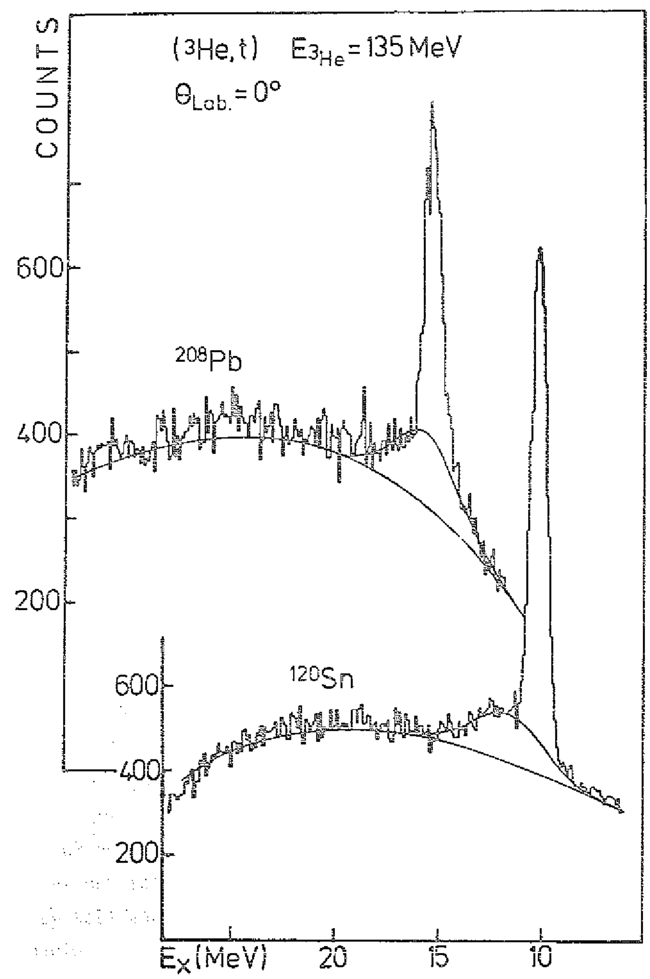

Figure 1: 0° spectra of the (^{3}He,t) reaction on ^{120}Sn and ^{208}Pb. Background and GT resonance fits are indicated.

a) Excitation of the IAS

This is related to the study of nuclear densities, in particular of the neutron excess density in heavy nuclei. Information on neutron densities has been recently extracted from 0.8 and 1 GeV proton scattering[2-5] and also from α scattering. More details on proton-neutron density differences may be obtained in a reaction in which only the neutron excess contributes. Further this reaction should have a different sensitivity to nuclear interior and surface parts. Both of these requirements are fulfilled in the (^{3}He,t) charge ex-

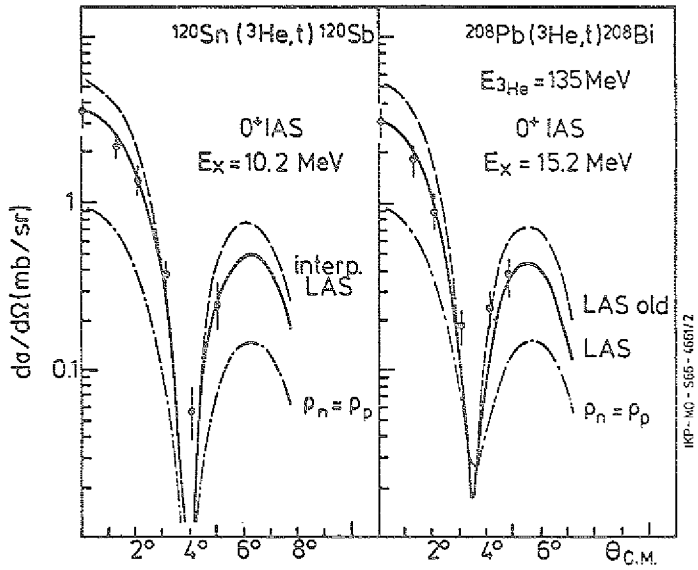

Figure 2: Differential cross sections from the (^{3}He,t) reaction exciting the IAS in comparison with DWBA calculations. Solid lines: best fit description, for ^{208}Pb this is identical to the use of the neutron density of ref. 3; dot-dashed lines: $\rho_n(r)=\rho_p(r)$ and dashed lines: older Los Alamos neutron densities from ref. 2.

change reaction exciting the IAS. Angular distributions for ^{120}Sn and ^{208}Pb are given in fig. 2, they show the strong cross section rise at 0^o typical of L=0 excitation. The data have been analysed within a DWBA approach using folding type form factors. For the effective isospin interaction a Gaussian form with a range of 1.68 fm was used. The strength is obtained from the (p,n) reaction at the same energy per nucleon of 45 MeV[6]. The data could be well described by use of microscopic and macroscopic transition densities. In the microscopic approach the absolute cross sections were found to be strongly dependent on the radius parameter r_o of the bound state potential. Good fits are obtained using r_o = 1.22 fm for ^{208}Pb and 1.23 fm for ^{120}Sm, the other bound state parameters were V_{so} = 6 MeV, a = 0.65 fm and V_o fitted to reproduce the experimental binding energies. In the macroscopic approach the transition density $\rho_{TR}(r)$ may be related to the neutron excess density $[\rho_n(r)-\rho_p(r)]$ by $\rho_{TR}(r) = \frac{G(r)}{\sqrt{N-Z}}[\rho_n(r) - \rho_p(r)]$. The correction function G(r) takes into account the fact that the IAS transition requires a neutron-proton transition density rather than a neutron excess density. It includes Coulomb effects as well as effects from the different binding of protons and neutrons. In a consistent description of microscopic and macroscopic densities the data are well described (solid lines in fig. 2). For ^{208}Pb these results are very similar to the cross sections obtained using the neutron density of ref. 3 derived from the Los Alamos 800 MeV proton scattering data. The older Los Alamos results[2] yield in both cases (^{3}He,t) cross sections larger by about 50 % (dashed lines in fig. 2). To demonstrate the strong sensitivity of the (^{3}He,t) cross sections to the neutron excess density in fig. 2 cross sections are also given for $\rho_n(r) = \rho_p(r)$ which are smaller by a factor of three. In the case of ^{208}Pb discrepancies in the extraction of $\Delta r_{np} = \langle r^2\rangle_n^{1/2} - \langle r^2\rangle_p^{1/2}$ exist between the 800 MeV Los Alamos (Δr_{np} = 0.14 - 0.16 fm) and 1 GeV Gatchina and Saclay results[4,5] ($\Delta r_{np} \sim 0.05$ fm). Our results support the Los Alamos results yielding $\Delta r_{np} \sim 0.13 - 0.20$ fm in agreement with theoretical studies.

b) 1^+ GT resonance

This excitation which has been studied systematically in the (p,n) charge-exchange reaction at proton energies up to 200 MeV[7] can be used to determine the spin-isospin part of the effective nucleon-nucleon interaction. Using a transition density for ^{208}Pb from the dominant $(\pi i_{11/2})^1(\nu i_{13/2})^{-1}$ and $(\pi h_{9/2})^1(\nu h_{11/2})^{-1}$ components and adjusting the L=0 strength to reproduce the GT peak in the high energy (p,n) data[7] (35 - 40% of the GT sum rule 3 (N-Z)) the cross sections in fig. 3 are well described by $V_{\sigma\tau} \sim 8.5$ MeV which corresponds to a ratio $V_{\sigma\tau}/V_0$ of about 0.5 in good agreement with the study of 1^+ states in 45 MeV (p,n)[8]. In fig. 3 contributions due to the nuclear tensor force are added characterized by L=2 angular distributions. These are adjusted to the cross section minimum at 3-4^o.

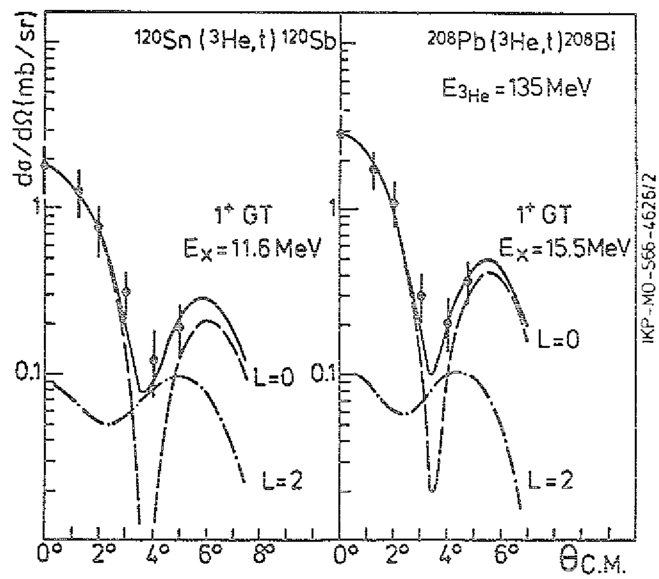

Figure 3: Differential cross section for the (^{3}He,t) reaction exciting the GT resonance. The dashed and dot-dashed lines represent microscopic DWBA calculations for central spin-isospin and tensor interaction, respectively.

c) Excitation of isovector giant resonances

After a detailed investigation of isoscalar giant resonances in α scattering[1] the primary motivation for the study of the (^{3}He,t) reaction was the possibility to investigate pure isovector giant resonances in this channel. As the spectrometer BIG KARL has a limited momentum bite of about 10 %, to investigate the continuum features in the (^{3}He,t) reaction one has to run with different field settings. This requires a careful correction of efficiency changes in the spectrometer and the detection system. Efficiency corrected spectra are given in fig. 4 for triton angles of 0^o and 3^o. Apart from the IAS peak the spectra indicate giant

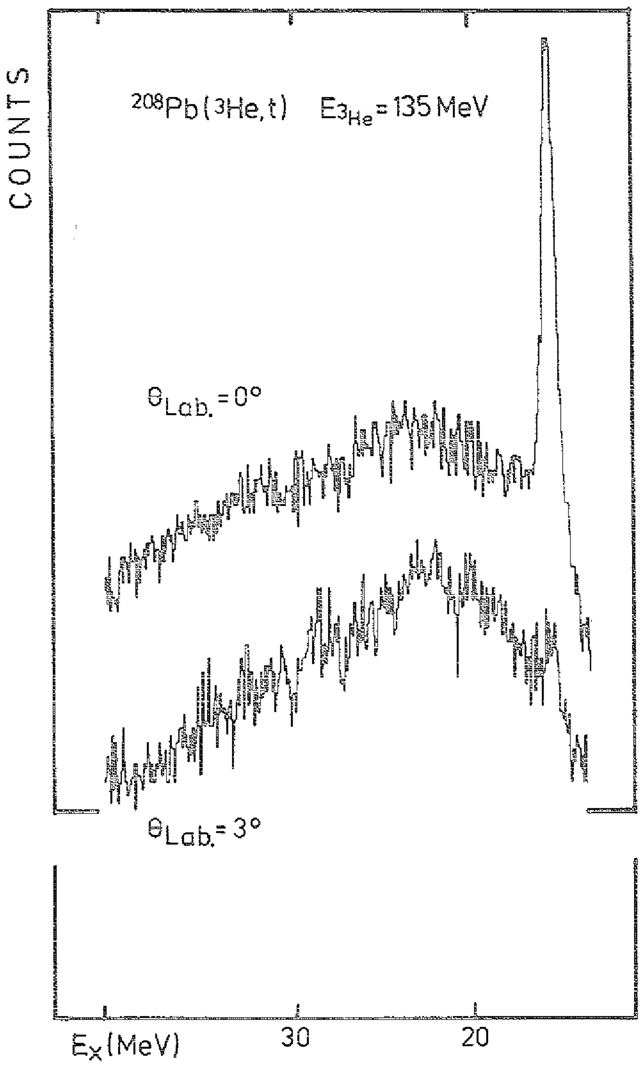

Figure 4: Efficiency corrected spectra for the reaction $^{208}Pb(^3He,t)^{208}Bi$ taken at triton angles of 0^0 and 3^0.

resonance structures which are significantly broader than in the inelastic channel. This can be explained by the fact that in the charge exchange channel mainly (T-1) components are excited which have large spreading widths. The IAS and GT excitations show the strong forward peaking whereas at higher energies a pronounced structure is observed which has the largest yield at 3^0. This indicates L=1 excitations containing the antianalog excitation of the giant dipole resonance and a dipole spin-flip resonance[7]. At higher excitation energies the angular dependence suggests L=2 excitation.

References

1) H.P. Morsch, P. Decowski, M. Rogge, P. Turek, L. Zemło, G.P.A. Berg, J. Meißburger, J.G.M. Römer and J.L. Tain, Annual Report 1982, IKP, KFA Jülich, Jül-Spez-202 (1983) 15

2) L. Ray, Phys. Rev. C19 (1979) 1855

3) G.W. Hoffmann, L. Ray, M. Barlett, J.McGill, G.S. Adams, G.J. Igo, F. Irom, A.T.M. Wang, C.A. Whitten, R.L. Boudrie, J.F. Amann, C. Glashausser, N.M. Hintz, G.S. Kyle and G.S. Blanpied, Phys. Rev. C21 (1980) 1488

4) G.D. Alkhazow, S.L. Belostotsky, O.A. Bomchenkov, Y.u V. Dotsenko, N.P. Kuropatkin, V.N. Nikulin, M.A. Shuvaev and A.A. Vorobyov, Nucl. Phys. A381 (1982) 430

5) A. Chaumeaux, V. Laly, and R. Schaeffer, Ann. Phys. 116 (1978) 247

6) R.R. Doering, D.M. Patterson and A. Galonsky, Phys. Rev. C12 (1975) 378

7) C. Gaarde, Nucl. Phys. A396 (1983) 127c and refs. therein

8) W.A. Sterrenburg, S.M. Austin, U.E.P. Berg and R. de Vito, Phys. Lett. 91B (1980) 337

1.16. Study of momentum transfer, mass distributions and total kinetic energies in the reaction $^{238}U(\alpha,\alpha' f_1 f_2)$

P. Decowski, H.P. Morsch, L. Zemło, M. Rogge, P. Turek, G. Hlawatsch

In $^{238}U(\alpha,\alpha' f_1 f_2)$ coincidence experiments the parallel momentum transfer deduced from fission angle measurements was found to be significantly smaller than obtained from two-body kinematics[1]. In order to obtain more complete information on the momentum transfer and also on the properties of the fission decay in α scattering we measured angle and velocities of the fission products using parallel plate detectors discussed in sect. 13.4. . From these data momentum transfers parallel ($p^{||}$) and perpendicular ($p^{\perp}$) to the beam direction were deduced as well as mass distributions and total kinetic energies of the fission fragments. Average momenta $p_m^{||}$ and $p_m^{\perp}$ relative to two-body kinematics (missing momentum transfer) as a function of α' energies are shown in fig. 1. The results for $p_m^{||}$

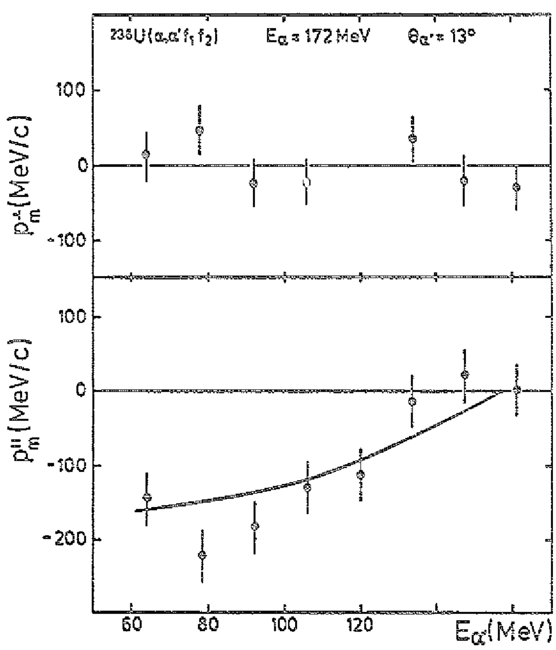

Figure 1: Average missing momentum transfer parallel ($p_m^{||}$) and perpendicular ($p_m^{\perp}$) to the beam axis as a function of α' energy. The solid lines indicate calculations assuming fast emission of uncorrelated particles.

are consistent with those in ref. 1, they indicate a sizable missing of momentum transfer to the fissioning nucleus for lower α' energies. For all α' energies the average value of $p_m^{\perp}$ is consistent with zero. Fig. 2 shows the distribution of $p^{||}$ for different bins of α' energies.

The experimental observations can be well understood by assuming emission of a fast prefission nucleon. Calculations have been performed for uncorrelated emission of fast particles. Such a process describes the damped component seen in the $(\alpha,\alpha' p)$ correlation experiment[1]. In such a case the yield is peaked in beam direction and is described by the angular distribution of emitted nucleons taken from the singles (α,p) data[2]. The calculations reproduce the distributions of $p^{||}$ in fig. 2 and the centroids of $p^{||}$ and $p_m^{\perp}$ in fig. 1 rather well.

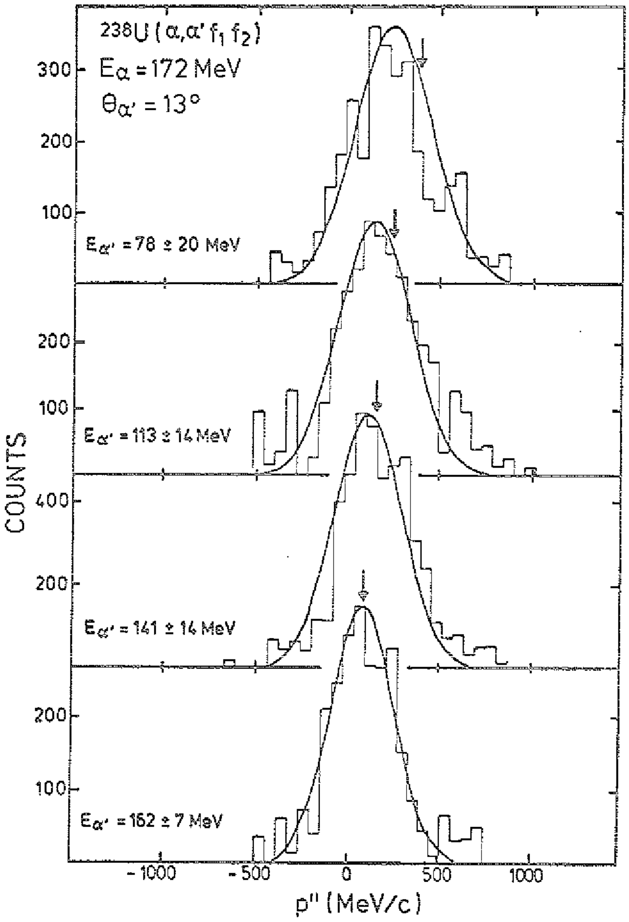

Figure 2: Distributions of momentum transfer parallel to the beam direction ($p^{||}$) for different bins of α' energies. The arrows indicate $p^{||}$ in two-body kinematics.

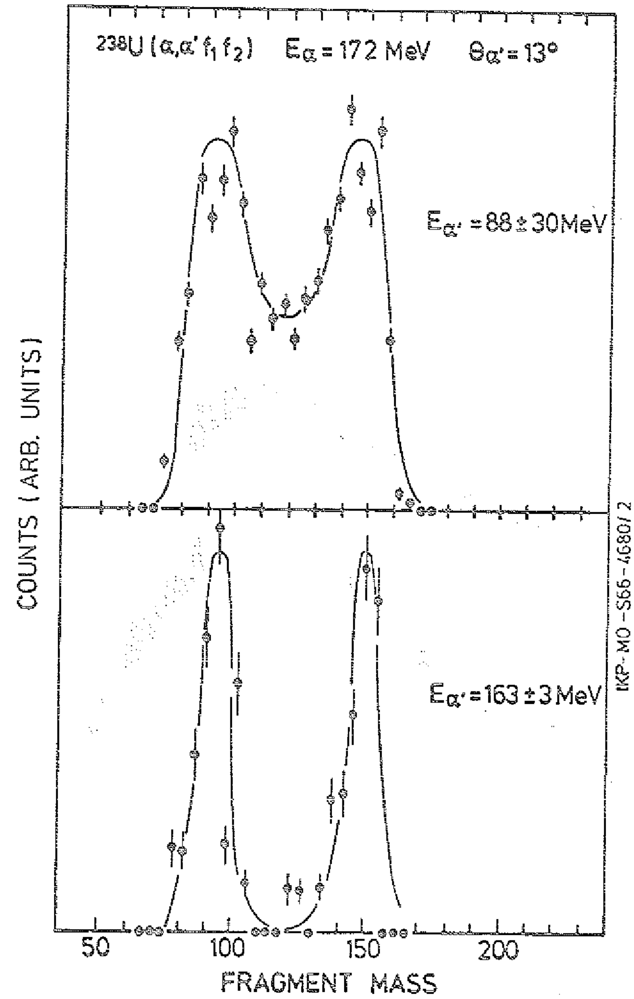

Figure 3: Fission fragment mass distributions for two bins of α' energies.

Mass distributions are given in fig. 3 for excitation energies around the fission barrier and for large negative Q-values of about -80 MeV. Even for the lowest α' energies measured in our experiment the mass distribution shows a sizable asymmetry with a ratio of asymmetrix to symmetric fission yield of about two. This may indicate that in the fission induced by inelastic α scattering the excitation energy of the fissioning nucleus is not exceeding about 40 MeV even at large energy transfers of ∿ 80 MeV. The average total kinetic energies changes in the whole α' energy region measured by about 20 MeV.

References

1) P. Decowski, H.P. Morsch, L. Zemło, M. Rogge, P. Turek, W. Schumacher, G. Gaul, R. Glasow, B. Ludewigt and R. Santo, Annual Report, IKP, KFA Jülich, Jül-Spez-202 (1983) 20

2) B. Ludewigt, R. Glasow, H. Löhner and R. Santo, Nucl. Phys. A408 (1983) 359

1.17. Three-body versus four-body contributions in α break-up on ^{58}Ni

R. Siebert, H.P. Morsch, P. Decowski, M. Rogge, P. Turek

Direct break up of the projectile gives an important contribution to the reaction cross section of fast α particles scattered on medium and heavy nuclei[1,2]. In the interpretation of this process in general a three-body mechanism is assumed. This concept may not be always realistic since in a hard collision it should be as easy to knock out a particle from the target. In order to study details of the break up of α into ^{3}He and neutron and to investigate nucleon knock out from the target we measured the reactions ^{58}Ni(α,^{3}He p) and ^{38}Ni(α,α'p). For the detection of the protons we used plastic detectors described in detail elswhere (sect. 13.5.). In the (α,^{3}He) singles spectrum (fig. 1) the α break up

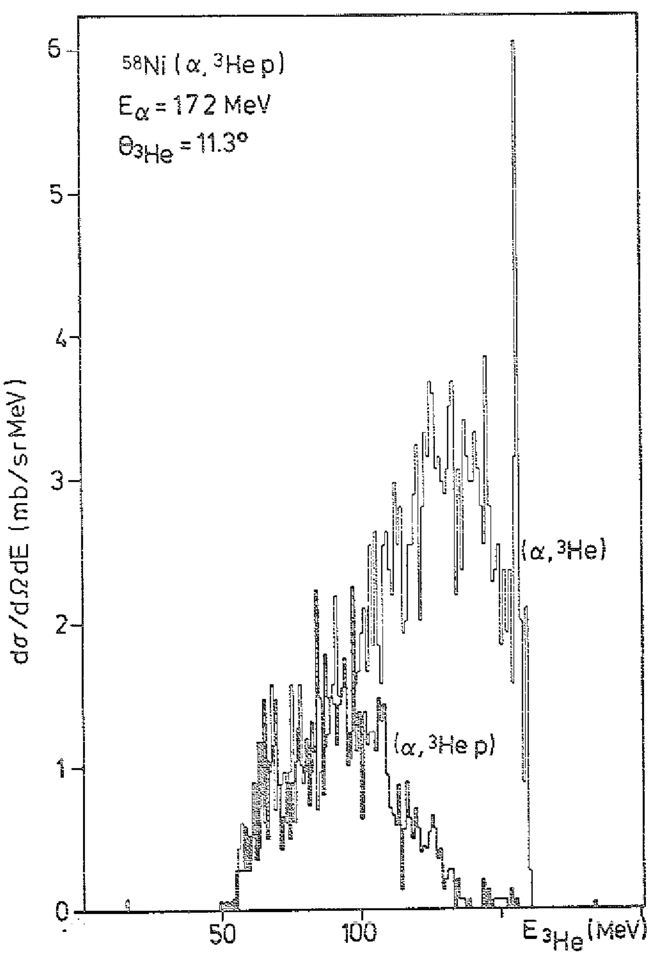

Figure 1: Comparison of normalized ^{3}He spectra from the singles (α,^{3}He) and the (α,^{3}He p) reaction.

peak is quite pronounced. Also is shown a ^{3}He spectrum coincident with emitted protons normalized to the singles (α,^{3}He) spectrum. As the three-body break up α → ^{3}He + n does not involve the emission of protons the detection of coincident protons indicates four-body contributions in which in addition to α break up a nucleon (proton) on the target is knocked out. This contributes to about 35 % of the total ^{3}He rate, which gives the probability to knock out a nucleon in the α → ^{3}He + n break up reaction. In comparing ^{3}He-proton and α-proton coinci-

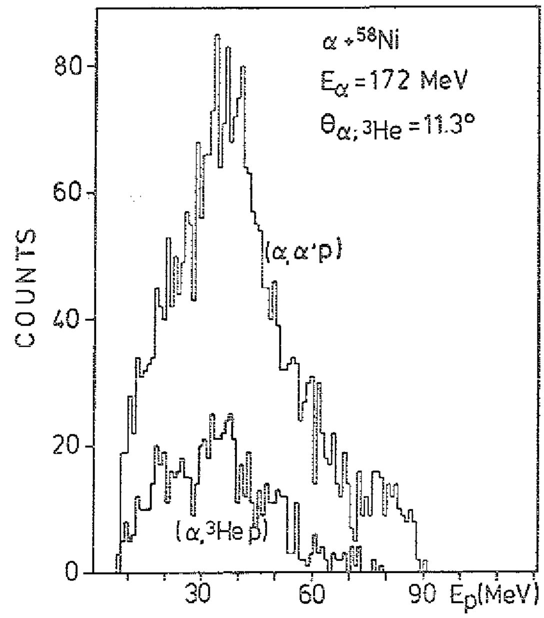

Figure 2: Proton spectra coincident with outgoing α' and ^{3}He particles.

dence yields one can get information on the α break up probability in the proton knock-out reaction. Proton spectra coincident with α' and ^{3}He particles are given in fig. 2. They have rather similar distributions indicating a similar origin in both cases; this is confirmed by the same ^{3}He and α' velocity distributions in the knock out channel. The relative yields are 4 : 1 indicating a break up probability of 20 %. The fact that the probability of three to four body break up is similar to the projectile break up probability in the knock-out channel indicates that apart from structure effects there is no distinction in the mechanism of break up and knock-out processes.

References

1) J.R. Wu, C.C. Chang, and H.D. Holmgren, Phys. Rev. Lett. 40 (1978) 1013

2) A. Budzanowski, G. Baur, C. Alderliesten, J. Bojowald, C. Mayer-Böricke, W. Oelert, P. Turek, F. Rösel and D. Trautmann, Phys. Rev. Lett. 41 (1978) 635

1.18. Investigation of light nuclei at high excitation energies with three-body break-up reactions

R. Franke, H. Machner, B. Steinheuer*, K. Wingender* and W. von Witsch**

Various three-body break-up reactions resulting from the bombardment of ^{7}Li with 120 MeV ^{3}He have been measured simultaneously in a kinematically complete experiment. Reaction products were detected and identified by means of four ΔE-E telescopes and coinciden events recorded on magnetic tape.

The main aim of the experiment was the search for highly excited states in light nuclei. In particular, the hope was that a comparison of the reactions $^{7}Li(^{3}He;\ ^{3}He,t)^{4}He^{*}$ and $^{7}Li(^{3}He;\ d,\alpha)^{4}He^{*}$ might reveal the existence of a state with T = 2 in ^{4}He since its formation would be isospin allowed in the ^{3}He+t channel but forbidden in the d+α channel. The excitation energy of the lowest T=2 state in ^{4}He has been estimated to be 38 ± 2 MeV[1]. No clear evidence for such a state has been found (fig. 1) although there is some evidence for a relatively narrow peak near 47 MeV.

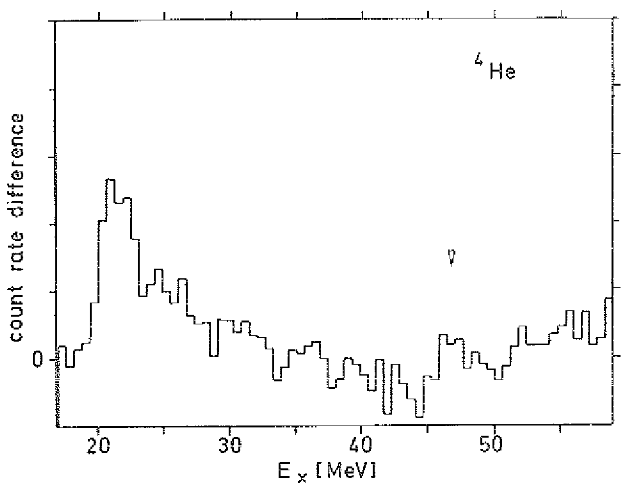

Figure 1: Missing-mass difference spectrum $^{7}Li(^{3}He;^{3}He,t)^{4}He$ minus $^{7}Li(^{3}He;d\alpha)^{4}He$.

In ^{4}H , a strong transition to the ground state was observed in the $^{7}Li(^{3}He;\ ^{3}He,^{3}He)^{4}H$ reaction which is well described by the P-wave phase shift $\delta_{1,\frac{2}{1}}$ alone (fig. 2), using for the yield Y_1 the expression[2] $Y_1=\sin^2\beta_1/P_1$, where β_1 is the resonant phase shift calculated from the total phase shift[3] $\delta = \beta + \varphi$, P_1 is the Breit-Wigner penetrability (for l = 1), and φ the hard sphere phase shift. No evidence for a T = 2 state is seen here which would be expected to lie about 12 MeV above the ground state of ^{4}H. In comparison, the ground state of ^{4}Li is populated much more weakly in the analog $^{7}Li\ (^{3}He;t,t)^{4}Li$ reaction.

In the reaction $^{7}Li(^{3}He;d,^{3}He)^{5}He$ the well established narrow state at 16.8 MeV as well as a broader one at 20 MeV (fig. 3) are strongly excited in ^{5}He while the same states are not seen in the analog $^{7}Li(^{3}He;d,t)^{5}Li$ reactions. This can be understood if ^{3}He is viewed as

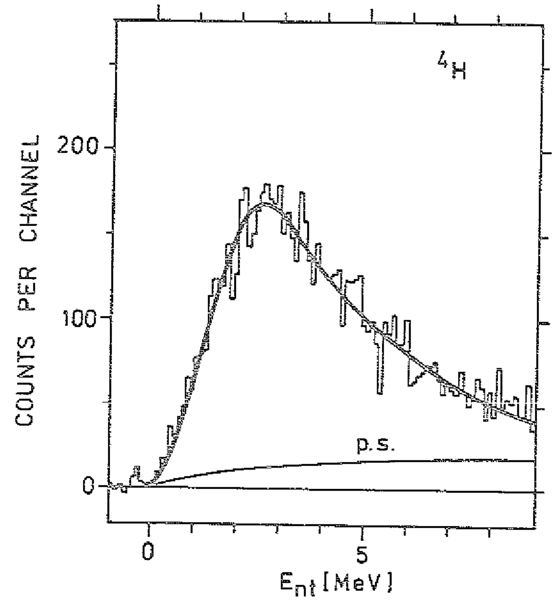

Figure 2: Missing mass spectrum of the $^{7}Li(^{3}He;^{3}He,^{3}He)^{4}H$ reaction. The fit is explained in the text. P.S. is the contribution from simultaneous four-body break-up.

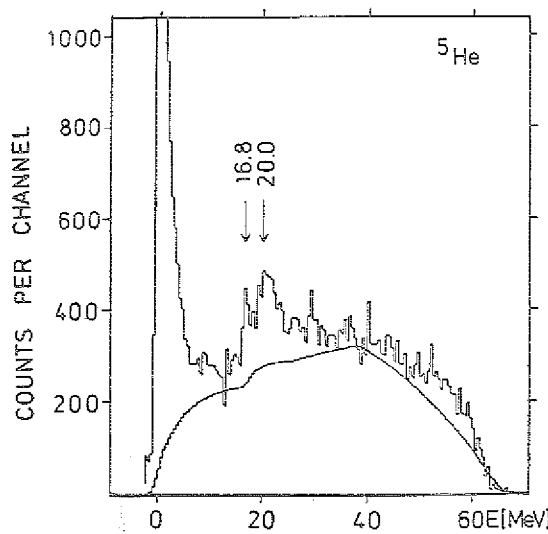

Figure 3: Missing mass spectrum for ^{5}He. The curve is a sum of the phase space distributions for simultaneous break-up into n + d + ^{3}He + ^{4}He and d + d + t + ^{3}He; break-up into more than four particles has not been taken into account.

(d+p), with the proton picking up two nucleons from the $^{2}P_{3/2}$ target; the 2-neutron transfer leading to the $^{4}S_{3/2}$ state in ^{5}Li (16.7 MeV) would then be S-forbidden[4]. The same is true for the D-wave interaction around 20 MeV excitation energy. In both reactions, there is evidence for a peak (width approximately 4 MeV) at 36 MeV and 34.5 MeV, respectively.

In ^{6}He, investigated through the reaction $^{7}Li(^{3}He;p,^{3}He)^{6}He$, a broad peak was observed at 16 MeV excitation energy which might consists of two or three narrower states (fig. 4). It is explained as being due to the knock-out of a 1s proton from ^{7}Li. Corresponding structure was found in the $^{7}Li(n,d)^{6}He$ and $^{7}Li(p,2p)^{6}He$ reactions (ref. 5 and refs. therein).

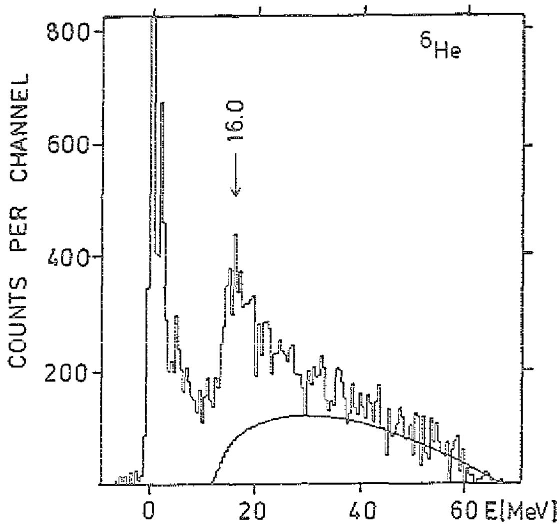

Figure 4: Same as fig. 3 but for the residual nucleus ^{6}He. The phase space distribution is for p + t + t + ^{3}He only.

References

1) L.A. Arnold, Technical report OSU-TR 79-402, Ohio State University, 1979
2) H.T. King et al., Nucl. Phys. A178 (1972) 337
3) T.P. Tombrello, Phys. Rev. 143 (1966) 772
4) J. Cerny et al., Phys. Rev. 152 (1966) 950
5) F.P. Brady et al., Phys. Rev. C16 (1977) 31

*Institut für Strahlen- und Kernphysik der Universität Bonn.

This work was supported by the Bundesministerium für Forschung und Technologie.

1.19. Light Particle Correlations

H. Machner

To study the nuclear continuum up till now mainly excitation functions of spallation products and inclusive energy spectra of secondaries have been measured. It is only recently that more exclusive data have been produced[1]. To explain these data the generalized exciton model has been extended[2]. During the equilibration cascade more than one fast particle may be emitted. The dynamics of the process is governed a set of master equations for the occupation probabilities $P(n,\Omega,t)$ and $Q(m,\Omega,t)$ of the composite system and the residual system after one particle emission, respectively. The starting condition is

$$P(n,\Omega,t) = \delta(n,n_0)A(n_0,\Omega)\sigma_0 \tag{1}$$

for the primary process with n_0 being the number of initially excited excitons, $A(n_0,\Omega)$ the direction of the scattered fast nucleon and σ_0 the absorption cross section. The transition rates between exciton states are those of ref. 4. Then the cross section for a particle consisting of n_i excitons is

$$\frac{d^2\sigma(\vartheta_i)}{d\varepsilon\, d\Omega} = \sum_{\substack{n=n_0\\ \Delta n=2}}^{\bar{n}} f(n,i)W_i(n,\varepsilon_i,E)\int_0^{t_{eq}} P(n,\Omega_i,t)dt$$

$$= \sum_{\substack{n=n_0\\ \Delta n=2}}^{\bar{n}} B_i(n,\varepsilon_i,E,\vartheta_i) \tag{2}$$

with $\bar{n}$ the exciton number characterizing statistical equilibrium. W_i is the emission rate and $f(n,i)$ an isospin mixing factor.

Because in the generalized exciton model there is no way to distinct between the strack and the scattered nucleon in a residual interaction, one has after one collision two "fast" particles. We therefore assume that hadron number conservation is sufficient[3] to give the initial condition for the secondary process:

$$Q(m,\vartheta_i,t=0)=\delta(m,m_0=n-n_i)B_i(n,\varepsilon_i,E,\vartheta_i)\ . \tag{3}$$

The cross section is thus independent from the linear momentum already carried away by the first particle . The second chance cross section into the direction Ω_j is then

$$\frac{d^2\sigma(\vartheta_i,\vartheta_j)}{d\varepsilon\, d\Omega} = \sum_{\substack{n=n_0\\ \Delta n=2}}^{\bar{n}} \sum_{\substack{m=m_0(n)\\ \Delta m=2}}^{\bar{n}} \int_0^{E-B} dU \int_0^{t_{eq}} Q(m,\vartheta_i,t)dt$$

$$\times\ f(m,j)W_j(m,\varepsilon_j,U)A(m+n_i,\Omega_j)\ . \tag{4}$$

We can then calculate the coincident cross section according to

$$\frac{d^4\sigma(\vartheta_i,\vartheta_j)}{d\varepsilon_i d\Omega_i d\varepsilon_j d\Omega_j} = \frac{d^2\sigma(\vartheta_i)}{d\varepsilon_i d\Omega_i}\ \frac{d^2\sigma(\vartheta_i,\vartheta_j)}{\sigma_0 d\varepsilon_j d\Omega_j}$$

$$+ \frac{d^2\sigma(\vartheta_j)}{d\varepsilon_j d\Omega_j}\ \frac{d^2\sigma(\vartheta_j,\vartheta_i)}{\sigma_0 d\varepsilon_i d\Omega_i}\ . \tag{5}$$

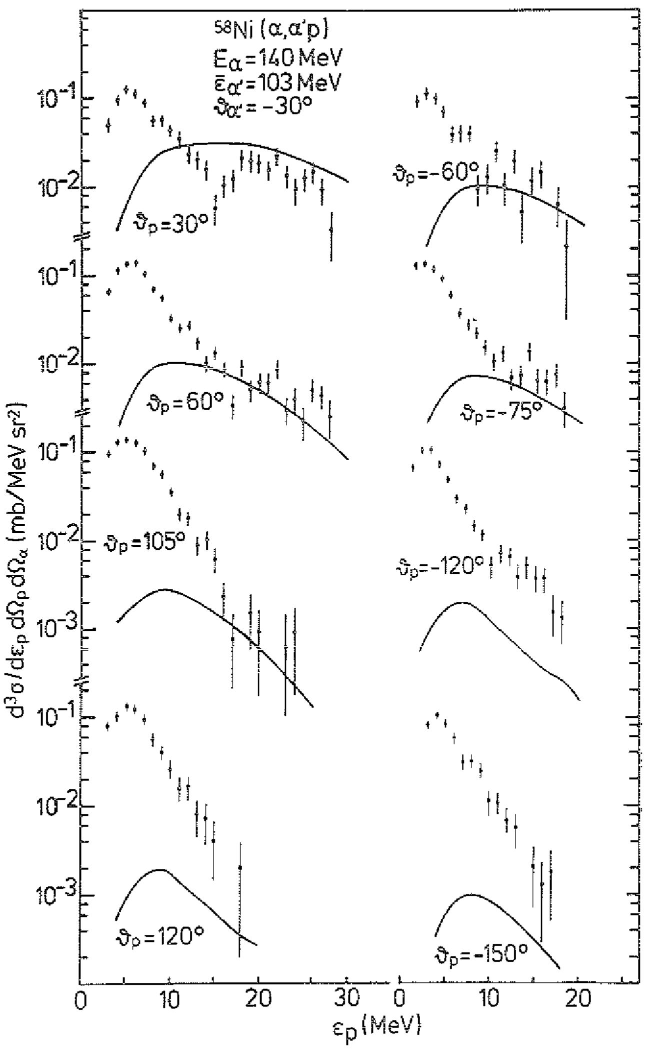

Figure 1: Coincident proton cross sections from the indicated reaction are compared with model predictions for $\varepsilon_{\alpha'} = 103 \pm 9.5$ MeV.

In the figure data[1] are compared with calculations. The free model parameter for complex particle emission - the coalescence radius P_0 (ref. 5) - has been adjusted to the inclusive data. There is no further adjustment.

The calculations presented in this contribution predict coincident cross sections peaked in beam direction. This is in contradiction to two body kinematics. However, the data support this prediction.

References

1) U. Bechstedt et al., Phys. Rev. C25 (1982) 3221
2) C. Ciangaru et al., to be published
3) H. Machner, accepted by the Physical Rev. C, and references therein
4) H. Machner, Z. Physik A302 (1981) 125
5) H. Machner, Phys. Lett. 86B (1979) 129

1.20. Search for nuclear structure effects in continuous spectra

G. Seniwongse, H. Machner, P. Jahn, M. Nolte, M. Rogge and P. Turek

Although the models for pre-equilibrium decay[1] are more or less phase space models they reproduce a wealth of data extremely well[2]. However, it is of great interest to now at what extend nuclear structure contributes to pre-equilibrium decay.

To study this question we have started a series of experiments in which angle dependent energy spectra of fast charged particles from nuclear reactions with target nuclei and 100 MeV α-particles will be measured. The target nuclei chosen are $^{24,25,26}Mg$, ^{27}Al and ^{28}Si. We can therefore study the effects of changing neutron number and proton number as well.

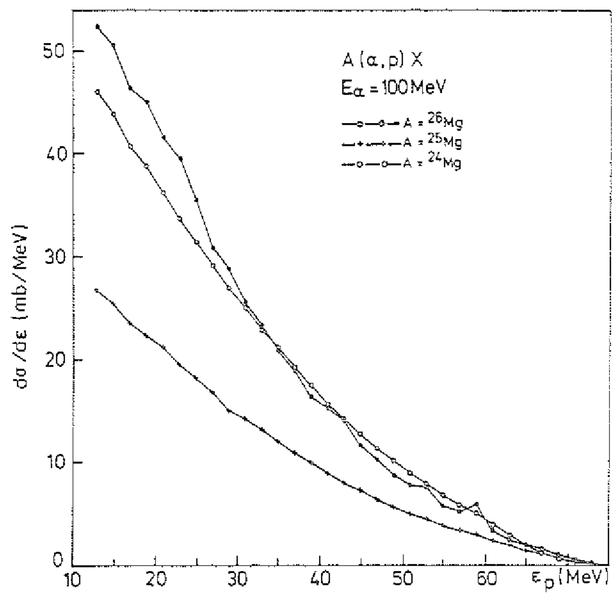

Figure 1: Angle integrated cross sections for the $^{24,25,26}Mg(\alpha,p)X$ reactions at E_α = 100 MeV.

In the figure preliminary data of angle integrated cross sections for the $^{24,25,26}Mg(\alpha,p)X$ reactions are shown. A dominant odd-even effect shows up which is also to be seen in the other particle channels. The investigation will be continued.

References

1) M. Blann, Annu. Rev. Nucl. Sci., 25 (1974) 123
2) H. Machner, Proc. Int. Conf. on Highly Excited States and Nuclear Structure, to appear in Edition Physique

1.21. Study of the fragment-mass-distribution of ^{4}He-induced fission

A. Buttkewitz, H.H. Duhm*, H. Machner and W. Strauß**

In continuation of a study of ^{3}He-induced fission on ^{169}Tm ($E_{^3He}$ = 42 MeV) we measured α-induced fission at E_α = 140 MeV on Gold, Holmium and Silver. Two silicon detectors of 30 mm diameter were used to determine the fragment energies. Figure 1 shows the two-dimensional energy spectra of fission products from Au, Ho in a symmetric left-right counter position relative to the incident beam and two spectra of Silver in a symmetric ($75.5^o/75.5^o$) and an asymmetric position ($62^o/90^o$). Unfortunatley the Silver spectra show considerable background from pile up. Preliminary mass spectra are shown in fig. 2. The mass spectrum of Silver is of particular interest since the fissility parameter $x = Z^2/(50.13 \cdot A)$ is rather close to the critical Businaro Gallone point[1,2] x = 0.4, where asymmetric mass fragmentation may occur. The obtained mass spectrum for the Silver target shows only symmetric fragmentation. It should be considered, however, as a very preliminary result because of background problems already mentioned and energy and angle cutoffs. We intend to continue the experiment using a position sensitive ionization chamber. Figure 3 shows the measured cross-sections together with a data compilation given by Moretto[3].

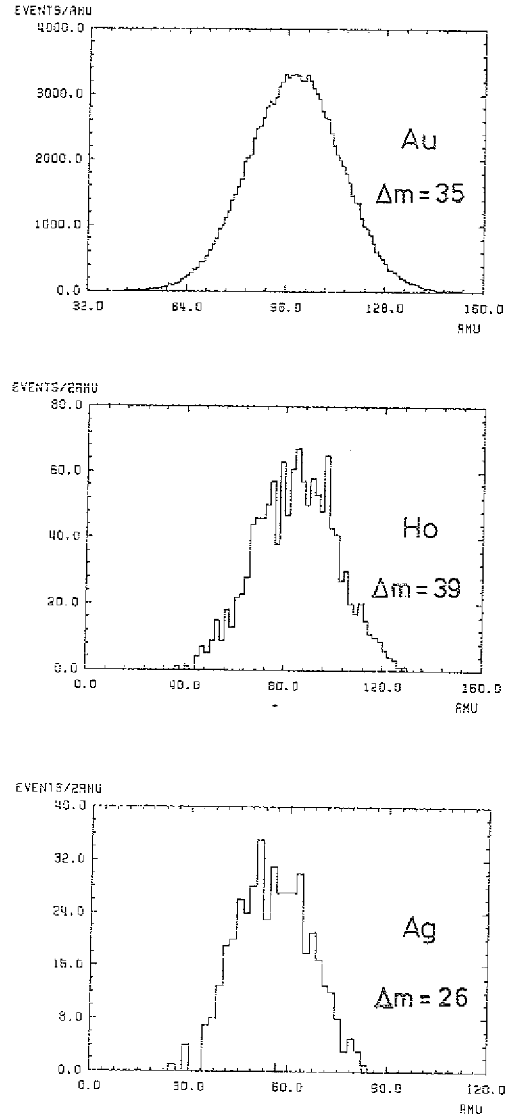

Figure 2: Mass spectra of the fission products.

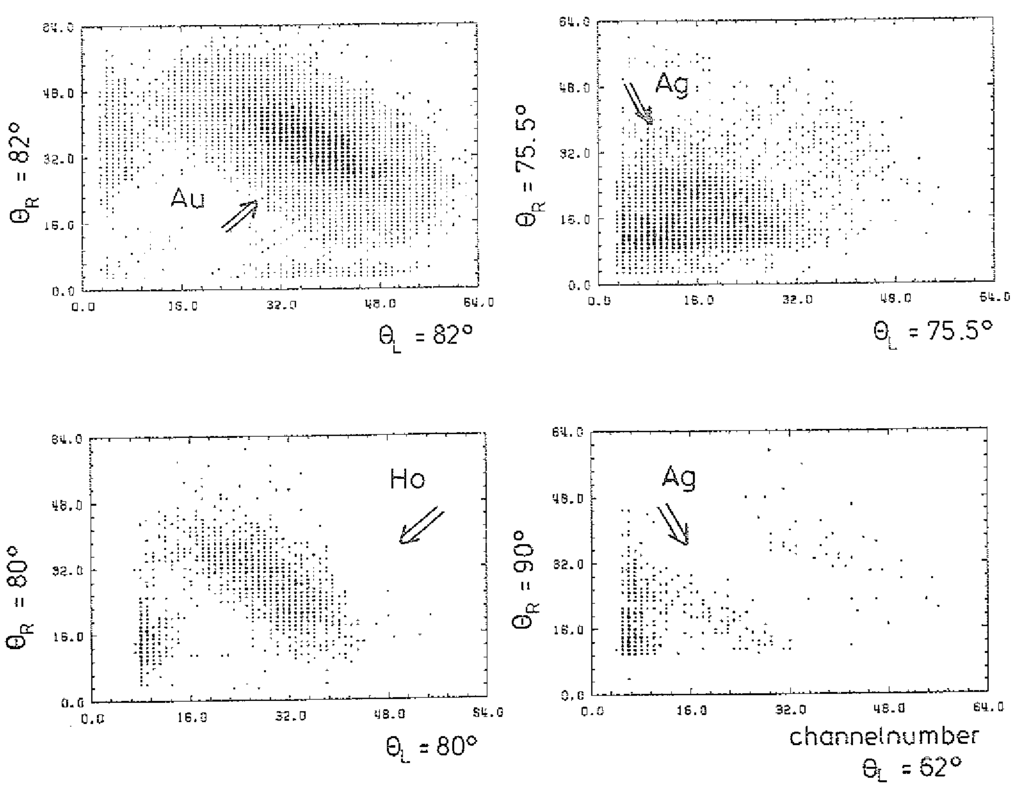

Figure 1: Two-dimensional energy spectra of fission products from the target nuclei studied. The detection angleshas been symmetric to the beam axis. One asymmetric case for silver is also shown (down right).

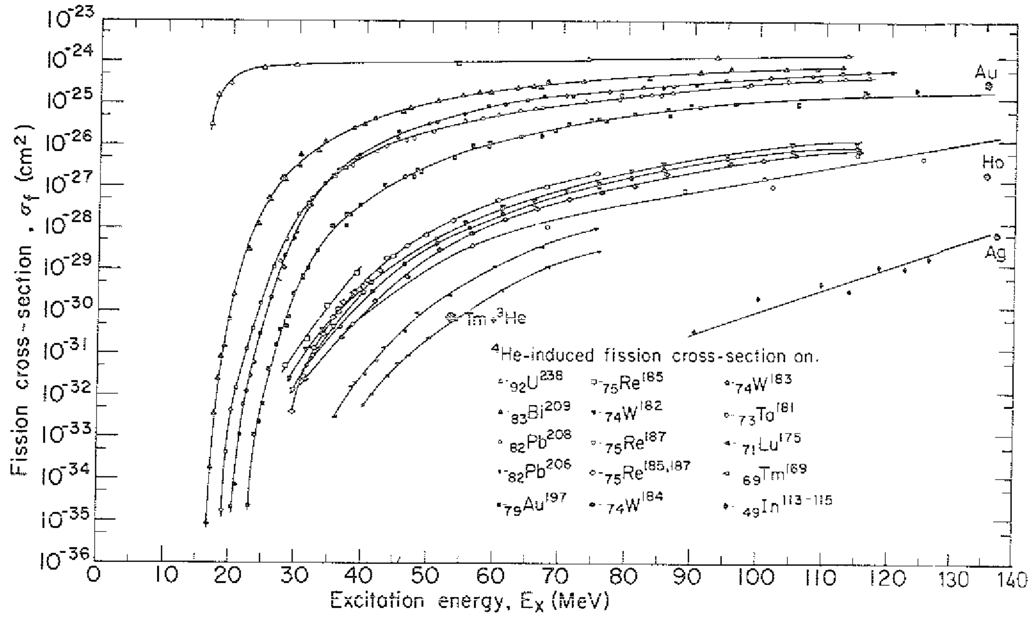

Figure 3: Fission cross section for the three target nuclei studied in comparison to lower energy data[2]. Also shown is the cross section for ^3He induced fission at lower energy from a previous experiment.

References

1) V.L. Businaro and S. Gallone, Nuovo Cim. 1 (1955) 1102

2) S. Cohen and W.J. Swiatecki, Ann. Phys. 19 (1962) 67

3) L.G. Moretto, Physics and Chemistry of Fission
Proc. Symp. Rochester 1973, Vol. I, p. 329

*I. Institut für Experimentalphysik, Universität Hamburg

1.22. Fast Nucleon Emission from Heavy Ion Induced Reactions

H. Machner

It has become very popular to parametrize spectra of fast light isotopes emerging from heavy ion bombardement of nuclei in terms of moving equilibrated sources. However, it is hard to believe that projectile energies of a few tens of MeV/nucleon can lead to a clear cut fireball geometry. Another possibility is to invoke models which have been extremely successful in reproducing light ion induced reactions like the exciton model[1].

After a first target-projectile interaction the system equilibrates via nucleon-nucleon collisions. This process is described by a system of master equations[2]:

$$\frac{dP(n,\Omega,t)}{dt} = \lambda_+(n-2,\Omega',E)P(n-2,\Omega',t) + \lambda_-(n+2,\Omega',E)P(n+2,\Omega',t) - [\lambda_+(n,\Omega,E)+\lambda_-(n,\Omega,E)+\lambda_c(n,E)]P(n,\Omega,t) \quad (1)$$

with P being the occupation probability of a state with n excitons (n = particles + holes) with respect to the Fermi surface and $\Omega = (\vartheta,\varphi)$ the direction. The transition rates for exciton-exciton interactions $\lambda_\pm$ and for emission into the continuum λ_c are those from refs. 3 and 4.

Since heavy ions are large objects compared to light ions some modifications in the model are expected to occur. In light ion induced reactions data analysis suggests an initial 1p + 1h excitation in the target nucleus leading to

$$n_o = A_p + 2 \ . \quad (2)$$

Here, in a first phase nucleus-nucleus interaction may lead to a xp+xh excitation depending on the overlap the two nuclei have. From such a picture two conjectures emerge:

- x will be an increasing number with increasing bombarding energy,
- x will not be a function of the target mass as long as $A_p << A_T$.

To test these conjectures we have analyzed data[5,6] with

$$n_o = A_p + 2x \ . \quad (3)$$

By varying x it turns out that x is a well defined quantity because spectral shape as well as absolute height are strongly depending on x.

The data analysis is in agreement with the conjectures stated above. As an example for the quality of agreement between model calculations and data we compare both in figure 1. In addition to the high energy part an evaporation calculation using the code JULIAN is also shown.

References

1) M. Blann, Annu. Rev. Nucl. Sci. 25 (1974) 123
2) G. Mantzouranis et al., Z. Physik A276 (1976) 145
3) H. Machner, Z. Physik A302 (1981) 125
4) H. Machner, Phys. Lett. 86B (1979) 129
5) E. Holub et al., Phys. Rev. C28 (1983) 252
6) H. Machner, Phys. Rev. C28 (1983) 2173

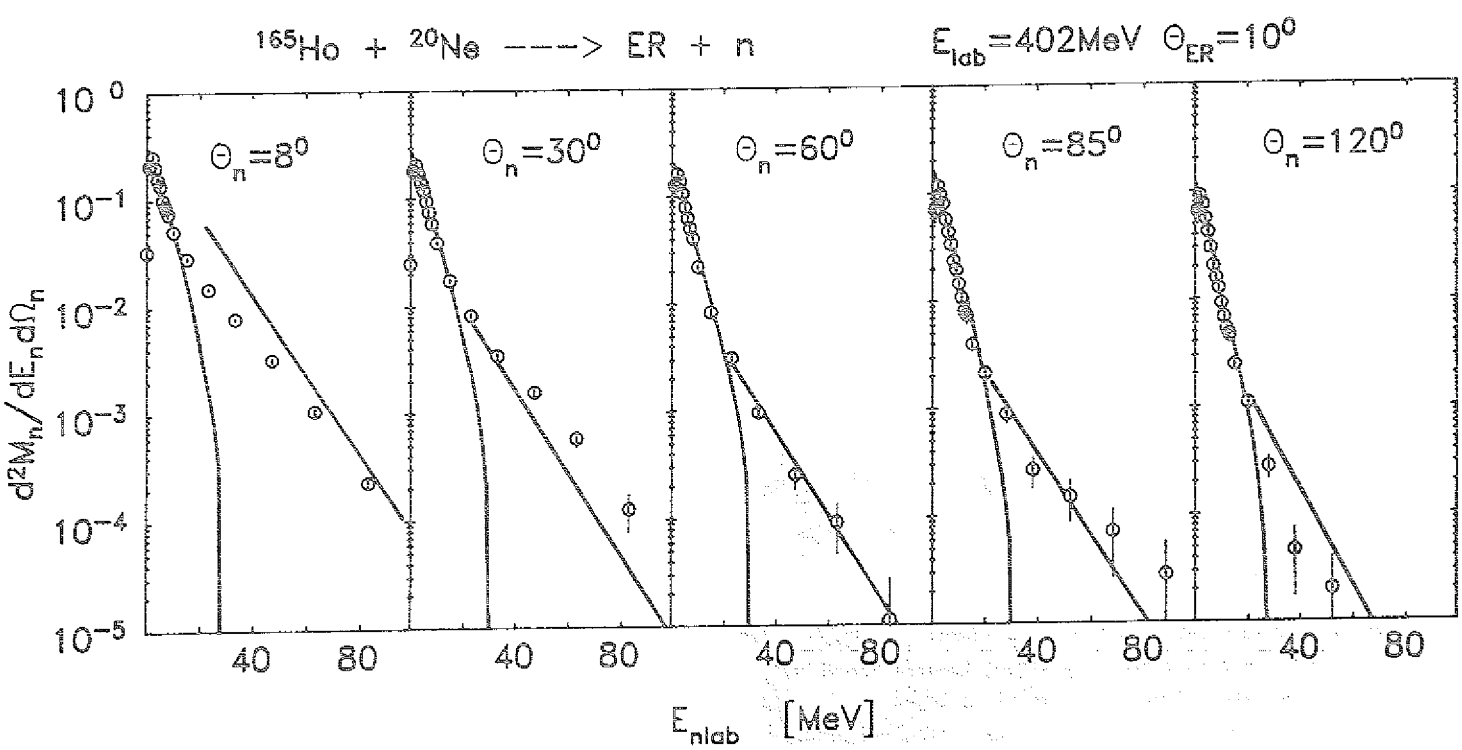

Figure 1: Neutron multiplicities measured at the indicated angle in coincidence with evaporation residues (ER) are compared with compound nucleus (low energy part) and exciton model calculations (high energy part).

1.23. How does the optical potential depend on nuclear excitations ?

H. Machner

With the appearance of medium energy heavy ion reactions the question how nuclear properties depend upon temperature has been becoming an important one. In this contribution only the temperature dependence of optical model parameters and the corresponding absorption cross sections will be discussed.

The mean free path Λ of a nucleon in nuclear matter is

$$\Lambda = \frac{v}{2W} \qquad (1)$$

with v being the asymptotic nucleon velocity and $W > 0$ the imaginary part of the optical potential. The classical relation is

$$\Lambda = (\rho\bar{\sigma})^{-1} \qquad (2)$$

with ρ the medium density and $\bar{\sigma}$ the cross section. For infinite nuclear matter $\bar{\sigma}$ should be replaced by $\langle\sigma\rangle$, the cross section including effects of the Pauli-principle. To derive at such a quantity we make the ansatz[1)]

$$\langle\sigma\rangle = \bar{\sigma}\,[1-f(\rho)e^{-\lambda T}] \ . \qquad (3)$$

The function $f(\rho)$ is the Pauli blocking function which can be derived under the assumption[2,3)] that in momentum space only states with momenta k_F larger than the Fermi momentum k_F are allowed as final states. The exponential weakens the influence of the Pauli-blocking at high temperatures T, because in a highly excited nucleus a large fraction of states below k_F are not occupied. The results of Collins and Griffin[4)] are reproduced for a value $\lambda = 0.02$.

For a real potential depth $V = 50$ MeV and assuming an effective mass $m^* \gtrsim 0.5$ m the imaginary part of the optical potential derived by Bohr and Mottelson[5)] for only volume absorption is approximately reproduced[1)]. In fig. 1

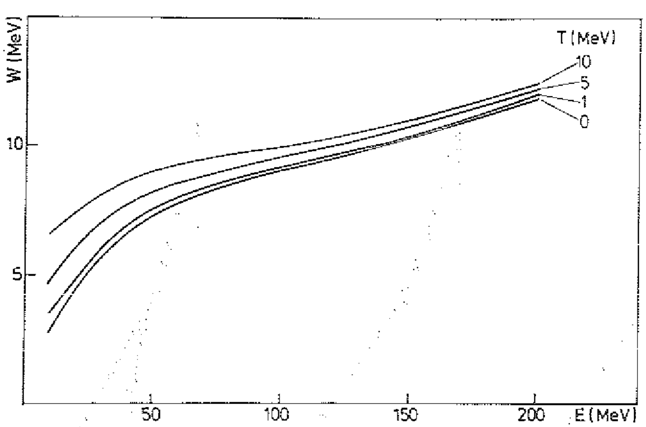

Figure 1: Imaginary parts of the optical potential as function of the incident neutron energy and for different nuclear temperatures T.

the temperature dependence of W is shown. Obviously, only for small energies there is a strong temperature dependence. From these imaginary potentials together with real parts and geometry from ref. 5 we can calculate absorption cross sectins. While at zero temperature there is a substantial interference between the incident and transmitted waves (nuclear Ramsauer effect) these corresponding fluctuations the cross sections are washed out at high temperatures. This is shown in figure 2. It is ob-

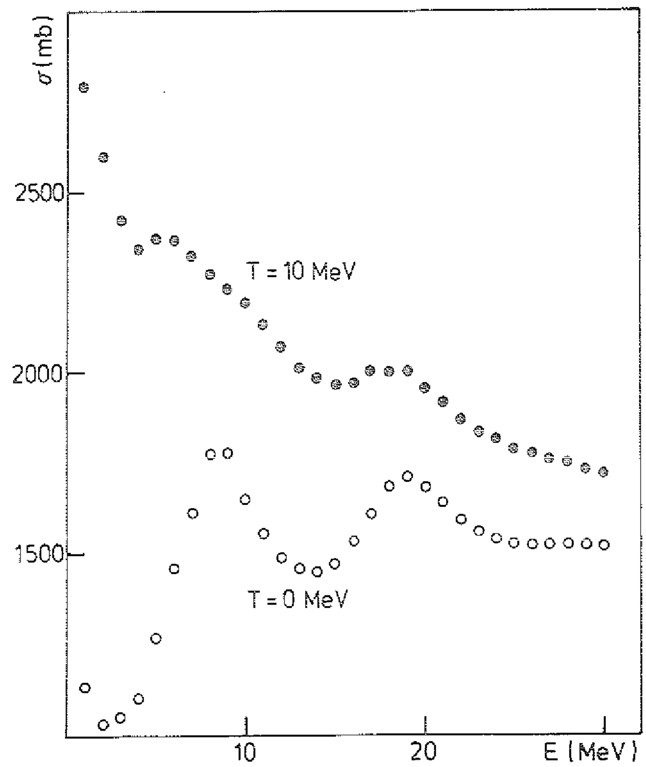

Figure 2: Absorption cross sections for low energy neutrons and an A = 100 nucleus are shown for the indicated temperatures.

vious from this figure that for high temperatures the common practice to approximate the cross section for time reversed reactions by ground state absorption cross sections to calculate the compound nucleus decay is not justified.

References

1) H. Machner, accepted by Z. Physik
2) E. Clementel and C. Villi, Nuovo Cim. 2 (1955) 176
3) K. Kikuchi and M. Kawai, Nuclear Matter and Nuclear Reactions, North Holland Publ., Amsterdam 1968
4) M.T. Collins and J.J. Griffin, Nucl. Phys. A348 (1980) 63
5) A. Bohr and B.R. Mottelson, Nuclear Structure Vol. I, W.A. Benjamin, Inc., New York 1969

1.24. Mean angular momenta involved in the preequilibrium charged particle emission

B. Bochev, T. Kutsarova, R.M. Lieder, J.-P. Didelez and T. Morek

The central collision models such as promptly emitted particles[1], exciton[2] and coalescence[3] models were used to interprete the emission of protons[4,5], deuterons and tritons[6] in alpha induced reactions at E_α = 45, 75 and 110 MeV studied in this laboratory. Furthermore it has been shown[7] that peripheral collisions, e.g. break-up fusion may contribute to the cross sections at least for deuteron and triton reaction channels. An important information about the reaction mechanism and hence about the applicability of a given model can be obtained from the angular momentum balance. In the following we shall present some estimation of the angular momenta involved in the reactions ^{159}Tb(α,charged particle xnγ) at E_α = 45, 75 and 110 MeV.

The input angular momentum is defined as

$$I_{in} = \frac{b}{\hbar}\sqrt{2\,\mu(E^{CM}-B)}\quad, \qquad (1)$$

where μ is the reduced mass, E^{CM} the beam energy in the CM system, B the Coulomb barrier between the target and the projectile nuclei and b the impact parameter. The input angular momentum is shared between the angular momenta taken away by the ejectile I_e, the emitted neutrons I_{xn}, and the gamma ray cascade I_γ. It is known[8], that the emission of a fast (preequilibrium) particle takes a time which is shorter than 10 fm/c, while the rotational time is longer than 100 fm/c. One can expect, therefore, that the preequilibrium charged particle is emitted from the same impact parameter b. Therefore, we can express I_{in} in a form independent of I_e as

$$I_{in} = \frac{I_{xn} + I_\gamma}{1 - \dfrac{\sqrt{\mu_e(E_e^{CM} - B_e)}}{\sqrt{\mu(E^{CM} - B)}}} \qquad (2)$$

with E_e^{CM} being the ejectile energy in the CM system. The quantities μ_e and B_e are the reduced mass and Coulomb barrier for the system ejectile-residual nucleus, respectively.

Considering for a given reaction channel the peak region of the cross section[4] the charged particle take away so much excitation energy that the subsequent neutrons are evaporated. Hence, the neutrons have very small kinetic energies of 0.5 - 2.5 MeV (ref.4) and carry away an angular momentum of the order of $I_{xn} = \frac{x}{2}\hbar$ (ref. 9). To deduce I_γ, the γ-ray multiplicity M_γ has been measured at E_α = 45 MeV, where the different reaction channels are well separated[10]. The values of M_γ together with the associated angular momentum $I_\gamma = 2\,(M_\gamma - 3)$ (ref. 11) are listed in table 1. The angular momentum released by the whole γ-ray cascade I_γ can be expressed as the sum of the mean observed yrast cascade spin I^Y and the γ-ray side feeding spin I^S. The yrast spin I^Y for the ^{159}Tb(α,ch.p.xnγ) reaction at E_α = 45 MeV and the sum $I^Y + I^S$ are shown in table 1, where the side feeding spin I^S has been taken from ref. 12 for the reaction ^{160}Gd(α,4n)^{160}Dy at E_α = 45 MeV. One can see an agreement of I_γ and $I^Y + I^S$ for the channels (α,p2nγ) and (α,pγ). This comparison shows that I^S in the channels (α,pxnγ) is close to that of the (α,xnγ) reaction in agreement with the conclusion of ref. 13. A good agreement can be also seen for the major deuteron channel (α,dnγ). For the (α,tγ) channel I^Y

Channel	(α,pγ)	(α,pnγ)	(α,p2nγ)	(α,dγ)	(α,dnγ)	(α,tγ)	(α,tnγ)
M_γ	8±1	9±1	10±1	9±1	10±2	6±1	9±1
I_γ	10±2	12±2	14±2	10±2	14±2	6±1	10±1
I^Y	7.5±2.5	-	8.0±0.5	-	7.2±0.6	5.7±0.5	-
I^Y+I^S	12.0±2.7	-	12.5±1.0	-	11.7±1.0	10.2±1.0	-

Table 1: Comparision of the angular momenta released by the whole gamma ray cascade I_γ for the ^{159}Tb(α,ch.part.xnγ) reaction at E_α = 45 MeV and particle detection angle of 45° with $I^Y + I^S$. The yrast spins I^Y are deduced from the particle-gamma coincidence data and the side feeding spin I^S = 4.5 ± 0.9 is taken from an experiment using the ^{160}Gd(α,4nγ) reaction at E_α = 45 MeV (ref. 12). M_γ is the measured multiplicity.

E_α (MeV)	45			75				110			
Channel	E_e (MeV)	$d\sigma/d\Omega$ (μb/sr)	I_{in} ($\hbar$)	E_e (MeV)	$d\sigma/d\Omega$ (μb/sr)	I^Y ($\hbar$)	I_{in} ($\hbar$)	E_e (MeV)	$d\sigma/d\Omega$ (μb/sr)	I^Y ($\hbar$)	I_{in} ($\hbar$)
(α,pγ)	30.4±0.5	200±20	18.1±3.6	59.2±0.5	17.1±3.0	6.5±2.0	23.3±4.0	92.2±1.0	2.5±1.1	∿6	∿30
(α,pnγ)	21.6±0.5	2040±87	18.8±3.0								
(α,p2nγ)	14.4±0.5	8250±80	16.3±2.5	41.6±0.5	1930±73	7.7±1.3	23.3±2.8	73.0±1.0	219±15	9.7±3.0	28.5±5.7
(α,p4nγ)				20.5±0.5	7282±67	8.4±0.6	20.5±1.7	51.5±1.0	4264±83	10.5±1.1	27.9±2.6
(α,p6nγ)								27.5±1.0	8737±73	9.2±0.7	23.1±2.0
(α,p8nγ)								∿10.5	1983±100	8.8±1.4	∿19
(α,dγ)	24.0±1.0	279±43	21.3±4.3								
(α,dnγ)	18.6±1.0	2320±30	17.9±3.4	45.6±1.0	433±32	7.5±1.9	32.2±5.2	77 ±2	275±25	8.5±3.0	38.9±8.6
(α,d3nγ)				26.3±1.0	2020±35	8.3±0.7	25.4±2.2	56 ±2.5	1613±60	10.1±2.0	35.7±5
(α,d5nγ)				13.0±1.0	>85	7.5±1.9	18.9±2.7	35 ±2.5	3294±70	8.6±0.9	27.5±2.6
(α,d7nγ)								15 ±2.5	1121±45	7.9±1.7	20.7±2.7
(α,tγ)	28.6±1.0	930±22	26.1±4.1	57.0±1.0	162±30	5.6±1.7	>30	84 ±2	220±30	6.3±1.5	>41
(α,tnγ)	16.8±1.0	550±50	19.5±3.7								
(α,t2nγ)				35.6±1.0	866±72	7.5±0.9	35.4±4.0	67.5±2.0	1070±50	8.5±1.3	51 ±6
(α,t4nγ)				16.0±1.0	518±30	7.5±1.2	21.6±2.4	45 ±2.5	1580±50	7.9±0.9	35.2±3.4
(α,t6nγ)								21 ±2.5	980±30	7.9±1.0	24.2±2.4
$\langle I(\alpha,pxn\gamma)\rangle$	16.8			21.1				24			
$\langle I(\alpha,dxn\gamma)\rangle$	21.4			26.3				28.9			
$\langle I(\alpha,txn\gamma)\rangle$	23.6			30.2				37			
ℓ_{lim}	20.5			26.2				31.6			
R_p	0.82			0.81				0.76			
R_d	1.04			1.00				0.92			
R_t	1.11			1.15				1.17			

Table 2: Input angular momenta I_{in} as calculated from eq. (2) for the ^{159}Tb(α,ch.part.xnγ) reaction channels at E_α = 45, 75 and 110 MeV, mean angular momenta $\langle I \rangle$ and the ratios R.

a) I_γ is taken from table 1; b) I_γ is calculated as $I^Y + I^S$ with I^S = 5.7 ± 1.1 $\hbar$ (ref. 12), except for the (α,tγ) channel, where I^S = 0; c) I_γ is calculated as $I^Y + I^S$ with I^S = 5.8 ± 1.3 $\hbar$ (ref. 12), except for the (α,tγ) channel, where I^S = 0.

is lower than for all other channels and it is close to I_γ suggesting a smaller value of the side feeding spin I^S than anticipated. Because of the lack of better data we shall use the side feeding spin I^S deduced for the reaction $^{160}Gd(\alpha,6n\gamma)^{158}Dy$ [12] to estimate the angular momenta I_γ removed by the γ-ray cascade for all reaction channels at E_α = 75 and 110 MeV except for the $(\alpha,t\gamma)$ channels. The calculated input angular momenta I_{in} are shown in table 2. The mean angular momenta <I> weighted by the cross sections $d\sigma/d\Omega$ have been calculated and compared with the limiting angular momentum ℓ_{lim} for complete fusion[14] at a given beam energy. The ratios $R = \frac{\langle I(\alpha,ch.p.xn\gamma)\rangle}{\ell_{lim}}$ are included in table 2. Several interesting features can be observed:

1) The input angular momentum I_{in} is a decreasing function of the number of emitted neutrons. This is due to the increasing ejectile energy which overbalances the effect of angular momentum release by the neutrons.

2) The ratios R for a given ejectile are independent on the beam energy. From the value of $R_p \sim 0.8$ it seems that the proton emission occurs predominantly at medium impact parameters. Such a result supports the applicability of the central collision models for the description of nonequilibrium protons. On the other hand the angular momentum ratios $R_d \sim 1$ and $R_t \sim 1.15$ indicate more peripheral character of the interactions followed by emission of deuterons and tritons.

References

1) J.P. Bondorf, N. De, G. Fâi, A.O.T. Karvinen, B. Jakobsson and J. Randrup, Nucl. Phys. A333 (1980) 285

2) M. Blann, Ann.Rev.Nucl.Sci. 25 (1975) 123

3) H. Machner, Phys. Lett. 86B (1979) 129

4) R.M. Lieder, B. Bochev, T. Kutsarova, H. Beuscher, D.R. Haenni, T. Morek, M. Müller-Veggian, A. Neskakis, C. Mayer-Böricke and J.-P. Didelez, Physica Scripta 24 (1981) 123

5) B. Bochev, R.M. Lieder, T. Kutsarova, T. Morek, A. Neskakis and J.-P. Didelez, Proc. of the 6th Int. School on Nuclear and Neutron Physics and Nuclear Energy, Sept. 1983, Varna

6) Unpublished results from IKP, KFA Jülich 1981

7) T. Kutsarova, B. Bochev, J.-P. Didelez, R.M. Lieder, T. Morek, M. Müller-Veggian and C. Mayer-Böricke, Annual Report 1980, IKP, KFA Jülich, Jül-Spez-99 (1981)

8) W.W. Morison, S.K. Samaddar, D. Sperber and M. Zielińska-Pfabe, Phys. Lett. 93B (1980) 379

9) T.D. Thomas, Nucl. Phys. 53 (1964) 577

10) J.-P. Didelez, B. Bochev, R.M. Lieder, T. Kutsarova, T. Morek, A. Neskakis, M. Müller-Veggian and C. Mayer-Böricke, Annual Report 1981, IKP, KFA Jülich, Jül-Spez-146 (1982) p. 36

11) Claudine Gerschel, Conference internationale sur quelques aspects des réactions entre ions lourds, Saclay (Mai 1982)

12) M.J.A. de Voigt, W.J. Ockels, Z. Sujkowski, A. Zglinski and J. Mooibroek, Nucl. Phys. A323 (1979) 317

13) T. Udagawa, Lecture given at Int. RCNP-Kikuchi Summer School on Nucl. Physics held at Kyoto, Japan, May 23-27, 1983

1.25. Simulation Experiments for Planetary Spectroscopy: Neutron-Induced Gamma-Rays from Thin Targets

P. Englert[+], J. Brückner[*], H. Wänke[*] and R.C. Reedy[++]

One of the important goals in planetology is the determination of the chemical composition of planetary surfaces, which can provide important clues on their origin and evolution. Such information can be obtained from gamma-rays emitted from the extraterrestrial bodies by means of orbital remote sensing gamma-ray spectroscopy[1].

Cascade particles produced by the interaction of the galactic cosmic radiation with extraterrestrial matter, and here especially neutrons, are important for the production of gamma-rays. Nonelastic scattering and neutron capture reactions produce many characteristic gamma-ray lines of discrete energy, which can be used to determine the abundances of the elements from which they are emitted. Proposed missions to Mars, Moon, comets and asteroids suggest simulation experiments which should lead to a better understanding of the production of gamma-rays by energetic neutrons, both in the planetary object observed itself and in the observing spacecraft. This will be useful for planning as well as for interpreting spectra obtained from such missions.

To investigate the gamma-rays induced by neutrons, experiments were carried out with 14 MeV neutrons. A characteristic spectrum of these irradiations is presented in figure 1, which shows 0.1-4.1 MeV gamma-rays from an Al-tar-

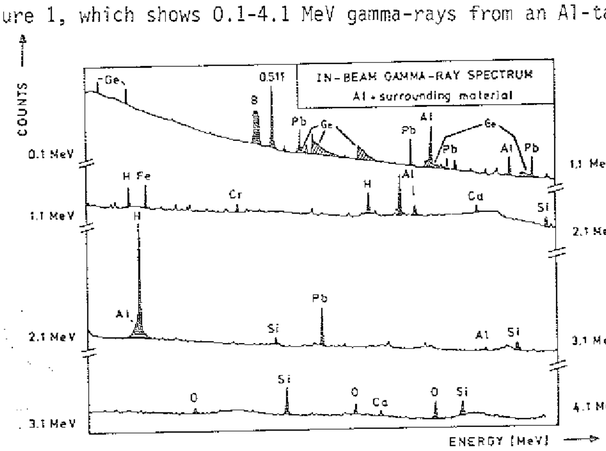

get irradiated with generator-produced neutrons[2]. Neutron energy spectra and neutron fluxes at the target location were roughly calculated from threshold monitor reactions[3]. A considerable flux of neutrons between 5 and 14 MeV was found, however, the majority had thermal and epithermal energies. From the linear generator-target-detector arrangement, the closeness of concrete walls and shielding with paraffin, an extreme degree of thermalization was expected at the target location. Therefore it is not surprising that neutron capture reactions produced most of the gamma-ray lines[2]. The ratios of the fluxes of the strongest neutron capture lines from Fe, Al, Mg and Si-targets agreed well with the ratios of measured yields for the capture of thermal neutrons. Background corrections were made for all lines and the flux of each line from a target was corrected for absorption in the detector shielding.

As expected, a broad 4.439 MeV gamma-ray peak made by inelastic scattering reactions with ^{12}C and a flat-topped peak at 0.478 MeV caused by the $^{10}Be(n,\alpha\gamma)^{7}Li$ reactions in shielding components were observed in all spectra. However, 5 wide asymmetric peaks between 0.5 and 1.1 MeV were unexpected. These peaks were generated in the detector and have a rapid drop at the lower energy side, but a very slow drop at the higher energy side. The energies at the lower edges correspond to various Ge-isotopes: 563 keV in ^{76}Ge, 596 keV in ^{74}Ge, 691 and 834 keV in ^{72}Ge, and 1040 keV in ^{70}Ge. These broad peaks were made by prompt processes, which occur when an energetic neutron excites a Ge nucleus in the detector to a level that rapidly deexcites. The energy from this deexcitation is often increased in the detector by the addition of energy from the recoil of the excited nucleus[4]. Fortunately, these background peaks occur in energy regions where there are not expected to be many gamma-ray lines of interest from a planetary surface. The 844 and 874 keV inelastic scattering gamma-rays from Al and Fe could be affected by serious interference with the tail of the relatively weak Ge-peak at 834 keV.

A more realistic simulation of the conditions in planetary surfaces was expected from irradiations with neutrons of higher energy produced via the Be(d,n)-reaction, a better neutron source-target-detector arrangement and less detector shielding. By positioning the targets and the detector closer and at angles of 45° and 90° with respect to the neutron source the necessary paraffin shielding could be reduced considerably. This led to a reduction of the neutron capture background, but did not affect the occurrence of C, Pb and Ge inelastic scattering gamma-ray lines. Another advantage is that the total neutron flux can be estimated from Faraday cup measurements. Preliminary results from a developmental run with a current of 0.5 nA of 78 MeV deuterons on Be for a Fe-target are presented in table 1 and compared with the 14 MeV results[2].

Energy keV	Reaction	normalized peak areas at max. neutron energy 39 MeV (6)	14 MeV (2)
846.7	$^{56}Fe(n,n\gamma)$	1196	8.1
931.2	$^{56}Fe(n,2n\gamma)$	126	0.31
1238.3	$^{56}Fe(n,n\gamma)$	225	2.3
1316.4	$^{56}Fe(n,2n\gamma)$	85	0.22
1407.7	$^{56}Fe(n,n\gamma)$	106	0.32
1810.9	$^{56}Fe(n,n\gamma)$	61	0.04
2112.9	$^{56}Fe(n,n\gamma)$	27	0.11
6609.1	$^{56}Fe(n,\gamma)$ d	1.2	1.4
7120.1	$^{56}Fe(n,\gamma)$ s	2.3	1.7
7631.1	$^{56}Fe(n,\gamma)$	1.5	1.1
6623.5	$^{56}Fe(n,\gamma)$ d	1.7	1.8
7134.5	$^{56}Fe(n,\gamma)$ s	1.4	1.4
7645.5	$^{56}Fe(n,\gamma)$	1.0	1.0

s - single escape peak
d - double escape peak

Table 1: Comparison of in-beam gamma ray-spectra from iron target.

Background, absorption and neutron flux corrections were applied. The peak areas for the inelastic scattering, (n,2n) and neutron capture gamma-ray lines are normalized to the 7645.5 MeV $^{56}Fe(n,\gamma)$ line. As expected, scattering and (n,2n) gamma-rays dominate the spectra taken during the 39 MeV maximum n-energy irradiation of Fe. The measured fluxes exceed those of the neutron capture gamma-rays by 2 to 3 orders of magnitude. A direct comparison with results from the 14 MeV maximum n-energy irradiation[2] makes the effect of the higher energy neutrons apparent.

As medium and high energy-neutrons contribute considerably to the secondary particle fluxes in the moderator-free planetary surfaces down to 150 g/cm^2 [5], the experiments with neutrons between 22.5 and 45 MeV maximum energy will improve knowledge of gamma-ray production in planetary surfaces and so help to develop tools for the interpretation of gamma-ray spectra obtained from such bodies.

References
1) R.C. Reedy (1978) Proc. Lunar Planet. Sci. Conf. 9th, 2961-2984
2) J. Brückner (1983) Ph. D. Thesis, Univ. Mainz
3) E. Rantanen, J.T. Routti and B. Bars (1975) Atomkernenergie 26, 103-106
4) R.L. Bunting and J.J. Kraushaar (1974) Nucl. Instr. and Meth. 118, 565-572
5) T.W. Armstrong and R.G. Alsmiller (1971) Proc. Second Lunar Sci. Conf., 1729-1745
6) This Work

+ Institut für Kernchemie, Universität Köln, F.R. Germany
* Max-Planck-Institut für Chemie, Mainz, F.R. Germany
++ Los Alamos National Laboratory, USA

1.26. Measurement and Hybrid Model Analysis of Integral Excitation Functions for Light Particle Induced Reactions

R. Michel[+], *M. Galas*[+], *F. Peiffer*[+], *R. Stück*[+]

In order to extend our earlier studies of p- and α-induced reactions on medium weight elements (e.g. 1-3) to other projectiles we measured integral excitation functions for the production of radionuclides ($44 \leq A \leq 61$) by ^{3}He- and ^{2}H-induced reactions on cobalt for energies up to 45 MeV per nucleon. The experimental data were compared with calculations using the computer code "OVERLAID ALICE"[4] combining the statistical theory of Weisskopf and Ewing with the hybrid model of preequilibrium reactions. For ^{3}He-induced reactions an unambiguous choice of the initial exciton configuration was possible using the reaction $^{59}Co(^{3}He,n)^{61}Cu$ (fig. 1). While an initial exciton

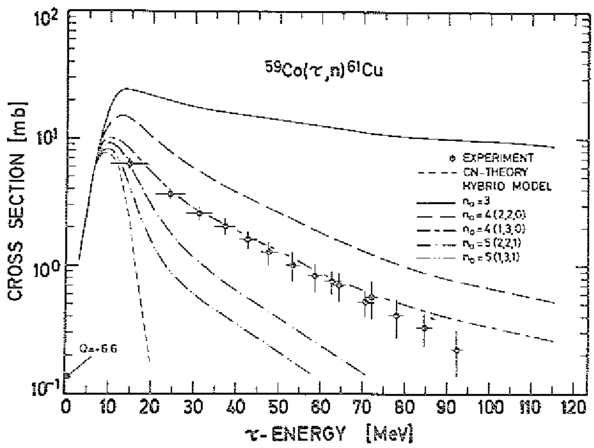

Figure 1: Experimental cross sections and theoretical predictions of the excitation function for the reaction $^{59}Co(^3He,n)^{61}Cu$.

configuration of $n_0 = 4(1,3,0)$ exclusively described the experimental data for this reaction, for other reactions partially extreme discrepancies between theory and experiment were observed. Exemplarily this is shown in fig. 2

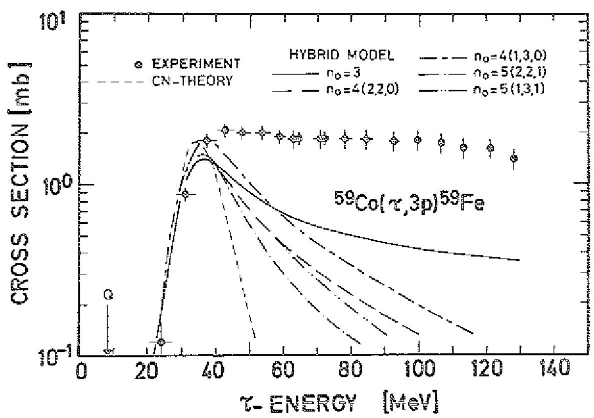

Figure 2: Experimental cross sections and theoretical predictions for the reaction $^{59}Co(^3He,3p)^{59}Fe$.

for the reaction $^{59}Co(^3He,3p)^{59}Fe$. For energies above 40 MeV the calculations underestimate the experimental data up to a factor of 5. For nearly all reactions of the type $\{(^3He,xpyn), x = 1,2\}$ the experimental cross sections are considerably higher than the theoretical ones in their high energy parts by up to one order of magnitude. For the explanation of the observed discrepancies break-up of the incoming ^{3}He-particle as well as double stripping may be assumed. Moreover, contributions of preequilibrium α-emission were to be seen giving rise to discrepancies between theory and experiment in the low energy part of the excitation functions. All the results[5] indicate that the initial states of ^{3}He-induced reactions are more complicated than assumed by the present forms of preequilibrium theories, as it was also stated earlier for α-induced reactions[2,3].

In contrast, the theoretical predictions of integral excitation functions for ^{2}H-induced reactions on cobalt[6] were in much better agreement with our new experimental data than for ^{3}He- and ^{4}He-induced reactions[2,3,5]. An example is given in fig. 3 for the reaction $^{59}Co(d,p2n)^{58m+g}Co$.

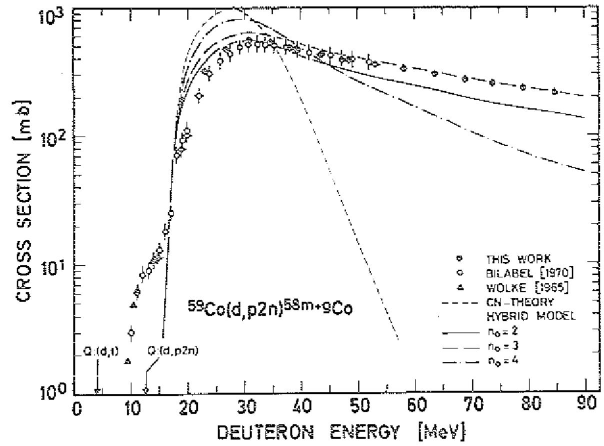

Figure 3: Experimental cross sections and theoretical predictions for the reaction $^{59}Co(^2H,p2n)^{58m+g}Co$. For the work of other authors see references in[6]

In general, the $\{(d,xpyn)\ x = 0\text{-}7,\ y = 0\text{-}8\}$-reactions are well described by the calculations and the agreement between theory and experiment is similarly good as observed for p-induced reactions earlier[1]. Only very particular reaction types, e.g. $(^2H,p)$ and $(^2H,2p)$ are affected by direct reactions, resulting in discrepancies between theory and experiment.

Furthermore, we started to measure integral excitation functions for the production of radionuclides from lutetium by p-induced reactions between 15 and 45 MeV. Lu is of particular interest, since it is supposed to be useful as a flux monitor in medium energy experiments for the evaluation of primary and secondary nucleon fluxes. Up to now, integral excitation functions for $\{(p,pxn), x=1\text{-}4\}$ and $\{(p,xn), x = 1, 3\text{-}5\}$ were mearsured. Also these experimental cross sections were compared with calculated ones based, however, on the new version of the computer code for the hybrid model "ALICE LIVERMORE 82"[7]. The particular advantage of this new code is the inclusion of multiple preequilibrium emission and the use of experimental mass data, in spite of those from mass formulas over wide mass ranges. Although these investigations are not yet finished, a preliminary data analysis showed that for Lu the theoretical cross sections are not as good as for the light elements[1]. In most cases, the predicted values were too small by a factor of 2. A detailed analysis of the experimental data will be necessary, however, before final conclusions can be drawn.

References

1) R. Michel, G. Brinkmann, H. Weigel, W. Herr, Nucl. Phys. A322 (1979) 40
2) R. Michel, G. Brinkmann, Nucl. Phys. A338 (1980) 167
3) R. Michel, G. Brinkmann, R. Stück, Radiochimica Acta 32 (1983) 173
4) M. Blann, COO-3494-10 (1973), COO-3494-29 (1976)
5) R. Michel, M. Galas, Nucl. Phys. A404 (1983) 77
6) R. Michel, M. Galas, Int. J. Appl. Rad. Isot. 34 (1983) 1325
7) M. Blann, LLNL-Report (1982) UCID-19614

+Institut für Kernchemie der Universität zu Köln, F.R. Germany

2. NUCLEAR SPECTROSCOPY

2.1. Study of ^{75}Se by Neutron Capture and SU(3) - SU(5) Transition in Quadrupole-Phonon Representation

Y. Tokunaga, H. Seyfarth, O.W.B. Schult, S. Brant[+], *V. Paar*[+], *D. Vretenar*[+], *H.G. Börner*[++], *G. Barreau*[++], *H. Faust*[++], *Ch. Hofmeyr*[*], *K. Schreckenbach*[++] *and R.A. Meyer*[**]

The γ- and e^- spectra following thermal neutron capture in ^{74}Se were studied with curved-crystal, β, and pair spectrometers. Precise energies have been obtained for the transitions and levels at low energies[1,2]. Two primary E2 transitions were found. The neutron separation energy for ^{75}Se was determined as 8027.6 keV. Precise γ energies following the electron capture decay of ^{75}Se were also measured, resulting in precise level energies in ^{75}As.

The calculation of the energy levels in ^{75}Se has been performed in the SU(6) particle-vibration model (PTQM) and 27 theoretical states have been tentatively assigned to the experimental levels. The spectrum of the core nucleus ^{74}Se has been calculated in the SU(6) quadrupole phonon model (TQM). The structure of theoretical states, the relation to SU(3) and SU(5) limits and potential energy surface are discussed[3]. Also, an overview is presented to theoretical explanations of the I=j, j-1, j-2 anomalous triplet emphasizing the rule with shell-model classification corrected for quadrupole phonons.

The level scheme of ^{75}Se and the information on the observed states and their mode of decay derived directly from the obtained (n,γ)-data have been given in a contribution in the last Annual Report[4]. In the present contribution the emphasis will be on the theoretical calculation and the comparison with the observed level energies.

Theoretically the levels in ^{75}Se are described by coupling a quasi-neutron to the anharmonic quadrupole vibrational core ^{74}Se, which is calculated in the truncated quadrupole phonon model[5,6]. The TQM Hamiltonian

$$H_{TQM} = h_1 \hat{N} + h_2 \{(b^+b^+)_0 \,|(N-\hat{N})(N-\hat{N}-1)|^{1/2} + H.C.\}$$
$$+ h_3 \{(b^+b^+\tilde{b})_0 \,(N-\hat{N})^{1/2} + H.C.\} +$$
$$+ \sum_{L=0,2,4} h_{4L} \{(b^+b^+)_L \,(\tilde{b}\tilde{b})_L\}_0$$

is diagonalized[3] in the basis $|n\ v\ I\rangle$, where n is the number of quadrupole phonons. With N=8 the anharmonicity parameters h_1, h_2, h_3, h_{4L} have been obtained from a fit to the levels of ^{74}Se. These parameters can now be compared with what is expected in the SU(5) limit (h_1 should be large and $h_2 = h_3 = 0$) or in the SU(3) limit, where four linearly independent relations between the parameters yield only two to be chosen as free parameters. It turns out that the fitted h_1 is large[3] and h_2 and h_3 are quite small, indicative of SU(5) character of ^{74}Se. On the other hand, taking the fitted h_3 and h_{4L} as input values for the SU(3) scheme, one obtains a set of parameters which agree in sign with those obtained in the fit. This suggests a SU(3) - SU(5) transition.

The calculation of the potential energy surface yields for ^{74}Se a prolate but not very pronounced minimum and γ-softness.

The levels of ^{75}Se are calculated in SU(6) particle-quadrupole phonon model PTQM[6] with

$$H_{PTQM} = H_p + H_{TQM} + H_{PVI},$$

where the last term is the SU(6) particle-vibration interaction[3,6]. Only the strength parameters Γ_0, Λ_0 and A_0 and the occupation probability $v^2_{\tilde{g}_{9/2}}$ were fitted to the experimental levels[3]. The calculated PTQM wave functions[3] show complete breaking of the weak-coupling classification. The largest quasiparticle-phonon component of $|9/2^+_1\rangle$ is $0.64|\tilde{g}_{9/2}, 46; 9/2\rangle$ which contains 4 phonons coupled to I=6. For the wave functions of the low-lying states a systematic shift of the largest components is seen towards the middle ($n \sim N/2 = 4$) of the phonon space. This is characteristic of the SU(6) quadrupole phonon wave functions in the SU(3) limit[6]. However, the wave functions for ^{75}Se exhibit pronounced leading components which implies that the SU(5) character is still present.

References

1) Y. Tokunaga, Thesis, University of Köln, Jül-Spez 158 (1982)
2) Y. Tokunaga and H.G. Börner, Jül-Spez 145 (1982)
3) Y. Tokunaga, H. Seyfarth, O.W.B. Schult, S. Brant, V. Paar, D. Vretenar, H.G. Börner, G. Barreau, H. Faust, Ch. Hofmeyr, K. Schreckenbach and R.A. Meyer, submitted for publication to Nucl. Phys.
4) Y. Tokunaga, H.G. Börner, G. Barreau, H. Faust, Ch. Hofmeyr, K. Schreckenbach, H. Seyfarth and O.W.B. Schult, IKP-Annual Report (1982), Jül-Spez 202
5) D. Janssen, R.V. Jolos and F. Dönau, Nucl. Phys. A224 (1974) 93
6) V. Paar, S. Brant, L.F. Canto, G. Leander and M. Vouk, Nucl. Phys. A378 (1982) 41

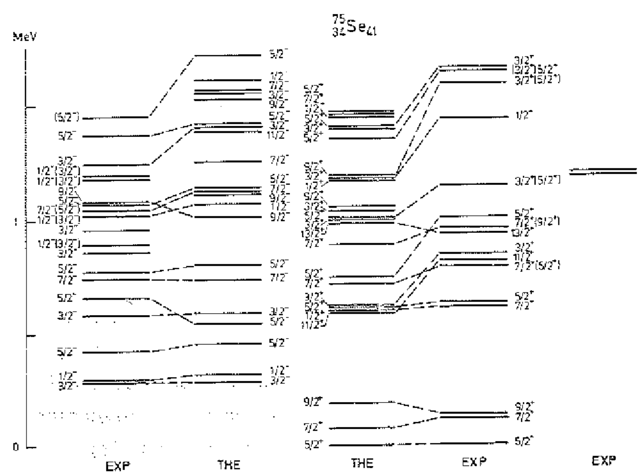

Fig. 1: Calculated and experimental levels in ^{75}Se. The assignments of the calculated levels are tentative.

[+] Prirodoslovno-matematicki fakultet, University of Zagreb, Marulicev trg 19, Zagreb, Yugoslavia

[++] Institut Laue-Langevin, F-38045 Grenoble, France

[*] NUCOR, Private bag X256, Pretoria 0001, Republic of South Africa

[**] permanent address: Nuclear Chemistry Division, Lawrence Livermore Laboratory, Livermore, Ca. 94550, USA

2.2. The $^{75}Se(n,\gamma)^{76}Se$ Reaction and the Low-Lying Level Structure of ^{76}Se

Y. Tokunaga, H. Seyfarth, O.W.B. Schult, H.G. Börner[+]*, Ch. Hofmeyr*[++]*, G. Barreau*[+]*, R. Brissot*[+]*, U. Kaup*[+++] *and Ch. Mönkemeyer*[+++]

The $^{75}Se(n,\gamma)^{76}Se$ reaction was studied through consecutive neutron capture with the use of pair and curved crystal spectrometers[1)]. The high-resolution data have allowed construction of a very well established level scheme including many new levels above ≈ 2.8 MeV excitation energy[2,3)]. The resulting neutron binding energy, 11154.0 ± 0.3 keV, is lower than the value given in the mass table[4)]. The $^{75}Se(n,\gamma)$ cross section was determined to be 330 ± 100 b. The level scheme and branching ratios were compared with results from IBM calculations.

These calculations were carried out both in IBM-1[5)] and in the framework of IBM-2[6)] which treats protons and neutrons separately. In this model, which has some connection to the shell model, we have tried to keep as close as possible to microscopic formulas for the parameters of the hamiltonian which have been derived by Otsuka, Arima and Iachello[7)] under the simplifying assmuption of a degenerate major shell. The calculations have been performend systematically for $^{72-80}Se$ and $^{74-82}Kr$, trying to give a description with few constants only. By using the microscopic formulas only two parameters had to be fitted to each nucleus, while three more parameters could be determined without fitting. However, it turned out[8)] that this program can be carried out only if one does not attempt to describe the 0_2^+ excitation in any of these nuclei. Hence we assumed that this state is an intruder. Of course, in this way we cannot prove that it is not possible to reproduce these states in the IBM. This is rather a consequence of the requirement that the model parameters should vary smoothly and regularly. Had we used more free parameters in the calculations, we could have obtained agreement at least for the level energies. We have to show, therefore, that in this case we obtain poor wave functions for the excited 0^+ states. This has been done by means of an IBM-1 calculation with all 6 parameters of the model hamiltonian varied freely. If the mixing of the noncollective degrees of freedom of the 0_2^+ state with the collective space is strong, IBM-1 could even work better than IBM-2. Both attempts rely on rather crude assumptions, and it is not clear a priori that any of the standard collective models is suited for the description of the selenium isotopes. The branching ratios measured in the (n,γ) experiments and B(E2) values and quadrupole moments from other measurements served for testing the model wave functions.

Further details about the calculations are given elsewhere[3)]. The models reproduce the level energies quite well (see Fig. 1). IBM-1, with more parameters fits better only the 0^+ states. The other levels agree better with IBM-2, which fails to explain the 0^+ levels. This suggests that the structure of the excited 0^+ states contains a significant fraction of noncollective degrees of freedom. This is obvious also from the fact that the models cannot explain satisfactorily the measured branching ratios[3)].

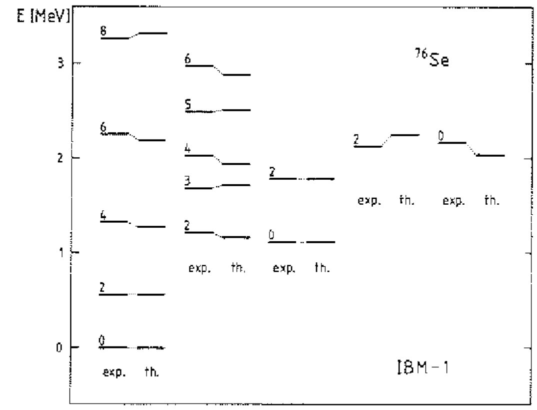

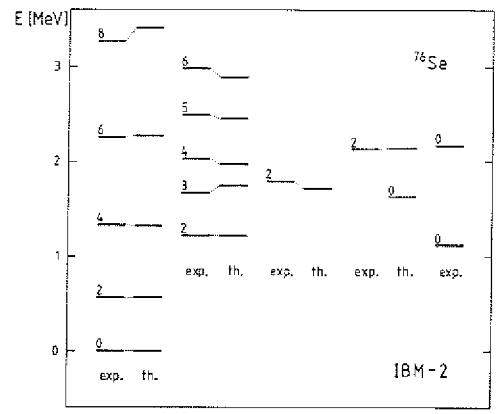

Fig. 1: Comparison of the experimental level energies with energies calculated in the framework of IBM-1 and IBM-2.

References

1) Y. Tokunaga, H.G. Börner, Ch. Hofmeyr, G. Barreau, R. Brissot, H. Seyfarth and O.W.B. Schult, Annual Report 1982, Jül-Spez 202 (1983) 38
2) Y. Tokunaga, thesis University of Köln, Jül-Spez 158 (1982) and Y. Tokunaga and H.G. Börner, Jül-Spez 145 (1982)
3) Y. Tokunaga, H. Seyfarth, O.W.B. Schult, H.G. Börner, Ch. Hofmeyr, G. Barreau, R. Brissot, U. Kaup and Ch. Mönkemeyer, Nucl. Phys. A411 (1983) 209
4) A.H. Wapstra and K. Bos, Atomic Data and Nuclear Data Tables 19 (1977) 231
5) A. Arima and F. Iachello, Ann. Phys. 99 (1976) 253, 111 (1978) 201, 123 (1979) 468
6) T. Otsuka, A. Arima, F. Iachello and I. Talmi, Phys. Lett. 76B (1978) 139
7) T. Otsuka, A. Arima and F. Iachello, Nucl. Phys. A309 (1978) 1
8) M. Matoba, M. Hyakutake, N. Katori and Y. Irie, Nucl. Phys. A325 (1979) 389

[+] Institut Laue-Langevin, F-38045 Grenoble, France
[++] NUCOR, Private bag X256, Pretoria 0001, Republic of South Africa
[+++] Institut für Kernphysik, Universität zu Köln, D-5000 Köln 1, West Germany

2.3. Low-lying levels of ^{77}Se studied through thermal neutron capture and evidence for a new term in the E2 operator of TQM(IBM)

Y. Tokunaga, H. Seyfarth, R.A. Meyer[+]*, O.W.B. Schult, H.G. Börner*[++]*, G. Barreau*[++]*, H. Faust*[++]*, K. Schreckenbach*[++]*, S. Brant*[+++]*, V. Paar*[+++]*, M. Vouk*[+++] *and D. Vretenar*[+++]

A high resolution study of the ^{76}Se(n,γ) reaction was carried out with curved crystal spectrometers at the ILL, Grenoble, and with a pair spectrometer at Jülich. Also conversion electrons were measured at the ILL following slow-neutron capture. The resulting data[1] yield very precise level energies and allow a detailed study of the decay scheme[2]. Spin and parity assignments were obtained for most of the levels, and their decay modes could be clarified. The neutron separation energy of ^{77}Se was measured as 7418.85 keV. The calculation of the energy levels in ^{77}Se has been performed in the SU(6) particle-vibration model (PTQM), by using ^{76}Se as a SU(5) vibrational core and the same particle-vibration interaction strengths as in the PTQM calculation for ^{75}Se. In this frame there is evidence for a $\Delta n = 2$ term in the E2 operator. This term has not been included so far in TQM and IBM calculations.

A short report on the experimental results has been given elsewhere[3]; also the obtained level scheme has been presented in this report. In the present report the emphasis is on the comparison of the experimental data with the PTQM[4]. The TQM calculation of the ^{76}Se core was performed in the SU(5) limit. In the PTQM calculation for ^{77}Se we have used BCS quasiparticle energies and occupation probabilities obtained by solving the BCS gap equations. These values were assumed to be the same as in the previous calculation for ^{75}Se. Also the same particle-vibration strengths have been taken as for ^{75}Se: $A_0 = 0.1$ MeV, $\Gamma_0 = 0.4$ MeV, $\Lambda_0 = 24.35$ MeV and $\chi = -\sqrt{7}/2$. In this way no parameters were fitted, the only difference being in the cores, ^{76}Se being close to SU(5) and ^{74}Se being between SU(3) and SU(5).

Thus the phonon distributions in the wave functions of the $5/2_1^+$, $7/2_1^+$ and $9/2_1^+$ states of ^{77}Se are rather narrow[5] but more spread out in the non-SU(5) nucleus ^{75}Se.

Wave functions with a narrow phonon distribution pose an intriguing problem in describing transitions. Namely, if the singularly large components in the initial and final states differ by two phonons, there emerges the possibility to have coherent and sizeable contributions to the matrix elements of $\Delta n = 2$ operators; and these have not been included so far in IBM-IBFM and TQM-PTQM calculations.

The E2 operator of PTQM reads

$$M_\mu^{PTQM}(E2) = M_\mu^{SP}(E2) + M_\mu^{TQM}(E2).$$

Here, $M_\mu^{SP}(E2)$ is the standard single-particle (quasiparticle) E2 operator and $M_\mu^{TQM}(E2)$ is the quadrupole phonon E2 operator of TQM:

$$M_\mu^{TQM}(E2) = e_v\left[b_\mu^+\sqrt{N-\hat{N}} + \sqrt{N-\hat{N}}\,\tilde{b}_\mu + \chi(b^+\tilde{b})_{2\mu}\right],$$

with conveniently defined effective charge $e_v = \frac{3}{4\pi}\, e^{VIB}(eR_0)^2$.

However, using RPA for quadrupole phonons of TQM and including diagrams up to the second order there arises the following corrected form of E2 operator[6]:

$$M_\mu^{cTQM}(E2) = M_\mu^{TQM}(E2) + M_\mu^{TQM,\Delta n=2}(E2).$$

Here, $M_\mu^{TQM}(E2)$ is the standard E2 operator of TQM and the additional term of $\Delta n = 2$ type reads

$$M_\mu^{TQM,\Delta n=2}(E2) = e_v\chi'\left[(b^+b^+)_{2\mu}\sqrt{(N-\hat{N})(N-\hat{N}-1)} + \sqrt{(N-N)(N-N-1)}\,(\tilde{b}\tilde{b})_{2\mu}\right].$$

In the microscopic derivation the new, $\Delta n = 2$ term arises in the same diagrammatic order as the standard $\Delta n = 0$ term $\chi(b^+\tilde{b})_{2\mu}$, giving a hint that this additional term has to be included in the E2 operator of TQM/IBM. In this light, it will be interesting to reinvestigate the calculations for E2 properties in IBM and TQM performed so far.

The new term gives sizeable contributions to the E2 transitions with large $\Delta n = 2$ overlaps between the wave functions of the initial and final state. Such a case is the $5/2_1^+ \to 9/2_1^+$ E2 transition in our PTQM calculation for ^{77}Se; the $\Delta n = 2$ contribution amounts to more than 99 % of the overlap between the wave functions of $5/2_1^+$ and $9/2_1^+$ states. Therefore, B(E2, $5/2_1^+ \to 9/2_1^+$) is very small (10^{-5}) if one employs the standard E2 operator of PTQM, which is contrary to experiment (0.09). On the other hand, including new $\Delta n = 2$ term in the E2 operator we get sizeable coherent contributions (0.11).

References

1) Y. Tokunaga and H.G. Börner, Jül-Spez.145 (1982)

2) Y. Tokunaga, Thesis, University of Köln, Jül-Spez 158 (1982)

3) Y. Tokunaga, H.G. Börner, H. Seyfarth, G. Barreau, H. Faust, K. Schreckenbach and O.W.B. Schult, Annual Report IKP, KFA Jülich, Jül-Spez 202 (1983)

4) V. Paar, S. Brant, L.F. Canto, G. Leander and M. Vouk, Nucl. Phys. A378 (1982) 41

5) Y. Tokunaga, H. Seyfarth, R.A. Meyer, O.W.B. Schult, H.G. Börner, G. Barreau, H. Faust, K. Schreckenbach, S. Brant, V. Paar, M. Vouk, D. Vretenar, to be published

6) V. Paar and S. Brant, to be published

+ Permanent address: Nuclear Chemistry Division, Lawrence Livermore National Laboratory, Livermore, California 94550, USA

++ Institute Laue-Langevin, F-38045 Grenoble, France

+++ Prirodoslovno-matematicki fakultet, University of Zagreb, Marulicer trg 19, Zagreb, Yugoslavia

2.4. Rotation-Like $5/2^+$ Bands in Odd-Mass A ∼ 100 Nuclei as Coherent-State Structures of Quadrupole Phonons in PTQM

R.A. Meyer$^+$, *V. Paar*$^{++}$, *S. Brant*$^{++}$

Recent investigations of nuclei far from stability have pointed to the possibility of odd-mass symmetric-rotational nuclei in the medium mass region of the nuclear chart (70 ≤ A ≤ 120). Among the odd-proton nuclei, a $5/2^+$ ground state (g.s.) band with members to $19/2^+$ has been found[1] for $^{99}_{39}Y_{60}$ and similar bands (with a smaller number of identified members) have been observed[2-4] in ^{101}Y, ^{101}Nb and ^{103}Nb. These bands have been discussed within the context of a |422 5/2| Nilsson band[1,2-5]. Here we investigate them within the PTQM[6].

This quadrupole phonon model employes a spherical representation (particle-phonon coupling). The PTQM Hamiltonian which is a particular (SU(6)-type) anharmonic quadrupole phonon model and particle-vibration interaction is diagonalized in a standard particle-vibration basis. The calculations have been performed for ^{99}Y which is taken as typical for this region. The TQM vibrational core has been determined in order to reproduce the low lying levels in ^{98}Sr. The maximum number of quadrupole phonons is N=7, the particle-vibration interaction strengths were fitted to ^{99}Y and are with $A_0 = 0$, $\Gamma_0 = 0.477$ and $\Lambda_0 = 4.77$ close to the values used[7] for $^{101}_{42}Mo_{59}$.

The low lying spectrum is presented in fig. 1 together with part of the experimental level scheme[1,8] of ^{99}Y. The ground state band is well reproduced and several side bands are predicted. Candidates for members of these bands are available[8]. It should be pointed out that K has not the conventional geometrical meaning in PTQM but is defined quantum-mechanically[9].

In the quadrupole-phonon representation, a deformed rotational state appears as a quantum-mechanical coherent state with the number of quadrupole phonons N → ∞. The coherent state has a Gaussian-type distribution of quadrupole phonons centered[6] around $\bar{n} \sim \frac{2}{3}N$. The phonon distribution is the same for all states of the g.s. rotational band.
In the odd-mass nucleus the PTQM analogs of Nilsson bands exhibit a similar type of phonon composition which can be interpreted as a supersymmetric pattern[10].

The phonon compositions of the states of the "K" = 5/2 band are shown in fig. 2. There is indeed an apparent similarity to the quantum-mechanical coherent state with the maximum at $\bar{n} \sim \frac{2}{3} \cdot 7 \sim 5$. The concept of a true static deformation which would correspond to N → ∞ is far from being realized.

It is interesting to note the difference in the phonon compositions for ^{99}Y and for $^{75}_{34}Se_{41}$, which is also shown in fig. 2. For the latter the $\bar{n}$ shifts to lower N and is more strongly peaked although ^{75}Se is a unique parity $g_{9/2}$ nucleus with a $5/2^+$ ground state. It apparently does not belong to the SU(3) class of nuclei.

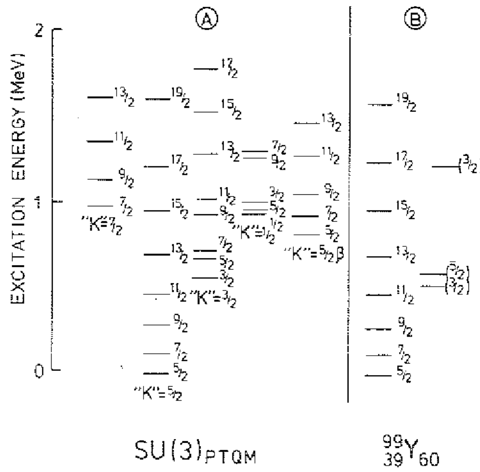

Fig. 1: Comparison of calculated and measured levels in ^{99}Y.

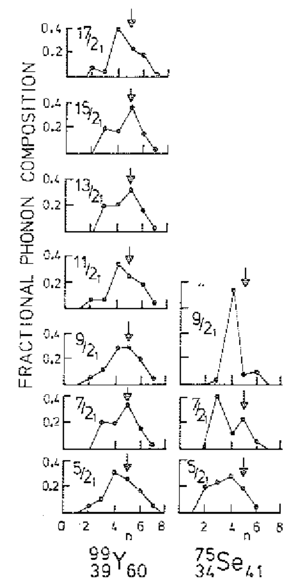

Fig. 2: Quadrupole phonon composition of the PTQM wave functions of the states of "K" = 5/2 band. PTQM wave function of the state $|J_K\rangle$ in the standard particle-vibration basis reads:

$$|J_K\rangle = \sum_{jn\nu I} \xi^{J_K}_{jn\nu I} \, |j, n\nu I; J\rangle$$

There, in the basis state $|j, n\nu I; J\rangle$ the single-particle state of j and the n-phonon state of angular momentum I are coupled to the total angular momentum J; the quantity $\xi^J_{jn\nu I}$ denotes the amplitude of the basis state $|j, n\nu I\rangle$ in the wave function $|J_K\rangle$. a) In the ^{99}Y calculation there is $j = g_{9/2}$, $n \le N = 7$. For each we present the phonon composition given by

$$A(n) = \sum_{\nu I} (\xi^{J_1}_{9/2, n\nu I})^2$$

b) Similar plot for lowest $5/2_1$, $7/2_1$, $9/2_1$ ... in ^{75}Se.

References
1) E. Monnand et al., Z. Physik A306, 183 (1982)
2) F.K. Wohn et al., Phys. Rev. Lett. 51, 873 (1983)
3) A.-M. Schmitt et al., Contribution to this Annual Report, p. 41
4) T. Seo, et al., to be published in Z. Physik and contribution to this Annual Report
5) R.A. Meyer et al., submitted to Nucl. Phys.
6) V. Paar et al., Nucl. Phys. A378, 41 (1982)
7) S. Brant et al., to be published
8) B. Pfeiffer, ILL Grenoble, private communication
9) D. Sunko et al., to be published
10) G. Winter et al., Z. Physik A309, 243 (1983)

+ 1982/83 on leave of absence from Lawrence Livermore National Laboratory, Livermore, Ca. 94550, USA

++ Visitors from University of Zagreb, Zagreb, Yugoslavia

2.5. New Excited 0^+ State in ^{100}Zr

K. Sistemich, R.F. Petry[+]*, J.C. Hill*[++]*, F.K. Wohn*[++]*, R.L. Gill*[+++]*, H. Mach*[+++]*, A. Piotrowski*[+++]

The nucleus $^{100}_{40}Zr_{60}$ has very remarkable features. It is the first heavy Zr isotope which shows rotational properties[1)] while its immediate even-even neighbour $^{98}_{40}Zr_{58}$ has shell-model character[2)] ($E_{2_1^+}$ = 1223 keV). The first excited 0^+ state of ^{100}Zr has been observed at 331 keV which indicates an asymmetric nuclear shape[3)]. This level cannot be the head of a β band.

In order to get more information on the level scheme and thus on the structure the nucleus ^{100}Zr has been reinvestigated through the β decay of ^{100}Y at the fission product separator TRISTAN[4)] at the High Flux Beam Reactor of the Brookhaven National Laboratory. Many new γ transitions in ^{100}Zr have been observed and the construction of an extended level scheme is in progress.

A first result is the evidence for the existence of a second excited 0^+ level at 830 keV. A γ-γ angular correlation measurement has been performed using a four-Ge detector setup[5)]. The result is shown in fig. 1. The correlation pattern of the 617-213 keV cascade is the same as the one for the well known 0^+-2^+-0^+ cascade of 119-213 keV. The depopulation of the 830 keV level only by the transition of 617 keV into the 2_1^+ state is consistent with the assignment of 0^+ for the spin and parity of this level. (It should be pointed out that the existence of the 617 keV transition had been observed already in recent investigations at the separators OSTIS[6)] and JOSEF.)

As far as its energy is concerned the new 0^+ level is a good candidate for being the head of a β band. The further analysis of the results from the experiments at TRISTAN will show whether other members of this band are present. Shell model calculations[7)] on the shape transition in the heavy even Zr and Mo isotopes could reproduce the drop of the 0_2^+ levels between ^{98}Zr and ^{100}Zr as well as the existence of three excited 0^+ levels in ^{98}Zr below 2 MeV. It would be of interest to see whether this type of calculations could also explain the existence of the new 0_3^+ level in ^{100}Zr.

References
1) E. Cheifetz et al., Phys. Rev. Lett. 25, 38 (1971)
2) K. Sistemich et al., Z. Physik A281, 169 (1977)
3) T.A. Khan et al., Z. Physik A284, 313 (1978)
4) D.S. Brenner et al., in Proc. Int. Symp. on Future Directions in Studies of Nuclei far from Stability, Nashville, Tennessee, 1979, ed. J.H. Hamilton et al., (North Holland, Amsterdam, 1980) p. 389
5) A. Wolf et al., Nucl. Instr. Meth. 206, 397 (1983)
6) B. Pfeiffer, ILL Grenoble, private communication
7) P. Federman and S. Pittel, Phys. Rev. C20, 820 (1979)

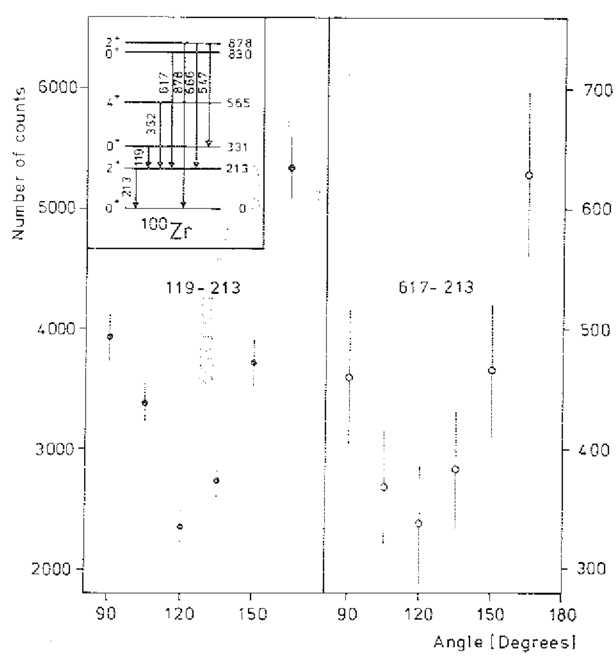

Fig. 1: Preliminary result of the γγ angular correlation measurements. The inset shows a partial level scheme of ^{100}Zr.

+ University of Oklahoma, Norman, Ok 73069, USA

++ Ames Laboratory DOE and Iowa State University, Ames, Ia 50011, USA

+++ Brookhaven National Laboratory, Upton, NY 11973, USA

2.6. Angular correlation measurements on ^{100}Mo

G. Menzen, H. Gietz[+]*, G. Lhersonneau, P. Kohl, H. Lawin, T. Seo*[++]*, K. Sistemich, N. Kaffrell*[+]

The determination of the angular momenta of the excited states is of importance for the understanding of the onset of deformation at the neutron rich nuclei with $A \sim 100$. In particular, the identification of 0^+-levels provides crucial probes for theoretical description of the shape transition in this nuclear region. Fig. 1 shows a partial level scheme of the nucleus ^{100}Mo.

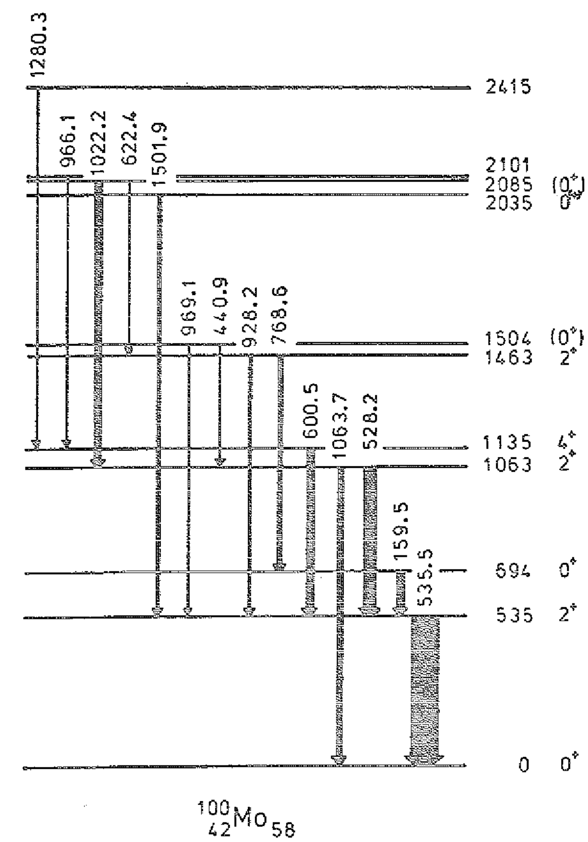

Fig. 1: Partial level scheme of ^{100}Mo

To study the spins of excited states of ^{100}Mo γ,γ-angular correlation measurements have been performed at the fission product separator JOSEF[1]. An arrangement of three Ge(Li) detectors, one being movable, on a goniometer-table was used, which is similar to the one described in ref. 2. The analysis of the data has been carried out and the first results show an I = 0 assignment to the state of 2035 keV. The data were normalized with the well known angular correlation of the 0-2-0 transition of the 159-535 keV cascade, measured simultaneously. Fig. 2 shows the 0-2-0 angular distribution for the latter (left) and for the 1500-535 transition (right hand side). The dotted curve gives a fit to the experimental values and the solid curve the theoretical pattern for a 0-2-0 cascade (solid angle corrections of the detectors have been taken into account).

The measurements indicate also I = 0 for the state at 2085 keV. Recent TQM calculations of Paar et al.[3] on ^{100}Mo give a 0^+-state at 1720 keV and another one at 2250 keV. Probably the experimental I = 0 states can be assigned to these predicted 0^+-levels. To get more information about the ^{100}Mo-structure, it is of interest to proof the parity of the I = 0 states and to look for bands built on them.

References

1) H. Lawin, J. Eidens, J.W. Borgs, R. Fabbri, J.W. Grüter, G. Joswig, T.A. Khan, W.D. Lauppe, G. Sadler, H.A. Selic, M. Shaanan, K. Sistemich, P. Armbruster, Nucl. Instr. Meth. 137 (1976) 103

2) H.A. Selic, G. Sadler, T.A. Khan, W.D. Lauppe, H. Lawin, K. Sistemich, Z. Physik A289 (1979) 197

3) V. Paar, S. Brant, University of Zagreb/Yugoslavia, private communication

[+] Institut für Kernchemie, University of Mainz, F.R. Germany

[++] On leave from Kyoto University, Japan

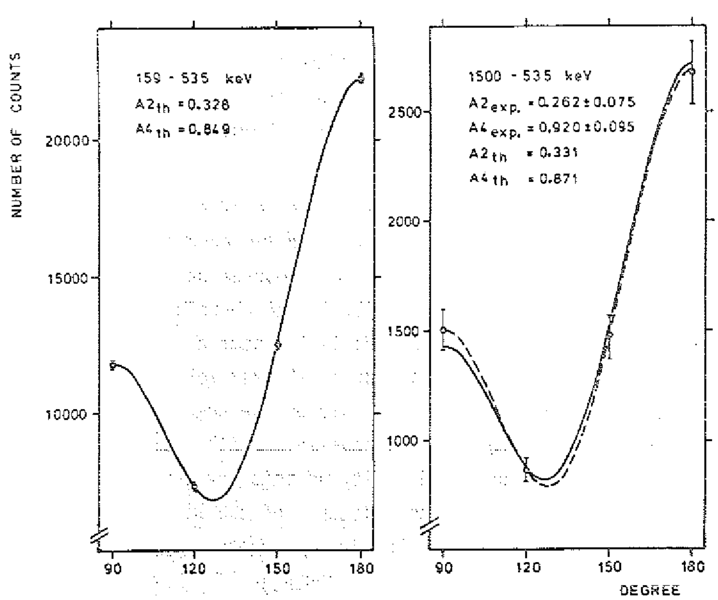

Fig. 2: Angular distribution for the 535-159 keV cascade (left) and for the 1500-535 keV cascade (right).

2.7. Nanosecond-Half-Lives of Nuclear Levels near A = 100

G. Lhersonneau, T. Seo+, H. Lawin, G. Menzen K. Sistemich

The study of the properties of deformed odd-mass nuclei around A = 100 which is currently performed at JOSEF, makes the knowledge of the half-lives of the lowest levels of these nuclei desirable. Therefore a systematic search for delayed γ-γ coincidences was undertaken using two intrinsic-Ge detectors with surfaces of 19 cm^2 and a Ge(Li) diode with a volume of 61 cm^3.

The half-lives in the ns region have been deduced from the measurements with the centroid shift method. The determination of the centroids for prompt coincidences as a function of the γ-ray energy was obtained from simultaneously measured γ-γ cascades of fission products with known level-lifetimes. Especially the γ radiation of ^{97}Zr, Ref. 1), and of ^{99}Nb, Ref. 2), with energies between 50 and 200 keV was used. Between these experimental points the centroid vs energy curve was interpolated with a simple smooth function.

For each γ-γ cascade which was used for the determination of an unknown level-half-life, two time distributions were obtained by starting the time-to-amplitude converter with each γ ray. After subtracting the influence of the γ-ray energy the difference of the centroid positions of these two distributions is equal to twice the mean-lifetime of the level which is fed and depopulated by them. An example for two such distributions is shown in Fig. 1.

The results for the Mo isotopes are given in Table 1 as examples. They are in part average values out of the data for more than one γ-γ cascade. The uncertainties include statistical as well as estimated systematic errors. The $t_{1/2}$ values for ^{100}Mo and ^{104}Mo agree well with those of other authors[3)] which shows the reliability of the applied procedure. The value for the 103 keV level of ^{103}Mo is considerably smaller than the result of Ref. 4) which points to a considerable deformation of this nucleus, see separate contribution to this Annual Report. Also the present half-life for the 95 keV level of ^{105}Mo is smaller than the one from an earlier measurement[5)]. Since the uncertainties almost overlap, the discrepancy is not as pronounced as in ^{103}Mo, but also here the new value indicates a stronger deformation (ε = 0.29(6)) than the one which corresponds[6)] to $t_{1/2}$ = 1.1 ns (ε = 0.21).

References

1) H.A. Selič, Thesis, Universität zu Köln (1977), Report Jül 1431 of KFA Jülich, F.R. Germany
2) G. Battistuzzi, K. Kawade, H. Lawin, K. Shizuma, K. Sistemich, Z. Physik A - Atoms and Nuclei 306, 113 (1982)
3) C.M. Lederer, V.S. Shirley, Table of Isotopes, Seventh Edition, New York: A. Wiley Sons Inc. 19
4) H.A. Selič, E. Cheifetz, J.B. Wilhelmy.: Jül-Spez-99, 69 (1981), Annual Report 1980 of IKP, Kernforschungsanlage Jülich, Germany
5) R.L. Watson, J.B. Wilhelmy, R.C. Jared, C. Rugge, H.R. Bowman, S.G. Thompson, J.O. Rasmussen: Nucl. Phys. A141, 449 (1970)
6) K. Shizuma, H. Ahrens, J.P. Bocquet, N. Kaffrell, B.D. Kern, H. Lawin, R.A. Meyer, K. Sistemich, G. Tittel and N. Trautmann, Z. Physik A - Atoms and Nuclei, 315, 65 (1984)

Table 1: Measured half-life values

Isotope	Level (keV)	$t_{1/2}$ (ns) present work	previous work	
^{103}Mo	103	0.45(16)	1.7(3)	(4)
^{105}Mo	95	0.54(25)	1.1(2)	(5)
^{100}Mo	695	1.81(23)	1.7(2)	(3)
^{104}Mo	192	1.05(15)	0.91(3)	(9)

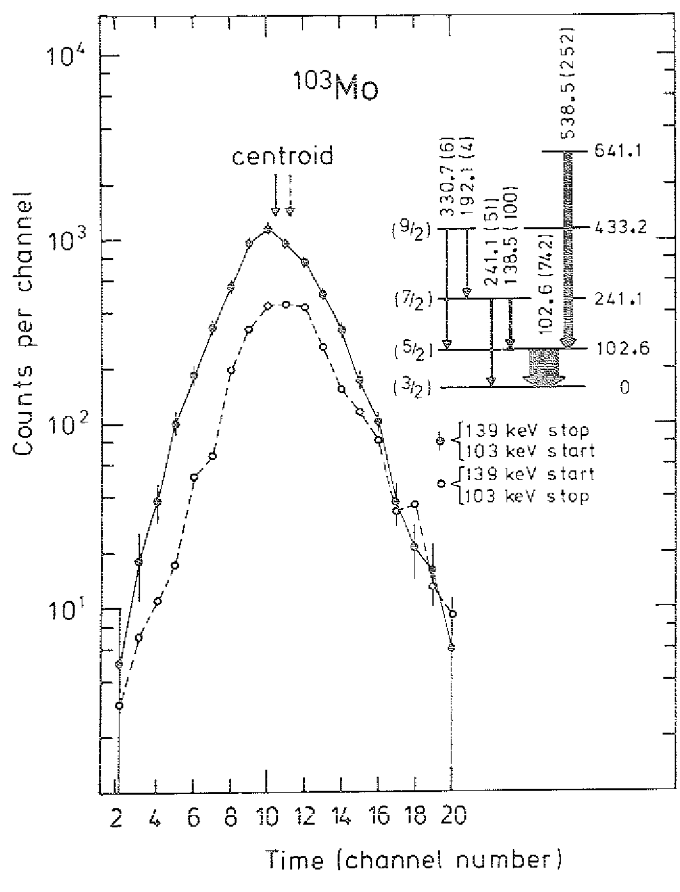

Fig. 1: Measured time distributions for γ-γ cascades in ^{103}Mo

+ on leave of absence from Kyoto University, Japan

2.8. The Deformation of $^{103}_{42}Mo_{61}$

T. Seo⁺, *G. Lhersonneau, H. Lawin, R.A. Meyer*⁺⁺, *G. Menzen, K. Sistemich*

In a recent publication[1] it was shown that the lowest levels of ^{103}Mo (and of ^{105}Mo) fit into a rotational band which shows fingerprints of a ν[411 3/2] Nilsson configuration, see Fig. 1. The half-life of (1.7 ± 0.3) ns of Selič et al.[2] was used to deduce the reduced transition probability B(E2) of 44 spu for the 102.6 keV ground-state transition and the intrinsic quadrupole moment of $|Q_0|$ = 1.92 barn as well as the deformation parameter of $|\varepsilon| \sim 0.17$. It was pointed out that these values are small compared to the corresponding quantities for the neighbouring even-even nuclei and that the value for $t_{1/2}$ (102.6 keV) of Ref. 2 has to be considered as an upper limit.

In order to clear up this apparent discrepancy between the rotational pattern of the levels and the low values of the above-mentioned quantities, the half-life of the 102.6 keV level has been re-measured at JOSEF. The experiment is described in the preceding contribution to this Annual Report. The result of $t_{1/2}$ = (0.45 ± 0.16) ns deviates indeed, considerably from the old value. The latter one had been determined through measuring the time behaviour of the emission of the 102.6 keV transition with respect to the fission events of ^{252}Cf and it might have been contaminated[1] by γ radiation which feeds into the 102.6 keV level.

The new result leads to values of

B(E2: 103 keV) = (176 ± 63) spu

Q_0 = 3.9(0.7) barn

ε = 0.3(0.05)

which are consistent with a strong deformation of ^{103}Mo.

References

1) K. Shizuma, H. Ahrens, J.P. Bocquet, N. Kaffrell, B.D. Kern, H. Lawin, R.A. Meyer, K. Sistemich, G. Tittel and N. Trautmann, Z. Physik A - Atoms and Nuclei 314,

2) H.A. Selič, E. Cheifetz, J.B. Wilhelmy, Annual Report of the IKP, KFA Jülich 1980, Report JÜl-Spez-99, ISSN0170-8937, p. 69

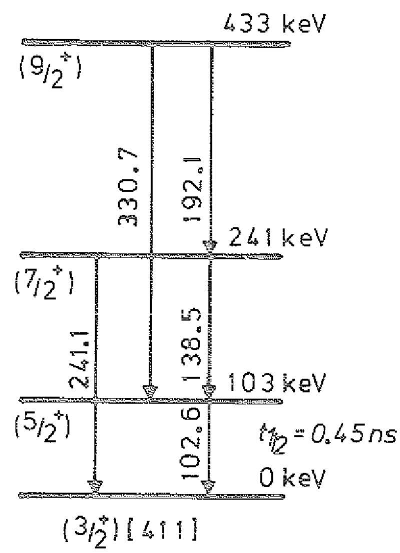

Fig. 1: The proposed[1] ground state band of ^{103}Mo

⁺ on leave of absence from Kyoto University, Japan

⁺⁺ on leave of absence (1982/83) from Lawrence Livermore National Laboratory, USA

2.9. Band Structures in $^{101}_{41}Nb_{60}$

A.-M. Schmitt[+], *T. Seo*[++], *H. Ahrens*[+++], *J.P. Bocquet*[*], *N. Kaffrell*[+], *H. Lawin*, *G. Lhersonneau*, *R.A. Meyer*[**], *K. Shizuma*[***], *K. Sistemich*, *G. Tittel*[+], *N. Trautmann*[+]

It has been observed recently that the level schemes of neutron-rich nuclei with odd masses in the region of A ~ 100 contain well developed rotational patterns. An outstanding example is ^{99}Y with a ground state band of eight members[1]. Evidence for band structures (or deformations) has also been reported for $^{97}_{37}Rb_{60}$, $^{99}_{38}Sr_{61}$, $^{101}_{40}Zr_{61}$, $^{103}_{42}Mo_{61}$, $^{105}_{42}Mo_{63}$, and single particle configurations could be assigned to the individual band heads in accordance with the standard Nilsson-model calculations. Here and in the following contribution to this Annual Report it is shown that also the odd-mass Nb isotopes with 60 or more neutrons can be interpreted in this frame.

The level scheme of ^{101}Nb has been studied through the β decay of ^{101}Zr with the fission product separators LOHENGRIN at the high flux reactor of the Institut Laue-Langevin in Grenoble and JOSEF at the reactor DIDO of the Kernforschungsanlage Jülich. The experiments have been described in ref. 2) and a level scheme has been proposed in ref. 3). The low lying levels up to 593 keV can all be grouped into three bands as is shown in fig. 1. Tentative Nilsson assignments are proposed for the band heads in agreement with the orbitals which are available near the Fermi surface at ε ~ 0.3, see fig. 1 of the contribution on ^{103}Nb to this Annual Report.

The attribution of the individual levels to the bands is based on the fact that the energies show a I(I+1) dependence with the proposed values of K and on the fact that all the expected intraband transitions have been observed.

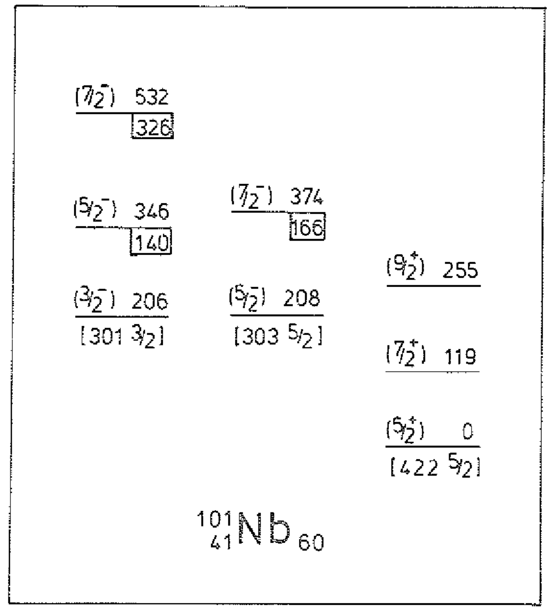

Fig. 1: Band structures in ^{101}Nb. Level energies and Nilsson-orbit assignments are given. Numbers below the levels indicate energies relative to the band heads.

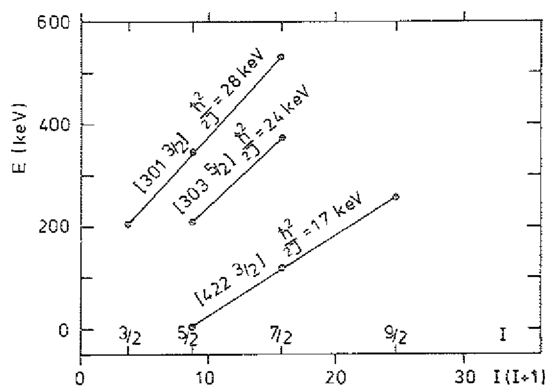

Fig. 2: Excitation energies of the band members vs. I(I+1).

[+] Universität Mainz, F.R. Germany
[++] on leave from Kyoto University, Japan
[+++] GSI Darmstadt, F.R. Germany
[*] Université de Grenoble, France
[**] on leave from Lawrence Livermore National Laboratory, USA
[***] on leave (1980-1982) from Hiroshima University, Japan

References
1) E. Monnand, J.A. Pinston, F. Schussler, B. Pfeiffer, H. Lawin, G. Battistuzzi, K. Shizuma, K. Sistemich, Z. Physik A - Atoms and Nuclei 306, 183 (1982)
2) K. Shizuma, H. Ahrens, J.P. Bocquet, N. Kaffrell, B.D. Kern, H. Lawin, R.A. Meyer, K. Sistemich, G. Tittel and N. Trautmann, Z. Physik A - Atoms and Nuclei 315, 65 (1984)
3) A.M.Schmitt, N. Kaffrell, N. Trautmann, Jahresbericht 1979 of Institut für Kernchemie, Universität Mainz

2.10. Rotational Bands in $^{103}_{41}Nb_{62}$

T. Seo+, *A.-M. Schmitt*++, *H. Ahrens*+++,
*J.P. Bocquet**, *N. Kaffrell*++, *H. Lawin*,
G. Lhersonneau, *R.A. Meyer***, *K. Shizuma****,
K. Sistemich, *G. Tittel*++, *N. Trautmann*++

As has been stated in the preceding contribution to this Annual Report, the observation of deformed structures in heavy isotopes of Rb, Sr, Y, Zr and Mo has initiated the search for rotational patterns in the neutron-rich Nb isotopes. An extended level scheme of ^{103}Nb has been obtained and the properties of the levels have been inspected with regard to their possible affiliation to bands.

The studies of ^{103}Nb were performed at the fission product separators JOSEF and LOHENGRIN through the β^- decay of ^{103}Zr. Gamma-ray singles and γ-γ as well as X ray-γ coincidence spectra were determined in experiments described in Ref. 1. At JOSEF the half-lives of individual levels have been measured with delayed γ-γ coincidences[2]. (A first level scheme from the results of LOHENGRIN has been given in Ref. 3.) Almost all of the levels below 750 keV can be placed in three rotational bands, see Fig. 1.

The energies of the band members show a linear I(I+1) dependence if the values of K = 5/2, 5/2 and 3/2 are assumed for the band heads at 0, 164 and 248 keV, respectively. All expected transitions inside the bands have been observed.

The Nilsson orbitals which are available[4] at the Fermi surface are depicted in the inset of Fig. 1. Since deformations around ε = 0.3 have been observed for the neighbouring even-even nuclei the probable proton configurations for the band heads in ^{103}Nb are [422 5/2], [303 5/2] and [301 3/2], respectively. The ratios $|(g_K - g_R)/Q_o|$ which can be deduced[1] from the relative intensities of the intraband transitions allow a sensitive test for the proposed configurations: Assuming Q_o = 3.6 barn (for $\varepsilon \sim 0.3$) and $g_R \sim Z/A$ the values of g_K have been determined for the different bands. As can be seen from the boxes in Fig. 1, they agree well with the theoretical estimates for the proposed Nilsson configurations.

Further support of the proposed interpretation of the low-lying levels in ^{103}Nb is the fact that the measured[2] half-lives of the band heads at 164 and 248 keV agree well with the Nilsson-model estimates[4] (including pairing), see Table 1.

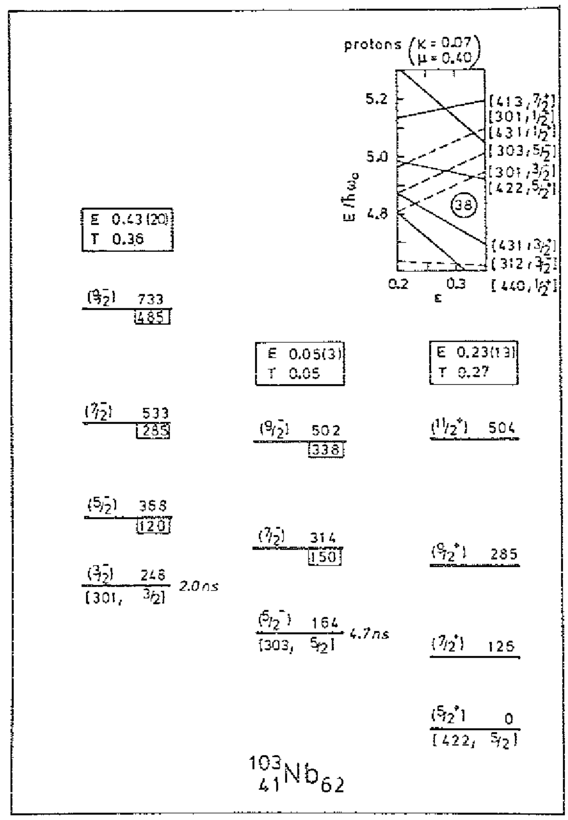

Fig. 1: Band structures in ^{103}Nb. Level energies and Nilsson-orbital assignments are given. Numbers below the levels indicate energies relative to the band heads. The boxes contain the experimental (E) and calculated (T) values of $|(g_K - g_R)/Q_o|$.

References

1) K. Shizuma et al.: Z. Physik A314, (1983)
2) G. Lhersonneau et al.: Contribution to this Annual Report, p. 39
3) A. Schmitt et al.: Jahresbericht 1979 des Inst. für Kernchemie, Universität Mainz, p. 34
4) I. Ragnarsson: Leysin Conference (1970), Report CERN 70-30, Vol. II, p. 847

+ on leave of absence from Kyoto University, Japan
++ Institut für Kernchemie, Universität Mainz, F.R.G.
+++ GSI Darmstadt, F.R.G.
* Université de Grenoble, France
** on leave of absence from Lawrence Livermore National Laboratory, USA
*** on leave of absence (1980-82) from Hiroshima University, Japan

Table 1: Measured and calculated half-lives of levels in ^{103}Nb

Level (keV)	Assignment	$t_{1/2}$(exp) (ns)	$t_{1/2}$(W) (ns)	$t_{1/2}$(N) (ns)	$t^P_{1/2}$(N) (ns)	F_W	F_N	F^P_N
164	[303 5/2] [422 5/2]	4.7(5)	$7.0\cdot10^{-5}$	2.8	20	$6.7\cdot10^{4}$	1.7	0.24
248	[301 3/2] [422 5/2]	2.0(6)	$2.0\cdot10^{-5}$	0.13	4.7	$1.0\cdot10^{5}$	15	0.43

$t_{1/2}$(W), $t_{1/2}$(N) and $t^P_{1/2}$(N) are the Weißkopf, Nilsson and Nilsson-with-pairing estimates, respectively.
$F_W = t_{1/2}(exp)/t_{1/2}(W)$, $F_N = t_{1/2}(exp)/t_{1/2}(N)$, $F^P_N = t_{1/2}(exp)/t^P_{1/2}(N)$

2.11. The level scheme of ^{134}Cs

M. Bogdanović [+], *H. Seyfarth*

The odd-odd ^{134}Cs with 55 protons and 79 neutrons is situated near to the closed shells Z = 50 and N = 82. Its knowledge therefore offers the possibility to study the interaction of protons and neutrons in the field of the spherical (or only weakly deformed) vibrating core.

The low-lying states of ^{134}Cs have been previously studied by means of the $^{133}Cs(n,\gamma)$ reaction using thermal and resonance neutrons[1]. In addition $^{133}Cs(d,p)^{134}Cs$ and $^{135}Ba(t,\alpha)^{134}Cs$ reactions have recently been studied[2].

The present measurements on the $^{133}Cs(n,\gamma)^{134}Cs$ reaction have been made at the High-Flux Reactor of the ILL in Grenoble with the bent crystal spectrometers GAMS1 and GAMS2/3, the magnetic beta spectrometer BILL and the pair-spectrometer. The additional experiment with the γ-γ coincidence spectrometer has been performed at the WWR-M reactor of LNPI in Gatchina. At the Brookhaven National Laboratory 5.9 eV and 22.6 eV resonance neutron-capture has been investigated. The $^{133}Cs(d,p)^{134}Cs$ reaction has been studied with the Q3D spectrograph at the tandem accelerator of the University and Technical University at München.

A careful analysis of all available experimental data has led to the levels with spin and parity assignments collected in table 1.

Table 1: Energies, spins and parities of the ^{134}Cs levels

Level energy (keV)	I^π	Level energy (keV)	I^π
0	4^+		
11.2445(18)	5^+	434.1737(31)	$6^-,7^-$
60.0296(13)	$3^+,4^+$	450.2371(22)	5^-
138.7437(29)	8^-	451.4241(17)	$3^+,4^+,5^+$
173.7938(15)	$2^+,3^+,4^+$	454.0870(22)	$2^-,3^-,4^-$
176.4047(16)	$3^-,4^-$	483.6571(29)	$2^-,3^-,4^-$
176.6409(29)	$1^+,2^+,3^+$	502.8410(29)	$3^+,4^+,5^+$
190.2626(28)	$3^+,4^+,5^+$	519.3151(48)	$3^+,4^+$
193.6156(20)	4^-	539.8731(56)	$4^-,5^-$
197.7812(16)	$2^+,3^+,4^+$	570.8259(27)	4^-
209.5450(17)	4^+	579.1314(37)	$2^+,3^+,4^+$
234.3332(18)	$3^+,4^+$	584.1795(26)	$2^+,3^+,4^+$
257.1074(23)	6^-	613.0199(54)	$3^-,4^-,5^-$
267.6616(25)	$4^-,5^-$	624.0069(31)	5^-
271.3482(15)	$2^+,3^+,4^+$	643.9636(28)	$4^-,5^-$
290.9670(20)	$2^+,3^+,4^+$	684.5039(49)	$2^-....5^-$
344.3593(25)	7^-	688.6202(44)	$2^+,3^+,4^+$
377.1020(20)	$3^+,4^+$	693.8371(52)	$2^+,3^+,4^+$
382.9832(24)	6^-	701.9983(27)	$3^-,4^-$
715.8220(37)	$2^-,3^-,4^-$	948.1386(46)	$3^-,4^-$
720.7100(51)	$2^+,3^+,4^+$	976.3094(37)	$3^-,4^-$
741.2755(33)	$3^+,4^+$	991.8764(57)	$4^-,5^-$
752.7016(30)	4^-	1014.346 (13)	
801.2353(79)	$2^-....5^-$	1043.5253(77)	$2^+....5^+$
821.6104(78)	$2^+,3^+,4^+$	1088.4214(46)	$2^-,3^-,4^-$
831.6822(40)	$4^-,5^-$	1094.5535(44)	$2^-....5^-$
835.7113(45)	$2^{(+)}...5^{(+)}$	1100.3376(87)	$3^-,4^-$
839.8136(35)	$2^-,3^-,4^-$	1142.8627(49)	$3^-,4^-$
880.3468(38)	$3^+,4^+,5^+$	1162.481 (11)	3,4,5
912.5989(68)	$3^+,4^+$	1239.467 (12)	3,4,5
916.1778(76)	$3^-,4^-$	1254.2028(54)	$2^-,3^-,4^-$
937.6296(48)	$4^-,5^-,6^-$	1266.1642(75)	$3^-,4^-$
942.025 (21)	2,3,4		

The spin assignments given in table 1 allow more ambiguity than those given in ref. 1 and our preliminary assignments[3] which were by part based on those of ref. 1. The spin assignments to the 60.0 and 176.6 keV state are of crucial importance for spin assignments to other states on the basis of transition characters. In spite of 3^+ and 1^+, respectively, being strongly favoured for these two states, no direct experimental evidence excludes the alternative spin assignments to these states which are given in table 1, too, and then allow a wider ambiguity in spin values of other states.

For the interpretation of the present level scheme beyond an earlier attempt[4] a model is used[5] which couples quasiproton and quasineutron to a vibrating core via exchange of one quadrupole and one magnetic dipole phonon. In this lowest-order approximation the multiplet energy splitting is equivalent to that resulting from long range singlet and triplet two-body residual interaction[4]. It can be written[6,7] as

$$\frac{2}{b_2^2} \cdot \Delta E(j_p,j_n,J_{pn}) = \mp P_2(x) - \frac{a}{c} \cdot x \qquad (1),$$

where $$x = \frac{J_{pn}(J_{pn}+1) - j_p(j_p+1) - j_n(j_n+1)}{2 \cdot (j_p(j_p+1) \cdot j_n(j_n+1))^{1/2}}$$

The parameters b_2^2 and a/c are determined[7] by the quadrupole and magnetic dipole interaction. The sign of the Legendre polynomial refers to quasiproton and quasineutron being of the same (-) or opposite (+) particle-hole character.

In figs. 1 and 2 the calculated energy splittings of the lowest multiplets with negative and positive parity are shown together with the splittings of the experimental excitation energies of those states which are interpreted as members of the multiplets. These assignments are based on the energetic positions and in addition on the branching ratios of E2 and M1 transitions and spectroscopic factors which have been calculated within the model[8], too. Besides an overall agreement fig. 1 shows an odd-even staggering pattern. This pattern cannot be reproduced by including higher order terms in the particle-vibration coupling, one has presumably to use a short range residual interaction which contributes higher multipoles[8]. The coupling constants which are fixed by the multiplet splittings of figs. 1 and 2 can be used to predict those of the $\pi g_{7/2}\ h_{11/2}$, $\pi d_{5/2}\ \nu d_{3/2}$, $\pi g_{7/2}\ \nu s_{1/2}$ and $\pi d_{3/2}\ \nu s_{1/2}$ multiplets. The energetic positions and decay patterns of the experimental states[7] indicate considerable mixing not included in the present simple model.

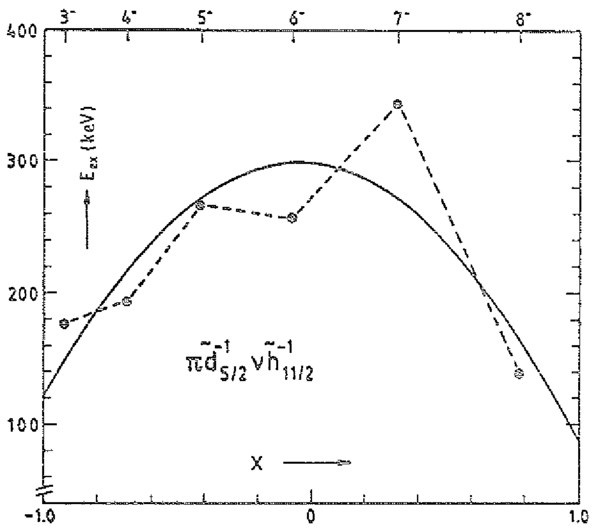

Fig. 1: Least-square fit of a second-order polynomial (eq. 1) to the experimental energies of the $\pi \tilde{d}^{-1}_{5/2}\ \nu \tilde{h}^{-1}_{11/2}$ multiplet states. The fit yields b_2^2 = 267 keV and a/c = 0.14.

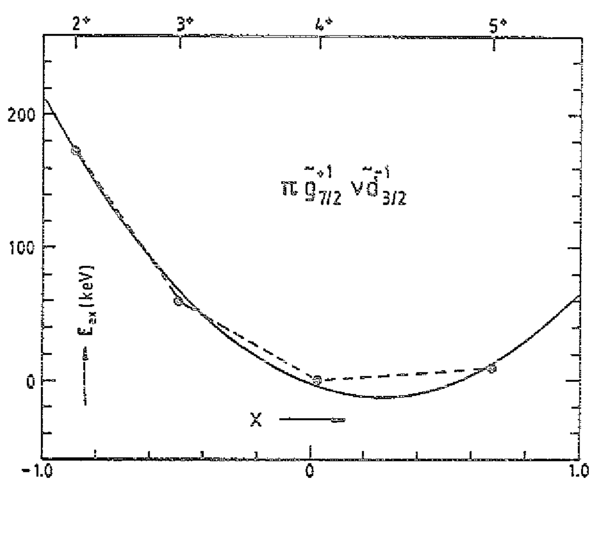

Fig. 2: Least-square fit of a second-order polynomical (eq. 1) to the experimental energies of the $\pi \tilde{g}^{+1}_{7/2}\ \nu \tilde{d}^{-1}_{3/2}$ multiplet states. The fit yields b_2^2 = 223 keV and a/c = 0.66.

References

1) Nucl. Data Sheets 15 (1975) 203; 34(1981) 475
2) A.G. Lee and R.G. Summers-Gill, McMaster Accelerator Laboratory, Annual Report 1980, p. 37 and 1982, p. 10
3) M. Bogdanovic et al., KFA Jülich, Institut für Kernphysik, Annual Report 1982, Jül-Spez 202 (1983) p. 45
4) V.L. Alexeev et al., Nucl. Phys. A297 (1978) 373
5) V. Paar, Nucl. Phys. A331 (1979) 16
6) J.P. Schiffer, Ann. Physics 66 (1971) 798
7) M. Bogdanović, R. Brissot, G. Barreau, K. Schreckenbach, S. Kerr, H. Börner, I.A. Kondurov, Yu.E. Loginov, V.V. Martynov, P.A. Sushkov, H. Seyfarth, O.W.B. Schult, T. von Egidy, P. Hungerford, H.H. Schmidt, H.J. Scheerer, A. Chalupka, W. Kane, to be published
8) G. Alaga, to be published

+ Boris Kidrič Institute for Nuclear Sciences, Belgrade, Yugoslavia

2.12. In-beam study of the odd-odd nuclei in ^{134}La and ^{136}La

T. Morek, H. Beuscher, B. Bochev, T. Kutsarova, R.M. Lieder, M. Müller-Veggian and A. Neskakis

The level schemes of the nuclei $^{134,136}La$ have been studies by means of in-beam γ-ray spectroscopic methods following the (γ,3n) and (p,3n) reactions. The beams were delivered by the Jülich isochronous cyclotron JULIC. Since little was known about the level schemes of $^{134,136}La$ extensive excitation function measurements and cross bombardments have been carried out. To establish the level schemes and to determine spins and half lives of the levels γ-γ coincidences, γ-ray angular distributions and time spectra in the ns- and ms-regimes have been measured. The resulting partial level schemes for $^{134,136}La$ are shown in figs. 1a, 1b and 2a, 2b. The low-spin parts

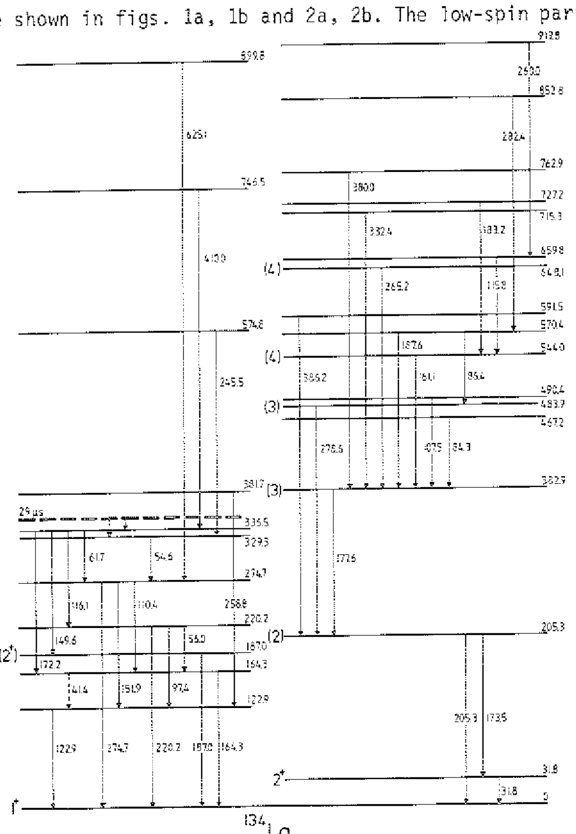

Figure 1a: Partial scheme of low-spin levels in ^{134}La.

of the level schemes are shown in figs. 1a and 2a. Long living isomers with half lives of 29 μs and 115 ms exist in $^{134,136}La$, respectively. A spin of 7 or 8 was tentatively assigned to the 115 ms isomer in ^{136}La. The level sequences shown in figs. 1b and 2b are considered to consist of high-spin states since they are much more strongly populated in the α- rather than the p-induced reactions. It has been assumed that they are to be placed on the 29 μs and 115 ms isomers in $^{134,136}La$, respectively. In ^{136}La furthermore an isomer with a half life of 17 ns was established and a spin of 3 was tentatively assigned to it.

Low-lying levels of odd-odd nuclei are usually treated in terms of proton-neutron configurations deriving from the lowest single-particle orbitals. It is known from the neighbouring nuclei that the lowest-lying proton orbitals

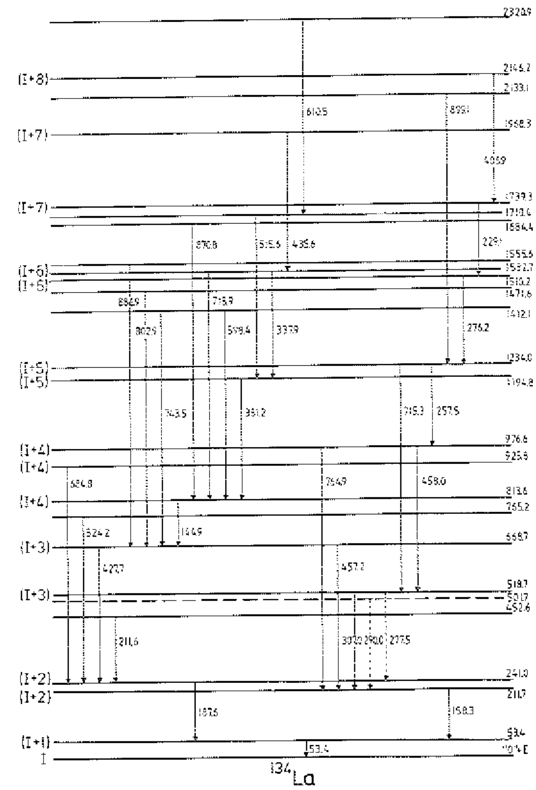

Figure 1b: Partial scheme of levels probably based on the 29 μs isomer in ^{134}La.

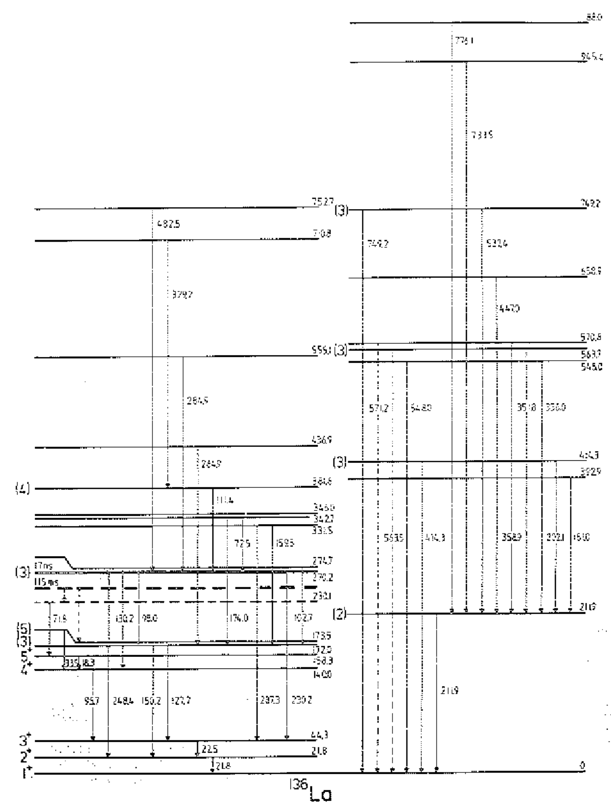

Figure 2a: Partial scheme of low-spin levels in ^{136}La.

of ^{134}La and ^{136}La have $2d_{5/2}$ and $1g_{7/2}$ shell model configurations. The lowest-lying neutron orbitals have $2d_{3/2}$, $3s_{1/2}$ and $1h_{11/2}$ shell model configurations. The following configurations may arise from the coupling of

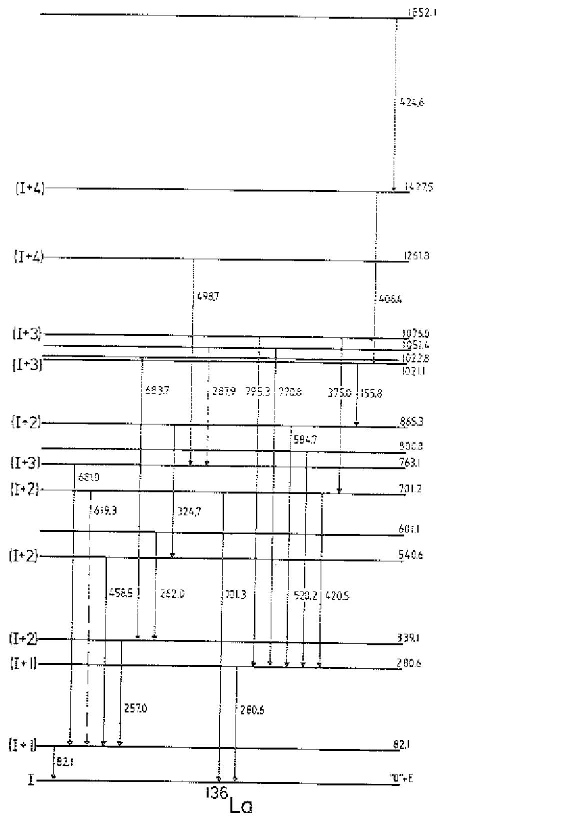

Figure 2b: Partial scheme of levels probably based on the 115 ms isomer in ^{136}La.

one proton and neutron:

$\pi d_{5/2}\nu d_{3/2}$, $\pi d_{5/2}\nu s^{-1}_{1/2}$, $\pi g_{7/2}\nu d_{3/2}$, $\pi g^{-1}_{7/2}\nu s_{1/2}$, $\pi d_{5/2}\nu h^{-1}_{11/2}$.

The levels arising from each of these configurations are degenerate if independent particle motion is considered but they split due to the residual interaction between the proton and the neutron. To interprete the experimentally observed states of $^{134,136}La$ simple calculations were performed for the above configurations in which the matrix elements of the proton-neutron interaction was assumed to be a δ force using the formalism of Sasaki[1]. Sasaki[1] applied the formalism only to odd-odd nuclei with one particle or hole outside the closed neutron and proton shells, respectively. Since the nuclei $^{134,136}La$ have several particles outside the closed shell, calculations using his formalism are not expected to reproduce the level energies but a correct level order may result. As result the relative excitation energies of the multiplets resulting from the proton-neutron configurations mentioned above are plotted in fig. 3 as a function of the mixture parameter α which characterizes the residual proton-neutron interaction.

The lowest-lying levels in $^{134,136}La$ result from the $(\pi d_{5/2}\nu d_{3/2})$ and $(\pi d_{5/2}\nu s^{-1}_{1/2})$ configurations. In both nuclei the ground state has a spin and parity of 1^+. In the calculations only one level with a 1^+ configuration was found being the lowest-lying member of the $(\pi d_{5/2}\nu d_{3/2})$ multiplet. The $(\pi d_{5/2}\nu d_{3/2})_{2^+}$ and $(\pi d_{5/2}\nu s^{-1}_{1/2})_{3^+}$ configurations may be assigned to the 21.8 and 44.3 keV levels, respectively and the $(\pi d_{5/2}\nu d_{3/2})_{3^+}$ configuration to the 172.0 keV state. The 140.0 keV level can be interpreted as having a $(\pi d_{5/2}\nu d_{3/2})_{4^+}$ configuration.

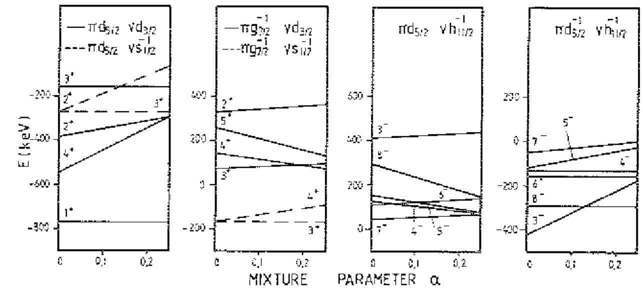

Figure 3: Theoretical calculations of excitation energies of proton-neutron multiplets using the formalism of Sasaki[1]. The excitation energy is plotted vs. the mixture parameter α which characterizes the residual proton-neutron interaction.

The two isomers in ^{136}La may be as well interpreted in the framework of the calculations discussed above. Both isomers result probably from the same multiplet and a high-spin configuration has to be involved, viz. the $\nu h_{11/2}$ configuration. Therefore the $\pi d_{5/2}\nu h^{-1}_{11/2}$ configuration is taken into consideration. However, since the nucleus ^{136}La lies 7 protons above the closed shell the $\pi d^{-1}_{5/2}\ \nu h^{-1}_{11/2}$ two-hole configuration may be regarded as well. The calculations for these configurations are included in fig. 3. The $(\pi d_{5/2}\nu h^{-1}_{11/2})$ configurations of $I^\pi = 7^-$ and 4^- or the $(\pi d^{-1}_{5/2}\nu h^{-1}_{11/2})$ configurations of $I^\pi = 8^-$ and 3^- may be assigned to the 115 ms and 17 ns isomers, respectively. Both assignments may allow to understand the decay pattern of the 17 ns isomer. The 21.8, 140.0 and 172.0 keV levels, which are populated by the isomeric decay, result all from the $(\pi d_{5/2}\nu d_{3/2})$ multiplet. Therefore, the orbital angular momentum changes by $\Delta\ell = 3$ for the isomeric transitions which causes the retardation. However the decay to the 44.3 keV level of $(\pi d_{5/2}\nu s^{-1}_{1/2})$ configuration is prohibited since $\Delta\ell = 5$. It is resonable to assume that also the 29 μs isomer in ^{134}La is a high-spin member of the $(\pi d_{5/2}\nu h^{-1}_{11/2})$ multiplet.

Reference

1) K. Sasaki, Nucl. Phys. 71 (1965) 95

2.13. Interaction between Neutron Particle-Hole and Octupole Core Coupled States in N = 83 Nuclei

R.A. Meyer[+], *K. Heyde*[++], *P. Van Isacker*[++], *M. Waroquier*[++], *J. Moreau*[++], *and J.L. Wood*[*]

For the N=83 odd neutron nuclei, the natural parity states have negative parity and the low-lying levels can be described as resulting from the neutron single-particle excitations, i.e. $2f_{7/2}$, $3p_{3/2}$... and their coupling to the low-lying $J^{\pi} = 2^+$ quadrupole state of the even-even N=82 core nuclei. Recently, there has been a growing body of experimental evidence for a number of positive-parity states below $E_x \approx 3$ MeV in the N=83 nuclei. Two distinct mechanisms can give rise to such states: (i) particle octupole core-coupled configurations ($|2f_{7/2} \otimes 3^-; 1/2^+ ...., 13/2^+\rangle$), (ii) 2p-1h intruder states, described by a neutron excited from the filled neutron orbitals below the N=82 closed shell into the unfilled orbitals above N=82. Because the octupole state steadily decreases in energy as ^{146}Gd is approached, the two types of configurations will occur at approximately the same unperturbed energy in the $Z \geq 60$ nuclei. Thus, we can investigate the extent of their interaction provided we have detailed experimental data for ^{145}Sm and ^{147}Gd. The energy spectra of ^{145}Sm have been known only to a limited extent even though early studies revealed a number of levels below $E_x \sim 3$ MeV. The properties (such as J^{π}, etc.) of these levels has not been known even though a number of low-energy conversion electrons, originally measured by Avotina[1], could be associated with intra-level transitions. Unfortunately, these transitions have been discarded in data compilations because their counterparts in γ-ray studies have not been found[2]. In our studies we have produced mass-separated sources of ^{145}Eu and measured high-statistics Ge(Li) singles and Ge(HP) Compton suppression spectra.

Analysis of these data, particularly the Compton suppression data, have revealed over a dozen previously unobserved γ-rays of low energy ($E_{\gamma} \lesssim 0.9$ MeV) which in conjunction with the conversion electron data of Avotina et al.[1] provides multipolarities. These transitions can be placed among levels up to $E_x \sim 3$ MeV, and as shown in fig. 1, provide a J^{π} determination for levels below $E_x \sim 2$ MeV.

In the present study, the particle-(hole)-core coupling calculations are carried out in each subspace separately. The coupling between the N=(82+particle) and the N=(84+hole) configurations is obtained by using the simplifying assumption that the core states in the N=84 nuclei specified by the collective quantum number (R'), are connected with the corresponding core states in the N=82 nuclei, specified by the collective quantum number (R), via the two-particle shell-model wavefunction[†]. That is, the $J^{\pi} = 0^+$ N=84 and N=82 ground states, are related by:

$$|N = 84(R')\rangle = \sum_{j_p} d\,(j_p^2;0^+)\,|N = 82(R)\rangle\,\delta_{RR'}.$$

Here, the summation j_p runs over all available single-particle states in the N=82-126 valence space.

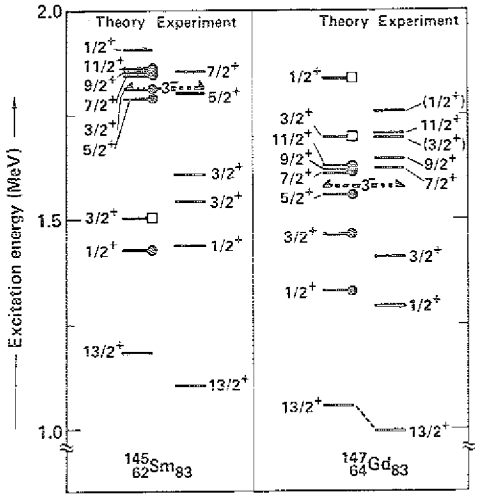

Fig. 1: Comparison of the results of the particle(hole)-core coupling calculations with the experimental data for positive parity states in ^{145}Sm and ^{147}Gd.

In fig. 1 we compare the experimental results with the calculations for ^{145}Sm and ^{147}Gd. The experimental data for ^{147}Gd are from the recent results of refs. 3, 4. For ^{145}Sm we calculate a large mixing between the 2p-1h and the $|2f_{7/2} \otimes 3^-; J^{\pi}\rangle$ core-coupled states for the $J^{\pi} = 1/2^+$, $3/2^+$ and $13/2^+$ levels. The influence of such mixing for the $J^{\pi} = 13/2^+$ levels has already been discussed in detail before. In this same figure octupole-core coupled states are observed to follow rather well the centroid value $\hbar\omega_3$ as obtained from the $J_1^{\pi} = 3_1^-$ excitation energy in the adjacent even-even nuclei. The single-hole states, on the other hand, cannot easily be connected to a single J^{π} level, but show a large fragmentation. The interaction between $1/2^+$ states need to be, on the average, a factor of ~ 3 stronger than the $3/2^+$ configuration mixing matrix elements in order to reproduce the experimental data. In comparing the relevant reduced matrix elements $\langle 3s_{1/2}||Y_3||2f_{7/2}\rangle$ and $2d_{3/2}||Y_3||2f_{7/2}\rangle$ the former is a nonspin-flip matrix element thus accounting for the difference in a simple way.

† Here R and R' represent all collective quantum numbers $(N_qR_q, N_oR_o)R$ defined in the N = 82 and N = 84 nuclei, respectively. The indices q and o denote quadrupole and octupole phonons, N the number and R the angular momentum.

References

1) M.P. Avotina, E.P. Gregorev, Zh.T. Zhelev, A.V. Zolotaven and V.O. Sergeev, Preprint OERE 2272, Dubna (1965)
2) J. Tuli, Nucl. Data Sheets 29 (1980) 533
3) E. Newman, K.S. Toth, D.C. Hensley and W.D. Schmitt-Ott, Phys. Rev. C9 (1974) 674
4) M. Piiparinen, T. Komppa, R. Komu, A. Pakkanen and J. Blomqvist, Z. Phys. A309 (1982) 87 and ref. therein

+ 1983 visiting scientist, permanent address: Nuclear Chemistry Division, Lawrence Livermore National Laboratory, Livermore, Ca. 94550, USA

++ Lab. voor Kernfysica, Proeftuinstraat 42, B-9000 Gent, Belgium

* School of Physics, Georgia Institute of Technology, Atlanta, Georgia 30332, USA

2.14. The 10^+ States of $\nu h_{11/2}^{-2}$ and $\pi h_{11/2}^2$ character in the N = 80 Nucleus ^{142}Sm

M. Lach, J. Styczen, H. Beuscher, P. Kleinheinz, J. Blomqvist***

In the N = 80 isotones $^{138}_{58}Ce$ and $^{140}_{50}Nd$, isomers of $(\nu h_{11/2}^{-2})_{10^+}$ character have been firmly identified[1-3] at ≈ 3.5 MeV excitation from in-beam γ-ray- and g-factor measurements. In the isotones above Z = 64, $^{146}_{66}Dy$ and $^{148}_{68}Er$, the 10^+ isomers lie[4,5] at much lower energy, ≈ 2.9 MeV, and they are naturally interpreted as $h_{11/2}^2$ two-proton excitations. The lowest 10^+ state in $^{144}_{64}Gd$, a 145 ns isomer at 3.433 MeV[6], has been shown[7] to be a $\pi h_{11/2}^2$ excitation, and we have recently[8] identified the ^{144}Gd $(\nu h_{11/2}^{-2})_{10^+}$ state 264 keV above, at 3.697 MeV. In the $^{142}_{62}Sm_{80}$ nucleus the situation was so far not clear. Earlier studies[9,10] and more recent experiments[2] with ^{24}Mg and ^{19}F beams could observe a long-lived isomer at 3.662 MeV, but its half life and spin parity could not be firmly established from these data. Also an attempt[2] to measure the g-factor remained unsuccessful since the main yrast γ-ray cascade bypasses the state.

We have now investigated ^{142}Sm through the (α,4n) and (^3He,3n) reactions. These reactions often provide more detailed level scheme information due to their lower angular momentum transfer to the compound nucleus. As a result the main side-feeding intensity populates the energy levels in the I = 9 to 16 region which therefore can be investigated more completely. In the experiment we used > 60 MeV α-particles and 32 to 50 MeV ^3He beams. For both reactions the γ-ray excitation functions and angular distributions were measured, and detailed four-parameter γγ-coincidence measurements with 140 ns separated beam bursts were carried out.

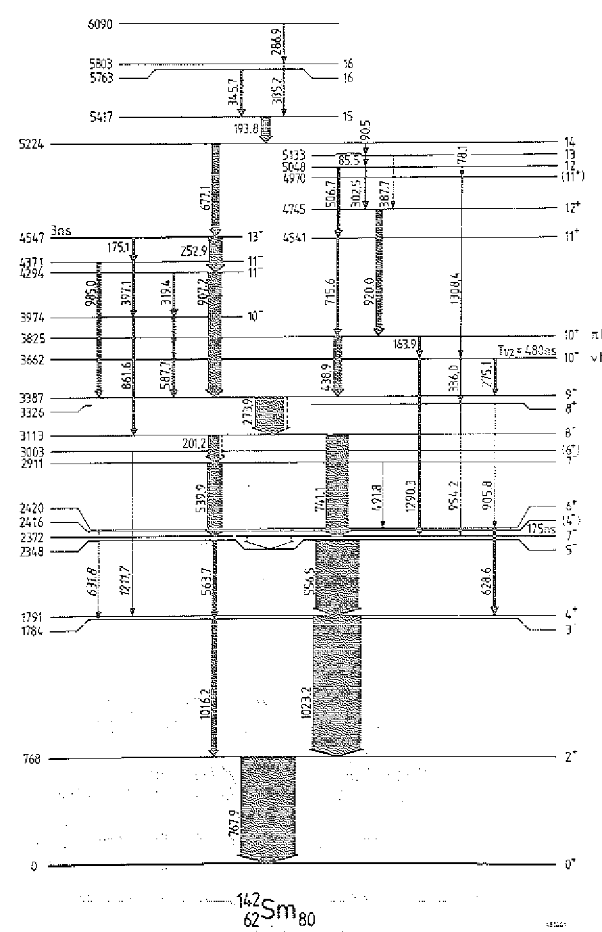

Fig. 1: High spin states in ^{142}Sm as observed in the present (α,4n) study. The two transitions labelled with *italics* were only seen in the (^3He,3n) spectra.

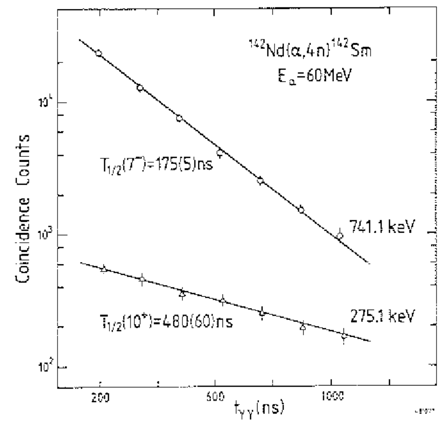

Fig. 2: Half life measurement for the 7^-(2.372 MeV) and 10^+(3.662 MeV) isomers in ^{142}Sm.

These data establish the ^{142}Sm level scheme up to 6 MeV and I ≈ 16 (fig. 1). Firm spin-parities could be assigned for most of the levels below 4.8 MeV excitation. Our data confirm the earlier tentative[9,10] assignment for the 3.662 MeV isomer and we identify a second 10^+ state 164 keV higher in energy, at 3.825 MeV. The previously unknown isomeric half life was determined from the $t_{\gamma\gamma}$ data (fig. 2) as

$$T_{1/2}(10^+, 3.662 \text{ MeV}) = 480 \pm 60 \text{ ns};$$

the same data give for the lower-lying 7^- isomer

$$T_{1/2}(7^-, 2.372 \text{ MeV}) = 175 \pm 5 \text{ ns}$$

in close agreement with the earlier[11,10] result. We also confirm the short-lived isomer[9,10] at 4.547 MeV. A $t_{\gamma\gamma}$ centroid shift analysis involving exclusively events with full-energy absorption in both detectors gives

$$T_{1/2}(13^-, 4.547 \text{ MeV}) = 2.6 \pm 0.6 \text{ ns}.$$

The two 10^+ level energies are in good agreement with the systematics of the N = 80 isotones, but since they occur close in energy additional evidence is needed to determine their configurations. The present results clearly characterise the lower (isomeric) 10^+ state as the $\nu h_{11/2}^{-2}$ excitation. The strengths of its three isomeric transitions are listed in table 1 and compared to isomeric transition strengths in other close-lying nuclei.

Table 1: Selected Isomeric Transition Strengths in ^{142}Sm and in Neighbouring Nuclei

Nucleus	Eγ (keV)	Multi-polarity	B_W	E_x^i	Initial and final state configurations	ref.
$^{142}_{62}Sm_{80}$	1290.3	E3	0.18(2)	3662	$(\nu h^{-2}_{11/2})_{10^+} \rightarrow (\nu h^{-1}_{11/2}\ d^{-1}_{3/2})_{7^-}$	this work
	336.0	E2	$1.3(2)\cdot 10^{-3}$	3662	$(\nu h^{-2}_{11/2})_{10^+} \rightarrow (\pi d^{-1}_{5/2}\ g^{-1}_{7/2})_{6^+}\ (\nu^{-2}_j)_{2^+}$	this work
	275.1	E1	$7.0(1.0)\cdot 10^{-9}$	3662	$(\nu h^{-2}_{11/2})_{10^+} \rightarrow (\pi h_{11/2}\ g^{-1}_{7/2})_{9^-}$	this work
$^{146}_{66}Dy_{80}$	127.0	E3	0.32(4)	2936	$(\pi h^{2}_{11/2})_{10^+} \rightarrow (\pi h_{11/2}\ d_{3/2})_{7^-}$	4
$^{149}_{66}Dy_{83}$	110.4	E3	0.32(2)	2661	$(\pi h^{2}_{11/2}\ \nu f_{7/2})_{27/2^-} \rightarrow (\pi h_{11/2}\ d_{3/2}\ \nu f_{7/2})_{21/2^+}$	12
$^{138}_{58}Ce_{80}$	430.0	E2	$1.08(6)\cdot 10^{-2}$	3538	$(\nu h^{-2}_{11/2})_{10^+} \rightarrow (\pi d^{-1}_{5/2}\ g^{-1}_{7/2})_{6^+}\ (\nu^{-2}_j)_{2^+}$	1

In our interpretation the 1290 keV E3 transition connects the $(\nu h^{-2}_{11/2})_{10^+}$ and $(\nu h^{-1}_{11/2}\ d^{-1}_{3/2})_{7^-}$ neutron hole configurations. This transition has not been observed in other nuclei in this region, but the analogous E3 for proton particles, $(\pi h^{2}_{11/2})_{10^+}$ to $(\pi h_{11/2}\ d_{3/2})_{7^-}$, is known[4,12] in the Dy isotopes with 80 and 83 neutrons and found to have comparable strength. A much higher E3 retardation for the 1290 keV transition would be expected for the alternative $(\pi h^{2}_{11/2})_{10^+}$ isomeric state assignment.

Additional evidence for the proposed 10^+ configurations comes from the feeding transitions. In ^{144}Gd it was found[8] that two higher-lying 11^+ and 12^+ levels exclusively decay to the $(\pi h^{2}_{11/2})_{10^+}$ state through transitions of 711 and 1018 keV. We interpret these levels as the yrast members of the $(\pi h^{2}_{11/2})_{10^+} \times (\nu^{-2})_{2^+}$ multiplett which is expected in that energy region. In ^{142}Sm, analogous γ rays, with 716 and 920 keV, connect 11^+ and 12^+ levels to the higher-lying 10^+ state which therefore must be the $\pi h^{2}_{11/2}$ excitation since analogous 11^+ and 12^+ levels cannot occur with the two valence neutron holes in $(\nu h^{-2}_{11/2})_{10^+}$.

A surprising result is the extreme retardation of a factor 10^3 for the 336 keV $10^+ \rightarrow 8^+$ isomeric E2 transition. Such a large hindrance requires high configuration-forbiddenness, which suggests a $(\pi d^{-1}_{5/2}\ g^{-1}_{7/2})_{6^+} \times (\nu^{-2}_j)_{2^+}$, v = 4 assignment for the 3.326 MeV 8^+ state. In agreement with expectations a corresponding 8^+ state was not found in ^{144}Gd in this energy region. Further support for this v = 4 8^+ assignment comes from a study[1] of the N = 80 ^{138}Ce nucleus, where the 3.538 MeV $(\nu h^{-2}_{11/2})_{10^+}$ isomer decays through an analogous $10^+ \rightarrow 8$ transition, but due to the unexpected large retardation (cf. table) the authors hesitated to adopt E2 multipolarity and positive parity for the 3.108 MeV I = 8 level in ^{138}Ce.

In summary the present study has completed the systematics for 10^+ excitations in the N = 80 isotones from $^{138}_{58}$Ce to $^{148}_{68}$Er. As one would expect the $(\nu h^{-2}_{11/2})_{10^+}$ excitation, now known from Ce to Gd, lies at rather constant energy, whereas the $(\pi h^{2}_{11/2})_{10^+}$ state drops conspicuously when crossing Z = 64 and stays constant for the nuclei above.

---

* Institute of Nuclear Physics, Cracow, Poland

** Research Institute of Physics, Stockholm, Sweden

References

1) M. Müller-Veggian, Y. Gono, R.M. Lieder, A. Neskakis, C. Mayer-Böricke, Nucl. Phys. A304 (1978) 1

2) J.C. Merdinger, Physica Scripta 24 (1981) 249

3) J.C. Merdinger, F.A. Beck, E. Bozek, T. Byrski, C. Gehringer, Y. Schutz, J.P. Vivien, Nucl. Phys. A346 (1980) 281

4) S.Z. Gui, G. Colombo, E. Nolte, Z. Physik A305 (1982) 297

5) E. Nolte, G. Colombo, S.Z. Gui, G. Korschinek, W. Schollmeier, P. Kubik, S. Gustavsson, R. Geier, H. Morinaga, Z. Physik A306 (1982) 211

6) M.A.J. Mariscotti, H. Beuscher, W.F. Davidson, Y. Gono, H.M. Jäger, R.M. Lieder, M. Müller-Veggian, A. Neskaskis, D.R. Haenni, D.R. Zolnowski, Nucl. Phys. A311 (1978) 395

7) O. Häusser, P. Taras, W. Trautmann, D. Ward, T.K. Alexander, H.R. Andrews, B. Haas, D.Horn, Phys. Rev. Lett. 42 (1979) 1451

8) M. Lach, J. Styczen, R. Julin, M. Piiparinen, P. Kleinheinz, Proc. Inst. Conf. on High Angular Momentum Properties of Nuclei, Oak Ridge, November 2 - 4, 1982, vol. 1, p. 74

M. Lach, J. Styczen, R. Julin, M. Piiparinen, P. Kleinheinz, Annual Report 1982, IKP-KFA Jülich, p. 47

9) F.A. Beck, T. Byrski, C. Gehringer, A.Z. Hrynkiewicz, J.C. Merdinger, Y. Schutz, J.P. Vivien, Proc. Int. Conf. on the Structure of Medium-Heavy Nuclei, Rhodos, May 1 - 4, 1979, p. 289

10) H. Beuscher, D.R. Haenni, B. Bochev, R.M. Lieder, T. Morek, M. Müller-Veggian, A. Neskakis, C. Mayer-Böricke, Proc. Int..Conf. on the Structure of Medium-Heavy Nuclei, Rhodos, May 1 - 4, 1979, p. 290

11) G.G. Kennedy, S.C. Gujrathi, S.K. Mark, Phys. Rev. C12 (1975) 553

12) A.M. Stefanini, P. Kleinheinz, M.R. Maier, Phys. Lett. 62B (1976) 405

2.15. High-Lying Yrast States in ^{145}Eu and its Mass

B. Rubio, R. Julin, A. Ercan, P. Kleinheinz, J.L. Tain, G.P.A. Berg, G. Hlawatsch, J. Meißburger, D. Paul, J.G. Römer and J. Blomqvist[+]

The nuclear shell model relates the energies of multiparticle states to the pertinent one- and two-particle excitations observed in neighbouring nuclei, and to the ground state masses. Such analyses are particularly applicable for maximum aligned multiparticle yrast states which are well separated in energy from other levels with the same spin and parity and therefore expected to be little affected by configuration mixing. These states might therefore be used to deduce specific ground state masses if the interactions are known from experiment[1)].

In the N=82 nucleus ^{145}Eu one expects a $27/2^+$ yrast state at ≈ 4 MeV of the configuration $\pi h^2_{11/2}\, g^{-1}_{7/2}$ which is well suited for such an analysis. Previous ^{145}Eu in-beam studies[2-4)] gave firm results only up to a $19/2^-$ level at 2.836 MeV, but for the level scheme above this energy the transition orderings and the level parities remained unclear due to severe spectral complexities. We have therefore carried out additional measurements using the ^{144}Sm(α,p2n) reaction with ∿ 50 MeV α-particle beams. The excitation function results of fig. 1 clearly specify the ordering of the four yrast transitions above the 2.836 MeV $19/2^-$ state as shown. The large negative A_2 values (Table 1) and intensity balance suggest M1-character for the three low-energy γ-rays and E1 multipolarity for the 794 keV line has been firmly established from conversion electron measurements[4)]. The new data for the transition multipolarities give firm spin-parity assignments for the associated yrast levels. In particular the 4123 keV level has $I^\pi = 27/2^+$ and we interpret it as the $(\pi h^2_{11/2}\, g^{-1}_{7/2})27/2^+$ state mentioned above. The 25/2 member of this configuration is calculated to lie .1 MeV lower in energy, and the 3977 keV level is identified as this state. It might however admix with the $(\pi h^2_{11/2}\, d^{-1}_{5/2})25/2^+$ state expected .3 MeV above the $27/2^+$ level, and we therefore will not consider it in the analysis below. The 3183 keV $23/2^-$ state is the fully aligned member of the $\pi h_{11/2}\, d^{-1}_{5/2}\, g^{-1}_{7/2}$ configuration.

Table 1: Properties of four high-lying yrast transitions in ^{145}Eu measured in the (α,p2n) reaction at 45 MeV.

E_γ	$I_\gamma^{a)}$	A_2	A_4	Multipolarity
75.2(2)	12(1)	-0.23(3)	0	M1
146.5(1)	15(1)	-0.30(8)	+0.03(10)	M1(+E2)
271.9(1)	59(3)	-0.50(4)	+0.09(6)	M1+E2
793.7(2)	42(2)	-0.42(5)	+0.03(7)	E1$^{b)}$(+M2)

a) normalised to 100 units for the 386.7 keV $11/2^- \rightarrow 7/2^+$ M2 transition

b) from α_K measurements of ref. 4

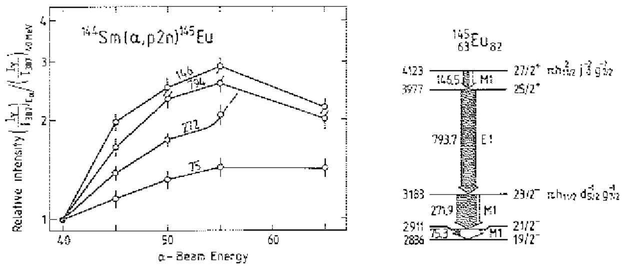

Fig. 1: Gamma-ray excitation functions of four high-lying yrast transitions relative to the 387 keV $11/2^- \rightarrow 7/2^+$ transition in ^{145}Eu, and the resulting ^{145}Eu level scheme. Above 55 MeV, the 272 keV line is confused by a ^{143}Eu transition.

A shell model reduction of the $27/2^+$ state involves the $(\pi h^2_{11/2})10^+$ level in ^{146}Gd, the $(\pi h_{11/2}\, g^{-1}_{7/2})8^-$ and 9^- states in ^{144}Sm, and the $(h_{11/2})11/2^-$ and $(g_{7/2})7/2^+$ single proton states in ^{145}Eu and ^{143}Pm. With the experimental energies for these levels the analysis gives for the combination of the four ground state masses

$$S^{calc}_{27/2} = M(^{146}Gd) - 3M(^{145}Eu) + 3M(^{144}Sm) - M(^{143}Pm) = -4924(50)\ \text{keV}.$$

Another decomposition, for the 17^- yrast state[5)] of ^{146}Gd at 7165 keV gives

$$S^{calc}_{17} - 2S^{calc}_{27/2} = -9822(100)\ \text{keV},$$

in good agreement with the above result.

The ground state masses of ^{144}Sm and ^{143}Pm are primary mass values in Wapstra's tables[6)]; the ^{146}Gd mass was recently measured in three independent two-nucleon transfer experiments[7-9)]. Using these mass data and the above S-value we obtain

$$M^{calc}(^{145}Eu) = -78034(14)\ \text{keV},$$

which differs by more than four standard deviations from the tabulated[6)] value.

In order to clear up this discrepancy we carried out a direct mass determination with the ^{144}Sm(^{3}He,d)^{145}Eu single proton transfer reaction using the magnet spectrograph Big Karl. Calibration reactions were performed with ^{208}Pb and ^{58}Ni targets. The sequence of spectra taken for the ^{145}Eu mass determination included several measurements with the Sm target runs always sandwitched between runs with the two calibration targets. Independent determinations were carried out at two laboratory angles, 15.5°, and 21.3°. For all runs the magnet settings were kept unaltered.

A particular problem was the accurate determination of the reaction angle. It was extracted from cross-over measurements of the ^{13}N ground state and the 3.118 MeV ^{209}Bi state populated in the (^{3}He,d) reactions on ^{12}C and ^{208}Pb.

Examples of deuteron spectra are shown in fig. 2. The excitation energies calculated from these spectra for the ^{145}Eu lines with the Wapstra[6] masses and the calibration function are 59(4) keV lower than the known real values, which requires a corresponding 59(4) keV correction to the ground state Q-value. Combining our result with the tabulated ^{144}Sm mass the new value for the ^{145}Eu ground state mass defect becomes

$$M(^{145}Eu) = -77995(7) \text{ keV},$$

which differs by -59(17) keV from the Wapstra value but lies somewhat closer to the result derived from the shell model analyses discussed above, from which it differs by 39(16) keV.

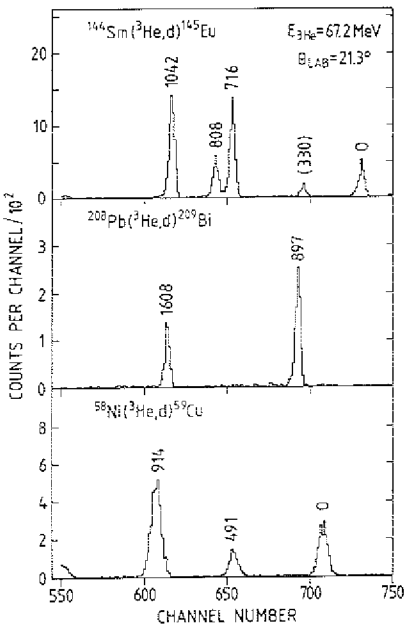

Fig. 2: Examples of deuteron spectra for determination of the ^{145}Eu mass with the (^{3}He,d) reaction. Peaks with excitation energies given in parentheses were not used in the analysis.

Since the ^{146}Eu mass was not yet measured by transfer reactions we used the same ^{3}He beam for a ^{144}Sm(^{3}He,p) experiment at θ = 12.3°. The (^{3}He,p) reactions on ^{207}Pb and ^{209}Bi targets provide suitable calibration Q-values. Examples of spectra are given in fig. 3. The energy resolution of the proton peaks is ∼ 30 keV fwhm. Of crucial importance for identification of the ^{146}Eu peaks was the knowledge of the excitation energies for the low-lying ^{146}Eu energy levels which only recently were determined[10] through in-beam γ-ray studies. Although the cross sections are much smaller for these two-nucleon transfer reactions it was possible to extract the Q-value as $Q(^{146}Eu) = Q(^3He,p)^{exp} - Q(^3He,p)^{Wapstra} = +8(12)$ keV, giving the ^{146}Eu mass defect as

$$M(^{146}Eu) = - 77119(13) \text{ keV},$$

apparently in near agreement with the Wapstra value - 77111(11) keV.

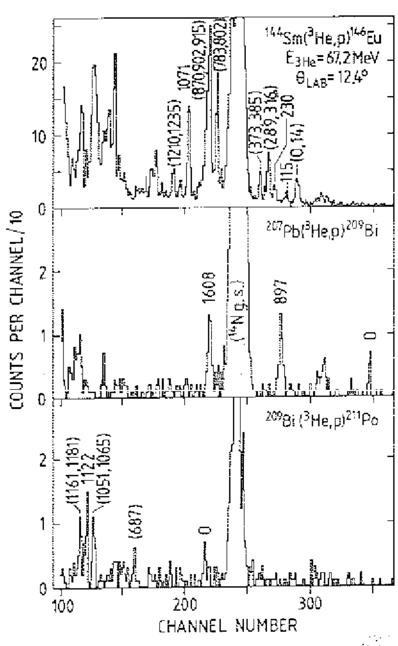

Fig. 3: Proton spectra for determination of the ^{146}Eu mass with the (^{3}He,p) reaction (cf. caption to fig. 2).

+ AFI, Stockholm, Sweden

References

1) J. Blomqvist, P. Kleinheinz, P.J. Daly, Z. Phys. A - Atoms and Nuclei 312, 27 (1983)
2) D.R. Haenni, H. Beuscher, R.M. Lieder, M. Müller-Veggian, A. Neskakis, C. Mayer-Böricke, Nucl. Phys. A331, 141 (1979)
3) D. Bazzacco, A.M.I. Haque, K.O. Zell, P. von Brentano, C. Protop, Phys. Rev. C21, 222 (1980)
4) D.A. Rakel, R. Kaczarowski, E.G. Funk, J.W. Mihelich, Phys. Rev. C21, 595 (1980)
5) R. Broda, P. Kleinheinz, S. Lunardi, J. Blomqvist, Proc. ASHPIN, Argonne, 1979, ANL/PHY-79-4, p. 389
6) A.H. Wapstra, K. Bos, At. Data Nucl. Data Tables 19, 177 (1977)
7) W.P. Alford, R.E. Andersen, P.A. Batay-Csorba, R.A. Emigh, D.A. Lind, P.A. Smith, C.D. Zafiratos, Nucl. Phys. A 321, 45 (1979)
8) R.C. Pardo, S. Gales, R.M. Ronningen, L.H. Harwood, Phys. Lett. 91B, 41 (1980)
9) E.R. Flynn, J. van der Plicht, J.B. Wilhelmy, L.G. Mann, G.L. Struble, R.G. Lanier, Phys. Rev. C28, 97 (1983)
10) A. Ercan et al., Proc. Int. Conf. Nucl. Phys. Florence, Aug. 1983, Vol. I, p. 154

2.16. Study of Particle-Hole Multipletts in ^{146}Gd through (α,2n) in-beam Measurements

S.W. Yates, P. Kleinheinz, R. Julin, W. Stöffl[+], *E. Henry*[+], *L. Mann*[+], *D. Decman*[+], *J. Blomqvist*[++]

Energy levels in the ^{146}Gd closed core nucleus so far were investigated through (α,5n) in-beam measurements[1,2] and in decay[3] of ^{146}Tb. The (α,5n) studies specified the yrast levels up to ~ 9 MeV excitation; the β-decays selectively proceed to specific particle-hole excitations via allowed GT transitions. From these studies one knows that the proton particle-hole multipletts lie in the 2.6 to 3.8 MeV region, whereas the neutron particle-hole states occur at somewhat higher energies (> 3.4 MeV). These energy levels provide basic input information for shell model analyses in this region, but so far only for one configuration, $\pi h_{11/2}\, d^{-1}_{5/2}$, the complete multiplett is identified. The yrast experiments, in addition, located the $\pi h^2 j_0^{-2}$ 10^+ state and the 9^- and 8^- members of the $\pi h_{11/2}\, g^{-1}_{7/2}$ configuration, and in β decay three neutron particle-hole states are populated.

To identify additional multiplett members we used the (α,2n) reaction at low beam energy which is suitable to populate levels above the yrast line. Detailed excitation function measurements, carried out at the MPI Heidelberg Tandem accelerator, suggested a number of new ^{146}Gd non-yrast transitions, as well as their approximate location in the level scheme which could be deduced from the excitation function thresholds (fig. 1). These data suggested 25.8 MeV as an optimum bombarding energy for an (α,2n) study to locate non-yrast levels in ^{146}Gd. At this energy the (α,2n) and (α,n) reactions have comparable cross sections, whereas other exit channels are quite weak. In collaboration with the LLNL Nuclear Structure Group extensive in-beam experiments were carried out with α-particle beams from the LANL Tandem Accelerator. From extensive 3-parameter γγ-coincidence data (10^8 events) many new ^{146}Gd transitions could be identified and placed

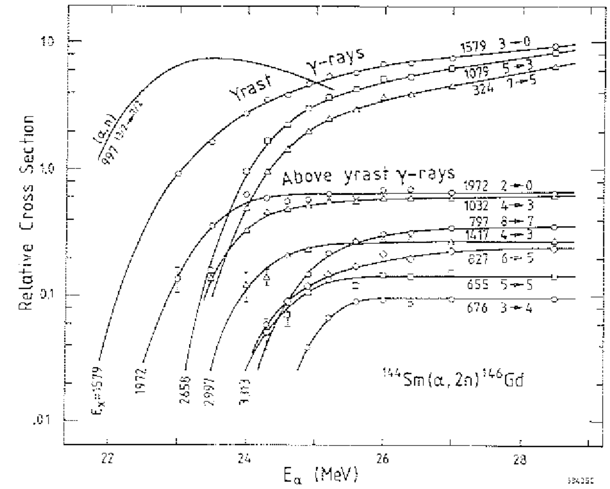

Fig. 1: Selected (α,2n) excitation functions for yrast and above-yrast transitions in ^{146}Gd. The 997 keV ^{147}Gd ground state transition is included.

in the level scheme, and firm data were obtained for transitions as weak as 0.3 % of the (α,2n) exit channel. Transition multipolarities have been deduced from angular distribution data, also taken at 25.8 MeV, and from conversion electron measurements where many of the new transitions are observed. These electron spectra were measured with a superconducting solenoid operated in swept-current lens mode.

The level scheme resulting from these data is given in fig. 2, with the yrast decay known from the earlier studies shown to the left. The new ^{146}Gd γ-rays are quite weak, in general < 5 % of the (α,2n) channel, but due to the high quality of the coincidence data most of the levels could be firmly located. In many cases the level spins and parities could be characterised from the transition

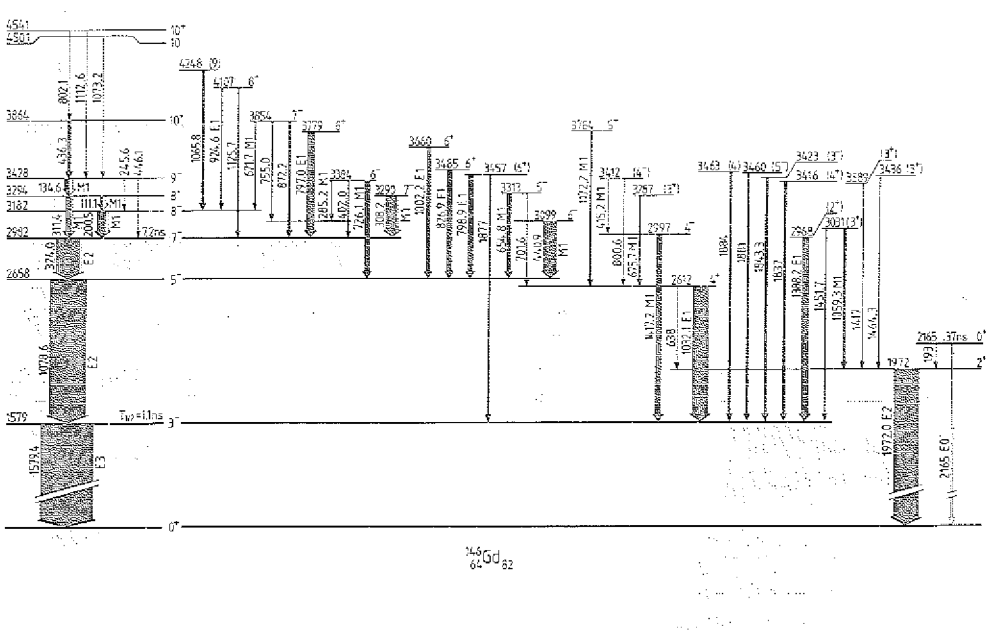

Fig. 2: Level scheme of ^{146}Gd observed in the (α,2n) reaction at 25.8 MeV. The previously known yrast-decay is shown to the left; the intensities in the right part of the figure are drawn five times thicker than the yrast γ rays to the left.

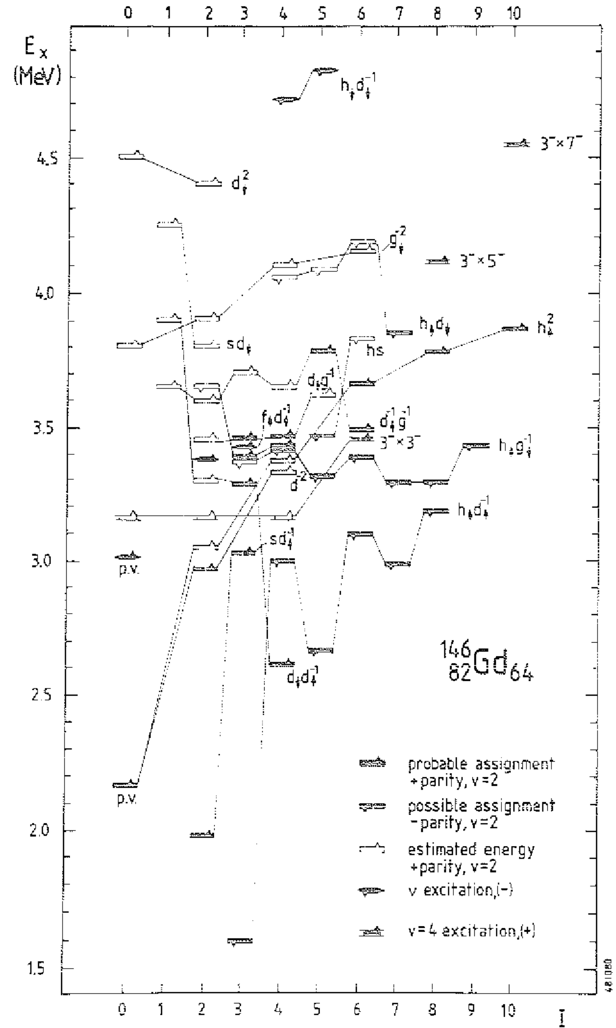

Fig. 3: Two-proton multipletts in ^{146}Gd. Non-observed multiplett members are drawn at their estimated energies. Known neutron excitations, and selected v = 4 levels are also included.

properties; feeding intensity arguments have also been considered. Many levels however are specified through only one γ-transition and a number of I^{π} assignments for such monopode levels remain tentative.

The proposed configuration assignments are given in fig. 3 where all known ^{146}Gd levels below 4.8 MeV excitation are included. These assignments are primarily based on energy considerations. The figure includes all $v = 2$ $\pi^{+1}\pi^{-1}$, $\pi^{2}j_0^{-2}$ and $\pi^{-2}j_0^{+2}$ multipletts provided by the five proton orbitals between 50 and 82. Yet unobserved multiplett members are drawn at estimated energies. It is apparent that the (α,2n) experiment located levels up to ≈ 1 MeV above the yrast line; knowledge of higher-lying low-spin states remains still limited. Neutron particle hole multipletts are expected above 3.4 MeV excitation. Included in the figure are only the 3 known $\nu^{+1}\nu^{-1}$ states, and the neutron pairing vibration observed in a recent[4] (p,t) experiment. A few v = 4 states expected below 4.8 MeV which involve the 3^- octupole phonon are also shown. Of these, the $(3^- \times 7^-)10^+$ and $(3^- \times 5^-)8^+$ assignments are reasonably firm, whereas the $(3^- \times 3^-)6^+$ identification is still highly tentative.

+ LLNL Livermore, Ca., USA

++ AFI Stockholm, Sweden

References

1) P. Kleinheinz, R. Broda, P.J. Daly, S. Lunardi, M. Ogawa, J. Blomqvist, Z. Phys. A290 (1979) 279

2) R. Broda, P. Kleinheinz, S. Lunardi, J. Blomqvist, ASHPIN, Argonne, 1979, ANL/PHY-79-4, page 389

3) J. Styczen, P. Kleinheinz, M. Piiparinen, J. Blomqvist, HECFOS, Helsingör 1981, CERN 81-09, 20. July 1981, page 548

4) E.R. Flynn, J. van der Plicht, J.B. Wilhelmy, L.G. Mann, G.L. Struble, R.G. Lanier, Phys. Rev. C28 (1983) 97

2.17. Single- and Double Octupole Excitations in ^{148}Gd

S. Lunardi, P. Kleinheinz, M. Piiparinen, M. Ogawa, J. Blomqvist[+]

The study of particle-phonon coupling phenomena in nuclei provides the basic understanding for the vibrational anharmonicities, which in turn are of crucial importance for the properties of two-phonon excitations. A number of recent in-beam studies have provided first results on particle-octupole coupling for the neighbours of ^{146}Gd which has a 3^- first excited state at 1.6 MeV. Of the $\nu f_{7/2} \times 3^-$ septuplett in ^{147}Gd one knew[1)] so far the $13/2^+$ member which occurs as low as 1.0 MeV due to the interaction with the close-lying $\nu i_{13/2}$ single-particle state. In a recent[2)] experiment five of the remaining six multiplett members were observed, all within < 180 keV of the 1.58 MeV core phonon energy. These results evince that here the $\nu f_{7/2} \times 3^-$ coupling is weak, comparable to ^{209}Bi, where the splitting of the $\pi h_{9/2} \times 3^-$ septuplett[3)] is < 250 keV.

We have now studied the coupling of two $f_{7/2}$ valence particles to the 3^- phonon. In the nucleus ^{148}Gd such excitations should occur not far from the yrast line and we could show that they are populated in (α,xn) reactions. In these experiments we have also observed two further two-phonon octupole states, which involve the stretched coupling of valence particles and core phonons, analogous as in the known[4)] $19/2^-$ two-phonon octupole state in ^{147}Gd. We had earlier[5)] investigated ^{148}Gd with the $(\alpha,4n)$ reaction, but due to severe spectral complexities only incomplete information was obtained on the level properties. We have now performed additional $(^3He,3n)\gamma$ and e^- experiments

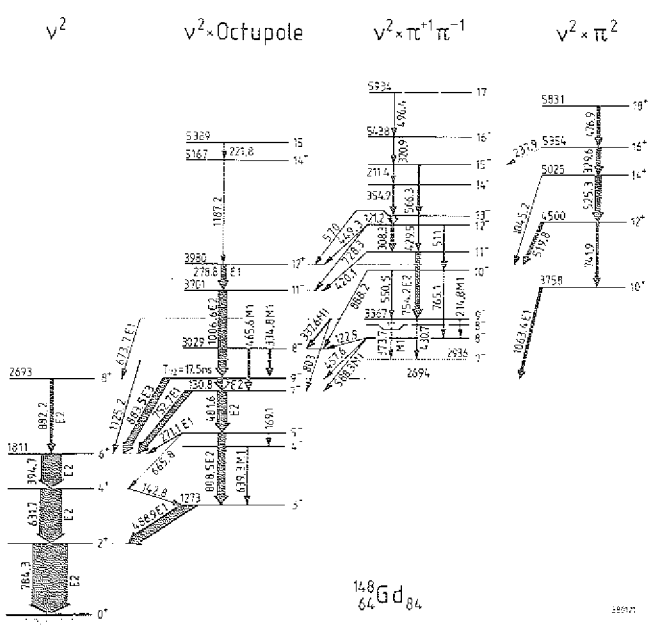

Fig. 1: The energy levels of ^{148}Gd arranged according to their structural configurations as shown above. Transition multipolarities derived from conversion electron data are given.

which completely specify the ^{148}Gd high spin states up to 18^+ and 6 MeV excitation. In fig. 1 the ^{148}Gd levels are arranged in four groups of different configurational character as labelled on top of the figure. The two groups to the right are high-spin shell model excitations involving the two valence neutrons coupled either to proton particle hole core excitations or to the $(\pi h^2_{11/2}\ j^{-2})10^+$ core excited state. Here we consider only the levels shown to the left, vz the pure two valence neutron states ($\nu f^2_{7/2}$, J = 0, 2, 4, 6^+, and $\nu f_{7/2}\ h_{9/2}$, J = 8^+), and the coupling of these states to the ^{146}Gd octupole phonon.

Ten octupole states were observed and are given in the second group in fig. 1, including the $T_{1/2}$ = 17.5 ns 9^- isomer at 2.694 MeV which decays to the 6^+ state through an E3 transition with 55 (6) B_W. The octupole nature of the 8^-, 11^-, and 12^+ levels is deduced from decay branching ratios which strongly suggest that these levels cannot be of multiparticle character as the levels shown to the right. The highly selective decay of the two high-lying 14^+ and 15 states also suggests octupole nature, but the upper one has no parity assigned yet and is therefore not considered in the discussion below.

For calculating the $f^2_{7/2} \times 3^-$ energies in ^{148}Gd we first consider the one-particle x phonon spectrum observed in ^{147}Gd which also specifies the coupling of two $f_{7/2}$ neutrons to the 3^- phonon (fig. 2). In the calculations we diagonalise the strong interaction of the $(\nu f_{7/2} \times 3^-)13/2^+$ septuplett member with the $\nu i_{13/2}$ single particle state using the matrix element $\langle i_{13/2}|H_{coupl}|f_{7/2} \times 3^-, 13/2\rangle$ = .8 MeV and the $\nu i_{13/2}$ single particle energy of 2.1 MeV.

In contrast to the one-particle case of ^{147}Gd, where the $i_{13/2}$ excitation affects only one multiplett member, the analogous mixing in the two-neutron case of ^{148}Gd involves the $3^- \leq I \leq 9^-$ members of the $\nu f_{7/2}\ i_{13/2}$ two-neutron multiplett which lie high above the ^{148}Gd yrast line and have not been observed. For the calculation we assume

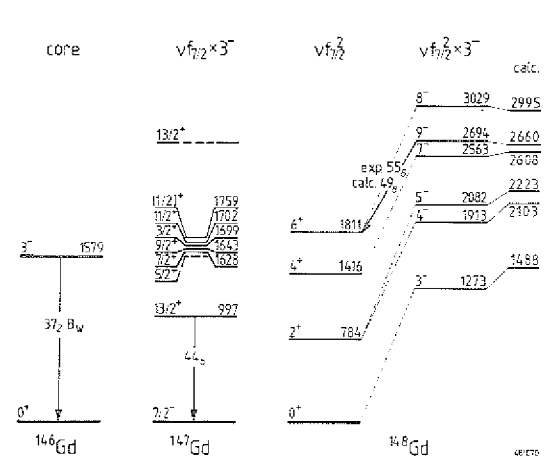

Fig. 2: Observed $\nu f^2_{7/2} \times 3^-$ octupole excitations in ^{148}Gd compared with calculated results. Empirical input data used for the calculation are shown to the left.

that the $4^- \leq I \leq 9^-$ νfi states lie 2.1 MeV above the $(\nu f^2_{7/2})6^+$ level, and that the νfi 3^- state is 600 keV lower. These assumptions fully specify the diagonal energies for calculation of the $\nu f \times 3$, νi interactions in the $\nu f^2 \times 3^-$ multiplett; the much smaller anharmonicities of the $\nu f_{7/2} \times 3^-$ couplings with $1/2 < j < 11/2$ are included as a perturbation. We diagonalise the interaction matrix within the basis states $|(f^2)_{J=0,2,4,6} \times 3^-|_I$ and $(fi)_I$, where in each case the appropriate geometrical factor is taken into account for the off-diagonal $i_{13/2}$ coupling matrix element as well as for the perturbation contributions to each diagonal element. The fig. 3 shows the complete results of the diagonalisation. Numerical results are given in fig. 2. So far only high spin members of each $f^2_J \times 3^-$ group were observed, but we note that their energies are well reproduced, and also that the calculated relative energy shifts within each J-group agree excellent with experiment in the two cases where more than one group member is known.

To the $9^- \rightarrow 6^+$ E3 strength two components contribute, vz the core octupole E3 and the $\nu i_{13/2} \rightarrow \nu f_{7/2}$ single particle E3 transition. The latter can be extracted as 8.5(4.5) B_W from the observed 44(6) B_W of the 997 keV transition in ^{147}Gd and the known core strength of 37(2) B_W. With this result, and the 9^- wave function obtained above, the $9^- \rightarrow 6^+$ BE3 value becomes 49(8) B_W in good agreement with the observed 55(6) B_W.

The 11^- level at 3.701 MeV is assigned as a stretched one-phonon octupole excitation built on the $(\nu f_{7/2}\ h_{9/2})8^+$ state. The coupling of the $(\nu h_{9/2} \times 3^-)13/2^+$ level to the $i_{13/2}$ single neutron state will be very weak since the $\nu i_{13/2} \rightarrow \nu h_{9/2}$ E3 transition involves a spin-flip. The 11^- octupole state energy should therefore be completely analogous to the $\nu f_{7/2} \times 3^-$ excitation in ^{147}Gd.

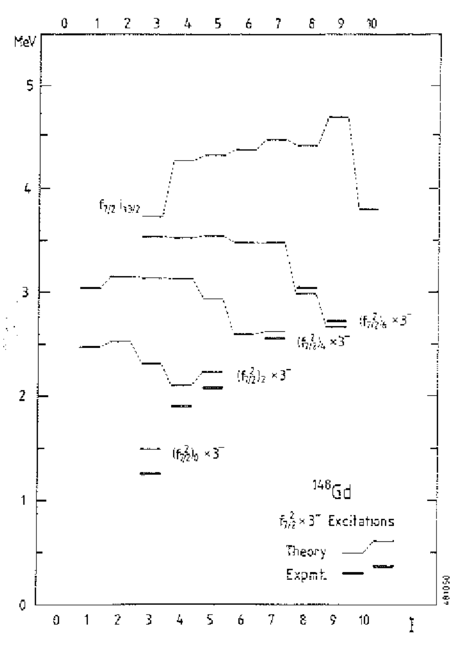

Fig. 3: The complete $\nu f^2_{7/2} \times 3^-$ energy spectrum calculated for ^{148}Gd. Also shown are the two-neutron states from the $\nu f_{7/2}\ i_{13/2}$ configuration. Observed octupole states are included.

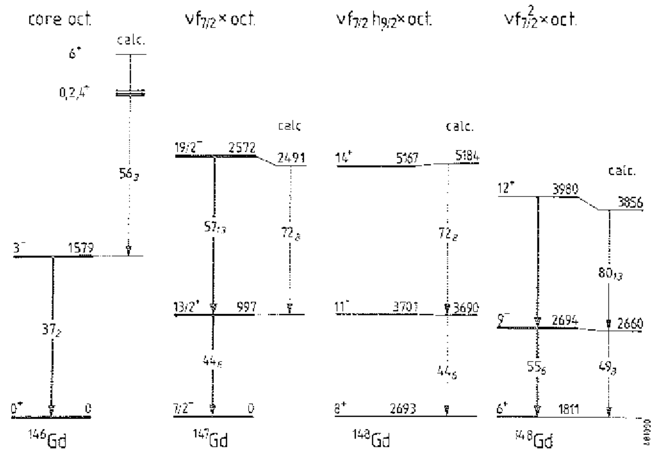

Fig. 4: Single- and double-octupole excitations in Gd-nuclei with 82 to 84 neutrons compared with calculated results.

The observed 1008 keV 8^+ to 11^- energy separation in ^{148}Gd is indeed in close agreement with the 997 keV $13/2^+$ energy in ^{147}Gd (fig. 4).

We assign the 12^+ and 14^+ levels at 3.980 and 5.167 MeV as the stretched two-phonon octupole excitations built on the aligned $(\nu f^2_{7/2})6^+$ and $(\nu f_{7/2}\ h_{9/2})8^+$ two-neutron states. Their energies can be predicted from the experimental information[4] on the $(f_{7/2} \times 3^- \times 3^-)19/2^-$ two-phonon octupole level in ^{147}Gd. The fig. 4 gives a synopsis of the three observed double octupole states. The unharmonicities for the ^{147}Gd $19/2^-$ excitation have been discussed[4] in a recent article, where it was shown that a 0.41 MeV upwards shift for the 6^+ two-phonon state arises from Pauli-blocking of the dominant $\pi h_{11/2}\ d^{-1}_{5/2}$ amplitude of the 3^- phonon. This shift, as well as the associated Pauli-reduction of the BE3 value, are taken into account in the calculated results of fig. 4.

In the calculation of the 14^+ two-phonon state of ^{148}Gd we again ignore the presence of the $h_{9/2}$ spectator neutron. The 14^+ energy is thus evaluated analogous as for the $19/2^-$ two-phonon state[4] in ^{147}Gd, giving E_x = 5.184 MeV for this $\nu f_{7/2}\ h_{9/2} \times 3^- \times 3^-$ double octupole state. In the $(\nu f^2_{7/2} \times 3^- \times 3^-)12^+$ state, the presence of two $f_{7/2}$ neutrons causes non-stretched contributions. The configurations present in that 12^+ level are $\nu f^2 \times 3 \times 3$, $\nu fi_{10} \times 3$, $\nu fi_9 \times 3$, and i^2. We diagonalise the interaction with the fi-states within this 4 x 4 matrix and again include the Pauli blocking shift as well as the pertinent contributions due to the anharmonicities from the $(f \times 3)_{j < 11/2}$ couplings by perturbation. Both calculated two-phonon level energies are in nice agreement with experiment (fig. 4).

References

1) P. Kleinheinz, R. Broda, P.J. Daly, S. Lunardi, M. Ogawa, J. Blomqvist, Z. Phys. A290 (1979) 279

2) M. Piiparinen, T. Komppa, R. Komu, A. Pakkanen, J. Blomqvist, Z. Phys. A309 (1982) 87

3) J. Ungrin, R.M. Diamond, P.O. Tjom, B. Elbek, Mat. Fys. Medd. Dan. Vid. Selsk. 38, no. 8, 1971

4) P. Kleinheinz, J. Styczen, M. Piiparinen, J. Blomqvist, M. Kortelahti, Phys. Rev. Lett. 48 (1982) 1457

5) S. Lunardi, M. Ogawa, M.R. Maier, P. Kleinheinz, ASHPIN, ANL/PHY-79-4, p. 393

2.18. Search for Rotational Band Members in ^{152}Eu

P.T. Prokofjev[+], *L.I. Simonova*[+], *H. Mattheß*, *F. Soramel-Stanco*, *J. Styczen*, *A. Ercan*, *P. Kleinheinz*

Originally it was thought that both deformed as well as spherical shapes occur among the low-lying levels of the doubly odd $^{152}_{63}Eu_{89}$ nucleus, but the results of very detailed (n,γ) studies supplemented by single-nucleon transfer reactions suggest[1)] rotational bands with $A \approx 11$ keV and thus a stably deformed nuclear shape. Since however the ^{152}Eu capture state has[1)] the rather low spin of 3^+ it was not possible to observe more than two rotational excitations for each band, except for the ground band where a third rotational state with $I^\pi = (6)^-$ was tentatively assigned.

The ^{152}Eu energy levels can also be populated in the $^{154}Sm(p,3n)$ reaction where ≈ 10 ħ are transferred to the compound nucleus. At this moderate angular momentum input the γ-decay is not yet sharply concentrated along the yrast line and it might be possible to extend the known near-yrast bands towards higher spin. Our results show however that this is very difficult in a nucleus with very high level density like ^{152}Eu. The (p,3n) measurements were carried out with proton beams from the IKP cyclotron and a 4.9 mg/cm^2 thick self-supporting 98.7 % enriched ^{154}Sm target. Gamma-ray excitation functions were measured from 26 to 35 MeV proton energy, the angular distributions were determined from measurements at six optimally spaced angles ranging from 90° to 165°, and four-parameter two-detector γγ-coincidence measurements were performed with 120 ns beam burst separation. Planar Ge detectors of 20 cm^3 and 30 cm^3 with < 750 eV fwhm at 122 keV were used in all measurements. The optimal beam energy was found to be 29 MeV, where ≈ 55 % of the compound nuclei lead to formation of ^{152}Eu. The (p,4n) exit channel at this energy is about twice as strong as the (p,2n) channel, but due to the higher γ-ray multiplicity in the deformed ^{153}Eu nucleus the transitions from the two odd-A Eu nuclei were equally strong in the coincidence projections. Of the known ^{152}Eu transitions the unresolved 89.4 and 89.6 keV ground state transition doublett strongly dominated the spectra; the second strongest ^{152}Eu line was > 10 times weaker. This quite unusual observation in an in-beam γ-ray experiment is clearly related to the high ^{152}Eu level density and re-emphasizes the difficulties to study this nucleus through the (p,3n) reaction.

The figure one shows a fraction of the ^{152}Eu level scheme which could be extracted from the coincidence data. Clear-cut results were obtained for the K = 3 ground band, although it is extremely weakly populated in the (p,3n) reaction. In the $t_{\gamma\gamma}$ time distribution measured with the 89.6 keV doublett no prompt contribution due to the 89.6 keV ground state transition is apparent, and one can conclude that its contribution to the coincidences is < .7 %. However, three ground band transitions, 110.0, 131.8, and 156.3 keV, clearly occur in the coincidence spectra when appropriately sharp prompt and in-beam gate settings were set for the $t_{\gamma\gamma}$ and $t_{\gamma RF}$ time parameters. A 193 keV γ-ray could possibly be the next higher ground band transition, but this could not be ascertained since in the neighbouring ^{153}Eu nucleus an intense 193.1 keV line is also in coincidence with transitions of 111.6, 131.6, and 156.1 keV (!). The properties of the ^{152}Eu ground band transitions extracted from the singles spectra are listed in Table 1. The measured negative A_2 values are consistent with M1 cascade transition character. Our 131.8(1) keV $6^- \to 5^-$ γ-ray energy is clearly higher than the 131.16 keV line tentatively assigned in the (n,γ) study.

The coincidence spectra give tentative evidence for two further bands, built on a known[1)] 3^+ state at 221.2 keV, and on the 384 ns 4^+ isomer at 89.8 keV. The proposed π|532↑|ν|505↑|K = 3^+ configuration assignment is in accord with the regular rotational spacings and the A-parameter of ≈ 8.2 keV. We have here however reinterpreted the I = 4 state as a rotational state, whereas in the (n,γ) work it was assigned as a $K^\pi = 4^-$ bandhead. The proposed new band built on the π|513↓|ν|402↓|K = 4^+ 384 ns isomer has strongly staggering rotational spacings, indicative of a significant ν|651↑| admixture. Bands with this $i_{13/2}$ neutron orbital in ^{154}Eu show similar energy spacings. Since however γ-ray angular distribution and intensity data are not yet available, these two band assignments must remain tentative.

Table 1: Ground band transitions of ^{152}Eu observed in the (p,3n) reaction at E_p = 29 MeV

E (keV)	Iγ	A_2/A_0	A_4/A_0	E_x^i	$I_i^\pi \to I_f^\pi$
89.86(6)[a]	1000[a]	+.00(1)[a]	-.03(2)[a]	89.61(0)[b]	$4^- \to 3^-$
111.0 (1)	10.6(7)	-.13(6)	-.09(6)	200.75(0)[b]	$5^- \to 4^-$
131.8 (1)	7.8(6)	-.14(4)	-.00(5)	332.55(10)	$6^- \to 5^-$
156.5 (3)	3.2(5)	-.17(18)	-.02(20)	489.05(14)	$7^- \to 6^-$

[a] fitted for doublett; [b] from (n,γ), ref. 1

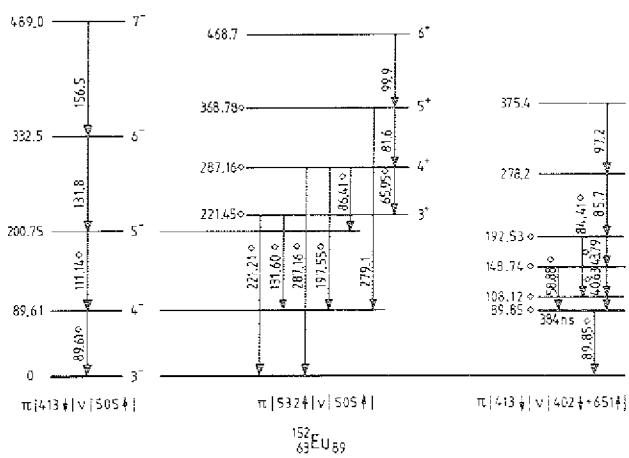

Fig. 1: Selected rotational bands in ^{152}Eu observed in the (p,3n) reaction. Energies labelled with ◇ are taken from the (n,γ) work[1)].

Reference

1) T. von Egidy et al. Z. Phys. A286(1978) 341

+ Latvian SSR Academy of Sciences, Institute of Physics, Riga

2.19. Study of the band structure in the odd-odd nucleus ^{180}Re

*Ts. Venkova, B. Bochev, W. Gast, T, Kutsarova, R.M. Lieder, T. Morek and G. Sletten**

The investigation of crossings bands in ^{180}Os showed[1] that the second crossing has a different characteristic frequency for negative- and positive-parity bands. It has been demonstrated[2] that this frequency shift is caused by a configuration-dependend residual interaction between quasineutrons and quasiprotons. In order to learn more about the residual interaction the study of the odd-odd nucleus ^{180}Re has been started. In this way the features of bands containing one quasiproton and one quasineutron can be studied, the simplest system to investigate residual proton-neutron interactions. The odd-odd nucleus $^{180}_{75}Re^{105}$ has been produced by means of the $^{181}Ta(\alpha,5n)^{180}Re$ reaction using a 62 MeV α-beam from the isochronous cyclotron JULIC. Measurements of the γ-γ coincidences were carried out using four large Ge detectors and a multiplicity filter consisting of four 3"x3" bismuth germaniate detectors. A large member of discrete γ-lines have been observed giving rise to a complex γ-ray spectrum.

A careful analysis of the γ-γ coincidence spectra was necessary to establish the level scheme. Seven rotational bands have been identified. In order to establish their deexcitation to the 1^- $\pi5/2^+[402]\uparrow - \nu7/2^-[514]$ ground state of ^{180}Re[3], which involves low energy γ-transitions four-parameter γ-γ coincidence measurements have been carried out using a large (60 cm^3) and a planar (20 cm^3) detector. The parameters were the two γ-ray energies, the time $t_{\gamma\gamma}$ between the emission of two γ-rays and the time $t_{\gamma beam}$ which elapses between the formation of the nucleus and the deexcitation of its levels. A partial level scheme of ^{180}Re is shwon in fig. 1, including those bands, which definitely belong to ^{180}Re. They are of strongly coupled nature. The remaining four bands are of rotational alignment character. More experiments are necessary to proof that they belong to ^{180}Re. Before an interpretation of the bands can be given their spins and parities have to be determined involving the clarification of their decay to the ground state and the measurement of γ-ray angular distributions. Corresponding experiments are in progress.

References

1) A. Neskakis, R.M. Lieder, G. Sletten and J.D. Garrett, Phys. Lett. 118B (1982) 49
2) R.M. Lieder, A. Neskakis, G. Sletten and J.D. Garrett, Contribution to this annual report, p. 58
3) P.F.A. Goudsmit, J. Konijn and F.W.N. de Boer, Nucl. Phys. A104 (1967) 497

*Niels Bohr Institute, Copenhagen

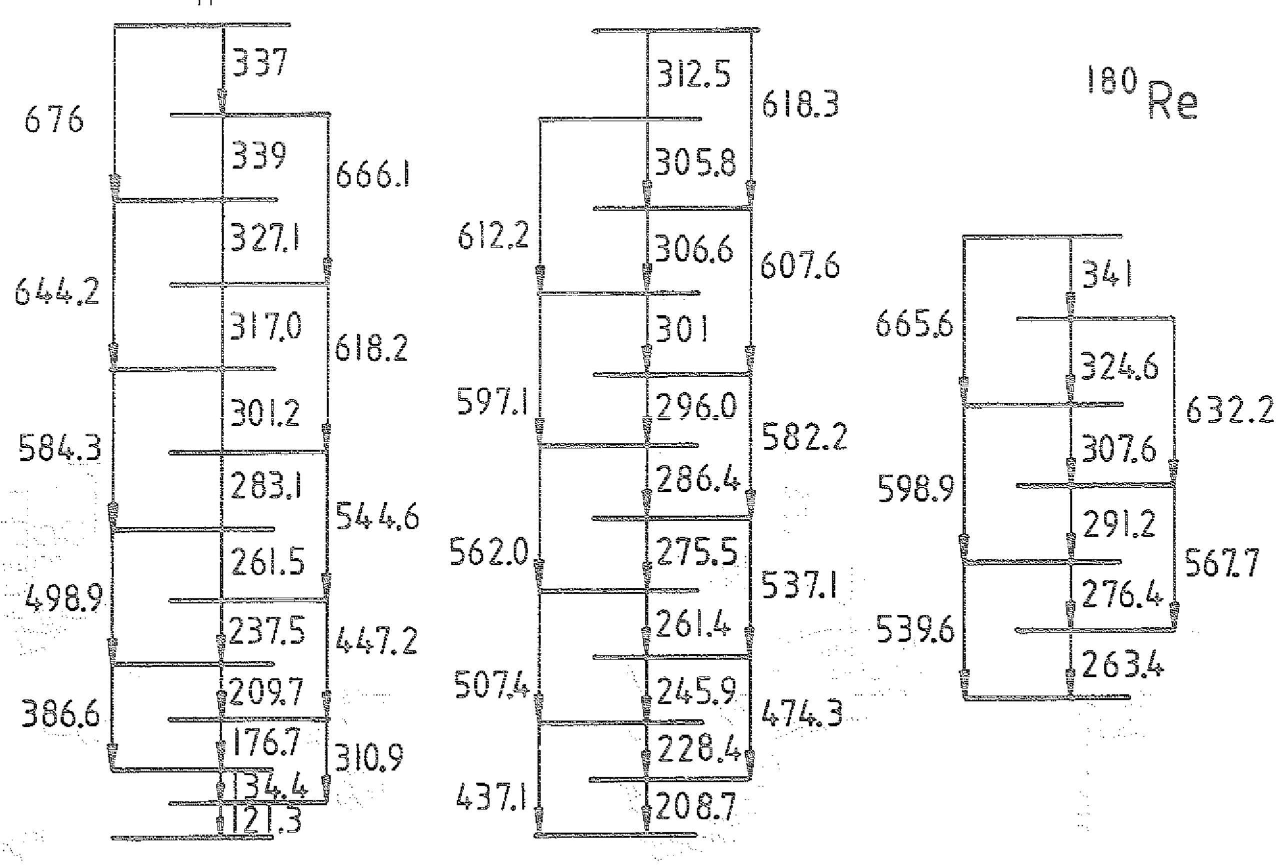

Figure 1: Partial level scheme of ^{180}Re.

2.20. Investigation of band structures and crossings in ^{181}Os

R.M. Lieder, A. Neskakis, G. Sletten and J.D. Garrett**

In the investigation of high-spin states in ^{180}Os nine bands have been observed. Detailed information about six of them has been published previously[1]. They have the following features:

1) Two crossings exist in the bands which are caused by the rotation alignment of a pair of $i_{13/2}$ quasineutrons and $h_{9/2}$ quasiprotons, respectively.
2) The second crossing has a characteristic frequency which is 60 keV smaller for the negative parity bands than for the positive-parity bands, probably due to residual interactions depending either on the configuration or on the number of quasiparticles.
3) The bands $(-,0)_2$ and $(-,1)_3$ (the labelling $(\pi,\alpha)_n$ indicates the parity π and signature α of each band and the number n is used to distinguish various bands), which have the same configuration, show a significant signature splitting not being expected in the framework of the axially symmetric cranked shell model.
4) The $(+,0)_0$ band forming the yrast sequence at low spins is crossed by the $(-,1)_3$ band at a spin of I=19.

In order to obtain additional information on these features the neighbouring nucleus ^{181}Os has been investigated. It was produced by bombarding a ^{167}Er target with 81.5 MeV ^{18}O ions delivered by the FN Tandem accelerator of the Niels Bohr Institute, Copenhagen. A γ-γ coincidence experiment has been carried out with 5 anti-Compton spectrometers. The angular distributions have been measured with an anti-Compton spectrometer consisting of a large Ge detector and a cylindrical suppression shield made of bismuth germanate. A partial level scheme resulting from this investigation is shown in fig. 1. In total 13 bands have been observed. The previously known[2] $(+,\pm)_1$, $(-,\pm)_2$ and $(-,+)_3$ bands (for odd-mass nuclei the signature is $\alpha = \pm\frac{1}{2}$; here the abbreviation $\alpha = \pm$ is used) have been extended up to a spin of $61/2^+$. At least one side band has been found for each of these bands consisting of a few members only. Of special interest is the side band feeding into the $(-,+)_3$ band. It represents most likely the missing $(-,-)_3$ band which is shifted considerably upwards in energy because of their $1/2^-|521|$ configuration.

For the most prominent bands the aligned angular momentum is plotted in fig. 2 as function of the rotational frequency. All bands show two crossings. They are caused, as in ^{180}Os, by the rotation alignment of a pair of $i_{13/2}$ quasineutrons and $h_{9/2}$ quasiprotons, respectively. Of special interest is to compare the characteristic

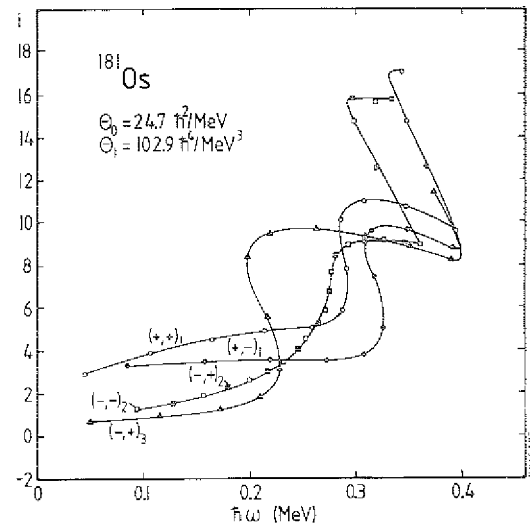

Figure 2: Plot of aligned angular momentum vs. rotational frequency for bands in ^{181}Os. A diabatic reference has been used. The parameters of the Harris expansion were obtained by fitting the g band in ^{184}Os.

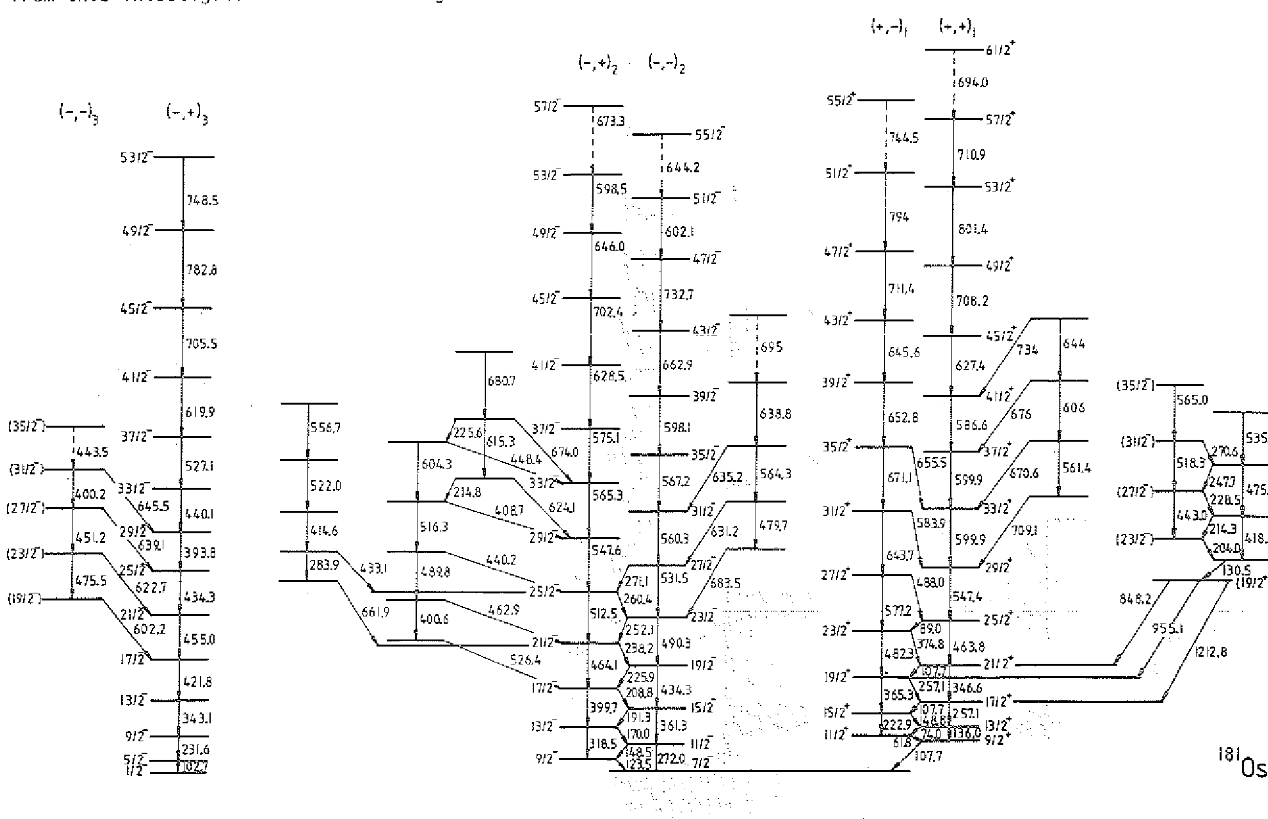

Figure 1: Partial level scheme of ^{181}Os.

frequencies of the second crossings in ^{181}Os and ^{180}Os. They are $\hbar\omega_c$ = 0.32 MeV and $\hbar\omega_c$ = 0.38 MeV, respectively, for the negative- and positive-parity bands in ^{180}Os (ref. 1) and $\hbar\omega_c$ = 0.32 MeV and $\hbar\omega_c$ = 0.37 MeV, respectively, for the $(-,\pm)_2$ and $(+,\pm)_1$ bands in ^{181}Os. Not only the absolute values but also the frequency shifts are almost the same in both cases. This result allows to rule out that the frequency shift depends on the number of quasi-particles involved in the configurations of the bands since in ^{181}Os all the second backbendings result from the crossing of three- and five-quasiparticle bands. It may be concluded, therefore, that the residual interaction, causing the shift, is configuration dependend. Since the configurations of the $(-,\pm)_2$ and $(+,\pm)_1$ bands in ^{181}Os differ by a $7/2^-|514|$ quasineutron it may be assumed that the residual interaction between this configuration and the $1/2^-|541|$ quasiproton configuration produces the frequency shift.

Another interesting feature is the signature splitting between the $(+,+)_1$ and $(+,-)_1$ bands in ^{181}Os. It is very similar to that of the $(-,0)_2$ and $(-,1)_3$ bands in ^{180}Os which are considered to have the configurations $|(+,-)_1\ (x)\ (-,+)_2|$ and $|(+,+)_1\ (x)\ (-,+)_2|$, respectively. It is, therefore, reasonable to assume that the signature splitting is due to the $(+,\pm)_1$ configuration. In order to find an explanation for the signature splitting calculations have been carried out in the framework of the axially asymmetric cranked shell model[3]. In fig. 3

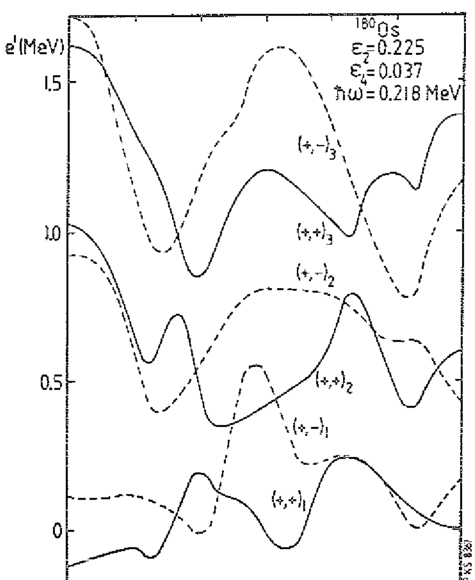

Figure 3: Plot of the quasiparticle energy vs. deformation parameter γ for $i_{13/2}$ quasineutron configurations as calculated in the framework of the axially asymmetric cranked shell model.

the quasiparticle energy is plotted vs. the deformation parameter γ. In the "Lund convention" (ref. 4) used here for the definition of the deformation γ an angle between 0^o and -60^o means a change from a prolate to an oblate shape, for which the nucleus rotates around an axis perpendicular to the symmetry axis. The calculations have been carried out for a rotational frequency of $\hbar\omega$ = 0.218 MeV at which the experimental value of the signature splitting is $\Delta e'$ = 0.15 MeV. It can be seen that the calculated signature splitting depends strongly on the γ deformation. Already a small γ value of $\gamma = -8^o$ is sufficient to explain the experimentally observed signature splitting. A deformation of this order of magnitude is expected for the Os nuclei since they lie at the border of the deformed region.

References

1) A. Neskakis, R.M. Lieder, G. Sletten and J.D. Garrett, Phys. Lett. 118B (1982) 49
2) A. Neskakis, R.M. Lieder, M. Müller-Veggian, H. Beuscher, W.F. Davidson and C. Mayer-Böricke, Nucl. Phys. A261 (1976) 189
3) S. Frauendorf and F.R. May, Phys. Lett. 125B (1983) 245
4) G. Andersen, Nucl. Phys. A268 (1976) 295

*Niels Bohr Institute, Copenhagen

2.21. Search for the two photon decay of light penetrating bosons with the use of a rotatable detector arrangement

H.Bechteler[+], *W.Ermer*, *H.Faissner*[+], *H.R.Koch*, *O.W.B.Schult*, *H.Seyfarth*, *R.Yogeshwar*[++]

The question of the existence of light penetrating bosons (LPB) and their emission by excited nuclei is of fundamental interest. A search for their two-photon decay at the FRJ-1 reactor (Merlin) was performed with a improved rotatable set-up shown in fig.1.

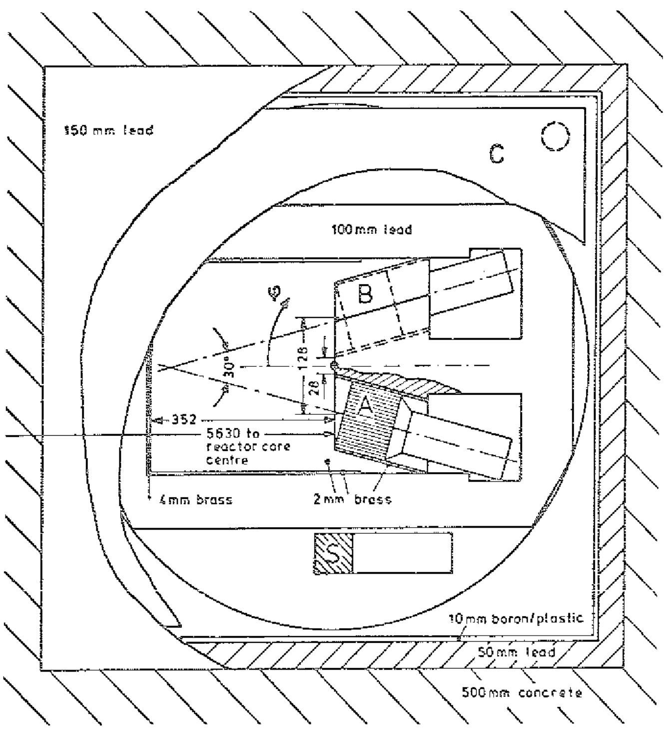

Fig. 1: Rotatable unit installed at the 10 MW light-water reactor FRJ-1 and located within a conventional tight shield. The NaI(Tl) detectors A and B (5" dia x 4") serve for the observation of the two γ quanta which are expected from the decays occuring in the 352 mm long decay region. The whole rotation unit is covered by the veto counter C. The monitor counter S (2" dia x 2") serves to detect any anisotropy of the background within the stationary shield.

Compared to our preceding experiment[1,2] the two NaI(Tl) detectors A and B now are inclined with respect to each other. By this and the reduction of the minimum-distance between both detectors the detection efficiency for the two photon decay of a light particle (assumed rest mass 250 keV/c^2) was improved by a factor of 2.9, with respect to the earlier set-up. The energy spectrum of the nuclear transitions, which served as input for the Monte-Carlo calculations, was assumed to be directly proportional to the reactor γ-ray spectrum[3]. In the earlier experiment[1,2]

the veto-counter C had been positioned between the top cover of the rotating inner 100 mm lead shielding and the stationary 50 mm lead top cover. The installation of the veto-counter C below the total top cover of 150 mm lead results in an increase of the veto-efficiency against cosmic-ray induced coincidences by a factor of 2 (the ratio $AB\bar{C}/AB$ decreases from 0.29 to 0.14) Measurements were performed in 4 different positions: $\varphi = 0^0$, 90^0, 180^0, 270^0. Only in the 0^0 position the simultaneous detection of the two decay photons is possible. In the other 3 positions, conservation of transverse momentum would not allow the two photons to hit directly the two detectors and to be registered as a decay event. Measurements in the effect position (0^0) and in the 3 non-effect positions (90^0, 180^0, 270^0) were performed at both reactor ON and OFF conditions permitting an empirical background subtraction.

Systematic changes of the coincidence rate show a correlation with the atmospheric pressure in agreement with our previous experiment[1,2]. The measured rates were corrected with respect to atmospheric pressure variations.

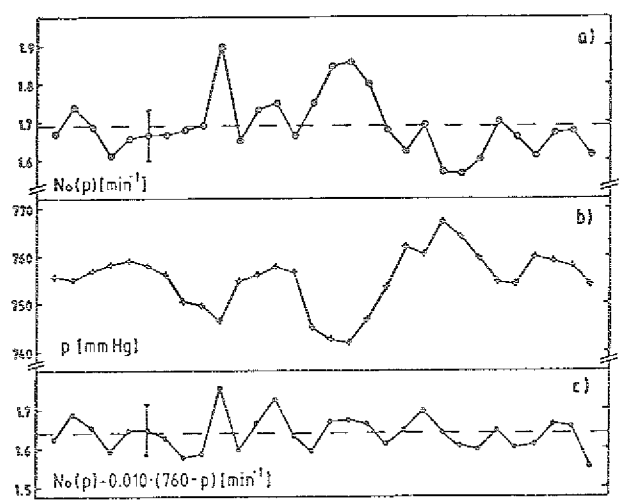

Fig. 2: Effect of atmospheric pressure on the measured coincidence rates and their correction (50 keV ≤ E_A,E_B ≤ 3 MeV, explanation see text).

As an example, Figure 2 demonstrates the effect of this correction for $\varphi = 0^0$ and reactor ON: In fig. 2a the time dependence of the original counting rates $N_0(p)$ is plotted. It is correlated to the atmospheric pressure p (Fig. 2b). The systematic changes in $N_0(p)$ are reduced after correction (Fig. 2c). The corrected counting rates are normalized to 760 mm Hg.

In Fig. 3 all mean coincidence rates for the different angular positions without and with pressure correction are collected together with the reactor ON-OFF differences.

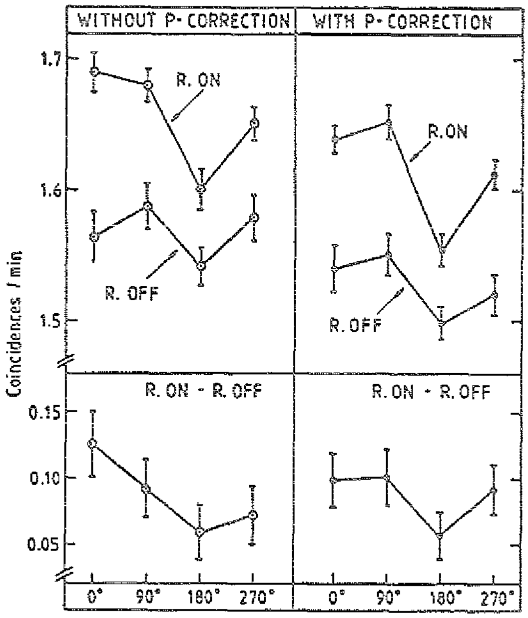

Fig. 3: Mean coincidence rates for the different angular positions at reactor ON and OFF conditions and their differences (50 keV $\leq E_A, E_B \leq$ 3 MeV). An example for the atmospheric pressure correction is given in fig. 2.

To minimize time dependent systematic effects, e.g. changes in the coincidence rates due to atmospheric pressure variations, the angular positions were changed after a preset time by an automatic driving system. Table 1 shows the mean differences deduced from the coincidence rates which have been measured at subsequent effect (0^o) and non-effect (180^o) positions. Mean differences are given which result without and with correction for variations in atmospheric pressure. Table 1 also contains mean differences which are determined using mean coincidence rates measured at subsequent non-effect positions 90^o, 180^o and 270^o.

Table 1: Mean differences between effect and non-effect coincidence rates (50 keV $\leq E_A, E_B \leq$ 3 MeV, all rates in events per minute).

Difference	Rate without p-corr.	Rate with p-corr.
	R.ON	
0°-180°	0.072+/-0.015	0.082+/-0.015
0°-(90,180,270)	0.030+/-0.011	0.030+/-0.011
	R.OFF	
0°-180°	0.020+/-0.020	0.040+/-0.021
0°-(90,180,270)	-0.009+/-0.014	0.014+/-0.015
	R.ON - R.OFF	
0°-180°	0.052+/-0.025	0.042+/-0.026
0°-(90,180,270)	0.039+/-0.018	0.016+/-0.019

The coincidence rate difference of (0.016 ± 0.019)/min yields an upper limit of 0.054/min (95 % confidence level) for the coincidence rate due to two-photon decay of LPB.

This upper limit can be interpreted in the framework of standard axion theory[4]. An overall 15 % contribution of M1 transitions to the total spectrum of nuclear transitions in the reactor[3] is assumed superposed by a 2.4 % M1 contribution from the (n,p)-capture line at 2.23 MeV. From the measured coincidence rate $R_{\gamma\gamma} \leq 5.4 \cdot 10^{-2}$/min and assuming 250 keV axion rest mass we deduce $\Gamma_a/\Gamma_\gamma \leq 3 \cdot 10^{-8}$ for the ratio of axion to γ-ray emission widths.

A new experiment is being set up at the nuclear power station Biblis. This experiment has a superior detection efficiency.

One of us (H.B.) is grateful to the Minister für Wissenschaft und Forschung, Düsseldorf, for support.

References

1) H. Bechteler, W. Ermer, H.R. Koch, O.W.B. Schult, H. Seyfarth, R. Yogeshwar, Annual Report 1982, IKP/KFA, Jül-Spez 202 (1983), p. 62
2) H.R. Koch, O.W.B. Schult, H. Seyfarth, H. Bechteler, R. Yogeshwar, Z. Phys. A313 (1983) 239
3) H. Bechteler, H. Faissner, H. Seyfarth, R. Yogeshwar, contribution to this report, p. 62
4) T.W. Donnelly, S.J. Freedman, R.S. Lytel, R.D. Peccei, M. Schwartz, Phys. Rev. D18 (1978) 1607

+ III. Physikalisches Institut, Technische Hochschule, Aachen, F.R. Germany
++ III. Physikalisches Institut, Technische Hochschule, Aachen and IKP/KFA Jülich, F.R. Germany

2.22. The Spectrum of γ Radiation Emitted in the FRJ-1 (Merlin) Reactor Core and Moderator Region

H. Bechteler[+], *H. Faissner*[+], *H. Seyfarth*, *R. Yogeshwar*[++]

Nuclear reactors might be strong sources of light, penetrating bosons[1] which have been suggested by some theories[1,2] unifying strong and electroweak interactions. A crucial issue in the interpretation of experiments,which search for the decay of such particles at a nuclear reactor[3], is the energy distribution of the nuclear transitions,which could lead to the emission of these particles instead of γ radiation. In earlier papers (e.g. ref. 4) the total γ-ray spectrum emitted in the reactor has been approximated by the spectrum of prompt fission γ rays[5]. The γ rays from β decay of fission products, radiative neutron capture and inelastic neutron scattering had been neglected. However, they contribute about 50 % to the total reactor γ-ray spectrum as is shown in the present note.

In a horizontal cut fig. 1 shows the set-up of the core region of the 10 MW_{th} research reactor FRJ-1 (Merlin) of the KFA Jülich within the H_2O tank and the biological shield. The reactor core consists of 28 standard fuel elements (F), each containing 264 g ^{235}U enriched to 80 %, and 4 absorber/fuel elements (A). Each of them contains 192 g of ^{235}U, and admits for the fork-shaped absorbers,which are alloys of 80 % silver, 15 % indium and 5 % cadmium. During a standard 30 day reactor period their mean position is 70 % outcore. Three positions (P) are reserved for incore irradiations. Three sides of the core surface are covered for the most part by steel irradiation bars (St). Neutron-flux bridges made of aluminium (Al) prevent the decrease of the neutron flux towards the thermal columns which are situated within the biological shield in -X and +X direction. The experimental set-up, used to search for the two-photon decay of light, penetrating bosons,is situated outside the closed biological shield in +X direction at a distance of ∿ 5 m from the reactor core.

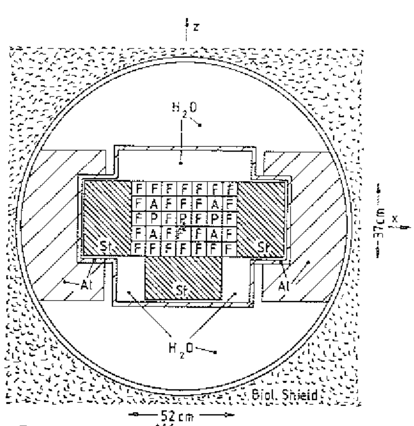

Fig. 1: FRJ-1 reactor core and moderator region (explanations see text).

The total energy release per thermal-neutron induced fission of ^{236}U except antineutrino energy amounts to 192 MeV/fission[6] (kinetic energy of fission products and neutrons, β and γ radiation of fission products). To maintain a thermal reactor power of 10 MW, 3.25×10^{17} fissions/sec are necessary. The average number of neutrons emitted after thermal-neutron induced fission of ^{236}U ($\nu = 2.47$[6]) yields the total neutron source strength of 8.03×10^{17}/sec. Of these 3.87×10^{17}/sec are absorbed by ^{235}U in (n,f) and (n,γ) processes. The total γ-ray spectrum per neutron absorbed in ^{235}U (including γ rays following β decay of the fission products) has been measured[7] and yields in total (13.6 ± 0.3) γ quanta/neutron.

The distribution of the neutron flux density in the set-up of fig. 1 has been calculated with the Monte Carlo program KENO[8] which follows the life history of neutrons through 53 neutron energy intervals (14.9 MeV ....10^{-5} eV), and 186 geometrical regions,into which the reactor core zone and its surrounding has been divided according to the distribution of materials. The thermal and epithermal neutron flux densities,together with the neutron capture cross sections[9], and the spectra of γ radiation emitted after neutron capture (low and high energy lines plus intermediate quasi-continuum, e.g. ref. 10) yield the local contributions of the different materials to the γ-ray spectrum. As an example fig. 2 shows the distribution of the (n,p) capture rate (i. e. the source strength of the 2.2 MeV γ rays) along the Z axis (fig. 1).

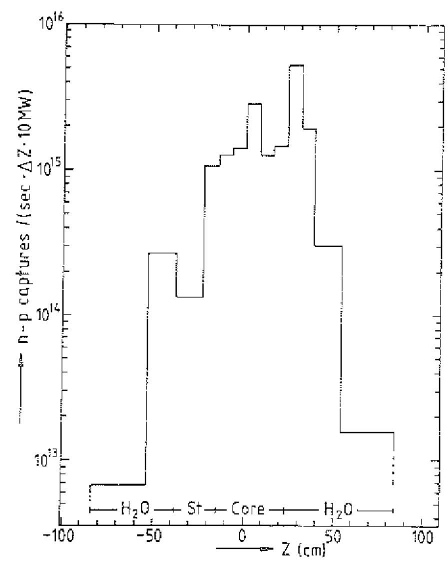

Fig. 2: Distribution of 2.23 MeV γ-ray source strength from n-p capture along Z axis (ΔZ = 1 cm)

Table 1 gives the neutron capture rates in the different materials, and their contributions to the total γ-ray source strength, at 10 MW reactor power.
Besides the materials already mentioned the fission products ^{135}Xe and ^{149}Sm with extremely high neutron capture cross section yield small contributions. The sum of 6.95×10^{17} neutron absorptions per second only covers 87 % of the full emission rate (8.03×10^{17}/sec). This may be explained with neutron leakage from the regarded volume.

Table 1: Contributions to the total neutron-absorption and γ-emission rates at 10 MW thermal reactor power (FRJ-1)

	neutron absorption (10^{17} n/sec)	γ-ray emission (10^{17} photons/sec)
$^{235}U(n,f)$	3.25	52.63
$^{235}U(n,\gamma)$	0.62	
^{238}U	0.05	0.25
H_2O	1.42	1.42
Al	0.47	1.37
Fe	0.57	0.90
^{135}Xe	0.28	1.21
^{149}Sm	0.06	0.24
Ag	0.10	0.51
In	0.04	0.22
Cd	0.09	0.33
Total	6.95	59.08

In fig. 3 the γ-ray spectra from neutron absorption in ^{235}U and from neutron absorption in the other materials (table 1) are shown together with the total spectrum. The first spectrum drops above the neutron binding energy of ^{236}U (B_n = 6.55 MeV[10]). The second one shows prominent peaks from β decay of ^{28}Al (1.78 MeV) and from neutron-capture in ^{1}H (2.23 MeV), ^{27}Al (6.10, 7.27 MeV), and ^{56}Fe (7.28, 7.63, 7.65 MeV).

The total spectrum $n(E_\gamma) = 5.60 \times 10^{18} \times e^{-0.956 E_\gamma}$ photons/(sec 1 MeV 10 MW), for E_γ in MeV, lies higher than that which results from the prompt fission γ-ray spectrum[5] as $3.0 \times 10^{18} \times e^{-1.14 E_\gamma}$ photons/(sec 1 MeV 10 MW).

To predict the energy spectrum of the emitted bosons, analysis of the total transition spectrum into its multipole components has to be performed. A rough preliminary estimate using experimental data on prompt fission γ-rays[11] and those from β decay of fission products[12] yields an overall (20 ± 5) % M1 contribution in the γ-ray spectrum. This estimate lies appreciably higher than an earlier one (1 %) which only had been based on general considerations on transition probabilities[4].

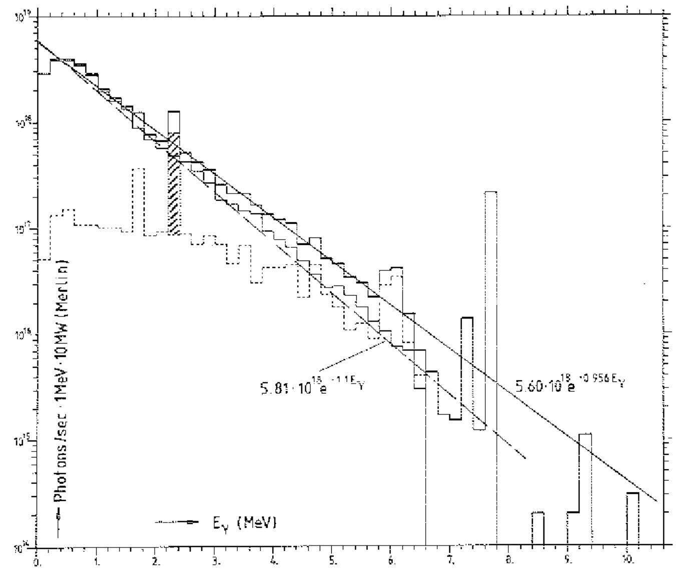

Fig. 3: The total γ-ray spectrum emitted in the FRJ-1 reactor core and moderator region (dark upper histogram) is approximated by $N(E_\gamma) = 5.60 \cdot 10^{18} \exp(-0.956\, E_\gamma)$. The lower full-line histogram shows the contribution from n capture in ^{235}U (fission, radiative capture and β decay of fission products) and is approximated by $N(E_\gamma) = 5.81 \cdot 10^{18} \exp(-1.1 \cdot E_\gamma)$. The dotted histogram represents the contribution from n capture in other materials except hydrogen. The dashed bar gives the intensity of the 2.23 MeV line from (n,γ) capture, which amounts to 2.4 % of the total spectrum.

References

1) S. Weinberg, Phys. Rev. Lett. 40 (1978) 223
2) F. Wilczek, Phys. Rev. Lett. 40 (1978) 279
3) H. Bechteler et al., contribution to this report, p. 60
4) T.W. Donnelly et al., Phys. Rev. D18 (1978) 1607
5) V.V. Verbinski et al., Phys. Rev. C7 (1973) 1173
6) J. Fassbender, Einführung in die Reaktortechnik (Thiemig Verlag, München, 1967)
7) P.J. Bendt and E.T. Jurney, in: Neutron Capture Gamma-Ray Spectroscopy, Edts. R.F. Chrien and W.R. Kane (Plenum Press, New York, 1979), p. 558
8) K.-J. Kalker, private communication
9) S.F. Mughabghab and D.I. Garber, BNL 325, 3rd Ed., vol. 1 (1973)
10) Nucl. Data A3 (1967) and A5 (1968)
11) R.W. Peelle and F.C. Maienschein, Phys. Rev. C3 (1971) 373
12) Table of Isotopes, Edts. C.M. Lederer and V.S. Shirley (1978)

+ III. Physikalisches Institut, Technische Hochschule Aachen, F.R. Germany

++ III. Physikalisches Institut, Technische Hochschule Aachen and IKP/KFA Jülich, F.R. Germany

3. NUCLEAR STRUCTURE

3.1. Quasiparticle RPA Calculations for $^{146}_{64}Gd_{82}$ with Effective Forces Including Meson Exchange Potentials

C. Conci, V. Klemt, J. Speth

The first application of our computer code[1], which allows the microscopic description of spherical superfluid nuclei, was meant for the nucleus ^{146}Gd and its neighbouring nuclei.

The theory we have used for this study is the quasiparticle random-phase approximation (QRPA)[2], which gives the possibility to treat collective and non-collective states of closed subshell nuclei within the same framework.

Our choice has been suggested by the fact that, even though there are some similarities between $^{146}_{64}Gd_{82}$ and the doubly-magic nucleus $^{208}_{82}Pb_{126}$, there exists however a qualitative difference between them: while the Z=82 and N=126 energy gaps are large enough to make negligible the nuclear pairing effect, the Z=64 gap is significantly smaller and consequently a relatively strong effect of proton pairing is present in the nucleus ^{146}Gd.

The ground state of a closed subshell nucleus, for which the pairing effect plays a significant role, corresponds to the Bardeen-Cooper-Schrieffer (BCS) ground state[3]. We have calculated the BCS wave function from a Woods-Saxon potential using a large single-particle basis and assuming pairing correlations between protons only.

The BCS-equations have been solved using a realistic pairing force like a density-dependent δ-force. The same force has been used as residual particle-particle interaction in the solution of the QRPA-equations.

As for the residual particle-hole interaction we have considered, in addition to a density-dependent zero-range force of Migdal type, also explicitly the finite-range contribution due to the one-pion and one-rho exchange potentials[4].

In this way we have studied the spectroscopic properties, viz. the excitation energies and the electric and magnetic transition probabilities of the doubly even nucleus ^{146}Gd, for which in recent years there have been extensive investigations[5]. The proton and the neutron levels for ^{146}Gd near the Fermi surface we used in the present calculations are drawn in Fig. 1.

The energy gap for protons is 3.4 MeV and for neutrons 3.7 MeV. Since the $\pi 1h_{11/2}$ level lies closer above the Z=64 gap than the neutron high-j levels above the N=82 gap, one expects that proton particle-hole excitations will form the yrast states of ^{146}Gd.

The measured ^{146}Gd yrast states are in full accordance with these expectations and so are the calculations which we present in Table 1 and in Fig. 2.

The comparison between experiment[5] and theory is done for the excitation energies and, in three cases, viz. 3_1^-, 2^+ and 0_2^+ also for the transition probabilities. In all cases the agreement between theory and experiment is good.

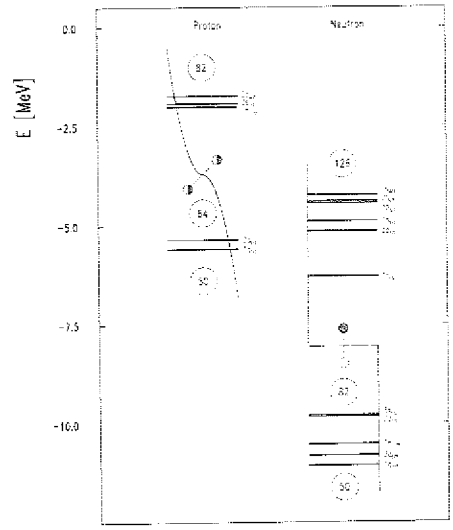

Fig. 1: Proton and neutron levels for ^{146}Gd. The dashed line indicates the Fermi surface, which for protons is smeared out due to the pairing correlations. The full and empty circles represent a particle-hole-like and the two half-full circles a quasiparticle-like excitation.

J^π	E_{exp} (keV)	E_{th} (keV)	$E_{exp}-E_{th}$ (keV)	B-value ($0^+ \to J^\pi$)	main config.	ϵ_{2qp} (keV)	X	Y
3_1^-	1579 a)	1555	24	0.363×10^6	$\pi 1h_{11/2}-2d^{-1}_{5/2}$	3428	0.7342	-0.2849
					$\nu 1h_{9/2}-2d^{-1}_{3/2}$	4930	0.3777	-0.1847
					$\nu 2f_{7/2}-3s^{-1}_{1/2}$	3500	0.2903	-0.1075
					$\nu 1i_{13/2}-1h^{-1}_{11/2}$	6280	0.2250	-0.1204
3_2^-	3423 b)	3561	-138	0.212×10^3	$\nu 2f_{7/2}-3s^{-1}_{1/2}$	3500	0.8086	0.0161
					$\nu 2f_{7/2}-2d^{-1}_{3/2}$	3530	0.5522	-0.0055
					$\pi 1h_{11/2}-2d^{-1}_{5/2}$	3428	-0.1122	0.0016
2^+	1972 a)	1968	4	0.446×10^4	$\nu 2f_{7/2}-1h^{-1}_{11/2}$	4230	0.5340	0.1837
					$\pi 2d_{3/2}-1g^{-1}_{7/2}$	3846	0.5074	0.1338
					$\pi 3s_{1/2}-2d^{-1}_{5/2}$	3349	0.3752	0.0785
					$(\pi 2d_{5/2})^{-2}$	3070	0.3463	0.0546
0_2^+	2165 d)	2524	-359	0.0117	$(\pi 1h_{11/2})^{-2}$	3786	-0.7006	0.1792
					$(\pi 1g_{7/2})^{-2}$	3530	0.5207	-0.1699
					$(\pi 2d_{5/2})^{-2}$	3070	0.5149	-0.1710
≤4	2612 c)	4^+:2456	146	0.856×10^7	$\pi 3s_{1/2}-1g^{-1}_{7/2}$	3579	0.4253	0.0665
					$\pi 2d_{3/2}-2d^{-1}_{5/2}$	3616	-0.3796	-0.0694
					$\pi 1g^{-1}_{7/2}-2d^{-1}_{5/2}$	3300	-0.3794	-0.0461
					$\nu 2f_{7/2}-1h^{-1}_{11/2}$	4230	-0.3647	-0.0885
					$(\pi 2d_{5/2})^{-2}$	3070	-0.3369	-0.0271
5^-	2658 a)	2845	-187	0.287×10^9	$\pi 1h_{11/2}-2d^{-1}_{5/2}$	3428	0.7655	-0.0714
					$\nu 2f_{7/2}-2d^{-1}_{3/2}$	3530	-0.3798	0.0532*
7^-	2982 a)	3379	-397	0.136×10^{12}	$\pi 1h_{11/2}-2d^{-1}_{5/2}$	3428	-0.9874	0.0068
4^-	2996 c)	3435	-439	0.890×10^6	$\pi 1h_{11/2}-2d^{-1}_{5/2}$	3428	0.9850	-0.0031
6^-	3099 c)	3468	-369	0.664×10^{10}	$\pi 1h_{11/2}-2d^{-1}_{5/2}$	3428	-0.9703	0.0064
8_1^-	3183 a)	3590	-407	0.360×10^{14}	$\pi 1h_{11/2}-2d^{-1}_{5/2}$	3428	-0.9151	0.0203
					$\pi 1h_{11/2}-1g^{-1}_{7/2}$	3658	0.4025	0.0045
8_2^-	3294 a)	3672	-378	0.760×10^{13}	$\pi 1h_{11/2}-1g^{-1}_{7/2}$	3658	0.9137	-0.0073
					$\pi 1h_{11/2}-2d^{-1}_{5/2}$	3428	0.4023	-0.0168
9^-	3429 a)	3825	-396	0.439×10^{15}	$\pi 1h_{11/2}-1g^{-1}_{7/2}$	3658	-0.9945	0.0528
10^+	3865 a)	3763	102	0.522×10^{16}	$(\pi 1h_{11/2})^2$	3786	0.9912	-0.0015

Table 1: Excitation energies and transition probabilities of the low-lying states in ^{146}Gd. (The B(EJ)-values are given in units of $e\ fm^{2J}$ and the B(MJ)-values in $(n\ m)^2\ fm^{2(J-1)}\ 10^{2J}$. B(E0) is dimensionless.)

The schemes of Fig. 2 indicate that the calculated level sequence agrees with the experimental one up to 9^-, but the levels from 5^- up to 9^- lie 300-400 keV higher than the experimental ones. We argue that these energy shifts are due to the fact that in the present calculations the residual Coulomb interaction has not been included.

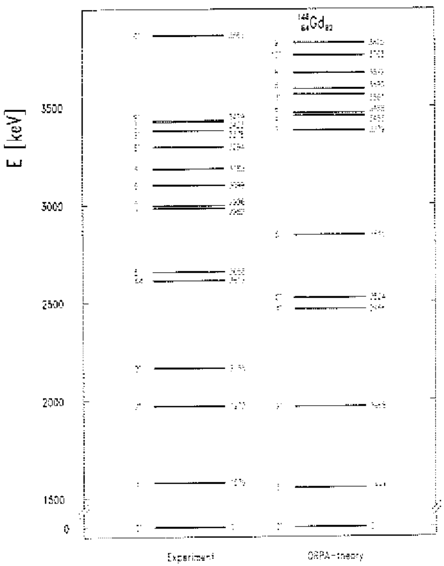

Fig. 2: Experimental and theoretical level schemes of the nucleus ^{146}Gd up to about 4 MeV. The second level scheme is calculated in the framework of the QRPA-theory with the inclusion of the π- and ρ-exchange potential.

Considering recent RPA-calculations performed for ^{208}Pb taking into account the contribution of the Coulomb force[6], we estimate that this effect leads to an attractive particle-hole and to a repulsive particle-particle interaction, whose order of magnitude in ^{146}Gd is around 250-350 keV. Applying these conclusions to the second level scheme of Fig. 2, we see that the agreement with the experimental one improves significantly.

References

1) C. Conci, V. Klemt, Annual Report 1982, Jül-Spez 202 (1983) 76.
2) B.L. Birbrair, K.I. Erokhina, I.Kh. Lemberg, Nucl. Phys. A145 (1970) 129;
D. Zawischa, J. Speth, D. Pal, Nucl. Phys. A311 (1978) 445.
3) J. Bardeen, L.N. Cooper, J.R. Schrieffer, Phys. Rev. 108 (1957) 1175.
4) J. Speth, V. Klemt, J. Wambach, G.E. Brown, Nucl. Phys. A343 (1980) 382.
5) P. Kleinheinz, R. Broda, P.J. Daly, S. Lunardi, M. Ogawa, J. Blomqvist, Z. Phs. A290 (1979) 279;
J. Styczen, P. Kleinheinz, M. Piiparinen, J. Blomqvist, Proc. 4th Int. Conf. on Nuclei far from Stability, Helsingør (1981), ed. by P.G. Hansen and G.B. Nielsen (CERN, Geneva, 1981) p. 548;
E.R. Flynn, J. Van der Plicht, J.B. Wilhelmi, L.G. Mann, G.L. Struble, R.G. Lanier, Phys. Rev. C28 (1983) 97;
R. Julin, J. Kantele, M. Luontama, A. Passoja, P. Kleinheinz, J. Blomqvist, Phys. Lett. 94B (1980) 123.
6) G. Co', J. Heisenberg, S. Krewald, J. Speth, preprint.

3.2. Spectroscopic Study of Low-Energy States of the N=82 Isotones $^{142}_{60}$Nd, $^{144}_{62}$Sm, $^{148}_{66}$Dy and $^{150}_{68}$Er in the Framework of the QRPA-Theory

C. Conci, V. Klemt, J. Speth

Within the formalism exposed in Ref. 1 and in the previous contribution to the present Annual Report it is possible to calculate also the spectroscopic properties of the even-even N=82 isotones around ^{146}Gd, changing only the proton number.

We have only to add or to take away two or four protons and to solve again the BCS- and the QRPA-equations[1] for the corresponding particle number.

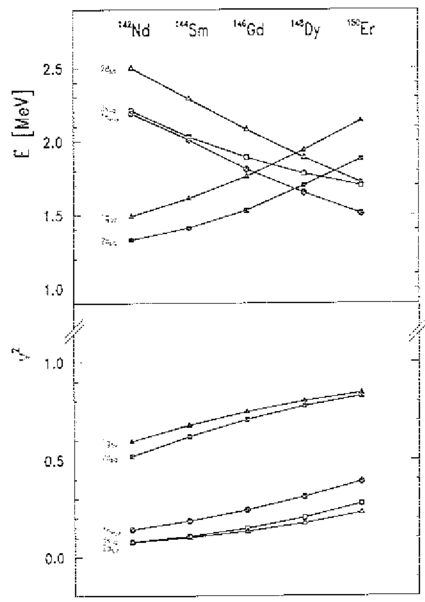

Fig. 1: Quasiparticle energies E and occupation probabilities v^2, obtained solving the BCS-equations using a realistic pairing force, for the N=82 isotones with 60<Z<68.

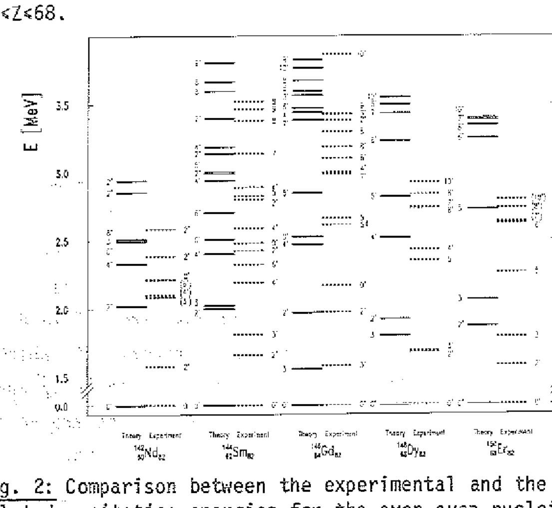

Fig. 2: Comparison between the experimental and the calculated excitation energies for the even-even nuclei ^{142}Nd, ^{144}Sm, ^{146}Gd, ^{148}Dy and ^{150}Er. All the measured levels up to about 4 MeV are represented.

In Fig. 1 it is shown how the occupation probabilities v^2 and the quasiparticle energies E change by increasing the proton number from Z=60 in ^{142}Nd to Z=68 in ^{150}Er for fixed neutron number N=82. Here we did not change the single-particle energies. The quasiparticle level sequence, which in ^{142}Nd is $d_{5/2}$-$g_{7/2}$-$h_{11/2}$-$s_{1/2}$-$d_{3/2}$ is reversed in ^{150}Er to $s_{1/2}$-$h_{11/2}$-$d_{3/2}$-$d_{5/2}$-$g_{7/2}$. This can be interpreted as a support for the good closure of the Z=64 subshell. Fig. 2 gives a complete overview of the results concerning the five N=82 isotones $^{142}_{60}$Nd, $^{144}_{62}$Sm, $^{146}_{64}$Gd, $^{148}_{66}$Dy and $^{150}_{68}$Er.

The nuclei ^{142}Nd and ^{144}Sm have four and two protons less in the $2d_{5/2}$-$1g_{7/2}$ subshell with respect to the doubly closed nucleus ^{146}Gd. The main configurations which will contribute to the yrast levels are the proton two-hole configuration $(\pi 2d_{5/2})^{-2}$, $(\pi 1g_{7/2})^{-2}$ and $(\pi 2d_{5/2}\text{-}1g_{7/2})^{-2}$. In both nuclei they give rise to the sequence of positive parity states: 2^+, 4^+, 6^+. For these states the agreement with the experimental values[2,3] is less than 300 keV. In the ^{142}Nd the only negative parity states which has been measured experimentally is the 3^- at 2084 keV with a B(E3)-value of 6.3×10^4 e^2fm^6 [2]. For this state we calculate an energy of 2501 keV and a B(E3)-value of 2.0×10^4 e^2fm^6.

The sequence of negative parity states with spin 3 to 9 in ^{144}Sm, which has been investigated a few years ago[3], is analogous to that of ^{146}Gd and is quite well reproduced in our calculations. In both nuclei the proton monopole pairing vibration state $0^+_{(2)}$ is reproduced, particularly well in ^{144}Sm.

In contrast to early calculations[4], we have now also calculated the negative parity states up to $J^\pi = 9^-$ and find good agreement with experiment for those. A few years ago the two proton nucleus $^{148}_{66}Dy_{82}$ was investigated[5] and its level scheme up to 4 MeV was established. Since the $1h_{11/2}$, $3s_{1/2}$ and $2d_{3/2}$ proton orbitals lie close together and are the only orbitals between the Z=64 and the Z=82 energy gaps, one expects that excitations involving the $\pi 1h_{11/2}$ level would form the complete sequence of the yrast states in ^{148}Dy. Our results reproduce the fact that the $(\pi 1h_{11/2})^2$ two-particle configuration contributes to all the positive parity states 2^+, 4^+, 6^+, 8^+, 10^+ and that the 10^+ is the fully aligned $(\pi 1h_{11/2})^2$ state.

Very recently two different groups[6] have determined the yrast states of the nucleus $^{150}_{68}Er_{82}$ up to 3 MeV. The positive parity spectrum of ^{150}Er up to $J^\pi = 10^+$ is described in our calculations as the sequence of the $(\pi 1h_{11/2})^4$ seniority two configurations. The 10^+ to 8^+ and 8^+ to 6^+ spacings agree well with experiment, which is in accordance with the experience that the fully and nearly fully aligned members of a j^2 multiplet are well reproduced by a δ-force, which we use for the particle-particle interaction. On the other hand, we calculate the 10^+ to 2^+ and 10^+ to 0^+ spacings about 300-400 keV larger than experiment, which corresponds to an overestimaed collectivity for these levels. In ^{148}Dy the 3^- lies higher than in ^{146}Gd, because the Fermi surface is shifted upwards by adding two protons. This tendency continues in the four valence-proton nucleus ^{150}Er, where the octupole vibration has still a dominant $(\pi 1h_{11/2}\text{-}2d^{-1}_{5/2})$ component.

From Fig. 2 we can observe that apart from ^{146}Gd, where the agreement between the experimental and the theoretical values is very good (see previous contribution to this Annual Report), one immediately observes that the calculated energy levels for all other nuclei lie systematically between 100 and 600 keV too high. We ascribe this effect to the simplicity of our choice for the particle-particle interaction, which is a density-dependent δ-force. This choice doesn't impair the results for ^{146}Gd, because here most of the states are dominantly of particle-hole structure. However, in the neighbouring nuclei, because of the added valence particles (or holes), the energy levels are more strongly dominated by particle-particle (or hole-hole) configurations and therefore their description demands a more realistic particle-particle interaction. The introduction of finite-range terms also in the particle-particle force will be one of the first tasks we intend to face in the future.

References

1) C. Conci, V. Klemt, Annual Report 1982, Jül-Spez 202 (1983) 76.
2) J.K. Tuli, Nucl. Data Sheets 25 (1978) 53.
3) C.M. Lederer, V.S. Shirley, Table of Isotopes, 7th Edition (J. Wiley, New York, 1978); R. Pengo, S. Lunardi, R. Tischler, Y. Nagai, R. Broda, P. Kleinheinz, Proc. Symp. on High-Spin Phenomena in Nuclei, Argonne Nat. Lab., Argonne, Illinois (1979) p. 385.
4) M. Waroquier, K. Heyde, Nucl. Phys. A164 (1971) 113.
5) P.J. Daly, P. Kleinheinz, R. Broda, S. Lunardi, H. Backe, J. Blomqvist, Z. Phys. A298 (1980) 173.
6) H. Helppi, Y.H. Chung, P.J. Daly, S.R. Faber, A. Pakkanen, I. Ahmad, P. Chowdhury, Z.W. Grabowski, T.L. Khoo, R.D. Lawson, J. Blomqvist, Phys. Lett. 115B (1982) 11; E. Nolte, G. Colombo, S.Z. Gui, G. Korschinek, W. Schollmeier, P. Kubik, S. Gustavsson, R. Geier, H. Morinaga, Z. Phys. A306 (1982) 211.

3.3. On the Nature of the 1^+ State at 3.48 MeV in ^{88}Sr

C. Conci, J. Speth

In the nucleus $^{88}_{38}Sr_{50}$ the partially occupied shell between Z=38 and Z=50 is made up by three negative parity states, $1f_{5/2}$, $2p_{3/2}$ and $2p_{1/2}$ and by the positive parity state $1g_{9/2}$. Because of the characteristic of semimagicity of ^{88}Sr, which has a closed subshell for protons at Z=38 and a closed shell for neutrons at N=50, in order to study the spectroscopic properties of this nucleus we have made use of the quasiparticle random-phase approximation[1].

Starting from a Woods-Saxon single-particle basis we solve the BCS-equations only for protons (see Fig. 1). We show in Table 1 the BCS-solutions, i.e. the energy gaps Δ and the occupation probabilities v^2, for the full configuration space we use in our calculations. The energy gaps are different for each level because our pairing force is a density-dependent δ-force which has, unlike the schematic pairing force, matrix elements that

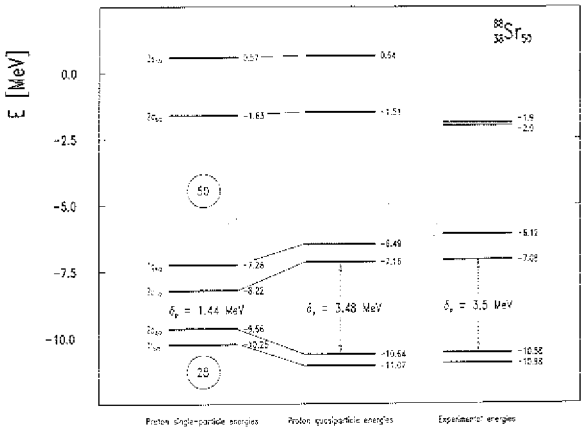

Fig. 1: To the left are represented the proton single-particle energies obtained from a Woods-Saxon potential; in the middle the corresponding quasiparticle energies obtained after the solution of the BCS-equations and to the right the experimental energies from Ref. 4.

orbit a	$\epsilon_{(sp)a}$ (MeV)	$\epsilon_{(qp)a}$ (MeV)	Δ_a (MeV)	v_a^2
$1s_{1/2}$	-35.90	-35.93	1.44	0.9993
$1p_{3/2}$	-29.93	-29.98	1.55	0.9986
$1p_{1/2}$	-28.35	-28.41	1.52	0.9985
$1d_{5/2}$	-23.05	-23.15	1.66	0.9966
$1d_{3/2}$	-19.60	-19.72	1.62	0.9944
$2s_{1/2}$	-19.01	-19.14	1.63	0.9937
$1f_{7/2}$	-15.45	-15.68	1.74	0.9833
$1f_{5/2}$	-10.25	-11.07	1.70	0.8121
$2p_{3/2}$	-9.66	-10.64	1.57	0.7188
$2p_{1/2}$	-8.22	-7.16	1.59	0.3039
$1g_{9/2}$	-7.26	-6.49	1.76	0.1600
$2d_{5/2}$	-1.63	-1.51	1.33	0.0082
$3s_{1/2}$	0.57	0.64	1.11	0.0034
$1g_{7/2}$	1.09	1.24	1.71	0.0072
$1h_{11/2}$	1.42	1.56	1.71	0.0067
$2d_{3/2}$	1.69	1.77	1.31	0.0038
$2f_{7/2}$	6.38	6.41	0.97	0.0010
$3p_{3/2}$	7.25	7.26	0.64	0.0004
$3p_{1/2}$	8.16	8.17	0.54	0.0003
$2f_{5/2}$	9.88	9.89	0.71	0.0004
$4s_{1/2}$	10.41	10.42	0.30	0.0001
$1i_{13/2}$	10.45	10.52	1.55	0.0016

Table 1: BCS-solution for proton states in ^{88}Sr: quasiparticle energies $\epsilon_{(qp)}$, energy gaps Δ and occupation probabilities v^2.

are not constant[1]. The quasiparticle energies are calculated as $E_a = \sqrt{(\epsilon_a-\lambda)^2+\Delta_a^2}$, where λ is the chemical potential. From these we obtain the quantities $\epsilon_{(qp)a}$ tabulated in Table 1 in the following way: $\epsilon_{(qp)a} = \pm E_a+\lambda$, where the positive sign is taken if the corresponding single-particle state a is a particle state and the negative sign for a hole state.

Using the same parametrization that we have used for ^{146}Gd (see previous contribution to this Annual Report) for the particle-hole and for the particle-particle force, which we need to solve the QRPA-equations, we can describe quite well the low-lying energy levels of the nucleus ^{88}Sr. Because of the big interest awaked recently for the nuclear magnetic transitions and the corresponding observed quenching[2], we have addressed our special interest to the results concerning the 3486 keV 1^+ state. From our calculations it turns out that the 1^+ is almost completely (~90 %) the proton spin-flip configuration $(\pi 2p_{1/2}-2p_{3/2}^{-1})$ with a small admixture (~9 %) of the $(\pi 1f_{5/2}-2p_{3/2})^{-2}$ two-hole configuration. In addition we obtain an excitation energy of 3361 keV and a $B(M1;0^+\rightarrow 1^+) = 0.32\ \mu_N^2$. This value is smaller than half the experimental value, which is equal to 0.92 ± 0.15 μ_N^2 [3]. We interpret the reduction of the theoretical B(M1)-value with respect to the experimental one as mainly due to the effect of the pairing coefficients $\gamma = (u_a v_b - v_a u_b)$, which enter the matrix elements of the magnetic multipole operator:

$$\langle J\|MJ\|0\rangle = -\sum_{a\geq b}\{(Z_{ab}^{+}+Z_{ab}^{-})^{*} + (-)^{J}(Z_{ab}^{+}-Z_{ab}^{-})^{*}\}(MJ)_{ab}(u_a v_b - v_a u_b) \qquad (1)$$

The value of this coefficient for the main configuration $(\pi 2p_{1/2}-2p_{3/2}^{-1})$ can be easily calculated from the occupation probabilities given in Table 1, obtaining a value of 0.41. It means that the transition matrix element of this configuration is reduced by a factor of 0.41 and that the corresponding reduction of the B(M1)-value, given from:

$$B(MJ;J\rightarrow 0) = \frac{1}{2J+1}\langle J\|MJ\|0\rangle^2 \qquad (2)$$

is of the order of $0.41^2 = 0.17$.

We check this assumption calculating the B(M1)-value by taking into account only the particle-hole configuration $(\pi 2p_{1/2}-2p_{3/2}^{-1})$ for two different values of γ: 0.41 (with) and 1 (without pairing correlations). The obtained B(M1)-values were respectively equal to 0.61 μ_N^2 and 3.56 μ_N^2, giving a reduction factor of exactly 0.17. This is only a rough estimate of the reduction effect due to the pairing coefficients, but the situation is much more complicated when we use the full configuration space.

Recently, L.T. van der Bijl et al.[2], discussing the electron scattering form factor of the 1^+ in ^{88}Sr, have reported that calculations performed in the two broken pair scheme give a B(M1)-value equal to 1.91 μ_N^2, which is twice the experimental value. They argue that non-nucleonic degrees of freedom like Δ-hole polarization are needed to explain the reduction of the M1-strength at low q. Unfortunately, we did not have the possibility to compare in detail our calculations with those quoted in Ref. 2.

Our next task will be the calculation of the electron scattering cross section with our QRPA-wave functions, to verify whether our reduction factor is enough to explain the experimental quenching or whether it is necessary to introduce subnucleonic degrees of freedom.

References

1) C. Conci, V. Klemt, Annual Report 1982, Jül-Spez 202 (1983) 76, and previous contributions to the present Annual Report, ps. 64, 65
2) L.T. van der Bijl, H.P. Blok, R. Frey, D. Meuer, A. Richter, P.K.A. de Witt Huberts, Z. Phys A305 (1982) 231.
3) R.F. Metzger, Nucl. Phys. A173 (1971) 141.
4) V.I. Isakov, S.A. Artamonov, L.A. Sliv, Sov. J. Nucl. Phys. 35 (1982) 173.

3.4. A Model to Include 2p2h as well as 1Δ1h States for the Magnetic Response of Heavy Nuclei

D. Cha, B. Schwesinger+, J. Speth and J. Wambach++

It is now established experimentally[1)] that at low momentum transfer spin flip transition strength is strongly suppressed. Theoretically two mechanisms have been proposed for this quenching: one is the Δ-hole effect and the other a conventional nucleonic 2p2h effect. Since both may be of the same order of magnitude, it is desirable to include them simultaneously in a model of magnetic strength functions. We extend the 2p2h formalism for the nuclear electric response by Schwesinger and Wambach[2)] to allow for the fact that magnetic isovector excitations can also couple to Δ-hole excitations.

Following the notation of Schwesinger and Wambach[2)], we write the response $S_Q(\omega)$ of a nucleus to a weak external field

$$Q(\omega) = \frac{1}{2}\,(Q^+e^{i\omega t}+Qe^{-i\omega t}) \tag{1}$$

as

$$S_Q(\omega) = -\frac{1}{\pi}\,\mathrm{Im}\{\langle|Q^+(\omega-H+E_0+i\eta)^{-1}Q|\rangle-(\omega+i\eta)^{-1}|\langle|Q|\rangle|^2\}\ . \tag{2}$$

H is the hamiltonian governing the dynamics of the system and E_0 the energy of the exact ground state $|\rangle$. Now we introduce the 1p1h vectors Q_N and Q_Δ the component of which is given by

$$\begin{aligned} Q_{N,\alpha} &= \langle 1p1h,\alpha|Q|0\rangle \\ &- \sum_\beta \langle 1p1h,\alpha|Q|2p2h,\beta\rangle\langle 2p2h,\beta|h_N^{-1}V_{NN}|0\rangle \qquad (3)\\ &- \sum_\gamma \langle 1p1h,\alpha|Q|1\Delta 1p2h,\gamma\rangle\langle 1\Delta 1p2h,\gamma|(M_\Delta-M_N)^{-1}V_{\Delta N}|0\rangle \end{aligned}$$

$$Q_{\Delta,\gamma} = \langle 1\Delta 1h,\gamma|Q|0\rangle \tag{4}$$

Here H has been split into a one-body part t plus a two-body potential V acting among nucleons and isobars

$$H = t_N+V_{NN}+t_\Delta+V_{\Delta\Delta}+V_{N\Delta}+V_{\Delta N} \tag{5}$$

and $|0\rangle$ is the Hartree-Fock ground state. h_N denotes the HF mean field to $t_N+V_{NN}-E_0$ and M_Δ, M_N are the masses of an isobar and a nucleon respectively. Note that we have included some effects of ground state correlations in the definition of Q_N. The diagramatic representation of eq. (3) is given by the first three graphs of Fig. 1c. The approximation implied by neglecting higher order terms in eqs. (3) and (4) leads to a projected response function $S_Q(\omega)$ onto the 1p1h- and 1Δ1h-subspace.

$$S_Q(\omega) = -\frac{1}{\pi}\,\mathrm{Im}\{(Q_N^+,Q_\Delta^+)\begin{pmatrix}\omega-C_{NN}+i\eta & -C_{N\Delta}\\ -C_{\Delta N} & \omega-C_{\Delta\Delta}+i\eta\end{pmatrix}\begin{pmatrix}Q_N\\ Q_\Delta\end{pmatrix}\} \tag{6}$$

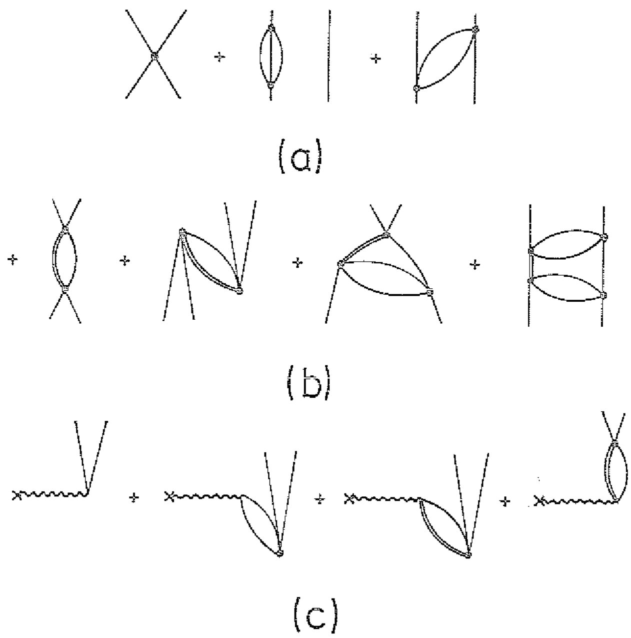

Fig. 1: Diagrams iterated in the effective 1p1h operator $(\omega-\tilde{C}_{\Delta\Delta}+i\eta)$ and the effective nucleonic transition operator $\tilde{Q}_N$. Group (a) summarizes the conventional nucleonic interactions, (b) polarization effects in the effective hamiltonian from isobars and (c) renormalization of the nucleonic transition matrix elements.

The submatrices $C_{AB}(\omega)$ stand for the one baryon-one hole matrix elements of the operators $\hat{C}_{AB}(\omega)$ defined by

$$\hat{C}_{NN} = t_N+V_{NN}+V_{NN}P(\omega-t_N-V_{NN}+E_0+i\eta)^{-1}PV_{NN}-E_0 \tag{7}$$

$$\hat{C}_{N\Delta} = V_{N\Delta}+V_{NN}P(\omega-t_N-V_{NN}+E_0+i\eta)^{-1}PV_{N\Delta} \tag{8}$$

$$\hat{C}_{\Delta\Delta} = t_\Delta+V_{\Delta\Delta}+V_{\Delta N}P(\omega-t_N-V_{NN}+E_0+i\eta)^{-1}PV_{N\Delta}-E_0 \tag{9}$$

where P is a projector on to npnh-states with n>1:

$$P = \sum_{n>1} P^{(n)} = \sum_{n>1}\sum_\beta |npnh,\beta\rangle\langle npnh,\beta|\ . \tag{10}$$

Since the 1Δ1h diagonal elements of $t_\Delta-E_0$ are mainly given by the isobar-nucleon mass difference (300 MeV), we can neglect terms of higher order in the isobar nucleon propagator $(\omega-C_{\Delta\Delta}+i\eta)$ inverting the matrix in eq. (6). This gives

$$S_Q(\omega) = -\frac{1}{\pi}\,\mathrm{Im}\{\tilde{Q}_N^+(\omega-\tilde{C}_{NN}+i\eta)^{-1}\tilde{Q}_N+Q_\Delta^+(\omega-C_{\Delta\Delta}+i\eta)^{-1}Q_\Delta\} \tag{11}$$

with the effective operators

$$\tilde{Q}_N = Q_N+C_{N\Delta}(\omega-C_{\Delta\Delta}+i\eta)^{-1}Q_\Delta \tag{12}$$

$$\tilde{C}_{NN} = C_{NN}+C_{N\Delta}(\omega-C_{\Delta\Delta}+i\eta)^{-1}C_{\Delta N} \tag{13}$$

We continue with following approximations. As the 1Δ1h diagonal elements of $t_\Delta-E_0$ are of the order of 300 MeV, we may neglect all other terms in $C_{\Delta\Delta}$ of eq. (9) which are of the order of one MeV. For the same reason, the frequency dependence of the 1Δ1h operator in eqs. (11)-(13) may be ignored for low energy excitations. Furthermore, we believe that it is a fairly good approximation to eqs. (7)-(9) to put

$$P(\omega-t_N-V_{NN}+E_o+i\eta)^{-1}P \rightarrow P^{(2)}(\omega-h_N+i\delta)^{-1}P^{(2)} \quad (14)$$

where the finite δ replaces the residual interaction among 2p2h-states and their coupling to even higher configurations.

To summarize, we propose to calculate the magnetic response function $S_Q(\omega)$ for $\omega \ll 300$ MeV by a matrix inversion of an effective hamiltonian $\tilde{C}_{NN}$ in the nucleonic subspace as

$$S_Q(\omega) = -\frac{1}{\pi}\,\mathrm{Im}\{\tilde{Q}_N^{+}(\omega-\tilde{C}_{NN}+i\eta)^{-1}\tilde{Q}_N\} \quad (15)$$

where $\tilde{Q}$ and $\tilde{C}$ are given by

$$\tilde{Q}_N = Q_N - \frac{1}{M_\Delta-M_N}\,C_{N\Delta}Q_\Delta \quad (16)$$

$$\tilde{C}_{NN} = C_{NN} - \frac{1+b}{M_\Delta-M_N}\,C_{N\Delta}C_{\Delta N} \quad (17)$$

In the zero frequency limit for the 1Δ1h propagator, b=1 if backward going graphs are included. Truncating at 2p2h, $\hat{C}_{NN}$ and $\hat{C}_{\Delta\Delta}$ are approximated by the one baryon-one hole matrix elements of the operators

$$\hat{C}_{NN} = t_N+V_{NN}+V_{NN}P^{(2)}(\omega-h_N+i\delta)^{-1}P^{(2)}V_{NN}-E_o \quad (18)$$

$$\hat{C}_{N\Delta} = V_{N\Delta}+V_{NN}P^{(2)}(\omega-h_N+i\delta)^{-1}P^{(2)}V_{N\Delta} \quad (19)$$

The diagrams iterated by this model are shown for illustration in Fig. 1.

References

1) J. Rapaport, contribution to the 1982 IUCF Workshop "The interaction between medium energy nucleons in nuclei";
A. Richter, invited talk presented at the Int. Conf. on Nucl. Phys., Florence (Italy), 1983.
2) B. Schwesinger, J. Wambach, Phys. Lett. in press;
B. Schwesinger, J. Wambach, submitted to Nucl. Phys. A.

+ SUNY at Stony Brook, Stony Brook, NY, USA
++ Univ. of Illinois, Urbana, IL, USA

3.5. Isobar-Hole and 2p2h Effects on the M1-Strength in ^{90}Zr and ^{208}Pb

D. Cha, B. Schwesinger+, J. Speth and J. Wambach++

Since both ^{90}Zr and ^{208}Pb are non spin-saturated, we expect a large amount of M1-strength. In ^{90}Zr the independent particle model (IPM) predicts a neutron $g_{9/2}\rightarrow g_{7/2}$ transition with a strength of 15.4 μ_N^2 and in ^{208}Pb two transitions: proton $h_{11/2}\rightarrow h_{9/2}$ and neutron $i_{13/2}\rightarrow i_{11/2}$ with B(M1)↑ values of 25.6 μ_N^2 and 22.1 μ_N^2 respectively. Experimentally, there has been some strength reported in ^{208}Pb 1) and about 40 % of IPM strength in ^{90}Zr has been identified recently by high energy proton scattering[2]. As can be seen from Table 1, most of the transition strength is purely spinflip. Convection current contributions are absent in ^{90}Zr and very small in ^{208}Pb. Therefore, we expect that effects of isobar-hole mixing are large, giving rise to a strong reduction of the transition strength.

We have performed RPA calculations by the matrix inversion technique which includes both the 2p2h and Δ-hole effects[3]. In contrast to the GT transition where RPA correlations are largely blocked, those have to be included in the other isospin branches. The inclusion of other correlations is summarized in Table 2. E_c denotes the centroid energy of the main peak and the percentages are obtained with respect to the IPM. In ^{90}Zr the results can be compared directly with experiment[4]. The amount of theoretical integrated strength in the vicinity of the peak varies between 38 % and 22 % depending on the additional zero-range coupling $\delta g_o'^*$. Our theoretical result has to be compared with the experimental one of 40±5 %. It favours somewhat the choice $\delta g_o'^* = 0$ but in view of the theoretical as well as experimental uncertainties it does not preclude the larger 1Δ1h mixing. In ^{208}Pb experiment is much less decisive. Definitely 8.5 μ_N^2, i.e. 17.4 % of the IPM strength have been located fragmented between 7 and 8 MeV [4]. Another tentative 8.5 μ_N^2 are located between 8 and 9.5 MeV increasing the percentage to 35 %. Our calculation yields centroid energies between 7.5 and 7.2 MeV depending on the 1Δ1h coupling strength with integrated transition strengths of 42 % and 26 % in the vicinity of the peak respectively. Like the GT strength, also the M1 strength functions

	configuration	spin μ_N^2	convection μ_N^2	B(M1)↑ μ_N^2
^{90}Zr	$\nu g_{9/2}\rightarrow\nu g_{7/2}$	15.4	0	15.2
	others	0.7	0.02	0.5
				15.7
^{208}Pb	$\pi h_{11/2}\rightarrow\pi h_{9/2}$	40.0	1.6	25.6
	$\nu i_{13/2}\rightarrow\nu i_{11/2}$	22.4	0	22.1
	others	1.6	0.05	1.1
				48.8

Table 1: Independent particle model M1 transition strength in ^{90}Zr and ^{208}Pb.

	^{90}Zr			^{208}Pb		
	E < 12 MeV			E < 11 MeV		
	E_c MeV	B(M1)↑ MeV	fraction	E_c MeV	B(M1)↑ μ_N^2	fraction
IPM	6.02	15.7	100 %	5.57 5.85	25.6 22.1	52.5 % 45.3 %
1p1h (RPA)	6.73	12.9	83.7 %	6.7	42.1	86.3 %
1p1h+2p2h (TDA)	8.0	10.17	66.0 %	7.6	37.79	77.4 %
1p1h+2p2h (RPA)	8.1	7.99	51.8 %	7.6	27.91	57.2 %
1p1h+2p2h +1Δ1h (RPA) $\delta g_o'^* = 0$	7.9	5.84	37.9 %	7.5	20.39	41.8 %
1p1h+2p2h +1Δ1h (RPA) $\delta g_o'^* = 0.5$	7.7	3.44	22.3 %	7.2	12.43	25.5 %
Exp.	8.9±0.2		40±5 %	~ 7.5		~ 17.4 %

Table 2: M1 strength in ^{90}Zr below 12 MeV excitation energy and in ^{208}Pb below 11 MeV excitation energy.

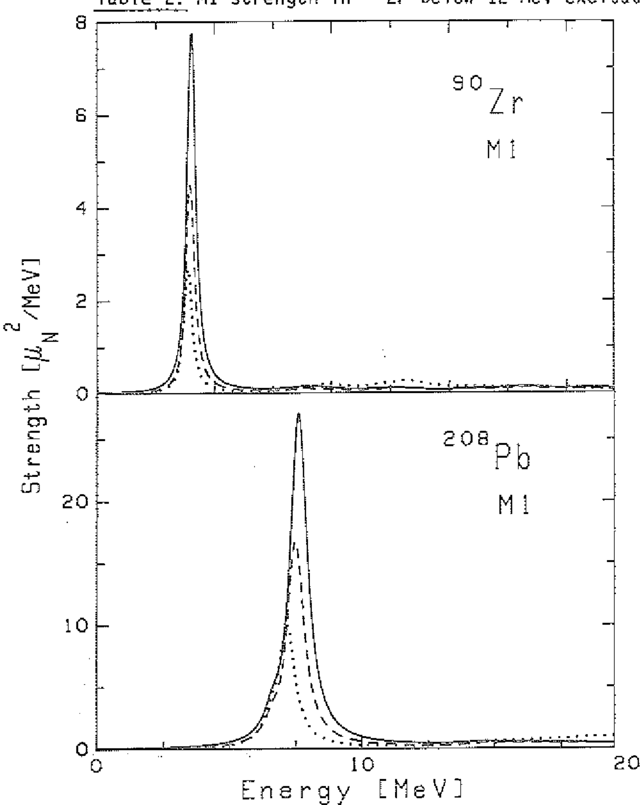

Fig. 1: M1 strength distribution in ^{90}Zr and ^{208}Pb. The full line denotes 1p1h+2p2h TDA results, while dashed and dotted lines include RPA and 1Δ1h correlations for $\delta g_o'^* = 0$ and 0.5 respectively.

exhibit long tails extending up to more than 50 MeV excitation energy (see Fig. 1). This naturally leads to an increase of the total energy weighted sum rule. In ^{90}Zr we have integrated the theoretical distribution up to 45 MeV and find 64 % more than the IPM value of 110.6 μ_N^2 MeV neglecting RPA correlations while including them gives 42 % enhancement. In these numbers isobar-hole admixtures are not included. Including those yields quenching of the EWSR. Relative to the 2p2h (RPA) value of 157.5 μ_N^2 MeV, we get 19 % reduction while $\delta g_o'^* = 0$ and 6 % reduction for $\delta g_o'^* = 0.5$ respectively.

References

1) G.E. Brown, S. Raman, Comments Nucl. Part. Phys. 9 (1980) 79.
2) C. Djalali et al., Nucl. Phys. A388 (1982) 1.
3) D. Cha et al., preceding contributions to this report.
4) N. Anantaraman et al., Phys. Rev. Lett. 46 (1981) 1318.

+ SUNY at Stony Brook, Stony Brook, NY, USA
++ Univ. of Illinois, Urbana, IL, USA

3.6. Isobar-Hole and 2p2h Effects on the M2-Strength in ^{90}Zr and ^{208}Pb

D. Cha, B. Schwesinger+, J. Speth and J. Wambach++

Experimental evidence for M2 resonances in ^{90}Zr and ^{208}Pb comes from (e,e') experiments[1]. In contrast to the M1 case, where contributions from the orbital operator are negligible, the orbital part of the M2 operator gives 1/5 of the total M2 strength[2]. Theoretically this orbital operator is of special interest because it excites a twisting oscillation of the nuclear density called the "twist mode"[3].

We have performed RPA calculations by the matrix inversion technique[4]. The new feature of our calculation as compared to previous ones[5] is the combination of 2p2h and 1Δ1h effects. As expected the addition of 1Δ1h states to the 1p1h+2p2h calculation in ^{208}Pb reduces only the spin strength. Therefore the relative importance of the twist peak at 7.9 MeV is enhanced with increased coupling to 1Δ1h states. This is displayed in Fig. 1 where the bottom graph gives the response of ^{90}Zr and ^{208}Pb to the spin part of the M2 operator, the middle section to the orbital part and the upper to the total M2 operator.

Table 1 gives the amount of M2 strength present in ^{208}Pb below 15.6 MeV as compared to the total sum rule.

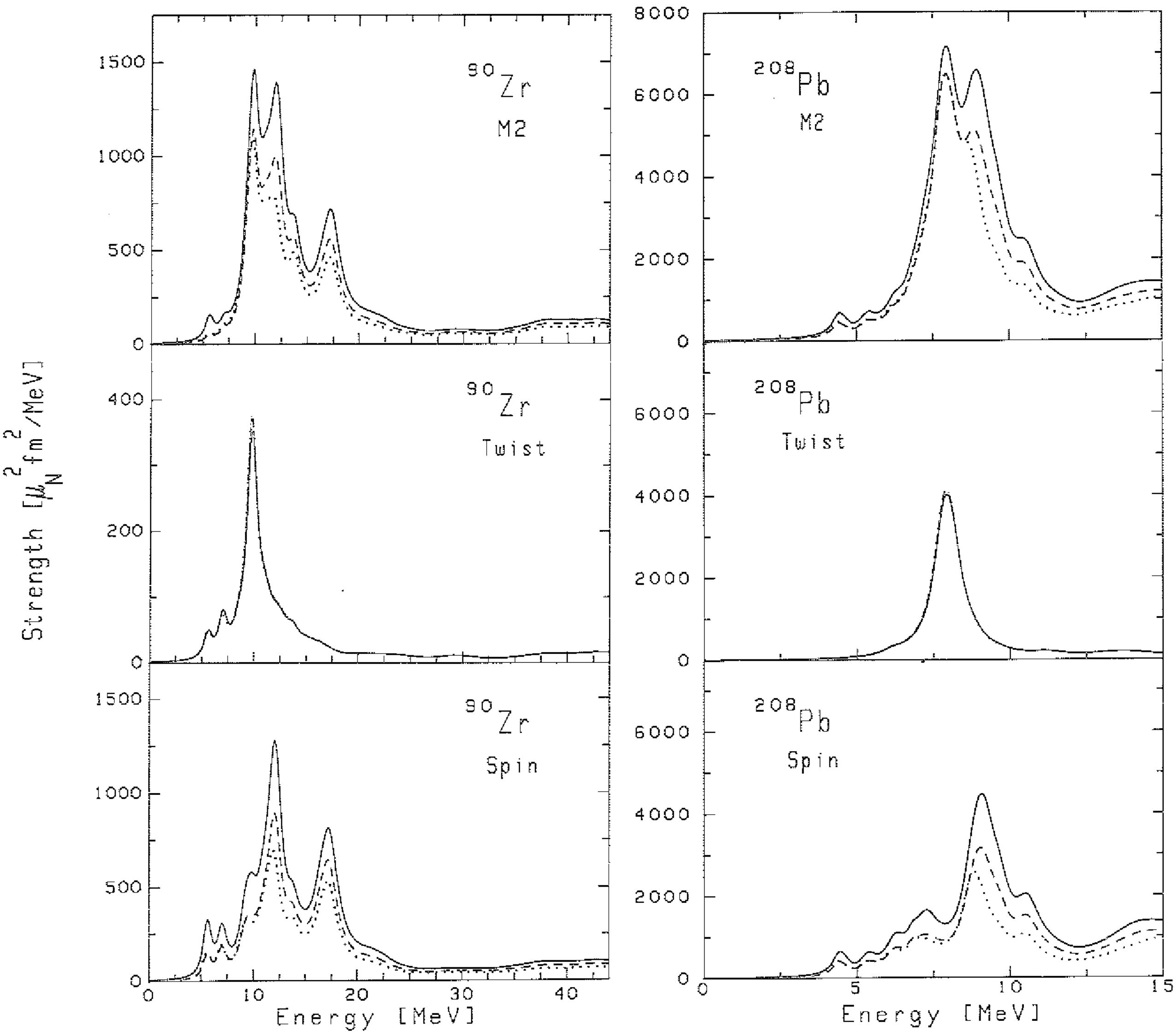

Fig. 1: Distribution of M2 strength in ^{90}Zr and ^{208}Pb. The upper part gives electromagnetic, the middle part twist and the lower part spin strength distributions. The full line denotes 1p1h+2p2h TDA results, while the dashed and dotted lines include RPA and 1Δ1h correlations for $\delta g_0'^* = 0$ and 0.5 respectively.

	elm $\mu_N^2 fm^2$	twist $\mu_N^2 fm^2$	spin $\mu_N^2 fm^2$
1p1h+2p2h (TDA)	2.9×10^4	0.7×10^4	1.9×10^4
1p1h+2p2h +1Δ1h (RPA) $\delta g_0'^* = 0$	2.4×10^4	0.7×10^4	1.4×10^4
1p1h+2p2h +1Δ1h (RPA) $\delta g_0'^* = 0.5$	2.1×10^4	0.7×10^4	1.1×10^4
total strength	3.9×10^4	0.8×10^4	3.1×10^4

Table 1: M2 strength in ^{208}Pb within the energy interval from 0 to 15.6 MeV.

Three cases, electromagnetic, twist and spin operators are considered. As may be seen the coupling to 2p2h states has already pushed larger amounts of spin strength up to higher excitation energies, whereas almost all twist strength is kept. On the other hand, the spin strength is strongly affected by the 1Δ1h admixtures. Below 10 MeV in ^{208}Pb there is only $.7\times10^{-4}$ $\mu_N^2 fm^2$ of the spin strength left, if 1Δ1h is included with $\delta g_0'^* = 0$. Now orbital strength accounts for 50 % of the total M2 strength below 10 MeV. The peaks to the twist and the spin response below 10 MeV are fairly well separated, the low-lying one between 7.5 and 8.5 MeV being due to the twist. These statements are in quantitative agreement to earlier findings[5].

References

1) R. Frey et al., Phys. Lett. 74B (1978) 45;
W. Knüpfer et al., Phys. Lett. 77B (1978) 367.
2) B. Schwesinger et al., Nucl. Phys. A341 (1980) 1.
3) T. Yukawa, G. Holzwarth, Nucl. Phys. A364 (1981) 29.
4) D. Cha et al., preceding contributions to this report.
5) B. Schwesinger, submitted to Phys. Rev. C;
D. Cha, J. Speth, submitted to Phys. Rev. C.

+ SUNY at Stony Brook, Stony Brook, NY, USA
++ Univ. of Illinois, Urbana, IL, USA

3.7. Isobar-Hole and 2p2h Effects on the Spin-Dipole Strength in ^{90}Zr and ^{208}Pb

D. Cha, B. Schwesinger+, J. Speth and J. Wambach++

In connection with the first forbidden $\beta_\pm$ decay, the distribution of isovector "spin-dipole" transition strength

$$Q \propto r[\sigma Y_1]^{0^-,1^-,2^-}_{\tau_{+,0,-}} \qquad (1)$$

is of importance. The τ_--branch has been investigated experimentally via medium energy (p,n) reactions[1]. The τ_0-branch has not been identified so far, but there are indications from 319 MeV (p,p') data in ^{90}Zr for substantial spin-flip strength at higher energy[2]. The τ_+-branch is accessible via (n,p) reactions but little is known up to now.

Here we have investigated the spin-dipole strength distribution in the parent nucleus (τ_0-part) using the matrix inversion technique of Ref. 3 which includes both 2p2h and 1Δ1h effects. Fig. 1 summarizes the results in ^{90}Zr (left part) and ^{208}Pb (right part). With increasing J the centroid moves to lower energy partly because the decrease in the average 1p1h energy but also the average interaction matrix elements are reduced because of the momentum dependence of the spin-isospin force. The effect of 1Δ1h mixing is depicted by the dashed ($\delta g_0'^* = 0$) and dotted ($\delta g_0'^* = 0.5$) lines in Fig. 1. While the 1^- and 2^- strength distribution is quenched for all cases, we find little effect on the 0^- for $\delta g_0'^* = 0$. In ^{90}Zr the strength is even slightly enhanced. This can be understood by remembering that spin-isospin response can be separated into a longitudial and transverse part excited by the operators

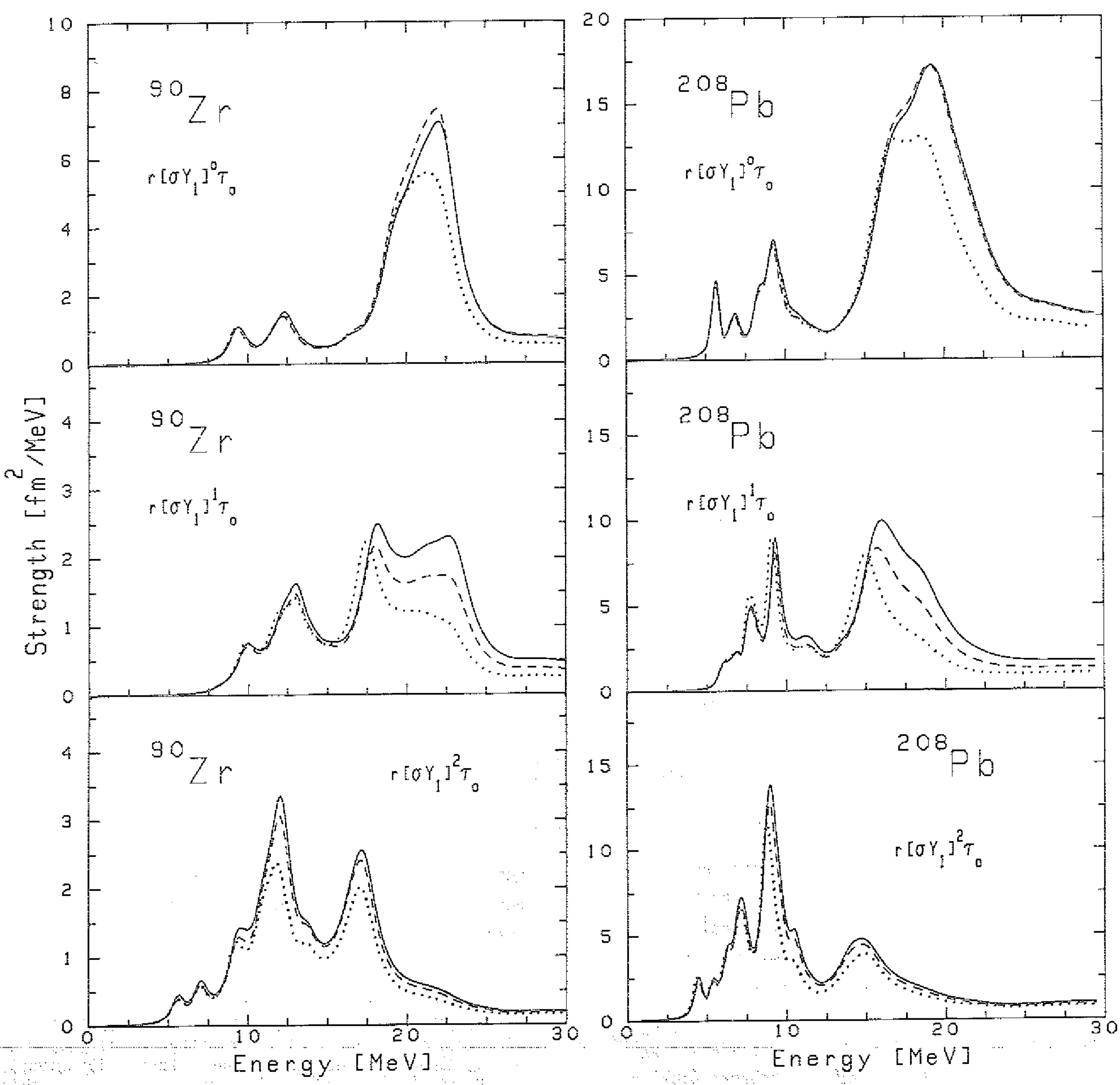

Fig. 1: Isovector spin-dipole strength distributions in ^{90}Zr (left part) and ^{208}Pb (right part). The full line denotes 1p1h+2p2h TDA results, while the dashed and dotted lines include RPA and 1Δ1h correlations for $\delta g_0'^* = 0$ and 0.5 respectively.

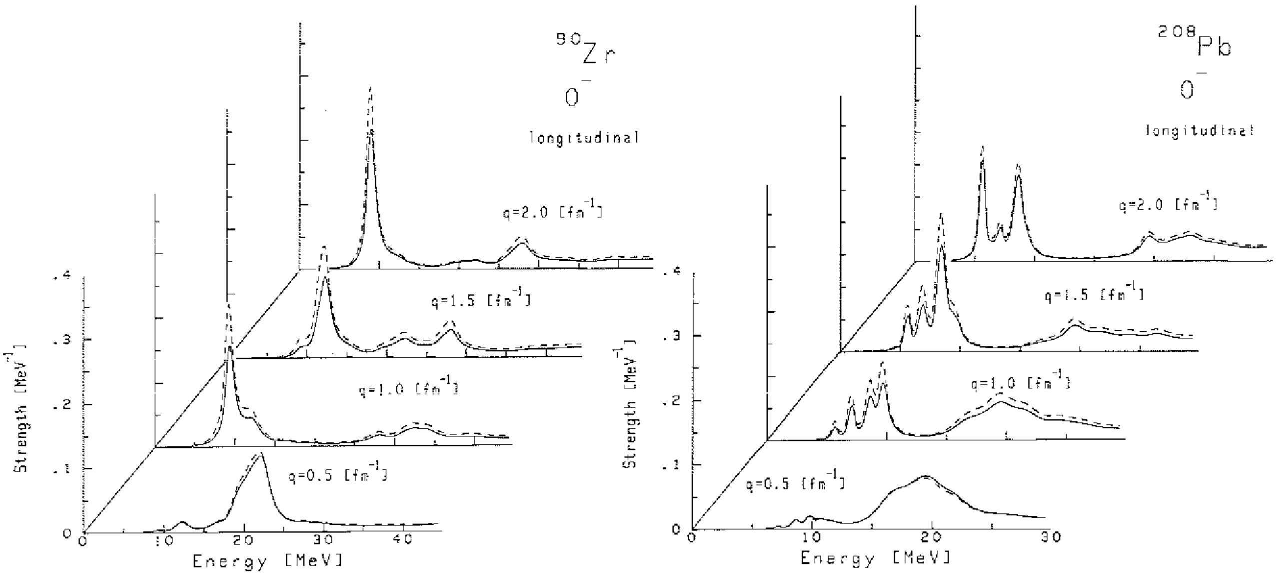

Fig. 2: Momentum and energy dependence of the 0^- longitudinal response functions in ^{90}Zr (left part) and ^{208}Pb (right part) normalized to the total strength at each momentum transfer. The full lines denote the 1p1h+2p2h results without 1Δ1h admixtures while they are included in the dashed lines ($\delta g_0'^* = 0$).

$$Q^{\ell g} = \sum_{i=1}^{A} \sigma(i)\cdot\hat{q}\; e^{iq\cdot r(i)}\tau(i) \qquad (2)$$

$$Q^{tr} = \sum_{i=1}^{A} \sigma(i)\times\hat{q}\; e^{iq\cdot r(i)}\tau(i) \qquad (3)$$

respectively. Due to the tensor piece in the π and ρ exchange potentials both modes propagate quite differently. The longitudical piece is driven by

$$V^{\ell g}_{\pi+\rho} = V^{central}_{\pi+\rho} + 2V^{tensor}_{\pi+\rho} \qquad (4)$$

which is strongly momentum dependent while the transverse part propagates according to

$$V^{tr}_{\pi+\rho} = V^{central}_{\pi+\rho} - V^{tensor}_{\pi+\rho}$$

for which the momentum dependence is much weaker. For 0^- which is not excited electromagnetically, the motion is purely longitudinal or "pion like" and a strong momentum dependence of the response function is expected. Fig. 2 shows the energy distribution of the 0^- longitudinal response functions for various q. With increasing q transfer, $V_{\pi+\rho}$ becomes strongly attractive shifting strength to lower energies. The 1Δ1h mixing indicaed by the dashed lines in Fig. 2 also exhibits a q dependence becoming more important at higher q.

References

1) C. Gaarde et al., Nucl. Phys. A369 (1981) 258.
2) S.K. Nanda et al., Phys. Rev. Lett. 51 (1983) 1526.
3) D. Cha et al., preceding contributions to this report.

+ SUNY at Stony Brook, Stony Brook, NY, USA
++ Univ. of Illinois, Urbana, IL, USA

3.8. Isobar-Hole and 2p2h Effects on the Gamow-Teller Strength in ^{90}Zr and ^{208}Pb

D. Cha, B. Schwesinger[+], J. Speth and J. Wambach[++]

Only recently, (p,n) experiments at intermediate energies have mapped out the spin-isospin resonse of nuclei. Particularly, the forward angle spectra are dominated by GT transitions as concluded from the ΔL=0 shape of the angular distribution characteristic for pure spin flip. A measure of the total observed transition strength is provided by the model independent Ikeda sum rule $S_{\beta_-}-S_{\beta_+} = 3(N-Z)$ [1]. In large neutron excess nuclei, S_{β_-} are largely Pauli blocked and small. Experimentally only a fraction of the sum rule (on the average 65 %) is observed up to excitation energy of 40 MeV [2].

We have studied the GT strength distribution in ^{90}Zr and ^{208}Pb employing the matrix inversion technique of Ref. 3 which includes both the 2p2h and Δ-hole effects. For the two-body interaction, we take a combined one-pion and one-rho exchange potential $V_{\pi+\rho}$ where the short range part has been cut out by a two-body correlation function. For numerical reasons, we approximated the coupling interaction to 2p2h states by a zero-range equivalent force taking both the direct and exchange terms. But an antisymmetrized zero-range nucleon-isobar transition interaction vanishes identically. This feature is not present in the finite range potential. We investigate the importance of these couplings by taking direct part of the additional zero-range force for the transition interaction. Our results will distinguish the two cases $\delta g_0'^* = 0$ and 0.5.

In the independent particle model, the GT response in ^{90}Zr is particularly simple with only two peaks of the transition from the $1g_{9/2}$-neutron holes to $1g_{9/2}$- and $1g_{7/2}$-proton particles. The energy separation is determined by the spin-orbit potential (upper left part of

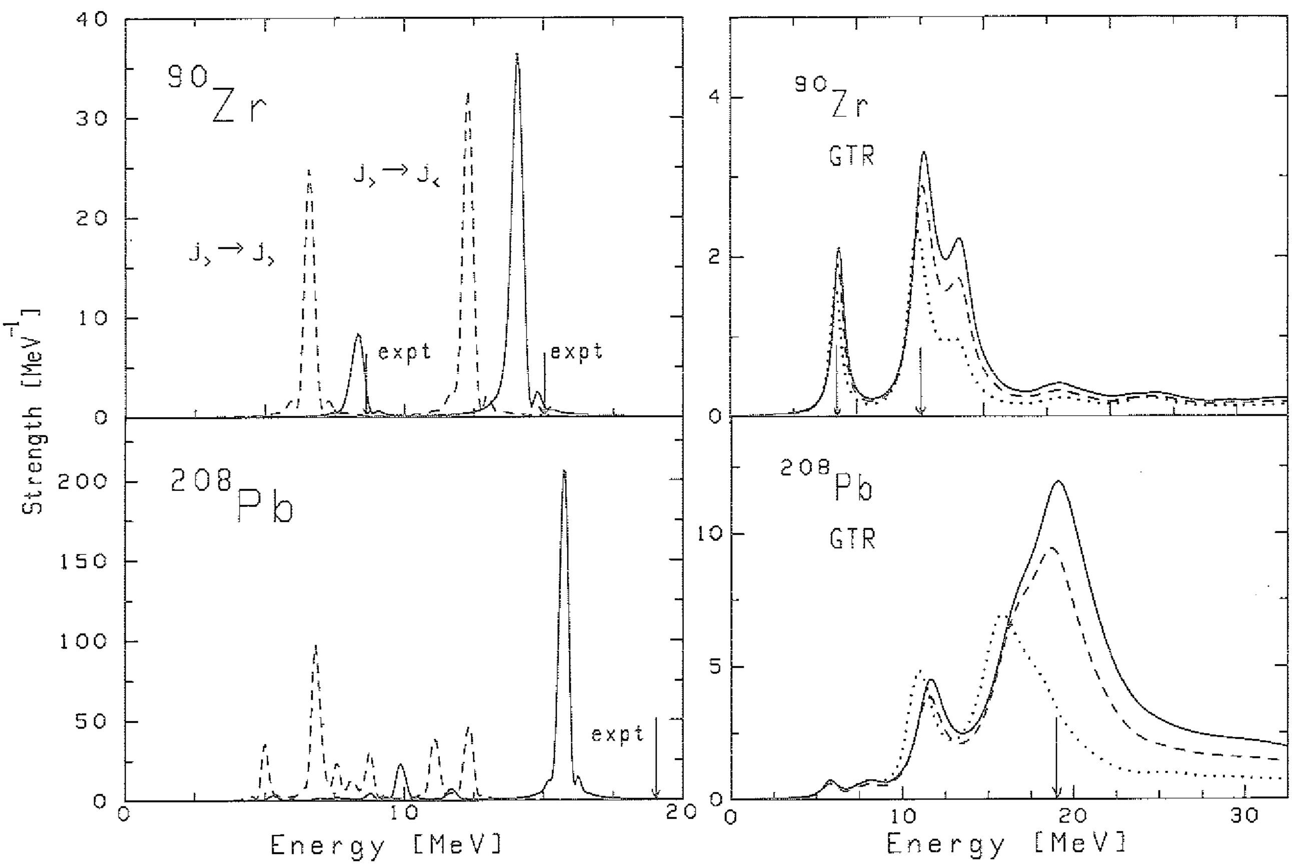

Fig. 1: Left part: Non interacting GT response (dashed lines) in ^{90}Zr and ^{208}Pb as comapred to inclusion of $V_{\pi+\rho}$ on the 1p1h level (full lines). The arrows indicate the experimental resonance energies. Right part: GT response functions in ^{90}Zr and ^{208}Pb including 2p2h- (full line) and in addition 1Δ1h-mixing (dashed line: $\delta g_0'^* = 0$, dotted line: $\delta g_0'^* = 0.5$). The arrows indicate the experimental resonance energies.

	^{90}Zr	^{208}Pb	^{90}Zr	^{208}Pb	^{90}Zr
2p2h (TDA)	63 %	68 %	77 %	84 %	4.5
2p2h+1Δ1h ($\delta g_0'^* = 0$)	53 %	54 %	63 %	66 %	4.2
2p2h+1Δ1h ($\delta g_0'^* = .5$)	38 %	39 %	47 %	49 %	3.4
energy window	0-25 MeV		0-40 MeV		

Table 1: Amount of non energy weighted sum rule strength 3(N-Z). The last column gives the ratios of integrated strength of the two peaks in ^{90}Zr.

Fig. 1). Because of the larger neutron excess, more single particle transitions are possible in ^{208}Pb with the largest carrying only about 20 % of the total strength. As the interaction $V_{\pi+\rho}$ is turned on, strength is pushed up to higher energies producing collective states in both ^{90}Zr and ^{208}Pb. Compared to experiment (indicated by the arrows in Fig. 1) the theoretical energies are too low. In order to reproduce the empirical centroid energies, sizable repulsive contributions have to come from second order (see right side of Fig. 1). Almost the entire contribution in second order comes from the ph linked diagram with a ph pair exchanged (bubble), the perturbative equivalent to the "induced interaction"[4]. The strong second order term provides an explanation for the ad hoc parameter $\delta g_0'^*$ used in Ref. 6 to describe M1 transitions in ^{48}Ca in a 1p1h space only. The inclusion of 2p2h-effects reproduces the empirical energies very well. Also the cross features of the measured (p,n) cross sections are reproduced. In ^{90}Zr the integrated strength ratio of the two peaks is 4.4 experimentally. A pure 1p1h calculation gives 4.2, whereas the inclusion of 2p2h increases the theoretical result slightly to 4.5 without 1Δ1h admixtures (Table 1). Including isobars we get 4.2 and 3.4 for $\delta g_0'^* = 0$ and 0.5 respectively. Both the GT strength functions in ^{90}Zr and in ^{208}Pb (right part of Fig. 1) exhibit long tails due to the 2p2h mixing. Isobar-hole excitations, indicated by the dashed ($\delta g_0'^* = 0$) and the dotted ($\delta g_0'^* = 0.5$) lines, quench the nucleonic transition strength (full line) almost uniformly over the whole energy range. The amount of GT sum rule strength which resides between 0-25 MeV and 0-40 MeV is listed in Table 1. Experimentally the sum rule fraction between 0 and 40 MeV has been determined by Rapaport[2]. On the average, he obtains 60±10 %. Our calculation indicates that 2p2h alone are not able to account for this value and 1Δ1h-mixing is needed. However, it seems difficult to pin down $\delta g_0'^*$. The two extremes $\delta g_0'^*$

= 0 and 0.5 give values comparable to the experimental uncertainties.

References

1) K.I. Ikeda et al., Phys. Lett. 3 (1963) 271.
2) J. Rapaport, contribution to the 1982 IUCF Workshop "The interaction between medium energy nucleons in nuclei".
3) D. Cha et al., preceding contribution to this report.
4) S. Babu, G.E. Brown, Ann. Phys. 78 (1973) 1.
5) C. Gaarde et al., invited talk presented at the Int. Conf. on "Spin Excitation in Nuclei", Telluride (USA), 1982.

+ SUNY at Stony Brook, Stony Brook, NY, USA
++ Univ. of Illinois, Urbana, IL, USA

3.9. Meson Exchange Current Effects in Heavy Nuclei

J.S. Dehesa+, S. Krewald, A. Lallena+ and T.W. Donnelly++

In light nuclei, very clear evidence for meson exchange current (MEC) effects is available. In heavy nuclei (i.e. A 4), however, our knowledge of nuclear structure suffers from uncertainties which are in general too large to allow unambiguous conclusion concerning MEC effects to be drawn. Nevertheless, one may argue in a qualitative way that at large momentum transfers, the MEC will become important even in heavy nuclei, because as two-body operators, the meson-exchange currents are able to accept larger momentum transfers than the electromagnetic one-body operators. The present lower limit of experimentally detectable cross sections in complex nuclei of 10^{-37}-10^{-38} cm^2/sr does permit an exploration of this interesting high momentum transfer region.

One of the major obstacles in evaluating MEC effects in heavy nuclei is contained in the treatment of the mean field. At the momentum transfers of interest for meson-exchange effects, the cross sections are very sensitive to small deviations in the mean field. So far, however, the mean field had to be approximated by a harmonic oscillator potential. In Ref. 1, a new method is suggested which permits to deal with selfconsistent mean fields.

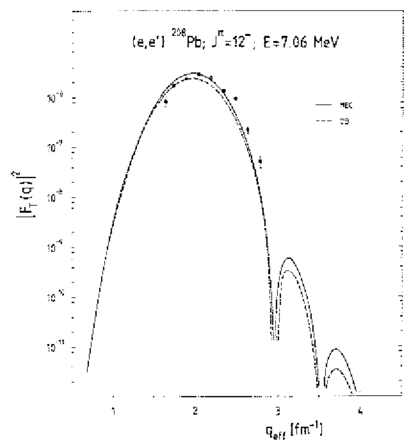

Fig. 1: Electroexcitation cross section for the 12^- state at 7.06 MeV in ^{208}Pb; pure one-body operator (dashed line) and pure one-body operator plus meson-exchange currents (solid line).

As an application, we present the effect of meson-exchange currents on the electroexcitation of the 12^- state at 7.06 MeV in ^{208}Pb (Fig. 1). The MEC are found to produce a smooth enhancement of the one-body cross section of the order of 10 % in the vicinity of the first maximum. At momentum transfers at 3.1 fm^{-1} (second maximum), the cross section due to one-body currents is expected to be enhanced by a factor of 1.8 due to MEC.

Reference

1) J.S. Dehesa et al., to be published.

+ Univ. de Granada, Spain
++ MIT, Cambridge, MA, USA

3.10. Description of Odd-Even Nuclei in the A=130 Region

E. Hammaren[+], K.W. Schmid[+] and F. Grümmer

After it has been shown that the MONSTER is a nuclear structure model which provides wave functions that are a good approximation to the exact shell model results[1], we planned to use the full power of the MONSTER computer-code for the description of many nuclei in one mass region. We chose the A=130 region out of the following reasons. First of all many interesting experimental data have been obtained here recently. Secondly this mass region contains nuclei, which are known to be well deformed rotors but also soft nuclei requiring a strong γ-deformation in a phenomenological description. Thus the ability of the MONSTER to describe all those nuclei can be tested. Finally the single particle basis which has to be used in these nuclei is not as large as for example in the rare earth region. Consequently the computer times to be used in the A=130 region will be not too large for a systematic study.

The single particle basis we use consists out of the $0g_{7/2}$, $1d_{5/2}$, $1d_{3/2}$, $2s_{1/2}$, $0h_{11/2}$, $0h_{9/2}$ and the $1f_{7/2}$ states for both protons and neutrons. This means we assume an inert core consisting of 50 protons and 50 neutrons. For this single particle basis we have to define effective single particle energies and effective two body matrix elements. For the latter we use an effective G-matrix which will be explained in more detail in the next report dealing with the even-even nuclei. The knowledge of the correct effective single particle energies is known to be very essential for the description of effects like the backbending in rotational bands which occurs in many of the nuclei under consideration. Since we cannot afford to fit the s.p. energies to the experimental data known in the mass region we have to try to fix them in such a way that some sensitive data are satisfactorily reproduced. This can for example be the low-lying states of the odd-even nuclei.

In the framework of the MONSTER odd-even nuclei are described by diagonalizing the effective hamiltonian in the space of spin- and number-projected one quasiparticle states with respect to the HFB-field of a neighbouring even-even nucleus.

$$|\mu;IMN_0Z_0\rangle = \hat{P}^I_M \hat{Q}_{N_0} \hat{Q}_{Z_0} a^+_\mu |HFB\rangle$$

This model definitely excludes the proper description of backbending and other band crossings in odd nuclei, but it should be sufficient for the description of band heads and low-lying states.

A good overall agreement of all spectra of the odd nuclei in the A=130 region is obtained with the single-particle energies listed in Table 1. Fig. 1 shows some bands for ^{129}Ba comparing the MONSTER results to the experimental data[2]. One realizes that the band heads and their relative positions are rather well reproduced.

level	neutrons	protons
$2s_{1/2}$	0.0	0.0
$1d_{3/2}$	0.209	-0.039
$1d_{5/2}$	-0.283	-0.394
$0g_{7/2}$	-0.221	-0.381
$1f_{7/2}$	0.320	0.580
$0h_{9/2}$	0.516	0.464
$0h_{11/2}$	0.012	-0.209

Table 1

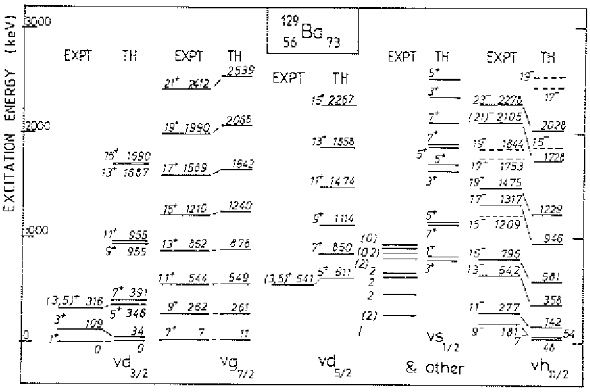

Figure 1

Keeping in mind that the description of the odd nclei does not include 3 q.p. states also the moments of inertia and the general structure of the different bands are in reasonable agreement with the experimental data. That the agreement of the energies is not an artifact of the model but reflects the correct structure of the states, can be seen in Fig. 2, where the spectroscopic amplitudes for the one particle transfer reaction ^{130}Ba(d,t)^{129}Ba are shown as a function of the excitation energy of ^{129}Ba [3].

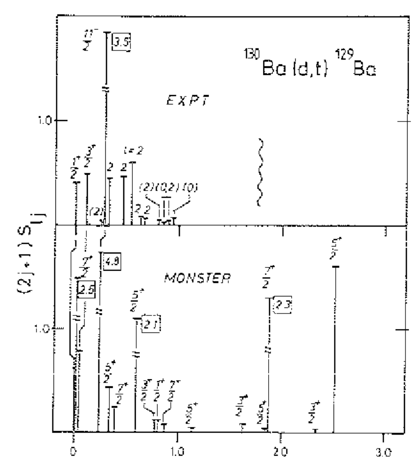

Figure 2

One can reproduce the strength distribution for all low-lying states rather well (note that the 7/2-level requires an l=4 transfer, which is strongly suppressed in the (d,t)-reaction and can hence not be disentangled from the strong l=0-transfer to the ½-ground state). Unfortunately above 300 keV experimental spin assignments have not been possible up to now and above about 1.8 MeV no data at all are available.

Summarizing one can say that low-lying states in odd nuclei may be rather well described with the MONSTER formalism and that the study of the spectra of the odd nuclei turns out to be very useful in order to fix the effective single particle energies.

References

1) K.W. Schmid, F. Grümmer, A. Faessler, Phys. Rev. C in press.
2) J. Gizon et al., Nucl. Phys. A277 (1977) 464.
3) R.D. Griffin and R.K. Sheline, Phys. Rev. C10 (1974) 624.

+ Inst. f. Theor. Physik, Univ. Tübingen,

3.11. Description of Even-Even Nuclei in the A=130 Region

K.W. Schmid+, E. Hammaren+ and F. Grümmer

During the last decade a large amount of experimental data has been obtained concerning the high spin states of deformed nuclei in various mass regions. Not only the yrast bands have been established up to very high angular momenta, but also various excited bands have been measured. In addition recently also data about the moments and transitions within these bands have been obtained.

Theoretically the data may be partially understood in terms of phenomenological models like the cranking model, the interacting boson model or particle rotor coupling models. The major problem of these models is the fact that they are all limited to a certain class of phenomena and that they do not have a sound microscopic justification. A model, which goes beyond those limitations is the MONSTER-model. It is a fully microscopic model, which may be used in any mass region provided an appropriate effective hamiltonian is known. The effective hamiltonian is diagonalized in the space of the spin- and number-projected HFB-mean-field

$$|A\rangle := |0;IMN_0Z_0\rangle = \hat{P}^I_M \hat{Q}_{N_0} \hat{Q}_{Z_0} |HFB\rangle$$

and the projected two quasiparticle excitations with respect to this field.

$$|A\rangle := |\mu\nu;IMN_0Z_0\rangle = \hat{P}^I_M \hat{Q}_{N_0} \hat{Q}_{Z_0} a^+_\mu a^+_\nu |HFB\rangle$$

This leads to the matrix equation

$$\sum_B \{\langle A|\hat{H}|B\rangle - E^{IM}_{N_0Z_0} \langle A|B\rangle\} f_B^{IM;N_0Z_0} = 0$$

which yields the energies $E^{IM}_{N_0Z_0}$ and the wave functions characterized by the $f_B^{IM;N_0Z_0}$.

The single particle basis we used for the study of the A=130 region is described in the previous report about the odd-even nuclei, where also the procedure to obtain the single particle energies is discussed. The effective interaction we employed in our calculations is a Brueckner G-matrix ($G=V+\tilde{G}$) which has been derived for nuclear matter starting with the Bonn potential[3] as the bare nucleon-nucleon interaction V, and using a parametrization in terms of Yukawa-functions of the Brueckner short-range term $\tilde{G}$ [4]. Since this force has been calculated for nuclear matter it has definitely to be renormalized in order to be used in finite nuclei and a finite single particle basis space. It was seen immediately in HFB-calculations performed with the original G-matrix that it does not provide enough pairing correlations. Thus we added an attractive short range force of Gaussian shape with a range of $\mu = 0.5$ fm, which contributes only to the proton-proton and neutron-neutron matrix elements. This part of the force influences strongly the alignment behaviour and thus the band crossing phenomena. It turned out that a good choice for the strengths of the two Gaussians is $V_{pp} = 80$ MeV and $V_{nn} = 50$ MeV.

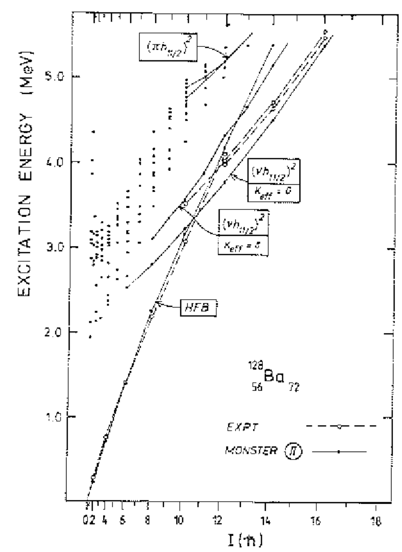

Figure 1

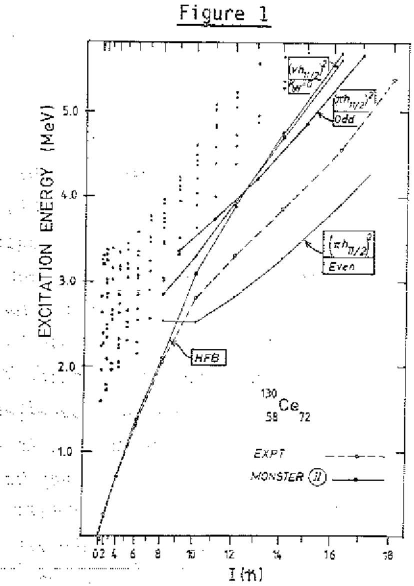

Figure 2

Fig. 1 and Fig. 2 show the results obtained with this force for the nuclei ^{128}Ba and ^{130}Ce. In both figures the energies of the lowest states for each spin are plotted as a function of I(I+1). The experimental data are represented by open circles and dashed lines[2], while the full dots are the theoretical results. In case of ^{128}Ba one obtains a very good agreement with the experimental data. The moment of inertia for the low spin states is reproduced very well and the backbending is theoretically explained by the crossing of a band with two aligned $h_{11/2}$-neutrons. The second nearly degenerate band above I=12 cannot be quantitatively reproduced by the theory, the only candidate for this band being another $h_{11/2}$-neutron quasiparticle band, since the proton bands turn out to be too high in energy. In case of ^{130}Ce (Fig. 2) the backbending is clearly caused by the crossing of a $h_{11/2}$-proton quasiparticle band, which occurs a little too early in the theory. The moment of inertia of the low spin states is again very well described. Some finetuning of the force parameters and the calculation of the other even-even nuclei in this region is still in progress. We hope that the results will help us in understanding the various experimental data available for excitation energies, g-factors and BE2-transitions.

References

1) K.W. Schmid, F. Grümmer, A. Faessler, Phys. Rev. C in press.
2) P.J. Nolan et al., Physica Scripta T5 (1983) 153; K. Schiffer et al., Z. Phys. A313 (1983) 245.
3) K. Holinde, K. Erkelenz, R. Alzetta, Nucl. Phys. A194 (1972) 161.
4) W.H. Dickhoff, Nucl. Phys. A399 (1983) 287.

+ Inst. f. Theor. Physik, Univ. Tübingen,

3.12. The Spin Dependence of the HFB-Mean Field

F. Grümmer and K.W. Schmid+

In the last years the MONSTER, a powerful code for the microscopic description of nuclear structure in large model spaces has been developed[1]. The idea of the underlying model is the use of a HFB mean field as a reference state with respect to which the additional correlations in the nuclear states may be described by two quasiparticle admixtures. In order to avoid spurious effects it is important to project the HFB wave function as well as the 2 qp states onto good angular momentum and particle number before one diagonalizes the many body hamiltonian in this basis. It was shown that this approach is a very good approximation to the exact shell model configuration mixing (SCM) method. Also effects like the backbending in heavy deformed nuclei, which is known to be a single particle effect, which may be described essentially by intrinsic two quasiparticle excitations with respect to the ground state, are rather well reproduced with the MONSTER in its present version[1].

The two major approximations used in the present version of the MONSTER are the assumption of a fixed mean field for all states to be described and the truncation of the configuration space to 2-q.p. configurations. This will cause problems if one wants to describe nuclear states, which are known to be essentially projected 4-q.p. excitations with respect to the ground state. Also all cases where the collective properties of the nucleus change rapidly and strongly within a band will cause difficulties.

A way to overcome those difficulties would be the use of a spin dependent mean field. Then the yrast state and the excited states for a given spin will always be described with respect to the optimal HFB-field for this spin. Since this HFB-state may be any many-quasiparticle excitation with respect to the intrinsic mean field wave function such a description will also include 4-q.p. states like they are for example necessary for the description of the second backbending in yrast bands of heavy nuclei.

The problem of calculating an optimal HFB-wave function for given angular momentum and particle number can be solved by a technique known as projection before the variation, which has been discussed already long ago but has been practically performed only in simple cases or with major approximations. We have developed a method, which performs a variation of the HFB-transformation after the projection onto good agnular momentum and particle numbers, the only approximation being the restriction to axial symmetric Slater determinants.

According to the generalized Thouless theorem any HFB-wave function may be expressed with respect to another one as

$$|\widetilde{HFB}\rangle = {}_{o} \cdot \exp\{ \tfrac{1}{2} \sum_{\mu\nu} d_{\mu\nu} a^{+}_{\mu} a^{+}_{\nu} \} |HFB\rangle$$

where d is an antisymmetric matrix. We assume here that $|HFB\rangle$ is an axial symmetric state and that the matrix d doesn't mix k-values, so that the matrices d span the space of all axial symmetric HFB-wave functions. The problem of projection before the variation now reduces to the problem of minimizing the spin- and number-projected energy

$$E^{IM}_{N_o Z_o}(d) = \frac{\langle\widetilde{HFB}|\hat{H}\hat{P}^{I}_{M}\hat{Q}_{N_o}\hat{Q}_{Z_o}|\widetilde{HFB}\rangle}{\langle\widetilde{HFB}|\hat{P}^{I}_{M}\hat{Q}_{N_o}\hat{Q}_{Z_o}|\widetilde{HFB}\rangle}$$

as a function of d. In order to perform this minimization efficiently we use the derivatives of $E^{IM}_{N_o Z_o}(d)$ with respect to the matrix elements $d_{\mu\nu}$

$$\frac{\partial E^{IM}_{N_o Z_o}}{\partial d_{\mu\nu}} = (Q^{T}\, g\, Q)_{\mu\nu}$$

Here g denotes the local gradient represented by the projected H_{20}-matrix

$$g_{\mu\nu} = \frac{\langle\widetilde{HFB}|\hat{H}\hat{P}^{I}_{M}\hat{Q}_{N_o}\hat{Q}_{Z_o} a^{+}_{\mu} a^{+}_{\nu}|\widetilde{HFB}\rangle - E^{IM}_{N_o Z_o}\langle\widetilde{HFB}|\hat{P}^{I}_{M}\hat{Q}_{N_o}\hat{Q}_{Z_o} a^{+}_{\mu} a^{+}_{\nu}|\widetilde{HFB}\rangle}{\langle\widetilde{HFB}|\hat{P}^{I}_{M}\hat{Q}_{N_o}\hat{Q}_{Z_o}|\widetilde{HFB}\rangle}$$

and Q is a matrix which orthonormalizes the HFB-transformation of $|HFB\rangle$ for a given d. It turns out that a simple steepest descent method is able to find the minimum of $E^{IM}_{N_o Z_o}(d)$, but the process is very slow since one has to use very small stepsizes. This is due to the fact that the projected energy depends more or less sensitively on different parameters of the HFB-wave function. A significant improvement is obtained by the use of a variable metric quasi Newton-method for the minimization.

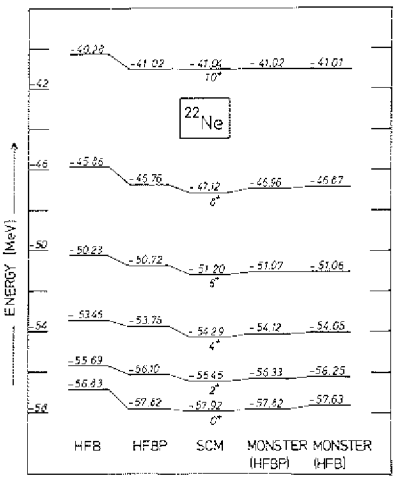

Figure 1

For the purpose of testing the program we applied it to the ground state band of ^{22}Ne. With the s-d shell as single particle basis and a modified surface delta interaction[2] as effective hamiltonian the results obtained with different models can be compared to the exact shell-model result. In Fig. 1 one sees the exact ground state band in the middle. To the left are the results of models using only one Slater determinant for each state. The band denoted by HFB results from the projection of spin and particle number from the intrinsic HFB-wave function. The energies differ by typically 1 MeV from the exact values. The band denoted by HFBP shows the result obtained with the new model, that means for each spin the optimal HFB-wave function has been calculated with the method described above. One finds a significant improvement of all the energies compared with the HFB result. To the right of the exact spectrum the results of two different MONSTER calculations are shown, one based on the intrinsic HFB-field while the other calculation uses different mean fields for each angular momentum. One sees that both spectra agree quite well with the exact one and with each other. It should be noted here that for the 0^+-ground state the HFBP-method yields a better energy than the MONSTER based on the intrinsic field. For the other states the MONSTER is still superior because of the mixing of different k-values, thus going beyond axial symmetry.

As a result one should stress that the HFBP-method to find an optimal HFB mean field gives a clear improvement of the usually used method of projection after the variation. In the case of ^{22}Ne the use of the optimal wave functions for each spin in a MONSTER-calculation doesn't improve the results of a MONSTER-calculation based on a fixed mean field very much. However, we know that in heavier nuclei and for different nuclear states this improvement should be an essential one.

References

1) K.W. Schmid, F. Grümmer, A. Faessler, Phys. Rev. C in press.
2) A. Plastino, R. Arvieu, S.A. Moszkowski, Phys. Rev. 145 (1966) 837.

+ Inst. f. Theor. Physik, Univ. Tübingen,

3.13. On Averaging in Iterative Hartree-Fock Solving Procedures

Vilmar Klemt

It is well known that iterative methods for the solution of Hartree-Fock (HF) equations do not always converge. It may turn out that the density $\rho^{(\nu+1)}(r)$ calculated in the iteration step number $\nu+1$ may be farer away from the true HF density than the density $\rho^{(\nu)}(r)$ of the ν-th step. In many cases, however, using, instead of $\rho^{\nu+1}(r)$, the average of the ν-th and the $(\nu+1)$-th density for the calculation of the respective $(\nu+1)$-th mean field leads to quick convergence.

In some cases this method does not seem to be directly applicable however. If we represent the HF single-particle orbits in form of an expansion into harmonic oscillators (ν = iteration number),

$$\zeta^{(\nu)}_{n\ell j}(r) = \sum_{n'=1}^{M} C^{(\nu)}_{n'}(n\ell j) R^{osc}_{n'\ell}(r) \quad , \qquad (1)$$

the HF-equations reduce to those for the expansion coefficients $C^{(\nu)}_{n'}(n\ell j)$:

$$\sum_{n_2} \{ \langle n_1 \ell_o j_o | t | n_2 \ell_o j_o \rangle + \sum_{n\ell j} \sqrt{\frac{2j+1}{2j_o+1}} \sum_{n_3 n_4} C^{(\nu)}_{n_3}(n\ell j) C^{(\nu)^*}_{n_4}(n\ell j) \times \langle n_1 \ell_o j_o (n_2 \ell_o j_o)^{-1}, 0 | V | n_3 \ell j (n_4 \ell j)^{-1}, 0 \rangle - \varepsilon^{(\nu+1)}_{n_o \ell_o j_o} \delta_{n_1 n_2} \} C^{(\nu+1)}_{n_2}(n_o \ell_o j_o) = 0 \ . \qquad (2)$$

Here t is the operator of the kinetic energy, V is the effective nucleon-nucleon interaction, whose particle-hole matrix elements, coupled to 0^+, appear in the equation. The sum $\sum_{n\ell j}$ runs over all the occupied HF orbits. The advantage of this method, which also has its drawbacks[1], is that one can calculate a set of 0^+ particle-hole oscillator matrix elements in principle once and for all (typically a 300x300 to 400x400 matrix for heavy nuclei), store them on a permanent data set and use them for arbitrarily many different HF-program runs. In this way realistic finite range forces (central and tensorial) can be used, whose matrix elements consume more computing time than the more schematic forces applied usually. On the other hand the nucleon density never appears directly in eq. (2) (except in density dependent forces which have to be recalculated in each iteration step), but only indirectly in form of the expansion coefficients $C_n^{(\nu)}(n\ell j)$. Therefore the question arises how an averaging procedure between two successive iteration steps can be carried out for the expansion coefficients. Now a transition from one basis (iteration number ν) in a space spanned by oscillator wave functions to another one (iteration number $\nu+1$) is always described by a unitary transformation U, which can be regarded as a generalization of a rotation. Therefore it suggests itself to assume that the procedure of averaging between the ν-th and $(\nu+1)$-th iteration should be related to a reduction of the "rotation angles" of that unitary transformation. It is well known that a unitary matrix can be transformed to diagonal form by a unitary transformation, what is equivalent to saying that the left-side and right-side eigenvectors of a unitary matrix are identical, and that the eigenvalues are of the form $\exp(iD_k)$, where the D_k's are real numbers. The resulting equation reads

$$\sum_n (U_{mn} - e^{iD_k}\delta_{mn})\langle n|\varphi^{(k)}\rangle = 0 \ , \qquad (3)$$

where the $\langle n|\varphi^{(k)}\rangle$ are the eigenvectors of the unitary matrix U specified in an arbitrary (in our case oscillator) basis $|n\rangle$. Let the iteration step (number ν, say) change the momentary HF basis $|u_i\rangle$ (i=1,2,...M according to eq. (1)) into the new basis $|v_i\rangle$, then the respective unitary matrix U that effects this is

$$U = \sum_i |v_i\rangle\langle u_i| \ , \qquad (4)$$

or in our oscillator basis:

$$U_{mn} = \sum_i \langle m|v_i\rangle\langle u_i|n\rangle \qquad (5)$$

Averaging between two iteration steps is achieved by multiplying the D_k's by a factor r with 0 r 1. Instead of U we get then the unitary transformation $U^{(r)}$ with

$$U_{mn}^{(r)} = \sum_k \langle m|\varphi^{(k)}\rangle\, e^{irD_k}\, \langle\varphi^{(k)}|n\rangle \ . \qquad (6)$$

$U^{(r)}$ leads from a basis $|u_i\rangle$ to a basis $|v_i^{(r)}\rangle$ with

$$|v_i^{(r)}\rangle = U^{(r)}|u_i\rangle \qquad (7)$$

The respective expansion coefficients are then

$$C_m^{(\nu+1,r)} = \langle m|v_i^{(r)}\rangle = \sum_n U_{mn}^{(r)}\langle n|u_i\rangle = \sum_n U_{mn}^{(r)} C_n^{(\nu,r)} \qquad (8)$$

Practical experience shows that this procedure is numerically fast (due to the small dimension of the matrices U, which is 8 for heavy nuclei) but not accurate enough numerically since the errors of the successive iteration steps accumulate. This problem can be easily cured however by reorthonormalizing the basis after each iteration step.

Reference

1) P.-G. Reinhard, R.Y. Cusson, Nucl. Phys. A378 (1982) 418

3.14. On a Relativistic Hartree-Fock Description of Magic Nuclei

Vilmar Klemt

In recent years the interest in relativistic Hartree-Fock (HF) theory for nuclei has grown since there is good evidence now that relativistic effects can no longer be considered small[1]. A relativistic HF-treatment of nuclei encounters many more problems with respect to its significance and justification[1,2] as well as concerning its numerical feasibility. While in nonrelativistic HF calculations rather schematic forces as those of the Skyrme type are frequently used, in a relativistic calculation one certainly has to cope with more realistic potentials that can be derived from meson exchange processes. Potentials of the latter kind however, especially their exchange (Fock) parts are much more difficult to handle analytically as well as numerically.

A nonrelativistic HF-code developed by the author (see another contribution of the author in this report) has made use of the oscillator expansion method, which allows to compute the relevant oscillator-space matrix elements only once, store them on a permanent data set and use them arbitrarily many times in subsequent HF runs.

It is tempting to examine how this method can be extended to relativistic HF calculation. The first difference is that the orbits of a relativistic HF Slater determinant consist of Dirac spinors of the form

$$\psi_{n\ell jm}(\vec r) = \begin{pmatrix} i g_{n\ell j}(r)\ \varphi_{\ell jm}(\Omega) \\ f_{n\ell j}(r)\ \ \vec\sigma\cdot\hat r\ \varphi_{\ell jm}(\Omega) \end{pmatrix} \qquad (1)$$

where the $\varphi_{\ell jm}$ are Pauli spinors and $g_{n\ell j}$ and $f_{n\ell j}$ are the radial wave functions of the large and small components, respectively. The operator $\vec\sigma\cdot\hat r$ (with $\hat r = \vec r/r$) has the property of changing the quantum number of the orbital angular momentum:

$$\vec\sigma\cdot\hat r\ \varphi_{j\pm 1/2, jm}(\Omega) = \varphi_{j\mp 1/2, jm}(\Omega) \qquad (2)$$

By considering the radial Dirac equation for a one-body Dirac Hamiltonian

$$H = \begin{pmatrix} m-U(r) & \vec\sigma\cdot\vec p \\ \vec\sigma\cdot\vec p & m\mp U(r) \end{pmatrix} \qquad (3)$$

for small arguments r one finds that the appropriate expansion of the radial Dirac functions into harmonic oscillators is

$$g_{n,j\pm 1/2,j}(r) = \sum_{m=1}^{M_a} a_m(n,j\pm 1/2,j)R^{osc}_{n,j\pm 1/2}(r) \qquad (4a)$$

and

$$f_{n,j\pm 1/2,j}(r) = \sum_{m=1}^{M_b} b_m(n,j\pm 1/2,j)R^{osc}_{n,j\mp 1/2}(r) \qquad (4b)$$

i.e. the small components $f_{n\ell j}$ correspond to a different ℓ than the large $g_{n\ell j}$.

The two-particle interaction, which in general consists of many different parts (scalar, vector, pseudoscalar, pseudovector etc.) now not only combines large with large and small with small components to a resulting mean field of 0^+ type (see another contribution of the author in this report) but also large with small and small with large components leading to a mean field of 0^- type:

$$\langle n_1\ell_o j_o|U^-|n_2\ell_o\pm 1 j_o\rangle$$

$$= \frac{1}{\sqrt{2j_o+1}} \langle n_1\ell_o j_o(n_2\ell_o\pm 1j_o)^{-1},0^-|\begin{pmatrix}\sigma\cdot\sigma' V_v \\ V_{ps}\end{pmatrix} \tag{5}$$

$$\times \sum_{n\ell j} \sqrt{2j+1} \begin{cases} \sum_{n_3n_4} a_{n_3}(n\ell j) b_{n_4}(n\ell j) |n_3\ell_j(n_4\ell\pm 1j)^{-1},0^-\rangle \\ \mp \sum_{n_3n_4} b_{n_3}(n\ell j) a_{n_4}(n\ell j) |n_3\ell\pm 1j)(n_4\ell j)^{-1},0^-\rangle \end{cases}$$

where the sum $\sum_{n\ell j}$ runs over occupied Dirac orbits and the $\mp$ in front of the $\sum_{n_3n_4}$ refers to the respective parts of the force (V_v for vector and V_{ps} for pseudoscalar). The extension to a relativistic HF thus leads to an approximate doubling of the dimension of the matrices to be diagonalized, which should not be prohibitive numerically, even for heavy nuclei.

References

1) M.R. Anastasio, L.S. Celenza, W.S. Pong, C.M.Snakin, Phys. Rep. 100 (1983) 327.
2) D. Schütte, Nucl. Phys. A411 (1983) 369.

3.15. A Microscopic Look at the Nuclear Twist

B. Schwesinger*

A microscopic description of nuclear excitations is used to confirm semiclassical predictions[1] on a collective twist motion. To this end specific properties of the excitation have been derived from Landau theory and are shown to persist on a microscopic level.

The microscopic calculation applied is a procedure which is equivalent to a diagonalization space of 1p-1h and 2p-2h states[2].

The main result is that ^{208}Pb shows two very sharp resonances in response to the twist operator which are located at 7.2 MeV and at 7.9 MeV. The position of these states is entirely fixed by experimentally measured single particle energies because the residual interaction does not affect the position of transverse zero sound modes.

According to the microscopic calculation ^{90}Zr is not heavy enough to exhibit a twisting motion.

The possibility of detecting the twist experimentally through electron scattering is also investigated. Despite this overwhelming contribution to the M2 sum, the competing spin flip[3] mode is so heavily fragmented that it cannot obscure the resonance peaks of the twist in (e,e') scattering experiments.

References

1) G. Holzwarth, G. Eckart, Z. Phys. A283 (1977) 219.
2) B. Schwesinger, J. Wambach, Phys. Lett. B in press; Phys. Rev. C in press.
3) B. Schwesinger, K. Pingel, G. Holzwarth, Nucl. Phys. A341 (1980) 1.

* Supported by a fellowship from the Scientific Committee of the NATO via the German Academic Exchange Service (DAAD)
Present address: SUNY at Stony Brook, Stony Brook, NY, USA

3.16. Effective Quasi-Particle G-Matrix Interaction

K. Nakayama, S. Krewald, J. Speth, and W.G. Love+

In the last decade considerable effort has been devoted to deriving an effective particle-hole interaction from a microscopic point of view. The main ingredient of such an interaction is the particle-hole irreducible kernel[1] which is usually approximated by the Brueckner G-matrix. This seems to be a reasonable approximation since ~ 85 % of the experimental binding energy is already explained by the Brueckner G-matrix. In addition to its traditional role in calculating ground state properties of nuclei, a Brueckner G-matrix (pion- and rho-exchange potential folded with a short-range correlation function) has recently been successfully applied to the description of magnetic states in nuclei[2]. In fact, a simple analysis of the Landau parameters derived from the Brueckner G-matrix shows qualitatively how the different components of an effective interaction influence the properties of the low-lying excited states. However, a more complete analysis of the Brueckner G-matrix and its momentum and density dependence are essential for understanding more quantitatively the properties of nuclei.

Using the method of deriving the operator structure[3] of the Brueckner G-matrix, an effective interaction (operator), based on a G-matrix in nuclear matter, derived from a one boson exchange potential, has been extracted. Once the operator structure of the Brueckner G-matrix is obtained, its analysis is substantially simplified compared with the methods used so far. Effects of the short-range correlations have been analyzed, showing that they are largely restricted to $^1S_0$ and $^3S_1$-$^3D_1$ states and affect predominantly the central components of the G-matrix interaction. The tensor forces are not affected by correlations due to the fact that the correlation functions in $^3S_1$-$^3D_1$ (L=L'=0) and $^3S_1$-$^3D_1$ (L=0,L'=2) states have opposite signs and therefore their contributions cancel each other almost exactly. The spin-orbit components are also weakly influenced by correlations (~ 10 %), since L=0 states cannot contribute to these channels. The non-locality of the G-matrix interaction has been explicitly verified. Although the short-range correlations introduce a very small amount of non-locality, the scalar-isoscalar channel is strongly nonlocal due to the ω- and σ-meson exchange potentials which have already such a behaviour. The density dependence of the G-matrix interaction has been mapped out using the local density approximation. A fairly simple density dependence is found. Based on these analyses a simplified momentum transfer and density dependent G-matrix interaction has been constructed. For further convenience, this interaction has been parametrized in terms of Yukawa type expressions

$$\frac{A}{q^2+m^2} \tag{1}$$

which reproduce the exact values within 0.2 % in the range of 0-2 fm^{-1} of the momentum transfer. Also a simple functional form for the density dependence has been suggested based on the analysis of an analytical G-ma trix, which gives an excellent quality of the fit (within 1 %) in the range of the density of 0.35 $\rho_0 < \rho < \rho_0$. The results of these parametrizations are shown in Table 1. There, SO(SE) and TO(TE) denote singlet-odd (even) and triplet-odd (even) channels of the G-matrix interaction, respectively. TNO(E) denotes the tensor-odd (even) component and LSO(E) the spin-orbit-odd (even) force. m is the mass of the effective mesons exchanged and A its coupling strength. The density dependence is fitted with an expression of the form

$$\frac{1}{1+\alpha(k_F-k_F^0)+\beta(k_F-k_F^0)^2} \tag{2}$$

where k_F is the Fermi momentum and $k_F^0 = 1.36\ fm^{-1}$. Λ is the cutoff parameter of the form factor given by $\left(\frac{\Lambda^2-m^2}{\Lambda^2+q^2}\right)$ for the tensor forces only.

We hope the momentum transfer and density dependent G-matrix interaction as constructed above may be used as a main ingredient of the full particle-hole interaction to describe the low-lying excited states of nuclei.

References

1) S. Babu, G.E. Brown, Ann. Phys. 78 (1973) 1.
2) J. Speth, V. Klemt, J. Wambach, G.E. Brown, Nucl. Phys. A343 (1980) 382.
3) K. Nakayama, S. Krewald, J. Speth, W.G. Love, Ann. Rep. 1982, Jül-Spez 202 (1982) 72.

+ Univ. of Georgia, Athens, USA

channel	$m_1 = 4.0\ fm^{-1}$			$m_2 = 2.5\ fm^{-1}$			$m_3 = 0.71\ fm^{-1}$	
SL	A	α	β	A	α	β	A*	Λ (MeV)
SO	3489.8578	-	-	-1072.6901	0.40738	-	1195.3360	-
SE	1332.2011	-0.21537	-0.61972	-1809.5155	-0.15600	-0.65536	-398.4453	-
TO	1253.1275	0.35298	-	-914.8167	0.45308	-	132.8151	
TE	2006.6900	0.82068	0.13303	-2627.8311	0.82708	0.05749	-398.4453	-
TNO	355.0412	-	-	79.9680	-	-	-132.8151	960
TNE	356.9312	-	-	-475.3378	-	-	398.4453	960
LSO	181.4617	-	-	135.5124	-	-	-	-
LSE	-852.9600	-	-	2[illegible].6745	-	-	-	

* OPEP, which has been added explicitly (not fitted).

Table 1: Fitted parameters. Coupling strengths A are in MeV fm^3; α in fm and β in fm^2.

3.17. The Effect of Nuclear Polarization on the Isotope Shift in Electronic Atoms

B. Hoffmann, G. Baur, and J. Speth

The isotope shift in electronic atoms is calculated in second order perturbation theory[1]. We consider multipole orders λ = 0, 1 and 2 for Z = 20-82 nuclei. The influence of the shape of the nuclear transition density on the polarization shift is investigated and found to be small. This can be seen in Fig. 1. In this figure, the contribution of different transition densities $\rho_{tr} \propto r^n$ (n=0,2,4,6) ($r<R_0$) to the quadrupole polarization energy is shown. To a good approximation, the polarization contribution is directly proportional to the electronic density at the nucleus. We study whether the polarization effect modifies the extraction of $\delta\langle r^2\rangle$ values from isotope shift measurements and find it to be small. It may not always be negligible, especially in the cases where very accurate optical measurements exist. We estimate the effect for the example of the Sm-isotopes, where a strong change of deformation occurs in the series of isotopes, which

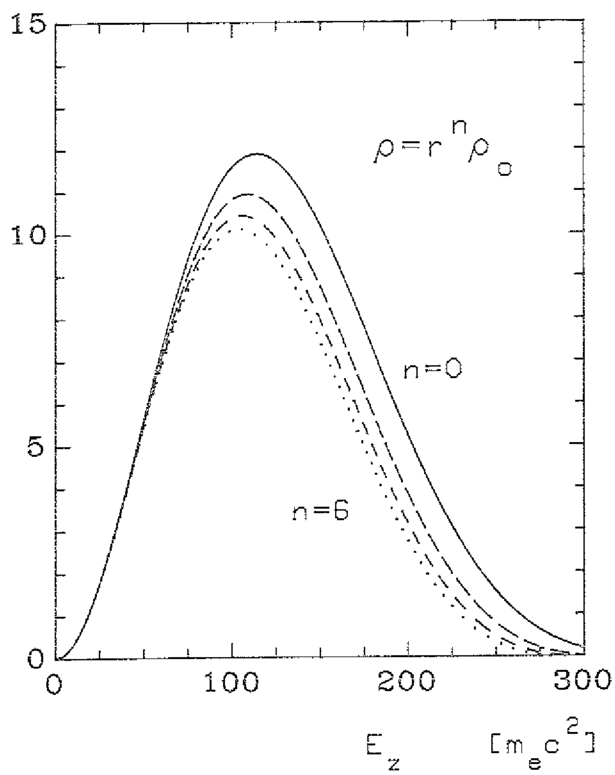

Fig. 1: Influence of the form of the transition density ρ_{tr} on the quadrupole polarization as a function of the intermediate electron energy.

causes changes in the quadrupole polarizability. In a recent paper by Bernabêu and Ericson[2] the effect of the dipole polarizability in electronic atoms was considered in the unretarded dipole approximation.

References

1) B. Hoffmann, G. Baur, J. Speth, Z. Phys. A in press.
2) J. Bernabêu, T.E.O. Ericson, Z. Phys. A309 (1983) 213.

3.18. Fission Barrier Calculation for Rotating Nuclei

J. Németh[+], J.M. Irvine[++], J. Okolowicz[++*]

Recent experiments concerning the fission of light rare earth nuclei[1] and the discovery of the "fast fission" phenomenon[2,3] made it important to reexamine the fission barrier dependence on the rotational angular momentum of the nuclei. We calculated the fission barrier of a rotating ^{144}Nb nucleus in constrained Hartree-Fock calculations, constraining the angular momentum and the quadrupole momentum values, and compared the results with the drop model calculation of Cohen et al.[4]. The results can be seen in Fig. 1 [5]. The fission barrier decreases with increasing angular momentum more rapidly than predicted by Ref. 4, in good agreement with experimental observations[1]. On the other hand, the maximum angular momentum for which the nucleus is still stable

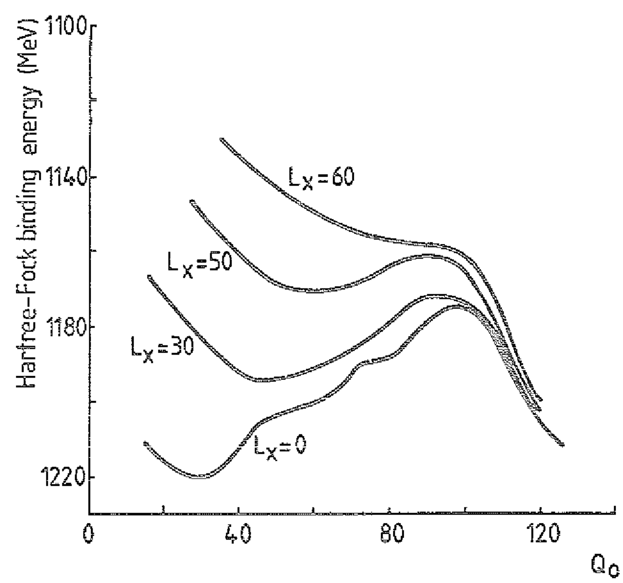

Fig. 1: The H.F. fission barrier as a function of the quadrupole constraint for L_x = 0, 30, 50 and 60 ħ.

against fission is about 60-80 % smaller than expected. This fact emphasizes even more the importance of the fast fission phenomenon, and makes it necessary to calculate the fission barrier for asymmetric rotating nuclei as well.

References

1) G. Andersson et al., Z. Phys. A293 (1979) 241.
2) C. Gregoire et al., Nucl. Phys. A387 (1982) 37c.
3) W.J. Swiatecki, Physica Scripta 24 (1981) 113.
4) J. Németh, J.M. Irvine, J. Okolowicz, to be published in Phys. Lett.
5) S. Cohen, F. Plasil, W.J. Swiatecki, Ann. Phys. 82 (1974) 557.

+ Eötvös University, Budapest, Hungary
++ Univ. of Manchester, Manchester, England
* Nuclear Physics Institute, Cracow, Poland

3.19. High Energy Proton Induced Fission of Rare Earth Nuclei

J. Németh[+], J.M. Irvine[++]

High energy (500-600 MeV) protons can induce fission of rare earth nuclei, while in the case of 200 MeV energy protons the fission probability of the same nuclei is practically negligible[1,2]. Since the fission barrier even for nuclei of mass number 150 is only about 50 MeV [3], this fact cannot be explained by energy considerations only. To examine the phenomenon in detail, it is useful to perform modified time dependent Hartree-Fock calculations. To solve the TDHF equations one has to start from an excited wave function, the excitation can be vibrational, rotational or thermal. However the usual TDHF equations cannot lead to fission, because there is no mechanism to change the filling order in a mean field approximation. To avoid this difficulty one has to introduce either unnaturally big pairing forces[4], or modified TDHF equations can be applied[5] to change the occupation probability of the levels and thus simulate the two-body dissipation. In case of ^{144}Nb giving the nucleus 400 MeV excitation either as vibrational or as thermal energy we got no fission within 10^{-20} sec. Giving the same amount of energy, but a part of it as rotation, the nucleus is fissioning in less than 10^{-21} sec. The reason for this is that high ($L_x \sim 30h$) angular momentum deformes the nucleus. Since this deformed shape is already close to the saddle point deformation, the nucleus can fission easily. Proton induced fission of light nuclei occurs in peripheral collisions with big impact parameters, and in our opinion the high energy of the protons is needed only to transfer high angular momentum to the nuclei. In fact there is experimental evidence that high angular momentum states can be excited with some probability in such collisions[2].

References

1) G. Andersson et al., Z. Phys. A293 (1979) 241.
2) S.B. Kaufman, E.P. Steinberg, Phys. Rev. C22 (1980) 167.
3) J. Németh, J.M. Irvine, J. Okolowicz, to be published in Phys. Lett.
4) J. Negele et al., Phys. Rev. C17 (1978) 1098.
5) J. Németh, J.M. Irvine, to be published in Acta Phys. Hung., and see Refs. there.

+ Eötvös University, Budapest, Hungary
++ Univ. of Manchester, Manchester, England

3.20. Effective Mass in Nuclei and the Level Density Parameter

M. Prakash[+], Z.Y. Ma[++] and J. Wambach

In generalizing the Thomas-Fermi approximation to finite temperatures, Barronco and Treiner[1] have given an expression for the level density parameter a involving local ground state quantities like the particle density $\rho_0(\vec{r})$, the local Fermi momentum $k_F(\vec{r})$ and the local effective mass $m^*(\vec{r})$. In terms of these fundamental quantities a is given by

$$a = \pi^2/4 \sum_i \int 2\rho_0^i(\vec{r}) m^{*i}(\vec{r})/(\hbar^2 k_F^i(\vec{r}))d\vec{r} \qquad (1)$$

The summation index distinguishes protons and neutrons. In the large A limit in which the $\vec{r}$-dependences disappear we get the familiar expression from Fermi liquid theory

$$a = \pi^2 2m^* A/(\hbar^2 k_F^2) \qquad (2)$$

Using $m^*=m$ and the equilibrium nuclear matter value $k_F = 1.36\ fm^{-1}$ $a = A/15$ much smaller than experiments in finite nuclei indicate for which on the average $a \sim A/7$. The deviation is solely due to the presence of the surface which acts as a static boundary as well as a dynamical variable adding extra degrees of freedom to the system.

To study the influence of these new degrees of freedom we have attempted to determine the volume, surface and curvature coefficients of the level density parameter a, expressed as

$$a = a_v A + a_\rho A^{2/3} + a_c a^{1/3} \qquad (3)$$

from empirical knowledge of the nuclear mean field Σ which in general is nonlocal and frequency dependent. In finite nuclei it furthermore depends on the c.m. coordinate $\vec{r}$ of two interacting particles. To arrive at the local quantities needed in (1) we expand Σ around the Fermi surface determined by the Fermi energy ε_F and the local Fermi momentum $k_F(\vec{r})$. First order is sufficient to determine the quasiparticle properties near the Fermi surface and therefore to specify the entropy. To this order the selfenergy Σ is given by

$$\Sigma(\vec{r},\vec{k},\omega) = \Sigma_0(\vec{r},k_F(\vec{r}),\varepsilon_F)+(\omega-\varepsilon_F)(\partial\Sigma/\partial\omega)\Big|_{\omega=\varepsilon_F} + (k^2-k_F^2(\vec{r}))(\partial\Sigma/\partial k^2)_{k^2=k_F^2} \qquad (4)$$

The zeroth order term determines the local Fermi momentum $k_F(\vec{r})$

$$k_F^2(\vec{r})/2m + \Sigma_0(\vec{r},k_F(\vec{r}),\varepsilon_F) = \varepsilon_F \qquad (5)$$

and the effective mass is given by the derivatives with respect to $\vec{k}$ and ω as

$$m^*/m(\vec{r}) = \left[1+2m\frac{\partial\sum(\vec{r},\vec{k},\varepsilon_F)}{\partial k^2}\right]^{-1}_{k^2=k_F^2} \cdot \left[1-\frac{\partial\sum(\vec{r},k_F(\vec{r}),\omega)}{\partial\omega}\right]_{\omega=\varepsilon_F} \quad (6)$$

Rather than deriving the mean field from an underlying two-body interaction we choose to parametrize $\sum_0$ by a Woods-Saxon potential. The first derivative of $\sum$ with respect to k^2 is proportional to the non-locality length α of the optical potential which has been determined empirically. The ω-derivative of $\sum$ is less known but can be obtained in principle from the ω-dependence of the absorptive part of the optical potential or equivalently from the spacing of single particle levels near ε_F. To finally obtain the level density parameter the one-body density ρ_0 is determined from the solutions of an equivalent Schrödinger equation which includes the selfenergy up to first order.

$$\{-\vec{\nabla}\hbar^2/2m^*(\vec{r})\vec{\nabla} + U(\vec{r})\}\phi_\nu(\vec{r}) = \varepsilon_\nu\phi_\nu(\vec{r}) \quad (7a)$$

$$U(\vec{r}) \sim m/m^*(\vec{r}) \textstyle\sum_0(\vec{r},k_F(\vec{r}),\varepsilon_F) \quad (7b)$$

In terms of these solutions one has

$$\rho_0(\vec{r}) = \sum_\nu n_\nu\phi_\nu^*(\vec{r})\phi_\nu(\vec{r}) \quad (8a)$$

$$n_\nu = \begin{cases} 1 & \varepsilon_\nu<\varepsilon_F \\ 0 & \varepsilon_\nu>\varepsilon_F \end{cases} \quad (8b)$$

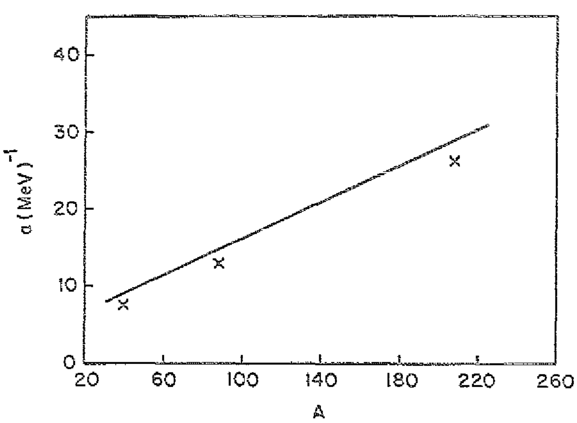

Fig. 1: A-dependence of the level density parameter. The crosses indicate results using expression (1) in ^{40}Ca, ^{90}Zr and ^{208}Pb. The straight line utilizes expression (9).

We have calculated the level density parameter for the three closed shell nuclei ^{40}Ca, ^{90}Zr and ^{208}Pb (indicated by the crosses in Fig. 1). To obtain the general A-dependence (3) we extracted from (1) the surface-, volume- and curvature coefficients deriving a general expression for a in terms of ε_F, $\rho_0(o)$, α and a parameter β characterizing the ω-derivative of $\sum$. The result can be expanded as

$$a = \pi^2/(4\varepsilon_F)A[(1-\alpha)+3(\alpha_0/r_0)\nu_0A^{-1/3} + 8(\alpha_0/r_0)^2\{\nu_1-(1-\alpha)\pi^2/6\}A^{-2/3} + \ldots] \quad (9)$$

Here α_0 denotes the diffuseness of the Woods-Saxon potential and r_0 = 1.2 fm. The coefficients ν_0 and ν_1 emerge from the analytical integration of (1) and are linear combinations of Fermi integrals. The A-dependence depicted as the solid line in Fig. 1 is close to experimental findings indicating that both frequency dependence in the mean field and curvature terms in a, usually neglected, are important.

References

1) M. Barranco, J. Treiner, Nucl. Phys. A351 (1981) 261.

$^+$ SUNY at Stony Brook, Stony Brook, NY, USA

$^{++}$ Institute of Atomic Energy, Beijing, China

3.21. Fragmentation of Nuclear Strength Distributions by Two-Particle Two-Hole Excitations

J. Wambach and B. Schwesinger[+]

The microscopic understanding of damping of nuclear collective motion has attracted theoretical interest in the past few years. For small amplitude vibrations two damping processes can be identified:

(1) pure mean field damping which gives rise to a spreading of 1p1h-transition strength due to shell structure ("fragmentation width") and a broadening above the continuum threshold due to prompt particle emission ("escape width") and is not described by mean field theories.

(2) damping from residual two-body collisions, which couple the 1p1h-doorway states to nuclear compound states ("spreading width").

Since both are of comparable importance especially as the frequency of the oscillation gets large, a proper many body theory of vibrational motion has to go beyond the mean field, i.e. the RPA-treatment. Based on linear response theory we have proposed an extension[1)] which treats the 1p1h- and 2p2h-subspaces explicitly and higher compound states on the average. Within the restricted model space all diagrams to order V^2 are iterated, where V denotes the residual interaction ($H = H_0+V$).

Implying that a one-body external field

$$Q(t) = \tfrac{1}{2}(Qe^{-i\omega t}+Q^+e^{i\omega t}) \quad (1)$$

couples only weakly to the 2p2h-space, the response to the perturbation Q, which in general is given by the ground state expectation value

$$S_Q(\omega) = -\lim_{\eta\to 0}\frac{\mathrm{Im}}{\pi}\{\langle|Q^+(\omega-H+i\eta)^{-1}Q|\rangle - \frac{|\langle Q|\rangle|^2}{\omega+i\eta}\} \quad (2)$$

can be approximated as

$$S_Q(\omega) = -\lim_{\eta\to 0}\frac{\mathrm{Im}}{\pi}\langle|Q^+P\{\omega-H_0-V+E_0+i\eta + V(1-P)(\omega-H_0-V+E_0+i\eta)^{-1}(1-P)V\}^{-1}PQ|\rangle \quad (3)$$

Here P denotes a projection operator onto the 1p1h-space

$$P = \sum_{1p1h} |1p1h\rangle\langle 1p1h| \qquad (4)$$

The operator 1-P projects of course onto the complementary space containing npnh-states. Since V is a two-body interaction it couples the P-space only to 2p2h-states which therefore act as the entrance channels for the compound decay. They are treated explicitly and all higher configurations are included on the average by making η finite in the 2p2h-propagator. Furthermore V is neglected in this propagator.

We have applied the above model to ^{90}Zr and ^{208}Pb by prescribing the mean field H_0 phenomenologically

$$H_0 = -\hbar^2/2m^*\nabla^2 + U(\underset{\sim}{r}) \qquad (5)$$

Here U is a Woods-Saxon potential and the effective mass m* an adjustable parameter. The residual interaction was approximated by zero-range density-dependent antisymmetrized terms

$$V(\underset{\sim}{r},\underset{\sim}{r}') = \{V_{00}[\rho]+V_{01}[\rho]\vec{\tau}\vec{\tau}'\}\, ½\,[1-P^{\sigma\tau}]\,\delta(\underset{\sim}{r}-\underset{\sim}{r}') \qquad (5a)$$

$$V_{\sigma\tau}(\rho) = V^{in}_{\sigma\tau}\rho(R) + V^{ex}_{\sigma\tau}(1-\rho(R)) \qquad (5b)$$

$$\rho(R) = (1+\exp(R-R_0)/\alpha)^{-1}\ ;\ (\underset{\sim}{R} = (\underset{\sim}{r}+\underset{\sim}{r}')/2) \qquad (5c)$$

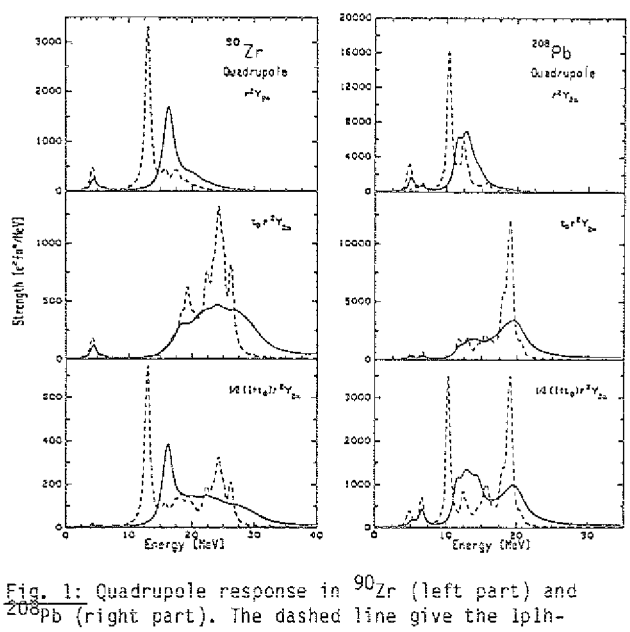

Fig. 1: Quadrupole response in ^{90}Zr (left part) and ^{208}Pb (right part). The dashed line give the 1p1h-response function alone while the full lines include coupling to 2p2h-states.

and the parameters adjusted to a few known resonances. As a typical example isoscalar and isovector transition strength distributions are displayed in Fig. 1. Here the dashed lines indicate a pure mean field (i.e. 1p1h-result) while the full line incorporates two-body collisions resulting in 2p2h-coupling. In general we find that isovector resonances are highly fragmented. Isoscalar modes suffer much less dispersion since large cancellations between the attenuation of the single particle motion (selfenergy insertions) and ph-linked processes (bubble diagrams) occur.

References

1) B. Schwesinger, J. Wambach, Phys. Lett. in press; B. Schwesinger, J. Wambach, to be published in Nucl. Phys.

+ SUNY at Stony Brook, Stony Brook, NY, USA

4. MEDIUM ENERGY PHYSICS

4.1. Δ-Isobar Effects on M2-Strength in ^{208}Pb

D. Cha and J. Speth

We have studied the M2-strength distribution in ^{208}Pb within the framework of the RPA including Δ-hole states. We want to clarify the influence of the Δ-resonances on the M2-strength. This is of special interest because the M2-strength in ^{208}Pb has a considerable contribution from the nuclear convection current in contrast to the M1-strength where the nuclear spin current dominates[1]. For the residual ph-interaction, we take a realistic one which includes the one-pion and one-rho meson exchange potential in the στ-channel explicitly with a two-body correlation function to account for the effects of the other mesons. In addition, we take phenomenological spin-dependent and spin-isospin-dependent zero-range terms, δg_0 and $\delta g_0'$ suggested by Suzuki et al.[2].

The M2-strength distribution between E_x = 6~8 MeV in ^{208}Pb has been measured by Frey et al.[3]. Eight prominent states were found sharing the total strength of $\Sigma B(M2)\uparrow = 8500\pm750\ \mu_N fm^2$. Our theory gives good agreement with the experiment as can be seen from Fig. 1. The

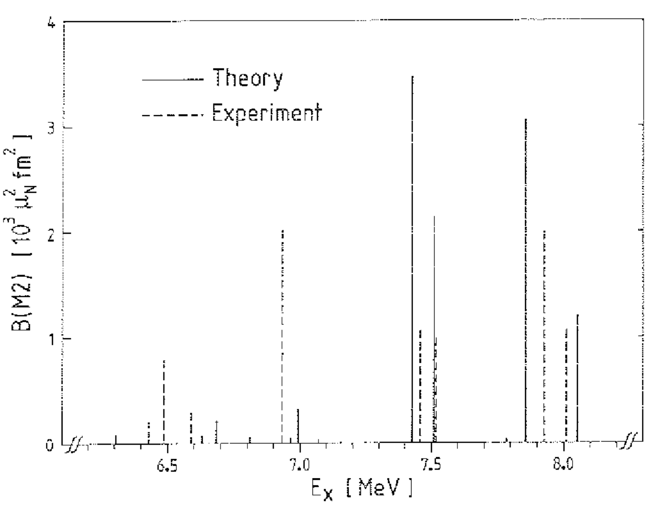

Fig. 1: M2-states between E_x = 6.2~8.2 MeV in ^{208}Pb. Theoretical states are obtained by the RPA including the Δ-hole states and experimental states are quoted from Ref. 3.

predicted total M2-strength within the measured excitation energy range is $\Sigma B(M2)\uparrow = 10808\ \mu_N fm^2$ when we include the Δ-hole states and $\Sigma B(M2)\uparrow = 11273\ \mu_N fm^2$ when they are not included. Therefore, we obtain in this energy range a quenching due to Δ-hole admixture of only 4 %. (If we use the bare g_ℓ factors, the theoretical strength including the Δ-hole effects is reduced to $\Sigma B(M2)\uparrow = 8975\ \mu_N fm^2$.)

To study this in more detail, we constructed histograms of the M2-strength by ΔE_x = 1 MeV bins in Fig. 2. The full columns illustrate the strength from the nuclear spin current only. The strong concentration of the unperturbed strength (Fig. 2a) which is dominated by the nuclear convection current in the E_x = 7~8 MeV bin is due to the proton $i_{13/2}h_{11/2}^{-1}$ single particle excitation, which has more than 40 % of the total unperturbed

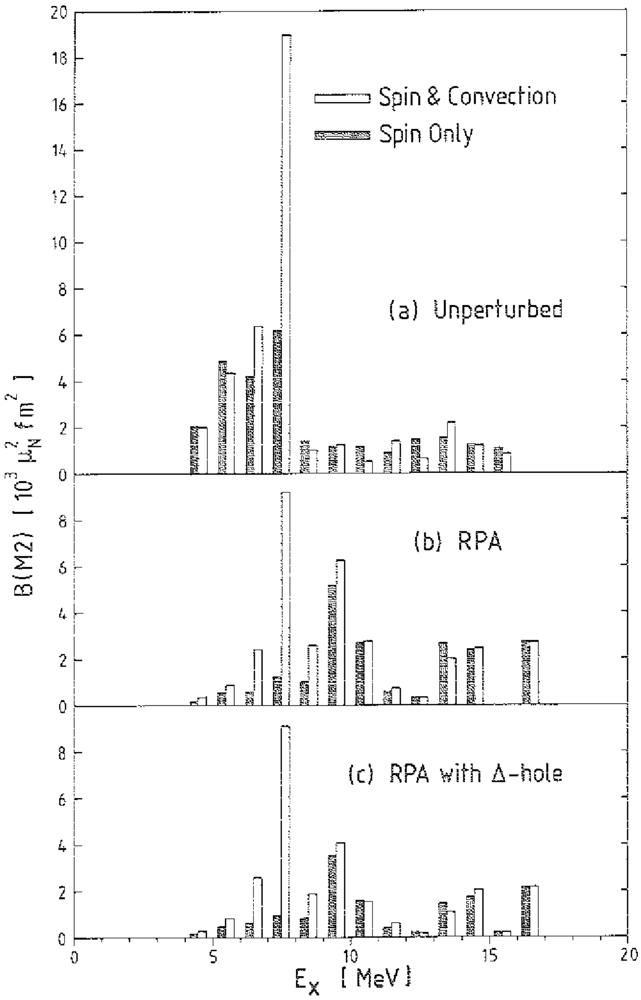

Fig. 2: Histograms of the M2-strength in ^{208}Pb by ΔE_x = 1 MeV bins.

strength. This state may be interpreted as the "twist mode" of Ref. 4. The strong repulsive interaction in the spin-isospin channel introduces two major effects: one is a reduction of about 20 % of the total strength which comes from ground state correlations and the other is a theft of the strength to higher energies. However, one can see that only the spin strength is removed from the lower excitation energy (below 8 MeV) into the higher energy region, while almost all the strength remained at low energies is from the nuclear convection current. That is because the ph-interaction is dominated by the repulsive spin-dependent component. We can also observe from Figs. 2b-2c that the strength below 9 MeV, which is mostly from the convection current, has been hardly affected by the Δ-hole admixtures (only 5 % quenching) while the spin dominated strength above 9 MeV has been significantly quenched (31 %). From our results we conclude that the renormalization of the nuclear spin current is not responsible for the quenching of the observed M2-strength below 9 MeV in ^{208}Pb [5].

References

1) B. Castel, I. Hamamoto, Phys. Lett. 65B (1976) 27.
2) T. Suzuki et al., Phys. Lett. 107B (1981) 9.
3) R. Frey et al., Phys. Lett. 74B (1978) 45.
4) G. Holzwarth, G. Eckart, Z. Phys. A283 (1977) 219.
5) W. Knüpfer et al., Phys. Lett. 95B (1980) 349.

4.2. Medium Polarization Effects: A Crucial Ingredient in the Δ(1232)-Nucleon Interaction

K. Nakayama, S. Krewald, J. Speth, G.E. Brown+

The Δ(1232) isobar has been suggested to play an important role in the reduction of spin-isospin strength in nuclei, especially after the experimental discovery of the Gamow-Teller giant resonance. The magnitude of the reduction of magnetic strength due to isobar-hole admixtures in the nuclear wave function depends strongly on the isobar-hole coupling strength. Here we present a microscopic derivation of the isobar-hole interaction for vanishing momentum transfer.

Due to the fact that nucleons carry spin and isospin 1/2, while the isobar has both spin and isospin 3/2, the two interacting nucleons must have total isospin T=1 and, in the spin-isospin channel, total spin S=1 in order to end up with isobar-nucleon in the final state. This implies that all even relative angular momenta of the interacting nucleons are suppressed in the spin-isospin channel, while in the isovector tensor channel all even or odd relative momenta are suppressed according to spin S being odd or even, respectively. This fact has an immediate consequence that the direct term of the isobar-hole interaction is largely cancelled by the exchange term if one approximates the full particle-hole interaction by a G-matrix. Therefore, Arima et al.[1] concluded that the isobar probably plays only a minor hole in explaining the reduction of magnetic strength in nuclei.

Now we would like to point out that the G-matrix is only a part of the full quasi-particle quasi-hole interaction. It is well known that employing the G-matrix as a residual particle-hole interaction leads to an instability in nuclear matter. Therefore one has to go beyond a simple Brueckner approach. It has been shown by Sjöberg[2] that the inclusion of screening effects in the so-called "crossed channel" reduces strongly the attraction of the G-matrix, e.g. the contributions are strongly repulsive. Therefore one expects also an additional repulsion in the spin-isospin channel. A general feature in many-body systems, and one which we shall show here, is that when an interaction is strongly repulsive (here that in the $\underset{\sim}{\sigma}\cdot\underset{\sim}{\sigma}'\underset{\sim}{\tau}\cdot\underset{\sim}{\tau}'$ channel), then the exchange term in the particle-hole interaction is strongly screened, whereas the direct term is unaffected.

The full ph-interaction can be written as[3]:

$$F^{ph} = K^{ph} + F_{induced}(F^{ph}) \qquad (1)$$

The so-called direct interaction K^{ph} may be approximated by an antisymmetrized G-matrix. The induced interaction $F_{induced}(F^{ph})$ sums all ph-bubbles in the crossed channel and thus makes the equation nonlinear.

The major effect of eq. (1) can be studied in the Landau limit, where the ph-interaction has the form

$$F^{ph} = C_0(f_0+f_0'\underset{\sim}{\tau}\cdot\underset{\sim}{\tau}'+g_0\underset{\sim}{\sigma}\cdot\underset{\sim}{\sigma}'+g_0'\underset{\sim}{\sigma}\cdot\underset{\sim}{\sigma}'\underset{\sim}{\tau}\cdot\underset{\sim}{\tau}') \qquad (2)$$

with the constant $C_0 = \frac{\hbar^2\pi^2}{mk_F} = 302$ MeV fm^3. In the isobar sector one has

$$(F^{ph})_{\Delta N} = C_0(g_0')_{\Delta N}\underset{\sim}{S}\cdot\underset{\sim}{\sigma}'\underset{\sim}{T}\cdot\underset{\sim}{\tau}' \qquad (3)$$

	f_0	f_0'	g_0	g_0'	$(g_0')_{\Delta N}$
G	-1.14	0.30	0.20	0.63	0.91
$F^{ph}(N+\Delta)$	-0.26	0.04	-0.06	0.75	1.45

Table 1: Landau parameters (in units of C_0 = 302 MeV fm^3) in both nucleon (f_0, f_0', g_0, g_0') and isobar $(g_0')_{\Delta N}$ sector based on HEA potential. The experimental value $(f^*/f) = 2$ was used. The row G denotes the G-matrix results, while $F^{ph}(N+\Delta)$ includes a selfconsistent coupling between isobars and nucleons.

The results of the generalized version[4] of eq. (1), which couples isobars and nucleons, are displayed in Table 1. The major effect of the induced interaction in the nucleon sector is to stabilize the parameter f_0, since all induced contributions (renormalizations coming from the other channels due to the exchange term) add coherently to compensate the attractive G-matrix contribution. In all other channels, however, the induced pieces cancel to a large extent. It introduces e.g. in the spin-isospin strength g_0' a correction of about 20 %. In the isobar sector, however, the situation is different for two reasons:

i) The isobar has to be excited via the spin-isospin channel. Therefore the cancellation of the induced pieces, which occur in the nucleon sector, does no longer exist.

ii) Since the induced interaction contributes only to the exchange term, the factor 1/4 (due to the exchange term), which reduces the induced pieces in the nucleon sector, does not occur, since $\underset{\sim}{S}\cdot\sigma' P_\sigma = \underset{\sim}{S}\cdot\sigma'$. Therefore the induced interaction causes a dramatic enhancement (~60 %) of the isobar-hole coupling strength $(g_0')_{\Delta N}$ by screening out the exchange term in the interaction.

References:

1) A. Arima et al., Phys. Lett. 122B (1983) 126.
2) O. Sjöberg, Ann. Phys. 78 (1973) 39.
3) S. Babu, G.E. Brown, Ann. Phys. 78 (1973) 1.
4) K. Nakayama, S. Krewald, J. Speth, to be published.

+ SUNY at Stony Brook, Stony Brook, NY, USA

4.3. A Deformable Chiral Bag

J. Wambach and Z.Y. Ma+

In connection with the difficulties of the nonrelativistic quark model to obtain the nucleon axial vector coupling constant g_A Glashow has speculated[1] upon intrinsic deformation of the nucleon ground state. Subsequently, it has been noted[2] that the Chiral Bag Model (CBM) of hadrons provides a mechanism for such deformations. The pseudo-scalar coupling between quarks and pions at the bag boundary adds a pressure term to the MIT bag model which is inhomogeneous across the surface. Motivated by these ideas we have developed a method to systematically study the question of hadron deformations in the CBM-framework.

The dynamics for arbitrary bag shapes is specified by the following Lagrange density (gluon fields are neglected)

$$\mathcal{L}(x) = \mathcal{L}_q(x) + \mathcal{L}_\pi(x) + \mathcal{L}_I(x) \quad (1a)$$

$$\mathcal{L}_q(x) = [\, 1/2\, \psi\partial\psi - B]\theta(R-r) - 1/2\, \bar{\psi}\psi n^\mu n_\mu\, \delta(r-R) \quad (1b)$$

$$\mathcal{L}_\pi(x) = 1/2\, (\partial\mu\vec{\pi})^2\theta(r-R) \quad (1c)$$

$$\mathcal{L}_I(x) = -i/(2f_\pi)\bar{\psi}\gamma_5\vec{\tau}\vec{\pi}\psi\ \delta(r-R)$$

where $\mathcal{L}_q$ and $\mathcal{L}_\pi$ correspond to the free field quark and pion Lagrangians and $\mathcal{L}_I$ to the coupling term. The pion field has been linearized. Requiring the action

$$S = \int d^4x\, \mathcal{L}(x) \quad (2)$$

to be stationary ($\delta S=0$) with respect to arbitrary variations of the fields and the boundary leads to the equations of motion

$$\not{\partial}\,\psi = 0 \qquad r<R(\vartheta,\varphi) \quad (3a)$$

$$\partial^2\vec{\pi} = 0 \qquad r>R(\vartheta,\varphi) \quad (3b)$$

and to the boundary conditions

$$\underset{\sim}{n}\underset{\sim}{\gamma}\psi = (1+i\gamma_5\vec{\tau}\vec{\pi}/f_\pi)\psi \qquad r=R(\vartheta,\varphi) \quad (3c)$$

$$\underset{\sim}{n}\underset{\sim}{\nabla}\vec{\pi} = i\bar{\psi}\gamma_5\vec{\tau}/(2f_\pi)\psi \qquad r=R(\vartheta,\varphi) \quad (3d)$$

Here time independence of the bag shapes has been implied. Note that the surface normal is angular dependent. To arrive at dynamical deformations we use the propagator methods of Chin[3] which starts with the free field solutions for which quarks and pions decouple (i.e. $f_\pi\to\infty$). The free fields obey the boundary conditions

$$\underset{\sim}{n}\underset{\sim}{\gamma}\psi = \psi \quad (4a)$$

$$\underset{\sim}{n}\underset{\sim}{\nabla}\pi = 0 \quad (4b)$$

The solutions to (4a) and (4b) are used in a perturbative expansion of the full propagators. We are interested in the minima of the energy surface with respect to the deformation parameters and therefore have to compute corrections to the unperturbed ground state energy E_0 which always has a spherical minimum. To second order in $\mathcal{L}_I$ one has

$$\Delta E_0^{(2)} = 1/(8f_\pi^2)\int_{-\infty}^{\infty} dt\ d\underset{\sim}{r}_1 d\underset{\sim}{r}_2\ \Delta(\underset{\sim}{r}_1,\underset{\sim}{r}_2,t)$$
$$\langle\phi_0|\bar{\psi}(x_1)i\gamma_5\vec{\tau}\psi(x_1)\bar{\psi}(x_2)i\gamma_5\vec{\tau}\psi(x_2)\delta(r_1-R)\delta(r_2-R)|\phi_0\rangle \quad (5)$$

which is deformation dependent due to the γ_5-coupling. Δ denotes the pion propagator which can be expanded in terms of the stationary solutions of (4b) as

$$\Delta(\underset{\sim}{r},\underset{\sim}{r}',\omega) = \int_{-\infty}^{\infty} dt e^{i\omega t}\Delta(\underset{\sim}{r},\underset{\sim}{r}',t) = \int \frac{d\vec{k}\,\phi^*_{\vec{k}}(\underset{\sim}{r})\phi_{\vec{k}}(\underset{\sim}{r}')}{\omega^2-k^2+i\eta} \quad (6)$$

The solutions of the Dirac- and Klein-Gordon-equations (3a) and (3b) subject to the boundary conditions (4a) and (4b) are very difficult to obtain in general. For ellipsoidal cavities (characterized by two shape parameters R and D), however, they can be expanded in the analytically known MIT quark field solutions and the hard sphere wave functions for the pion field with the expansion coefficients easily obtained from matrix diagonalization. The deformation dependence of the lowest quark eigenenergies and mixing coefficients are displayed in Fig. 1. With the aid of the free solutions we can project onto the two component Pauli space to obtain

$$\Delta E_0^{(2)}(R,D) = \langle\,\square\square\square\,|\ \sum_{ij} V_{ij}(\omega)\,|\,\square\square\square\,\rangle \quad (7)$$

Here $|\square\square\square\rangle$ denotes symmetric combinations of Pauli spinors in ordinary and isospin space and V_{ij} is a frequency dependent two body interaction

$$V_{ij}(\omega) = 1/(2f_\pi^2R^3)\sum_{L,L',M}\tilde{\Delta}_{L,L',M}(D,\omega)$$
$$\underset{\sim}{\sigma}_i\hat{r}_i\underset{\sim}{\sigma}_j\hat{r}_j Y^*_{LM}(\Omega_i)Y_{L'M}(\Omega_j)\vec{t}_i\vec{t}_j \quad (8)$$

which is also deformation dependent. The calculated deformation dependence of $\Delta E_0^{(2)}$ for the nucleon (depicted in Fig. 2) indicates that indeed the ground state is intrinsically deformed.

References

1) S.L. Glashow, Physika 96A (1979) 27.
2) V. Vento, G. Baym, A.D. Jackson, Phys. Lett. 102B (1981) 97.
3) S.A. Chin, Nucl. Phys. A382 (1982) 355.

+ Institute of Atomic Energy, Beijing, China

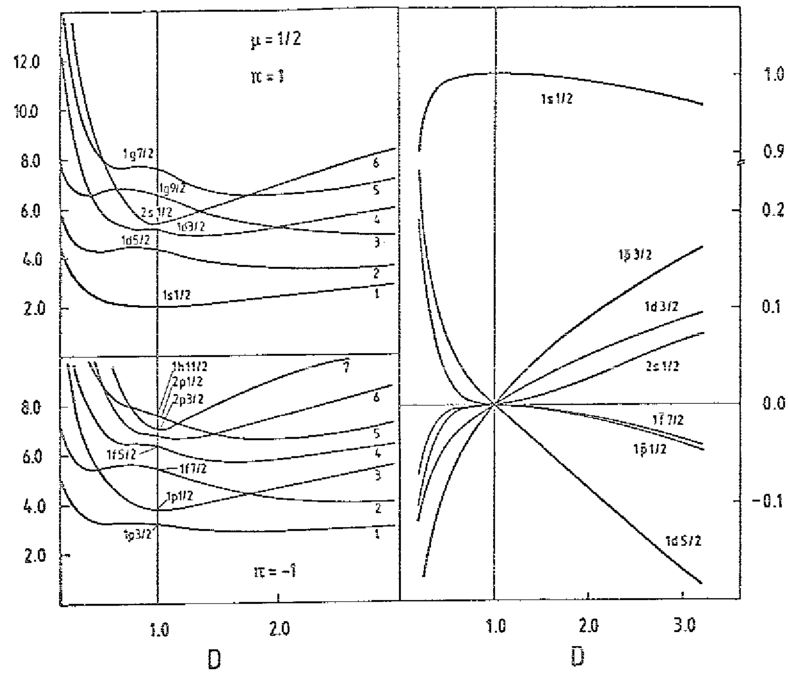

Fig. 1: Positive energy quark levels for $\mu = 1/2$ and $\pi = \pm 1$ (left part) and mixing amplitudes of spherical states in the lowest deformed state as a function of the deformation parameter D (the bar denotes negative energy spherical states).

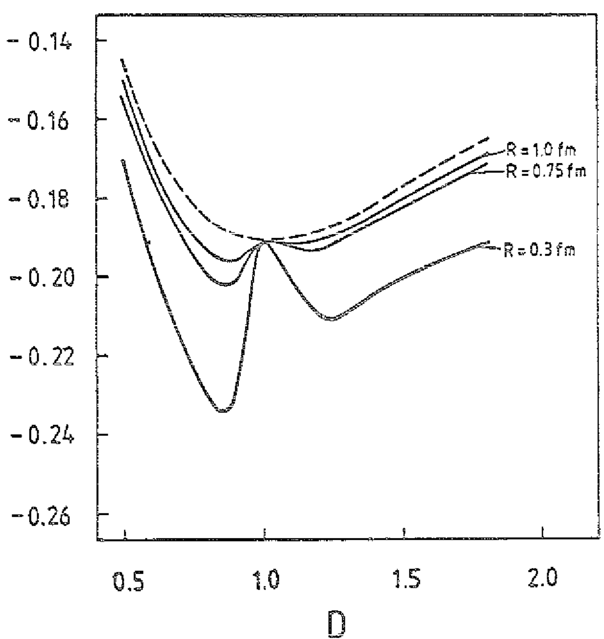

Fig. 2: ΔE_0 for the nucleon (in units $1/(f_\pi^2 R^3)$ as a function of D after configuration mixing. The dashed curve represents the result with all quarks in the lowest orbit.

4.4. Quantum Variational Approach to the Chiral Bag

J.N. Urbano+, K. Goeke

A quantum variational approach[1] to the chiral bag is formulated, in which the pion field is described by a quantum mechanical coherent state

$$|\pi(\xi)\rangle = \frac{1}{N}\exp\left(\sum_j \int d^3k\ \xi_j(\underline{k})a_j^+(\underline{k})\right)|0\rangle$$

The wave function of the bag of the nucleon is obtained by eliminating the quark degrees of freedom in favour of the colourless baryonic states assumed as a mixture of a proton and delta with z-components equal 1/2

$$|BN(\alpha)\rangle = \cos\alpha|N^+_{1/2}\rangle + \sin\alpha|\Delta^+_{1/2}\rangle$$

The total Hamiltonian of the system is given by

$$H = H_{MIT} + H_\pi + H_{coupl}$$

where the H_{coupl} is taken from the linearized version of the cloudy bag model[2]. The stability of the nucleon is achieved by taking into account the finite extension of the $q\bar{q}$-component of the pions in the cloud. This leads to an effective coupling constant depending on the radius n_π = 0.17 fm of the pion and on the radius R of the bag:

$$g_{\pi NN} \to g_{eff}(R) = g_{\pi NN}\left[1+1.2\left(\frac{n_\pi}{R}\right)^2\right]^{-3/2}$$

The variation of the total energy

$$E(\xi,\alpha) = \langle BN(\alpha)|\langle\pi(\xi)|H|\pi(\xi)\rangle|BN(\alpha)\rangle$$

with respect to the pion field amplitude yields for the variational solution

$$\bar{\xi}_j(\underline{k}) = i\,\frac{\rho(k)}{\sqrt{2(2\pi\omega(k))^3}}\, g_{eff}(R)\, G(\alpha)\, k_z\, \delta_{jz}$$

where $\rho(k)$ is the pion source and $G(\alpha)$ is given by

$$G^2(\alpha) = \cos^2\alpha + \frac{8}{5}\sqrt{2}\sin\alpha\cos\alpha + \frac{1}{5}\sin^2\alpha$$

The states $|BN(\alpha),\pi(\xi)\rangle$ do not possess the proper spin and isospin quantum numbers. However, they can be projected on them by Peierls-Yoccoz techniques involving rotations around the angles β and $\tilde{\beta}$ in spin and isospin space around the y-axis. This yields for the pion field

$$\pi(\bar{\xi},\beta\hat{\beta}) = \exp\left\{\sum_j \int d^3k\ \bar{\xi}_j(\underline{k},\beta\hat{\beta})a_j^+(\underline{k})\right\}|0\rangle$$

with

$$\bar{\xi}_j(\underline{k},\beta\hat{\beta}) = \sum_{j'}(R_2(\tilde{\beta}))_{jj'}\,\bar{\xi}_{j'}(R_y^{-1}(\beta)\underline{k})$$

The actual calculations show that the average number of pions and the selfenergy, the bag acquires due to its coupling to the pion cloud, are strongly dependent on the mixing angle α and, of course, on the bag radius R. The projection itself increases the number of pions in the cloud up to a factor of four in case of the nucleon quantum numbers. Thus both, a proper intrinsic wave function and quantum effects due to projection, are necessary ingredients for a stable nucleon solution[3] of small radii R 0.5 fm since there the pion field is strongest.

References

1) J.N. Urbano, K. Goeke, to be published.
2) S. Théberge, A.W. Thomas, G.A. Miller, Phys. Rev. C22 (1980) 2838.
3) G.E. Brown, M. Rho, Phys. Lett. 82B (1979) 177.

+ Univ. de Coimbra, Portugal

4.5. Effect of the Quantum Fluctuations of the Pion Field on the Chiral Bag Energy

J.N. Urbano+ and K. Goeke

As is well known, notwithstanding their remarkable success in predicting hadron properties, present day approaches to chiral bag models are still confronted with some difficulties. Indeed, either they use semiclassical methods to deal with the pion field or, if properly quantized, they are based on perturbative expansions, the validity of which relies on the assumption that the bag radius is fairly large ($R \gtrsim 0.8$ fm). In any case, it seems that some fundamental ingredient is missing from the very foundation of the models, since the bag of quarks collapses under the effect of the pion pressure.

Recently, a proposal was made to stabilize the Chiral Bag by taking into account the quark substructure of the pions themselves[1]. As a consequence, the upper limit to the MIT-bag-model parameter B could be raised, and minima for the bag energy could be found for bag radii $R < 0.5$ fm. Unfortunately, this interesting work is not free the above indicated difficulties, a fact that is particularly annoying in a context when one is dealing with very small radii. In this contribution we cover the same ground as the authors of Ref. 1, but we use a fully quantized variational approach.

Our starting point is a field theoretical Hamiltonian describing: quarks confined in an MIT-bag, free pions, and an interaction between quarks and pions. In this investigation we have considered, for the sake of simplicity, the linearized version of the Clowdy Bag Model Hamiltonian[2]. The second ingredient of our approach is a trial wave function consisting of a linear combination of properly chosen three-quark MIT-bag colourless configurations, multiplied by a coherent state of pions. For each set of values of the bag radius and of the linear combination coefficients, the trial wave function is separately projected onto states with definite angular momentum and isospin, using the Peierls-Yoccoz technique[3]. The total energy is then evaluated with the projected states, and is finally minimized with respect to the pion field amplitudes[3] and to the remaining parameters, bag radius included. In this work we have performed the variation with respect to the pion amplitudes before the projection was carried out.

Since we are interested in the lowest baryon state, only nucleon- and delta-bag configurations were considered. In this framework, we find that the best advantage is taken of the interaction's spin-isospin structure with special linear combinations of the nucleon- and delta-bag configurations[4]. With these, one has to perform three-dimensional projections in both spin and isospin states, but in this work we have simplified the calculations considering only bare bag configurations with spin up and charge +1. This provides the trial wave function with axial symmetry in both spaces.

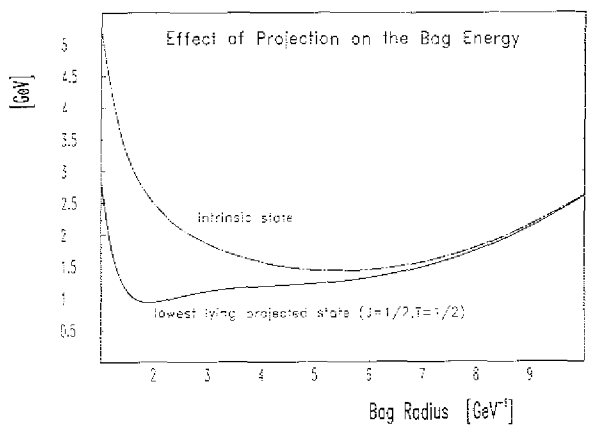

The figure shows the effect of projection on the bag energy for the following set of bag model parameters: $B^{1/4}$ = 148 MeV, Z = 0.244. The bare πNN-, πNΔ- and $\pi\Delta\Delta$-vertex coupling constants were related using the usual quark model predictions. The πNN-vertex coupling constant was then properly renormalized by ensuring that one gets the experimental value at the minimum energy.

We may conclude that it is quite necessary to consider the quantum fluctuation of the pion field when dealing with small bag radii; and that the possibility of having a small bag solution is favoured by the projection.

References

1) J. de Kam, H.J. Pirner, Nucl. Phys. A389 (1982) 640.
2) S. Théberge, G.A. Miller, A.W. Thomas, Can. J. Phys. 60 (1982) 59.
3) J. da Providencia, J. Urbano, Phys. Rev. C18 (1978) 4208.
4) See, e.g., sect. 4-2g, Vol. 2, A. Bohr, B.R. Mottelson, Nuclear Structure (Benjamin, New York). We are thankful to Prof. G.E. Brown to have called our attention to this point.

+ Univ. de Coimbra, Coimbra, Portugal

4.6. On the Hedgehoog Solution

J.N. Urbano+, K. Goeke

In recent years there has been frequently discussed a special ansatz for the intrinsic bare nucleon configuration coupled to a pion field, the so-called "hedgehoog" solution[1]. This is given, in an obvious notation, by

$$|BN\rangle = \frac{1}{\sqrt{2}} \left(|p\downarrow\rangle - |n\uparrow\rangle\right) \qquad (1)$$

Actually such an intrinsic nucleon state is considered to be compatible with a pion field, which in cartesian coordinates can be written as

$$\vec{\phi}(\underline{r}) = \hat{\underline{r}}\, G(r) \qquad (2)$$

i.e. which has a very special space-isospace structure facilitating very much the solution of the field equations.

In a recently formulated quantum variational model[2] of the chiral bag this concept can be checked in a variational way: We assume for the intrinsic solution of the bag a structure of

$$|BN\rangle = \frac{1}{N} \sum_{st} \alpha_{st} |\tfrac{1}{2}\, s\rangle |\tfrac{1}{2}\, t\rangle \qquad (3)$$

and the pion field is described by a coherent state

$$|\pi(\xi)\rangle = \frac{1}{N'} \exp\{ \sum_{s=1}^{s} \int d^3k\; \xi_j(\underline{k}) a_j^+(\underline{k})\} |0\rangle \qquad (4)$$

the total Hamiltonian of the system is assumed to be the one of the linearized clowdy bag model of Théberge et al.[3] with a coupling part of the form

$$H_{coupl} = i \int d^3k\; f(\underline{k}) \sum_j \{\hat{X}_j(\underline{k}) a_j(\underline{k}) - \hat{X}_k^+(\underline{k}) a_j^+(\underline{k})\} \qquad (5)$$

with

$$\hat{X}_j(\underline{k}) = g_{\pi NN} \sum_{st} (\underline{\sigma}\cdot\underline{k})_{ss'} (\tau_j)_{tt'} \hat{v}_{st}^+ \hat{v}_{s't'} \qquad (6)$$

where $\hat{v}_{st}^+$ creates a nucleon in spin state $|\tfrac{1}{2}\, s\rangle$ and isospin state $|\tfrac{1}{2}\, t\rangle$. The variation of the total energy of the system with respect to $\xi_j(\underline{k})$ and to α_{st} yields the following qualitative result: There is a continuous set of degenerate solutions which minimize the energy. The hedgehoog (1) is one of them. The selfenergy of these minimal solutions is 3 times larger than for a pure nucleon configuration (e.g. with $s = \tfrac{1}{2}$ and $t = \tfrac{1}{2}$), a result which corresponds to the findings of Bohr and Mottelson[4]. The field corresponding to the hedgehoog solution can be evaluated by

$$\phi_j(\underline{r}) = \langle \pi(\xi,\alpha) | \sum_j \int d^3k\; \omega(k) a_j^+(\underline{k}) a_j(\underline{k}) | \pi(\xi,\alpha)\rangle \qquad (7)$$

and it has indeed the structure given by eq. (2). The other solutions, being degenerate with the hedgehoog, show fields whose space-isospace structure is more complicated. They are presently under investigation.

References

1) V. Vento, M. Rho, E.M. Nyman, J.H. Jun, G.E. Brown, Nucl. Phys. A345 (1980) 413.
2) J.N. Urbano, K. Goeke, to be published.
3) S. Théberge, A.W. Thomas, G.A. Miller, Phys. Rev. D22 (1980) 2838.
4) A. Bohr, B. Mottelson, Vol. II, p. 20f.

+ Univ. de Coimbra, Portugal

4.7. Equilibrium between Anisotropic Normal and Pion Condensed Nuclear Matter

I. Lovas[+], J. Németh[++], K. Sailer[+++]

We investigated the properties of the pion condensed phase of nuclear matter at finite temperatures in the framework of a relativistic field theory. The solution of the field equations and the expectation value of the energy-momentum tensor were calculated in the mean field approximation. It was observed that the selfconsistent set of equations for the amplitudes of the mesonic fields obtained directly from the field equations are identical with the conditions of thermodynamical equilibrium. The pressure of the pion condensed phase was found to be isotropic in thermodynamical equilibrium. In Fig. 1 the binding energy of the nucleons $\varepsilon(\rho\text{-}m)$ MeV in pion condensed nuclear matter is given as function of the relative density ρ/ρ_0 and temperature. The density of nuclear matter in its ground state is $\rho_0 = 0.145$ fm^3 [1]. The values of the wave number are: k = 2.0 (a), k = 2.5 (b), k = 3.0 (c). The binding energy of the nucleons in normal isotropic nuclear matter is also shown by dashed lines. The equilibrium between anisotropic normal and pion condensed nuclear matter is indicated by asterisks.

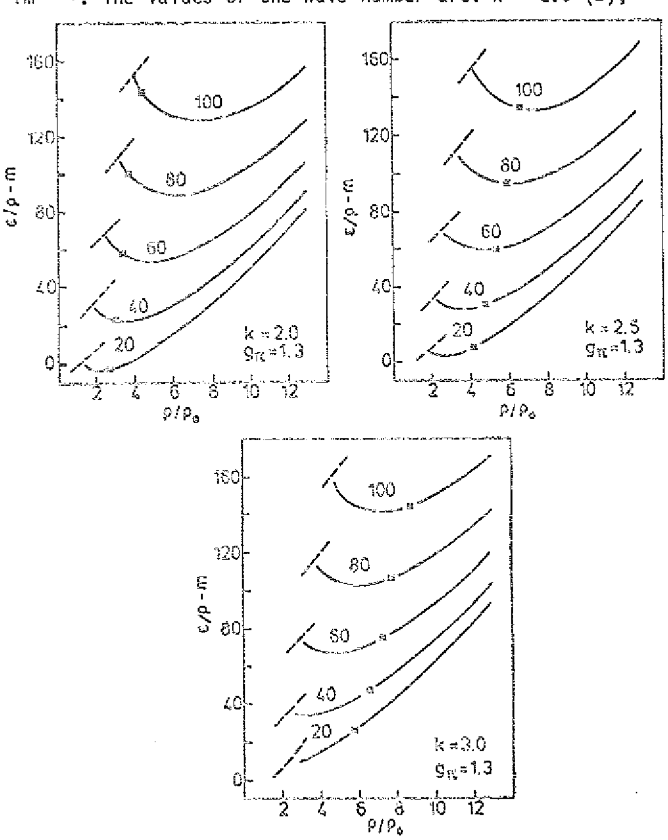

Fig. 1: The binding energy of the nucleons $\varepsilon(\rho\text{-}m)$ MeV as function of the relative density.

We studied the possibility of phase equilibrium between pion condensed and anisotropic normal nuclear matter. The nuclear matter produced in heavy ion collision is anisotropic and it is far away from thermodynamical equilibrium. During the collision process the anisotropy is decreasing and the system is approaching the thermodynamical equilibrium. It was shown that non-equilibrated pion condensed nuclear matter may have the same anisotropy as the normal one and they may be in phase equilibrium during the whole collision process. This circumstance allows us to draw the following conclusion: if there is a chance at all for the phase transition from normal to pion condensed phase then the anisotropy produced inevitabely in heavy ion collision does not prevent this transition.

+ Central Research Institute for Physics, Budapest, Hungary
++ Inst. for Theor. Physics, Eötvös University, Budapest, Hungary
+++ Inst. for Exp. Physics, KLTE Debrecen, Hungary

5. NUCLEAR REACTIONS

5.1. Theoretical Analysis of the Proton Decay of Electroexcited Carbon

G. Co', S. Krewald

The reaction $^{12}C(e,e'p)^{11}B$ was investigated in the giant resonance region within a theoretical model including final state interactions and all four interference terms between the charge and current operators. For details see Ref. 1.

All the positive and negative multipole excitations up to 4^+ and 4^- were included. We checked that in the giant resonance region multipoles higher than 4 were giving a negligible contribution.

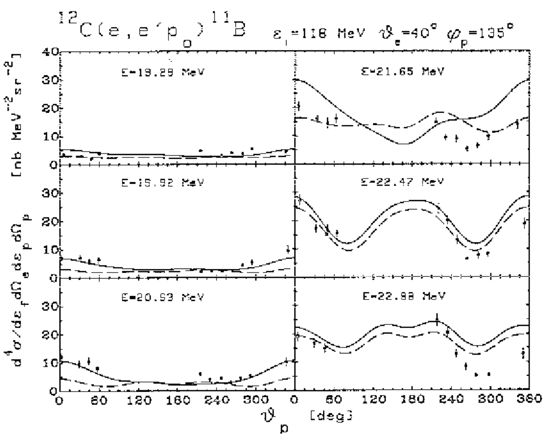

Fig. 1: The experimental double differential cross sections for the reaction $^{12}C(e,e'p)^{11}B$ as measured by Calarco et al.[2] are shown as a function of the angle ϑ_p between the momentum $\vec{p}$ of the emitted proton and the axis defined by the momentum transfer $\vec{q}$. The angle between $\vec{p}$ and the scattering plane is $\varphi_p = 135^o$. The cross sections for $\varphi_p = -45^o$ are represented within the interval between $\vartheta_p = 180^o$ and $\vartheta_p = 360^o$. The symmetry of the cross section around $\vartheta_p = 180^o$ is broken by the charge-current interference. Note that a direct knock-out reaction would have maximal cross section at $\vartheta_p = 180^o$. The solid line shows the theoretical cross section including all multipole modes up to $J^\pi = 4^+$ and 4^-. The dashed line represents the results obtained without monopole strength. The magnituds of all theoretical cross sections are scaled by a factor $\lambda = 0.4$.

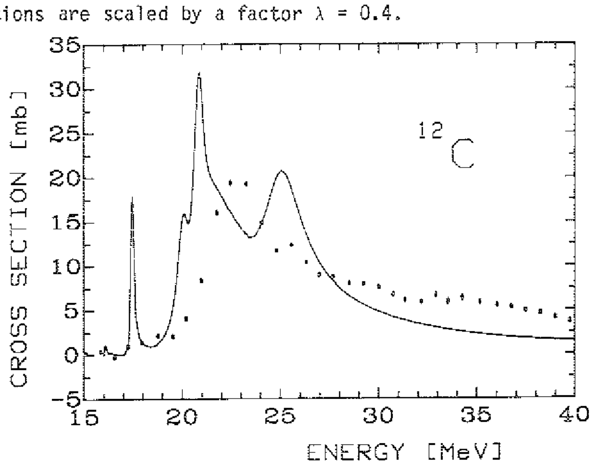

Fig. 2: The photoabsorption cross section of ^{12}C by Ahrens et al.[3] is compared with a continuum random-phase calculation described in the text.

In Fig. 1 the result of our computations (full line) is compared with the experimental points of Calarco et al.[2]. All the theoretical energies are shifted up by 1.5 MeV in order to compensate for the discrepancy between the experimental[3] and theoretical peak of the photonuclear cross section (see Fig. 2).

Since the theoretical angular distributions overshoot the experimental data and we were interested in the shape of the angular distribution of the emitted particle, we determined a scaling factor of λ=0.4 in order to facilitate the comparison between the theoretical and experimental angular distributions at the peak energy of 22.47 MeV of the dipole resonance. At all the other excitation energies the comparison was made using the same scaling factor which is effectively taking into account effects of 2p-2h degrees of freedom and branching to decay modes other than proton or neutron emission, phenomena which are not considered in the present version of our model.

The first result is that our model is able to reproduce the relative magnitudes of the coincidence cross section at all the experimentally investigated excitation energies. The theoretical angular distributions are reproducing rather well the experimental ones, only at the energies of 21.65 MeV and 22.98 MeV the agreement is poor. We explain this with the fact that our model, for the already mentioned lack of 2p-2h configurations, does not give the correct energy width of the dipole which results to be too concentrated around the peak energy of 22.47 MeV.

The strong forward (ϑ_p = 180^o)-backward (ϑ_p = 0^o) asymmetry at the three lower energies is a signature of the presence of positive parity states interfering with the giant dipole. Calarco suggested that in addition to the 2^+ also the 0^+ might be present.

In order to demonstrate the effects of 0^+ strength we repeated the calculation without monopole strength (dashed line).

Without 0^+ a series of bumps in forward and backward direction is found at the three lower energies while only the presence of the 0^+ is able to reproduce the large forward-backward asymmetry.

The large effect of the 0^+ does not imply that the monopole is a concentrated resonance.

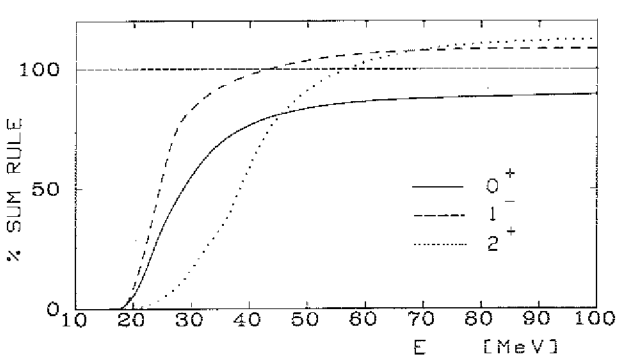

Fig. 3: The exhaustion of the energy-weighted sum rule as a function of the excitation energy for monopole (solid), dipole (dashed) and quadrupole (dotted) strength.

In Fig. 3 the energy weighted sum rule exhaustion for 0^+, 1^-, 2^+ is shown. One can see that the 0^+ needs an energy interval of approximately 20 MeV to exhaust its sum rule while for the dipole only 10 MeV are necessary.

Even though the monopole excitation is not a concentrated resonance the interference terms between monopole and dipole are large enough to be seen in a coincidence experiment.

References

1) G. Co', S. Krewald, J. Speth, Annual Report 1982, Jül-Spez 202 (1983) 71.
2) Calarco et al., Proc. Symp. on Highly Excited States in Nucl. Reactions, ed. by H. Ikegami and M. Muraoka, Osaka (1980) 543, and private communication.
3) J. Ahrens et al., Nucl. Phys. A251 (1975) 479, and private communication.

5.2. Theoretical Description of Electron Scattering Coincidence Experiments

G. Co', S. Krewald

With the advent of the new generation of electron accelerators (high-energy, high duty factor) it will become very common to perform experiments in which the scattered electron is detected in coincidence with a nucleon knocked-out from the target nucleus.

One of the problems concerning this kind of experiments is up to which extent one can control the nuclear reaction mechanism in order to get information about the nuclear excitation modes.

We developed a computer code to evaluate (e,e'p) cross sections based on a microscopic theoretical model we presented in the previous issue of this Annual Report. Input of our code is the solution of the continuum RPA equations we solved in the Fourier-Bessel formalism[1] using as residual interaction the zero range Landau-Migdal force in the parametrization of Rinker and Speth[2]).

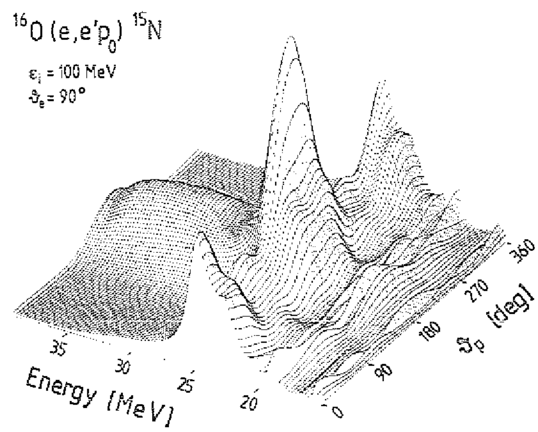

Fig. 1: Angular distribution of the emitted proton against excitation energy of the nucleus for the reaction $^{16}O(e,e'p_0)^{15}N$ obtained keeping fixed the incoming energy of the electron ε_i and the scattering angle ϑ_e. The proton is emitted in the scattering plane and ϑ_p is measured with respect to the axis defined by the momentum transfer direction which is, in our conventions, at $\vartheta_p = 180^0$. In the computation all the excitation multipoles up to 4^+ and 4^- are included.

We studied the reaction $^{16}O(e,e'p_0)^{15}N$ and Fig. 1 shows the angular distribution of the emitted particle versus the nuclear excitation energy: the incoming energy of the electron is fixed at 100 MeV, the scattering angle has the value of 90^0 and the emitted proton, leaving the ^{15}N in its ground state, is detected on the scattering plane.

From the continuum threshold up to 21 MeV the figure shows narrow resonances typical of discrete excited states lying in the continuum, from 21 up to 29 MeV there is the large bump of the giant resonance. Then, after 29 MeV, the angular distribution of the emitted particle is concentrated around the direction of the transferred momentum ($\vartheta_p = 180^0$ in our conventions).

We interpreted the behaviour in the region beyond the giant resonance as quasifree scattering: The virtual photon exchanged between electron and nucleus interacts only with the emitted particle, and there is no collective excitation of the nucleus; in the extreme situation the particle is emitted mainly along the transfer momentum direction. To test this hypothesis we performed a computation switching off the residual interaction.

We chose two different excitation energies: 25 MeV, in the peak of the giant resonance and 40 MeV where the quasifree scattering, in our hypothesis, should take place.

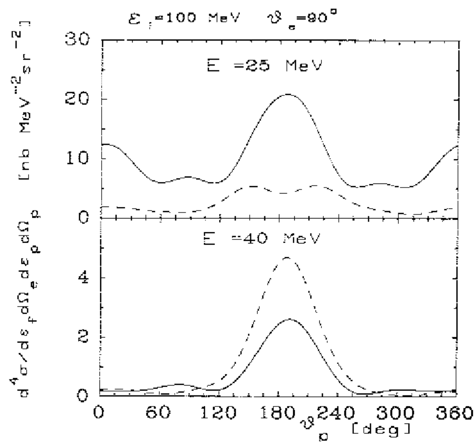

Fig. 2: Angular distribution of the emitted proton for the reaction $^{16}O(e,e'p)^{15}N$ at two different excitation energies. The dashed line shows the result obtained switching off the residual interaction (see text).

In Fig. 2 the results obtained with and without residual interaction are compared.

While at 25 MeV the shape of the two angular distributions is rather different, then the residual interaction plays an important role, i.e. there is a collective excitation of the nucleus, at 40 MeV the shape of the two angular distributions is rather similar, which makes it difficult to distinguish a collective excitation from quasi-free scattering in a model-independent way. Note, however, that the role of the residual interaction in this energy region is by no means negligible, since it modifies the absolute magnitude of the coincidence cross section by a factor of two.

From this analysis it turns out that (e,e'p) is a good tool to investigate the nuclear excitation modes in the giant resonance region (the following report will show a practical application) but for energies above the giant resonance the reaction mechanism really dominates the process and no information about nuclear excitations can be extracted from the angular distribution of the emitted particle.

References

1) R. de Haro, S. Krewald, J. Speth, Nucl. Phys. A388 (1982) 265.
2) G.A. Rinker, J. Speth, Nucl. Phys. A306 (1978) 360.

5.3. Microscopic Calculation of the Imaginary Optical Potential for $^{208}Pb(p,p)$ at 14 MeV

H. Dermawan, F. Osterfeld, V.A. Madsen+

In the nuclear structure approach[1] the calculation of the imaginary optical potential is made in second order in an effective two-nucleon interaction, taking into account finite nuclear effects such as shell structure and collectivity of excited states. In earlier calculations[2,3,4], which used the density independent, finite-range Eikemeier-Hackenbroich t operator[5] as an effective interaction and RPA transition densities[6] to describe the intermediate state of ^{40}Ca, the local equivalents[7] $\tilde{W}(R)$ of the resulting imaginary optical potentials were surface peaked like phenomenological potentials but at a radius too small by about .6 fm.

We report here a similar calculation undertaken for $^{208}Pb(p,p)$, for which the $B(E\lambda)$ values and transition densities have been well tested[8] by comparison with electron scattering[9]. For propagation of the intermediate projectile we used a real folding potential. The exchange part was calculated in a zero-range pseudopotential approximation, the strength of which was determined to agree with exchange scattering amplitudes in an exact calculation[10]. Other aspects of the calculation were the same as has been carried out and reported in our earlier work[2-3] on $^{40}Ca(n,n)$ and $^{40}Ca(p,p)$.

λ^π	W(7.6,7.6) [MeV fm^{-3}]
0^+	-0.0043
1^-	-0.0034
2^+	-0.0436
3^-	-0.082
4^+	-0.0358
5^-	-0.0367
6^+	-0.0108
3^{-*}	-0.0735

Table 1: Contribution of various multipoles to the diagonal nonlocal imaginary potential $W(r,r)$ at the peak radius r = 7.6 fm. * = low-lying 3^- collective state only.

Table 1 shows the contribution of the different multipolarities of natural parity states to the diagonal nonlocal potential at r = 7.6 fm. The low-lying 3^- collective state is a very important contributor to the absorption, but, as is seen in the table, there are several other essential contributions. Although less important and not shown in the table, unnatural parity states were also included in the final determination of the absorptive potential.

In Fig. 1 the equivalent local potential $\tilde{W}(R)$ is compared to the phenomenological potential[11]. The calculated potential is surface peaked and, in contrast to $^{40}Ca(p,p)$ and $^{40}Ca(n,n)^{2-4)}$, the surface peak position r = 7.6 fm is in good agreement with r = 7.8, that of the phenomenolgical potential. The shift in the peak position by about 0.2 fm can easily be accounted for by a density dependent effective projectile-target nucleon interaction[2]. This result shows that good structure

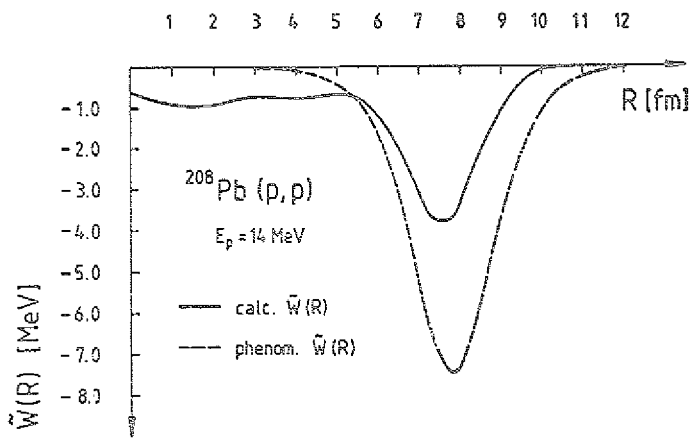

Fig. 1: Comparison of the microscopic local equivalent imaginary potential with the phenomenological potential of Ref.

wave functions are needed for the description of the intermediate excited states in order to obtain the right form of the microscopic absorptive potential. The volume integral per nucleon J_W of the microscopic potential amounts to 33 MeV fm^3 and that of the phenomenological potential to 73 MeV fm^3. A deficiency of a factor of 2 was also found in our former studies of the microscopic imaginary potentials for $^{40}Ca(p,p)$ and $^{40}Ca(n,n)$ scattering[2-4].

Similar calculations of $\tilde{W}(R)$ for $^{208}Pb(p,p)$ have been performed by Bernard and Van Giai[12]. They used the Skyrme interaction to generate the Hartree-Fock mean field, the RPA-excited states and the projectile-target nucleon coupling. In their calculations they included only inelastic natural parity states with spin-parities $J^\pi \leq 5^-$. The resulting imaginary potential of Ref. 12 is also too weak both in the nuclear interior and at the nuclear surface. The volume integral of their calculated potential is about 4 times smaller than the empirical value, which, considering the smaller space of intermediate states used in Ref. 12, is quite consistent with our result.

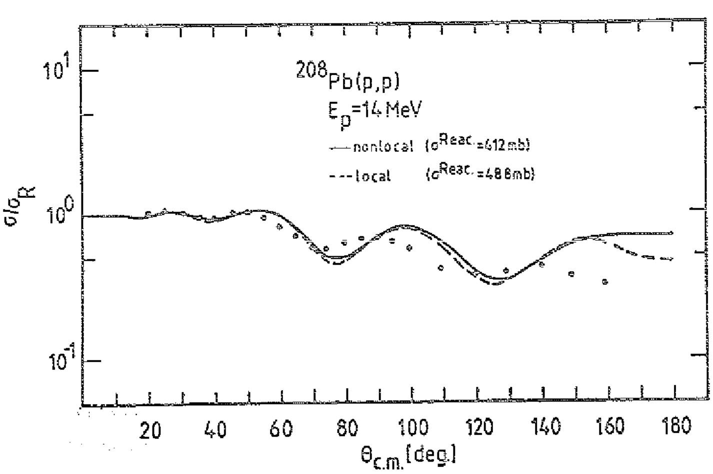

Fig. 2: Comparison of calculated $^{208}Pb(p,p)$ differential cross sections at 14 MeV to the experimental data of Ref. 11. The full line is the exact nonlocal calculation. The dashed line is the calculation with the equivalent local imaginary potential.

To further test our microscopic imaginary optical potential, we used it directly to calculate the differential scattering cross section for 14 MeV $^{208}Pb(p,p)$ scattering using a newly developed[4,13] program for solving the Lippmann-Schwinger equation in momentum space. Angular distributions due to a local real potential plus the calculated nonlocal potential $W(r,r')$ or its local equivalent $\tilde{W}(R)$ are compared to experimental data[11] in Fig. 2. Both calculated angular distributions agree well with the data up to 80°, but at larger angles the calculated cross sections are too high, indicating too little absorption.

References

1) N. Vinh Mau, A. Bouyssy, Nucl. Phys. A257 (1976) 189.
2) F. Osterfeld, J. Wambach, V.A. Madsen, Phys. Rev. C23 (1981) 179.
3) F. Osterfeld, V.A. Madsen, Phys. Rev. C24 (1981) 2468.
4) H. Dermawan, F. Osterfeld, V.A. Madsen, Phys. Rev. C27 (1983) 1474.
5) K.A. Amos, H.V. Geramb, R. Sprickmann, J. Arvieux, M. Buenerd, G. Perrin, Phys. Lett. 52B (1974) 138.
6) S. Krewald, J. Speth, Phys. Lett. 52B (1974) 295.
7) F.G. Perey, D.S. Saxon, Phys. Lett. 10 (1964) 107.
8) J. Speth, A. van der Woude, Rep. Prog. Phys. 44 (1981) 719, and references cited therein.
9) J. Heisenberg, Nucl. Phys. A396 (1983) 171, and references cited therein.
10) J. Atkinson, V.A. Madsen, Phys. Rev. C1 (1970) 1377.
11) J.S. Eck, W.J. Thompson, Nucl. Phys. A237 (1975) 83.
12) V. Bernard, N. Van Giai, Nucl. Phys. A327 (1979) 397.
13) H. Dermawan, Ph.D. Thesis, University of Bonn (1982).

+ Oregon State Univ., Corvallis, OR, USA

5.4. Calculation of the Background below Gamow-Teller Resonances

F. Osterfeld, A. Schulte

Recent (p,n)-experiments at intermediate energies at the Indiana University Cyclotron have shown that the total Gamow-Teller (GT) strength in nuclei is quenched by roughly 40 % with respect to the model independent Ikeda sum rule. The accurate determination of the quenching of the total GT-strength, however, is severely limited by the subtraction of the background below the GT-resonances.

We have calculated[1] this background in a microscopic particle-hole doorway model assuming that the background is a superposition of all cross sections of inelastic excitations to bound, quasibound and continuum states.

The particle-hole doorway model includes the nuclear continuum exactly but treats nuclear collectivity explicitly only for certain selected states like the GTR or IAS. We argue that for our purpose such a limited inclusion of nuclear collectivity is sufficient. Our argument is based on the fact that for $\Delta S=1$-, $\Delta T=1$ transitions collectivity plays only a role for low multipolarities, i.e. for 0^-, 1^+, 1^- ($\Delta S=1$) and, maybe, 2^- states[2]. This is simply an effect of the finite range residual particle-hole (ph)-interaction in the $\Delta S=1$-, $\Delta T=1$-channel[2] which is strongly repulsive for low spin states and weak for high spin states ($J^\pi \geq 2^-$). Therefore states with large J^π are nearly unaffected by the residual ph-interaction.

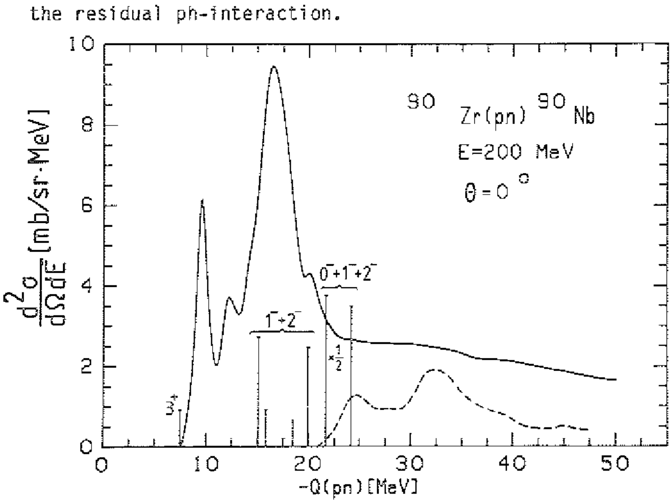

Fig. 1: Zero degree spectrum for the reaction $^{90}Zr(p,n)$. The data (thick full line) are taken from Ref. 3. The discrete lines are calculated cross sections due to bound and quasibound states. The theoretical cross sections due to GTR and IAS are not plotted. The optical parameters for the cross section calculations have been taken from Ref. 6.

In Fig. 1 we show the 0^o-spectrum of the reaction $^{90}Zr(p,n)$. The experimental data (full curve) have been taken from Ref. 3. The dashed curve represents the calculated continuous background. As in the case for $^{48}Ca(p,n)$ we sum all cross sections with multipolarities $\Delta L=0$ through $\Delta L=3$ ($J^\pi = 0^-,1^-,1^+,2^-,2^+,3^-,3^+,4^-$) and include therefore at least all $3\hbar\omega$-1p1h-excitations in the calculations. The calculated spectrum shows resonance type structures around Q-values Q = -25 and Q = -31 MeV. Both bumps are essentially due to ($\Delta L=2$) $J^\pi = 1^+,2^+,3^+$ excitations and form the building "blocks" for the $\Delta L=2$ resonance. It should be mentioned that the bumps would be appreciably smeared out if we would also include a spreading width in the calculations.

There is one important difference between the results for the continuous spectra in $^{48}Ca(p,n)$ and the present one for $^{90}Zr(p,n)$. While the background calculations reproduce the experimental data at high negative Q-values for $^{48}Ca(p,n)$ they fail to do so for $^{90}Zr(p,n)$ and underestimate here the data by a factor of about 2. The "missing" cross section in the calculated spectrum around Q = -28 MeV is not really missing since most of the cross section due to 0^-, 1^-, and 2^- states which appear in our model at lower excitation energies (the discrete lines in Fig. 1) would be shifted to this energy region if we would include nuclear collectivity in our calculations.

The sum of 0^-, 1^-, and 2^- cross sections in Fig. 1 amounts roughly to ~14 mb, from which 6.6 mb are due to 0^-, 1.4 mb due to 1^-, and ~6 mb due to 2^- transitions (see Table 1). Using the results of Bertsch et al.[4] for the strength distribution of 0^-, 1^-, 2^- in ^{90}Zr we find a maximum of about 7.4 mb $\Delta L=1$ cross section directly below the GT-resonance. This means that also in $^{90}Zr(p,n)$ we have practically no background below the GT-resonance, i.e., all the cross section in the Q-value range $-12 \geq Q \geq -20$ is GT-strength. A real problem, however, is that the calculated continuous spectrum underestimates the experimental data in the Q-value range $-32 \geq Q \geq -50$. One could argue that this "missing" cross section might be produced by $\Delta L=4$ excitations not included in our calculations. We have checked this point and have found that these states make a negligible contribution to the cross section at forward angles. Furthermore, if the missing cross section would be due to $\Delta L=4$ transitions the discrepancy between experimental and calculated cross section should increase with angle since cross sections of $\Delta L=4$ shape give the biggest contribution at larger scattering angles. This behaviour, however, is not seen in the spectra. There is actually just the opposite tendency in that the different between measured and calculated cross section becomes smaller with increasing scattering angle. We therefore conclude that this "missing" cross section at large Q-values and forward angles can only be produced by another mechanism. An explanation consistent with the suggestions of Bertsch and Hamamoto[5] is that this cross section not described by the background calculations is actually GT-strength which was shifted to this high excitation energy region due to the mixing of the "low-lying" 1p-1h GT-state with high-lying 2p-2h configurations. Corresponding to our calculations the amount of GT-strength located in the energy range $-20 < Q < -50$ could be as large as 25 mb. One might ask why the 2p-2h polarization effect seems to be more important for ^{90}Zr than for ^{48}Ca. This

θ	$\sum_i \sigma^i (0^-)$ [mb]	$\sum_i \sigma^i (1^-)$ [mb]	$\sum_i \sigma^i (2^-)$ [mb]	$\sum_i \sigma^i (0^-,1^-,2^-)$ [mb/sr]	$\sigma_{exp}-\sigma_{calc}$ [mb/sr] -20>Q(p,n)≥-50 MeV
0^o	8.8	1.4	6	16.2	40
4.5^o	12	23	28	63	52
9.5^o	10	17	21	48	38
12.8^o	2.7	6.3	12	21	20

Table 1: Sum of cross sections of all 1ħω ΔL=1 transitions with spin-parities $J^\pi = 0^-, 1^-$, and 2^- obtained for different scattering angles θ. Column 4 shows the sum of 0^-, 1^-, and 2^- cross sections while column 5 shows the cross section obtained by subtracting the calculated continuous cross section from the experimental one in the Q-value range -20>Q≥50 MeV.

is probably due to a simple shell structure effect. The damping mechanism of the GT-state due to 2p-2h states is much more efficient in heavy than in light nuclei due to the larger density of 2p-2h states in heavy nuclei.

References

1) F. Osterfeld, Phys. Rev. C26 (1982) 762.
2) J. Speth, V. Klemt, J. Wambach, G.E. Brown, Nucl. Phys. A343 (1980) 282.
3) C. Gaarde, J. Rapaport, T.N. Taddeucci, G.D. Goodman, C.C. Forster, D.E. Bainum, C.A. Goulding, M.B. Greenfield, D.J. Horen, E. Sugarbaker, Nucl. Phys. A369 (1981) 258.
4) G. Bertsch, D. Cha, H. Toki, Phys. Rev. C24 (1981) 533.
5) G. Bertsch, I. Hamamoto, Phys. Rev. C26 (1982) 167.
6) A. Nadasen et al., Phys. Rev. C23 (1981) 1023.

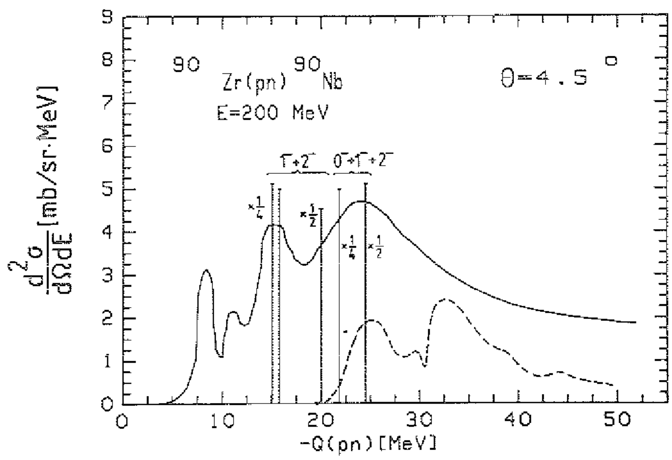

Fig. 1: Same as Fig. 1 in previous contribution but for $\theta_{CM} = 4.5^o$.

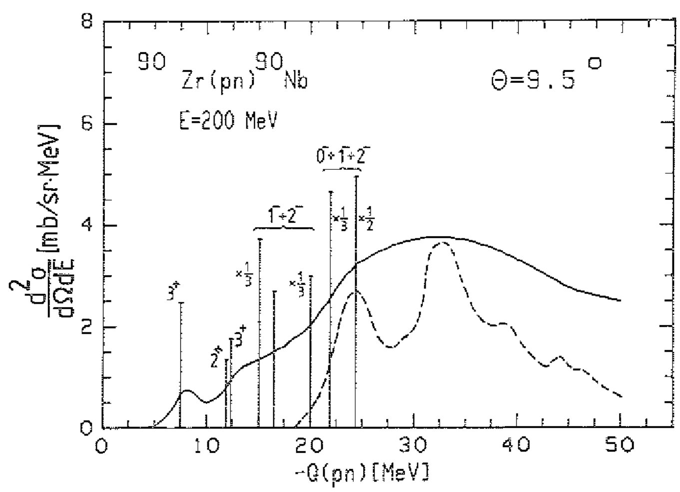

Fig. 2: Same as Fig. 1 in previous contribution but for $\theta_{CM} = 9.5^o$.

5.5. Calculation of the Background below the Giant Dipole (ΔL=1)-Resonance

F. Osterfeld, A. Schulte

Within the microscopic particle hole doorway model[1] we have calculated the ^{90}Zr(p,n)-spectra for angles of 4.5^o and 9.5^o, respectively. They are shown in Figs. 1 and 2. The data (full line) have been taken from Ref. 2 and the dotted lines represent the calculated continuous spectrum. The peaks at Q-values of Q = -24 and Q = -32 MeV are again due to the (ΔL=2) $J^\pi = 1^+,2^+,3^+$ resonance. As is seen from the figures the (ΔL=1) $J^\pi = 0^-,1^-,2^-$ resonance gives a large contribution to the cross section (discrete lines in the figures). The summed cross section of all 1ħω 0^-, 1^-, and 2^- excitations amounts to 63 mb at the scattering angle of 4.5^o and to 48 mb at 9.5^o (see also Table 1 in the previous contribution). Most of the ΔL=1 strength will be shifted into the energy region around Q = -26 MeV when the residual ph-interaction is switched on. As one can see from Figs. 1 and 2 we have now, however, a big problem since we have much more (ΔL=1) cross section to distribute than the experimental data permit. This is especially striking for the 9.5^o spectrum. If we subtract in the Q-value range from 20 to 50 MeV the calculated continuous cross section from the experimental one we obtain roughly ~31 mb. The calculated ΔL=1 cross section, on the other hand, amounts to 48 mb which is by a factor of ~1.5 larger than the estimated cross section above. This happens although we have implicitly assumed already that the ΔL=1 strength is distributed over the whole Q-value range from -20 to -50 MeV. The latter amounts to the assumption that high-lying 2p-2h configurations[3] couple to the ΔL=1 resonance in a similar way as to the GT-resonance and spread out the ΔL=1 strength over a wide energy range. In spite of this assumption we still need a quenching of about 50 % in order to reconcile the theoretical and experimental cross sections. Part of this quenching is certainly due to ground state correlations not included in our calculations. Ground state correlations will reduce both the ΔL=1 cross section and also the calculated continuous cross section being therefore an effective agent to diminish the surplus cross section mentioned above. If we assume a reduction of ~25 % for both the background and the ΔL=1 cross sections then the experimental and calculated cross sections would just agree. It may, however, also well be that this is an overestimate and that an additional quenching due to admixtures of Δ(1232) isobar-nucleon hole configurations into the ΔL=1 resonance is needed to describe the data as has been repeatedly pointed out in the analysis of 2^- states measured in inelastic electron scattering experiments[4].

References

1) F. Osterfeld, Phys. Rev. C26 (1982) 762.
2) C. Gaarde, J. Rapaport, T.N. Taddeucci, G.D. Goodman, C.C. Forster, D.E. Bainum, C.A. Goulding, M.B. Greenfield, D.J. Horen, E. Sugarbaker, Nucl. Phys. A369 (1981) 258.
3) G. Bertsch, D. Cha, H. Toki, Phys. Rev. C24 (1981) 533.
4) N. Anantaraman et al., Phys. Rev. Lett. 46 (1981) 1318;
C.M. Crawley et al., Phys. Rev. C26 (1982) 87;
C. Djalali et al., Nucl. Phys. A388 (1982) 1.

5.6. The Tensor Force in (^{3}He,t)-Scattering with Exact Treatment of Knockout Exchange

T. Udagawa+, F. Osterfeld

The (^{3}He,t)-reaction at intermediate energies seems to be a very promising tool to study στ-excitations in nuclei[1]. It shows the same selectivity in exciting the low-lying nuclear excitation spectrum as the (p,n)-reaction at similar energies. Moreover, high energy (^{3}He,t)-scattering at 2 GeV incident energy very strongly excites the Δ-resonance in nuclei[1]. For the analysis of these data it is very important to have a computer program which can handle a large number of partial waves and which can treat knockout exchange processes exactly. Knockout exchange describes the process where the incoming projectile nucleon hits a target nucleon which is ejected from the nucleus while the originally incoming nucleon gets stuck in the nucleus. Because of numerical complications this process has never been calculated exactly for composite particle scattering. We have developed a method and a program which permit to calculate knockout exchange amplitudes also for composite particle scattering exactly[2]. Until recently only central forces could be handled, but now we have extended the program so that we can treat also tensor forces. Tensor forces are very important for the study of στ- and Δ-excitations in nuclei. First results show that the tensor force is dominant in exciting the Δ. This is an effect of the large momentum transfer involved in exciting states of high excitation energy of $E_x \sim 300$ MeV.

References

1) C. Ellegaard et al, Phys. Rev. Lett. 50 (1983) 1745.
2) T. Udagawa, F. Osterfeld, KFA Annual Report 1982, Jül-Spez 202 (1982) 82.

+ Univ. of Texas, Austin, Texas, USA

5.7. Calculation of Proton-Neutron Coincidence Cross Sections in 56 MeV Deuteron-Induced Breakup Reactions by Post Form Distorted-Wave Born Approximation

G. Baur, F. Rösel+, R. Shyam++, and D. Trautmann+

Recently measured neutron-proton angular correlations in the deuteron-induced breakup reactions at 56 MeV incident energy have been analyzed[1] in terms of the post form distorted-wave Born approximation theory of breakup reactions[2]. Comparison of the present results is made with those of the prior form distorted-wave Born approximation calculations[3]. It is found that the results of the post form distorted-wave Born approximation calculations are in better agreement with the experimental data than the prior form distorted-wave Born approximation results.

References

1) G. Baur, R. Shyam, F. Rösel, D. Trautmann, Phys. Rev. C28 (1983) 946.
2) G. Baur, F. Rösel, D. Trautmann, R. Shyam, Phys. Rep. to be published;
G. Baur, R. Shyam, F. Rösel, D. Trautmann, Helv. Phys. Acta 53 (1980) 506.
3) N. Matsuoka, K. Hatuanaka, T. Saito, T. Itahashi, K. Hosono, A. Shimizu, M. Kondo, F. Ohtani, O. Cynshi, Nucl. Phys. A391 (1982) 357.

+ Inst. f. Theor. Phys., Univ. Basel
++ GSI Darmstadt

5.8. Coulomb Dissociation at Nonrelativistic and Relativistic Energies[1]

B. Hoffmann and G. Baur

We discuss various characteristics of Coulomb dissociation at low and high bombarding energies by means of model calculations. The sub-Coulomb breakup of the deuteron is generally quite well understood in the DWBA framework[2], however, for very low energies of the emerging protons, the experimental data of the Bonn group[3] cannot be reproduced by our theoretical models. The experimentally observed deviation of (d,p) breakup yields for intermediate (E_d = 56 MeV) energy deuterons from the $A^{1/3}$ dependence is tentatively explained in terms of the Coulomb dissociation mechanism. In view of the current experiments at the BEVALAC[4] and forthcoming accelerators with relativistic projectiles, we illustrate by means of typical examples the various effets arising in relativistic electromagnetic excitation[5].

References

1) B. Hoffmann, G. Baur, to be published.
2) J. Kleinfeller, J. Bisplinghoff, J. Ernst, T. Mayer-Kuckuk, G. Baur, B. Hoffmann, R. Shyam, F. Rösel, D. Trautmann, Nucl. Phys. A370 (1981) 205.
3) B. Seligmann, J. Ernst, H. Gemmeke, K. Keller, J. Kleinfeller, L. Lassen, W. Lücking, R. Schreck, Annual Report 1981-2 Institut für Strahlen- und Kernphysik der Universität Bonn, p. 25.
4) J. Hill, private communication.
5) A. Winther, K. Alder, Nucl. Phys. A319 (1979) 518

5.9. On the Dynamics of the $^{16}O+^{16}O \rightarrow ^{32}S$ Fusion Process

J. Friedrich[+], K. Goeke, D.H.E. Gross[++],
F. Grümmer and P.-G. Reinhard[+++]

For a reproduction of fusion data by means of microscopic theories there are two important properties of the interaction which have to be well described. First the binding energies of the fragments and of the compound system must be correct, and second the surface thickness must be accurate. Both properties, to be tested in static calculations, determine the position and the height of the barrier and the depth of the collective potential. The presently often used Bonche-Koonin-Negele interaction (BKN) does not fulfil these re-

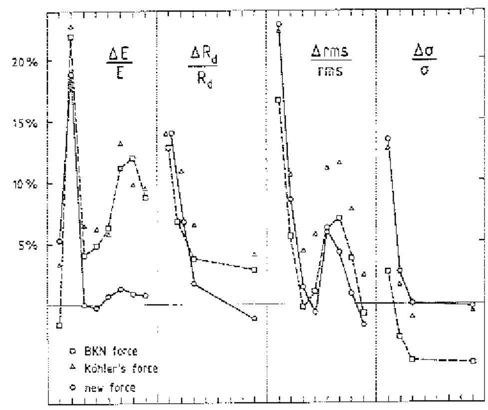

Figure 1

quirements well. This can be seen at Fig. 1 where the relative deviations of the HF-results from the experimental data are given. One notices the improvement of the so-called "new force". This one has the general structure of the BKN force, however, the power α of the density dependent term is not fixed to $\alpha = 1.0$. The parameters of the force, including α, have been fitted[2] by reproducing the binding energies and the electron scattering form factors of $^{16}O+^{16}O$-system. The mass parameter and the heavy ion interaction potential calculated by quantized ATDHF[3] are given in Fig. 2. One realizes a lower saddle at larger separation distances and a deeper bound state. This has a drastic effect on the fusion cross section as one can see at Fig. 3. The subbarrier fusion cross section, expressed by the astrophysical S-factor is in very much better agreement with experiment that before, where the BKN force was used. By means of

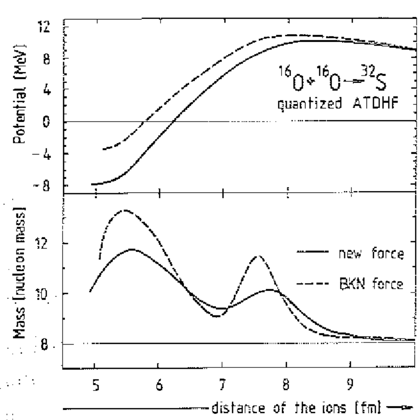

Figure 2

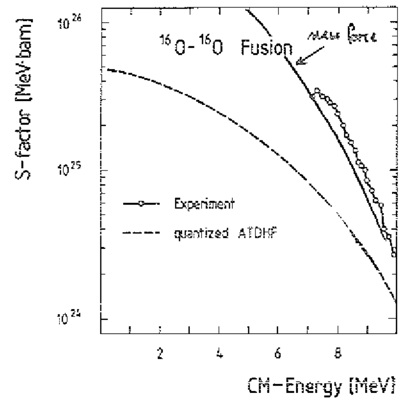

Figure 3

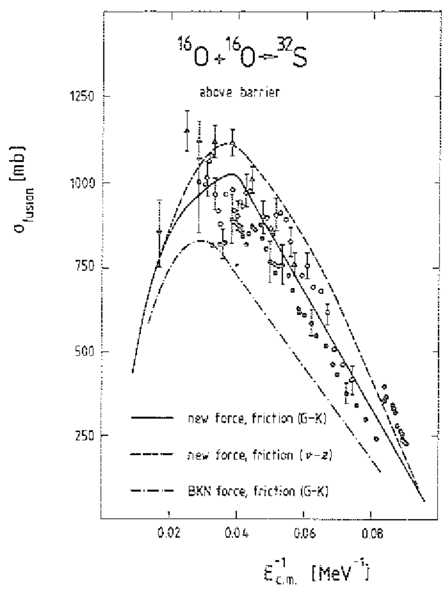

Figure 4

trajectory calculations also the fusion cross section above the barrier can be calculated. The results are given in Fig. 4. There the solid line gives the theory with the new force and the dash-dotted with the BKN interaction. Again only the curve with the new force is in good agreement with the data. It seems to be that the dynamics of the $^{16}O+^{16}O \rightarrow ^{32}S$ fusion process is understood and that, maybe, one can believe the theory also at energies, which are not accessible to experiments, e.g. at thermonuclear burning temperatures.

References

1) P. Bonche, S. Koonin, J. Negele, Phys. Rev. C13 (1976) 1226.
2) P.-G. Reinhard, J. Friedrich, K. Goeke, F. Grümmer, D.H.E. Gross, to be published.
3) K. Goeke, F. Grümmer, P.-G. Reinhard, Ann. Phys. 150 (983) 504.

+ Inst. f. Kernphysik, Univ. Mainz
++ HMI Berlin
+++ Inst. f. theor. Physik, Univ. Erlangen

5.10. ATDHF Calculation on the ^{4}He-^{16}O System

D. Provoost, F. Grümmer, K. Goeke

The ATDHF code[1] has been extended to allow for asymmetric configurations. The ^{4}He-^{16}O system has been intensely studied with use of the BKN force and a modification of it[2].

The collective path in the quantized ATDHF theory is determined by the following differential equation[1]:

$$\frac{d}{dq}|\phi_q\rangle = c(q)[H,H_{ph}]_{ph}|\phi_q\rangle \tag{1}$$

The labelling q of the Slater determinants along the path turned out to be an interesting point.

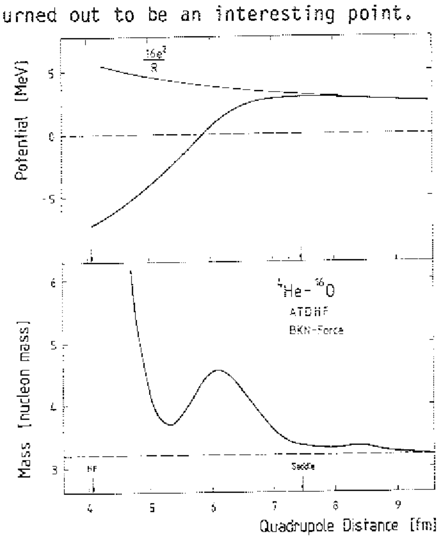

Fig. 1: Collective mass M and potential V for α-^{16}O-^{20}Ne as a function of the quadrupole distance using the BKN interaction.

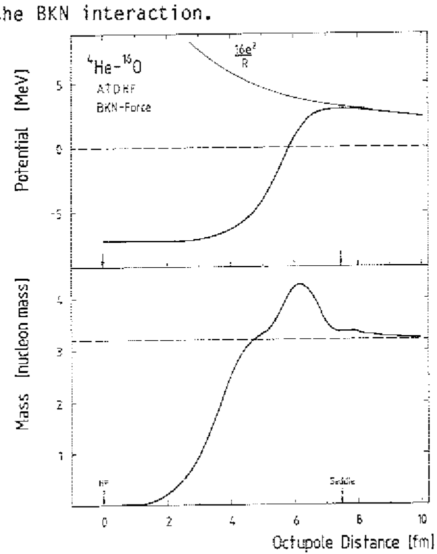

Fig. 2: Collective mass M and potential V for α-^{16}O-^{20}Ne as a function of the octupole distance using the BKN interaction.

In Fig. 1 the classical potential V and mass parameter M are shown as a function of a coordinate called quadrupole distance which is derived from the quadrupole moment in the following way:

$$R_2 = \sqrt{\langle Q_2\rangle/2\mu} \tag{2}$$

which ensures that R_2 is equal to the cluster distance in the asymptotic region for separate clusters.

In Fig. 2 a transformation is made to another coordinate derived from the octupole moment of the system:

$$R_3 = \sqrt[3]{\frac{(A_1+A_2)}{2\mu(A_2-A_1)}\langle Q_3\rangle} \tag{3}$$

and is called octupole distance. This coordinate has the advantage to start from zero for the symmetric ^{20}Ne HF ground state and is again equal to the cluster distance in the asymptotic region. Although the curves shown are rather different the physical content is identical. This is explicitly demonstrated if one transforms from both coordinates to a third one in which the mass parameter is constant and identical to the reduced mass. Both coordinates yield the same result.

The next step of the ATDHF method consists in the solution of the collective Schrödinger equation[1]

$$\left\{-\frac{\hbar^2}{2\mu}\frac{d^2}{dq^2} + V(q) - Z(q) + \frac{h^2}{2\theta}\ell(\ell+1)\right\}g_\ell(q) = E\, g_\ell(q) \tag{4}$$

Z takes the quantum corrections into account and the centrifugal term has been added by hand since we do not make an explicit angular momentum projection. The ground state rotational band obtained after solution of eq. (4) is shown in Fig. 3 and compared with experiment and with pure HF + centrifugal term.

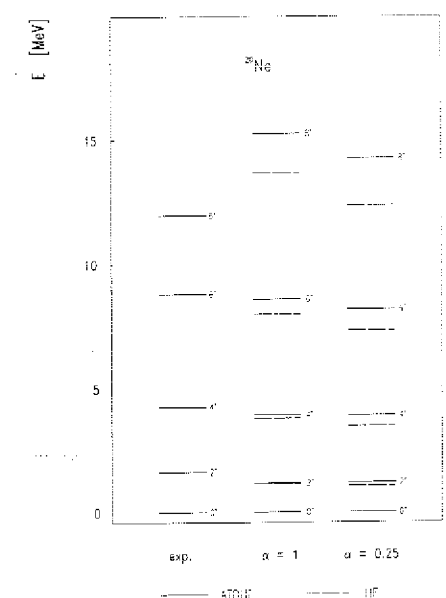

Fig. 3: Ground state rotational band of ^{20}Ne. Experimental values, ATDHF calculation with BKN interaction (α=1) and with modified force (α=0.25) are compared. The results obtained with ^{20}Ne HF ground state plus centrifugal term are also given.

The agreement for the 2^+-, 4^+- and 6^+-state is reasonable. The 8^+ however has no longer a rotational structure, so we cannot find agreement for this state with experiment.

The elastic differential scattering cross sections for α on ^{16}O are shown in Fig. 4. The upper part shows the comparison experiment-BKN calculations, the middle part experiment-modified force calculations, and the lower

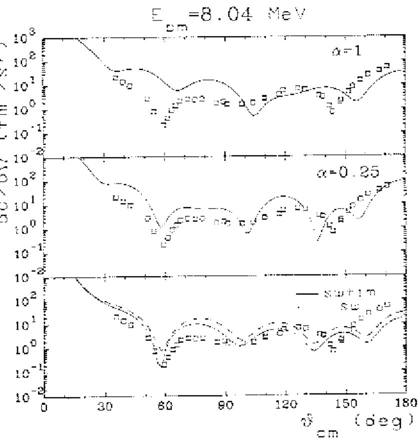

Fig. 4: Differential scattering cross sections for the elastic scattering of α on ^{16}O for a CM bombarding energy of 8.04 MeV. The experimental data are taken from Ref. 3 and compared with the BKN and modified force calculations (α=1 and α=0.25 resp.) and with the Woods-Saxon fit to the experimental data once with and once without imaginary part.

part compares experiment with the Saxon-Woods fit to the experimental data[3]. One sees that the α-scattering data can be reproduced without adjusting any free parameters at least as good as the Saxon-Woods fit (without imaginary part). Further investigations in particular focused on angular momentum properties and channel coupling are in progress.

References

1) K. Goeke, F. Grümmer, P.-G. Reinhard, Ann. Phys. 150 (1983) 504.
2) P.-G. Reinhard, J. Friedrich, K. Goeke, F. Grümmer, D.H.E. Gross, to be published.
3) M.K. Mehta, W.E. Hunt, R.H. Davis, Phys. Rev. 160 (1967) 791.

5.11. ATDHF Calculations with Skyrme Interaction

R. Gissler, K. Goeke, and F. Grümmer

The quantized ATDHF theory[1] allows to derive for a given effective microscopic interaction, the collective path $\{|\phi_q\rangle\}$ associated to the lowest large amplitude collective mode. The collective path is determined by solving a differential equation in finite steps, thus obtaining a discrete series of states $|\phi_{q_n}\rangle$ on the path, labelled by the collective coordinate q_n. In the numerical treatment we handle the Slater determinants $|\phi_{q_n}\rangle$ by handling the corresponding set of occupied single particle states $\{|\psi_{\alpha q,n}\rangle, \alpha=1,\dots,A\}$. We obtain:

$$|\psi_{\alpha q,n+1}\rangle = (1-\varepsilon\hat{S})|\psi_{\alpha q,n}\rangle$$

with

$$\hat{S}|\psi_{\alpha q,n}\rangle = (1-\rho)\{W_0(1-2\rho)W_0+W_1\}|\psi_{\alpha q,n}\rangle$$

W_0 and W_1 depend on the effective microscopic interaction used. We use for our calculations the Skyrme interaction without ℓs-term and a direct Coulomb force. Differently from the commonly used interactions, as e.g. Bonche-Koonin-Negele force, the W_1 does not vanish, and W_0 depends on an effective mass $m^*(r)$ and the kinetic energy density $\tau_0(\vec{r})$. In detail we obtain[2] the usual expression for the mean field Hamiltonian W_0 and for the linear response operator W_1:

$$W_1 = \frac{1}{32}(3t_1+5t_2)(\vec{\nabla}\cdot\vec{j}+\vec{j}\cdot\vec{\nabla})$$

$$\vec{j}(\vec{r}) = 8\sum_{\alpha}\{(\vec{\nabla}W_0^{ph}\psi_{\alpha q})(\vec{r})\psi_{\alpha q}(\vec{r})-(\vec{\nabla}\psi_{\alpha q})(\vec{r})(W_0^{ph}\psi_{\alpha q})(\vec{r})\}$$

t_1 and t_2 are parameters of the Skyrme force. W_0^{ph} is the 1p-1h and 1h-1p part of W_0 with respect to $|\phi_q\rangle$.

The calculations have been performed for the α-^{16}O system using the Skyrme III force[3].

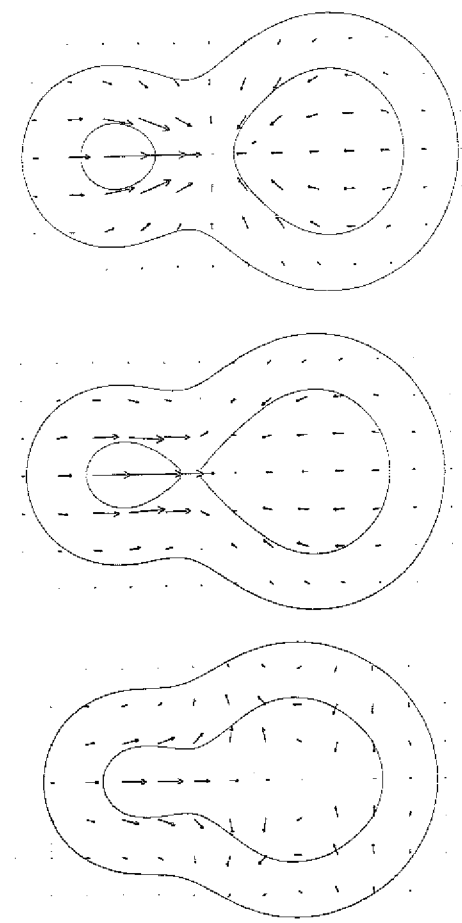

Fig. 1 shows the current distributions together with the lines of 10 % and 70 % nuclear matter density plotted for three distances of the ions in the approaching region.

The current $\vec{j}$ allows the representation of the density movement along the collective path. The Figures 1 and 2 show the current distributions. The scales have been chosen such that the x-component is enlarged by a factor of 10 compared to the z-component, where the z-axis coincides witht the collision axis. The main and interesting feature is that in the approach phase first matter from the halo of the system flows into the centre, then at smaller separation distances the neck between the ions grows by flow in outward directions.

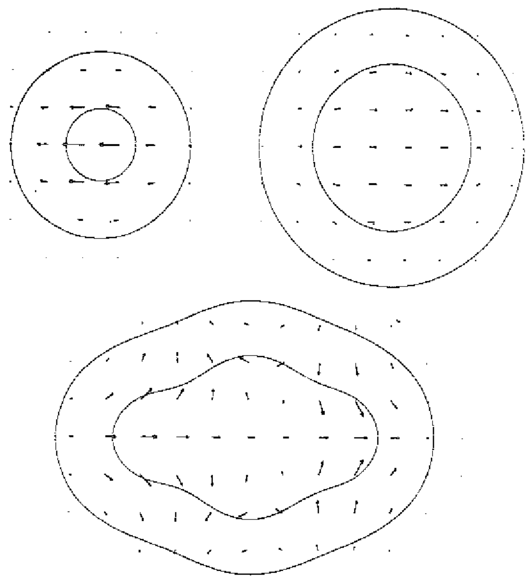

Fig. 2 gives similar results at configurations close to the HF-point of the ^{20}Ne-system and in the asymptotic region with separate fragments.

References

1) K. Goeke, F. Grümmer, P.-G. Reinhard, Ann. Phys. 150 (1983) 504.
2) Y.M. Engel et al., Nucl. Phys. A249 (1975) 215.
3) M. Beiner et al., Nucl. Phys. A238 (1975) 29.

5.12. Extended Time-Dependent Mean-Field Theories from the Maximum Entropy Principle

H. Reinhardt[+], R. Balian[++] and Y. Alhassid[+++]

The time-dependent Hartree-Fock (TDHF) theory is supposed to give an adequate description of low energy nuclear dynamics where the two-body collisions are essentially suppressed by the Pauli principle. In fact, numerical application of the TDHF theory reproduced satisfactorily well the mean-values of s.p. observables but failed (even at low energies) to reproduce the data on two-body correlations. With increasing energies the Pauli principle becomes more and more ineffective in preventing two-body collisions. In high energy heavy ion reactions ($E_{lab}/A \sim 100$ MeV) two-body collisions are so frequent that they may lead to an almost instantaneous thermalization of the system.

The present paper is devoted to the inclusion of the effect of two-body collisions in a mean-field description. The approach is guided by the maximum entropy principle, according to which the system is described by a density matrix which maximizes the entropy under the constraint that the mean-value of the observables of the system which are considered as relevant are exactly reproduced. Combining the maximum entropy principle with a recently developed form[1] of the time-dependent projection method for statistical systems, we derive several collision extended time-dependent mean-field (ETDMF) equations which differ in the extent of how detailed the evolution is described, i.e. how many observables of the system are considered as relevant for its evolution[2].

If all single particle observables are considered as relevant one obtains an evolution equation for the s.p. density matrix with a collision term where also off-diagonal matrix elements of the s.p. density matrix (in the TDHF s.p. basis) enter. This equation is perhaps intractable for heavy ion collisions but its linearized form is expected to describe adequately the width of giant resonances. Furthermore this equation also serves as a starting point to include two-body collisions into an adiabatic time-dependent mean field description[3].

A less detailed (and, hence, more practicable) description is obtained by considering as relevant observables not all the s.p. observables of the time-dependent mean-field description, but only the occupation number operators of the time-dependent mean-field s.p. states. This yields a master equation for the occupation numbers.

A further reduction of the description is achieved by considering only the energy and the particle number as relevant observables. The resulting set of evolution equations may be characterized as time-dependent temperature mean-field theory.

The present approach, which presents different extended mean-field approximations from a unified viewpoint, exhibits a general recipe to construct adequate but practicable extensions of the time-dependent mean-field theory.

References

1) R. Balian, Y. Alhassid, H. Reinhardt, to be published in Phys. Rep.
2) H. Reinhardt, R. Balian, Y. Alhassid, submitted to Nucl. Phys. A.
3) K. Goeke, P.-G. Reinhard, H. Reinhardt, to be published.

+ ZfK Rossendorf, Dresden, GDR
++ CEN Saclay, France
+++ Yale Univ., New Haven, CT, USA

6. ATOMIC COLLISIONS

6.1. Inner Shell Ionization Processes in Asymmetric Collision Systems

G. Baur, F. Rösel+, and D. Trautmann+

The ionization of inner shells in heavy particle induced reactions is a basic process in atomic physics. This effect can be well described by semiclassical methods using a Coulomb or a screened Coulomb trajectory for the incoming particle[1]. In some cases it becomes important to include the effect of the projetile-electron interaction in the wave function of the target electrons[2,3]. Especially for the explanation of L_3-subshell alignment data it will be important to include higher order effects in the projectile-target interaction. This is done in a coupled channels formulation[4].

The excitation of bound, high-lying states (Rydberg states) with large principal quantum number n was studied in Ref. 5, where the scaling of the cross section with n^{-3} could indeed be verified.

A fully quantal theory of ionization induced by neutrons is given in Ref. 6. The semiclassical limit treated by Migdal[7] could be obtained as a special case. The expression for the T-matrix for this process depends on the on-shell neutron-target scattering amplitudes at the energies E_{inc} and $E_{inc}-\Delta$, where $\Delta = E_{el}+E_{bind}$ denotes the transferred energy. The observation and study of this neutron induced ionization process would thus yield interesting insight into the correlation width of the autocorrelation function of the nuclear scattering matrix. This may become possible with the advent of the new high intensity neutron sources[8]. In contrast to the study of time delay effects in charged particle induced reactions[9], where an overwhelming background of ionization processes is present in which no nuclear reaction occurs, such a problem will not exist in the neutron induced ionization process.

References

1) A. Jakob, F. Rösel, D. Trautmann, G. Baur, Z. Phs. A309 (1982) 13.
2) D. Trautmann, F. Rösel, G. Baur, Nucl. Instr. and Methods 214 (1983) 21.
3) A. Jakob, D. Trautmann, F. Rösel, G. Baur, Nucl. Instr. and Methods, to be published.
4) R. Lamprecht, Diplomarbeit 1983 Institut für theoretische Physik, Basel (unpublished).
5) B. Leibundgut, Diplomarbeit 1983 Institut für theoretische Physik, Basel (unpublished).
6) G. Baur, F. Rösel, D. Trautmann, J. Phys. B16 (1983) L419-423.
7) A.B. Migdal, Qualitative Methods in Quantum Mechanics (Reading, Mass., Benjamin 1977) p. 108.
8) Realisierungsstudie zur Spallations-Neutronenquelle Jül-Spez-113 (1981).
9) W. König, K.W. McVoy, H.A. Weidenmüller, P. Kienle, Phys. Lett. 123B (1983) 279.

+ Inst. f. Theor. Physik, Univ. Basel

6.2. Excitation of Inner Shells in Collisions of Charged Particles with Atoms

B. Hoffmann and G. Baur

Ion-atom collisions play a significant role in plasma physics, laser physics, physics of interstellar media and in many other fields. The general theoretical description of these collisions is too complex to be solved, therefore various approximations are applied. Collisions involving many-electron ions and atoms involve, due to the molecular effects, additional approximations, whose validity cannot be proved until the basic assumptions are well understood. A good testing ground for the primary approximations are collisions of charged particles with hydrogen or hydrogen-like atoms.

One of the approximations which are quite often used in ion-atom collisions is the semiclassical approximation, where the movement of the projectile is described by a classical trajectory, whereas the excitation process is treated quantum mechanically. Full quantum mechanical calculations exist up to now only in the high energy regime in terms of Born approximation or Glauber theory.

In the present approach the ion-atom collision is treated fully quantum mechanically in terms of DWBA. The DWBA connects the regimes where the Born approximation is good with the regime where the semiclassical theory works well and it may be used to test the limitations of the latter theories. Nevertheless this DWBA approach is a first order theory and it does not consider molecular effects which play an important role for very low energies.

The DWBA T-matrix element for excitation of an inner shell by a projectile with charge Z_p is given by:

$$T_{if} = \langle \psi_f^{(-)} | \frac{Z_p e^2}{\vec{R}-\vec{r}} | \psi_i^{(+)} \rangle \qquad (1)$$

where

$$\psi_j^{(\pm)} = \phi_j(\vec{r})\chi^{(\pm)}_{\vec{Q}_j}(\vec{R}).$$

$\phi_j(\vec{r}) := \phi_{n_j \ell_j m_j}(\vec{r})$ denotes the bound electron wave function and

$$\chi^{(\pm)}_{\vec{Q}_j}(\vec{R})$$

denotes the Coulomb wave function of the projectile with the appropriate boundary conditions.

Eq. (1) may be written more explicitly as:

$$T_{if} = \sum_{\lambda\mu} \frac{Z_p e^2}{2\lambda+1} W_{\lambda\mu} \int d^3R \, \chi^{(-)}_{\vec{Q}_f}(\vec{R}) G^{\lambda}_{if}(R) Y^*_{\lambda\mu}(\vec{R}) \chi^{(+)}_{\vec{Q}_i}(\vec{R}) \qquad (2)$$

G^{λ}_{if} is the electronic form factor for the transition $n_i \ell_i m_i \xrightarrow{\lambda\mu} n_f \ell_f m_f$ and $W_{\lambda\mu}$ is a factor absorbing all the angular momentum coupling coefficients.

The electronic form factor G^{λ}_{if} is a function of the type

$$G^{\lambda}_{if} = \sum_k a_k R^k e^{-\varkappa_k R} \qquad (3)$$

where the a_k and $\varkappa_k$ can be easily calculated using non-relativistic hydrogenic electron wave functions.

In order to compute the matrix element of G_{if}^{λ} with the Coulomb waves, we expand the $\chi_{\vec{Q}}$ in partial waves. Then one has to calculate the generalized Coulomb matrix elements, defined by:

$$M_{\ell_i,\ell_f}^{-\lambda-1,\varkappa} := \frac{1}{Q_i Q_f} \int dr\, F_{\ell_i}(Q_i R) \frac{e^{-\varkappa R}}{R^{\lambda+1}} F_{\ell_f}(Q_f R) \qquad (4)$$

For small ℓ_i, ℓ_f it is possible to compute these integrals directly in terms of F_2-functions[1]. But in atomic physics problems one needs typically many ten thousands partial waves, which can be calculated in finite time only by means of recursion relations.

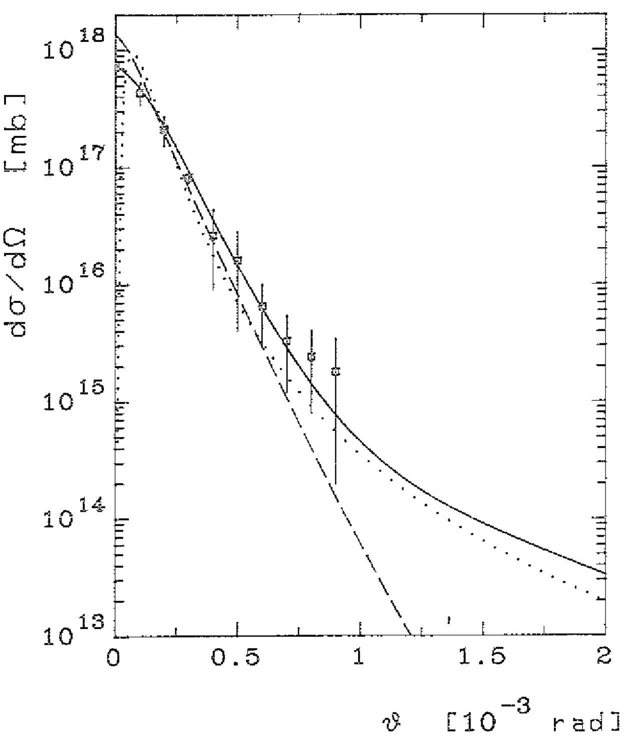

Fig. 1: The measured differential cross section[2] for the reaction p+H(1S) p+H(2P), E_p = 100 keV, is compared to Coulomb-DWBA (full line), Born approximation (dashed line), and semiclassical theory (dotted line).

In Fig. 1 we compare the results of this approach for the reaction p+H(1S) p+H(2P) with experimentally measured differential cross sections[2], with Born approximation and semiclassical theory. It can be seen that the Born approximation drops much too fast with increasing angle compared with experiment. The Coulomb DWBA approach outlined above shows better agreement with experiment.

At angles not too near to zero the Coulomb DWBA and semiclassical theory agree reasonably well with each other, despite of the fact that the Coulomb parameter η is quite small (η = 0.5) in this case. At angles near to zero the semiclassical theory fails. The reason for this phenomenon lies in the fact that in deriving the semiclassical approximation via stationary phase methods, an asymptotic expansion of the spherical harmonics $Y_{\ell m}(\vartheta,\varphi)$ was used, which is valid only for ϑ greater than some finite ε.

References

1) K. Alder, D. Trautmann, Ann. Phys. 66 (1971) 884.
2) J.T. Park, J.E. Aldag, J.L. Peacher, J.M. George, Phys. Rev. A21 (1980) 751.

7. ASTROPHYSICS

7.1. Electron Capture in Stellar Collapse

J. Cooperstein+ and J. Wambach

The center of a large star becomes dynamically unstable when it exhausts its nuclear fusion fuels. The mass of the ashes of the most strongly bound Fe peak nuclei grows larger than that which electron degeneracy pressure is able to support. Triggered by endothermic photodisintegration, catastrophic implosion ensues on a timescale of milliseconds, to be reversed only when the center surpasses nuclear matter density. The ability of the shock wave produced at the edge of the central core to succcessfully expell the outer regions of the star is extremely sensitive to the core's profile during the final collapse stages. The two most important quantities are the number of leptons per nucleon Y_e and the entropy S as was first pointed out by Bethe et al.[1]. It has been demonstrated that a high lepton fraction and low entropy are essential if the shock is to succeed.

Both Y_e and S change during the collapse entirely due to electron capture and neutrino interactions because the weak interaction processes are not equilibrated on the collapse timescale. Neutrinos are emitted after capture of relativistically degenerate electrons from the few free protons present in the infalling matter

$$p+e^- \rightarrow n+\nu_e \tag{1a}$$

or after neutronization of heavy nuclei via

$$(N,Z)+e^- \rightarrow (N+1,Z-1) + \nu_e \tag{1b}$$

Therefore the complete capture rate $dY_e/dt \equiv \dot{Y}_e$ will be given by two pieces

$$\dot{Y}_e = \dot{Y}_{e_p} + \dot{Y}_{e_H} \tag{2}$$

where the first arises from the protons dripped out of heavy nuclei and the second includes contributions from all of the heavy nuclei according to their abundances. The relative abundances are thermodynamically prescribed with the assumption of nuclear statistical equilibrium with a distribution function derived from a liquid drop model equation of state[2] as

$$\phi(A)/\phi_0 = \exp[-\tfrac{1}{2}((A-A_0))/(\sigma_A))^2] \tag{3a}$$

$$A_0 \cong \tfrac{1}{2} W_{surf}/W_{Coul} \tag{3b}$$

and

$$\sigma_A = A_0 \sqrt{3T/(W_{surf}A^{2/3})} \tag{3c}$$

$$W_{surf} = 290(Z/A)^2\,[1-(Z/A)]^2 \tag{3d}$$

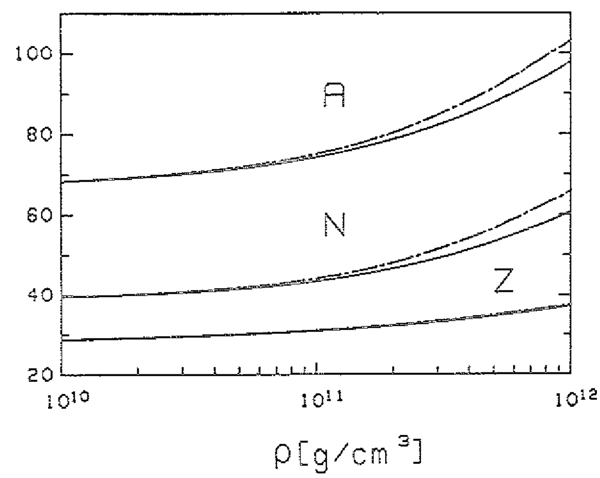

Fig. 1: Mass number A, number of neutrons N and number of protons Z for the mean nucleus as a function of matter density. The full and dash-dotted lines correspond to two different assumptions about the capture rates.

Here A_0 denotes the mean nucleus, W_{surf} and W_{Coul} the surface and Coulomb energies, Z the nuclear charge and T the temperature. The evolution of A,N,Z with matter density ρ are depicted in Fig. 1. With $\phi(A)$ the total e^--capture rate from heavy nuclei in the extremely relativistic limit is given by

$$\dot{Y}_{e_H} = \int \phi(A)/(\phi_0 \cdot A) \sum_f \int_{Q_{if}}^{\infty} d\varepsilon_e\, G(\varepsilon_e,\varepsilon_\nu;T)\sigma_{if}(A,\varepsilon_e;T) \tag{4}$$

where G is the lepton-neutrino phase space factor and σ_{if} the total e^--capture cross section from state i to state f for nucleus A. Q_{if} denotes the Q-value of the reaction.

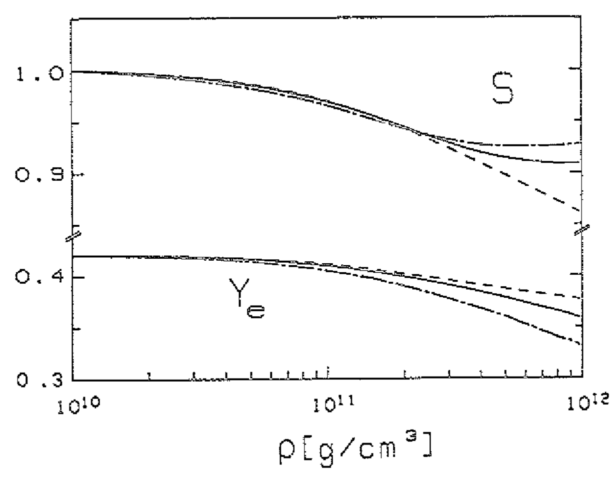

Fig. 2: Density dependence of the entropy S and the electron fraction per baryon Y_e. The dashed line includes capture from free protons only, while the dash-dotted and full lines include capture from heavy nuclei as well with two different assumptions about the rates.

The total cross section σ_{if} contains Gamow-Teller (GT) contribution arising from thermal unblocking mechanisms in the nuclear ground state and proceeds energetically mainly beneath the T=0 threshold, as well as parity forbidden contributions particularly the 2^- "unique forbidden" transitions. Those are generally of comparable strength to the unblocked allowed transitions. We have calculated[3] σ_{if} for each A in a finite temperature nuclear single particle model and evaluated $\dot{Y}_{e_H}$ (eq. 4).

Fixing the initial conditions at the beginning of the collapse the evolution of the entropy S and Y_e have then been traced in a one zone hydrodynamical collapse model. The results are given in Fig. 2. They indicate that the electron fraction at neutrino trapping densities is not much reduced from its initial value. In contrast to previous work, the entropy is shown to decrease via neutrino cooling from below threshold GT-transitions as well as free protons. Heating from "forbidden transitions" above threshold capture cannot compensate for this. The small amount of e^--capture and entropy decrease are useful in producing successful supernova explosions.

References

1) H.A. Bethe et al., Nucl. Phys. A324 (1979) 487.
2) H.A. Bethe et al., Nucl. Phys. A403 (1982) 625.
3) J. Cooperstein, J. Wambach, to be published in Nucl. Phys. A

+ Nordita, Copenhagen, Denmark

III. SOLAR ENERGY

8.1. Solar Heating Plant at Mount Zugspitze

H.J. Stein, M. Köhnen

The German Federal Post has installed a new radio transmission station at Mount Zugspitze/Garmisch. The service building of this station has been equipped with a solar heating plant.[1] We have overtaken the task of monitoring the solar system, in order to get reliable data on system performance as a basis for an optimum operational strategy and possible technical improvements.

The construction housing the telecommunication systems consists of a weather protecting cover made of aluminium under which the well-insulated windowless service building is located. Plastic windows are integrated into the aluminium cover. Behind the plastic windows single-glazed solar collector modules have been placed, Fig. 1. The entire solar heating system consists of an array of 48 collectors (field aperture area 53 m^2), two storage vessels (2,35 m^3 each), and an electrically driven heat pump (3 to 4 kW driving power). The whole system is

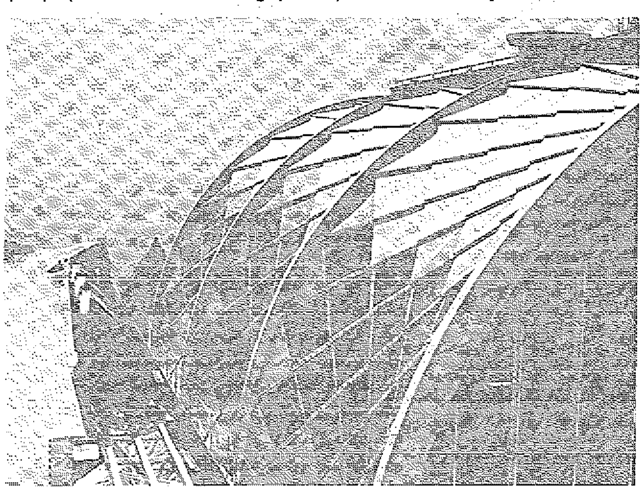

Fig. 1: Solar heating plant in service building of the Zugspitze radio transmission station.

filled with antifreeze 70% glycol/30% water. The heating system of the building is based on air ventilation including regenerative heat exchanging with fresh air. Back up energy is delivered via electric resistor heaters in the ventilation system. Electric resistor heating in the storage using low tariff electricity is also applied. The solar system has two operating modes, Fig. 2.

i) above 30 °C storage temperature heat is directly fed into the air ventilation system,

ii) below 40 °C the heat pump is switched on, operating down to a storage temperature of -5 °C.

Data taking for monitoring the solar system is performed in a twofold way,

i) All energy fluxes as solar radiation, heat from the collector field, the storage, and the heat pump, as well as the various electric energy inputs are measured by appropriate sensors and transmitted to numerical registers centrally placed in a telltale board showing the energy fluxes in the system. Readings are automatically photographed every day before midnight.

ii) In parallel, these energy fluxes are also recorded by a specially developed computer-based data acquisition system which records also temperatures and system status information. Data are integrated every 10 minutes or hourly, stored on flexible disk, and retrieved weekly by mailing the flexible disk, and/or daily by telephone communication to a central computer at the KFA Jülich.

The solar system together with the energy counters has been in full operation since beginning of April 1982. The computer system for data taking has been operating since end of June 1982. Yearly performance data were expected to be promising due to the fact that in an altitude of 2964 m there is a heating load also during the

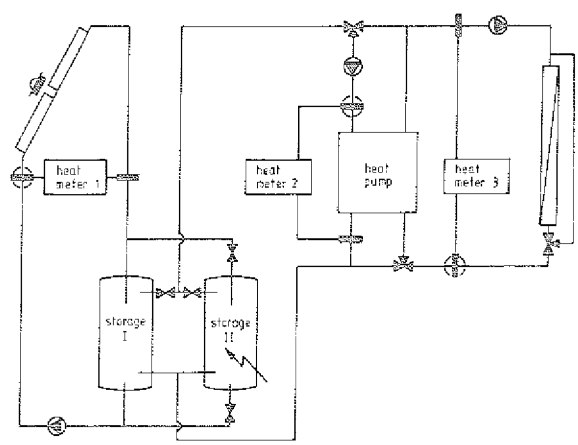

Fig. 2: Scheme of the solar heating system with basic instrumentation.

summer months and a high solar radiation input all over the year. Data based on the daily photographed energy flux measurements gave 40 % savings in the period from April to October 1982, Fig. 3. In the following winter time a dramatic reduction in system performance was observed. Analysing the high time resolution computer data the reason was found to be a malfunction of fluid dynamics and regulation related to the twin storage system. As a consequence the storage temperatures were always too high causing high losses of electrically generated heat and low collector efficiencies. Since the simple repair of these defects in February 1983 the system has been operating properly. From the available data, Fig. 3, it can be concluded that the plant has the potential of 35-40 % year-long savings.

References

1) BMFT, Annual Report 1980 on New Sources of Energy, Project No. ET 4315 Z/2, 4.1, p. 1616.

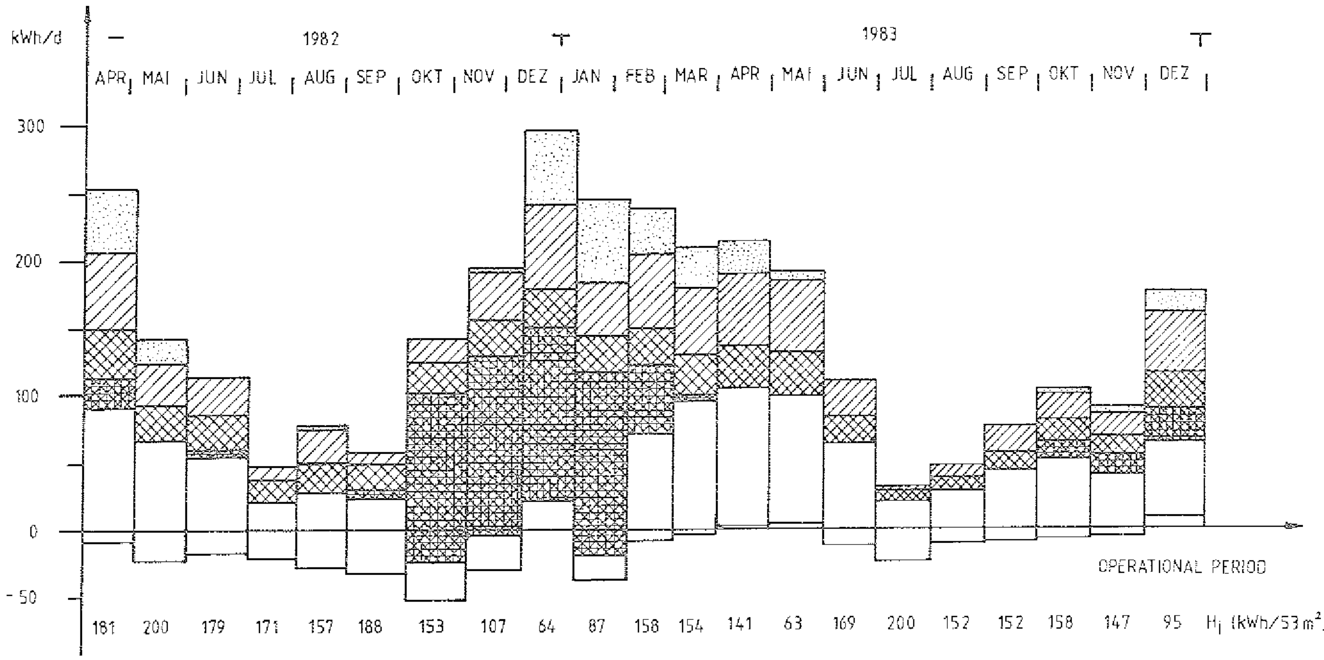

Fig. 3: Result of energy balance measurements of the solar heating plant Mount Zugspitze in the period from April 4, 1982 to Jan. 5, 1984. The plot shows the mean daily heating load over approximately monthly periods. Substracted from the heating load are back up heating energy ▒, heat pump compressor energy ▨, auxiliary energy ▩, stored electrical energy ▦, and collector heat output □. The numbers below give the incident solar energy available within the weather protecting cover related to 53 m3 collector aperture area. The white bars above zero define the savings relative to 100 % electrical heating. Values below zero describe system losses, mainly due to thermal losses of the storage.

8.2. Methodical Developments in Solar Collector Testing

J.-D. Witt, P. Schmidt, H.J. Stein

Due to heat capacity effects standard test procedures like DIN 4757/4 or ASHRAE 93-77 require steady state conditions for the solar irradiation E in order to determine the instantaneous efficiency η of a solar collector. The time periods for outdoor tests are, therefore, restricted to clear sunny days which do not occur very often under middle European weather conditions.

Our attempt to overcome this restriction is to integrate the collector heat output $\dot{Q}$ and the solar irradiation E over time periods which are longer than the heat capacity time constant of the collector.

$$\bar{\dot{Q}} = \frac{\dot{m}c}{t_2 - t_1} \int_{t_1}^{t_2} (\vartheta_e - \vartheta_i)\,dt$$

$$\bar{E} = \frac{1}{t_2 - t_1} \int_{t_1}^{t_2} E\,dt$$

$$\eta = \bar{\dot{Q}}/\bar{E}$$

$\dot{m}$ = mass flow rate
c = specific heat capacity of the collector fluid
ϑ_i = collector inlet temperature
ϑ_e = collector outlet temperature
$t_{1/2}$ = start/stop time of the integration period

Since $\dot{m}$ and ϑ_i are held constant by the test loop only the outlet temperature ϑ_e fluctuates when the solar irradiation is a fluctuating function with time. Choosing appropriate time marks for start and stop of the integration, i.e. the measured temperature difference $\vartheta_e - \vartheta_i$ has to be the same at the beginning and the end of the integration period, heat capacity effects can be minimized already within integration times of less than one hour.

This method was successfully applied with a bilaterally operated collector test loop at the University of Ljubljana/Yugoslavia. Based on an agreement between the KFA Jülich and the University of Ljubljana, the Institute for Mechanical Engineering at Ljubljana[1] was equipped with a versatile test unit usable for absolute and comparative tests of two collectors, Fig. 1. The equipment for this test unit corresponds to the standard IKP test stand consisting of a loop for series connection of two collectors, a thermostat to stabilize and regulate collector inlet temperatures, electronics comprizing PT 100 $\Delta\vartheta$ amplifiers, electronic integrators for $\Delta\vartheta$ and E signals, and a multi-channel strip chart recorder. Two flat plate collectors were comparatively tested outdoors, i.e. the efficiency curves for both collectors were determined simultaneously under the same climatic conditions.

Collector 1: single glazed, black paint absorber, aluminium rollbond absorber, commercially available in Germany.

Collector 2: single glazed, special absorber structure similar to the construction of heat exchangers for air conditioning units, Yugoslavian prototype for commercial solar water heaters.

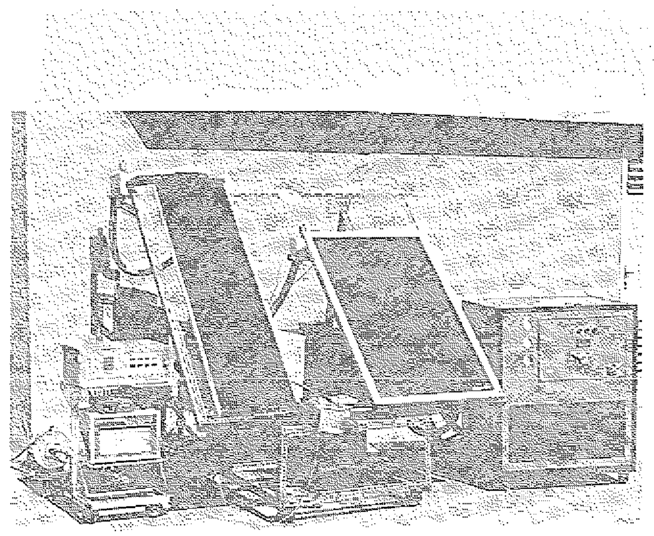

Fig. 1: Comparative collector test loop at University of Ljubljana equipped with electronic integrators for the precise determination of the mean values of collector heat output and solar radiation input.

Measured data points and fitted efficiency curves are shown in Fig. 2. The measurements were done in only two days of bright sunshine by moving the test loop according to the location of the sun. Data scattering is much smaller as compared to earlier measurements under similar conditions. The advantage of electronically determined mean values of $\dot{Q}$ and E is clearly demonstrated.

A second possibility to prove the technical quality and the methodical advantages of the KFA-IKP collector test unit has been the temporary use of our original test loop at the Nuclear Research Center Demokritos in Athens, Greece. Here, Greek authorities have started activities to build up a national solar energy test center. Our task is to give technical support to our colleagues at Demokritos[2]. Two commercially available flat plate collectors have already been tested in late 1983, Fig. 3.

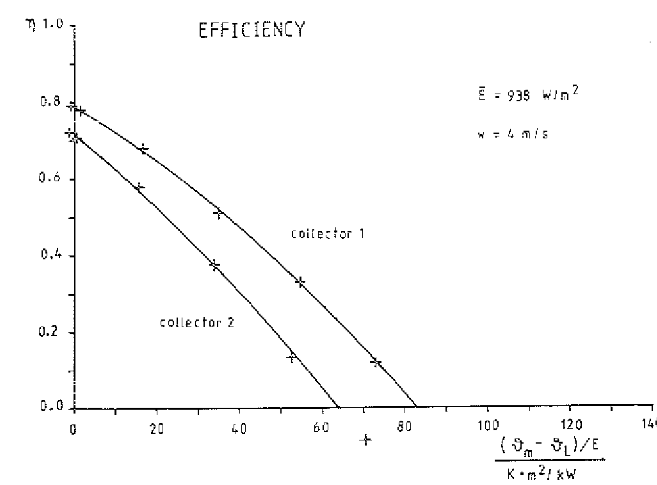

Fig. 2: Efficiency versus reduced temperature of two collectors comparatively tested following the rules of ASHRAE 93-77. Ljubljana, Sept. 26-27, 1983.

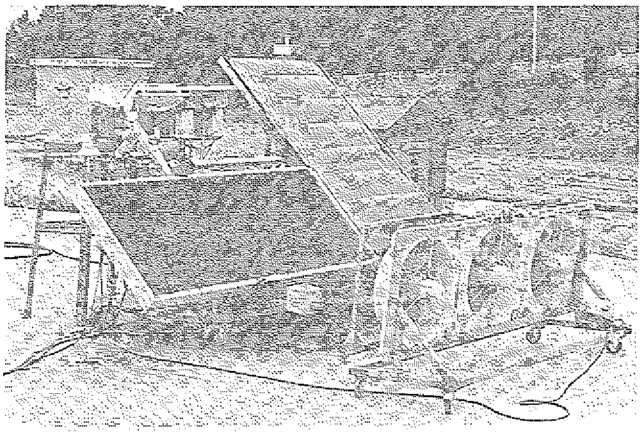

Fig. 3: The KFA-IKP collector test unit installed at the NRC Demokritos in Athens.

Collector 1: double plastic cover, black aluminium absorber with integrated stainless steel tubing.

Collector 2: single glazed, selective stainless steel absorber of the two sheet type.

Due to very bad weather at the time of the tests only a few efficiency points could be measured. Therefore, the method of additional heat loss measurements according to DIN 4757/4 was applied in order to get the total efficiency curve. The heat loss measurements were performed overnight under cloud covered sky. It is well-known that outdoor heat loss curves may be parallel shifted into the direction of higher losses caused by long wave atmospheric radiation effects. This was also observed here, Fig. 4. The correct heat loss curve is obtained by shifting the measured curve downwards until it crosses the zero point. Fig. 5 shows the efficiency curves of both collectors constructed from the near η_0 values and the heat loss data assuming solar irradiations of 600 and 1000 W/m^2. It is interesting to note that both collectors have the same effective heat loss coefficient. The efficiency of collector 2 is higher at all operating conditions due to a better conversion factor. Results of collector 1 do compare very well with earlier measurements at Jülich.

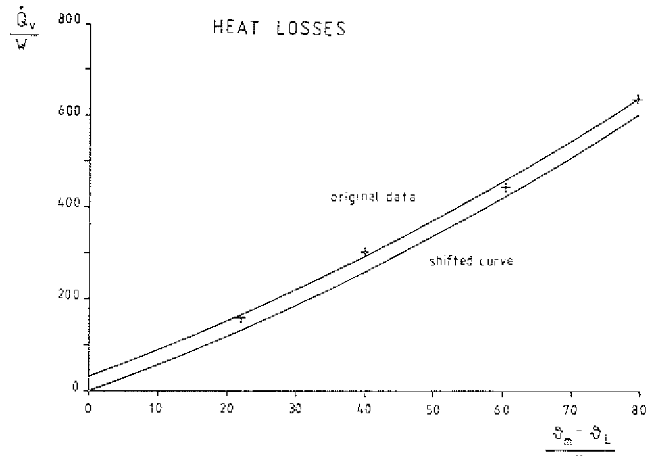

Fig. 4: Collector heat loss versus mean fluid temperature measured outdoors overnight. Athens, Nov. 23, 1983. A parallel shift of the measured heat loss curve is observed.

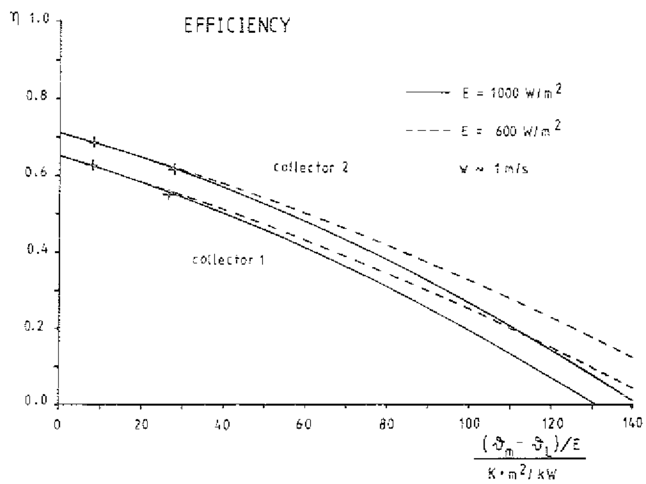

Fig. 5: Efficiency versus reduced temperature of two collectors comparatively tested following the rules of DIN 4757/4. Athens, Nov. 23-24, 1983.

References

1) The excellent cooperation with P. Novak and S. Medved, University of Ljubljana, is gratefully acknowledged.

2) We thank P. Andronikos and D. Haikalis, NRC Demokritos, for assistance and excellent cooperation.

8.3. Bilateral Cooperation in the Field of Collector Testing

B. Sack, H.J. Stein

A simple test loop for comparative testing[1] of thermal performance of solar collectors was developed at KFA Jülich and donated to partner institutions in several countries of the Third World. The aim of this project funded by the German Minister for Research and Technology[2] is to contribute to the development of the technical infrastructure of testing laboratories in these countries. Participating laboratories are today:

- Universidade Federal da Paraiba, UFPb, Joao Pessoa, Brasil,
- Universidade Federal do Rio Grande do Sul, UFRGS, Porto Alegre, Brasil,
- Egyptian Electricity Authority, EEA, Cairo, Egypt,
- SEDUE - Coordinaçion Administrativa y de Apoyo, La Paz, Mexico
- Faculty of Electrical Engineering, University of Split Yugoslavia.

Based on practical experiences during the running time of the project, several modifications and improvements of measuring techniques and methodical procedures are underway. Since in a comparative test using a reference collector the temperature difference of collector outlet and inlet temperatures is the remaining critical source of measuring errors, precise PT 100 temperature sensors (1/10 of DIN standards) and electronic temperature difference amplifiers have been introduced. Installations of the test loops at the partner institutes and comparative test results using the improved accuracy of $\Delta\vartheta$ measurements are shown in Figs. 1 through 4.

Using calibrated instruments for the solar radiation and the mass flow rate it is then also possible to determine collector thermal performance along the recommendations of internationally accepted standards. However, test runs are still restricted to days with excellent weather conditions. In the next step the thermal loop of the test stand will be replaced by a newly developed apparatus which guarantees very stable collector inlet temperatures also under fluctuating solar radiation conditions[3]. This will make possible the application of the "integration method"[4] which will considerably enhance the availability of testing time. Additional equipment necessary for this purpose, like electronic integrators for temperature difference and pyranometer signals als well as a pyranometer for determining the diffuse fraction of the solar radiation is already in use in most of the participating laboratories.

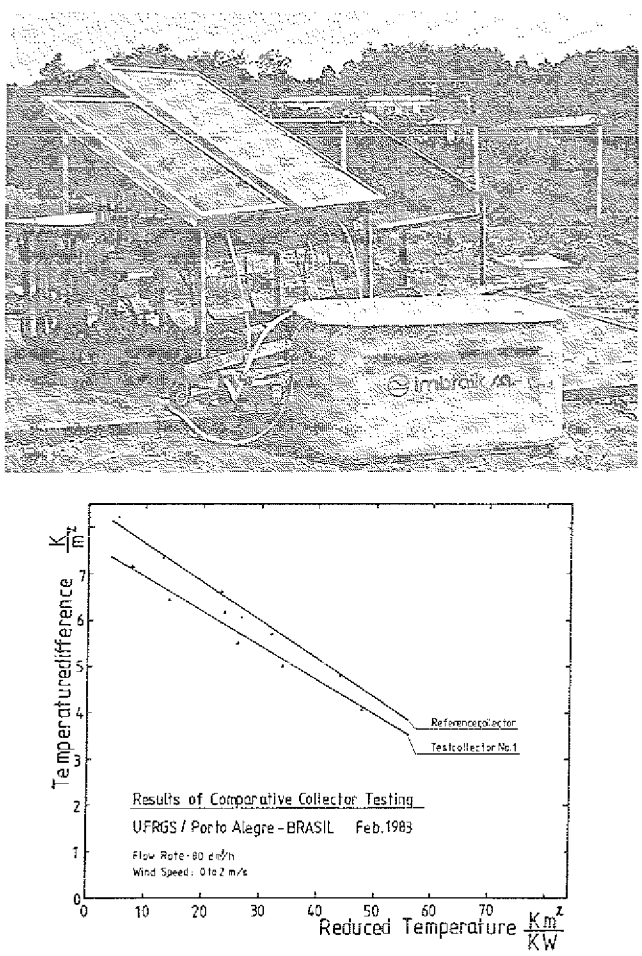

Fig. 1: Test loop installation at the University of Porto Alegre/Brasil, Febr. 1983, and results of comparative collector testing
- reference collector, black paint, single glass cover,
- test collector 1, black paint, double cover (acrylic)

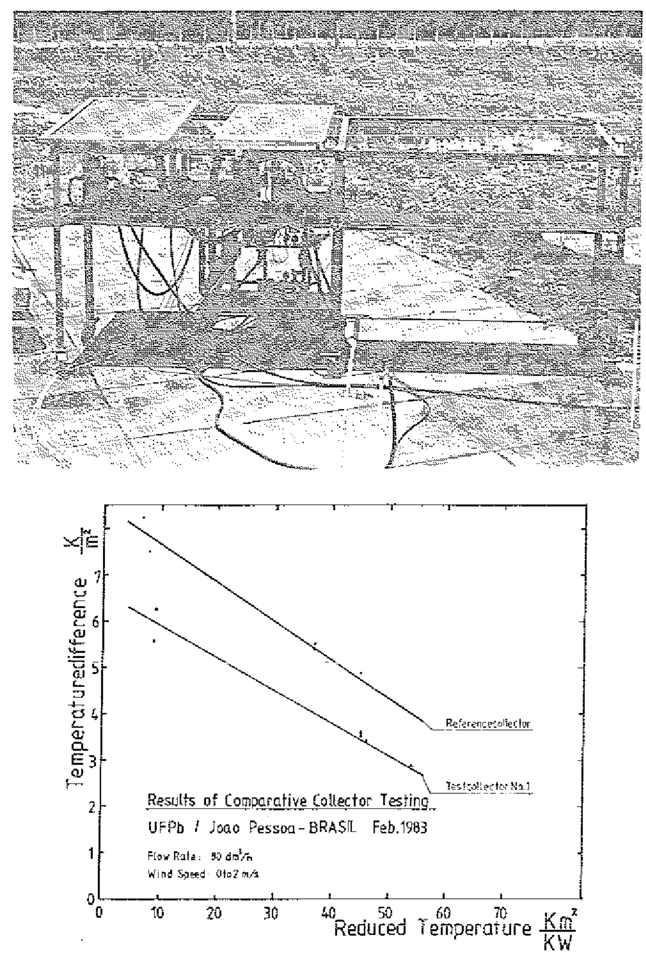

Fig. 2: Test loop installation at the University of Joao Pessoa/Brasil, Feb. 1983, and results of comparative collector testing
- reference collector, black paint, single glass cover,
- test collector 1, black paint, double glass cover.

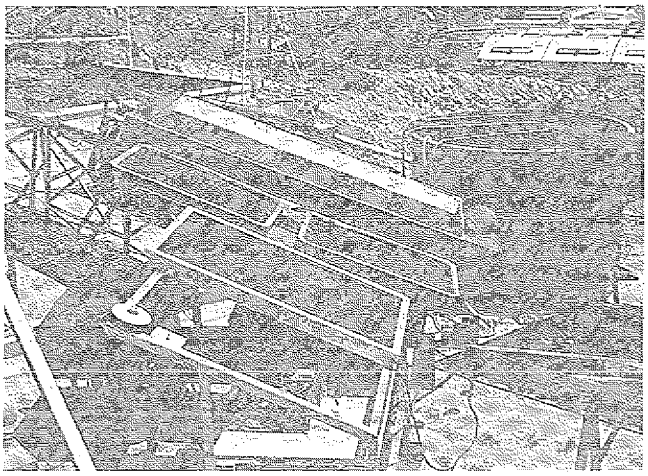

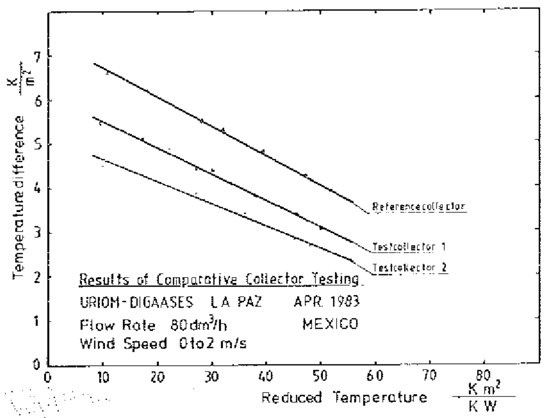

Fig. 3: Installation of the test loop at the Solar Laboratory La Paz/Mexico, April 1983, and results of comparative collector testing
- reference collector, black paint, single glass cover,
- test collector 1, plastic collector (complete), single cover (acrylic),
- test collector 2, Mexican collector, black paint, single glass cover.

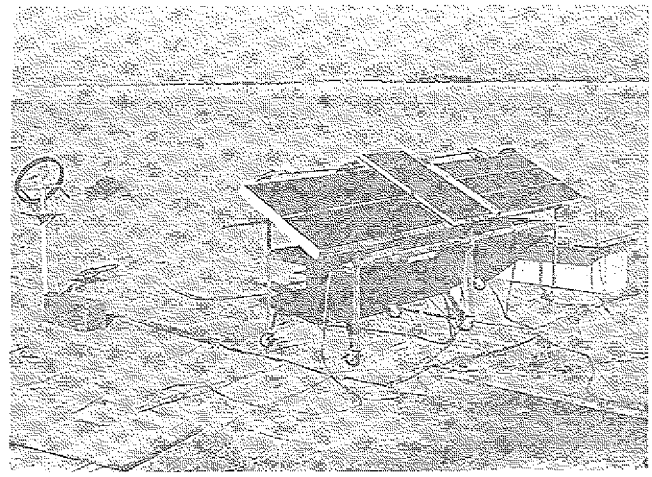

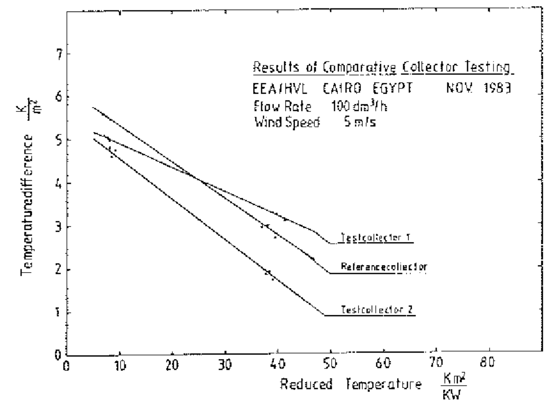

Fig. 4: Installation of the test loop at the High Voltage Laboratory/EEA, Cairo/Egypt, Nov. 1983, and results of comparative collector testing
- reference collector, black paint, single glass cover,
- test collector 1, selective, single glass cover,
- test collector 2, black paint, single glass cover.

References

1) B. Sack, H.J. Stein, Development of a Simple Test Unit for Comparative Testing of Solar Collectors, Annual Report 1981 of KFA-IKP, Jül-Spez-146, p.102.

2) BMFT Annual Report 1980 on New Sources of Energy, Project No. ET 4172 B, p. 969.

3) J.-D. Witt, P. Schmidt, to be published.

4) J.-D. Witt, P. Schmidt, H.J. Stein, Methodical Developments in Solar Collector Testing, cf. this Annual Report 1983, p. 111

8.4. Testing of a Solar Air Heating Collector

T. Zekorn

A test loop for measuring the efficiency of an industrially manufactured solar air heater was constructed at the collector test field of the IKP. The loop has been operational since June 1983. The collector consists of hollow-bodied plastic panels. The lower absorbing side is made of black, the upper side is made of transparent polycarbonate material, Fig. 1. Simultaneously the collector can serve as roofing for buildings. This solar air heater has been designed for heat pump applications or preheating domestic hot water. In both applications the collector will be used in an open cycle. With the ambient air temperature always being the inlet temperature, the collector works at low temperature levels with small thermal losses.

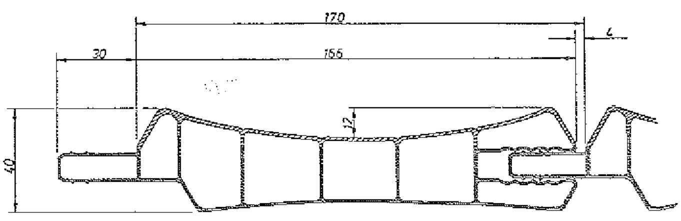

Fig. 1: Cross sectional view of an element of the air heating collector consisting of hollow bodied plastic panels. Dimensions in mm.

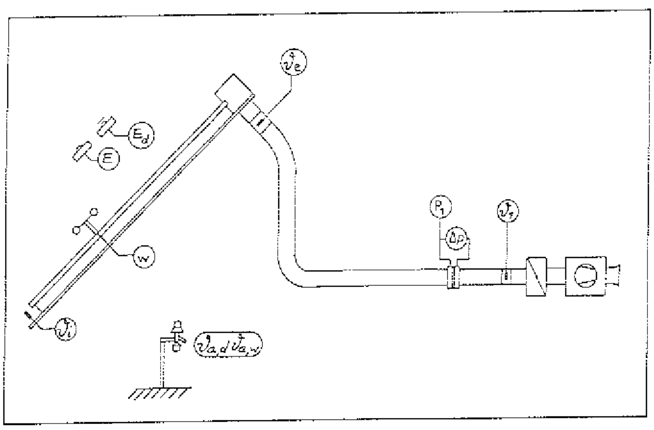

Fig. 2: Scheme of the test loop.

Therefore, the test loop, Fig. 2, has been designed as open loop in order to obtain test data under similar operating conditions as in practice. Calorimetric measurements of the useful energy output of a 10 m^2 collector module were carried out simultaneously with the recording of relevant meteorological data. Using the data acquisition system MADAS the following data are registered:

Collector loop:

ϑ_i = inlet temperature
ϑ_e = outlet temperature
Δp = pressure loss at the orifice plate of the air flow meter
ϑ_1 = temperature behind the orifice plate

Meteorology:

$\vartheta_{a,d}$ = dry bulb air temperature
$\vartheta_{a,w}$ = wet bulb air temperature
E = global solar radiation in the plane of the collector
E_d = diffuse solar radiation
w = wind speed
p_a = ambient air pressure

Based on a sampling rate of 1/20 s, 10-minutes mean values are directly computed by the data acquisition system. The useful heat output $\dot{Q}_u$ of the collector is calculated with the following equations:

$$\dot{Q}_u = \frac{\dot{m}}{1+x} c_{p,1+x} (\vartheta_e - \vartheta_i), \qquad c_{p,1+x} = c_{p,a} + x\, c_{p,v}$$

$$\dot{m} = \alpha\, \varepsilon \frac{d^2}{4} \sqrt{2 \Delta p\, \varrho_1}$$

$\dot{m}$ = mass flow rate
α = flow rate number
ε = $f(\vartheta_1)$ expansion factor
d = diameter of the orifice plate
ϱ_1 = air density at the location of the orifice plate
x = absolute humidity
$c_{p,a}$ = specific heat of air
$c_{p,v}$ = specific heat of water vapour

The efficiency written in usual terms as

$$\eta = \frac{\dot{Q}}{EA} = \eta_o - k_{eff} \frac{\vartheta_m - \vartheta_a}{E}$$

was determined with values of $E > 750$ W/m^2 and specific mass flow rates between 20 and 80 kg/hm^2. Since the specific heat capacity of air and the applied mass flow rates are relatively low, it is advisable to use the logarithmic mean temperature

$$\vartheta_m - \vartheta_a = (\vartheta_{stag} - \vartheta_a)\left(1 - \frac{1-e^{-x}}{x}\right)$$

with $\vartheta_{stag} - \vartheta_a = \frac{\eta_o}{k_{eff}} E$

and $x = \frac{A\, k_{eff}}{\dot{m}\, c_p}$

The experimental data are best fitted with η_o = 0.75 and k_{eff} = 13.3 W/m^2K. For practical purposes it is useful to plot the efficiency as a function of the specific mass flow rate, Fig. 3.

$$\eta = \eta_o \frac{1-e^{-x}}{x}$$

η is independent of E as long as k_{eff} can be assumed to be constant. Considering the small range of operating temperatures, $0 < (\vartheta_e - \vartheta_a) < 50$ °C, this simplified characterisation of the collector will be sufficient for the intended applications.

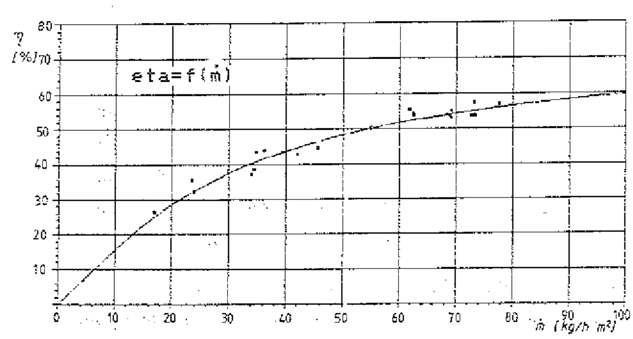

Fig. 3: Efficiency of the open loop air heating collector as a function of the specific mass flow rate.

8.5. Results of IEA-Task III Outdoor and Indoor Pyranometer Comparison

P. Ambrosetti, H.E.B. Andersson**, C. Fröhlich***, H.D. Talarek*

Five groups of pyranometers were investigated both indoors and outdoors. Calibration constants, day-long variability, tilt and seasonal effects were studied. Full characterization in laboratory was also performed for all 27 instruments.

- The experiments were designed very much from a consumer's point of view. The product in question was the pyranometer. Five groups of pyranometers were investigated, amounting to 27 pyranometers in total. With the exception of the K&Z CM5 instruments most of the other pyranometers were essentially new. (Serial numbers are indicative!)
- Manufacturers readily agreed to provide the instruments.
- The outdoor experiments were run at the World Radiation Center, Davos, Switzerland, providing the necessary World Radiometric Reference (WRR) on site.
- Indoor measurements to characterize the pyranometers were conducted at Statens Provningsanstalt, Boras, Sweden, providing the necessary fully automatized test equipment to cope with the extensive measurements.

The study was performed as part of the IEA Solar Heating and Cooling Program, Task III: Performance Testing of Solar Collectors.

With respect to the outdoor tests in Davos, Switzerland, a special set-up was required because of the large number of instruments: two bars of 5 m length were constructed and mounted on supports that allowed the instruments to be tilted towards the south. Four individual mounts were designed for the moving shadow bar pyranometers. An absolute radiometer PMO2 (used as the World Radiometric Reference) measured the direct radiation. Other meteorological parameters were also recorded. The entire system was connected to a sophisticated data acquisition unit that recorded all data including the mean of ten 1-second integrals read over a minute. The data analysis was performed on a CDC mainframe computer. Data were collected for more than 130 hours over a wide range of weather condition during summer and winter with the pyranometers in both horizontal and tilted positions.

For selected clear days, an absolute reference was available - that is the sum of the direct component measured with the PMO2 plus the diffuse component measured by the shaded pyranometer. For days with less favourable sky conditions, the arithmetic mean value of four instruments (2 Eppley PSP and 2 K&Z CM10) was used as a reference. The selection of these instruments was made on grounds of clear day performance.

Concerning the comparison of manufacturers and our calibration constants we first checked the calibration constants quoted by the manufacturers at standard calibration conditions, i.e. high irradiance, horizontal position, small incidence angle. (Table 1)

Pyranometer Manufacturer	Type	Instrument Number	Calibration Constants (mV/kWm⁻²) (Manufacturer)	(mV/kWm⁻²) (WRC Davos 81)	% - Deviation = (Manuf. Calibration / WRC Calibration) - 1 (-3 -2 -1 % +1 +2 +3 +4 +5)
EKO	STAR	81901	8.24	8.12	
EKO	STAR	81903	7.85	7.88	
EKO	STAR	81906	6.89	7.09	
EKO	STAR	81907	7.25	7.40	
EKO	STAR	81908	9.61	9.62	
EKO	STAR	81909	7.42	7.45	
EPPLEY	PSP	14806F3	9.81	9.78	
EPPLEY	PSP	17750F3	9.15	9.27	
EPPLEY	PSP	18135F3	8.78	8.92	
EPPLEY	PSP	20523F3	9.95	9.90	
EPPLEY	PSP	20524F3	10.10	10.01	
EPPLEY	PSP	20655F3	10.28	10.24	
KIPP & ZONEN	CM5	773656	11.94	11.72	
KIPP & ZONEN	CM5	773992	12.62	12.16	
KIPP & ZONEN	CM5	774120	13.41	12.80	
KIPP & ZONEN	CM5	785017	10.59	10.35	
KIPP & ZONEN	CM5	785047	12.23	11.87	
KIPP & ZONEN	CM10	790059	5.58	5.65	
KIPP & ZONEN	CM10	810119	4.58	4.59	
KIPP & ZONEN	CM10	810120	4.54	4.52	
KIPP & ZONEN	CM10	810121	4.66	4.62	
KIPP & ZONEN	CM10	810122	4.24	4.22	
SCHENK	STAR	1626	14.26	14.49	
SCHENK	STAR	2166	14.94	15.15	
SCHENK	STAR	2209	15.36	15.29	
SCHENK	STAR	2217	14.16	14.17	
SCHENK	STAR	2221	15.24	14.97	

Table 1: Comparison of calibration constants (mV/kWm^{-2})

We found best agreement for the new CM10 and PSP. The systematic bias of the CM5s is now widely recognized.

Short term values and day-long variability of pyranometers sensitivity are of prime interest for testing and monitoring purposes (Fig. 1 and Fig. 2)

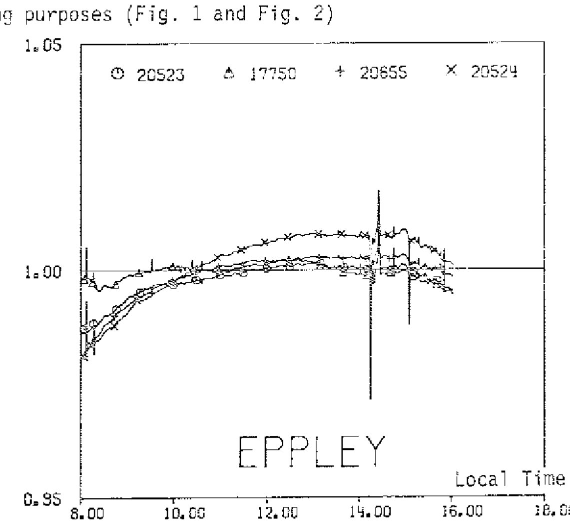

Fig. 1: Calibration constants, relative performance

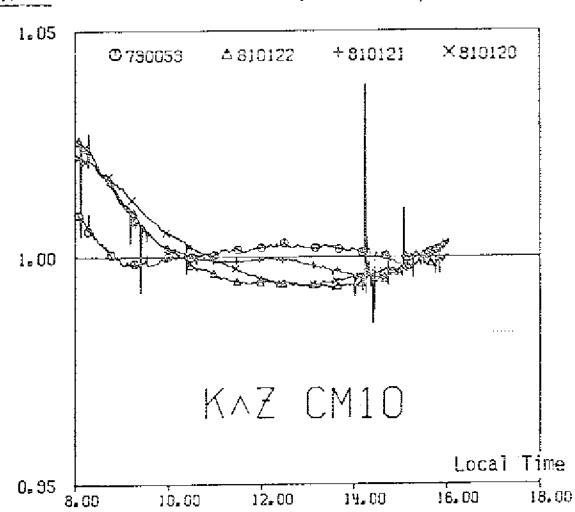

Fig. 2: Calibration constants, relative performance

The standard methods of testing the thermal performance of solar collectors require the same meteorological conditions as that for the pyranometer calibrations unless the collectors are tested in the tilted position. A possible sensitivity change of the pyranometer under inclined exposure is thus of major concern in collector testing applications. Tilt effects were, therefore, studied. The CM10, PSP and Swissteco did not show any appreciable change of sensitivity when the instruments were tilted, whereas the CM5, EKO and Schenk revealed a decrease of sensitivity.

The characterization of pyranometers took place in Boras, Sweden. Pyranometers of the thermoelectric type are designed to respond to short wave radiation. This sensitivity is cross correlated with interfering sensitivities of a number of parameters which are assumed to have a small combined effect on the instrument's performance. Many of these interfering sensitivities can be investigated by laboratory experiments which are designed to isolate a particular feature. Among those parameters which affect their sensitivity we find a number which are amenable to indoor measurements:

- the effect of tilt from the horizontal position (tilt effect)
- the effect of the intensity of solar radiation (deviation from the expected linear response, linearity)
- spectral distribution of the light source and the response of the instrument (spectral response)
- the temperature of the instrument body or the ambient air (temperature coefficient)
- the effect of transient irradiance and thermal shock (time constant)
- the effect of the angle of the incident solar radiation (azimuth and altitude, cosine error)

Results from the laboratory testing: the results of the temperature effects were encouraging. As found also by Dirmhirn (1979): the temperature effect was typical for a type or a group of instrument, the only exception being the EKO-star instruments where each instrument has its individual temperature coefficient.

The groups of K&Z CM5, Schenk Star and Swissteco instruments showed a "natural" temperature coefficient while the other groups of instruments (K&Z CM10, Eppley PSP) might be classified as slightly overcompensated.

The response of the instruments with respect to varying level of irradiance was linear to a very good degree (± 1 %). For the group of Eppley PSP, no deviations from a linear response could be observed.

The effect of tilt is most relevant for the application of pyranometers to solar collector testing purposes. The tilt effect is obviously cross-correlated with the level of irradiance. Three groups of instruments did not show any tilt effect: K&Z CM10, Eppley PSP, Swissteco. The K&Z CM5, the Schenk and EKO star instruments showed a tilt effect of comparable magnitude. It should be noted that these findings agree well with the outdoor investigations.

The directional response is rather unique to the instrument. However, all instruments showed a marked deviation from the ideal cosines response for angles of incidence greater than 60^{0}.

The intercomparison of indoor and outdoor results showed a remarkable correspondence between indoor characterization and outdoor performance of the pyranometers. However, this was usually only qualitative. The deviations found for some instruments could not be quantitatively accounted for by correction derived from indoor data.

We would not recommend use of pyranometers which show a tilt dependence. However, an instrument which is known to be tilt sensitive should be calibrated in a tilted position on the test site.

From our results, we would recommend that the Eppley PSP and the K&Z CM10 should be used for testing applications. The best instruments also demonstrated variability from summer to winter in typical test situations (clear sky) by ± 1 - 2 %. To account for the uncertainties of the calibration procedure, we claim an overall accuracy of ± 2.5 to ± 3 % for the measurement of global radiation under test condition for solar collectors.

Further investigators should strive to characterize the day-long performance of the pyranometer under study during a typical calibration day (referenced to a direct and diffuse measurement).

In addition, the following variables should be studied in the laboratory:

- temperature coefficient
- tilt effect (at different level of irradiance)
- the effect of irradiance level (linearity)

We do not recommend cosine measurements because of the present uncertainty associated with measurement technique.

ACKNOWLEDGEMENT

The authors would like to express their sincere appreciation to the fellow researchers of the IEA Solar Heating and Cooling Project for their assistance and support. The work was supported by the following institutions:

- The Swiss National Energy Research Foundation under coordination of the Swiss Federal Office of Energy,
- the Swedish Council for Building Research.

Participating laboratories:

* Swiss Federal Institute for Reactor Research, Würenlingen, Switzerland

** National Testing Institute, Boras, Sweden

*** World Radiation Center, Davos, Switzerland

References

1) M.R. Riches (ed) (1982). Proceedings of the International Energy Agency Conference on Pyranometer Measurements, 16-20 March, 1981, Boulder, Colorado, SERI/TR-642-1156R.

2) C. Fröhlich (1980). Results of a Pyranometer Comparison, IEA-Task III Report, Davos, 5-6 March, 1980.

3) I. Dirmhirn et al. (1979). Experience with Tests and calibrations of Pyranometers for a Mesoscale Solar Irradiance Network, Solar Energy, 22, 197-203.

4) K. Dehne (1980). Wichtige Spezifikationen von Pyranometern für Solarenergiebelange, Vol. 2, Proc. 2nd International Solar Forum, Hamburg.

5) R.J. Bahm, J.C. Nakes (1979). The Calibration of Solar Radiation Measuring Instruments, the University of New Mexico, Report BER 1 (79) DOE 184/.

6) J.R. Latimer (1971). Radiation Measurement, International Field Year for the Great Lakes, Technical Manual No. 2, Atmospheric Environment Service, Canada.

7) H.E.B. Andersson et al. (1981). Calibration and Testing of Pyranometers, National Testing Inst., Boras, Sweden.

IV. TECHNICAL DEVELOPMENT

9. ISOCHRONOUS CYCLOTRON

9.1. Cyclotron Operation and Improvement

*H.G. Böge, W. Bräutigam, H. Borsch, R. Brings, R. Fiedler, H.L. Hagedoorn**, *H. Hadamek, I. Jannakos, H. Lawin, J. Reich, A. Retz, N. Rotert, G. Schlienkamp, H. Schwan, P. Wucherer*

In 1983 the cyclotron JULIC was in operation for 43 weeks. The scheduled annual shut down time in the summer of normally 6 weeks had to be extended to 8 weeks because of two reasons: As there was an increasing demand for high intensity analysed beams at the magnetic spectrograph BIG KARL the cyclotron had to be operated over long times with high internal beam power. Because of the related radiation problems the maintenance and repair activities at the cyclotron could only be started after a delay of more than two weeks. Simultaneously a main transformer had to be exchanged against a bigger type to provide the power for the components of the ISIS-project. Therefore, essential equipment of the building was not available during this period. The beam time distribution for 1983 is given in table 1.

Cyclotron tuning and beam handling	490 h	6.8 %
Beam on target	4527 h	62.6 %
Beam time for experiments	5017 h	69.4 %
Beam development testing new components	671 h	9.3 %
CYCLOTRON OPERATIONAL	5688 h	78.7 %
SCHEDULED MAINTENANCE	213 h	2.9 %
SYSTEM FAILURES	1328 h	18.4 %
SCHEDULED OPERATING TIME	7229 h	100.0 %
BEAM TIME DISTRIBUTION		
Guest scientists (U.Bonn, U.Hamburg, U.Köln, U.Krakau, U.Mainz, U.Münster, U.Tübingen, GSI Darmstadt)	745 h	14.8 %
Scientist of KFA excluding IKP (ICH1-IME,-IRA)	575 h	11.5 %
Scientists of IKP	3697 h	73.7 %
BEAM TIME FOR EXPERIMENTS	5017 h	100.0 %

Table 1: Cyclotron time distribution in 1983.

Besides the routine operation and maintenance some modifications and improvements have been realized.

Several water leaks mainly at the tuning plates of the RF system caused severe vacuum problems. Even if the inner surfaces of the water channels in the aluminium plates of all dees have been coated with epoxy rersin some years ago, it could not be expected, that the corrosion was completely stopped by this measure. New elements consisting of copper plated aluminium sheet metal with soft soldered copper tubes were prefabricated as far as possible. The total variety of parts is available since spring 1983. So we could keep the losses in beam time short by exchanging the corroded elements subsequently against new devices. Special care had to be taken to operate old aluminium and new copper parts in one cooling circuit. To avoid possible corrosion problems the copper tubes are coated with epoxy resin too, up to the date the accelerating systems consists entirely of plates with copper water tubes. - The complete exchange is planned for the annual shut down period 1984.

The modification of the beam line vacuum system is on the way. A first set of six new turbomolecular pumps is in operation since the 1983 shut down period. Pumps and the associated measuring and control equipment perform well. The subsequent exchange of another 10...12 pumps has to be carried on.

A protection circuit for the septum was developed and installed. Even if a septum completely made of tungsten wires is used, which can stand approximately 3 kW internal beam power (instead of 1 kW with a septum of tungsten sheet metal) it is necessary to have a rapid beam switch off when working at the upper limits. Signals from the phase probes are used to stop the beam in the center region when the current becomes excessive.

Some measurements at the cyclotron beam were done to study the correlations between instabilities of important cyclotron parameters and external beam quality. These investigations have to be continued in order to define the stability of the Dee voltage and the frequency needed for a good and reproducible beam quality from the cyclotron.

First tests proved that the acceleration of fully stripped ions in 9ω-mode of operation of the cyclotron is possible. Deuteron beams of 8 MeV could be successfully extracted from the cyclotron with intensities of up to 100 nA (see also chapter 9.6).

Besides these activities related to the operation of the cyclotron the major part of work was dedicated to the realisation of the project ISIS (see chapter 9.3).

*Eindhoven University of Technology, Netherlands

9.2. Measurement of Transfer Coefficients and Improvements in the Beam Handling System

M. Rogge, J. Reich, L. Zemło, J.G.M. Römer,
G. Berg, H. Hagedoorn, G. Hlawatsch, H. Lawin,*
J. Meißburger, W. Oelert, G. Riepe, P. v. Rossen,
D. Protić, M.D. Trivedi, P. Turek

The measurement of the beam line properties was continued[1] with a two dimensional position-sensitive Si-detector with improved spatial resolution. The center of gravity could be determined with an accuracy of about 0.05 mm. A thick foil at the entrance slit DS1 (Fig. 1) of the monochromator was used to become independent of changing cyclotron beam properties. Essentially the dispersive plane (x-coordinate) was investigated.

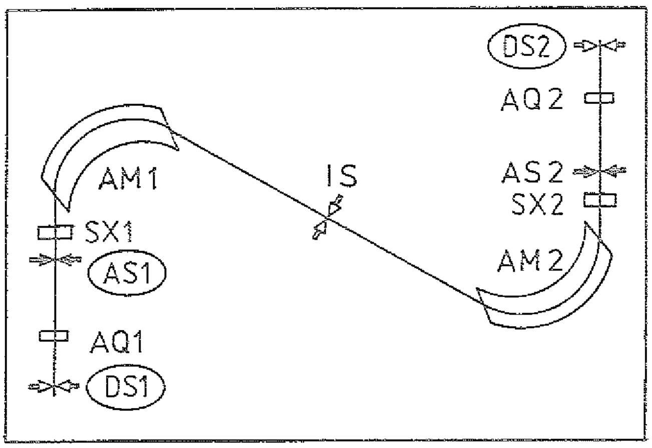

Figure 1: Double monochromator system with the arrangement of quadrupoles (AQ), sextupoles (SX) and slits (DS, AS, IS).

The measurements allowed to improve the beamline mainly in two points:

1. The monochromator was adjusted to second order for focussing from DS1 to DS2 in the horizontal plane as shown in fig. 2. The achieved accurary was $\Delta x(\theta_{in}) = 0.15$ mm. Here $\Delta x(\theta_{in})$ means the shift of the center of gravity of a pencil beam within the working range of $\theta_{in} = \pm 6$ mrad.

   The measured second order aberration was simulated in the calculations by thin identical sextupole lenses at the entrance of the dipole AM1 and the exit of AM2. The upper part of fig. 2 shows the original situation. The measured points correspond to centers of gravity of a typically 0.5 mm wide beam spot. The background is calculated with the simulated sextupoles only. In the middle part second order effects are compensated by the sextupoles SX1 and SX2 in calculation and measurement. The lower part shows the result of first and second order final adjustment for energies corresponding to Bρ-values of 698, 1590, 1913 kG·cm, respectively. (In the $E_p = 23$ MeV-curve the effect of a small deadjustion of the Bρ-values of the dipoles AM1/AM2 is demonstrated.) The strong deviations from the design values can thus be explained by inherent quadrupole and sextupole components, but their origin cannot be localized by the position of simulated lenses in TURTLE[2]-calculations.

There is still one free parameter in the sextupole and quadrupole-settings of the monochromator, corresponding to a not measured image at IS. Concerning the second order focussing all sextupole fields which follow the relation

$$B(SX1) + B(SX2) = C; \; C = -0.8\cdot(B\rho/2000)$$

give the same quality of the focus at DS2 for a B(SX1) variation from 0 to 100 % of C in the measured Bρ-range. A similar formula holds for first order focussing and all Bρ-values up to the region of saturation. Both relations have been measured to be valid with the same precision $\Delta x(\theta_{in}) = 0.15$ mm.

For the formerly used settings of the sextupoles the constant C was practically zero. This explains that almost no change was seen before[1], if the field strength of SX1 and SX2 was varied simultaneously from 0 to 600 % of the calculated value.

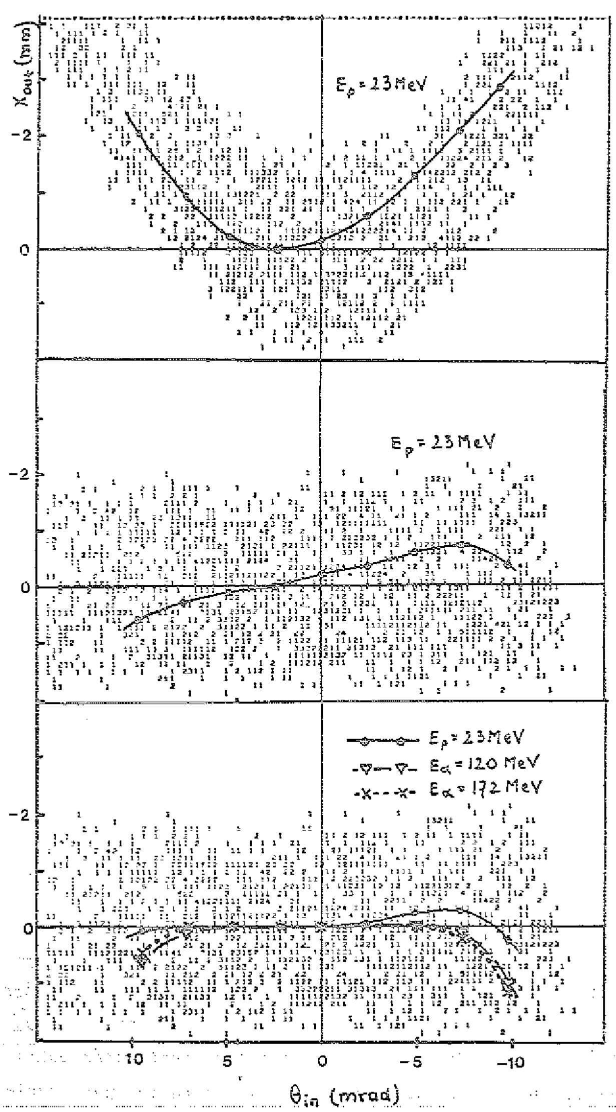

Figure 2: Stepwise improvement in adjustment of monochromator focussing in comparison with TURTLE[2] calculations in the background, θ_{in} = entrance angle of the beam at DS1, x_{out} = exit position of the beam at DS2.

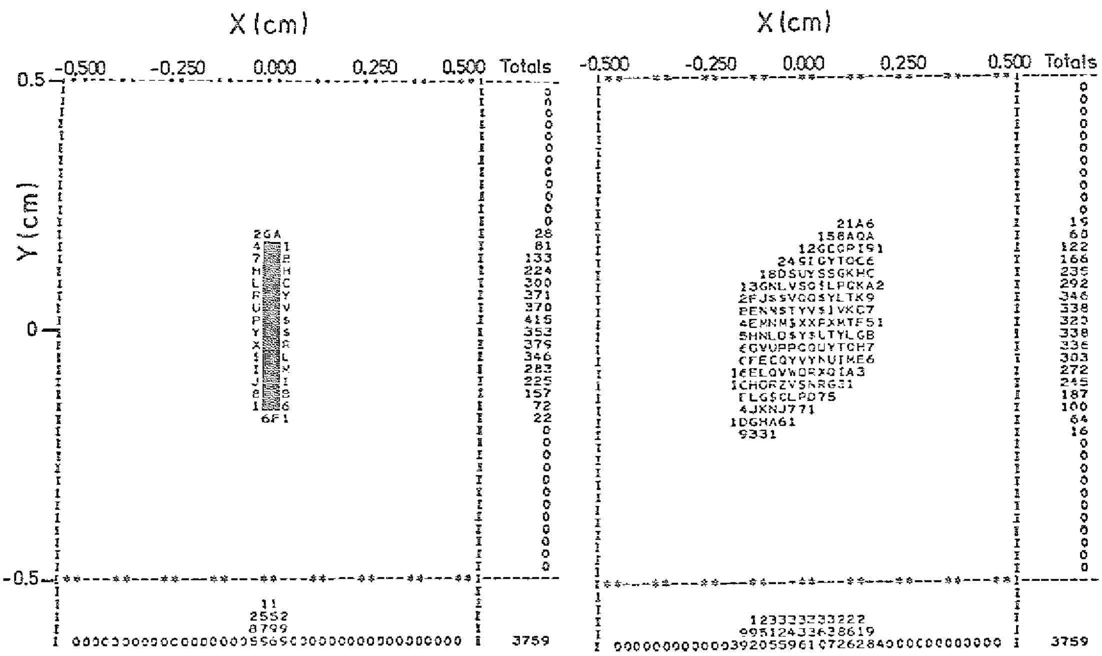

Figure 3: Influence of a small turn of the second quadrupole lens before the target on the beam profile (TURTLE calculations). Angle of turn around the beam axis $\psi = 0.4^{o}$. Left side: on the target, dark area represents the beam size for $\psi = 0$. Right side: 10 cm behind the target.

2. A "tilting" of the image on the target was eliminated. After the correct first and second order focussing at DS2 it became evident, that the "tilt" or "blow-up" of the image of DS2 was a first order effect. It was traced back to the misalignment of (at least) one quadrupole in the beam line, which was rotated around the beam axis by only 0.4^{o}. The extreme sensitivity to such rotation is demonstrated in fig. 3.

At the image point the main effect is a broadening of the image changing the dispersion of the beam. If the field strength in one of the quadrupoles (not necessarily the misaligned one) is changed by $\approx$ 1 % the shift of the focus point results in an apparent "tilt" of the image which easily can amount to 120^{o}. The coupling between x and y-coordinates transfers changes in x to y and results in a characteristical additional "steering".

A correction of the misalignment by a weak quadrupole which is turned by 45^{o} around the beam axis is in principle possible. Here a mechanical correction was preferred.

After these two adjustments the focussing from DS1 through the whole beam line to the target at the magnetic spectrometer BK was measured to be $\Delta x(\theta_{in}) \approx 0.15$ mm. This is to be compared with a 0.5 mm (monoenergetic) image of a 1 mm aperture in DS1.

References

1) H.G. Böge, W. Oelert, J. Reich, G. Riepe, J.G.M. Römer, M. Rogge, P. Turek, L. Zemło, IKP-Annual Report 1982, KFA, Jül-Spez-222 (1983) 102

2) K.L. Brown, Ch. Iselin, Report CERN 74-02, February 1974

*Eindhoven University of Technology, Netherlands

9.3. Progress of ISIS

The progress of the project ISIS[1-4] (Injektion schwerer Ionen nach EZR-Stripping: Injection of heavy ions after ECR-stripping) in 1983 is described for the different subsystems (see figure 1).

1. ECR-Source

H. Beuscher, W. Briell, R. Fiedler, W. Krauss-Vogt, H.-G. Mathews, A. Retz, U. Rindfleisch

The superconducting magnet system of the ECR-source[2] has been delivered in July. A cold leak in the He-tank of the cryostate had already been detected at the factory at LN_2-temperature. The system has been set up in Jülich to test the magnetic properties of the superconducting coils and to determine the He losses to decide whether the He-tank had to be repaired or not. The solenoid coils have been energized to the full current without any quench supplying a magnetic field required for ECR (electron-cyclotron-resonance) at 18 GHz microware frequency. The training of the hexapole has been interrupted at 60% of the full current. Since the He consumption was a factor of 5 to 6 higher than proposed a search was started to localize the cold leak first at the institute (IKP) and later at the BBC factory. In the meantime the leak has been found and repaired. If another leak test at LN_2-temperature is successfull the magnet system will be back at the institute in the beginning of 1984.

The main vacuum chamber, which was built by the company "Balzer Hochvakuum GmbH", has been delivered in fall.

A first plasma stage designed for an overdense plasma[5] and a flexible extraction system are under construction.

A power supply including remote control and safety system for a 14 GHz 2 kW Klystron (Thomson CSF) will be delivered by the "Laboratorium für Mikrowellenanwendungen, Dr. Beerwald" in March 1984.

Computer calculations have been started to optimize the ion extraction from a plasma in a strong magnetic field. First results are presented in chapter 9.5.

The work on the Pre-ISIS test sources has been continued. The results of the latest version Pre-ISIS 2* are reported in chapter 9.4.

2. Beam Handling and Axial Injection System

W. Bräutigam, W. Briell, R. Fiedler, A. Retz, J. Reich, U. Rindfleisch, P. Wucherer, M. Agena[+], K. Euler[+], D. Rosendahl[+]

The magnetic elements and power supplies for the beam handling and axial injection system have been manufactured by the company "Bruker Analytische Meßtechnik GmbH" (except the components LH_0, LM and H, see figure 1). Emphasis has been given to watch and accompany the various magnetic field measurements of the elements done by the manufacturer by appropriate TRANSPORT[5] and TURTLE[7] ion optics calculations[8]. At the end of the year the magnetic field measurements and their evaluation was completed and the main parts of the system, the 180°-bending system and the 90°-bending system with matching section in front, were under assembly and adjustment on separate bases partly with vacuum chambers.

Together with the manufacturer a cycling procedures has been tested successfully for a reproduction of the magnetic fields within ± 0.3 G.

After it has been confirmed that the pre-ISIS 2*-source (see also chapter 7.4) is also a powerful external light ion source (LIS) the related beam handling and charge analysis components have been determined to be another solenoid (LH_0) and a Wien-filter in an adjacent box (see figure 1).

All adjustment bases and supports for the beam line components including those for quick access to the ones in the 4 m thick wall have been designed and are now manufactured.

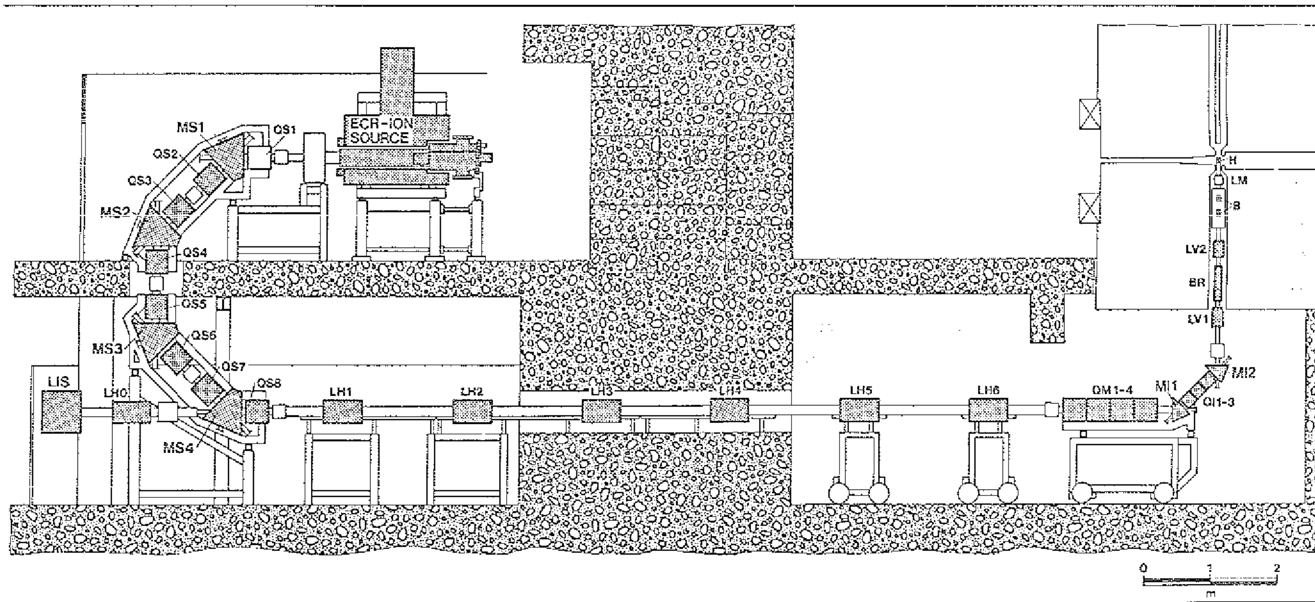

Figure 1: Layout of the project ISIS at JULIC: LIS-light ion source; QS, QM, QI-quadrupole magnets; MS, MI-dipole magnets; LH, LV-solenoid lenses; BR-beam rotation solenoid; B-bunching system; LM-magnetic lens; H-hyperboloid inflector.

The design of the vacuum system has been revised[9] and the logic of the process generating and surveying a vacuum of better than 10^{-7} mbar with cryo-pumps[10] in the beam pipe has been worked out.

The complex axial hole insert which will house the solenoids LV1, 2 and BR, the bunching system B, the magnetic lense LM, the cyclotron pole insert and the hyperboloid inflector H has been designed and given for manufacturing by the end of the year.

The design of the strong magnetic lense LM (17 cm focal length) has been revised. The glaser-type lense has been built in the IKP.

A system consisting of two double gap bunchers built at and for the Bonn isochronous cyclotron has been investigated. The bunchers related with appropriate amplitude and phase shift to the first and second harmonic of the cyclotron frequency gave a very satisfactory beam intensity enhancement of a factor 6. The Bonn cyclotron crew will built a similar device for the ISIS project.

The former ion source test magnet is being modified to serve as a test bench at a temporary position just after the 180°-bending system for debugging the axial hole insert prior to the installation in the cyclotron.

Prototypes of the beam diagnosis and steering elements to be used for beam tuning[11] are being tested.

3. Cyclotron

H.G. Böge, W. Bräutigam, W. Briêll, A. Retz, U. Rindfleisch, P. Wucherer

The original h=3 RF-center region design[4] has been revised and corrected using Runge-Kutta orbit calculations following threedimensional relaxation to generate realistic electric fields (see also chapter 9.6.). The mechanical center region design requires that the minimum distance in axial direction between RF-conducting and grounded parts is reduced considerably. Using a spacer between Dee and Dummy Dee the electric field has been increased from 18 to 30 kV/cm. No reduction in the conditionned RF-voltages has been encountered during several months of cyclotron operation. The mechanical center region design also requires that the upper and lower magnetic pole insert are no longer mirror symmetric to the cyclotron midplane[12]. In a first step of an iterative procedure the magnetic field in the cyclotron center has been mapped for a first set of pole inserts. The evaluation of the data with respect to midplane distortion is in progress.

The necessity for an improvement of the cyclotron vacuum system becomes evident from table 1 which gives the transmission TR for some typical ions from the ISIS ECR-source at different cyclotron energies at two different tank pressures p. The table has been calculated from

Ion	T/A MeV/A	K_1	K_2	K_3	K	Transmission $5\cdot10^{-6}$ mbar	Transmission $2\cdot10^{-6}$ mbar
$^{20}Ne^{10+}$	22	19.8	-	-	19.8	48%	74%
$^{20}Ne^{10+}$	44	6.8	-	-	6.8	77%	90%
$^{20}Ne^{7+}$	22	9.1	1.6	4.7	15.4	56%	79%
$^{12}C^{4+}$	22	2.8	1.9	9.0	13.7	60%	81%

Table 1: Beam transmission through the cyclotron for some ion species and energies for two different tank pressures.

$$TR=EXP(-3.35\cdot10^{16}\cdot p\int_0^L\sigma(s)ds)=exp(-K\cdot10^4 p) \quad (1)$$

evaluating the above integral from available data for three energy regions during acceleration as K1, K2, K3 for which the conditions $\sigma_c \gg \sigma_1$ (K1) and $\sigma_c \ll \sigma_1$ (K3) hold. σ_c denotes the cross section for an ion charge change by electron capture, σ_1 the one by electron loss.

Calculations and associated measurements reveal that a figure of $<2\cdot10^{-6}$ mbar can be expected if the present pumping speed of 12... 13000 l/s will be improved by the installation of three cryopumps with pumping speeds of 10000 l/s each. Two of these pumps have already been installed at the cyclotron and worked well during first tests.

4. Instrumentation

H. Borsch, W. Bräutigam, R. Brings, K.P. Kruck, A. Müller, N. Rotert

The universal control module UFB[13] which mainly will handle the manual and computer control of the ISIS power supplies has been tested successfully. A driver has been written for its CAMAC interfacing and tested at the same time. A set of 30 modules for the ISIS project but also for the external beam line is presently under fabrication.

In a factory acceptance test 5 power supplies different in type have been tested[14]. The non sufficient long term stability of two types has been cured meanwhile.

Some of the existing hard- and software for the computer control of the external beam line has already been extended or modified to serve for ISIS purposes, especially the FLUKE-scanning system for data aquisition.

The newly developed module for beam current monitoring is now used very satisfactorily in the external beam line. A set of 10 modules is under fabrication.

The control logic for the ECR-source vacuum system comprising 4 pumping sections equipped with 4 cryo- and 2 turbomolicular pumps has been worked out[15]. It is now being implemented using the SIEMATIC S5 system (Siemens programmable logic control system).

The automated control of the ISIS beam line vacuum system[16] comprising 3 beam path sections equipped with 8 cryo- but also some turbomolecular pumps uses the Siemens SMP-microprocessor system. The related prototype hardware and the basic software written in PL/M-85 have been tested successfully at one vacuum test section. The fabrication of the complete hardware and the implementation of the final software is under way.

5. Installation and Building

H. Pabich[*], A. Retz, G. Schlienkamp

To provide the power for the ISIS components (400 kW connected power in total) one of the main transformers has been exchanged. The different power lines are now ready as well as the various cable racks. The existing water-cooling system has been extended for the ISIS purposes. The floor plans for placing the ISIS electronic and auxiliary devices have been worked out and the 20 racks have been ordered.

The shielding against the expected Roentgen-radiation from the ECR-source has been delivered and partly errected.

References

1) Erläuterungsbericht und Planungsunterlagen zum Projekt ISIS, März 1981
2) H. Beuscher, H.G. Mathews, C. Mayer-Böricke, J. Reich, Proc. 9th Int. Conf. on Cyclotrons and their Applications (Caen, 1981), Hrsg. G. Gendreau (1982) p. 285
3) R.K. Bhandari, J. Reich, Proc. 9th Int. Conf. on Cyclotrons and their Applications (Caen, 1981), Hrsg. G. Gendreau (1982) p. 261
4) L. Aldea, J. Reich, P. Wucherer, Proc. 9th Int. Conf. on Cyclotrons and their Applications (Caen, 1981), Hrsg. G. Gendreau (1982) p. 461
5) H.-G. Mathews, H. Beuscher, C. Mayer-Böricke, Physica Scripty, Vol. T3, p. 52, 1983
6) K.L. Brown, D.C. Cary, Ch. Iselin, F. Rothacker, Report CERN 80-04, March 1980
7) K.L. Brown, Ch. Iselin, Report CERN 74-02, February 1974
8) J. Reich, ISIS-note 1, April 83
9) P. Wucherer, ISIS-note 5, April 83
10) P. Wucherer, ISIS-note 4, April 83
11) J. Reich, ISIS-note 2, April 83
12) P. Wucherer, U. Rindfleisch, ISIS-note 7, May 83
13) W. Bräutigam, ISIS-note 8, October 82
14) W. Bräutigam, ISIS-note 10, June 83
15) R. Fiedler, A. Müller, ISIS-note 11, December 83
16) K.P. Kruck, N. Rotert, ISIS-note 9, May 83

[+]University of Bonn, F.R. Germany

[*]KFA Jülich

9.4. Pre-ISIS 2 * - a two stage ECR source for highly stripped light heavy ions

H.-G. Mathews, H. Beuscher, R. Fiedler, W. Krauss-Vogt

Because of the delay for the delivery of the ISIS ECR source[1,2] superconducting magnet system the development of the small ECR source pre-ISIS 2 [3,4] could be continued in 1983.

Based on a proposal of the Berkeley ECR source group the easy axis of the Sm Co_5-hexapole bars inside the pre-ISIS 2 source was turned by 90 degrees to achieve an azimutal magnetization of the hexapole. In this way the heating up of the vacuum chamber was considerably reduced. Replacing the so far used O-ring gaskets, which had sometimes been destroyed because of microwave absorption, by copper or indium seals the background vacuum pressure of the source was lowered to $5 \cdot 10^{-8}$ mbar resulting in a better output especially for the higher ion charge states.

A new support structure for the extraction system gave more pumping speed to the ion extraction area. The problems associated with neon cryopumping have been solved by the installation of an adequate thermal buffer plate between the condensation surface and the head of the second refrigerator stage of the cryopump.

Tests with an overdense plasma stage at 2.45 GHz[5] as an injector stage for the pre-ISIS 2 source had failed - probably because the plasma density injected into the second stage was above the cut-off density for 5 GHz. The energy of the ions from the overdense stage was found to be well below 5 eV, therefore the decision was made to try the overdense plasma stage as injector for the higher frequency 14-GHz-ECR stage of the superconducting ISIS source[1]. For pre-ISIS 2 a 5 GHz ECR-injector stage was set up, which worked very satisfactorily. Figure 1 shows a schematic drawing of the new two stage source, pre-ISIS 2 *, together with the axial and the radial magnetic field distribution. The magnetic resonance field for the

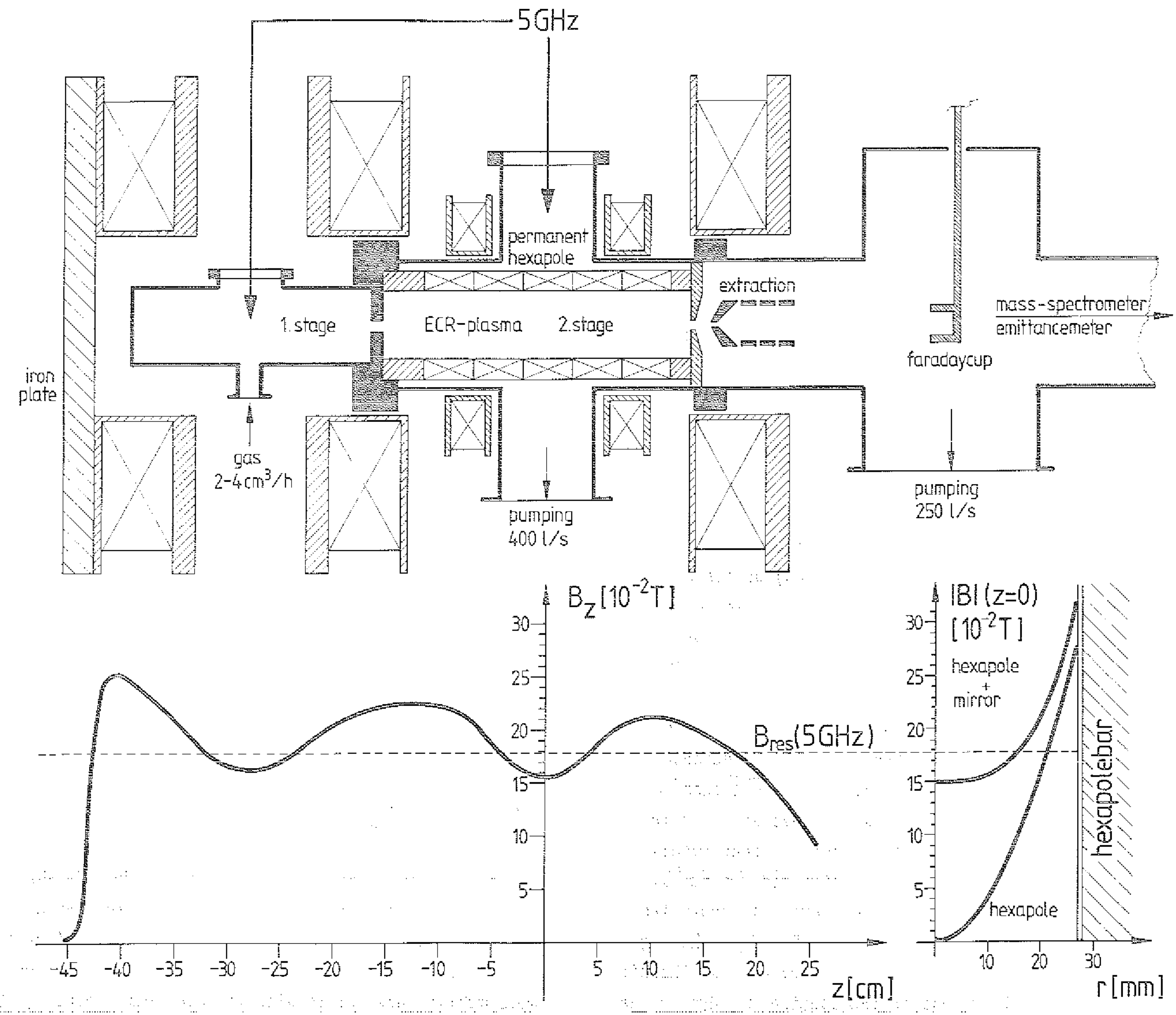

Figure 1: Schematic drawing of the pre-ISIS 2 * ECR-source including the axial and the radial magnetic field distribution.

injector stage was achieved by adding another watercooled solenoid and an iron endplate to the original pre-ISIS 2 arrangement. The power consumption of the 3 main coils and the 2 additional coils, which determine the mirror ratio of the second stage, is about 46 kW.

The microwave power for the injector plasma stage is delivered by the same 5 GHz klystron as for the hot plasma stage. By means of an E-H-tuner and a circulator a defined part of the incident microwave power to the second plasma stage is reflected and guided through a quartz window into the first stage. The reflected power from this plasma stage is dumped in an isolator. The microwave power consumption for the production of carbon, nitrogen and oxigen ions was in the order of 300 W and for argon ions less than 600 W.

The ions produced inside the injector stage - mainly charge state 1 - enter the second plasma stage through an 8 mm bore. There is no additional pumping needed for the first stage.

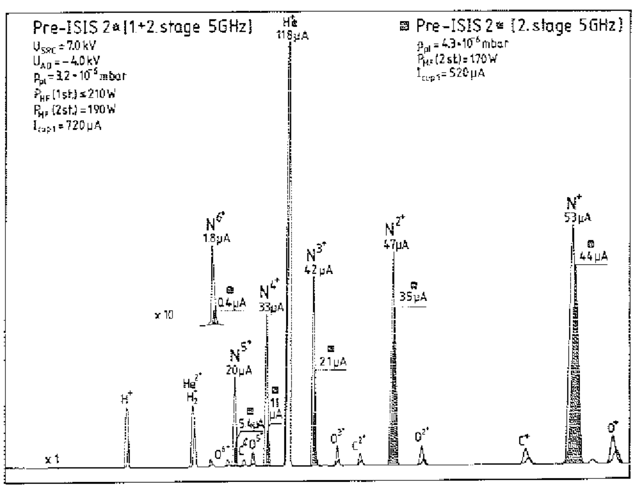

Figure 2: Spectra of nitrogen ions from pre-ISIS 2 * with and without plasma in the injector stage.

Figure 2 gives two nitrogen spectra from pre-ISIS 2 * showing the improvement by the injector plasma stage. A remarkable increase in higher nitrogen charge states is observed, when the first stage is turned on. In connection with this effect a drop of neutral gas pressure in the second stage is found. This indicates that mainly ions enter the second stage, which leads to a reduced probability for charge exchange with neutral atoms. At the same time the total ion intensity from the source increases by about 40 %. The numbers attached to the nitrogen peaks in figure 2 are measured currents obtained at 1.3 m from the source exit in a mode with strongly reduced resolving power of the analysing system and optimized transmission. Figs. 3 and 4 are typical spectra of carbon-13 and nitrogen-15 enriched gas mixtures from pre-ISIS 2 *, showing also the fully stripped carbon and nitrogen ions. The high contribution of helium ions in the spectra is due to the addition of helium gas to the working gas nitrogen, which leads to a more stable and effective operation of the source. Fig. 5 demonstrates the effect of mixing a lighter gas to the gas to be ionized in pre-ISIS 2 *. Adding nitrogen to argon strongly shifts the charge distribution for

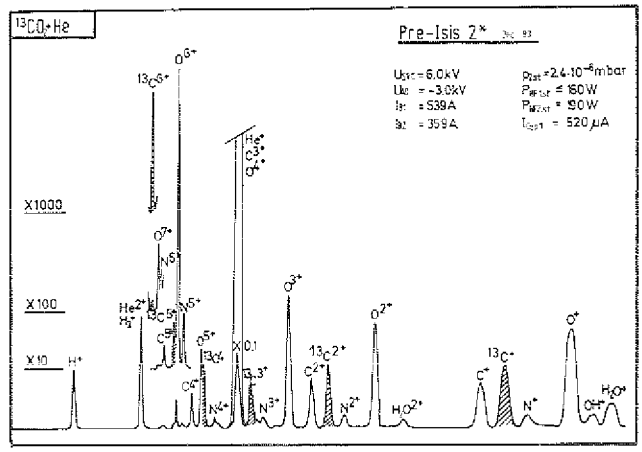

Figure 3: Spectrum of carbon-13 ions from pre-ISIS 2 *.

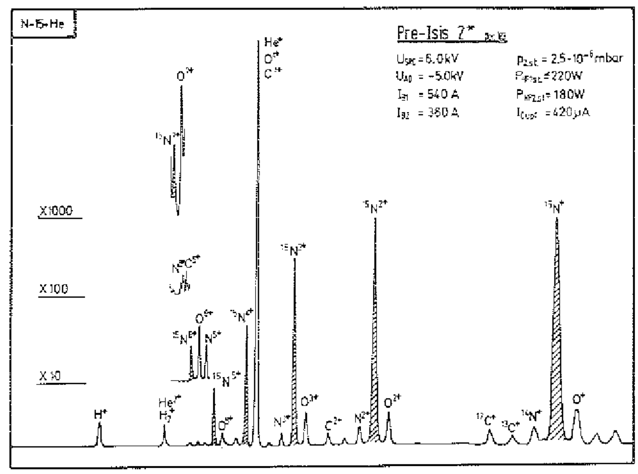

Figure 4: Spectrum of nitrogen-15 ions from pre-ISIS 2 *.

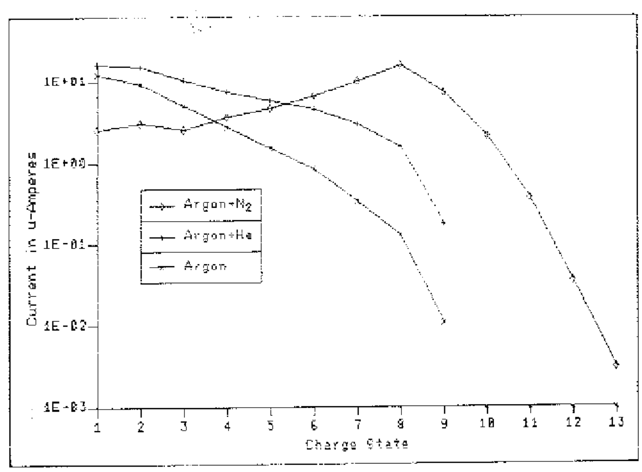

Figure 5: Argon charge states from pre-ISIS 2 * for different gas compounds.

the argon ions to higher charge states, whereas the charge distribution for nitrogen gets worse compared with fig.2. This leads to the assumption, that the heavier ions may achieve a better confinement at the cost of the lighter, more mobile ones. It is also visible from figure 5, that helium is less efficient than nitrogen as additional gas. As another result it can be stated, that the accepted microwave power rises with the effectiveness of the compound gas (Ar: 160 W, Ar + He: 250 W, Ar + N_2: 580 W), probably leading to a higher average energy of the plasma electrons.

The energy spread of the extracted beam was investigated for ions from the injector plasma stage and from the second plasma stage with both stages in operation. Due to the low electron energies and the poor confinement the energy spread for ions from the injector plasma stage is about 2 eV. For ions leaving the hot plasma stage of the source the energy spread was determined to be about 5 eV. Because of the sheeth potential between the confined plasma and the wall of the second stage vacuum chamber the energy of the extracted ions is about 20 to 30 eV per charge higher than given by the source potential power supply. The value for the sheeth potential strongly depends upon the microwave power applied to the source.

The radial emittance of the extracted nitrogen beam after momentum separation was measured to be $\varepsilon_{90\%}$ = (294±45) mm mrad for N^{1+}, $\varepsilon_{90\%}$ = (241±36) mm mrad for N^{2+} and $\varepsilon_{90\%}$ = (200±30) mm mrad for N^{3+} with 6 kV source potential. The emittance of the total beam from the source at 6 kV lay within a phase space of $\varepsilon_{90\%}$ = (420±63) mm mrad. This indicates, that almost the total beam out of pre-ISIS 2 * can be accepted by the Jülich cyclotron, which has an acceptance of 500 mm mrad due to the hyperboloid inflector.

Table 1 comprises the intensities per charge state for the different gases obtained from pre-ISIS 2 * as a source for light heavy ions.

For the light ions up to α-particles pre-ISIS 2 * works best as a single stage source with the first stage solenoid not energized. The ion intensities obtained in this way after momentum separation are represented in fig. 6.

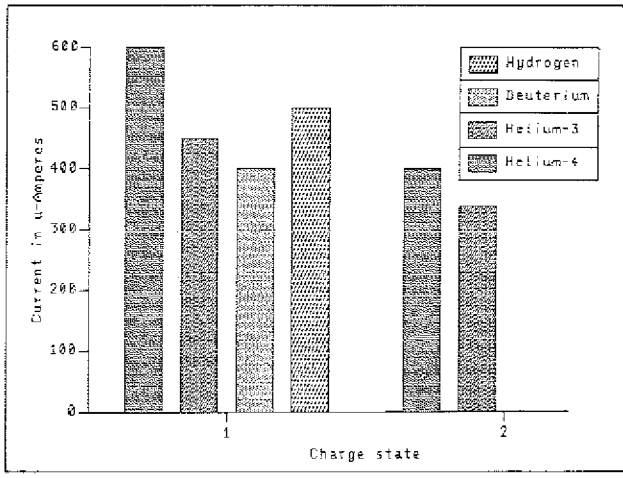

Figure 6: Beam currents from pre-ISIS 2 * working in the light ion source mode.

With a total power consumption of about 60 kW and a gas consumption of less than 5 cm^3 per hour pre-ISIS 2 * is one of the less expensive sources for α-particles in the hundreds of μA range and highly stripped light heavy ions.

GAS \ charge state	1-3	4	5	6	7	8	9	10	11	12	13
C-13	>30μA	17μA	1.6μA	30nA							
N-15	>40μA	36μA	18μA	1μA	16nA						
O-16	>40μA	37μA	36μA	11μA	170nA	( )					
Ne-20	>40μA	36μA	12μA	2.1μA	340nA	15nA					
Ar-40	>20μA	8μA	6μA	7μA	10μA	15μA	7μA	2.2μA	370nA	35nA	3nA

Table 1:
Intensities of light heavy ion species obtained from pre-ISIS 2 * at 6 kV after momentum separation.

References

1) H. Beuscher, H.-G. Mathews, C. Mayer-Böricke, J. Reich, Proc. 9th Int. Conf. on Cyclotrons and their Applications, Caen, 1981, Hrsg. G. Gendreau (1982) 285

2) H. Beuscher, H.-G. Mathews, J. Reich, IKP-Annual Repoert 1980, Jül-Spez-99 (1981) 152

3) H.-G. Mathews, H. Beuscher, R. Fiedler, W. Krauss, IKP-Annual Report 1982, Jül-Spez-202 (1983) 109

4) H.-G. Mathews, H. Beuscher, W. Krauss-Vogt, Proc. Int. Ion Engineering Congress - ISIAT '83 & IPAT '83, Kyoto/Japan (1983) 209

5) H.-G. Mathews, H. Beuscher, C. Mayer-Böricke, Proc. Symp. on Production and Physics of Highly Charged Ions (Stockholm 1982), Physica Skripta, Vol. T3 (1983) 52

9.5. Computer Calculation on the ECR Ion Source extraction

W. Krauss-Vogt, H. Beuscher, H.-G. Mathews

A computer code has been installed to study the ion extraction and beam formation for the ISIS ECR-source[1]. The code determines the ion trajectories in combined electrostatic and magnetic field configurations[2].

Of special interest is the influence of the strong axial magnetic field of the source. This field decreases in the case of 14 GHz microwave frequency for the ECR-plasma from 7.6 kG at the exit of the source to 0.14 kG at about 1 m downstream where the ions enter the 180° bending system of the beam line to the cyclotron[3]. If the ions would follow the diverging field lines of the decreasing field the result would be a strongly diverging beam. Under such conditions an efficient beam transport to the cyclotron could be difficult.

Therefore the first calculations have been carried out to understand this influence of the decreasing magnetic field on the extracted ions. The results are given in figure 1. An accel-decel extraction geometry consisting of the plasma electrode, a puller and a decel electrode has been used. Figures 1a) and b) show the ion trajectories along the first 30 cm behind the source, part a) is the case with and b) without magnetic field.

These results indicate that the fringing field has no defocussing effect but acts like a magnetic lens producing a beam waist at a distance of about 17 cm from the exit of the source in this special case. In the case without field (Figure 1b) this waist does not appear but the ion trajectories are steadily diverging behind the acceleration gap.

For program technical reasons it was necessary to start a second run in order to follow the beam envelope over the full distance from the plasma electrode to the entrance of the bending system. Because of the focussing effect of the fringing field only one additional optical device, namely a solenoid lens at z = 98.5 cm behind the plasma electrode has been inserted. Figure 1c), which is the continuation of figure 1a), shows that the slightly diverging beam can be focussed before entering the bending system, but further calculations are necessary to investigate the emittance matching of the extracted beam to the adjacent injection line.

Another point to study is how the beam quality is determined by the geometry of the plasma electrode.

References

1) H. Beuscher, H.-G. Mathews, C. Mayer-Böricke, J. Reich, Proc. 9th Int. Conf. on Cyclotron and their Applications (Caen, 1981) p. 285
2) W.B. Herrmannsfeld, SLAC-226 UC28 1979
3) R.K. Bhandari and J. Reich, Proc. 9th Int. Conf. on Cyclotrons and their Applications (Caen, 1981) p. 261

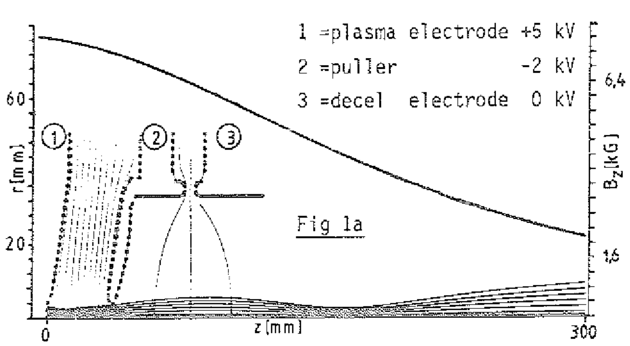

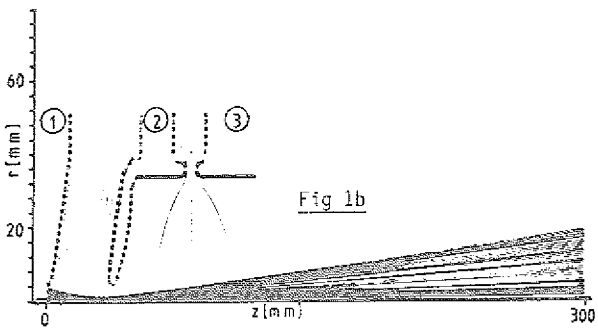

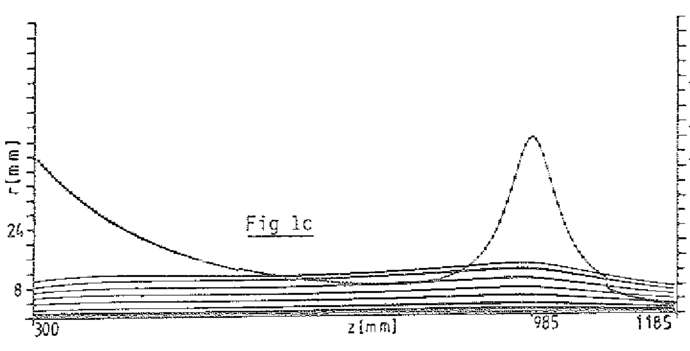

Fig. 1: Ion trajectories behind the ECR-source for M/Q = 2

a) First 30 cm behind the plasma electrode with magnetic field

b) Same part without field

c) Continuation of part a) from 30 cm behind the plasma electrode to the entrance point of the 180° bending system with an solenoid lens.

9.6. Check of the ISIS-center-region

P. Wucherer, H.L. Hagedoorn, U. Rindfleisch*

The center region had to be redesigned for the project ISIS[1]. The principal physical design was already fixed in 1980 [2], because the coordinates of the beam entrance hole in the pole plate had to be fixed early for technical reasons. The details of the center region geometry, however, can be changed more easily: e.g. a puller change takes only a few hours to get the cyclotron operational again. The design has therefore been performed in two steps: For the first step a self optimizing procedure[2] (IONAN) was used having a fast analytical calculation of the orbits. This, however, requires a simplification for the fields: the magnetic field must be homogeneous and the electric field shape sharply cut off at the boundaries of the acceleration gaps. In the second step, reported here, the electric field distribution in the regions of the first and second gap is calculated by a 3-dimensional relaxation code (RESEKT) and the orbits are integrated by the Runge-Kutta method. The output parameters from the IONAN-procedure were used as input parameters for the Runge-Kutta integration but with realistic electric fields.

The beam envelope of 27 particles representing a phase space area of $160 \cdot \pi$ mm·mrad and $\pm 20^0$ RF-phase width at the start (exit of the inflector) are shown in fig. 1 (upper part, case A, hatched area). For comparison the envelope of the IONAN-calculation is displayed as well (blackened area).

As a result of a mechanical design study[3] it turned out that the designed puller did not match with the necessary spatial shape of the hyperboloid inflector casing. This fact is not yet taken into account in the upper part of fig. 1. The beam is off centered by 6-7 mm. The energy gain is too small and the envelopes are much broader because of a higher degree of nonlinearity for the acceleration in the first gaps. This has been investigated more closely and confirmed by looking at the energy gain, RF-phase, etc. as a function of gap number, geometrical phase space, etc. Two examples of such figures are presented. In fig.2, the energy gain per turn for deuterons is diplayed vs. the number of the accelerating gaps. In the IONAN-calculations with sharp cut off electric fields the energy gain is close to the maximum of 41 keV except in the first gap (not shown in fig. 2). Using realistic electric field shapes but the identical input parameters the energy gain is much too less and oscillates within a period of six gaps i.e. one turn. This corresponds with the motion of the orbit centers in the median plane shown in fig. 3. The motion inside a gap is represented by a straight line showing the energy gain (length) and gap angle (direction) but the orbits do not move in between two gaps. The center of gravity of the orbit centers of the last (six) gaps is a measure for the beam centering. The parameters of case A in fig. 3 are identical with those of fig. 2 (case A). The off centering of 7 mm clearly is caused by the low energy gain in the gaps number 3, 4 and 5 but it originates already in the first two gaps from

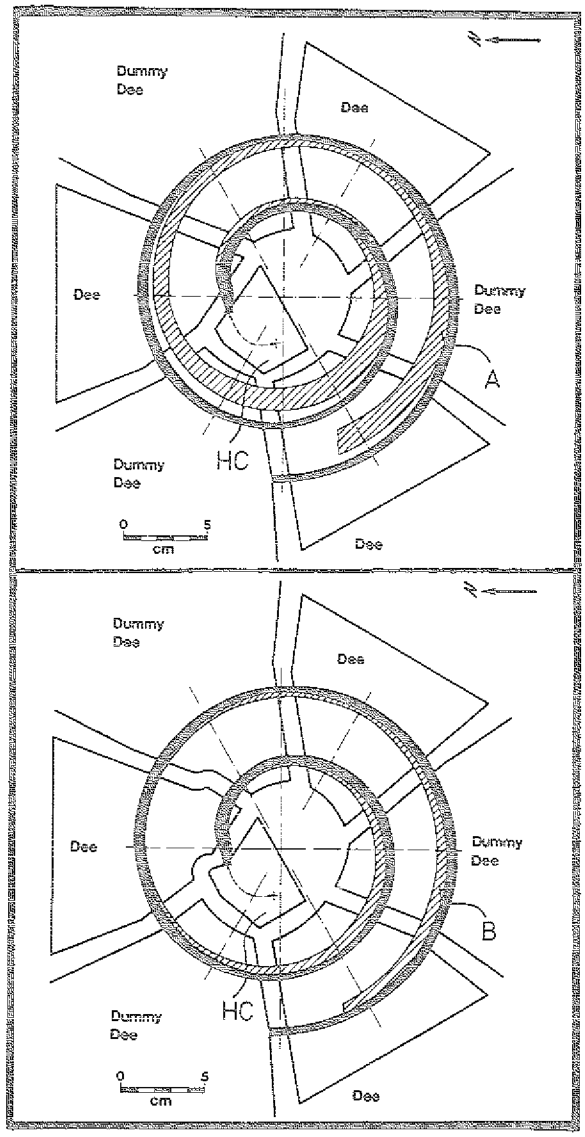

Figure 1: Dee-structure of the ISIS-center-region and envelopes (hatched areas) of the beam for input parameters from the IONAN-calculations (upper part, case A) and for a modified geometry of the first and second gap (lower part, case B). The blackened areas represent the results of the IONAN-calculations. HC-hyperboloid inflector casing.

the severe difference in the electric field shapes in comparison to the idealized sharp cut off assumption in the IONAN-calculations.

The necessary modification of the inflector and puller shape (fig. 1 , lower part, case B) mainly rotates a little the direction of the electric field in the region close to the exit of the inflector. The consequence is that the energy gain in the gaps number 3 - 5 is improved essentially. The center of curvature of the orbit centers is shifted to a point for which mainly a rotation of the second gap can shift it towards the machine center (MC in fig. 3). A rotation of only the second gap is feasible because of a sufficient turn separation (compare fig. 1). The necessary angle for this was derived from

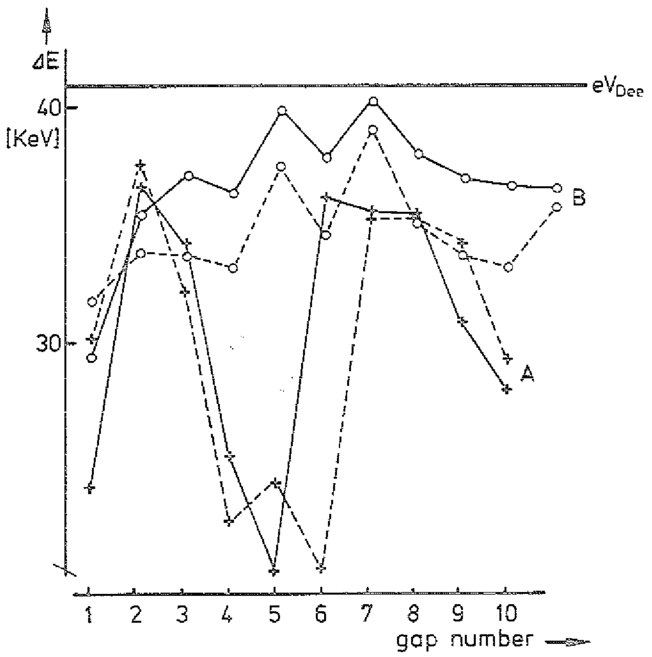

Figure 2: Energy gain ΔE per gap vs. the gap number for the cases A and B (see fig. 1) for RF-phases at start of -125° (full lines) and -85° (dotted lines). e V_{DEC}=41 keV is the upper limit for the energy gain ΔE.

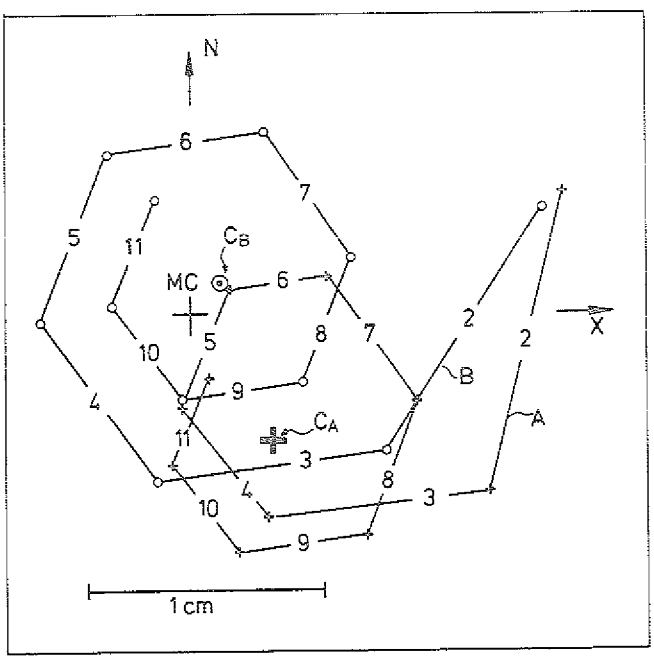

Figure 3: Orbit centers in the median plane as a function of the gap number for the cases A and B (see fig. 1). MC = machine center. C_A and C_B = centers of gravity for the last six orbit centers. The lines represent the action of the gaps; the numbers are the corresponding gap numbers.

fig. 3. Additionally the width of the second gap is reduced from 10 to 8 mm. The results of the modifications in the first and the second gap are shown in the figs.1-3 denoted as case B. The radii of the orbits now are sufficiently large to avoid the hitting of physical boundaries. The envelopes are smaller. The energy gain and the orbit centering are nearly as good as in the IONAN-calculations.

A more detailed investigation of the optical properties of the center region would need a lot of systematical and elaborate calculations for the first two gaps.

References

1) H. Beuscher, H.-G. Mathews and J. Reich, Annual Report 1980, IKP, KFA Jülich, Jül-Spez-99 (1981) 152;
R.K. Bhandari, J. Reich, Annual Report 1980, IKP, KFA Jülich, Jül-Spez-99 (1981) 154;
L. Aldea, P. Wucherer, Annual Report 1980, IKP, KFA Jülich, Jül-Spez-99 (1981) 156

2) L. Aldea, J. Reich, P. Wucherer, Proc. 9th Int. Conf. on Cyclotrons and their Applications, Caen, 1981, 461

3) W. Bräutigam, U. Rindfleisch, P. Wucherer, Annual Report 1982, IKP, KFA Jülich, Jül-Spez-202 (1983) 109

*Eindhoven University of Technology, Netherlands

9.7. First Experimental Results of an Operation in the 9ω-Mode

P. Wucherer

The cyclotron JULIC originally was designed for an operation in the 3ω-mode from an internal ion source for energies between 22.5 and 45 MeV/A.

The project ISIS[1-5] now under progress delivers heavier ions to the cyclotron center region by means of an ECR-source[1,2] and a beam handling and axial injection system[3-5]. However, for many nuclear spectroscopy experiments as e.g. proposed in the project OSIRIS[6] energies as low as 4-5 MeV/A are favourable. This energy range would match with that of the cyclotron if operated in the 9ω-mode.

Before the external injection system becomes operational first experiments with the internal ion source have already been performed and some basic properties and side constraints have been discussed[7]. Basic problems being involved with the 9ω-mode operation are:

1) To extract ions with A ≥ 20 Q/A ≈ 1/4 at a beam current of ≫ 100 nA from the source and to transport them to the cyclotron. The inflection into the median plane of a compact type cyclotron requires very low injection energies of ≈ 0.5 keV/A in this mode.
2) The modification of the center region for both the harmonic numbers h=3 and h=9. The most practicable design would be not to change the Dee geometry. However, a puller change may be necessary.
3) Beam dynamic problems i.e. the proper Dee angle, trim coil configuration (currents and setting and RF-stability).
4) Gas stripping of the necessarily not totally stripped ions during accelleration.

The first two problems are not yet investigated in detail for the external injection but it has been found out experimentally that the present center region with an internal source really works in the 9ω-mode. The needed RF-amplitudes are much higher than one would expect from the scaled orbit-philosophy in the 3ω-mode. This, however, is very helpful for the last two problems as it reduces the total turn number and therefore the beam path length, too.

The very first experiments have been performed with deuterons to get rid of the stripping problem. By iterative corrections of the cyclotron frequency and the trim coil currents the beam is brought to extraction radius. For a possible future routine operation of the 9ω-mode the trim coil settings have to be calculated from field maps.

Since the shape of the averaged main magnetic field (i.e. the pole face geometry) had been adapted to a relativistic mass increase of 4.1% (i.e. 77 MeV deuterons) the trim coil currents are on a high negative level for the very low mass increase in the 9ω-mode of ≈ 0.4%. Practically, this means there is a lower limit for the charge state of the ions or an upper limit for the energy, resp. As so far it is clear that for 4-5 MeV/A Q/A must be > 1/4 for the present maximum trim coil currents of 20 A.

By the measurement of the 12 phase probe signals the normally used optimization procedure (matrix method)[8] could be successfully applied. In figure 1 the turn patterns (upper part) and the corresponding phase deviations are shown (lower part). Only the first two phase deviations

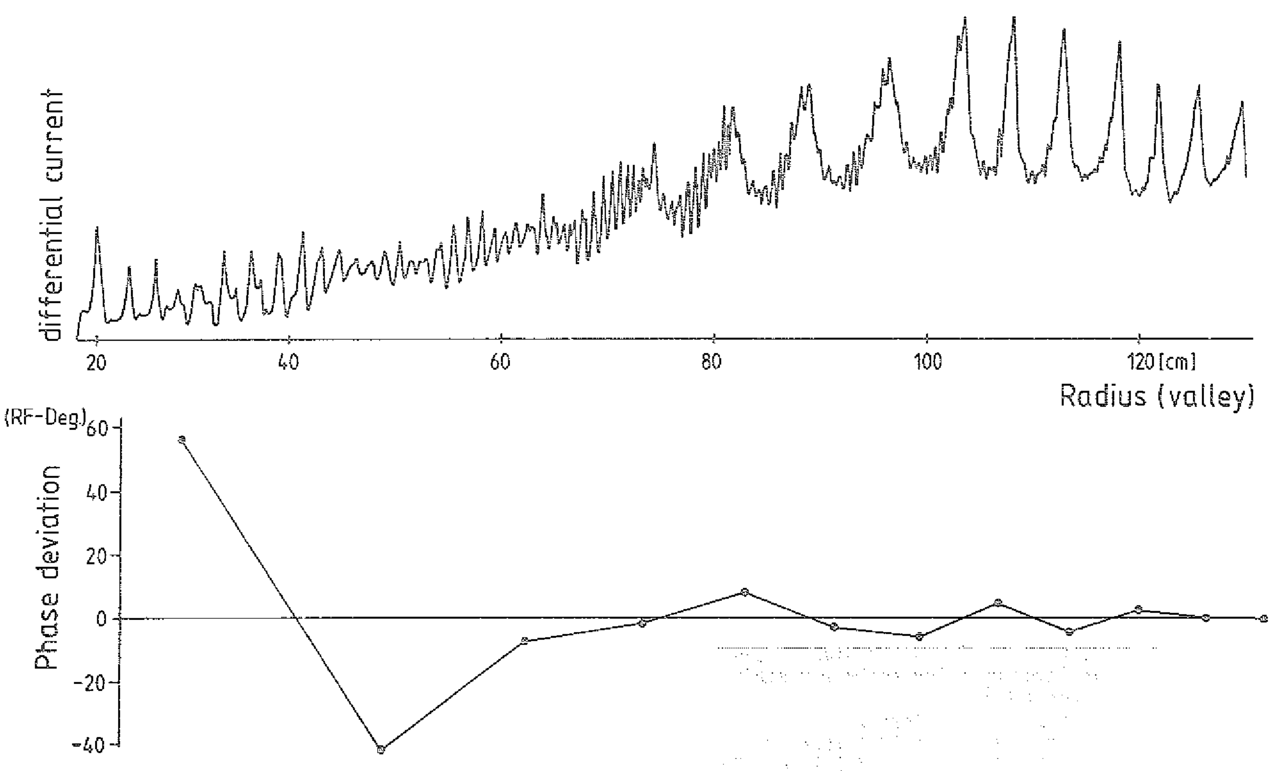

Figure 1: The upper part of the figure shows the turn patterns for deuterons accelerated in the 9ω-mode for f=26.3 MHz (3.7 MeV/A) and the lower part the corresponding phase history vs. the radius of the valley probes (V_{Dee} = 22 kV).

are significant and further investigations will show if they can be avoided. Since center region features turned out to be coupled with at least the first phase signal (e.g. necessary rf-amplitude) the problem is more complex as that for the larger radii. The coherent amplitude is in the normal range ($\lesssim$ 2 mm) and extraction efficiency $\approx$ 30% i.e. not too far from routine operation in the 3ω-mode.

The beam loss on the first 4 orbits is about a factor of 10 and is strongly dependent on the RF-amplitude, ion source position and trim coil setting.

The gas stripping problem was investigated with $^4He^{1+}$. The ion sources used in routine α operation have broad extraction slits and the He-gas pressure in the cyclotron vacuum chamber therefore rises to $\approx 6\cdot10^{-5}$ Torr. Already at 1/3 of the total beam path length (1.6/3 km) the spill beam of $^4He^{2+}$ ions exeeds that of the properly accelerated $^4He^{1+}$ ions. The beam current drops according to $I = I_0\cdot\exp(-a\cdot p\cdot t)$ (I= beam current, p= pressure in Torr, t= acceleration time in s, a is a constant).

The constant is proportional to σ_{loss}/v (σ_{loss}= stripping cross section, v = particle velocity). This advantageous fall off of the cross section[8-9] for this energy range is demonstrated in figure 2 in which lg I/I_0 is displayed vs. R^2 (since $R^2 \sim t$). Curve I is taken at a pressure of $\approx 6\cdot10^{-5}$ torr and 85% He-gas content. The constant derived from the slope of curve I and the roughly estimated turn numbers from figure 1 is $a \geq 1.1\cdot10^9$ Torr^{-1} s^{-1} whereas the previous figures are $5\text{-}40\cdot10^9$ [9-10].

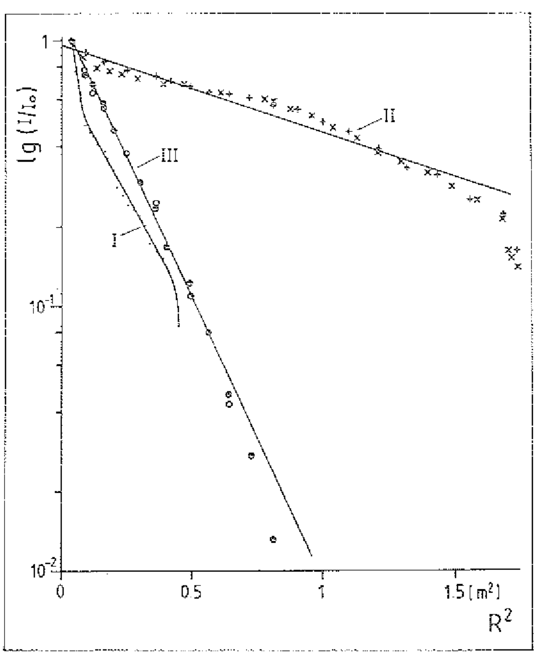

Figure 2: The beam current vs. R^2 (R = radius of the valley probes) is displayed on a log scale for different gas pressures and compositions:
Curve I 85% He-gas at p $\approx 6\cdot10^{-5}$ Torr
Curve II mixed composition at p $\approx 8\cdot10^{-6}$ Torr
Curve III 12% He-gas, $\approx$ 80% N_2-gas at p $\approx 2.9\cdot10^{-5}$ Torr
+,x and 0⊗, resp., mark different measurements for the identical conditions (f = 23 MHz, V_{Dee} = 27 kV)

By using an ion source with a small slit the pressure was reduced to $\approx 8\cdot10^{-6}$ Torr. The trim coil set was scaled according to the magnetic field levels from that of the deuterons (Figure 1). This is a good guess because of the low realivistic mass increase of both ions. By phase optimization the final phase history was similar to that in the lower part of figure 1. Curve II in figure 2 shows the resulting decrease of lg I/I_0 vs. R^2. So far it is not clear why the slope is not a straight line; presumably the pressure p and the gas composition are not constant. By inlet of nitrogen gas to p $\approx 2.9\cdot10^{-5}$ Torr the strong decrease of curve III in figure 2 was measured and a value of $a \approx 3.5\cdot10^9$ Torr^{-1} s^{-1} is derived from the slope. Up to 100 nA $^4He^{1+}$ could be extracted from the cyclotron with an extraction efficiency of 44%.

The author wishes to thank for the support of H. Lawin, H.L. Hagedoorn and the operators of the cyclotron JULIC.

References

1) H. Beuscher, H.G. Mathews, C. Mayer-Böricke and J. Reich, Proc. 9th Int. Conf. on Cyclotrons and their Applications (Caen 1981), Hrsg. G. Gendreau (1982)
2) H.G. Mathews, H. Beuscher, R. Fiedler, W. Krauss-Vogt, this Annual Report, contribution 7.4
3) Erläuterungsbericht und Planungsunterlagen zum Projekt ISIS, März 1981
4) R.K. Bhandari, J. Reich, Proc. 9th Int. Conf. on Cyclotrons and their Applications (Caen, 1981), Hrsg. G. Gendreau (1982) p. 261
5) L. Aldea, J. Reich, P. Wucherer, Proc. 9th Int. Conf. on Cyclotrons and their Applications (Caen, 1981) Hrsg. G. Gendreau (1982) p. 461
6) R.M. Lieder, H.M. Jäger and C. Michel, IKP-Annual Report 1982, Jül-Spez 202 (April 1983)
7) H.L. Hagedoorn, P. Wucherer, ISIS-note 12, Dec. 1983
8) J. Linz, IKP Annual Report 1977, Jül-Spez-15 (June 1978), p. 123
9) R.S. Lord et al. Proc. 5th Cycl. Conf. Oxford (1969) Hrsg. R.W. McIllroy (1971) p. 453
10) W. van Genderen and H.L. Hagedoorn, Internal Report of the Technical University Eindhoven VDF/Nk 83.34 (Sept. 1983)

10. COOLER RING COSY

10.1. The Cooler Storage Ring COSY

G. Berg, G. Gaul[+]*, H. Hagedoorn*[++]*, J.A. van der Heide*[++]*, F. Hinterberger*[*]*, S. Martin*[**]*, T. Mayer-Kuckuk*[*]*, F. Osterfeld, H. Paetz gen. Schieck*[***]*, D. Prasuhn, M. Rogge, P. v. Rossen, P. Turek*

The concept of a cooler storage ring (COSY = Cooler Synchrotron) has been worked out which includes recent accelerator and experimental developments for future nuclear reactions research and which will make efficiently use of the SNQ-LINAC. The presented storage ring allows a variety of novel experiments and covers a large field of interests of nuclear reaction physicists in Nordrhein-Westfalen. The intention is to build COSY at the IKP of the KFA with the support of the Institutes for nuclear physics of the Universities of Bochum, Bonn, Eindhoven, Köln and Münster.

The three essential properties of the storage ring are:

1) Very efficient use of the beam by internal target techniques in the storage ring.
2) Energy variability by RF-acceleration.
3) Extremly high beam resolution by electron cooling.

COSY will satisfy the requirements of nuclear physicists for high resolution experiments also with polarized particles in the so called energy window of the nucleon-nucleon interaction at 150 - 300 MeV. Other possible experimental techniques will be pointed out below.

With the existing cyclotron JULIC, the ISIS source for light ions which is under construction and the successfully working high resolution magnet spectrometer BIG KARL there are very favourable circumstances for a successful use of the proposed storage ring.
Two ways of injection are planned:

1) From the SNQ-LINAC energy variable protons with energies $E_p \gtrsim 100$ MeV in particular for more than $\sim 10^{11}$ particles in the ring. High resolution spectroscopy with BIG KARL up to about 500 MeV is possible. This secondary SNQ-beam should be polarized.
2) From the cyclotron JULIC (p,d,^{3}He,α with 22.5-45 MeV/N). Later ISIS-particles (ECR source with external injection). The external injection under construction will also allow the installation of a polarized ion source.

Figure 1 shows the principal lay out of the storage ring. The lattice consists of 6 unit cells with 2 quadrupole and one dipole magnets and 2 straight sections which are designed for the installation of the electron cooler and the spectrometer target area. Details of the lattice are given in another contribution to this report. It should be mentioned that the electron cooling is a novel development in accelerator technology with so far unused potentialities allowing extremly high momentum resolution of $\Delta p/p \approx 10^{-5}$ (refs.1-3). With COSY we want to make use of these developments for nuclear research experiments. For the proposed concept we assume that the frequency of the RF-structures can be varied within a factor of 2. This allows for example the following energy variations:

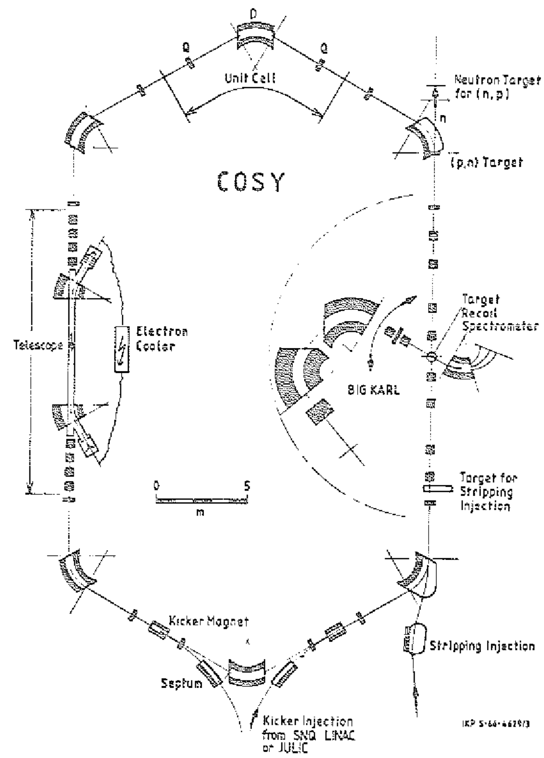

Figure 1: Schematic view of the COSY storage ring with the essential elements of the ion optical system, the electron cooler, the injection and some of the experimental instruments.

- protons: 10 - 200 MeV for injection of max. JULIC energy E_p = 45 MeV
- protons: 100 - 500 MeV for SNQ-injection at assumed E_p = 350 MeV
- α-particles: 20 - 350 MeV for injection of min. JULIC energy E_α = 90 MeV.

Further energy variations are possible by different harmonic modes of the cyclotron. The cooled emittance is expected to be as small as 0.1 π mm mrad (for $\Delta\theta \sim 1$ mrad this means a target spot of $\Delta x \sim 0.3$ mm!). For 10^9 particles in the ring the attainable momentum resolution will be $\Delta p/p \sim 10^{-5}$. For a revolution periode of 0.4 μsec ($E_p \approx 400$ MeV) the circulating current is 0.4 mA. For higher currents the momentum resolution becomes worse and will be $\Delta p/p \lesssim 10^{-4}$ for 100 mA. The straight section in the ring offers sufficient space for the installation of a 6 m long cooler device, e.g. 6 m long Fermilab design[4].

Target stations:

In the ring one target station is intended for high resolution experiments (BIG KARL). It should be possible to measure reaction products at very forward scattering angles ($\theta_{lab} = 0^o - 20^o$). With a second spectrometer (recoil spectrometer) indicated in Fig. 1 the experimental possibilities could be extended significantly, in particular because the extremely thin internal targets (e.g. gas jets[5]) allow the measurements of recoil nuclei. The use of gas jet or atomic beam targets is also possible in the short sections in the ring, also parallel with other experiments, in particular when extremely high luminosities are required, i.e. parallel cooling and measuring on very thin targets ($\lesssim$ 0.1 μg/cm^2).

For conventional scattering chamber experiments the cooled beam can be extracted. This SLOW-EXTRACTION is already used at LEAR, CERN[6]. For 100 mA circulating current there will be available about 30 nA externally with a duty factor of 1:3, i.e. in the average about 10 nA. Higher currents are possible, but one has to bear in mind that this will deteriorate the good momentum resolution.

Beam properties:

The outlined cooler ring accelerator has the following main properties:

- Very high luminosity for experiments with extremely thin targets ($\lesssim 10^{17}$ atoms/cm^2).
- Variable duty factor up to 100 % (DC beam).
- Fine tuning of the primary energy (1 MeV/min) with the electron cooler.
- Very accurate absolute energy definition by measurement of electron energy.
- For stripping injection efficiency nearly 100 %, i.e. measurement during injection.
- No beam stop in the recirculation mode (internal target), hence reduced background.
- As internal targets also polarized atomic beams including existing polarized heavy ion beams can be used.
- Target materials with high evaporation temperature might be usable as target by sputtering techniques.

Possible experiments:

With this accelerator concept many novel experiments might become possible:

- Fine energy tuning for sharp resonances and threshold energies.
- Measurement of heavy recoil nuclei and reaction products at large angles.
- Tagging of secondary beams by recoil measurement (e.g. tagged neutrons).
- Reaction measurements with extremely high resolution.
- High coincidence count rate with good energy resolution in three body reactions.
- Life time measurements (using the variable duty factor).
- Experiments with polarized atomic beams as target.
- Storage of exotic reaction products (e.g. tritons, ^{6}He).
- Nuclear reactions and γ-spectroscopy with low background and very small cross sections.
- Spin excitations in the energy window of 150 - 300 MeV.
- Production of neutrons with good energy resolution by ^{7}Li or ^{12}C(p,n) reactions at 0^o for (n,p) measurements.
- Low lying hole states at E_p = 400 - 500 MeV.
- Polarization transfer experiments, spin-spin interactions with high resolution.
- Pion production at Δ_{33}-resonance energy.
- Coherent pion production with light ions near the threshold energy.

Realization:

The construction and operation of the outlined storage ring COSY could be realized in the following steps:

1) Construction of the storage ring with RF-structures for the correction of the average energy loss in the target, matching and installation of the BIG KARL spectrometer at the ring, injection from cyclotron. Operation of the system in the recirculation mode[7].
2) Installation of RF-structures (frequency range ±100 %). Operation in the extended energy range.
3) Installation and operation of the electron cooler ($E_e \lesssim$ 100 keV) for $E_p \lesssim$ 180 MeV. Use of gas jet and atomic beam targets. Test for cooling of light ions (d, ^{3}He, α, ISIS-particles). Development of new target techniques.
4) Development and construction of an electron cooler for proton energies up to 500 MeV and injection from SNQ-LINAC.

References

1) G. Budker, Y. Derbenev, N. Dikansky, I. Meshkov, V. Parkhomchuk, D. Pestrikov, R. Salimov, A. Skrinsky, and B. Sukhina, CERN 77-08, PS Division, 13. April 1977
2) M. Bell, J. Chaney, H. Herr, F. Krienen, P. Møller-Peterson, and G. Petrucci, Nucl. Instr. Meth. 190 (1981) 237
3) R. Forster, T. Hardek, D.E. Johnson, W. Kells, V. Kerner, H. Lau, A.J. Lennox, F. Mills, Y. Miyahara, L. Oleksiuk, R. Peters, T. Rhoades, and D. Young, IEEE/NS 28 No. 3 (1981) 2386
4) Fermilab Electron Cooling Experiment, Design Report, FERMILAB, August 1978
5) H.W. Becker, L. Buchmann, J. Görres, K.U. Kettner, H. Kräwinkel, C. Rolfs, P. Schmalbrock, H.P. Trautvetter, and A. Vlieks, Nucl. Instr. Meth. 198 (1981) 277
6) D. Möhl, and K. Kilian, private communication (1983)
7) S. Martin, W. Schott, and C.-A. Wiedner, Workshop on Electron Cooling, Jül-Spez-159, Juli 1982, 7.1

+ IKP, Universität Münster
++ Universität Eindhoven
* ISKP, Universität Bonn
** ABT-SNQ, KFA Jülich
*** IKP, Universität Köln

10.2. Lattice studies for the Cooler Storage Ring COSY

G. Berg, A. Magiera, S. Martin, D. Prasuhn

The layout of the COSY ring is shown in figure 1 of the contribution "The Cooler Storage Ring COSY". The ring consists of 6 identical unit cells and 2 straight sections. Each unit cell contains a set of two quadrupoles and one 60^o bending dipole magnet ("combined function"). The straight sections are telescopes with magnification $\pm$ 1 in order to be invisible to the ring. At the target the straight section consists of a combination of 2 telescopes, providing an adjustable dispersion and beam spot at the target position without changing the other ring elements. The telescope in the electron-cooling section has to produce a wide and parallel beam in order to get a minimum cooling time.

Fig. 1 shows the amplitudes of the betatron oscillations (betatron functions) in horizontal (β_H) and vertical direction (β_V) as well as the dispersion function $D = \partial r/(\partial p/p)$ as function of the position in one unit cell. Further data are given in the following table:

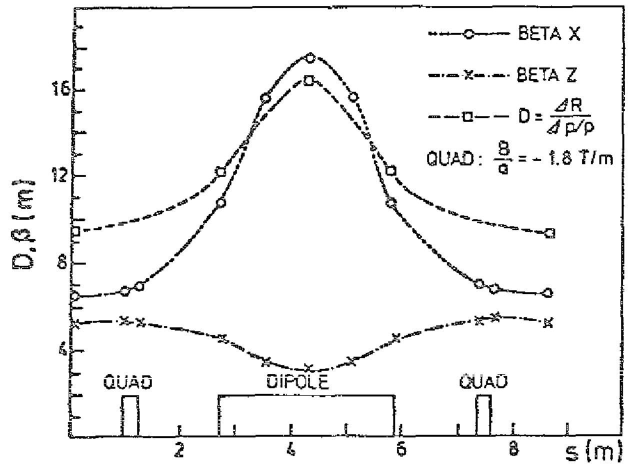

Fig. 1: The horizontal and vertical betatron functions (β_x and β_y) and the dispersion as function of the position in one unit-cell.

Parameters of the preliminary COSY lattice

6 unit cells of the structure O D O F O D O The "F" characterizes the horizontal focussing action of the combined function magnet. One telescope of 20 m length with magnification - 1 Two telescopes of 10 m length with magnification- 1		
Circumference:		88.75 m
Dipolefield for 500 MeV protons ($p = 1.09 \frac{GeV}{c}$):		12.1 kG
Free length for cooling section:		9.8 m
Free length for BIG KARL:		2.25 m
Acceptance uncooled:	$\epsilon_x = 33\ \pi$ mm mrad	$\epsilon_y = 34\ \pi$ mm mrad
cooled:		$\epsilon_x = 0.15\ \pi$ mm mrad
Dispersion at target:		variable: 2 - 20 cm/%
The following values correspond to the dispersion D = 11 cm/%		
β-function	β_{target}:	$0.6 \leq \beta_x \leq 60$ m
Maxima in unit cell:	$\beta_{horizontal}$:	$\beta_x = 18.7$ m
	$\beta_{vertical}$:	$\beta_y = 5.2$ m
Q-values	$Q_{horizontal}$:	3.16
	$Q_{vertical}$:	3.95

Calculations are done using the design programs MAD[1], TRANSPORT[2], AGS[3], RAYTRACING[4], HARMON[5]. Definitions and formulas use the notation from Bovel et al.[6].

References

1) F.Ch. Iselin, The MAD Program, Computing in Accelerator Design and Operation, Berlin, Sept. 1983

2) K.L. Brown, D.C. Carey, Ch. Iselin and F. Rothacker, TRANSPORT a computer program for designing charged particle beam transport systems, CERN-80-04 (Geneva 1980)

3) E. Keil, Y. Marti, B.W. Montague, and A. Sudboe, AGS-The ISR Computer Program for Synchrotron Design, Orbit Analysis and Insertion matching, CERN 75-13 (Geneva 1975)

4) H.A. Enge, S. Kowalski, private communication, 1982

5) M. Donald, Chromaticity Correction in Circular Accelerators and Storage Rings, PEP-Note - 311, Juli 1979

6) C. Bovet, R. Gouiran, I. Gumowski, K.H. Reich, CERN/MPS-SI/Int. DL/70/4, Geneva 1970

11. γγ SPECTROMETER OSIRIS

11.1. Compton Suppression array for High Resolution In-Beam Spectroscopy

R.M. Lieder, W. Gast, H. Jäger, J. Schaeffler-Kräh, K.H. Maier, P. von Brentano**, J. Eberth**, K. Schiffer**, H. Hübel+, K.P. Blume+ and C. Michel++*

One of the principal methods of in-beam spectroscopy has always been the study of the electromagnetic radiation, which is emitted from highly excited nuclei. In a coded form it contains the information about the structure of the nuclei. The more detailed the properties of the γ-radiation can be determined, the more of the included information can be uncoded. In the so called conventional spectroscopic studies this has been attempted by measuring the γ-radiation with the maximum energy, angular and time resolution possible.

Although the instruments used in such studies have been continuously improved, a limit seems now to be approached. It turned out, that the conventional type of spectroscopy is restricted to the investigation of the nuclear structure in the vicinity of the yrast line. This is because in (HI,xn) compound nuclear reactions, which may impart up to $\simeq 70\,\hbar$ of angular momentum into the compound system before it is disrupted by the Coriolis and centrifugal forces, the final nucleus decays through several parallel cascades before the yrast states are reached. Thus in contrast to the low spin part of the decay path, where the total intensity of the decay concentrates on the yrast transitions, it spreads over a large number of parallel transitions in the high spin part. As a result we obtain in addition to the large number a very weak intensity of the individual high spin transitions, which instead form an apparent continuum in the conventional γ-ray spectra.

Several new techniques have been developed to study at least the gross average properties of this continuum, e.g. large sum-energy crystals, multiplicity filters, or large NaI(Tl) detector systems in various coincidence arrangements[1]. However, while these average properties are quite interesting, they cannot fully elucidate the physics behind the behaviour of fast rotating nuclei. As we have learned from our conventional spectroscopic work this elucidation can come only with the resolution of the spectrum.

One year ago therefore a γ-γ coincidence spectrometer was designed which combines the positive features of these newly developed techniques with the acknowledged advantages of the conventional discrete spectroscopy. It has been named OSIRIS (COmpton Suppression array for hIgh Resolution In-beam Spectroscopy). It will be built in a collaboration between the Universities of Cologne and Bonn, the Hahn-Meitner Institute in Berlin, and the KFA Jülich. Let us briefly recapitulate the salient features of the present design:

1. The optimum energy resolution of the spectrometer shall be obtained by the use of Ge detectors.
2. The rather small detection efficiency of these detectors shall be compensated by arranging at least 12 detectors in two rings as close as possible around the target (Fig. 1).
3) A reduction of the two main components of the γ-ray background shall be achieved in the following way: The Compton background will be suppressed using an anti-Compton shield made of bismuth-germanate (BGO). The quasicontinous background arising from the statistical decay shall be reduced by an additional sum-energy and γ-ray multiplicity filter detector located in the center of the spectrometer. It consists of 38 BGO scintillators.
4) The neutron background will be reduced since the employed BGO detectors are much smaller compared to e.g. NaI detectors of the same γ efficiency, while having about the same detection efficiency for neutrons.

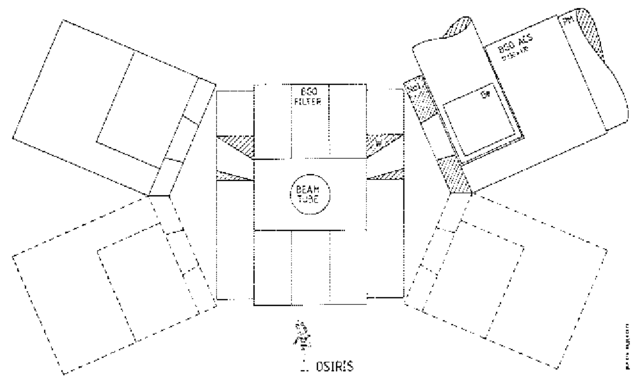

Figure 1: Side view of the γ-γ coincidence spectrometer consisting of a sum-energy and γ-multiplicity filter (BGO Filter) and an array of Ge detectors surrounded by anti-Compton shields (ACS) each.

Concerning the design of the physical and technical details of the different parts of the spectrometer we started with the anti-Compton shield (ACS) as the most important one.

With a given detection efficiency of the scintillator material used, the suppression power of an ACS physically depends on its shape, dimension and the system configuration; the latter shall also take into account all collimating, absorbing and scattering passive material in the system. In order to optimize these parameters, Monte Carlo calculations using the EGS code have been carried out[2]. Their results favoured an asymmetric configuration of the shield, in which the γ-radiation enters the Ge detector from the side. In this configuration the front face of the ACS has a square shape reflecting the rectangular side view cross section of the Ge detector (c.f. Fig. 1).

The technical realization of such a BGO shield is connected with two main problems: up to now BGO single crystals are available only in relative small sizes and BGO has a ten times smaller light output compared to NaI as well as a very high refraction index of n = 2.15. Hence the problems of light collection, transfer to the photomultiplier and detection have to be treated very carefully, especially as the whole ACS has to be made up of several pieces of BGO while no optical coupling materials for such high refraction indices are available up to now. Regarding these problems the front part of our shield has been designed to consist of NaI. In this way the detection probability for the backscattered γ-rays which have the lowest energies may be enhanced.

In order to check the predicted physical properties and to study the above mentioned technical problems a prototype of the shield has been ordered. Various test experiments have been performed at the different collaborating institutes up to now:

1. Initial test of energy and time resolution:
   After a preliminary test of their specified energy and time resolution ($\lesssim$ 20 % and $\lesssim$ 15 ns respectively) the individual BGO crystals and the NaI(Tl) crystal have been glued together and canned at the factory. The ACS was then delivered as a complete unit including a 5" RCA 583006 EMI photomultiplier tube. For this original set up the timing was measured against a plastic scintillator. A time resolution of fwhm $\simeq$ 16 ns was obtained for a ^{60}Co source disregarding the weak long-term component of the BGO scintillation decay of 300 ns. An energy resolution could not be determined. The light collection or detection properties for the individual crystals appeared to be too different as to give an uniform pulse height at the anode of the photomultiplier tube (PMT).

2. Test of lower threshold setting:
   Although a good energy resolution is not required for an ACS, it will affect the lower threshold setting (LTS); lower threshold is defined here as lowest γ-ray energy significantly detectable. Since the light output of BGO is very small the LTS is limited by the light collection and transfer properties and by the photomultiplier noise in our system. It was measured by taking energy spectra of a ^{241}Am source for various positions of the source. As the width and position of the 60 keV line in the spectra shifted as a function of the source position, a position dependent value of 30 keV - 50 keV was obtained. These values are estimated from the depth of the minimum between the 60 keV line and the noise tail.

3. Investigation of the position dependent response of the shield to different γ-ray energies:
   In order to study the observed pulse height variations in more detail, the position dependent response of the shield to various γ-ray energies (^{60}Co, ^{137}Cs, ^{241}Am) has been measured. The position of the source practically determines, in which of the individual crystals the γ-rays mainly are absorbed. A strong dependence was observed in so far, as the lowest output pulse heights were obtained for those crystals with the smallest area of optical contact to the PMT cathode. The effect is the stronger the lower the incident γ-ray energy is. From this one may conclude that the light generated in one individual crystal stays more or less inside this crystal during its transfer to the photomultiplier; only a small amount of light can penetrate into the neighbouring crystals although they are glued together with optical cement. This may be due to the large ratio of refraction indices of BGO to optical cement (2.15/1.6) giving an angle of total reflection of less than 45^{0}.

As a final test of the system in its original configuration the Compton-suppression for a reverse electrode (γ-X) detector of 19 % efficiency has been measured. The ACS was shielded against the ^{60}Co source by a tungsten (densimet) collimator of 30 mm thickness. The maximum suppression factor of 5.6 was obtained for the energy region of 350-400 keV. In the following experiments we tried to improve this result by changing the configuration of the system.

4. Test of different photomultipliers and photomultiplier-light-guide configurations:
   From the previous measurements an imperfect light collection due to the incomplete area of optical contact to the photomultiplier cathode was observed for some of the outer crystals with respect to the others. Diffuse reflector material applied on those parts of the crystals not covered by the photocathode did not give a gain in light collection. Hence several light-guides (lucite) has been fabricated in order to improve the adaption of the 133 x 133 mm square shaped extrance window of the BGO to different configurations of PMT's with round shaped photocathodes: two light-guides of 30 mm and 50 mm length, respectively, for the adaption to one 5" PMT and four light-guides of 35 mm length for the adaption to four 3" photomultiplier tubes. The test measurements of the various photomultiplier-light-guide configurations have been performed using the 30 mm tungsten collimator and a ^{60}Co source with the light-guides covered by reflector powder. They are summarized in table 1.

Photomultiplier	Background suppression for light guide:			
type	30 mm	50 mm	4x35 mm	no
RCA 58300 6 EMI	6.9*)	7.2		5.6
RCA 8854	6.4*)			
Valvo XP 2041		5.8		5.2
Hamamatsu R 1307			6.2	
Valvo PM 2312			5.2	

Table 1: Photomultiplier-light guide configurations tested for the BGO anti-Compton shield. The suppression factors for the ^{60}Co Compton background at $\approx$ 350 keV are given.
*)Different collimator (see text)

The use of the light-guides leads to a substantial improvement of the uniformity of light collection; nevertheless only a slight increase of suppression factor was obtained in general. The bad performance of the XP2041 is ascribed to its bad noise characteristics. For the configurations with four photomultipliers the influence of different coincidence conditions between the photomultipliers on the lower threshold setting has been tested, too. A satisfying result is obtained only for the combination of the original PMT with the 50 mm light guide. It reproduces the calculated suppression factor to nearly 90 %. However, this is true only for the energy region above 500 keV. For the low energy region a value of 7.6 measured at 150 keV competes with a value of 14.5 predicted for this energy. Since a relativ strong backscatter preak was observed in the experimental spectra we ascribed this discrepancy to scattering problems. A γ-ray which is already scattered, e.g. at the collimator, before it enters the Ge detector produces true background which cannot be suppressed by the ACS. For the high theoretical suppression factors predicted for our shield even a small amount of such true background reduces the measurable suppression factor drastically.

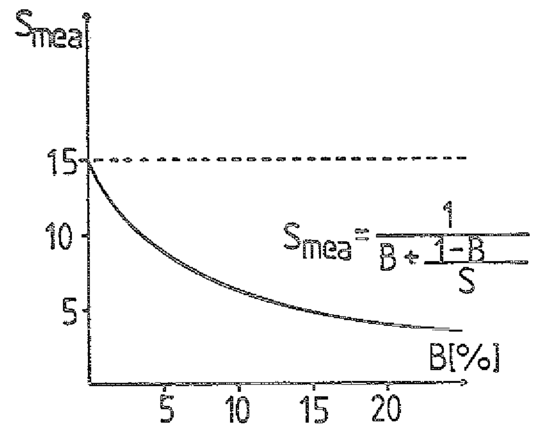

Figure 2: Experimentally measurable suppression factor Smea as a function of the contamination of the Compton background with true background B for a theoretical suppression factor of S=15.

Figure 2 shows for a theoretical suppression factor of 15 the experimentally measurable factor as a function of the contamination of the Compton-background with true background.

5. Test of different collimators:

In order to study this effect experimentally background spectra and suppression factors for different collimators have been measured. A conical lead collimator of 150 mm thickness led to a significant improvement of the results. The experimental suppression factor of a configuration which consists of this collimator, the 50 mm light guide and the RCA 58300 6 EMI photomultiplier, is compared to the theoretical predictions for different dimensions of the shield (c.f. ref. 2) in Fig. 3a. The present prototype compares to B = 80 mm. The backscattering was not accounted for in the theoretical calculations. In Fig. 3b the corresponding suppressed and unsuppressed spectra are shown.

6. In beam studies:

Several in-beam test have been performed at the accelerators of the different institutes. Suppression factors of 3-5 obtained for in-beam singles spectra are not a measure of the capabilities of the shield since an appreciable amount of true background occurs in in-beam experiments. The promising features of a spectrometer consisting of such ACS's can be better read off from the comparison of an unshielded with a shielded detector for an in-beam coincidence measurement as given in Fig. 4. As the coincidence condition reduces the true background the observed suppression improves again with respect to singles spectra. Thus a lot of new lines occur in the projection of the suppressed detector which are not observable at all in the unsuppressed spectrum.

References

1) B. Herskind, J. de Phys., Colloque C10, Suppl. no. 12, p. 106

2) C. Michel et al., preprint, GSI Darmstadt 1982

* HMI, Berlin

** IKP, Universität Köln

+ ISKP, Universität Bonn

++ GSI, Darmstadt

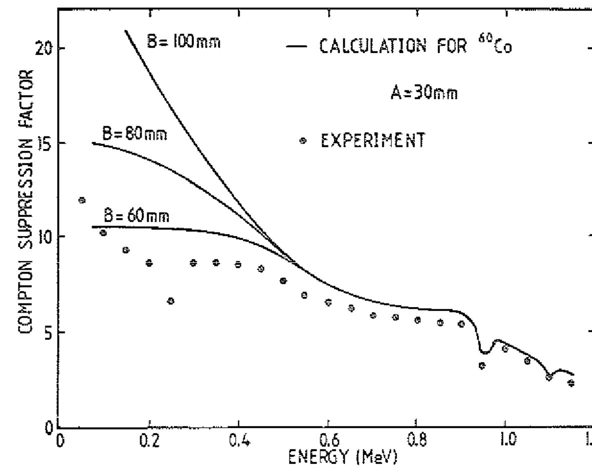

Figure 3a: Comparison of the theoretical suppression factors with the experimental results obtained with the prototype of the ACS.

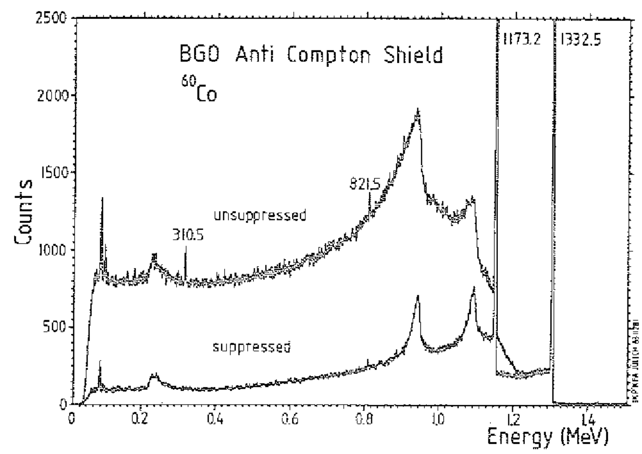

Figure 3b: Comparison of the corresponding γ-ray spectra.

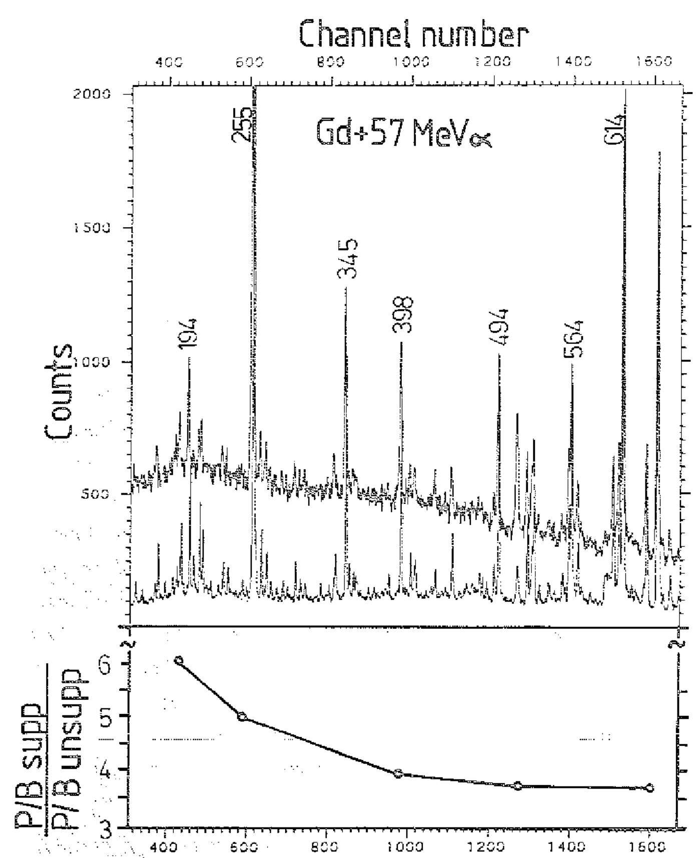

Figure 4: Coincidence projections of an in-beam coincidence measurement between a shielded and unshielded detector of the same γ-ray efficiency. The ratio of corresponding peak-to-background ratios (P/B) for different γ-ray energies are given in the lower part.

12. BIG KARL

12.1. The Magnet Spectrometer BIG KARL

G.P.A. Berg, B. Brinkmöller, G. Hlawatsch, A. Magiera, J. Meißburger, D. Paul, D. Prasuhn, J.G.M. Römer, P. von Rossen, O. Schult, J.L. Tain

Since the magnetic spectrograph BIG KARL has been put into operation in 1979 it has been the main user of the cyclotron beam and has proven to be very dependable.

Various nuclear physics experiments were performed which are presented in detail elsewhere in this report:

- Gamow-Teller resonances
  (^{3}He,t) on ^{90}Zr
- Two nucleon transfer
  (d,^{6}Li) on ^{12}C and (^{3}He,^{6}Li) on ^{11}B
- high lying 1^{+} states
  (p,p') on ^{40}Ca
- study of proton hole states
  (d,^{3}He) on ^{62}Ni
- $T=\frac{1}{2}$ states close to the lowest $T=\frac{3}{2}$ states via
  (^{3}He,α) on ^{14}C
- study of collective excitations
  (^{3}He,t) on ^{120}Sm and ^{208}Pb
- spin-flip reactions to unnatural parity states
  (p,p') and (d,d') on ^{58}Ni
- (p,p') on ^{143}Nd

Spectrograph Development and Improvements:
During the yearly maintenance period the cryo-vacuum system was overhauled after being used for five years. In addition each of the cryopumps has been equipped with a vacuum valve that seals the pump from the vacuum chamber during regeneration.

The central concrete shielding of the scattering chamber (IGLOO) was dismanteled to replace six of its sixteen air bearings. Before reassembling, a steel cover has been added to its lower part to prevent premature wear down of those air bearings.

To eliminate the effects of ground movement all elements of the spectrograph and the last four quadrupoles of the beam line were optically realigned.

Significant improvements were done on the detector system. Two large area (8 cm x 90 cm) focal plane detectors allow position and angle discrimination giving an improved background reduction and larger energy range. Extensive software has been developed for fast on-line operation of the new delay-line readout drift-chambers and the off-line data analysis. An additional ΔE-gas-detector with the same active area as the Morris-drift-chambers improves the identification between different reaction products.

Especially for the reduction of background under extreme forward angle the antiscattering slits have obtained scintillation detectors at their edges (active slits) to mark and suppress slit-scattered particles.

BIG KARL CONTROL AND DATA ACQUISITION

12.2. Spectrometer Control

B. Brinkmoeller, K. Kruck, J. Meissburger

A new 128 bit optocoupler box was installed and connected to various status and error lines of the vacuum and power supply systems. This will improve visual and automatic monitoring of the spectrometer status.

A program TTCYC was written to test overall power supply performance with high accuracy in order to detect malfunction of either host computer, CAMAC I/O or internal power supply electronics.

Another program QBCYC supports test measurements on the beamline optics. It allows correlated scaling of the four last beamline quadrupoles according to user-defined data and function tables. This will eventually be included in CYCLE as a new command to vary spectrometer dispersion and reaction angle in a way to preserves matching conditions.

In order to save money on PDP11 hardware and to speed up program development under RSX-11/M the complete PDP11/40 environment was transferred to the VAX-11/780 computer in a fully compatible way. Camac I/O is simulated on the VAX by a set of CAmac SIMulating Interface Routines CASIMIR which provide for all necessary IKP Camac library calls.

12.3. Data Acquisition and Analysis

B. Brinkmoeller, R. Korthues, J. Meissburger, D. Paul

The VAX is now running VMS 3.3 supporting a new 470 MBytes Winchester disk. All terminals support screen editing, four of them provide national languages to print on a letter printer in DIN-A4 format.

A new BRHO plotting utility was written to produce multicolour plots of various combinations of variables in reaction kinematics for multilayer or impure targets including energy loss.

The BKARLO energy loss program now accepts symbolic and structured data input that makes preparation of a spectrometer description file a few minutes job.

Major efforts went into the development of all the software tools to handle the new Morris detector. The utility MOCAL provides for interactive data manipulation on calibration spectra as well as for the complex organization around on- and offline sorting utilities. This includes the online data acquisition program ACON with it's realtime subprocess ACQUIRERT, the user-parameter definition utility ACPARAM, the hardware configuration utility MEMPHIS, the offline sorting program PLSORT and finally the documentation utilities ACSTATUS and ACSAVE. A total of 36 different files are managed by the system in a user transparent way. Complete and portable documentation of hard- and software status is guaranteed at all times for later offline reanalysis.

12.4. MOrris chamber CALibration utility MOCAL

J. Meissburger, D. Paul

A one-coordinate particle position in the Morris multiwire drift chamber is constructed from three measured parameters: The "wire number" delay line signal determining which anode wire fired next to the particle track (8 mm spacing), the drift time signal providing the position in between the wire and a sign signal to resolve the left/right ambiguity. The true particle position is constructed from these values on- or offline by a table lookup technique. The program MOCAL has been developed as a fast generation utility for these so-called calibration tables. The calibrations are done within MOCAL by an autofit routine and by an integrating binning routine. MOCAL further offers interactive graphics for proving or manipulating the data and uses Big Karl standard command parsing with some tutorial support. A special initialisation routine MOINI assembles all necessary data tables and corresponding software modules for the on- and offline sorting utilities ACON and PLSORT and for hardware configuration in MEMPHIS.

12.5. Detectors at the BIG KARL Spectrometer

G. Hlawatsch, D. Paul, G.P.A. Berg, P. von Brentano[+], *B. Brinkmöller, J. Meißburger, C.F. Moore*[++], *C.L. Morris*[+++], *J.G.M. Römer, M. Rogge, S.J. Seestrom-Morris*[+++], *G. Sondermann*[*], *J.L. Tain, L. Zemlo*[**]

Some effort has been spent to maintain and improve the detection possibilities at BIG KARL for a variety of experiments. The operation of the Morris detector[1)] and the necessary calibration programs in particular for different reaction products (p, d, ^{3}He, t, α) has been improved considerably. An additional large ΔE-gas detector for particle identification purposes covering the active area of the Morris detector was built. A time of flight (TOF) start detector for the background reduction in exotic reactions e.g. (^{3}He, ^{6}He) was installed and tested at the entrance of dipole D1. The existing ΔE-E plastic scintillator blocks had to be replaced due to surface aging effects. In order to reduce slit scattering into the spectrometer the entrance slits behind Q1 and Q2 have been equipped with plastic scintillation counters which will be tested in the next beam time. In the following some details of these detectors are given:

Morris detector: For the flexibility of handling this detector[1)] which operated at atmospheric pressure a new detector concept was initiated. A new detector front chamber was built and installed with an exit window of 100 cm x 10 cm dimension consisting of 35 - 50 μm Mylar supported by 0.5 mm Nylon wires. Several detectors can be mounted behind this window. For this purpose six optical bench slides adjustable in height have been mounted on the steel ground plate behind the window. All detectors have optical bench feet and can now be positioned in and behind the focal plane allowing quickly assembling an optimum set-up for a variety of experiments.

More experience has been gained with the Morris detector. Problems like high voltage sparks in the detector, unefficiencies, and operation instabilities have been solved. Corresponding investigations showed that mainly gas impurities and electronic drifts caused the malfunctions. A special start-up procedure with detector and gas system cleaning by vacuum pumping and a proper gas flow as well as new electronic modules, especially new matched preamplifiers have improved the stability. The development of calibration and operation software for the detector[2)] has been completed. Details are described in another place in this report. Several combinations of one or two (for angle determination) of these detectors with ΔE-gas, ΔE-plastic and E-plastic detectors have been used in various experiments (see this report) for a variety of particles (p, d, ^{3}He, t).

ΔE-gas detector: For the identification of particles (e.g. ^{4}He in the ^{14}C(^{3}He, ^{4}He) experiment) a ΔE-gas detector was built. It consists of a frame with a volume of 100 cm x 10 cm x 3.5 cm closed by 6 μm aluminized Mylar foils at entrance and exit. Eight 20 μm gold plated tungsten wires are stretched horizontally along the middle plane of the windows with a spacing of 1 cm. The wires, electrically connected together, lead into an ORTEC 970 D charge sensitive preamplifier. The outgoing signals are processed with conventional spectroscopy electronics. As detector gas mixture P10 (10 % Methane, 90 % Argon) was used at ca. 1700 V in the proportional region. Fig. 1 shows the ΔE spectrum that allows clear separation of deuterons and ^{4}He particles.

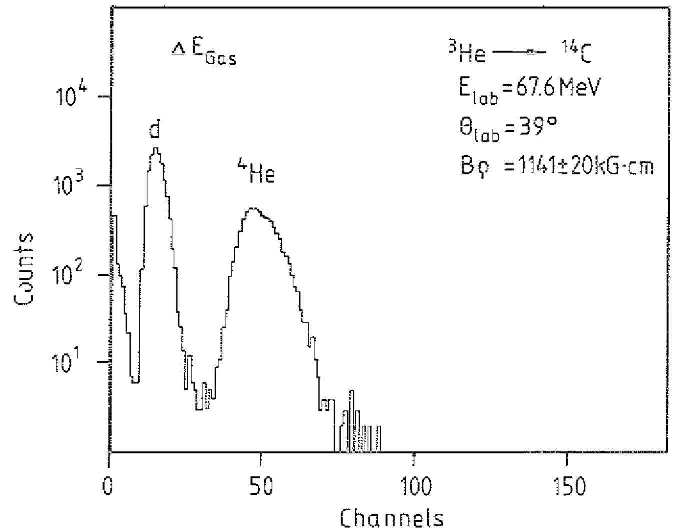

Fig. 1: Spectrum of the ΔE-gas detector in a ^{14}C(^{3}He,α)^{13}C experiment at an angle of Θ_{lab} = 39° showing clearly separated peaks of deuteron and α-particles of the same Bρ-value reaching the focal plane.

Avalanche Counter: For background reduction in exotic reactions (e.g. the ^{26}Mg(^{3}He, ^{6}He) experiment) the time start of a newly developed transmission Parallel Plate Avalanche Counter (PPAC) situated at the entrance of dipole D1 was used to generate time of flight (TOF)

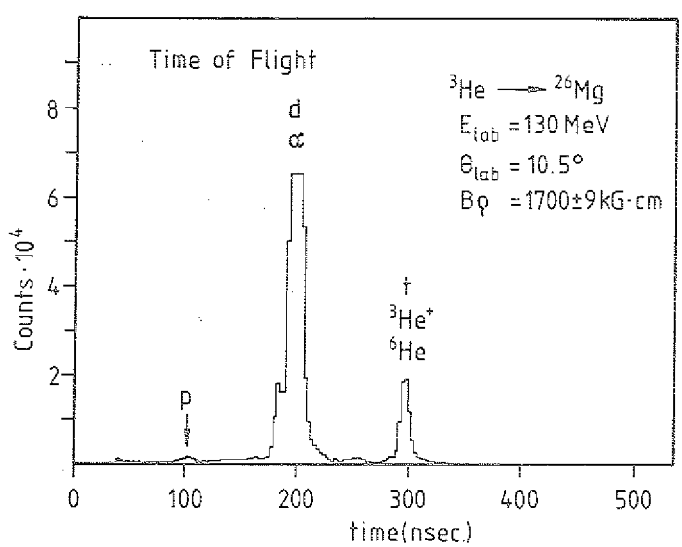

Fig. 2: Time of flight spectrum measured with a PPAC against the plastic scintillator. Particles with the same mass to effective charge ratio have the same flight time through the spectrometer.

spectra with the plastic scintillator as stop detector. It consists of two thin stretched (ca. 40 $\mu g/cm^2$) polycarbonate foils (area: 7 cm x 10 cm) with a 100 $\mu g/cm^2$ gold layer evaporated on one side. Their spacing is 6 mm. The detector was operated with pure isobutane at a pressure of 30 mbar and an voltage of 1550 V. In fig. 2 a time spectrum is displayed which shows sufficient time resolution for the separation of ^{6}He from p, d, and α particles. Significant reduction of background could be obtained by gating the ^{6}He spectra from the particle identification with the ΔE-gas detector with the corresponding ^{6}He line in the TOF spectrum.

Active slits: Another device for background reduction, so called active slits have been installed and put into operation at the end of the current year. They consist of four plastic scintillators (0.4 cm x 5 cm x 16,5 cm with light guides ca.3,5 cm long) at the front surfaces of the entrance slits (copper bars: 5 cm x 16 cm x 16,5 cm) behind Q1 and Q2. The signals from the attached Photo Multiplier Tubes (PMT) are used in anticoincidence to the EVENT signal eliminating hereby all particles that were scattered at the slit surface and reached the focal plane.

Plastic scintillators: The existing plastic ΔE and E counters were now five years in operation and showed cracked surfaces originating from material aging. The resulting deterioration of the energy signals made a replacement necessary. In order to maintain the modular detector concept, two ΔE (0.3 cm and 0.8 cm thick) and one E counter (10 cm thick) have been built, each in a separate housing. They are matched in size with the other focal plane detectors having an active area of 10 cm x 100 cm. As plastic material PLEXIGLAS scintillator (type 1921 and 1923, Röhm) was chosen. The PMT's are specially selected for good energy resolution and sharp timing (XP2230, VALVO).

References

1) G.P.A. Berg, P. von Brentano, B. Brinkmöller, G. Hlawatsch, J. Meissburger, C.F. Moore, C.L. Morris, D. Paul, J.G.M. Römer, M. Rogge, S.J. Seestrom-Morris, J.L. Tain and L. Zemlo, Annual Report 1982, Jül-Spez 202 (1983) 116

2) Diplomarbeit D. Paul, Univ. Münster, 1983, unpublished

+ Institut für Kernphysik, Universität zu Köln

++ University of Austin, Texas, USA

+++ Los Alamos Scientific Laboratory, New Mexico, USA

* Institut für Kernphysik, Universität Münster

** Institute of Nuclear Research, Warsaw, Poland

13. DETECTORS, TARGETS, SPECTROMETERS

13.1. Semiconductor Detectors

A. Hamacher, T. Künster, E. Lawin, H. Metz, K. Nicoll, D. Protić, G. Riepe

To be used for charged particle spectroscopy and particle identification in nuclear reaction experiments (IKP and visiting groups) 5 large cryostats of different design (each with 2 detectors) for the 100 cm scattering chamber and 5 monitor cryostats were kept available. They were equipped with side-entry Ge(Li)-detectors made by the detector laboratory. Radiation damaged detectors were regenerated or replaced by new ones. A series of commercial Si ΔE-detectors, position-sensitive Si-detectors and Si(Li)-detectors were tested before and after use in the experiments.

Two cryostats designed to be mounted at the bottom of the 100 cm scattering chamber were completed. One of them was equipped with a digitally position-sensitive ΔE-detector and a side-entry E-detector (for particles of up to 30 mm range), both made from HPGe (Figure 1). The structure of

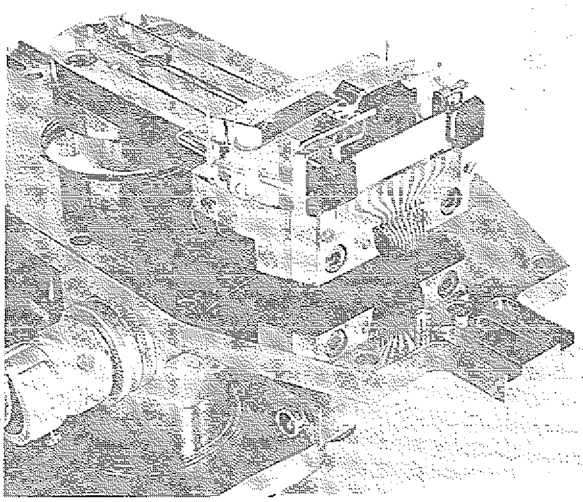

Figure 1: Detector arrangement inside the cryostat to be mounted at the bottom of the 100 cm scattering chamber.

the ΔE-detector (with a thickness of 1.5 mm) consists of 9 elements (2.6 msr each) with an angular spacing of 2.5°, surrounded by a guard-ring (active collimator). The ΔE-information for all elements can be derived from the rear side of the detector.

The improved version of a multi-detector cryostat (Figure 2) was equipped with 6 HPGe detectors of a total thickness of 83 mm (corresponding to the range of 200 MeV protons).

For the fabrication of digitally position-sensitive detectors the technology of photolithography was introduced. This process combined with plasma etching (SF_6) in a planar geometry (resulting in anisotropic etch rates) now enables much finer structures.

For the use in ion beam diagnostics at the cyclotron and at the beam line Si strip detectors (about 4 mm thick) with two different patterns were fabricated. These patterns consisted of rows of 14 or 28 strips having a length of 10 mm inside an area of 10 by 7.1 mm^2, resulting in values for the pitch of 510 and 250 μm.

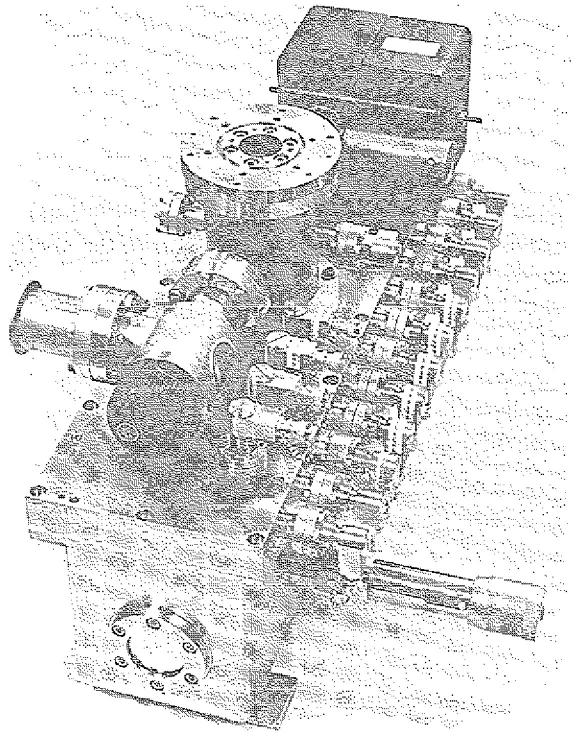

Figure 2: The improved version of a multi-detector cryostat

To investigate inhomogeneities of thick materials through gamma-ray (^{60}Co) transmission, a one-dimensional strip detector (10 mm thick) was made from HPGe having a lithium contact on the rear side. The boron-implanted contact was divided into 60 strips of 300 μm width and 3 mm length with grooves of 50 μm width in between, surrounded by a guard-ring (Figure 3). Each strip will be connected to an individual preamplifier to enable a fast and simultaneous read-out (high count rates).

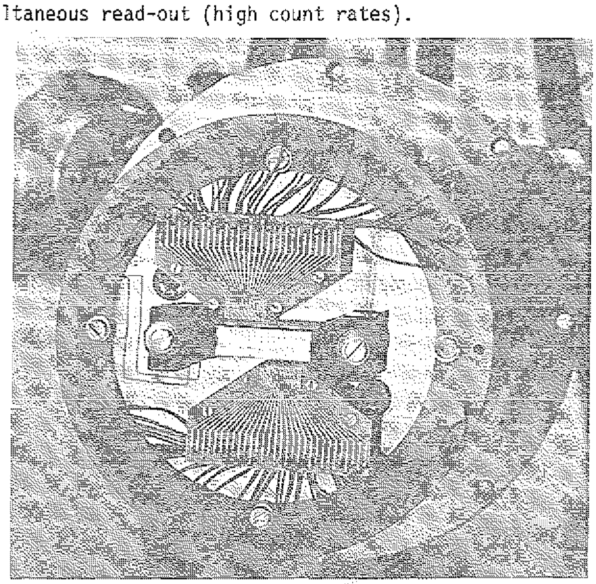

Figure 3: The one-dimensional strip detector.

A detailed study of strip detectors with α-particles yielded several interesting results. An α-particle incident to the groove is not lost but recorded by the two adjacent strips. Summing both signals one arrives at the nominal α-energy with a loss of only 3%. Processing the signals in appropriate electronics can be used to obtain position-information.

Various types of Ge or Si detector-systems - most of them commercial ones - were regenerated of repaired.

13.2. Target Laboratory

J. Pfeiffer, G. Riepe

To be used in experiments (IKP and visiting groups) at the cyclotron, at the research reactor, at the crystal spectrometer, and at university laboratories about 170 targets (with and without backing) were prepared from 30 different elements, mostly by vacuum deposition or rolling (after reduction or melting). The thicknesses were in the range from 3 $\mu g/cm^2$ to 20 mg/cm^2, and the areas were between 10 and 250 mm^2.

Again, as in the last year, most of the targets, especially those of large area and minor thickness, were prepared for experiments at the magnet spectrograph (BIG KARL).

13.3. Light particle detection by BGO-scintillators with photodiode readout

*R. Glasow**, *K.H. Kampert**, *H. Löhner** *and G. Gaul**

The applicability of a BGO crystal coupled to a photodiode for detection of light charged particles from medium energy nucleon reactions in the particle energy range of some ten to some hundred MeV, was investigated in an experiment using the 172 MeV α-beam.

Due to the high density (ρ = 7.13 g/cm^3) of BGO, the 1 x 1 x 1 cm^3 crystals used are able to totally stop protons of about 70 MeV and α-particles of about 275 MeV$^{+)}$. The particle identification was achieved by the usual ΔE-E-technique with a 1000 μm Silicon surface barrier detector.

The ΔE-E_{rest}-scatterplot of such an arrangement demonstrates the particle resolution between p, d, t, ^{3}He- and α-particles (Fig. 1). A peculiarity of this device is

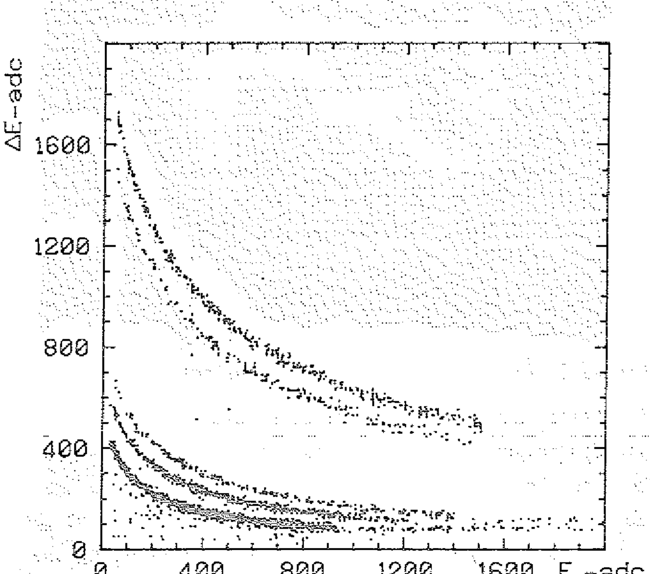

Figure 1: ΔE-E_{rest}-scatterplot for the reaction α(172 MeV) + ^{58}Ni at θ_{lab} = 35^0.

that the punch through particles which directly hit the depletion layer of the photodiode, give a very high E_{rest}-signal which therefore does not disturb the lower mass particle spectra but can potentially be used as an anticoincidence signal. To determine the energy resolution of the BGO-detector, the kinematical coincidence between protons and the recoil α-particles was used.

Figure 2 shows the inclusive (upper part) and the coincident (lower part) proton spectrum, which were measured at θ_{lab} = 45^0 with a Mylar target. The derived energy resolution of this elastic proton peak at E_p = 52 MeV is about 1.5 MeV (fwhm) and therefore comparable to the values observed with NaI(Tl) scintillators coupled to photomultipliers.

The great advantages of this detector which make it attractive as a replacement for classical scintillation counters, is the very compact construction due to the high stopping powers of BGO and the small size of the photodiode, the insensitivity

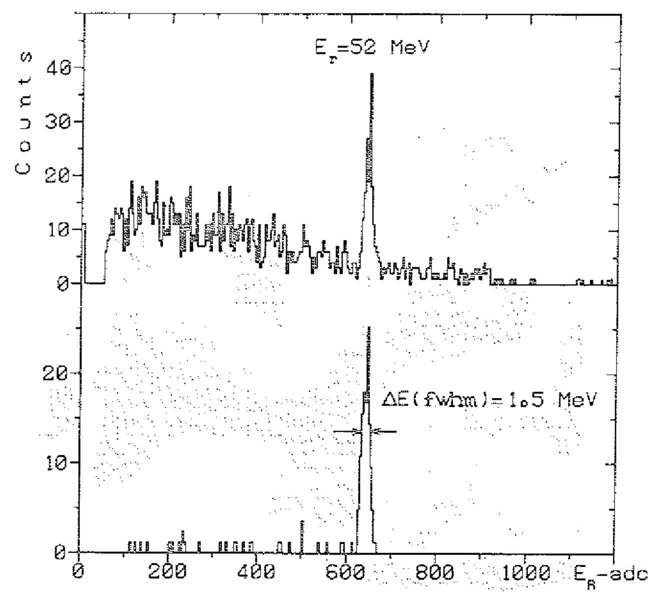

Figure 2: Inclusive (upper part) and coincident (lower part) spectra of the reaction p(α,α)p for E_α = 172 MeV and θ_{lab} = 45^0.

insensitivity to magnetic fields and the absence of a voltage divider and a high voltage supply.

Further investigations concerning the differential light output and the quenching factors of BGO are in progress.

$^{+)}$In our experiment the BGO crystal (HARSHAW) was glued to a S1723-04 Silicon photodiode (HAMAMATSU).

*Institut für Kernphysik, Universität Münster

13.4. Position Sensitive Parallel Plate Avalanche Detectors for Fission Fragments

L. Zemło, G. Hlawatsch, P. Decowski, H.P. Morsch

To proceed with earlier studies of the fission channel in nuclear reactions five position sensitive fission detectors were constructed. They are parallel plate gas counters[1)] with entrance window openings 30 x 60 mm^2 (see fig. 1). The cathode consists of 31 strips 1.8 mm

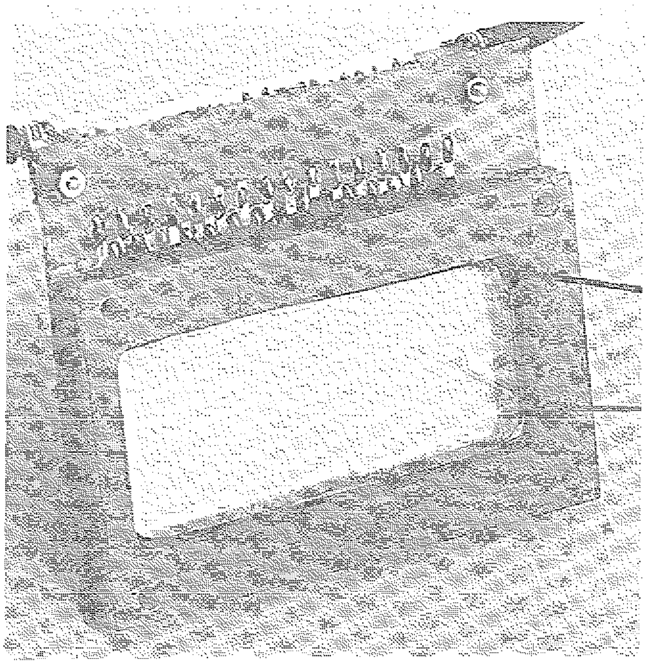

Figure 1: Front view of the parallel plate detector.

broad separated by 0.2 mm connected with the delay line with a structure 3 ns/strip. The anode is made from gold coated 1.0 μm Mylar foil placed at a distance of 2 mm from the cathode plate. A fast anode signal serves for triggering purposes. The counters are filled with isobutan gas at a pressure of 8 mbar. The operating voltage (∿ 500 V) corresponds to the proportional region of the gas amplification which helps to discriminate fission events from those of light particles. The counters were successfully applied in the $^{238}U(\alpha,\alpha' f_1 f_2)$ experiment described in sect. 1.16. in which fission fragment velocities and folding angles were measured.

Reference

1) H. Stelzer, Nucl. Instr. & Meth. 133 (1976) 409

13.5. Small size plastic scintillation counters for measurement of protons up to 100 MeV

R. Siebert, P. Decowski, H.P. Morsch, M. Rogge and P. Turek

For coincidence experiments with the BIG KARL spectrometer small size detectors are needed which can stop rather high energy particles (protons up to 100 MeV) and have a good time resolution. For this purpose we have made 4 scintillation counters (fig. 1) from plastic material

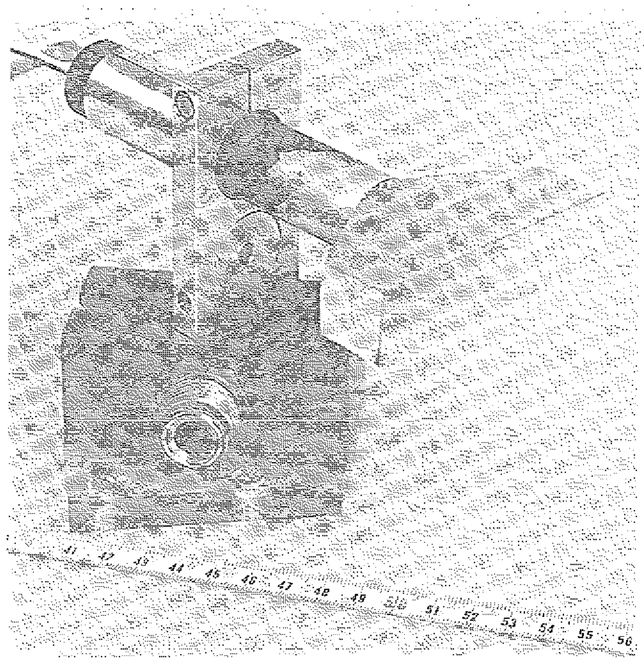

Figure 1: View of the scintillation detector.

NE 102 A (2 cm x 2 cm x 8 cm) attached to plexiglass light guides and small size photomultipliers of the type RCA 4516 2c (with integrated voltage divider). The parts are glued together and coated with 2.5 μm aluminum. Total dimensions are 8 cm long and 16 cm wide.

In test measurements the energy resolution was 5 % for protons of energies of 30 - 90 MeV, the time resolution was 800 psec. The total efficiency from 90 % at 30 MeV proton energy decreased to 70 % at 90 MeV. The detectors were successfully applied in measurements of the reactions $^{58}Ni(\alpha,\alpha' p)$ and $^{58}Ni(\alpha,{}^3He\ p)$ discussed in sect. 1.17.

13.6. High Resolution Spectrographs

H. Ikegami+

In measurements of reaction particle momenta, the ultimate resolution is limited by several factors rather than a well constructed spectrograph itself. Therefore, one has so far been involved with preparation of uniform and/or thin targets, matching of the spectrograph with an associated beam line - and even accelerator - system and so on.

In general, the momenta of reaction particles emitted from the target vary with the reaction angle, which in turn results in the kinematical line broadening. It should be noted here that the so called dispersion matching between the spectrograph and the beam line is no longer useful when the kinematical effect is appreciable[1]. This means that one has to achieve dynamic focussing control of the spectrograph as well as its associated beam line, that is, adjust magnetic multipole fields in the beam line and the spectrograph on line.

One may use, in such cases, several magnetic elements for individual multipoles. The practical considerations on the actual layout, however, usually restrict the dimensions and shapes of the space in which multipole fields have to be generated. This limitation sometimes makes it even impracticable to use desired sets of multipoles or to use ordinary magnets with conventional pole configurations. The spectrographs RAIDEN[2] (QDMDQ type at RCNP, Osaka), ENMA[3] (QMDMDM type at Japan Atomic Energy Research Institute) and BIG KARL[4] (QQDDQ type at IKP, KFA Jülich) have especially powerful multipole-field generating devices. Here, the abbreviations D, Q and M stand for dipole-, quadrupole and multipole-magnets, respectively.

In fig 1 is shown the cross-sectional view of the multipole magnet M installed in the spectrograph RAIDEN. Four sets of coils have been included to realize the current distributions, as determined in the way described below, for the quadrupole (MQ), sextupole (MS), octupole (MO) and decapole (MD) fields. Each set of coils is connected to an independent power supply so that each field component can be generated independently. An example of the lines of force distribution calculated numerically for MQ is shown in fig. 2 together with the coil configuration assumed.

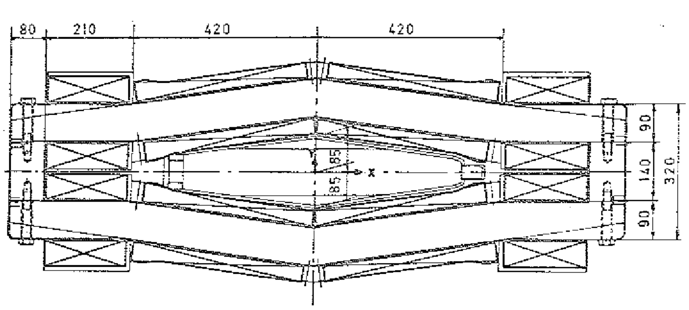

Fig. 1: Cross-sectional view of the multipole magnet

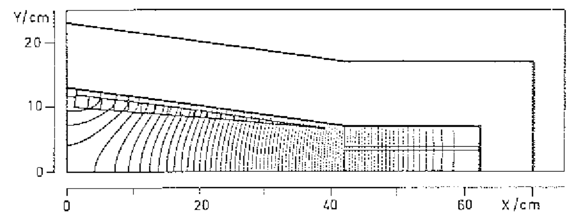

Fig. 2: Lines of force distribution in the multipole magnet, calculated for the quadrupole (MQ) component.

In fig. 3 are the field distributions measured in the symmetry plane at the middle position in the magnetic axis that is the particle beam direction. It seems to be clear from these figures that perfect distributions have been obtained in the entire aperture of the magnet.

The multipole magnets M have been designed following the concept of the "Current Sheet Magnet". This concept has an important advantage of allowing us not only to design any multipoles in a given space but also to obtain several multipoles integrated in a single magnet[5]. Magnets with three dimensional configurations are describable through any current sheet on the basis of the present theory; we shall be concerned here with the two dimensional cases in the x,y-plane, for simplicity.

Let us consider a cavity of which the contour is denoted by C, in a magnetic medium having infinitely large permeability, as seen in fig. 4. Suppose that the cavity has a thin layer of electric current (current sheet) on the surface and the magnetic field generated inside the cavity is described by a magneto-static potential ϕ. In such cases the desired current j which flows normal to the

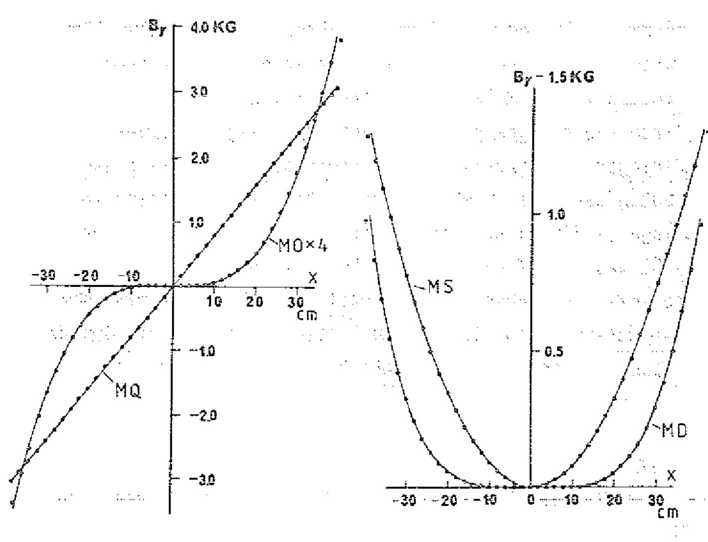

Fig. 3: Field distributions in the multipole magnet, measured along the x-axis at the middle of the magnet

x,y-plane has a density distribution along the contour C given by

$$j = d\phi/ds, \qquad (1)$$

where s denotes the arc length measured along the contour C.

For the 2N-pole field, the potential can be written as

$$\phi_{2N} = - k_{2N}\, r^N \sin(N\Theta)$$
$$r = \sqrt{x^2+y^2}\,, \quad \Theta = \tan^{-1}(\tfrac{y}{x}) \qquad (2)$$

where k_{2N} is an appropriate coefficient representing the strength of the field.

By inserting eq. (2) into eq. (1) one finds

$$j = N k_{2N}\, r^{N-1} \sin|\alpha+(N-1)\Theta|, \qquad (3)$$

where α denotes the inclination angle of the tangent of the contour C with respect to the x-axis.

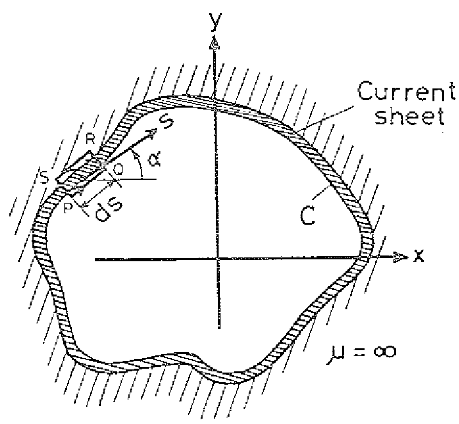

Fig. 4: Cross section of the cavity in the magnetic medium with infinitely large permeability. The current sheet is schematically presented by the shaded area along the contour.

So far we have confined ourselves to the cases where the current sheet is very thin and the permeability of the magnetic medium is infinitely large. The risk of oversimplification has been found to be small from the model calculation in which a finite size of the current sheet or a finite permeability have been taken into account in a somewhat simplified way. The results have shown that the fractional deviations of the order of $(c/l)^2$ and $1/\mu$ in the field distribution might be caused by the finite thickness (c) and extension (l) of the current sheet and by the finite permeability (μ), respectively.

Now, let us define the quantity F, as figure of merrit of magnets as,

$$F = (\text{Area of field space}) \div (\text{total current})$$
$$= (\text{Area of space enclosed by C}) \div (\oint |j|\, ds) \qquad (4)$$

For the 2N-pole field, eq. (4) can be rewritten

$$F = (\text{Area of space enclosed by C}) \div (\Sigma|\phi_i - \phi_{i+1}|) \qquad (5)$$

Here, ϕ_i and ϕ_{i+1} denote the potential where j=0, that is where the current j changes its flow direction.

The figure of merrit defined above was calculated for several kinds of multipole magnets. It was found that except for the dipole case, the figure of merrit strongly depends on the shape of the contour C, that is the configuration of the magnet especially for higher multipole cases.

As an example, let us compare two quadrupole magnets which have the same quadratic magnet aperture. One is a special case of the well known Panofsky magnet. For the other one, the magnet yoke is set at 45^o with respect to the x-axis. This magnet with skew quadratic aperture gains in figure of merrit even more than a factor of two compared to the Panofsky type magnet yielding remarkable savings in construction of the coils and the associate power supply system.

References

1) H. Ikegami, Nucl. Instr. and Meth. 175 (1980) 335
H. Ikegami, S. Morinobu, Y. Sugiyama and S.A. Martin, to be published in Nucl. Instr. and Methods

2) H. Ikegami, S. Morinobu, I. Katayama, M. Fujiwara and S. Yamabe, Nucl. Instr. and Methods 187 (1981) 13

3) Y. Sugiyama, N. Shikazono, H. Ikezoe and H. Ikegami, Nucl. Instr. and Methods 187 (1981) 25

4) S.A. Martin et al., Nucl. Instr. and Methods 214 (1983) 281

5) H. Ikegami, Proc. 6th Int. Conf. on Magnet Technology (Bratislava, 1977), p. 904

† Visiting Scientist, present address: Research Center for Nuclear Physics, Osaka University, Japan

14. COMPUTER DEVELOPMENT

14.1. Computer Configurations

K.-H. Watzlawik, M. Karmadi, R. Hellen

Besides work on the VAX-11/780 off-line computer serving the evaluation of experimental data and the development of programs for user application throughout the Institute as well as on the PDP-11/34 minicomputer used for developing PDP-11 user software, the DP-group is engaged in the development of softwars systems and experimental interface hardware on the following on-line process computer systems:

- 4-parameter analyzer system, SCORPIO, using the process computer PDP-11/34,
- multiparameter analyzer system, Nuclear-Data ND6660,
- on-line process computer PDP-11/34 for the acquisition and evaluation of data from the isochronous cyclotron and data of the beam line system,
- analyzer system of the high-resolution crystal spectrometer using the process computer PDP-11/10,
- analyzer system of the detector laboratory, Nuclear Data ND620, which is linked with the PDP-11/10 process computer for the control of experiments,
- 8-parameter analyzer system using the process computer PDP-11/24 and CAMAC for the discovery of new types of particles on reactors,
- analyzer system of the low-energy crystal spectrometer using the process computer PDP-11/10.

The off-line computers VAX-11/780 and PDP-11/34 as well as the analyzer systems SCORPIO and Nuclear-Data ND6660 have been spatially rearranged according to future requirements and received a new configuration with regard to hardware architecture.

After the evaluation software in operation on the PDP-15/50 under the RSX operating system and on the PDP-15/35 under DOS V3.3 has been implemented on the VAX-11/780 under the VMS V3.3 operating system, both PDP-15 off-line computers were put out of service as involving too much cost and technical support.

A user room was provided for interactive user operation on the VAX-11/780, accommodating at present four raster graphic terminals, three alphanumeric display terminals and two hard copy terminals.

A DATA SWITCH was conceived in cooperation with the Site Planning Department and the Central Institute for Mathematics and commissioned to enable selective communication between terminals and connected computer systems at our Institute and the Central Institute for Mathematics.

14.2. Off-Line Data Evaluation

K.-H. Watzlawik, M. Karmadi

The performance of the off-line computer VAX-11/780 has been increased for purposes like the off-line evaluation of experimental data and the development of software by hardware expansions such as

- installation of a Winchester disk RA81 (456 M byte capacity) with UDA 50 controller,
- expansion of the main memory to 4 M byte,
- installation of a terminal multiplexer DMF 32 with DMA capability and three additional display terminals (TAB 132/15).

A further increase in system performance was achieved by installing and optimizing the operating system VMS Release 3.3 and by implementing the FORTRAN Compiler V3.3 and the PASCAL Compiler V2.0.

Software development has been further facilitated by the implementation of a Tektronix 4010/4012/4014 compatible graphic library GRAFIX[1] on the VAX-11/780. This software package makes it possible to generate high-level two- and three-dimensional graphs and software character sets in FORTRAN and PASCAL. Selective clearing and modification of image parts for the raster graphic terminal WESTWARD 1015 has been implemented as an additional option in the library.

Conversion routines were created and the existing MTIKP and SORT4PAR programs expanded to the individual data structure of external analyzer systems (such an GSI-Darmstadt and ORSAY-Paris) for the evaluation of list mode data and spectra files of such analyzers.

A single spectra mode for list mode data of the CANBERA80 analyzer system was implemented in the universal Sort Program SORT4PAR.

The fit program SPTFIT for the evaluation of giant resonances which, in the past, has been capable of being run on the PDP-15/35 under the DOS V3.3 operating system was rewritten for the operating system VAX-11/780 and largely implemented. For this purpose, the program system was restructured and the areas of data handling, graphical representation on the screen and plotter as well as interactive communication were redeveloped. SPTFIT is a general FIT program of flexible design with regard to functional capability and application. Spectra can be evaluated in the interactive mode according to the following criteria:

- Background fitting,
  the background is fixed by one or more polynomials of the degree 1 to 5, which were calculated according to the least squares method using preset grid points (max. 50) within one spectrum. A background spectrum can be devided into several regions with different polynomials. Grid points were fixed by cursor positioning or numerical coordinate input on the terminal.
- Peak fitting
  A maximum of 10 Gaussian peaks of random position can be fitted simultaneously within one spectrum. The peak position, peak width and peak center are preset in the interactive mode by cursor positioning or numerical input.

- Spectra modification comprises the compessing of spectra (e.g. 4 k to 2 k or 4 k to 1 k) by the addition of consecutive channels and the division of spectra according to the algorithm ($(spectrum_i + A_i)/(spectrum_j + A_j)$). A_i and A_j are preset factors.
- Data handling comprises the storage of background spectra, modified spectra as well as peak fit parameters on disks and the plotting of spectra on the CALCOMP plotter.

The interactive dialog is effected via a graphic and an alphanumeric (hard copy) terminal. While the alphanumeric terminal is used for the global dialog and log printout, spectra are represented and graphical operations performed on the graphic terminal.

The IBM program "AUTOFIT" was implemented on the VAX-11/780 for the evalutation of nuclear reaction spectra. This implementation comprises:
- transcoding of the software according to the requirements of the VMS operating system as well as
- modification of the program from batch to interactive operation.

The interactive operation comprises control functions such as terminal dialog during program flow, representation of fitted spectra or spectrum sections on the graphic terminal as well as plotting the spectra on the CALCOMP plotter.

Furthermore, the development of a program system for the evaluation of data from the emittance measuring equipment "EMA" was started, which will be used for beam diagnostics on the beam line system of the isochronous cyclotron. Current work covers
- the investigation of methods for direct emittance calculation from the measured data by approximation of an ellipse in the (x,x') or (y,y') coordinates as a function of the rel. beam current as well as
- the development of models for approximating the beam profile by means of three-dimensional Gaussian functions from which the emittance and other relevant variables were calculated.

Both methods still exhibit unsatisfactory convergence properties in threshold regions.

14.3. On-Line Processing and Data Acquisition

K.-H. Watzlawik, R. Nellen, H. Diesburg

All the analyzer and computer systems with PDP 11 computers (4 systems), except for the SCORPIO system, were provided with RL02 disks (10 M byte each) for the purpose of standardizing and expanding the storage capacity. This action included both the conversion of existing RL01 disk drives and the replacement of some RK05 disks by RL02 disk drives.

Obsolete operating systems on PDP-11 systems were replaced by new operating systems optimized for certain units, i.e.:
- the operating system RT11 Single-Job Vers. 4.0 was installed on the analyzer systems of the detector laboratory and the high- resolution crystal spectrometer and the user systems were implemented accordingly,
- the foreground background operating system RT11 Vers. 4.0 was installed for program development on the PDP-11/34 of the DP-group.
- the operating systems RSX-11M Vers. 4.0 with FORTRAN IV V2.5 or FORTRAN IV Plus V3.0 were installed on the PDP-11/34 of the isochronous cyclotron and the DP-group.

A CAMAC driver[2] for the CAMAC controller DEC CA11A (branch controller) as well as single crate controller BORER type 1533AJ and DEC CA11F was implemented and tested on the DP-PDP-11/34 under the operating system RSX-11M for the acquisition of data and control of experiments. This driver permits the programming of CAMAC systems in the high-level language FORTRAN.

A new operating and user system MIDAS+E was installed on the multiparameter analyzer system ND6660. A one-week multiparameter data acquisition workshop was held for users and operators in cooperation with Nuclear Data. Lectures and practical exercises covered the operating system MIDAS of the analyzer ND6660, programming in FORTRAN and assembler as well as data acquisition in the MPA system.

The data acquisition software required for collecting experimental data on the magnetic spectrograph BIG KARL via 12-fold NIM counter, type 342, and CAMAC I/O modules Borer 1031 was developed and implemented on the on-line VAX-11/780 of the BIG KARL system.

The analyzer system MEMPHIS II[3] for the requirements of the nuclear reaction and nuclear spectroscopy groups were further developed in cooperation with the Central Electronics Laboratory (ZEL). An 8-parameter system was completed, new computing function modules (e.g. the 2D Window Unit) were defined and the overall system was conceived in conformity with extended requirements. A CAMAC driver[4] for the crate controller Borer, type 1533A, was implemented on the DP-VAX under the operating system VMS V3.3 for connection to this overall system.

A CAMAC-oriented 8-parameter analyzer system was conceived for the acquisition of data and control of an experiment to discover new types of particles on reactors. The hardware configuration of this system comprises:
- the process computer PDP-11/24 with 256k byte memory, two disks RL02 (10 m byte capacity each), a programmable clock KW11P,
- 2 terminals, the system console LA100 and a graphic terminal WESTWARD 1015 with the hard copy printer ANADEX DP-9500 A as well as
- a CAMAC crate with crate controller Borer 1533AJ and CAMAC modules for data acquisition and experiment control as interface hardware for the experiment.

The analyzer system works under the real-time operating system RSX-11M V.4.0. A CAMAC driver[2] has been implemented for CAMAC operations permitting the programming of CAMAC functions in FORTRAN IV. Data of a multi-detector arrangement mounted on a rotating telescope are collected during the experiment as a function of the telescope position. Experiment control comprises telescope positioning and measuring time presetting. The following is carried out for each measuring point defined by the measuring position and measuring time:

- acquisition of coincident multiparameter events as list mode data,
- generation of projection spectra for each detector as well as
- acquisition of summation count rates for detectors and experiment-accompanying pulse sources.

During the period under review, the computer and CAMAC hardware of the analyzer system was built up and component tests of the interface hardware, especially of CAMAC components, were carried out. The creation of the data acquisition and control system was commenced.

Furthermore, the development of an analyzer system for the new low-energy crystal spectrometer was started. The hardware configuration of this system comprises:

- the process computer PDP-11/10 with 64k byte memory, a programmable clock KW11P, a terminal interface DL11E and an RL02 disk,
- 2 terminals, a VT55 video terminal and an LA100 printer as well as
- CAMAC interface hardware for data acquisition and experiment control.

References

1) Graphisches System Grafix, HMI Berlin D/M 130, Nov. 1982

2) E. Busse, K.-H. Degenhardt, U. Vidic, Mumpti a Multi-User-Multi-Task-Interpreter for process-control application with CAMAC, HMI-B338, October 1980

3) K.-H. Watzlawik, R. Nellen, On-line Processing and Data Acquisition, IKP-Annual Report 1982, Jül-Spez 202, April 1983, p. 127

4) H. Heer, H. Stoff, CAMAC-Driver unter VAX-11/780 VMS 2.1, Betriebssystem für PDP11 CAMAC Crate Controller Borer 1533AJ, Jül-Spez 116, Juni 1981

14.4. Software Development

B. Hoffmann

A graphics package for 2-dim representation of data was designed and implemented on a HP 9836 computer. The program was designed in such a way that it is easy to use even by novice users without giving up the flexibility that an experienced user needs. This is achieved by using menu techniques and a lot of graphical feedback.

Here is a short list of main features:

- up to 10 different datasets can be handled simultaneously
- each of them may contain up to 9 graphs (1 x-column, 9 y-columns)
- picture may consist of 1 to 8 different viewports
- axes can be chosen to be linear or logarithmic
- Greek character fond
- data manipulation routines including: editor, sorter, calculator ...

Hardcopies can be produced on the HP 9872 (DIN A3, 4-pen) plotter or on a HP 2631 graphics printer. Utility programs for data transfer from TSS, CMS and VSPC are available.

A short introduction to this plot program is in preparation.

14.5. Data Analysis Developments at JOSEF

G. Lhersonneau, M. Karnadi, W. Tenten[+] *and T. Seo*[++]

Most of the experiments performed at JOSEF involve γ-γ-t coincidences where the data are written in event mode on magnetic tapes. Therefore much effort was devoted in 1983 to improve the sorting procedure for these coincidence events as well as for the subsequent data processing.

New routines for On/Off-line sorting at the Mega Channel Analysator MECCA at the reactor DIDO were implemented, which allow more flexibility in the selection of gates. Of particular interest for the life-time determination of nuclear levels is the facility of sorting up to 2048 time spectra from a gate matrix with 32 x 64 energy windows.

For Off-line analysis at the VAX computer of the IKP a sort program was developed starting from an existing standard routine. Owing to a new sort algorithm, the execution speed has been increased by a factor typically of 4, when compared to the previous version.

In order to minimize manual input, which is always a source of errors, the data processing has been highly automatized. One of the crucial steps in the analysis of coincidence data is the correction for the background caused in the projections by Compton and random events. For this purpose we have implemented an algorithm[1] which estimates exactly the correction, irrespective of the width and position of the gating windows. The basic assumptions are that background windows are chosen on both sides of the 'peak' window (see fig. 1) and that in this channel range the background has a linear behaviour according to the following formula:

$$B(x,y,z) = B_0(z) + A_x(z)(x - x_0) + A_y(z)(y - y_0) \qquad (1)$$

Here x,y (resp. z) are channel numbers on the gating (resp. projected) parameters of the γ-γ-t event. The channels x_0, y_0 are chosen close to the peak centroids. The coefficients B_0, A_x, A_y describe a projection gated by the channel pair x,y.

It is shown in ref. 1) that the background corrected projection C(z) can be expressed as a linear combination of the various projections $P_i(z)$ obtained by combining the gating windows in all possible ways as shown on fig. 1. This yields an expression of the form:

$$C(z) = \sum_{i=1}^{9} \alpha_i P_i(z) \qquad (2)$$

The index i is shown on fig. 1. The coefficients α_i are functions of the gating window limits only. If a window is missing the α_i's in the corresponding row or column will be zero. (Note that the accuracy will be reduced since then a constant background is assumed.)

The standard error σ(z) on C(z) is no longer given by Poisson's statistics but instead by:

$$\sigma(z) = \left| \sum_{i=1}^{9} \alpha_i^2 P_i(z) \right|^{1/2} \qquad (3)$$

In the case of unfavourable peak to background ratios the deduced errors might be substantially underestimated if one ignores eq. 3. Therefore, a separate σ(z) spectrum is also generated and the peak analysis routine has been adapted in order to extract the errors from it.

To conclude, the present set of routines allows a faster and more accurate data analysis of γ-γ-t coincidence events. An example is the background correction described above. The formalism is presented for 3-parameter events, but might be easily extended to more dimensions. Therefore, it can have a broader range of applications in other coincidence experiments.

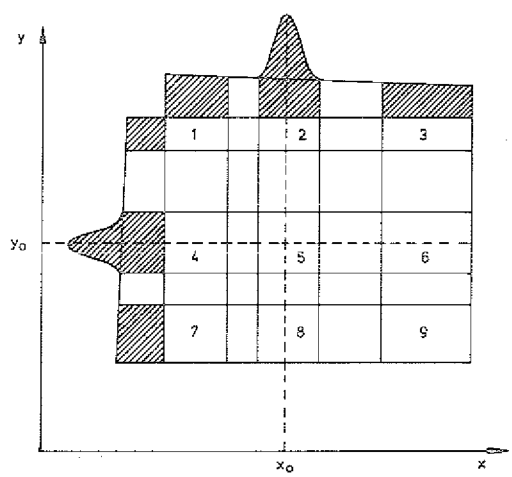

Fig. 1: Gate matrix

Reference

1) G. Lhersonneau, Nucl. Instr. Meth. 157 (1978) 349

[+] Zentrallabor für Elektronik, KFA Jülich
[++] on leave from Research Reactor Institute, Kyoto University, Kumatori-cho, Osaka, Japan

15. Electronic Division

H. Labus, J. Bojowald

1. Soft- and hardwaremodules were developed for the new low energy bent crystal spectrometer where three rotary motions must be controlled simultaneously. The actual values of the motions are the Bragg angle, which is measured by a 1" resolution HAIDENHAIN encoder, the angle position of the multiwire detector chamber, which is measured by a 1' resolution encoder and the direction of the detector plane which is measured by a potentiometric resolver. To make possible the use of the control and data acquisition concept of the older high energy bent crystal spectrometer a special double EURO-SMP input module was built to convert the encoder data. The software was written in PL/M-80 on our INTEL-DS246-software development system and partially tested. In the vincinity of the position balance point the set values of the analogue velocity control circuits are reduced monotonically to zero which gives excellent settling behavior even at large dead times. Printed boards were developed and tested for the multiwire detector chamber to supply its forty hybrid preamplifiers and to shape their output signals.
(H. Labus, G. Lürken, K. Winkler)

2. The set up to the BIBLIS multidetector AXION-experiment was supported. A special photomultiplier base for the EMI-9808K tube was developed with very small volume and mechanisms to fasten the 16 units with constant pressure on large anti counters of PLEXIGLAS GS-2037. Six ORTEC model 276 bases were modified to fit for EMI-9813KB tubes. A MATTKE Serie MTRB servo-amplifier was used to build a motor control to rotate the 40 tons shielding box to the measurement positions by manual preset or by the PDP11/10-CAMAC data-acquisition system.
(N. Dolfus, W. Ernst, G. Lürken, K. Winkler)

3. Investigations were made to expand our INTEL-DS246 software development system to multiuser applications and to other languages than PL/M preferably PASCAL, and to 16-Bit-computers as INTEL-8086/8088. In this context other hard- and software products are being tested together with the central electronic lab ZEL. With the combination of SIEMENS-SMP-Hardware and DIGITAL-RESEARCH software PASCAL/MT + 85/86 and SPP running under CP/M or MP/M it seems to be able to configure low cost single or multiuser software development systems which would furthermore habe the advantage of using the same hardware as our application systems.
(N. Dolfus, G. Lürken, H. Labus)

4. The old electronic control of beam slit ASI within the JULIC beam guide system which could only change the width of two perpendicular, beam limiting windows was replaced by a new analogue control which allows to position each of the four jaws independently. Three switch selectable windows with preselectable width and centerposition can be choosen manually or by computer controlled DAC's.
(N. Dolfus, H. Labus, G. Lürken, K. Winkler)

5. About 75 repair, manitenance or modification jobs of NIM- and CAMAC modules, TV-cameras and monitors, power supplies of all categories, electronically controlled scattering chambers and beams slits and a great variety of special instruments from our own or external production were performed.
(N. Dolfus, W. Ernst, G. Lürken, K. Winkler)

16. Radiation Protection

16.1. Composition of the radioactive contaminations at JULIC and sensitivity of the contamination measuring devices

I. Uray+, *H.J. Probst*

The German Radiation Protection Ordinance prescribes contamination limits in radiation areas. If those limits are exceeded, certain measures (decontamination, sealing in foils etc.) have to be taken. In practice this implies that the amount of contamination have to be determined quickly during routine operation. For cases where one handles only a few radioactive nuclides this quick determination is possible. Either a methane/propane/butane gas flow or a Xe-filled proportional counter is used.

The situation at a cyclotron is really complex. It was therefore considered necessary to investigate whether the value (count rate) obtained through an usual contamination measuring device could possibly be used to determine the amount of the contamination in the cyclotron area also. For that purpose wipe samples were taken from many places in the cyclotron area as well as from outside. The nuclides present in those samples and their activities were determined by means of a Ge(Li)- or a Si(Li)-detector. Furthermore, the count rates produced by those different samples were registred using several contamination measuring devices. In all 19 wipe samples were analysed. The investigation furnished following essential results:

a) The number of the nuclides identified was large (even after a cooling time of few days at least 28 radioactive nuclides with half-lives between 2.7 days and 5 years were analysed).

b) The nuclidic composition differs strongly at least partly, from sample to sample. The highest contamination activities consisted of Re-, W- and Ta-nuclides (nuclides of the strongly activated tungsten wires of the deflector). However, partly ^{7}Be, ^{65}Zn, ^{75}Se, ^{169}Yb were also dominant nuclides.

c) The sensitivity of the contamination measuring devices varies by more than a factor of 10 for the different wipe samples. The trends in the sensitivities of the different measuring devices are the same for the different wipe samples.

d) The sensitivities are in some cases very low (only small fractions of the background count rate). The Xe-counter has by a factor of 3 to 6 higher sensitivity.

e) Small covers over the samples and distances of a few centimeters between sample and counter reduce the sensitivity strongly.

Details on points a) to e) are described in ref. 1), 2).

The results allow to make the following two important statements:

a) Because of the great differences in the sensitivity the value of the contamination activity cannot be deduced from the count rate of the usually used contamination measuring devices.

b) Because of the low sensitivity, in many cases the count rate of the contamination measuring devices corresponding to the contamination limits is so small that this value cannot be used for practical purposes.

References

1) I. Uray, H.J. Probst, Bericht der 17. Jahrestagung des Fachverbandes für Strahlenschutz e.V. über Strahlenschutzaspekte bei radioaktiven Kontaminationen, June 8-10, 1983, Aachen, FS-83-32-1, pp 505-518, Redaktion H. Bonka, H.-G. Horn

2) H.J. Probst, I. Uray, Proc. of the XI. Regional Congress of IRPA Austrian-Hungarian-Yugoslavian Radiation Protection Meeting on Recent Development and New Trends in Radiation Protection, Sept. 20-24, 1983, Vienna (in press)

+IAEA fellow, permanent address: Institute of Nuclear Research of the Hung. Acad. Sci., P.O.B. 51, H-4001 Debrecen, Hungary

16.2. Routine Duties

H.J. Probst, I. Uray[+]*, H.J. Hintzen, K. Krafft*

Since the personnel safety system operates well, in 1983 the major emphasis was placed on the dangers during handling of partly strongly activated cyclotron components. It is especially critical during the annual maintenance. This is evident from figure 1 which shows the distribution of the ß-γ-dose rate in the cyclotron vault at the beginning of the maintenance.

It is satisfying that in spite of the high dose rates and the extremely inhomogeneous distribution the resulting man-rem-dose amounts only to 0.11 Sv (11 rem), thereby showing a slow decrease in comparison to 1982. Only one person got a dose of 15 m Sv (1,5 rem). This is somewhat higher than the annual dose of 10 m Sv which we internally try to observe. Moreover, regulary examinations of the persons handling unsealed radioactive materials were performed but no incorporations were detected. Also the extremity doses were negligibly low. Contaminations could be kept within limits so that no special measures were necessary.

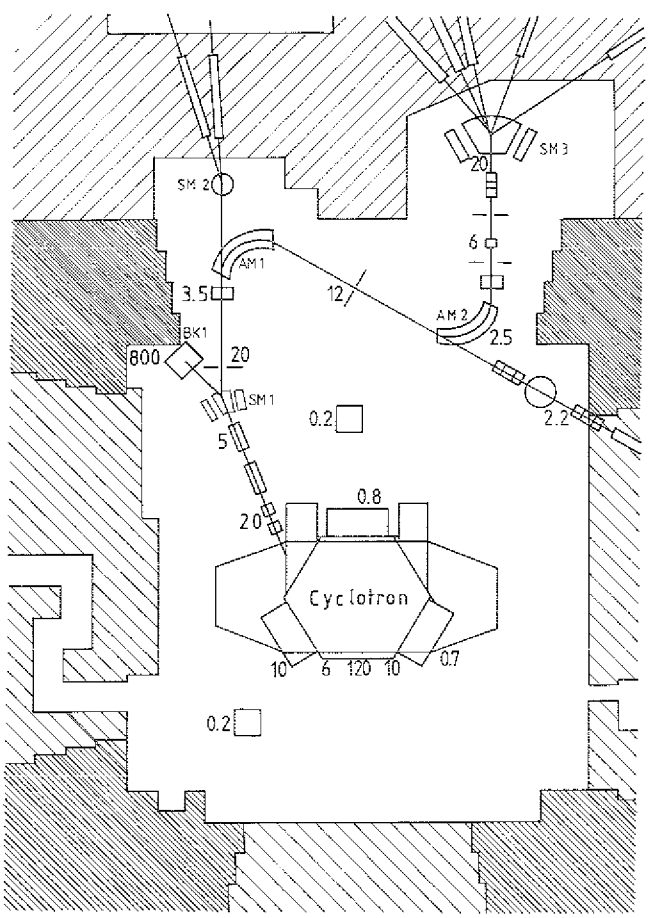

Figure 1: Distribution of the ß-γ-dose rate in the cyclotron vault at the start of the maintenance. The values are given in m Sv/h (1 m Sv/h = 100 mrem/h).

[+]IAEA fellow, permanent address: Institute of Nuclear Research of the Hung. Acad. Sci., P.O.B. 51, H-4001 Debrecen, Hungary

16.3. Gamma-Neutron Radiation Field in the Cyclotron Vault

I. Uray[+], *H.J. Probst*

The mixed gamma-neutron radiation field was investigated in the cyclotron vault of the JULIC isochronous cyclotron. Knowledge of this field at an accelerator operating long since provides us with important information for the accidental dosimetry which, often based on an incomplete measured data set, can give an uncertain estimation of the dose only. The goal of these studies was to obtain a comprehensive picture over the in-operation status of the cyclotron[1] and, to search for a possible way of a simple but sufficient control of the accidental doses[2].

The operating cyclotron is a very intense source of fast neutrons and, because of slowing down processes, intermediate and thermalized neutrons are always present, as well. Different kinds of nuclear processes are producing also considerable gamma radiation. According to our gamma dose measurements the proportion of the gamma dose near the accelerator is negligible compared to the neutron dose equivalent, amounting to a few per cent of it only. This means, that the control of the gamma dose alone is insufficient for the accidental dosimetry inside the shielded area.

A possible accidental dosimetrical use of activation detectors and thermoluminescent materials was investigated. Moreover to identify the produced neutron spectra the activation sets of In, Cu, Al and Fe materials were used. In first order the ratio of the thermal, epithermal and intermediate energy neutrons depends on the size of the room, while the type of the reaction investigated is only a modifying factor. In the measured thermal flux proportion moreover there is a significant difference when the measurements are carried out in air or on the surface of a moderating phantom or of the wall. However fast neutrons are giving the decisive part of the neutron dose because of their much higher biological harm. Consequently their dose contribution is responsible nearly for the whole neutron dose equivalent.

Long-term dose equivalent rate measurements were carried out employing a Studsvik 2002 B Neutron Radiation Meter, controling the radiation status and testing other measuring methods, respectively. Fig. 1 shows a characteristic fragment of these measurements. It has been found, that

1.) the neutron dose equivalent rate in the cyclotron vault can exceed the value of 1 mSv/h (100 mrem/h) even at the entrance of the cyclotron vault, where the radiation level is relatively low. (Close to the cyclotron the dose equivalent rate is much higher.)

2.) the operating conditions of this cyclotron influence the dose equivalent rate, which is frequently and considerably changing even at the same place. At such circumstances the common use of activation accidental dosemeters is unadvisable.

3.) the LiF thermoluminescent dosemeters offer a possible solution for the accidental dosimetry. Their gamma and thermal neutron responses can be selected on the basis of the differences of their glow curves. Furthermore it is possible from these data, having some knowledge about the neutron spectra, to give an acceptable estimation for the neutron dose equivalent, as well.

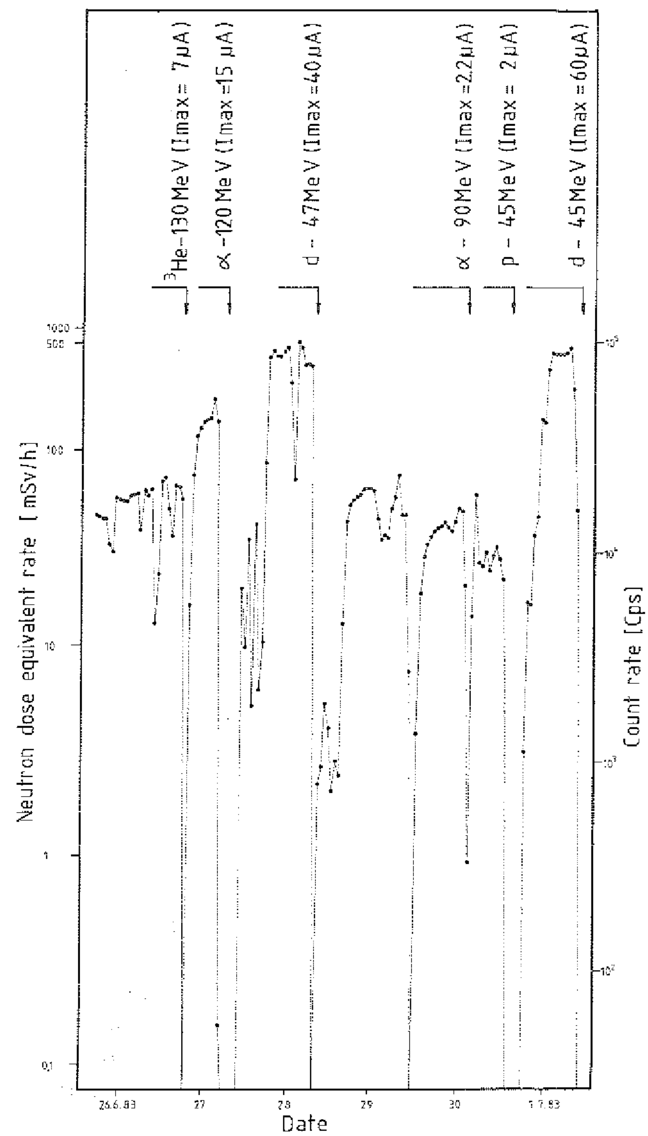

Figure 1: The hourly changes of the neutron dose equivalent rate $\dot{H}$ at the entrance of the cyclotron vault between 26.06.83 and 01.07.83 in mSv/h units (1 mSv = 100 rem). The particles accelerated, their energy and the highest internal currents are given.

References

1) I. Uray, P. Manngård, H.J. Probst, M. Heinzelmann, Characteristics of mixed neutron-gamma radiation field around cyclotrons, XI. Regional Congress of IRPA, Vienna, Sept. 20-24, 1983 (to be published)

2) I. Uray, E. Gyarmati, J. Fèlszerfalvi, H.J. Probst, M. Heinzelmann, Possible use of LiF dosemeters in mixed neutron-gamma fields, XI. Regional Congress of IRPA, Vienna, Sept. 20-24, 1983 (to be published)

[+]IAEA fellow, permanent address: Institute of Nuclear Research of the Hung. Acad. Sci., P.O.B. 51, H-4001 Debrecen, Hungary

16.4. Skin Dose of the Contaminations at JULIC

H.J. Probst, I. Uray⁺

In the first part of the Radiation Protection contribution it has been shown that the value of a contamination existing in the cyclotron area cannot be deduced from the count rate of a contamination measuring device. Long experience has shown that contaminations at JULIC are important almost exclusively for causing radiation dose to the skin. Therefore, for radiation protection reasons, it is important to know if and which relationship exists between the count rate of a contamination measuring device and the radiation dose to the skin caused by this contamination.

To clarify this question 7 wipe samples were taken from different places in the cyclotron area as well as from outside. In order to be able to measure the skin dose caused by these contaminations with the help of 3 layers of TLD[1,2] which are often used in the KFA, and to achieve rather good homogenity, disks of 12 mm diameter were punched out of the wipe samples. The subsequent investigations were carried out using these samples: determination of the nuclidic composition, of the activity and of the count rate of contamination measuring devices. The resulting sensitivity of the measuring devices varies considerably for the different samples, as shown in figure 1a (the sensitivities for $^{90}Sr/^{90}Y$ and ^{204}Tl are given for comparison). The skin dose produced by these samples was measured by means of 3 layers of TLD as mentioned above. The exposure was carried out for periods between 1 and 7 days depending on the activity of the sample. Figure 1b shows the skin dose rate factor. It is the quotient between the measured dose per exposure time and the measured activity per area. The values of $^{90}Sr/^{90}Y$ and ^{204}Tl are also given for comparison. As can be seen, the values differ rather strongly. The arrow at wipe samle no. 7 in the figure 1a and 1b denotes that due to the non-detection of all the γ-lines of the sample no. 7 the activity is a little higher than the value taken for calculating the sensitivity and the skin dose rate factor, respectively. Therefore, the sensitivity and the skin dose rate factor are a little smaller.

Finally, the quotient of the skin dose rate factor and the sensitivity of the measuring device was determined. This value describes the skin dose rate produced by a contamination corresponding to 1 cps per cm^2 of contamination area. It is noticeable that all the wipe samples have about the same quotient. Since this value is less than the values for $^{90}Sr/^{90}Y$ and ^{204}Tl, it offers an advantageous possibility to set count rate limits on the contamination measuring devices for contaminations of unknown composition: The count rate produced by a $^{90}Sr/^{90}Y$- or ^{204}Tl-calibration source having a known activity which is accepted or given as deciding value may be used for unknown contaminations, too. Of course, the activity of the unknown contamination is in general higher than the values given in the Radiation Protection Ordinance, as seen in figure 1a, but the skin dose produced by this contamination - and this should be the criterion - is less than the values of $^{90}Sr/^{90}Y$ or ^{204}Tl for instance, as seen in figure 1c).

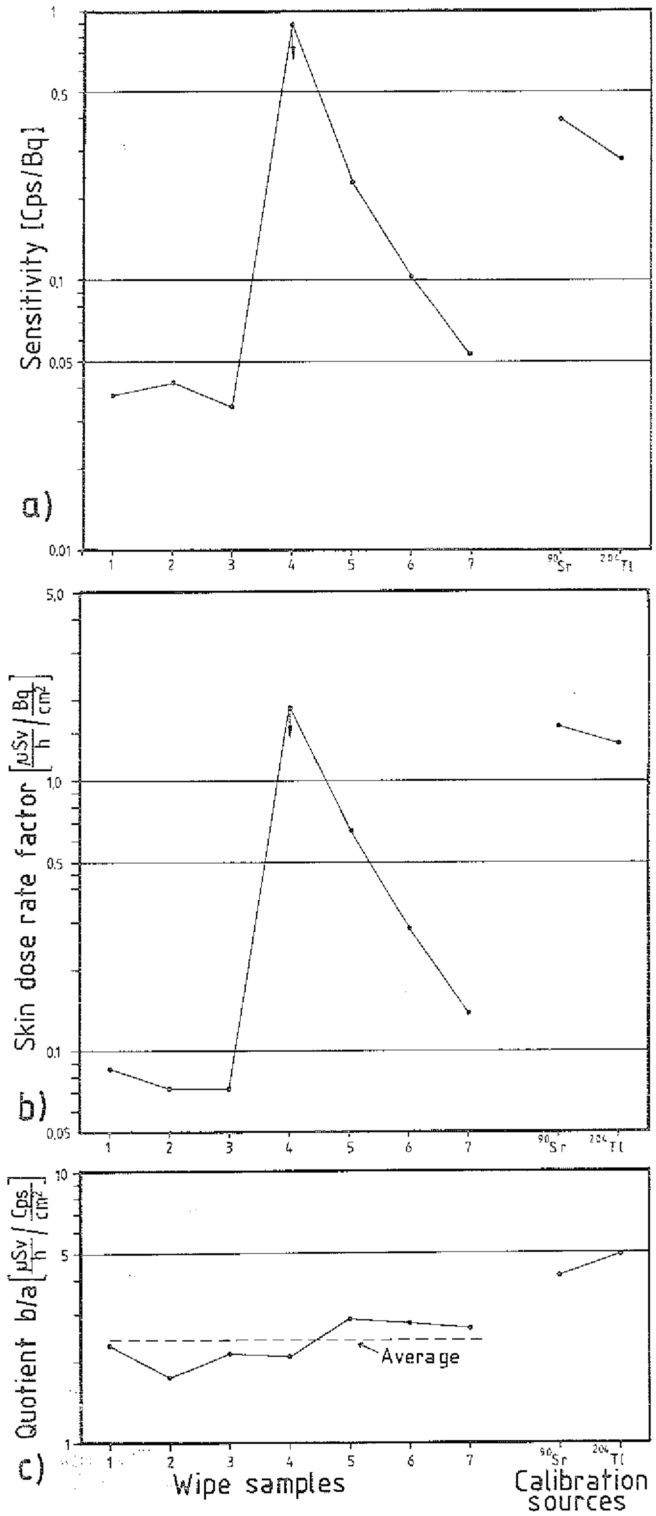

Figure 1:
a) Sensitivity of the contamination measuring device H1370 (Fa. Herfurth, F.R. Germany) for 7 different wipe samples and the calibration sources $^{90}Sr/^{90}Y$ and ^{204}Tl. For sample 4 see text.
b) Experimentally determined skin dose rate factors for 7 different wipe samples. The values for $^{90}Sr/^{90}Y$ and ^{204}Tl are given for comparison. For details see text.
c) Quotient of the skin dose rate factor (figure 1b) and the sensitivity (figure 1a). It describes the skin dose rate per count rate (of a contamination measuring device) normalized to the unit area. For details see text.

References
1) M. Heinzelmann, H. Schüren, M. Keller, Radiation Protection Dosimetry, Vol. 2 No. 2 p. 115-118 (1982)
2) M. Keller, Int. Report ZST-Bericht 0330, KFA Jülich (1980)

⁺IAEA fellow, permanent address: Institute of Nuclear Research of the Hung. Acad. Sci., P.O.B. 51, H-4001 Debrecen, Hungary

17. Engineering Office and Mechanical Workshop

W. Briëll, D. Gross, H. Hadamek, A. Retz, U. Rindfleisch, H. Schwan

In 1983 the work of the engineering office was concentrated on the realization of the ISIS project (see status report p. 122).

A great part of the mechanical workshop's capacity was dedicated to a complete service on the vacuum system of the magnet spectrometer BIG KARL and to a major repair of its air pads supporting the concrete shielding. A new vacuum chamber with a big (100 x 10 cm) window in front of the focal plane detectors went into operation. Active slits behind the first and second quadrupole were built in.

Besides the service and the scheduled maintenance of the cyclotron, improvements on the vacuum system were achieved during the annual shutdown period. For the installation of three 10.000 l/s cryo-pumps the cyclotron vacuum chamber was equipped with additional pump sockets (NW 500). Due to higher internal beam currents the radiation damage of the extraction elements increased significantly. Three new septum blades had to be produced since the repair of the highly activated components was not possible in most cases.

A new crystal spectrometer for experiments with low energy X-rays was designed. The production is in progress (see figure 1). To satisfy the requested accuracy for positioning and rotation, high requirements in bearing, measuring and production have to be met. The two independent supporting arms of the crystal and the detector are centered by a double wire ball bearing system and are positioned by separate driving elements. The relative angle measurement is performed by two angular encoders with an accuracy of less than 5 seconds of arc from the source to the crystal and less than 1 second of arc from the crystal to the detector. The detector support is rotatable around its center. Driving is done by 12 Volt DC motors.

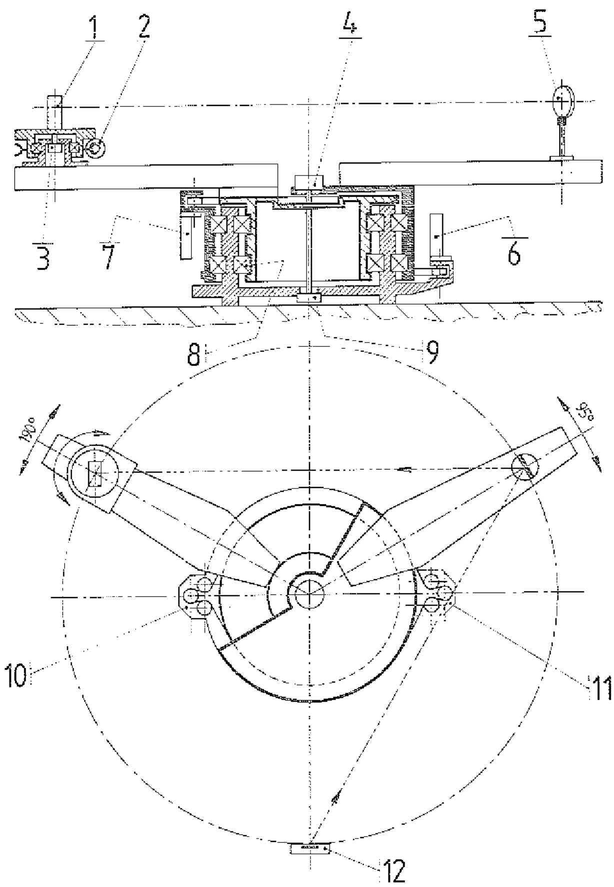

1) detector 2) detector rotation 3) encoder 4) detector angular encoder 5) crystal 6) motor for crystal movement 7) motor for detector movement 8) wire ball bearing 9) (source)-crystal angular encoder 10+11) gear system for crystal and detector drive 12) source

The mechanical components for two experiments searching for penetrating particles (axions) at nuclear reactors were designed and constructed. At the FRJ-1 reactor an experimental set-up was installed which changes the angular position of the radiation detectors and the shielding periodically. The construction of a similar improved device consisting essentially of a low radiation background rotatable chamber weighing 30 tons is in progress.

V. SCIENTIFIC ADVISORY COUNCIL OF THE INSTITUTE OF NUCLEAR PHYSICS

Prof. Dr. R. Bock	GSI Darmstadt
Prof. Dr. G.E. Brown	Dept. of Phys. SUNY at Stony Brook
Prof. Dr. P.G. Hansen	University of Aarhus
Prof. Dr. T. Mayer-Kuckuk	University of Bonn
Prof. Dr. R. Santo (Chairman)	University of Münster
Prof. Dr. R. Sizmann	University of München
Prof. Dr. H.J. Specht	University of Heidelberg
Prof. Dr. H. Vonach	Österreichische Akademie der Wissenschaften, Wien
Prof. Dr. H.A. Weidenmüller	MPI für Kernphysik, Heidelberg
Prof. Dr. L.E. Feinendegen	KFA Jülich

VI. EXTERNAL COMMITTEE FOR GUEST EXPERIMENTS

Prof. Dr. R. Santo	University of Münster
Prof. Dr. H.J. Specht	University of Heidelberg

VII. PERSONNEL

Institute for Nuclear Physics:

Dr. C. Mayer-Böricke	Director of the Institute for Nuclear Physics (Experiment I), till 30.9.1983 Professor of Physics at University of Bonn
Dr. P. Turek	Acting Director (Experiment I), since 1.10.1983
Dr. O. Schult	Director of the Institute for Nuclear Physics (Experiment II) Professor of Physics at University of Köln
Dr. J. Speth	Director of the Institute for Nuclear Physics (Theory) Managing director of the Institute for the year 1983 Professor of Physics at University of Bonn

Scientific Staff:

DP G. de Angelis (E2)
since Oct. 31, 1983

Dr. G. Baur (Th)
(Privat Dozent at the
Univ. of Basel)

Dr. G. Berg (E2)

Dr. H. Beuscher (LI)

Dipl. W. Bodewig (E2)
until Dec. 31, 1983

DP J. Bojowald (Ec)

Dr. G. Borchert (E2)

DI W. Bräutigam (LI)

Dipl. B. Brinkmöller (E2)

Dr. D. Cha (Th)
since Feb. 9, 1983

DP C. Conci (Th)

DI S. Dasgupta (LI)
until July 21, 1983
(BARC, Calcutta/India)

Dr. P. Decowski (E1)
(Warsaw University,
Warsaw/Poland)

DP H. Dermawan (Th)
until Aug. 14, 1983

Dr. A. Djaloeis (E1)

Dr. S. Drozdz (Th)
since Oct. 3, 1983

DP A. Ercan (E2)
until April 30, 1983

Dr. W. Gast (E1)

DP R. Gissler (Th)

Prof. K. Göke (Th)
(Prof. at the
Univ. of Bonn)

Dr. F. Grümmer (Th)

Dipl. G. Hebbinghaus (E1)

Dr. G. Hlawatsch (E2)

DP B. Hoffmann (Th)

Dr. P. Jahn (E1)

Dipl. A. von Kempis (Th)

Dr. P. Kleinheinz (E2)

Dr. V. Klemt (Th)

Dr. H.R. Koch (E2)

DP P. Kohl (E2)

Dipl. A. Krämer-Flecken (E1)

DP W. Krauss (E1)

Dr. S. Krewald (Th)

DP D. Kusnezov (E2)
until Aug. 31, 1983

Dr. H. Labus (Ec)

DP M. Lach (E2)

Dr. H. Lawin (LI)

Dr. G. Lhersonneau (E2)

Dr. R.M. Lieder (E1)
(Privat Dozent at the
Univ. of Bonn)

Dr. H. Machner (E1)

DP A. Magiera (E2)

DM K. Maßmeyer (E2)

Dr. H.G. Mathews (LI)

DP T. Massey (E2)

Prof. Dr. C. Mayer-Böricke (E1)
(Prof. at the Univ. of Bonn)
until Sept. 30, 1983

Dr. J. Meißburger (LI)

DP G. Menzen (E2)

Dr. R.A. Meyer (E2)
until Aug. 31, 1983
(Lawrence Livermore Nat.Lab.)

Dr. H.P. Morsch (E1)

DP K. Nakayama (Th)

Dr. A. Neskakis (E1)
until Apr. 14, 1983
(Univ. of Crete,
Iraklion/Greece)

Dipl. M. Nolte (E1)

Dr. W. Oelert (E1)

Dr. F. Osterfeld (Th)

Dr. G. Pâlla (E1)
(Hung. Academy of Sciences,
Central Res. Inst. for
Physics, Budapest)

Dipl. D. Paul (LI)
since Apr. 25, 1983

DI R. Posorski (E2)
until March 31, 1983

DP D. Prasuhn (LI)
since July 1, 1983

DP H.J. Probst (Rp)

DP D. Protić (Dt)

DP D. Provoost (Th)
since Aug. 1, 1983

DP J. Reich (LI)

Dr. G. Riepe (Dt)

DP J. Römer (LI)

Dr. M. Rogge (E1)

DP T. Rose (E2)

Dr. P. von Rossen (LI)
since Oct. 1, 1983

DP B. Rubio (E2)

DI B. Sack (E2)

Dipl. J. Schäffler-Krãh (E1)

Prof. Dr. O. Schult (E2)
(Prof. at the Univ.
of Cologne)

DP A. Schulte (Th)
since March 1, 1983

Dipl. G. Seniwongse (E1)

Dr. T. Seo (E2)

Dr. H. Seyfarth (E2)

Dipl. R. Siebert (E1)

Dr. K. Sistemich (E2)
(Privat Dozent at the
Univ. of Cologne)

DP G. Sondermann (E2)
from June 1 to July 31, 1983

Prof. Dr. J. Speth (Th)
(Prof. at the Univ. of Bonn)

Dr. H.J. Stein (E2)

DP J. Tain (E2)

Dr. H. Talarek (E2)

Dr. Y. Tokunaga (E2)
until May 6, 1983

Dr. P. Turek (E1)

DP T. Venkova (E1)
(Bulgarian Academy of
Sciences, Sofia, Bulgarien)

Dr. R. Wagner (E2)

Dr. J. Wambach (Th)
since June 13, 1983

Dr. K.-H. Watzlawik (Da)

Dr. P. Wucherer (LI)

Dipl. R. Yogeshwar (E2)

DP T. Zekorn (E2)

Dr. L. Zemlo (E1)
until Sept. 14, 1983
(Institute of Nuclear
Research, Warsaw/Poland)

Dr. K. Zuber (E2)

Research visitors
(for one week to six months):

Prof. J. Blomqvist (E2)
from June 26 to July 2, 1983 and
from Sept. 18 to Sept. 24, 1983
(Res. Inst. for Phys. Stockholm)

Dr. B. Bochev (E1)
from Apr. 18 to July 15, 1983
(Bulg. Academy of Sciences,
Sofia, Bulg.)

Dr. T. Bocheva (E1)
from June 13 to Aug. 31, 1983
(Bulg. Academy of Sciences,
Sofia, Bulg.)

Dr. M. Bogdanovic (E2)
from May 4 to Aug. 4, 1983
(Boris Kidric Inst., Zagreb)

Dr. S. Brant (E2)
from Oct. 1 to Oct. 31, 1983
(Boris Kidric Inst., Zagreb)

Prof. P.J. Daly (E2)
from Sept. 5 to Sept. 13, 1983
(Purdue Univ., W. Lafayeth,
Indiana)

Dr. J.P. Didelez (E1)
from July 2 to July 14, 1983
(Inst. Phys. Nucl., Orsay,
France)

Dr. C. Fiolhais (Th)
from Aug. 1 to Aug. 31, 1983
(Univ. of Granada, Spain)

Dr. J. Hanzlik (Dt)
from June 1 to June 30, 1983
(Tschechoslowakische Akademie
der Wissenschaften, Prag)

Prof. Dr. H. Ikegami (E2)
from Aug. 25 to Nov. 4, 1983
(Res. Center for Nucl. Phys.,
Osaka)

Prof. L. Jarczyk (E2)
from Nov. 15 to Dec. 16, 1983
(Jagellonian Univ. Cracow)

Dr. R. Julin (E2)
from Nov. 28 to Dec. 11, 1983
(Univ. of Jyväskylä)

Dr. Bohumil Krâl (E1)
from Nov. 25, 1982 to Febr. 24,
1983
(Techn. Hochschule Brno, Tsche-
choslowakei)

Dipl. A. Lallena (Th)
from May 9 to June 30, 1983
(Univ. of Granada, Spain)

Prof. Dr. I. Lovas (E1)
from March 28 to May 27, and
Sept. 2 to Oct. 8, 1983
(Hung. Academy of Sciences,
Budapest, Ungarn)

Prof. G. Love (Th)
from Sept. 1 to Sept. 30, 1983
(Univ. of Georgia, Athens, USA)

Dr. S. Lunardi (E2)
from Sept. 24 to Oct. 14, 1983
(Istituto Nazionale de Fisica Nucl., Padova)

Dr. Z.Y. Ma (Th)
from March 7 to Apr. 8, 1983
(SUNY at Stony Brook, USA)

Prof. Dr. A. Marinov (E1)
from July 1 to Sept. 30, 1983
(The Hebrew Univ. of Jerusalem, Jerusalem, Israel)

Dr. T. Morek (E1)
from May 15 to Aug. 15, 1983
(Warschau Univ.)

Dr. C. Morris (E2)
from Sept. 10 to Sept. 15, 1983
(LANL, Los Alamos)

Prof. J. Nemeth (Th)
from Jan. 21 to March 31, 1983
(Eötvös Univ., Budapest, Hungary)

Prof. V. Paar (E2)
from Oct. 1 to Oct. 31, 1983
(Boris Kidric Inst., Zagreb)

Prof. V.R. Pandharipande (Th)
from July 19 to Aug. 12, 1983
(Univ. of Illinois, Urbana, USA)

Prof. Dr. M. Piiparinen (E2)
from Jan. 3 to Jan. 23, 1983
(Univ. of Jyväskylä)

Prof. Dr. P.-G. Reinhard (Th)
from March 7 to 10, from Apr. 20 to 22, from Sept. 19 to 30 and from Oct. 17 to 28, 1983
(Univ. Erlangen)

Dr. H. Reinhardt (Th)
from Sept. 9 to Oct. 31, 1983
(ZfK Rossendorf, Dresden, DDR)

Dr. B. Schwesinger (Th)
from Sept. 1 to Oct. 31, 1983
(SUNY at Stony Brook, USA)

Dr. G. Sletten (E1)
from July 3 to July 9, 1983
(Niels Bohr Inst., Copenhagen)

Dr. F. Soramel-Stanco (E2)
from Apr. 5 to 12, and Oct. 5 to 9, 1983
(CSNSM, Orsay)

Prof. A. Strzalkowski (E2)
from Nov. 15 to Dec. 16, 1983
(Jagellonian Univ. Cracow)

Dr. B. Styczen (E2)
from Nov. 17 to Dec. 21, 1983
(Jagellonian Univ. Cracow)

Dr. J. Styczen (E2)
from Dec. 9 to Dec. 21, 1983
(Institute fo Nucl. Phys., Cracow, Poland)

Dr. C. Sükösd (E1)
from Jan. 3 to Febr. 4, 1983
und from July 18 to Aug. 17,1983
(Dept. of Atomic Physics, Roland Eötvös Univ. Budapest)

M.D. Trivedi (LI)
from Sept. 15, 1983 to Sept. 14, 1984
(Bhabba Atomic Research Centre, Calcutta, India)

Prof. T. Udagawa (Th)
from May 30 to June 30, 1983
(Univ. of Texas, Austin, USA)

Dr. I. Uray (Rp)
from Jan. 1, 1983 to June 30, 1984
(Hungarian Acad. of Sciences, Debrecen)

Prof. J.N. Urbano (Th)
from June 1 to Oct. 9, 1983
(Univ. of Coimbra, Portugal)

Technical and administrative staff:

K. Barth (Ec)
H.G. Böge (LI)
W. Borgs (E2)
H. Borsch (LI)
B. Brandes (Da)
since Sept. 1, 1983
W. Briêll (Cd)
R. Brings (LI)
G. Brittner (Ec)
E. Bröke1 (Th)
U. Burck (Ad)
J. But (Ws)
H. Diesburg (Ec)
A. Dohmen (Ad)
N. Dolfus (Ec)
F. Drees (LI)
R. Enge (Ws)
R. Engelbrecht (Ws)
since May 2, 1983
P. Engels (LI)
W.R. Ermer (E2)
W. Ernst (Ec)
R. Fiedler (LI)
G. Gad (LI)
G. Göbbels (Ws)
A. Golik (Ws)
E. Gollnick (E2)
E. Griesen (Ad)
D. Groß (Cd)
U. Hacker (LI)
until March 31, 1983
H. Hadamek (Ws)
M. Heese (Ad)
H. Heinrichs (LI)
K. Hieble (LI)
H. Hintzen (Rp)
W. Hoffmeister (LI)
K. Hütten (Ws)
H.M. Jäger (E1)
I. Jannakos (LI)
H.J. Jansen (Ws)
R. Janssen (Ad)
A. Jeglorz (E2)
M. Karnadi (Da)
M. Köhnen (E2)
R. Korthues (LI)
K. Krafft (Rp)
K.P. Kruck (LI)
T. Künster (Dt)
E. Lawin (Dt)
H.-G. Lemkamp (E2)
G. Lürken (Ec)
H. Metz (Dt)
H. Meuser (Ws)
A. Müller (LI)
R. Nellen (Da)
K. Nicoll (Dt)
J. Pfeiffer (Dt)
H.W. Pohl (E1)
A. Retz (Cd)
U. Rindfleisch (Cd)
N. Rotert (LI)
T. Sagefka (LI)
H. Sauer (Ad)
M. Scherer (Ad)
until Oct. 21, 1983
G. Schlienkamp (LI)
P. Schmidt (E2)
Jos. Schmitz (Ws)
Jürg. Schmitz (LI)
F. Schultheiß (Ws)
E. Schwaab (E2)
H. Schwan (Ws)
R. Seidemann (E2)
H. Sieling (Ad)
D. Weynen (LI)
since Sept. 1, 1983
K.P. Wieder (E2)
W. Wilms (LI)
K. Winkler (Ec)
M. Witteler (LI)
since Sept. 1, 1983
J. Wolanski (Ws)
R.A. Wollny (Ec)
from Jan. 20 to July 19, 1983

(E1) Institute for Experimental Nuclear Physics I
(E2) Institute for Experimental Nuclear Physics II
(Th) Institute for Theoretical Nuclear Physics
(LI) Large Nuclear Physics Instruments
(Ad) Administration
(Cd) Construction and Design
(Da) Data Acquisition Group
(Dt) Detector and Target Laboratory
(Ec) Electronics
(Rp) Radiation Protection
(Ws) Mechanical Workshop

VIII. PUBLICATIONS

IKP-100183
Bauhoff, W.; von Geramb, H.V.; Palla, G.
Study on nonlocal and local equivalent microscopic optical potentials
Phys. Rev. C27 (1983) 2466-2481
2o.o6.o

IKP-100283
Baur, G.; Shyam, R.; Rösel, F.; Trautmann, D.
Calculation of proton-neutron coincidence cross sections in 56 MeV deuteron-induced breakup reactions by post form distorted-wave Born approximation
Phys. Rev. C28 (1983) 946-949
2o.8o.o

IKP-100383
Baur, G.; Rösel, F.; Trautmann, D.
Ionisation induced by neutrons
J. Phys. B: At. Mol. Phys. 16 (1983) L419-423
2o.8o.o

IKP-100483
Berg, G.P.A.; Hürlimann, W.; Katayama, I.; Martin, S.A.; Meißburger, J.; Römer, J.G.M.; Styczen, B.; Tain, J.L.
Isoscalar character of the 1^+ state at 5.844 MeV in ^{208}Pb
Proc. 1983 RCNP Int. Symp. on Light Ion Reaction Mechanism, Osaka, Japan, 16.-20.5.83, ed. by H. Ogata, T. Kammuri, I. Katayama, RCNP Osaka (1983) 214-222
2o.o6.o

IKP-100583
Beuscher, H.; Mathews, H.-G.; Krauss-Vogt, W.
Status of the superconducting ECR-source of the Jülich cyclotron
Proc. 5th E.C.R. Ion Sources Workshop, Louvain-La-Neuve, Belgien (1983) 83-91
2o.o3.o

IKP-100683
Blomqvist, J.; Kleinheinz, P.; Daly, P.J.
Atomic masses above ^{146}Gd derived from a shell model analysis of high spin states
Z. Phys. A - Atoms and Nuclei 312 (1983) 27-41
2o.1o.o

IKP-100783
Borchert, G.; Rose, T.; Schult, O.W.B.
Evidence for intensity shifts of K X rays
Proc. Int. Conf. on X Ray and Atomic Inner-Shell Physics, Eugene, USA, 23.-27.8.82, ed. by B. Crasemann (American Inst. of Physics, New York, 1982) S. 115-120
2o.1o.o

IKP-100883
Borchert, G.L.; Schult, O.W.B.; Speth, J.; Hansen, P.G.; Jonson, B.; Ravn, H.L.; McGrory, J. B.; ISOLDE Collaboration
Differences of the mean square charge radii of the stable lead isotopes observed through electronic K X-ray shifts
Nuov. Cim. 73A (1983) 273-294
2o.1o.o; 2o.8o.o

IKP-100983
Brown, V.R.; Krewald, S.; Speth, J.
Crucial test for the Δ(1232)-hole effect: (n,p) vs. (p,n)
Phys. Rev. Lett. 50 (1983) 658-661
2o.8o.o

IKP-101083
Budzanowski, A.; Bechstedt, U.; Machner, H.; Jahn, P.; Mayer-Böricke, C.
Local excitation of the nucleus
Proc. 3rd Int. Conf. on Nucl. Reaction Mechanisms, Varenna, Italien, 14.-19.6.82, ed. by E. Gadioli, Ricerca Scientifica ed Educazione Permanente, Suppl. 28 (1982) 310-321
2o.o6.o

IKP-101183
Cunsolo, A.; Foti, A.; Immè, G.; Pappalardo, G.; Raciti, G.; Rizzo, F.; Saunier, N.; Baur, G.; Shyam, R.; Rösel, F.; Trautmann, D.
Deuteron inclusive and exclusive spectra in ^6Li + light nucleus collisions
Proc. 3rd Int. Conf. on Nucl. Reaction Mechanisms, Varenna, Italien, 14.-19.6.82, ed. by E. Gadioli, Ricerca Scientifica ed Educazione Permanente, Suppl. 28 (1982) 352-367
2o.8o.o

IKP-101283
Dehesa, J.S.; Guardiola, R.; Polls, A.; Ros, J.
Monopole resonances and Jastrow correlations
Phys. Lett. 118B (1982) 13-20
2o.8o.o

IKP-101383
Dermawan, H.; Osterfeld, F.; Madsen, V.A.
Cross section calculations for nucleon-^{40}Ca and α-^{40}Ca elastic scattering from microscopic nonlocal optical potentials
Phys. Rev. C27 (1983) 1474-1482
2o.8o.o

IKP-101483
Didelez, J.P.; Frascaria, N.; Gerlič, E.; Hourani, E.; Morlet, M.; Machner, H.; Protič, D.; Riepe, G.; Sükösd, C.
H and He ions production by 200 MeV protons
Proc. 3rd Int. Conf. on Nucl. Reaction Mechanisms, Varenna, Italien, 14.-29.6.82, ed. by E. Gadioli, Ricerca Scientifica ed Educazione Permanente, Suppl. 28 (1982) 237-242
2o.o6.o; 2o.2o.o

IKP-101583
Djaloeis, A.; Alderliesten, C.; Bojowald, J.; Mayer-Böricke, C.; Oelert, W.; Turek, P.
Role of the ^3He optical model potential ambiguity in the distorted-wave Born approximation description of the $^{58}Ni(^3He,d)^{59}Cu$ reaction at 130 MeV incident energy
Phys. Rev. C27 (1983) 1483-1488
2o.o6.o

IKP-101683
Djaloeis, A.; Bojowald, J.; Gopal, S.; Oelert, W.; Puttaswamy, N.G.; Turek, P., Mayer-Böricke, C.
Breakup of ^3He projectiles at an incident energy of 43.3 MeV/nucleon
Phys. Rev. C27 (1983) 2389-2392
2o.o6.o

IKP-101783
Djaloeis, A.; Gopal, S.; Bojowald, J.; Oelert, W.; Turek, P.; Mayer-Böricke, C.
$^{25}Mg(^3He,\alpha)^{24}Mg$ reaction at 130 MeV incident energy
Phys. Rev. C28 (1983) 67-72
2o.o6.o

IKP-101883
Djaloeis, A.; Gopal, S.; Bojowald, J.; Oelert, W.; Turek, P.; Mayer-Böricke, C.
High energy $(^3He,d)$ proton stripping by ^{27}Al and ^{28}Si nuclei: Transitions to excited states
Phys. Rev. C28 (1983) 561-573
2o.o6.o

IKP-101983
Gill, R.L.; Shmid, M.; Chrien, R.E.; Chy, Y.Y.; Wolf, A.; Brenner, D.S.; Sistemich, K.; Wohn, F.K.; Yamamoto, H.; Chung, C.; Walters, W.B.
Levels in ^{148}Ce from the decay of mass separated ^{148}La
Phys. Rev. C27 (1983) 1732-1744
2o.65.o

IKP-102083
Goeke, K.; Grümmer, F.; Reinhard, P.-G.
Three-dimensional quantized ATDHF calculations for heavy ion fusion
Proc. Topical Meeting on Nucl. Fluid Dynamics, Triest, Italien, 11.-15.10.82, IAEA-SMR-108 (1983) 153-160
2o.8o.o

IKP-102183
Goeke, K.; Speth, J.
Theory of giant resonances
Ann. Rev. Nucl. Part. Sci. 32 (1982) 65-115
2o.8o.o

IKP-102283
Goeke, K.; Cusson, R.Y.; Grümmer, F.; Reinhard, P.-G.; Reinhardt, H.
Time dependent Hartree-Fock and beyond
Prog. Theor. Phys., Suppl. 74+75 (1983) 33-65
2o.8o.o

IKP-102383
Goeke, K.; Grümmer, F.; Reinhard, P.-G.
Three-dimensional nuclear dynamics in the quantized ATDHF approach
Ann. Phys. 150 (1983) 504-551
2o.8o.o

IKP-102483
Goeke, K.; Grümmer, F.; Reinhard, P.-G.
Quantized ATDHF calculations for subbarrier fusion of heavy ions
Phys. Lett. 124B (1983) 21-25
2o.8o.o

IKP-102583
Jakob, A.; Rösel, F.; Trautmann, D.; Baur, G.
Screened Coulomb trajectory effects on inner shell ionization
Z. Phys. A - Atoms and Nuclei 309 (1982) 13-18
2o.8o.o

IKP-102683
Kalend, M.; Anderson, B.D.; Baldwin, A.R.; Madey, R.; Watson, J.W.; Chang, C.C.; Holmgren, H.D.; Koontz, R.W.; Wu, J.R.; Machner, H.
Energy and angular distributions of neutrons from 90 MeV protons and 140 MeV alpha-particle bombardment of nuclei
Phys. Rev. C28 (1983) 105-119
2o.o6.o

IKP-102783
Katayama, I.; Berg, G.P.A.; Hürlimann, W.; Martin, S.A.; Meißburger, J.; Oelert, W.; Rogge, M.; Römer, J.G.M.; Tain, J.; Styczen, B.; Gaul, G.
Charge transfer reactions of ^{3}He in carbon at 68, 99 and 130 MeV
Phys. Lett. 92A (1982) 385-388
2o.o6.o

IKP-102883
Katayama, I.; Berg, G.P.A.; Hürlimann, W.; Martin, S.A.; Meißburger, J.; Oelert, W.; Rogge, M.; Römer, J.G.M.; Tain, J.L.; Styczen, B.; Gaul, G.
Equilibrium charge states of ^{3}He ions emerging from solid targets at high incident energies
Phys. Rev. A27 (1983) 2738-274o
2o.o6.o

IKP-102983
Kicinska-Habior, M.; Decowski, P.; Dabrowska, M.; Grochulski, W.; Jaracz, P.; Matulewicz, T.; Sikora, B.; Töke, J.; Somorjai, E.
Analysis of the ^{27}Al(p,γ)^{27}Si reaction at subbarrier energies in terms of the direct-semi-direct model
Z. Phys. A - Atoms and Nuclei 312 (1983) 89-93
2o.o6.o

IKP-103083
Koch, H.R.; Schult, O.W.B.; Seyfarth, H.; Bechteler, H.; Yogeshwar, R.
Search for light penetrating bosons with the use of a rotatable detector arrangement at a nuclear reactor
Z. Phys. A313 (1983) 239-240
2o.1o.o

IKP-103183
Krewald, S.; Dehesa, J.S.
Meson-exchange current effects in heavy nuclei
Proc. 5th Topical School "Quarks, Mesons and Isobars in Nuclei", Motril/Granada, Spanien, 6.-10.9.82, ed. by R. Guardiola, A. Polls (World Scient. Publ. Co. Pte. Ltd., Singapore 1983) S. 266-277
2o.8o.o

IKP-103283
Krmpotić, A.; Nakayama, K.; Pio Galeao, A.
Giant first-forbidden resonances
Nucl. Phys. A399 (1983) 478-502
2o.8o.o

IKP-103383
Lieder, R.M.
Band crossings in ^{181}Os and comparison with features observed in ^{180}Os
Proc. Workshop on Nucl. Structure at High Spin, NBI Kopenhagen 1983, S. 49-51
2o.1o.o

IKP-103483
Lieder, R.M.
A γ-γ coincidence spectrometer with large efficiency and background suppression
Proc. Workshop on Development and Perspective of In-Beam Measurement of Particle-e-γ Spectroscopy and Particle-γ Correlation, Osaka, Japan, 1982, ed. by H. Ejiri, Y. Nagai, Osaka University (1983) 85-88
2o.1o.o

IKP-103583
Ma, Z.Y.; Wambach, J.
A deformable Chiral bag
Phys. Lett. 132B (1983) 1-6
2o.8o.o

IKP-103683
Ma, Z.Y.; Wambach, J.
Implications of a dynamical effective mass on the nuclear shell-model
Nucl. Phys. A402 (1983) 285-317
2o.8o.o

IKP-103783
Machner, H.
Continuous light ion spectra from heavy ion induced reactions
Proc. Int. Conf. on High Energy Nucl. Physics, Balatonfüred, Ungarn, ed. by J. Erö (1983) 209-217
2o.o6.o

IKP-103883
Machner, H.
Pre-equilibrium in heavy ion reactions
Phys. Rev. C28 (1983) 2173-2175
2o.o6.o

IKP-103983
Machner, H.
Study of particle emission following π^- absorption at rest
Nucl. Phys. A395 (1983) 457-470
2o.o6.o

IKP-104083
Machner, H.
Continuous spectra of light ions at incident energies above 15 MeV/nucleon
Proc. 3rd Int. Conf. on Nucl. Reaction Mechanisms, Varenna, Italien, 14.-19.6.82, ed. by E. Gadioli, Ricerca Scientifica ed Educazione Permanente, Suppl. 28 (1982) 131-155
2o.o6.o

IKP-104183
Machner, H.; Bechstedt, U.; Budzanowski, A.; Jahn, P.; Mayer-Böricke, C.
Pre-equilibrium and knock-out processes in (α,2α) reactions
Nucl. Phys. A400 (1983) 584c
2o.o6.o

IKP-104283
Machner, H.; Riepe, G.; Protić, D.; Bohlen, H.G.; Fuchs, G.
Light particle emission from $^{20}Ne+^{197}Au$
Nucl. Phys. A400 (1983) 584c
2o.o6.o; 2o.2o.o

IKP-104383
Madsen, V.A.; Suzuki, T.; Bernstein, A.M.; Brown, V.R.
Neutron and proton multipole matrix elements in ^{48}Ca and ^{208}Pb.
Phys.Lett. 123B (1983) 13-15
2o.8o.o

IKP-104483
Mairle, G.; Schindler, K.; Grabmeyr, P.; Wagner, G.J.; Schmidt-Rohr, U.; Berg, G.P.A.; Hürlimann, W.; Martin, S.A.; Meißburger, J.; Römer, J.G.M.; Styczen, B.; Tain, J.L.
Spectroscopic results from a high-resolution study of proton particle-hole states in ^{208}Pb
Phys. Lett. 121B (1983) 307-312
2o.o6.o

IKP-104583
Martin, S.A.; Hardt, A.; Meißburger, J.; Berg, G.P.A.; Hacker, U.; Hürlimann, W.; Römer, J.G. M.; Sagefka, T.; Retz, A.; Schult, O.W.B.; Brown, K.L.; Halbach, K.
The QQDDQ magnet spectrometer "Big Karl"
Nucl. Instr. Meth. 214 (1983) 281-303
2o.o6.o

IKP-104683
Mathews, H.-G.; Beuscher, H.; Krauss-Vogt, W.
ECR-ion-source development at the Jülich cyclotron
Proc. Int. Ion Engineering Congress - ISIAT '83 & IPAT '83, Kyoto, Japan (1983) 209-214
2o.3o.o

IKP-104783
Mathews, H.-G.; Kruger, A.; Penselin, S.; Weinig, A.
The new high intensity polarized proton and deuteron source for the Bonn isochronous cyclotron
Nucl. Instr. Meth. 213 (1983) 155-164
2o.3o.o

IKP-104883
Mathews, H.-G.; Beuscher, H.; Fiedler, R.; Krauss-Vogt, W.
Results of a 5 GHz ECR test device - Pre-ISIS 2
Proc. 5th E.C.R. Ion Sources Workshop, Louvain-La-Neuve, Belgien (1983) 70-82
2o.3o.o

IKP-104983
Mathews, H.-G.; Beuscher, H.; Mayer-Böricke, C.
Status of ECR-source development for ISIS at Jülich
Physica Scripta T3 (1983) 52-55
2o.3o.o

IKP-105083
Matulewicz, T.; Decowski, P.; Kicinska-Habior, M.; Sikora, B.; Toke, J.
Analysis of the $^{28}Si(p,\gamma)^{29}P$ reaction data in the region of the subbarrier single particle resonances
Acta Physica Polonica B14 (1983) 617-624
2o.o6.o

IKP-105183
Meyer, R.A.; Kaffrell, N.; Lawin, H.; Lhersonneau, G.; Monnard, E.; Poor, V.; Pfeiffer, B.; Pinston, J.A.; Ragnarsson, J.; Schussler, F.; Schmitt, A.; Seo, T.; Sistemich, K.; Trautmann, N.
Symmetric deformation in A~100 odd and odd-odd nuclei and its influence of fission product beta-decay rates
Proc. Experts Meeting on Fission Product Data, BNL, USA, Oktober 1983
2o.65.o

IKP-105283
Morsch, H.P.; Berg, G.P.A.; Decowski, P.; Tain, J.L.; Rogge, M.; Turek, P.; Zemlo, L.; Meißburger, J.; Römer, J.G.M.
Study of the (^3He,t) reaction on heavy nuclei
Proc. 1983 RCNP Int. Symp. on Light Ion Reaction Mechanism, Osaka, Japan, 16.-20.5.83, ed. by H. Ogata, T. Kammuri, I. Katayama, Osaka (1983) 294-298
2o.o6.o

IKP-105383
Morsch, H.P.; Rogge, M.; Turek, P.; Decowski, P.; Zemlo, L.; Mayer-Böricke, C.; Martin, S.A.; Berg, G.P.A.; Katayama, I.; Meißburger, J.; Römer, J.G.M.; Reich, J.; Wucherer, P.; Bräutigam, W.
The giant octupole resonance in deformed nuclei
Phys. Lett. 119B (1982) 311-314
2o.o6.o; 2o.3o.o

IKP-105483
Morsch, H.P.; Rogge, M.; Decowski, P.; Machner, H.; Sükösd, C.; David, P.; Debrus, J.; Hartfiel, J.; Janszen, H.; Schulze, J.
Fission decay of isoscalar giant resonances excited in 172 MeV α scattering from ^{238}U
Phys. Lett. 119B (1982) 315-319
2o.o6.o

IKP-105583
Morsch, H.P.; Decowski, P.; Rogge, M.; Turek, P.; Zemlo, L.; Martin, S.A.; Berg, G.P.A.; Hürlimann, W.; Meißburger, J.; Römer, J.G.M.
Isoscalar giant resonances in ^{208}Pb - in particular $2\hbar\omega$ L=0,2,4 and 6 excitations - studied in small angle α scattering
Phys. Rev. C28 (1983) 1947-1958
2o.o6.o

IKP-105683
Morsch, H.P.
Investigation of giant resonances in hadron scattering experiments
Proc. XXI Int. Winter Meeting on Nucl. Physics, Bormio, Italien, 24.-29.1.83, S. 66-81
2o.o6.o

IKP-105783
Neumann, B.; Rebel, H.; Gils, H.J.; Planeta, R.; Buschmann, J.; Klewe-Nebenius, H.; Zagromski, S.; Shyam, R.; Machner, H.
Inclusive break-up reactions of ^6Li at an incident energy of 26 MeV/nucleon
Nucl. Phys. A400 (1983) 585c
2o.o6.o

IKP-105883
Oelert, W.; Palla, G.
Ground state transitions in (d, Li) reactions on sd-shell nuclei
Proc. 1983 RCNP Int. Symp. on Light Ion Reaction Mechanism, Osaka, Japan, 16.-20.5.83, ed. by H. Ogata, T. Kammuri, I. Katayama, Osaka (1983) 420-429
2o.o6.o

IKP-105983
Oelert, W.; Berg, G.P.A.; Djaloeis, A.; Mayer-Böricke, C.; Turek, P.
(d,^6Li) alpha-transfer reaction on ^{32}S and ^{34}S at E_d = 80 MeV
Phys. Rev. C28 (1983) 73-81
2o.o6.o

IKP-106083
Osterfeld, F.
Quenching of Gamow-Teller resonances - a Δ-isobar effect or a background problem?
Proc. Int. Workshop XI on Gross Properties of Nuclei and Nucl. Excitations, Hirschegg, 17.-22.1.83, ed. by H. Feldmeier, TH + GSI Darmstadt (1983) 169-172
2o.8o.o

IKP-106183
Palla, G.; von Geramb, H.V.; Pegel, C.
Elastic and inelastic scattering of 25.6 MeV protons from even Sm isotopes
Nucl. Phys. A403 (1983) 134-155
2o.o6.o

IKP-106283
Posorski, R.
Thermisches Verhalten von Energieabsorbern als Wärmequellenanlage in Wärmepumpen-Heizungsanlagen
Jül-1864, August 1983, 121 Seiten
2o.6o.1

IKP-106383
Posorski, R.
Energieabsorber-Wärmeübergänge und Systemverhalten
ISES Tagungsbericht Erfahrungen mit Kollektor-Energieabsorber- und Wärmepumpenanlagen, Köln, 1.12.83, S. 137-153
2o.6o.1

IKP-106483
Prakash, M.; Wambach, J.; Ma, Z.Y.
Effective mass in nuclei and the level density parameter
Phys. Lett. 128B (1983) 141-146
2o.8o.o

IKP-106583
Puttaswamy, N.G.; Oelert, W.; Djaloeis, A.; Mayer-Böricke, C.; Turek, P.; Glaudemans, P.W. M.; Metsch, B.C.; Heyde, K.; Waroquier, M.; von Isacker, P.; Wenes, G.; Lopac, V.; Paar, V.
Structure of the energy levels of ^{53,55,57}Mn from the (d,^{3}He) reaction on iron isotopes at 80 MeV
Nucl. Phys. A401 (1983) 269-302
2o.o6.o

IKP-106683
Puttaswamy, N.G.; Oelert, W.; Djaloeis, A.; Mayer-Böricke, C.; Turek, P.
Energy levels of the odd Mn nuclei from the (d,^{3}He) reaction
IEEE Transactions on Nucl. Science NS-30 (1983) 1140-1142
2o.o6.o

IKP-106783
Reinhard, P.-G.; Cusson, R.C.; Goeke, K.
Time evolution of coherent ground-state correlations and the TDHF approach
Nucl. Phys. A398 (1983) 141-188
2o.8o.o

IKP-106883
Shizuma, K.; Lawin, H.; Sistemich, K.
Level structure of ^{106}Mo
Z. Phys. A - Atoms and Nuclei 311 (1983) 71-78
2o.65.o

IKP-106983
Shizuma, K.; Hill, J.C.; Lawin, H.; Shaanan, M.; Selic, H.A.; Sistemich, K.
Levels in ^{102}Zr populated in the decay of ^{102}Y
Phys. Rev. C27 (1983) 2869-2878
2o.65.o

IKP-107083
Shizuma, K.; Ahrens, H.; Bocquet, J.P.; Kaffrell, N.; Kern, B.D.; Lawin, H.; Meyer, R.A.; Sistemich, K.; Tittel, G.; Trautmann, N.
Odd neutron nuclei near A=100: Rotational Bands in ^{103}Mo and ^{105}Mo populated in the β^- decays of ^{103}Nb and ^{105}Nb
Z. Phys. A - Atoms and Nuclei 314 (1983)
2o.65.o

IKP-107183
Shyam, R.
Exact finite range calculations of one nucleon pick-up reactions induced by polarized deuteron
Proc. 3rd Int. Conf. on Nucl. Reaction Mechanism, Varenna, Italien, 14.-19.6.82, ed. by E. Gadioli, Ricerca Scientifica ed Educazione Permanente, Suppl. 28 (1982) 715-729
2o.8o.o

IKP-107283
Shyam, R.; Baur, G.; Rösel, F.; Trautmann, D.
Post-form DWBA description of coincidence spectra in light ion induced break-up reactions
Proc. 1983 RCNP Int. Symp. on Light Ion Reaction Mechanism, Osaka, Japan, 16.-20.5.83, ed. by H. Ogata, T. Kammuri, I. Katayama (1983) 541-557
2o.8o.o

IKP-107383
Shyam, R.; Baur, G.; Budzanowski, A.; Bojowald, J.; Dabrowski, H.; Mayer-Böricke, C.; Oelert, W.; Riepe, G.; Rogge, M.; Turek, P.; Rösel, F.; Trautmann, D.
Explanation of ^{3}He and triton rates in the alpha breakup inclusive cross sections
Phys. Rev. C27 (1983) 2393-2396
2o.o6.o; 2o.8o.o

IKP-107483
Soramel-Stanco, F.; Styczen, J.; Prokofjev, P.; Ercan, A.; Kleinheinz, P.
A 45 ns 8^{+} isomer in the doubly odd ^{150}Eu nucleus
Z. Phys. A317 (1983) 127
2o.1o.o

IKP-107583
Speth, J.
Δ(1236)-isobar degrees of freedom and the strength of spin-isospin resonances
AIP Conf. Proc. No. 97 "The Interaction between Medium Energy Nucleons in Nuclei - 1982", Indiana Univ. Cycl. Facility, ed. by H.O. Meyer (American Inst. of Physics, New York, 1983) S. 398-403
2o.8o.o

IKP-107683
Speth, J.
Electric and magnetic resonances in nuclei
Proc. 5th Topical School "Quarks, Mesons and Isobars in Nuclei", Motril/Granada, Spanien, 6.-11.9.82, ed. by R. Guardiola, A. Polls (World Scient. Publ. Co. Ltd., Singapore 1983) S. 102-145
2o.8o.o

IKP-107783
Speth, J.
Giant resonances
Nucl. Phys. A396 (1983) 153c-170c
2o.8o.o

IKP-107883
Schmid, K.W.; Grümmer, F.; Faessler, A.
Nuclear structure theory in spin- and number-conserving quasiparticle configuration spaces - Part I: General formalism
Phys. Rev.
2o.8o.o

IKP-107983
Schmid, K.W.; Grümmer, F.; Faessler, A.
Nuclear structure theory in spin- and number-conserving quasiparticle configuration spaces - Part II: The MONSTER-approach
Phys. Rev.
2o.8o.o

IKP-108083
Schult, O.W.B.
Nuclear studies at a high current spallation source
Proc. 1983 RCNP Kikuchi Summer School, Kyoto, Japan, ed. by H. Ogata, M. Fujiwara, A. Shimizu, Osaka (1983) 171-192
2o.1o.o

IKP-108183
Schwesinger, B.; Wambach, J.
The width of isovector monopole vibrations in charge exchange reactions
Phys. Rev. C28 (1983)
2o.8o.o

IKP-108283
Stein, H.J.; Köhnen, M.
Solarheizungsanlage zum Beheizen, Funkübertragungsstelle Garmisch II auf der Zugspitze - Meßprogramm
BMFT Statusbericht Nutzung der Sonnenenergie in bundeseigenen Gebäuden, Band I, Mai 1983, S. 76-84
2o.6o.1

IKP-108383
Styczen, J.; Nagai, Y.; Piiparinen, M.; Ercan, A.; Kleinheinz, P.
Deformed ground-band states in the N=86 nucleus ^{152}Dy
Phys. Rev. Lett. 50 (1983) 1752-1755
2o.1o.o

IKP-108483
Styczen, J.; Piiparinen, M.; Nagai, Y.; Kleinheinz, P.; Bazzacco, D.; Eberth, J.; Blomqvist, J.
Seniority-three yrast states in the N=82 nucleus ^{147}Tb
Z. Phys. A - Atoms and Nuclei 312 (1983) 149-154
2o.1o.o

IKP-108583
Trautmann, D.; Rösel, F.; Baur, G.
Accurate calculation of inner-shell ionization
Nucl. Instr. and Meth. 214 (1983) 21-27
2o.8o.o

IKP-108683
Trautmann, D.; Baur, G.; Rösel, F.
Fast evaluation of the relativistic ionisation form factor: Momentum space representation
J. Phys. B16 (1983) 3005-3013
2o.8o.o

IKP-108783
Tokunaga, Y.; Seyfarth, H.; Schult, O.W.B.; Börner, H.G.; Hofmeyr, Ch.; Barreau, G.; Brissot, R.; Kaup, U.; Mönkemeyer, Ch.
The ^{75}Se(n,γ)^{76}Se reaction and the low-lying level structure of ^{76}Se
Nucl. Phys. A411 (1983) 209
2o.1o.o

IKP-108883
Xiangfu, S.; Bazzacco, D.; Gast, W.; Gelberg, A.; Kaup, U.; Dewald, A.; Zell, K.O.; von Brentano, P.
Band crossing in ^{130}Ba
2o.1o.o

IKP-108983
Uray, I.; Probst, H.J.
Empfindlichkeit von Kontaminationsmeßgeräten für praktisch vorkommende Kontaminationen am Jülicher Isochronzyklotron - Problematik der Grenzwertfestlegung für Routinebetrieb
Tagungsbericht der 17. Jahrestagung des Fachverbandes für Strahlenschutz e.V. über Strahlenschutzaspekte bei radioaktiven Kontaminationen, Aachen, 8.-10.6.83, Redaktion: H. Bonka, H.-G. Horn, FS-83-32-T, November 1983, S. 505-518
2o.o5.o

IX. CONFERENCE CONTRIBUTIONS, TALKS

IKP-200183
Ahrens, H.; Bocquet, J.P.; Kaffrell, N.; Kern, B.D.; Lawin, H.; Shizuma, K.; Sistemich, K.; Tittel, G.; Trautmann, N.
Rotational structure in ^{101}Zr, ^{103}Mo, ^{105}Mo?
Frühjahrsgung der DPG, Sektion A: Kernphysik, Münster, 21.-25.3.83
2o.65.o

IKP-200283
Ambrosetti, P.; Andersson, H.E.B.; Fröhlich, C.; Talarek, H.D.
Results of IEA-Task III outdoor and indoor pyranometer comparison
Solar World Congress, Perth, Australien, 14.-19.8.83
2o.6o.o

IKP-200383
Anhalt, J.
Die Kollektorteststation Atibaia/Brasilien - Status und Perspektiven
Gesellschaft für Technische Zusammenarbeit, Eschborn, 8.6.83
2o.6o.1

IKP-200483
Baur, G.
Polarizability of nuclei in Sub-Coulomb scattering and in electronic atoms
MPI Heidelberg, 7.3.83
2o.8o.o

IKP-200583
Baur, G.; Hofmann, B.; Speth, J.
Nuclear polarization and isotope shift in electronic atoms
Frühjahrstagung der DPG, Sektion A: Kernphysik, Münster, 21.-25.3.83
2o.8o.o

IKP-200683
Baur, G.;
Fragmentation processes in nucleus-nucleus collisions
1983 RCNP Int. Symp. on Light Ion Reaction Mechanisms, Osaka, Japan, 16.-20.5.83
2o.8o.o

IKP-200783
Baur, G.; Budzanowski, A.; Bojowald, J.; Dabrowski, H.; Djaloeis, A.; Mayer-Böricke, C.; Oelert, W.; Riepe, G.; Rogge, M.; Turek, P.; Shyam, R.; Roesel, F.; Trautmann, D.
Alpha break-up inclusive cross sections to ^{3}He and triton
Frühjahrstagung der DPG, Sektion A: Kernphysik, Münster, 21.-25.3.83
2o.o6.o; 2o.2o.o; 2o.8o.o

IKP-200883
Baur, G.; Bojowald, J.; Djaloeis, A.; Mayer-Böricke, C.; Oelert, W.; Riepe, G.; Rogge, M.; Turek, P.; Budzanowski, A.; Dabrowski, H.; Shyam, R.; Rösel, F.; Trautmann, D.
^{3}He and triton rates in the alpha break-up inclusive cross sections
1983 RCNP Int. Symp. on Light Ion Reaction Mechanisms, Osaka, Japan, 16-20.5.83
2o.o6.o; 2o.2o.o; 2o.8o.o

IKP-200983
Baur, G.
Mechanisms of breakup reactions
RCNP Osaka, Japan, 24.5.83
2o.8o.o

IKP-201083
Baur, G.
Mechanismus von Aufbruchsreaktionen
DESY Hamburg, 14.6.83
2o.8o.o

IKP-201183
Baur, G.
Einfluß der Kernpolarisierbarkeit auf die Isotopieverschiebung in elektronischen Atomen
Univ. Mainz, 1.12.83
2o.8o.o

IKP-201283
Bechteler, H.; Faissner, H.; Koch, H.R.; Schult, O.W.B.; Seyfarth, H.; Yogeshwar, R.
Search for light penetrating bosons at a nuclear reactor with a set up of variable angular position
Frühjahrstagung der DPG, Sektion A: Kernphysik, Münster, 21.-25.3.83
2o.1o.o

IKP-201383
Bechteler, H.; Faissner, H.; Yogeshwar, R.; Koch, H.R.; Schult, O.W.B.; Seyfarth, H.
Search for the two-photon decay of penetraging particles emitted from a nuclear reactor
Frühjahrstagung der DPG, Sektion A: Kernphysik, Münster, 21.-25.3.83
2o.1o.o

IKP-201483
Bechteler, H.; Faissner, H.; Yogeshwar, R.; Koch, H.R.; Schult, O.W.B.; Seyfarth, H.
Suche nach dem Zwei-Photonen Zerfall leichter, durchdringender Teilchen am Forschungsreaktor MERLIN der KFA Jülich
Frühjahrstagung der DPG: Sektion B: Teilchenphysik, Wuppertal, 28.-30.3.83
2o.1o.o

IKP-201583
Bechteler, H.; Faissner, H.; Yogeshwar, R.; Koch, H.R.; Schult, O.W.B.; Seyfarth, H.
Spektrum leichter, durchdringender Teilchen aus Kernreaktionen
Frühjahrstagung der DPG, Sektion B: Teilchenphysik, Wuppertal, 28.-30.3.83
2o.1o.o

IKP-201683
Berg, G.
Isoscalar character of the 1^+ state at 5.844 MeV in ^{208}Pb
Int. Symp. on Light Ion Reaction Mechanisms, Osaka, Japan, 16.-20.5.83
2o.o6.o

IKP-201783
Berg, G.
The high resolution spectrometer BIG KARL and its use in nuclear and atomic physics
RCNP Osaka, Japan, 1.6.83
2o.o6.o

IKP-201883
Berg, G.
BIG KARL a high resolution spectrometer and its use in nuclear and atomic physics
Tandem Accelerator Center, Univ. of Tsukuba, Japan, 3.6.83
2o.o6.o

IKP-201983
Berg, G.
High resolution spectrometer "BIG KARL" and its use in nuclear and atomic physics
Jagiellonian Univ., Krakau, Polen, 13.7.83
2o.o6.o

IKP-202083
Beuscher, H.; Mathews, H.-G.; Mayer-Böricke, C.
ECR-source development at Jülich
Frühjahrstagung der DPG, Sektion A: Kernphysik, Münster, 21.-25.3.83
2o.3o.o

IKP-202183
Beuscher, H.; Mathews, H.-G.; Krauss-Vogt, W.
Status of the superconducting ECR-source for the Jülich cyclotron
5th E.C.R. Ion Sources Workshop, Louvain-La-Neuve, Belgien, 21.-22.4.83
2o.3o.o

IKP-202283
Beuscher, H.; Bräutigam, W.; Mathews, H.-G.; Reich, J.; Wucherer, P.
The project ISIS at JULIC
20th European Cyclotron Progress Meeting, Groningen, Niederlande, 7.-8.9.83
2o.3o.o

IKP-202383
Beuscher, H.; Mathews, H.-G.; Krauss-Vogt, W.
Results with the Pre-ISIS 2 E.C.R. source
20th European Cyclotron Progress Meeting, Groningen, Niederlande, 7.-8.9.83
2o.3o.o

IKP-202483
Blomqvist, J.; von Dincklage, R.D.; Ewan, G.T.; Hoff, P.; Jonson, B.; Kerek, A.; Klepper, O.; Lövhöjden, G.; Mattson, S.; Nyman, G.; Ravn, H.L.; Schardt, D.; Sistemich, K.
The single neutron nucleus $^{133}_{50}Sn_{82}$
Int. Conf. on Nucl. Physics, Florenz, Italien, 29.8.-3.9.83
2o.65.o

IKP-202583
Borgs, W.; Chatzipetros, J.; Lawin, H.; Lhersonneau, G.; Menzen, G.; Sistemich, K.; Wolf, A.
Set up for g-factor determination at JOSEF
Frühjahrstagung der DPG, Sektion A: Kernphysik, Münster, 21.-25.3.83
2o.65.o

IKP-202683
Brown, V.R.; Dermawan, H.; Krewald, S.; Osterfeld, F.; Speth, J.
A crucial test for the $\Delta(1232)$-hole quenching mechanism: (n,p) vs. (p,n) in heavy mass nuclei
Frühjahrstagung der DPG, Sektion A: Kernphysik, Münster, 21.-25.3.83
2o.8o.o

IKP-202783
Brown, V.R.; Krewald, S.; Speth, J.
Crucial test for the $\Delta(1232)$-hole effect
Int. Conf. on Nucl. Physics, Florenz, Italien, 29.8.-3.9.83
2o.8o.o

IKP-202883
Butsch, R.; Heck, B.; Pochodzalla, J.; Rabe, H.J.; Rosner, G.; Hlawatsch, G.
Fusion and incomplete fusion in reactions leading to the compound nucleus ^{59}Cu
Frühjahrstagung der DPG, Sektion A: Kernphysik, Münster, 21.-25.3.83
2o.o6.o

IKP-202983
Co', G.; Krewald, S.; Speth, J.
A theoretical approach to the electron scattering coincidence experiments for the study of the giant multipole resonances
Frühjahrstagung der DPG, Sektion A: Kernphysik, Münster, 21.-25.3.83
2o.8o.o

IKP-203083
Decowski, P.; Morsch, H.P.
Surface and volume vibrations in the giant monopole excitation of heavy nuclei
Frühjahrstagung der DPG, Sektion A: Kernphysik, 21.-25.3.83
2o.o6.o

IKP-203183
Decowski, P.; Morsch, H.P.; Zemlo, L.; Rogge, M.; Turek, P.; Schumacher, W.; Gaul, G.; Glasow, R.; Ludewigt, B.; Santo, R.
Contribution of quasifree scattering in 172 MeV α scattering from heavy nuclei
Frühjahrstagung der DPG, Sektion A: Kernphysik, Münster, 21.-25.3.83
2o.o6.o

IKP-203283
Decowski, P.; Morsch, H.P.; Zemlo, L.; Rogge, M.; Turek, P.; Gaul, G.; Glasow, R.; Ludewigt, B.; Santo, R.; Schumacher, W.
The role of fast nucleon emission in high energy α scattering studied by the parallel momentum transfer from fission angular correlations
Int. Conf. on Nucl. Physics, Florenz, Italien, 29.8.-3.9.83
2o.o6.o

IKP-203383
Decowski, P.
Giant collective excitations in nuclei
XV Masurian Summer School on Nucl. Physics, Mikolajki, Polen, 5.-17.9.83
2o.o6.o

IKP-203483
Dermawan, H.; Osterfeld, F.; Madsen, V.A.
Cross section calculations from microscopic nonlocal optical potentials
Frühjahrstagung der DPG, Sektion A: Kernphysik, Münster, 21.-25.3.83
2o.8o.o

IKP-203583
Djaloeis, A.; Gopal, S.; Bojowald, J.; Oelert, W.; Turek, P.; Mayer-Böricke, C.
The $^{25}Mg(^{3}He,\alpha)^{24}Mg$ reaction at E_i = 130 MeV
Frühjahrstagung der DPG, Sektion A: Kernphysik, Münster, 21.-25.3.83
2o.o6.o

IKP-203683
Ercan, A.; Broda, R.; Piiparinen, M.; Kleinheinz, P.; Blomqvist, J.
Proton-neutron multipletts in the one-particle one-hole nucleus $^{146}_{63}Eu_{83}$
Int. Conf. on Nucl. Physics, Florenz, Italien, 29.8.-3.9.83
2o.1o.o

IKP-203783
Goeke, K.
The quantized ATDHF approach: theory and application
Univ. Regensburg, 24.1.83
2o.8o.o

IKP-203883
Goeke, K.
The time-dependent Hartree-Fock-theory
Univ. Erlangen, 25.1.83
2o.8o.o

IKP-203983
Goeke, K.
The quantized ATDHF theory
Univ. Erlangen, 26.1.83
2o.8o.o

IKP-204083
Goeke, K.
Subbarrier fusion of $^{16}O+^{16}O$
Int. Conf. on Heavy-Ion Physics and Nucl. Physics, Catania, Italien, 21.-26.3.83
2o.8o.o

IKP-204183
Goeke, K.
Microscopic approach to subbarrier fusion
Univ. Tübingen, 28.6.83
2o.8o.o

IKP-204283
Goeke, K.
Meanfield methods in nuclear large amplitude collective motion
Vorlesungsreihe, 6th Granada Workshop on Nucl. Physics, Granada, Spanien, 3.-8.10.83
2o.8o.o

IKP-204383
Goeke, K.; Grümmer, F.; Reinhard, P.-G.
Quantized ATDHF calculations for the $^{16}O+^{16}O\rightarrow^{32}S$ fusion below and above the barrier
Vorlesungsreihe, VI Int. School on Nucl. and Neutron Physics and Nuclear Energy, Varna, Bulgarien, 12.-20.9.83
2o.8o.o

IKP-204483
Grümmer, F.
Microscopic description of nuclear excitations in deformed heavy nuclei
Int. Symp. on Nucl. Physics at Large Tandem Accelerators, Legnaro, Italien, 16.-18.3.83
2o.8o.o

IKP-204583
Grümmer, F.; Goeke, K.; Reinhard, P.-G.
Three-dimensional nuclear dynamics in the quantized ATDHF approach
Frühjahrstagung der DPG, Sektion A: Kernphysik, Münster, 21.-25.3.83
2o.8o.o

IKP-204683
de Haro, R.; Wambach, J.; Krewald, S.; Speth, J.
Microscopic description of decay and spreading width of giant resonances
Frühjahrstagung der DPG, Sektion A: Kernphysik, Münster, 21.-25.3.83
2o.8o.o

IKP-204783
Ikegami, H.
High resolution spectrographs
Workshop on the Physics Program at CELSIUS, Uppsala, Schweden, 8.11.83
2o.o6.o

IKP-204883
Jarczyk, L.; Kamys, B.; Magiera, A.; Strzalkowski, A.; Styczen, B.; Berg, G.P.A.; Hlawatsch, G.; Hürlimann, W.; Katayama, I.; Meißburger, J.; Oelert, W.; Römer, J.G.M.; Tain, J.L.; Krug, J.
Five nucleon transfer in the $^{12}C(d,^{7}Li)^{7}Be$ reaction at 78 MeV
Frühjahrstagung der DPG, Sektion A: Kernphysik, Münster, 21.-25.3.83
2o.o6.o

IKP-204983
Julin, R.; Yates, S.W.; Lunardi, S.; Soramel-Stanco, F.; Kleinheinz, P.; Gräf, H.; Chevallier, A.; Chevallier, J.; Haas, B.; Khazrouni, S.; Schulz, N.; Blomqvist, J.
The yrast states in the dysprosium nuclei with 82 and 83 neutrons
Frühjahrstagung der DPG, Sektion A: Kernphysik, Münster, 21.-25.3.83
2o.1o.o

IKP-205083
Kleinheinz, P.
Proton neutron residual interactions from inbeam studies of ^{146}Gd and ^{146}Eu in low spin compound reactions
Univ. of Jyväskylä, Finnland, 20.1.83
2o.1o.o

IKP-205183
Kleinheinz, P.
Multiparticle and octupole excitations in the nuclei around ^{146}Gd
Univ. Hamburg, 21.2.83
2o.1o.o

IKP-205283
Kleinheinz, P.
Teilchen-Phonon Austauschwechselwirkung bei Ein- und Zweiphonon Oktupolzuständen in ^{146}Gd
Expertentreffen in Schleching, 5.3.83
2o.1o.o

IKP-205383
Kleinheinz, P.
In-beam studies of the shell model nuclei around ^{146}Gd
Int. Symp. on Nuclear Physics at Large Tandem Accelerators, Padua, Italien, 16.-18.3.83
2o.1o.o

IKP-205483
Kleinheinz, P.
Deformed states in the spherical nucleus ^{152}Dy
Workshop on Nuclear Structure at High Spin, Kopenhagen, Dänemark, 24.-27.5.83
2o.1o.o

IKP-205583
Kleinheinz, P.
GT Zerfall des ^{147}Dy
GSI Darmstadt, 17.8.83
2o.1o.o

IKP-205683
Kleinheinz, P.
Aligned multiparticle yrast configurations and particle-octupole coupling phenomena in the nuclei around ^{146}Gd
Int. Symp. on Electromagnetic Properties of Atomic Nuclei, Tokio, Japan, 9.-12.11.83
2o.1o.o

IKP-205783
Kleinheinz, P.
Octupole excitations in Gd
Univ. Tokio, Japan, 14.11.83
2o.1o.o

IKP-205883
Kleinheinz, P.
Low-lying octupole and quadrupole collective states in the A=150 region
Inst. of Physical and Chemical Research, Saitama, Japan, 16.11.83
2o.1o.o

IKP-205983
Kleinheinz, P.
Nuclear structure in the ^{146}Gd region
Tokyo Inst. of Technology, Tokio, Japan, 17.11.83
2o.1o.o

IKP-206083
Kleinheinz, P.
Single and double octupole excitations observed in Gd nuclei
Research Center for Nucl. Phys., Osaka, Japan, 21.11.83
2o.1o.o

IKP-206183
Kleinheinz, P.
In-beam nuclear structure studies in the ^{146}Gd region
Osaka Univ. Lab. of Nucl. Studies, Osaka, Japan, 22.11.83
2o.1o.o

IKP-206283
Kleinheinz, P.
GT-β-decay and proton radioactivity in ^{147}Tb
HMI Berlin, 24.11.83
2o.1o.o

IKP-206383
Krewald, S.
The role of the isobar degree of freedom in the nucleus
5th Nordic Meeting on Intermediate and High Energy Nucl. Physics, Geilo, Norwegen, 10.-14.1.83
2o.8o.o

IKP-206483
Krewald, S.
(d,^{2}He) - a reaction for ICE?
5th Nordic Meeting on Intermediate and High Energy Nucl. Phys., Geilo, Norwegen, 10.-14.1.83
2o.8o.o

IKP-206583
Krewald, S.
Die Rolle der Δ_{33}-Resonanz im Kern
MPI Heidelberg, 19.1.83
2o.8o.o

IKP-206683
Krewald, S.
Zerfalls- und Spreizbreite von Riesenresonanzen
Expertentreffen für Kernphysik, Schleching, 2.-11.3.83
2o.8o.o

IKP-206783
Krewald, S.
Medium-Polarisationseffekte in der Δ_{33}-Loch Wechselwirkung
Univ. Bonn, 12.7.83
2o.8o.o

IKP-206883
Lieder, R.M.; Jäger, H.M.; Neskakis, A.; Venkova, T.; Michel, C.; Sletten, G.
Design study for a γ-γ coincidence spectrometer with large efficiency and background suppression
Frühjahrstagung der DGB, Sektion A: Kernphysik, Münster, 21.-25.3.83
2o.1o.o

IKP-206983
Lieder, R.M.
Band crossings in ^{181}Os and comparison with features in ^{180}Os
Workshop on Nucl. Struct. at High Spin, Kopenhagen, Dänemark, 25.5.83
2o.1o.o

IKP-207083
Lieder, R.M.; Neskakis, A.; Sletten, G.; Garrett, J.D.
Neutron and proton band crossings in ^{181}Os
Int. Conf. on Nucl. Phys., Florenz, Italien, 29.8.-3.9.83
2o.1o.o

IKP-207183
Lieder, R.M.; Jäger, H.; Neskakis, A.; Venkova, T.; Michel, C.
Design of a γ-γ coincidence spectrometer using BGO anti-compton spectrometers
Int. Conf. on Nucl. Phys., Florenz, Italien, 29.8.-3.9.83
2o.1o.o

IKP-207283
Lieder, R.M.
Design of BGO anti-compton spectrometers
Nordic Accelerator Workshop, Kopenhagen, Dänemark, 19.10.83
2o.1o.o

IKP-207383
Löwenich, K.; Dewald, A.; Gast, W.; Hanewinkel, H.; Zell, K.O.; Gelberg, A.; von Brentano, P.
High spin states and lifetime measurements in $^{120}Xe^{+}$
Frühjahrstagung der DPG, Sektion A: Kernphysik, Münster, 21.-25.3.83
2o.1o.o

IKP-207483
Löwenich, K.; Dewald, A.; Gast, W.; Hanewinkel, H.; Zell, K.O.; von Brentano, P.
High spin states in ^{120}Xe
Int. Conf. on Nucl. Phys., Florenz, Italien, 29.8.-3.9.83
2o.1o.o

IKP-207583
Ma, Z.Y.; Kuo, T.T.S.
A model-space BHF theory of nuclear matter.
Int. Conf. on Nucl. Phys., Florenz, Italien, 29.8.-3.9.83
2o.8o.o

IKP-207683
Machner, H.
Untersuchung des Reaktionsmechanismus mit Hilfe der ^{58}Ni(α,α'c), C=p,α Reaktion bei E_α = 140 MeV
Philipps Univ. Marburg, Februar 1983
2o.o6.o

IKP-207783
Machner, H.; Bechstedt, U.; Budzanowski, A.; Jahn, P.; Mayer-Böricke, C.
Pre-equilibrium and knock-out processes in (α,2α) reactions
Frühjahrstagung der DPG, Sektion A: Kernphysik, Münster, 21.-25.3.83
2o.o6.o

IKP-207883
Machner, H.; Didelez, J.P.; Riepe, G.; Protić, D.; Frascaria, N.; Gerlic, E.; Hourani, E.; Morlet, M.
Production of fast particles from nuclear reactions with high energy protons
Frühjahrstagung der DPG, Sektion A: Kernphysik, Münster, 21.-25.3.83
2o.o6.o

IKP-207983
Machner, H.; Riepe, G.; Protić, D.; Bohlen, H.G.; Fuchs, G.
Light charged particle emission from ^{20}Ne+^{197}Au
Frühjahrstagung der DPG, Sektion A: Kernphysik, Münster, 21.-25.3.83
2o.o6.o

IKP-208083
Machner, H.
Untersuchung kontinuierlicher Teilchenspektren bei mittleren Energien
TH Darmstadt, 31.5.83
2o.o6.o

IKP-208183
Machner, H.
Continuous light ion spectra from heavy ion induced reactions
Int. Conf. on High Energy Nucl. Phys., Balatonfüred, Ungarn, 5.-11.6.83
2o.o6.o

IKP-208283
Machner, H.
Test of a spreading width formula over a large energy range
Int. Conf. on Nucl. Phys., Florenz, Italien, 29.8.-3.9.83
2o.o6.o

IKP-208383
Machner, H.
New developments in the study of continuum spectra
Int. Conf. on Highly Excited States and Nucl. Struct., Orsay, Frankreich, 5.-8.9.83
2o.o6.o

IKP-208483
Mairle, G.; Grabmayr, P.; Schmidt-Rohr, U.; Wagner, G.J.; Berg, G.P.A.; Hürlimann, W.; Katayama, I.; Martin, S.A.; Meißburger, J.; Römer, J.G.H.; Styczen, B.; Tain, J.L.
Effective p-h interactions from the ^{209}Bi(d,^{3}He) ^{208}Pb reaction
Frühjahrstagung der DPG, Sektion A: Kernphysik, Münster, 21.-25.3.83
2o.o6.o

IKP-208583
Marinov, A.; Berg, G.P.A.; Gopal, S.; Hürlimann, W.; Katayama, I.; Martin, S.A.; Mayer-Böricke, C.; Meißburger, J.; Oelert, W.; Römer, J.G.M.; Rogge, M.; Tain, J.L.; Turek, P.; Zemlo, L.
Study of the ^{62}Ni(d,^{3}He)^{61}Co reaction
Frühjahrstagung der DPG, Sektion A: Kernphysik, Münster, 21.-25.3.83
2o.o6.o

IKP-208683
Mathews, H.-G.
ECR (Electron-Cyclotron-Resonance)-Ionenquellenentwicklung in Jülich
Univ. Bonn, 18.1.83
2o.3o.o

IKP-208783
Mathews, H.-G.; Beuscher, H.; Fiedler, R.; Krauss-Vogt, W.
Results of a 5 GHz ECR test device - Pre-ISIS 2
5th E.C.R. Ion Sources Workshop, Louvain-La-Neuve, Belgien, 21.-22.4.83
2o.3o.o

IKP-208883
Mathews, H.-G.; Beuscher, H.; Krauss-Vogt, W.
ECR-ion-source development at the Jülich cyclotron
7th Symp. on Ion Sources and Ion Assisted Technology - ISIAT '83, Kyoto, Japan, 12.-16.9.83
2o.3o.o

IKP-208983
Mathews, H.-G.
ECR source development at the Jülich cyclotron
IPCR Workshop, Tokio, Japan, 20.9.83
2o.3o.o

IKP-209083
Meyer, R.A.; Kaffrell, N.; Lawin, H.; Lhersonneau, G.; Monnand, E.; Paar, V.; Pfeiffer, B.; Pinston, J.A.; Ragnarsson, I.; Schussler, F.; Schmitt, A.; Seo, T.; Sistemich, K.; Trautmann, N.
Symmetric deformation in A∿100 odd and odd-odd nuclei and its influence of fission product beta-decay rates
Experts Meeting on Fission Product Data, BNL Upton, New York, USA, Oktober 1983
2o.65.o

IKP-209183
Morsch, H.P.
Investigation of giant resonances in hadron scattering experiments
XXI Int. Winter Meeting on Nucl. Phys., Bormio, Italien, 24.-29.1.83
2o.o6.o

IKP-209283
Morsch, H.P.; Decowski, P.; Rogge, M.; Turek, P.; Zemlo, L.; Martin, S.A.; Berg, G.P.A.; Meißburger, J.; Römer, J.G.M.; Tain, J.L.
New results from the study of giant resonances in small angle scattering
Frühjahrstagung der DPG, Sektion A: Kernphysik, Münster, 21.-25.3.83
2o.o6.o

IKP-209383
Morsch, H.P.
Direct excitation of higher multipole resonances in heavy nuclei
Int. Conf. on Highly Excited States and Nucl. Struct., Orsay, Frankreich, 5.-8.9.83
2o.o6.o

IKP-209483
Morsch, H.P.; Berg, G.P.A.; Decowski, P.; Tain, J.L.; Rogge, M.; Turek, P.; Zemlo, L.; Meißburger, J.; Römer, J.G.M.
Investigation of isovector giant resonances in (^{3}He,t) at $E_{^3He}$ = 135 MeV
Int. Conf. on Highly Excited States and Nucl. Struct., Orsay, Frankreich, 5.-8.9.83
2o.o6.o

IKP-209583
Morsch, H.P.
Surface and volume compression in the giant monopole resonances in heavy nuclei
Int. Conf. on Highly Excited States and Nucl. Struct., Orsay, Frankreich, 5.-8.9.83
2o.06.o

IKP-209683
Morsch, H.P.
Neue kollektive Anregungsmoden in schweren Kernen
Univ. Göttingen, 4.11.83
2o.06.o

IKP-209683
Nakayama, K.; Krewald, S.; Speth, J.; Love, W.G.
Exact operator structure of the Brueckner G-matrix
Frühjahrstagung der DPG, Sektion A: Kernphysik, Münster, 21.-25.3.83
2o.80.o

IKP-209783
Neskakis, A.; Lieder, R.M.; Sletten, G.; Garrett, J.D.
Neutron and proton band crossings in $^{179-181}Os$
Frühjahrstagung der DPG, Sektion A: Kernphysik, Münster, 21.-25.3.83
2o.1o.o

IKP-209883
Neskakis, A.; Beuscher, H.; Bochev, B.; Lieder, R.M.; Morek, T.; May, F.R.
Study of high-spin states in ^{188}Au
Int. Conf. on Nucl. Phys., Florenz, Italien, 29.8.-3.9.83
2o.1o.o

IKP-209983
Oelert, W.; Palla, G.; Mayer-Böricke, C.; Turek, P.
The (d,^{6}Li) alpha-transfer reaction on nuclei of the sd-shell
Frühjahrstagung der DPG, Sektion A: Kernphysik, Münster, 21.-25.3.83
2o.06.o

IKP-210083
Oelert, W.; Palla, G.
Ground state transitions in (d,^{6}Li) reactions on sd-shell nuclei
1983 RCNP Int. Symp. on Light Ion Reaction Mechanism, Osaka, Japan, 16.-20.5.83
2o.06.o

IKP-210183
Oelert, W.
Activities at the Nuclear Physics Laboratory in Jülich
Univ. Fukuoka, Japan, 30.5.83
2o.06.o

IKP-210283
Oelert, W.
Four-nucleon transfer reactions on sd-shell nuclei
Univ. Sendai, Japan, 3.6.83
2o.06.o

IKP-210383
Oelert, W.
Reaction mechanism of four-nucleon transfer reactions on sd-shell nuclei
Univ. Tokio, Japan, 7.6.83
2o.06.o

IKP-210483
Oelert, W.
The importance of considering coupled-reaction-channel mechanism in alpha transfer at sd-shell nuclei
INS Tokio, Japan, 9.6.83
2o.06.o

IKP-210583
Oelert, W.; Palla, G.; Betigeri, M.G.; Fortune, T.H.; Mayer-Böricke, C.; Rubio,B.; Turek, P.
Importance of two-step contributions in alpha transfer reactions on ^{22}Ne
Int. Conf. on Nucl. Phys., Florenz, Italien, 29.8.-3.9.83
2o.06.o

IKP-210683
Oelert, W.; Palla, G.
Alpha transfer of ground state transitions in sd-shell nuclei
Int. Conf. on Nucl. Phys., Florenz, Italien, 29.8.-3.9.83
2o.06.o

IKP-210783
Osterfeld, F.
Quenching of Gamow-Teller resonances - a Δ-isobar effect or a background problem?
Int. Workshop XI on Gross Properties of Nuclei and Nucl. Excitations, Hirschegg, 17.-22.1.83
2o.80.o

IKP-210883
Osterfeld, F.
Hochenergetische Protonenstreuung
Kernphysik-SNQ-Workshop, Bad Honnef, 1./2.2.83
2o.80.o

IKP-210983
Osterfeld, F.
Analyse von Gamow-Teller Resonanzen
Expertentreffen für Kernphysik, Schleching, 2.-11.3.83
2o.80.o

IKP-211083
Osterfeld, F.
Microscopic calculation of the background below Gamow-Teller resonances
Frühjahrstagung der DPG, Sektion A: Kernphysik, Münster, 21.-25.3.83
2o.80.o

IKP-211183
Osterfeld, F.
Microscopic background calculations for Gamow-Teller resonances
Symp. on Delta-Nucleus Dynamics, Argonne, IL, USA, 2.-4.5.83
2o.80.o

IKP-211283
Osterfeld, F.
Analysis of Gamow-Teller resonances
Kent State Univ., Kent, Ohio, USA, 6.5.83
2o.80.o

IKP-211383
Osterfeld, F.
Analysis of Gamow-Teller resonances
Indiana Univ., Bloomington, IN, USA, 9.5.83
2o.80.o

IKP-211483
Osterfeld, F.
Analysis of M1- and Gamow-Teller resonances
Michigan State Univ., East Lansing, MI, USA, 11.5.83
2o.80.o

IKP-211583
Osterfeld, F.
Is there evidence for Δ(1232) isobar-nucleon hole states in nuclei?
Lawrence Livermore Nat. Lab., Livermore, CA, USA, 20.5.83
2o.80.o

IKP-211683
Osterfeld, F.
Calculation of the imaginary optical potential in the nuclear structure approach
Workshop on Microscopic Approaches to Nucleon-Nucleus Scattering, Asilomar, CA, USA, 25.5.83
2o.8o.o

IKP-211783
Osterfeld, F.
Why do we need a high energy neutron facility?
Workshop on Microscopic Approaches to Nucleon-Nucleus Scattering, Asilomar, CA, USA, 27.5.83
2o.8o.o

IKP-211883
Osterfeld, F.
Untersuchung von Gamow-Teller-Resonanzen mit Hilfe von Ladungsaustauschreaktionen
Univ. Bonn, 18.7.83
2o.8o.o

IKP-211983
Osterfeld, F., Schulte, A.
Microscopic calculations of the background below giant resonances
Int. Symp. on Highly Excited States and Nucl. Struct., Orsay, Frankreich, 5.-8.9.83
2o.8o.o

IKP-212083
Osterfeld, F.
Physics with protons at intermediate energies
Workshop on the Physics Program at CELSIUS, Uppsala, Schweden, 8.11.83
2o.8o.o

IKP-212183
Osterfeld, F.
Quenching of Gamow-Teller and $\Delta L=1$-resonances, a Δ-isobar-effect or a damping and background problem?
NBI Kopenhagen, Dänemark, 15.12.83
2o.8o.o

IKP-212283
Palla, G.; Oelert, W.
Inelastic two-step processes in (d,^{6}Li) reaction on ^{24}Mg and ^{26}Mg at 80 MeV
1983 RCNP Int. Symp. on Light Ion Reaction Mechanism, Osaka, Japan, 16.-20.5.83
2o.o6.o

IKP-212383
Palla, G.; Oelert, W.
Population of $K^{\pi} = 2^{-}$-band states in ^{20}Ne via the (d,^{6}Li) reaction
1983 RCNP Int. Symp. on Light Ion Reaction Mechanism, Osaka, Japan, 16.-20.5.83
2o.o6.o

IKP-212483
Palla, G.; von Geramb, H.V.
A comparison of phenomenological and microscopic optical model potentials
Int. Conf. on Nucl. Phys., Florenz, Italien, 29.8.-3.9.83
2o.o6.o

IKP-212583
Palla, G.; Oelert, W.
Excitation of $K^{\pi} = 2^{-}$-band states in ^{20,22}Ne via the (d,^{6}Li) reaction
Int. Conf. on Nucl. Phys., Florenz, Italien, 29.8.-3.9.83
2o.o6.o

IKP-212683
Palla, G.; Oelert, W.
Coupled-channels effects in (d,^{6}Li) reaction on ^{24}Mg and ^{26}Mg at 80 MeV
Int. Conf. on Nucl. Phys., Florenz, Italien, 29.8.-3.9.83
2o.o6.o

IKP-212783
Posorski, R.
Energieabsorber - Wärmeübergangseigenschaften und Systemverhalten
BSE/ISES-Tagung: Erfahrungen mit Kollektor-, Energieabsorber- und Wärmepumpenanlagen, Köln, 1.12.83
2o.6o.1

IKP-212883
Probst, H.J.; Uray, I.
Die radioaktive Kontamination an einem Zyklotron
XI. Regional Congress of IRPA, Austrian-Hungarian-Yugoslavian Radiation Protection Meeting (Recent Developments and New Trends in Radiation Protection), Wien, 20.-24.9.83
2o.o5.o

IKP-212983
Reich, J.; Römer, J.; Rogge, M.; Zemlo, L.
Update of the JULIC beam handling system
20th European Cyclotron Progress Meeting, Groningen, Niederlande, 7.-8.9.83
2o.3o.o

IKP-213083
Römer, J.G.M.; Berg, G.P.A.; Hürlimann, W.; Katayama, I.; Martin, S.A.; Meißburger, J.; Oelert, W.; Tain, J.L.; Eversheim, P.D.; Hinterberger, F.; Trelle, P.; von Rossen, P.
Search for T = 5/2 double analog states in ^{23}Mg via the ^{26}Mg(^{3}He,^{6}He) reaction
Frühjahrstagung der DPG, Sektion A: Kernphysik, Münster, 21.-25.3.83
2o.o6.o

IKP-213183
Römer, J.G.M.; Berg, G.P.A.; Hlawatsch, G.; Magiera, A.; Meißburger, J.; Tain, J.L.; Hinterberger, F.; Brinkmöller, B.; Sondermann, G.
Search for 1^{+}-states in ^{88}Sr(p,p') and ^{90}Zr (p,p) at E_p = 45 MeV
Frühjahrstagung der DPG, Sektion A: Kernphysik, Münster, 21.-25.3.83
2o.o6.o

IKP-213283
Rösel, F.; Trautmann, D.; Baur, G.
Halbklassische Alignmentrechnungen bei Ion-Atom-Stößen
Frühjahrstagung der DPG, Sektion B: Atomphysik, Regensburg, 21.-25.3.83
2o.8o.o

IKP-213383
Rubio, B.; Julin, R.; Yates, S.W.; Kleinheinz, P.; Ercan, A.; Stoffl, W.; Henry, E.; Mann, L.; Struble, G.; Lanier, R.; Blomqvist, J.
An in-beam study of the one-hole nucleus ^{145}Eu
Frühjahrstagung der DPG, Sektion A: Kernphysik, Münster, 21.-25.3.83
2o.1o.o

IKP-213483
Seyfarth, H.
Grundlagen der Physik der Kernwaffenexplosion
Vorlesungsreihe "Verantwortung für den Frieden", RWTH Aachen, 26.10.83
2o.1o.o

IKP-213583
Sistemich, K.
Der Physiker in staatlichen Großforschungseinrichtungen
Wochenendseminar des Regionalverbands Hessen, Mittelrhein, Saar der DPG, Königstein, 4.-6.11.83
2o.65.o

IKP-213683
Sondermann, G.; Gaul, G.; Berg, G.P.A.; Hürlimann, W.; Katayama, I.; Martin, S.A.; Meißburger, J.; Römer, J.G.M.; Tain, J.L.; Styczen, B.
Search for 1^{+} states in ^{58}Ni(p,p') at E_p = 45 MeV
Frühjahrstagung der DPG, Sektion A: Kernphysik, Münster, 21.-25.3.83
2o.o6.o

IKP-213783
Speth, J.
Crucial test of the Δ(1232)-hole effect: (n,p) vs. (p,n)
School on Mesons, Isobars, Quarks and Nucl. Excitations, Erice, Sizilien, 6.-18.4.83
2o.8o.o

IKP-213883
Speth, J.
Δ-isobar effects in nuclei
CEN Orsay, Frankreich, 9.6.83
2o.8o.o

IKP-213983
Speth, J.
Quenching von Spin-Isospin-Moden in Kernen
Univ. Regensburg, 15.7.83
2o.8o.o

IKP-214083
Speth, J.
Nuclear giant resonances and nucleon-nucleon interaction
Vorlesungsreihe, Int. Summer School on Nucleon-Nucleon Interaction and Nuclear Manybody Problem, Changchun, China, 25.7.-1.8.83
2o.8o.o

IKP-214183
Speth, J.
Delta-isobar nucleon interaction
Indiana Univ. Cycl. Facility, Bloomington, IN, USA, 10.10.83
2o.8o.o

IKP-214283
Speth, J.
Mesonic and haryonic degrees of freedom in nuclear structure physics
Indiana Univ. Cycl. Facility, Bloomington, In, USA, 11.10.83
2o.8o.o

IKP-214383
Speth, J.
Mesonic and baryonic degrees of freedom in nuclear structure physics
Texas A&M Univ., College Station, TX, USA, 14.10.83
2o.8o.o

IKP-214483
Speth, J.
What is the role of quarks in nuclear physics?
Indiana Univ. Nucl. Phys. Workshop, Bloomington, IN, USA, 21.10.83
2o.8o.o

IKP-214583
Speth, J.
Mesonic and baryonic degrees of freedom in nuclear structure physics
Univ. of Pittsburgh, PA, USA, 27.10.83
2o.8o.o

IKP-214683
Speth, J.
Die Δ-Isobar-Nukleon-Wechselwirkung in Kernen
Univ. Heidelberg, 12.12.83
2o.8o.o

IKP-214783
Schmid, K.W.; Grümmer, F.; Faessler, A.; Fladt, B.; Ansari, A.
The first year with the MONSTER
Frühjahrstagung der DPG, Sektion A: Kernphysik, Münster, 21.-25.3.83
2o.8o.o

IKP-214883
Schult, O.
ISOLDE-Physik: Gegenwart und Zukunft
Kernphysik-SNQ-Workshop, Bad Honnef, 1./2.2.83
2o.1o.o

IKP-214983
Schult, O.
Nuclear physics at ISOLDE (CERN) and the ILL (Grenoble)
Tagung der Japanischen Physikalischen Gesellschaft, Osaka, Japan, 29.3.83
2o.1o.o

IKP-215083
Schult, O.
Thoughts about nuclear physics at an intense spallation source
Tokyo Inst. of Technology, Tokio, Japan, 31.3.83
2o.1o.o

IKP-215183
Schult, O.
Nuclear physics at an intense spallation source
Inst. for Nucl. Studies, Tokio, Japan, 1.4.83
2o.1o.o

IKP-215283
Schult, O.
Thoughts about nuclear physics at an intense spallation source
Inst. of Physical and Chemical Research, Tokio, Japan, 2.4.83
2o.1o.o

IKP-215383
Schult, O.
Thoughts about nuclear physics at an intense spallation source
Japan Atomic Energy Research Inst., Tokai, Japan, 4.4.83
2o.1o.o

IKP-215483
Schult, O.
Thoughts about nuclear physics at an intense spallation source
RI-Cyclotron Centre, Tohoku Univ., Sendai, Japan, 7.4.83
2o.1o.o

IKP-215583
Schult, O.
Thoughts about nuclear physics at an intense spallation source
Univ. Hiroshima, Japan, 12.4.83
2o.1o.o

IKP-215683
Schult, O.
Thoughts about nuclear physics at an intense spallation source
Kyushu Univ., Fukuoka, Japan, 14.4.83
2o.1o.o

IKP-215783
Schult, O.
Isotope shifts
Osaka Univ., Japan, 4.5.83
2o.1o.o

IKP-215883
Schult, O.
Plans for nuclear research at the spallation facility SNQ
Research Center for Nucl. Phys., Suita, Osaka, Japan, 11.5.83
2o.1o.o

IKP-215983
Schult, O.
Contributions of nuclear physicists to applied science
Dept. of Nucl. Engineering, Nagoya, Japan, 12.5.83
2o.1o.o

IKP-216083
Schult, O.
Nuclear studies at a high current spallation source
Vorlesung, RCNP-Kikuchi Summer School, Kyoto, Japan, 26.5.83
2o.1o.o

IKP-216183
Schult, O.
Gamma and X-ray measurements with crystal spectrometers
Europhysics Study Conf., Kreta, 27.6.-1.7.83
2o.1o.o

IKP-216283
Schult, O.
Nuclear structure studies with slow neutrons
Vorlesungsreihe, VI Int. School on Nucl. and Neutron Phys. and Nucl. Energy, Varna, Bulgarien, 12.-20.9.83
2o.1o.o

IKP-216383
Stein, H.J.
Solarheizungsanlage zum Beheizen, Funkübertragungsstelle Garmisch II auf der Zugspitze - Meßprogramm
BMFT Statusseminar: Nutzung der Sonnenenergie in bundeseigenen Gebäuden, Dieburg, 8.6.83
2o.6o.1

IKP-216483
Stein, H.J.; Köhnen, M.
Solar heating plant at mount Zugspitze
Solar World Congress, Perth, Australien, 14.-19.8.83
2o.6o.1

IKP-216583
Stein, H.J.
Solarenergienutzung in der Haustechnik - Ergebnisse und Perspektiven von KFA-Arbeiten
Insolar-Kolloquium, DFVLR-FZ-Zentrum, Stuttgart, 19.9.83
2o.6o.o

IKP-216683
Stein, H.J.
Solare Warmwasserbereitung und Wärmepumpen-Heizanlagen - Systemtechnische Aspekte
Philips Forschungslabor, Aachen, 19.10.83
2o.6o.1

IKP-216783
Stein, H.J.
Die Sonnenheizungsanlage der Deutschen Bundespost am Zugspitzgipfel
Univ. München, 25.11.83
2o.6o.1

IKP-216883
Tain, J.L.; Berg, G.P.A.; Decowski, P.; Katayama, I.; Martin, S.A.; Meißburger, J.; Morsch, P.; Römer, J.G.M.; Rogge, M.; Styczen, B.; Turek, P.
Investigation of the 1^+ state in ^{208}Pb at 5.84 MeV by inelastic hadron scattering
Frühjahrstagung der DPG, Sektion A: Kernphysik, Münster, 21.-25.3.83
2o.o6.o

IKP-216983
Tain, J.L.; Brinkmöller, B.; Berg, G.P.A.; Hlawatsch, G.; Magiera, A.; Meißburger, J.; Oelert, W.; Palla, G.; Römer, J.G.M.; Sondermann, G.
Gamow-Teller resonance in $^{90}Zr(^{3}He,t)$ at $E_{^3He}$ = 135 MeV
Int. Symp. on Highly Excited States and Nucl. Struct., Orsay, Frankreich, 5.-8.9.83
2o.o6.o

IKP-217083
Talarek, H.D.; Pescatore, M.
Supplemental thermal performance tests
DCS Workshop des SSPS Projekts, Almeria, Spanien, 6.-8.12.83
2o.6o.1

IKP-217183
Trache, L.; Wrzesinski, J.; Wesselborg, C.; Zell, K.O.; Bazzacco, D.; Moore, F.; von Brentano, P.; Berg, G.P.A.; Hürlimann, W.; Meißburger, J.; Römer, J.G.M.; Tain, J.; Katayama, I.
Particle-octupole coupling in the N=83 ^{143}Nd nucleus
Frühjahrstagung der DPG, Sektion A: Kernphysik, Münster, 21.-25.3.83
2o.o6.o

IKP-217283
Trautmann, D.; Rösel, F.; Baur, G.
Alignment bei der Ionisation innerer Schalen
Frühjahrstagung der DPG, Sektion B: Atomphysik, Regensburg, 14.-18.3.83
2o.8o.o

IKP-217383
Uray, I.; Gyarmati, E.; Felszerfalvi, J.; Probst, H.J.; Heinzelmann, M.
Possible use of LiF dosemeters in mixed neutron-gamma fields
XI. Regional Congress of IRPA, Austrian-Hungarian-Yugoslavian Radiation Protection Meeting (Recent Developments and New Trends in Radiation Protection), Wien, 20.-24.9.83
2o.o5.o

IKP-217483
Uray, I.; Manngard, P.; Probst, H.J.; Heinzelmann, M.
Characteristics of mixed neutron-gamma radiation fields around cyclotrons
XI. Regional Congress of IRPA, Austrian-Hungarian-Yugoslavian Radiation Protection Meeting (Recent Developments and New Trends in Radiation Protection), Wien, 20.-24.9.83
2o.o5.o

IKP-217583
Uray, I.; Probst, H.J.
Empfindlichkeit von Kontaminationsmeßgeräten für praktisch vorkommende Kontaminationen am Jülicher Isochronzyklotron - Problematik der Grenzwertfestlegung für Routinebetrieb
17. Jahrestagung des Fachverbandes für Strahlenschutz e.V. (Strahlenschutzaspekte bei Radioaktiven Kontaminationen), Aachen, 8.-1o.6.83
2o.o5.o

IKP-217683
Wambach, J.
Recent developments in Chiral bag models
Int. Symp. on Quarks and Nucl. Struct., Bad Honnef, 13.-16.6.83
2o.8o.o

IKP-217783
Wambach, J.; Schwesinger, B.
Damping of highly excited vibrations in heavy nuclei
Int. Symp. on Highly Excited States and Nucl. Struct., Orsay, Frankreich, 5.-8.9.83
2o.8o.o

IKP-217883
Wucherer, P.
The problems to realize an optimized RF central region for ISIS
20th European Cyclotron Progress Meeting, Groningen, Niederlande, 7.-8.9.83
2o.3o.o

IKP-217983
Xiangfu, S.; Bazzacco, D.; Gast, W.; Gelberg, A.; Kaup, U.; Dewald, A.; Zell, K.O.; von Brentano, P.
Excited states in $^{130}Ba^{+}$
Frühjahrstagung der DPG, Sektion A: Kernphysik, Münster, 21.-25.3.83
2o.1o.o

IKP-218083
Xiangfu, S.; Löwenich, K.; Dewald, A.; Gast, W.; Gelberg, A.; Hanewinkel, H.; Kaup, U.; Zell, K.O.; von Brentano, P.; Zemel, A.
B(Ew) anomaly in collective levels of Ba and Xe nuclei
Int. Conf. on Nucl. Phys., Florenz, Italien, 29.8.-3.9.83
2o.1o.o

IKP-218183
Yates, S.W.; Kleinheinz, P.; Julin, R.; Stöffl, W.; Henry, E.; Mann, L.; Decman, D.; Blomqvist, J.
Nucleon-nucleon interactions from particle-hole multipletts in ^{146}Gd
Frühjahrstagung der DPG, Sektion A: Kernphysik, Münster, 21.-25.3.83
2o.1o.o

IKP-218283
Yogeshwar, R.
Suche nach leichten, durchdringenden Teilchen am Forschungsreaktor MERLIN der KFA Jülich
RWTH Aachen, 29.4.83
2o.1o.o

IKP-218383
Yogeshwar, R.
Grundlagen der Physik der Kernwaffen
FH Aachen-Jülich, 20.10.83
2o.1o.o

INSTITUT FUER KERNPHYSIK

X . INTERNAL REPORTS

IKP-500183
Bodewig, W.
Bestimmung des Absorptionsvermögens von Energieabsorbern aus deren Leerlauftemperaturen
KFA-IKP-Sol IB 1/83
2o.6o.1

IKP-500283
Talarek, H.D.
Annual progress report task III - Performance testing of solar collectors
IEA Internal Report, Januar 1983
2o.6o.1

XI . INTERNAL TALKS

IKP-600183
Anhalt, J.
Die Kollektorteststation Atibaia/Brasilien - Status und Perspektiven
PLS-Seminar, IKP, 6.6.83
2o.6o.1

IKP-600283
Berg, G.P.A.
1^+-Spektroskopie in schweren Kernen an BIG KARL
9. Sitzung des wiss. Beirats des IKP, 28.6.83
2o.o6.o

IKP-600383
Krewald, S.
Hochenergetische Neutronenstreuung als Test auf die Δ_{33}-Resonanz im Kern
9. Sitzung des wiss. Beirats des IKP, 28.6.83
2o.8o.o

IKP-600483
Lieder, R.M.
Untersuchung von Bandenkreuzen in $^{180,181}Os$ mit Anti-Compton-Spektrometern
9. Sitzung des wiss. Beirats des IKP, 28.6.83
2o.1o.o

IKP-600583
Love, W.G.
Spin x current correlations in nuclei and their implications for (p,p') reactions
IKP, KFA Jülich, 21.9.83
2o.8o.o

IKP-600683
Ma, Z.Y.
Quark pion interactions in a deformed bag model
IKP, KFA Jülich, 31.3.83
2o.8o.o

IKP-600783
Mathews, H.-G.
Stand der ECR-Ionenquellenentwicklung für das Projekt ISIS am Jülicher Zyklotron
9. Sitzung des wiss. Beirats des IKP, 28.6.83
2o.o3.o

IKP-600883
Maßmeyer, K.
Variationen des Stromes fühlbarer Wärme in der atmosphärischen Grenzschicht
PLS-Seminar, IKP, 30.11.83
2o.6o.1

IKP-600983
Nemeth, J.
Pion condensate in heavy ion collisions
IKP, KFA Jülich, 17.3.83
2o.8o.o

IKP-601083
Probst, H.J.
Personensicherheit am Jülicher Isochronzyklotron
Fortbildungsseminar der KFA Jülich (Angewandter Strahlenschutz), Jülich, 11.5.83
2o.o5.o

IKP-601183
Reinhardt, H.
A geometric approach to dissipation in many-body systems
IKP, KFA Jülich, 22.9.83
2o.8o.o

IKP-601283
Stein, H.J.
Die Sonnenheizungsanlage der Deutschen Bundespost am Zugspitzgipfel
PLS-Seminar, IKP, 28.10.83
2o.6o.1

XII. INDEX TO AUTHORS